

Project title:
Integrated Flood and
Sediment Management in
River Basins for
Sustainable Development



CRRP2020-09MY-Kantoush

2022

Project Reference Number: CRRP2020-09MY-Kantoush

Project Duration: 2 Years

Funding Awarded: USD 87,000

Grant DOI: <https://doi.org/10.13039/100005536>

Date of Publication:31/01/2023

Project Leader and Contact Details:

| No. | Name | Organization | Email |
|-----|-----------------------------------|---|--------------------------------------|
| 1 | Assoc. Prof. Sameh Ahmed Kantoush | Disaster Prevention Research Institute (DPRI), Kyoto University (KU), Japan | kantoush.samehahmed.2n@kyoto-u.ac.jp |

Collaborators and Contact Details:

| No. | Name | Organization | Email |
|-----|-------------------------------|--|--|
| 1 | Prof. Sumi Tetsuya | Disaster Prevention Research Institute (DPRI), Kyoto University (KU), Japan | sumi.tetsuya.2s@kyoto-u.ac.jp |
| 2 | Dr. Mohamed Saber | | mohamedmd.saber.3u@kyoto-u.ac.jp |
| 3 | Dr. Khagendra Bharambe | | bharambe.khagendrapralhad.2k@kyoto-u.ac.jp |
| 4 | Dr. Bui Du Duong | Director of National Center for Water Resources Planning and Investigation, Vietnam | duongdubui@gmail.com |
| 5 | Dr. Dao Ngo | An Nhien Farm, Vietnam | daongolapat@gmail.com |
| 6 | Dr. Vo Cong Hoang | Thuy Loi University, Vietnam | hoangvc@tlu.edu.vn |
| 7 | Prof. Nguyen Canh Thai | | ncanhthai@tlu.edu.vn |
| 8 | Dr. Pham Hong Nga | | phamhongnga@tlu.edu.vn |
| 9 | Assoc. Prof. Vo Ngoc Duong | The University of Da Nang, Vietnam | vnduong@dut.udn.vn |
| 10 | Dr. Binh Doan Van | Vietnamese-German University, Vietnam | binhdv0708vl@gmail.com |
| 11 | Prof. Orlando F. Balderama | Isabela State University, Philippines | ofbalderama@gmail.com |
| 12 | C'zar M. Sulaik | Deputy Administrator for Engineering and Operations, National Irrigation Administration, Philippines | daeo17@yahoo.com |
| 13 | Susan P. Abaño | Chief of Program Division of the National Water Resources Board, Philippines | susan.abano@nwr.gov.ph |
| 14 | Prof. Jeffrey Lloyd R. Bareng | Isabela State University, Philippines | jlloydbareng@gmail.com |

| | | | |
|----|--------------------|---|----------------------|
| 15 | Sancho A. Maborang | Department of Science and Technology Region 02, Philippines | dost02.ord@gmail.com |
| 16 | Dr. Lanie A. Alejo | Isabela State University, Philippines | laalejo@up.edu.ph |

Recommended Citation:

Kantoush, S.A, Tetsuya, S., Saber, M., Duong D.B., Ngo, D., Hoang, V.C., Thai, N.C., Nga, P.H., Duong, V.N., Doan Van, B., Balderama, O., Sulaik, C.M., Abaño, S.P., Bareng, J.L., Maborang, S.A., Alejo, L.A. (2023). Integrated Flood and Sediment MAnagement in River basins for susTainable development (FSMART). Project Final Report. Asia-Pacific Network for Global Change Research.



Asia-Pacific Network for Global Change Research (APN)

© 2022 The authors. Published by the Asia-Pacific Network for Global Change Research (APN) under the Creative Commons Attribution-NonCommercial 4.0 International (CC-BY-NC 4.0) licence.

All opinions, findings, conclusions or recommendations expressed in this material are those of the authors and do not necessarily reflect the views of APN. While the information and advice in this publication are believed to be true and accurate at the date of publication, neither the editors nor APN accepts any legal responsibility for any errors or omissions that may be made. APN and its member countries make no warranty, expressed or implied, with respect to the material contained herein.

The use of geographic names, boundaries and related data on maps, and in lists and tables within this publication are not warranted to be error-free, nor do they imply any endorsement by APN.

1. Summary

The project aimed to assess the impacts of climate change and human interventions on reservoir sedimentation, flood inundation, agricultural practices, and river and coastal erosion in the Vu Gia-Thu Bon and Cagayan River basins of Vietnam and the Philippines, respectively, to establish an integrated flood and sediment management schemes for sustainable development. Over the recent decades, dam construction and anthropogenic activities have had increasingly profound effects on sediment load, bathymetry, and hydrological processes. Understanding these impacts is critical for the foundation of sustainable hydrogeomorphology management. Hence, this project was designed with the ultimate goal of transferring the project results to the stakeholders and policy decision-makers to implement them into the national laws. This also involved organizing some training courses, seminars, and workshops to train the young researchers, stakeholders, policymakers, land local communities and expand the collaborative network with other ASIAN countries and global change programs.

In regard to the proposed objectives, and activities planned, the project has collected all the required sets of data through various field visits and bathymetry surveys, and analysis has been performed to achieve the objectives. The results have been published in various high-impact factors international journals (***See the list of publications for more details***). Moreover, the project results, and research activities have been also shared, and discussed during the special APN/JASTIP session at the 2nd international conference on environmental sustainability and resource security (IC-ENSURES2022, during 08-09 March 2022), and during the special project closing symposium (1st international symposium on Integrated Flood and Sediment Management in River Basin for Sustainable Development (FSMaRT 2022), during 18-20 December 2022, Vietnam) by APN-Project researchers and collaborators from Japan, Vietnam, and the Philippines side counterparts (***See the Annex 1 for more details***).

Apart from this, the project also helped to establish an international commission (International Association on Climate Change Adaptation and Disaster Risk Reduction Management Inc. (IO-CCA-DRRM)) in the Philippines for more global collaboration, and networking (***see the Annex 2 for more details***). This project has also trained stakeholders, policymakers, and local communities on integrated water resource management by conducting a three-day face-to-face collaborative stakeholder forum on Integrated Flood Risk Management in the Philippines (***see annex 3 for more details***), and many young researchers on TELEMAC numerical simulation by organizing comprehensive four days training workshop hosted physically and virtually by Kyoto University and Isabela State University for the participants from the Philippines and Japan respectively (***see annex 4 for more details***). Overall, this initiative helped publish numerous papers in high-impact factor journals and prestigious international conferences (***annex 5.1-5.9, annexes 6.1-6.10, and annex 7***) and will continue such collaboration through future projects and multilateral fund collaboration.

2. Objectives

The main objectives of this proposed project are:

1. To assess climate change/climate variability and its impacts on the rainfall-runoff and sediment yield in the Vu Gia-Thu Bon and Cagayan River basins.
2. To quantify the consequences of changing climate on floods, droughts, agriculture activities, and river and coastal erosion; then to propose appropriate countermeasures.
3. To evaluate reservoir sedimentation and propose suitable sediment management techniques focusing on Cagayan (e.g., Magat dam) river basins.
4. To develop an integrated flood and sediment management for sustainable development.
5. To foster young research for leading such innovative networks for bridging Asia and Pacific region partners and have a significant input for such global issues;
6. To establish an association where the results can be transferred to the central government for implementation of “integrated river basin management” in the laws.

3. Outputs, Outcomes and Impacts

| Outputs | Outcomes | Impacts |
|---|--|--|
| Completed multiple field surveys and required data has been collected (Objective 1, 2, and 3). | Collected data on Bathymetry, dam operation rules, topographic, soil sampling, sediment, climate, historical flood, and damage data etc. (Objectives 1, 2, and 3). | Assessed the potential high-risk zones for drought, and flood across Cagayan & VGTB basins, and also developed first time new Land Use, Soil maps. Published results in high-impacts factor journal, and reputed international conferences. |
| Established SWAT, TELEMAC, and RRI Model (Objective 1, 2, and 3). | Hydrological modelling and data analysis (Objective 1, 2, and 3). | |
| Delivered and Installed Turbidity Meters (Objectives 3) | Instruments installation, and data measurements techniques (Objectives 3) | Real-time data measure, and analysis such as turbidity measurement, and analysis for water quality improvement, rainfall prediction and forecasting inundation areas ahead of any typhoon |
| Developed an ensemble rainfall prediction, and Decision Support System (DSS) (Objective 3, and 4) | Real-time Long-term rainfall prediction and web-based DSS for effective dam operation (Objectives 3, and 4) | |
| Completed Stakeholder Forum on Integrated Flood Risk Management (Objective 4) | Face-to-face collaborative workshop on scaling up community linkages (Objective 4) | Community involvement for integrated flood and sediment management for |

| | | |
|--|--|--|
| | | sustainable development |
| Completed onsite and online (physically and virtually) trainings (Objectives 3, 4 and 5) | Organized training programs on TELEMAC 2D and 3D numerical simulations, and UNESCO-IHP (Objectives 3, 4 and 5) | Trained young and early career researchers on integrated sediment management from project pilot countries |
| Established an International Organization on Climate Change Adaptation and Disaster Risk Management (IO-CCA-DRRM)- (Objective 6) | International organization for global collaboration, and networking (Objective 6) | Expanded FSMaRT Network, and an international association that can bridge in implementing an Integrated River Basin Management |
| Conducted International conference, and discussed the project results (Objective 4, and 5) | Organized an international conference (Objective 4, and 5) | Published and shared project results, networking, and well-formed a strong international research group for continuation of research, and future co-project funding applications |
| Completed the project closing symposium | Reporting the final results of the project and closing summary | |
| Completed a series of bi-annual meetings, seminars and workshops | Conducted a Kick-off meeting, project monitoring workshop, and project meetings | Helped time-to-time project monitoring, progress tracking, and successfully project submission |
| Successfully submitted annual and bi-annual project reports | Email communication, and submission of project reports | |
| Developed APN-project (FSMaRT) website, Social network page | Updated website with information on project activities, and research outputs | Shared project information with all the project members, and associated global networks |

4. Key facts/figures

- Trained more than 40 young/early career researchers through four-days (25-28 February 2022) training on TELEMAC 2D and 3D Numerical Models.
- Signed Memorandum of Understanding (MOU) between the Japan Water Agency (JWA) and the City of Santiago to establish a partnership in conducting collaborative activities and projects to achieve water security in Santiago City and sharing knowledge on water issues concerning flood and sediment management of Magat Dam and Cagayan River Basin, during the stakeholder forum held between July 14-16, 2022, at the Mango Suites, Santiago City, Philippines.

- Established an expanded FSMaRT Network, and an International Association on Climate Change Adaptation and Disaster Risk Management (IO-CCA-DRRM) for global collaboration and the formation of a larger network of agencies worldwide.
- Participated more than 70% young/early career researchers especially women during the project closing workshop (1st International Symposium on Integrated Flood and Sediment Management in River Basin for Sustainable Development (FSMaRT 2022)) held during 18th -20th December 2022 in Vietnam.
- The Stakeholder Forum on Integrated Flood Risk Management, held from 14 to 16 July 2022, was designed to train the stakeholders and enhance the capacities of policymakers, managers, and practitioners of river basin organizations on flood management through knowledge sharing, techniques, methodologies, and good practices to help achieve the effective implementation of integrated flood risk management.
- Project results on almost 10 different research topics were published and shared during the 2nd international conference on environmental sustainability and resource security (IC-ENSURES2022), held virtually from 08 to 09 March 2022.
- Assessed and supported young early career researchers from a new member country (Universiti Teknologi Malaysia, UTM Malaysia) for expanding the APN network and multilateral collaboration over the course of this two-year project.
- One super computer system for project data modeling and simulation has been purchased and transferred to the University of Danang (DU), Vietnam.
- Two turbidity meters have been delivered, and two turbidity measurement stations have been installed in the Cagayan River basin, Philippines.
- Throughout the project period, three bathymetry and field data surveys and one post-flood survey were conducted.
- A web-based ensemble rainfall prediction, and decision support system (DSS) has been developed for effective dam operation, and to support rainfall prediction over Cagayan River Basin, Philippines.
- Published nine numbers of journal articles and more than 20 numbers of conference proceedings articles.

5. Publications

1. Binh Quang Nguyen, Sameh Kantoush, Doan Van Binh, Mohamed Saber, Duong Ngoc Vo & Tetsuya Sumi (2023): Understanding the anthropogenic development impacts on long-term flow regimes in a tropical river basin, Central Vietnam, Hydrological Sciences Journal, DOI: 10.1080/02626667.2022.2153298
2. Binh Quang Nguyen, Sameh Kantoush, Mohamed Saber, Doan Van Binh, Duong Ngoc Vo & Tetsuya Sumi (2023): Quantifying the impacts of hydraulic infrastructures and contributions of the sub-basins on streamflow in a tropical river basin, Vietnam, Journal of Hydrological Processes.
3. Mohamed Saber, Tayeb Boulmaiz, Mawloud Guermoui, Karim I. Abdrabo, Sameh A. Kantoush, Tetsuya Sumi, Hamouda Boutaghane, Tomoharu Hori, Doan Van Binh, Binh

- Quang Nguyen, Thao TP Bui, Ngoc Duong Vo, Emad Habib & Emad Mabrouk (2023): Machine learning techniques and 2D rainfall-runoff inundation model for flood susceptibility and extent mapping, *Journal of geomatics natural hazards and risk* (Under Review)
4. Thanh, H. V., Binh, D. V., Kantoush, S. A., Nourani, V., Saber, M., Lee, K.-K., & Sumi, T. (2022). Reconstructing daily discharge in a megadelta using machine learning techniques. *Water Resources Research*, 58, e2021WR031048.
<https://doi.org/10.1029/2021WR031048>
 5. Doan Van Binh, Sameh A. Kantoush, Riadh Ata, Pablo Tassi, Tam V. Nguyen, J'ér'emy Lepasqueur, Kamal El Kadi Abderrezzak, Sébastien E. Bourban, Quoc Hung Nguyen, Doan Nguyen Luyen Phuong, La Vinh Trung, Dang An Tran, Thanh Letrung, Tetsuya Sumi (2022): Hydrodynamics, sediment transport, and morphodynamics in the Vietnamese Mekong Delta: Field study and numerical modelling, *Geomorphology*, <https://doi.org/10.1016/j.geomorph.2022.108368>
 6. Mata, C.B., Balderama, O.F., Alejo, L.A., Bareng, J.L.R., Kantoush, S.A. (2022). Satellite-based flood inundation and damage assessment. *J Robot Auto Res*, 3(2), 209-219. doi:10.33140/jrar.03.02.12
 7. Singson, C.L., Alejo, L.A., Balderama, O.F., Bareng, J.L., Kantoush, S.A. (2023) Modelling Climate Change Impact On The Inflow Of Magat Reservoir Using The Soil And Water Assessment Tool (Swat) Model For Dam Management (2023). *Journal of Water and Climate Change*.
 8. Felipe, A.J., Alejo, L.A., Balderama, O.F., Rosete, E.A. (2023) Climate change intensifies the drought vulnerability of river basins. *Journal of Water and Climate Change*. (Under Review)
 9. Alejandro, A.S., Alejo, L.A., Balderama, O.F., Bareng, J.L., Kantoush, S.A. (2023). Forecasting dam inflow and flood inundations under extreme rainfall events using the rainfall-runoff-inundation model. *Modeling Earth Systems and Environment*. (Under Review)

6. Media reports, videos, and other digital content

1. APN-Project (FSMaRT) Website updated with project information, and key research activities (<https://www.ifsm-ku.com/>)
2. 1st international symposium on Integrated Flood and Sediment Management in River Basin for Sustainable Development (FSMaRT) 2022 (<https://fsmart.dut.udn.vn/>)
3. Video contents of 1st international symposium on Integrated Flood and Sediment Management in River Basin for Sustainable Development (FSMaRT) 2022 (https://www.youtube.com/watch?v=mM7_Bc9W6uA)
4. The 2nd international conference on environmental sustainability and resource security (IC-ENSURES2022, during 08-09 March 2022, available at, <https://www.utm.my/ipasa/icensures2022/>)

5. Social networking site for activity reporting, and publications developed by project collaborator (Isabela State University (ISU), Philippines),
<https://www.facebook.com/APN.ISU.IFWARM>

7. Pull quotes

The APN FSMaRT project paved the way for a new paradigm shift in Asian river basins for integrated flood and sediment management by developing new monitoring techniques and generating accurate measurements that allow us to propose a suitable countermeasure. Furthermore, the APN-FSMaRT project plays a significant role in the multilateral collaboration between Japan, Vietnam, and the Philippines, with the addition of Malaysia as a new member, and it provides a future direction for young researchers and local/national governments to implement. The project was a driving force in raising funds for the APN project and establishing our network.

8. Acknowledgments

This work is supported by the Asia-Pacific Network for Global Change Research (APN) under the funder id- <https://doi.org/10.13039/100005536>. The project team would also like to thank all of the project collaborators, and member institutes who engaged in project activities, namely, Disaster Prevention Research Institute (DPRI), Kyoto University (Japan), Japan Weather Association (JWA), Ministry of Natural Resources and Environment (MONRE, Vietnam), National Center for Water Resources Planning & Investigation (NAWAPI) (Vietnam), Thuyloi University (Vietnam), The University of Da Nang (Vietnam), Vietnamese-German University (Vietnam), NGO An Nhien Farm (Vietnam), Isabela State University (Philippines), National Irrigation Administration (Philippines), National Water Resources Board (Philippines), DOST Region 2 Carig, Tuguegarao City (Philippines), NIA-MARIIS-DRD (Philippines).

9. Appendices

Annex 1: International Conference and Symposiums

Annex 2: IO-CCA-DRRM Inauguration

Annex 3: Stakeholder Forum on Integrated Flood Risk Management in Cagayan River Basin

Annex 4: Trainings, and capacity building programs

Annex 5.1: Journal article published in Hydrological Sciences Journal

Annex 5.2: Journal article published in Hydrological Processes journal

Annex 5.3: Journal article submitted to journal Geomatics Natural Hazards and Risk (Under Review)

Annex 5.4: Journal Article published in Journal of Water Resources Research

Annex 5.5: Journal Article published in Journal of Geomorphology

Annex 5.6: Journal article published in the Journal of Robotics and Automation Research

Annex 5.7: Journal article published in Journal of Water Science and Climate Change

Annex 5.8: Journal article submitted to Modeling Earth Systems and Environment (Under Review)

Annex 5.9: Journal article submitted to the Journal of Water and Climate Change. (Under Review)

Annex 6.1: Agenda_IC ENSURES 2022 International Conference (APN_Special Session)

Annex 6.1: Conference publication_AlejandroA_Philippines (IC-ENSURES 2022)

Annex 6.2: Extended_Abstract_Mata_GEE_IC_ENSURES 2022

Annex 6.3: Extended-Abstract_AIHC_Singson (IC-ENSURES 2022)

Annex 6.4: Abstract Khagendra Bharambe (ICENSURE-2022)

Annex 6.5: Abstract_APN_Project_KANTOUSH et al (ICENSURE-2022)

Annex 6.6: Abstract_Binh_APN-Project (ICENSURE-2022)

Annex 6.7: Abstract_Thao Bui_APN-Project (IC-ENSURES 2022)

Annex 6.8: Full Paper_Duy Luu_APN-Project (IC-ENSURES 2022)

Annex 6.9: Abstract_Mai Thi Thuy Duong (IC-ENSURES 2022)

Annex 6.10: Abstract_Truong_APN-Project (IC-ENSURES 2022)

Annex 7: Abstracts Book, and detailed agenda_1st FSMaRT2022

Annex 1: International Conferences, and Symposiums

The 2nd international conference on environmental sustainability and resource security (IC-ENSURES2022- 08-09 March 2022).

This conference aims to create an international platform to exchange views, learn best practices, and sharing knowledge between professionals and academicians on environmental sustainability and resource security (IC-ENSURES2022) related to the environment and water security, which also includes disaster related topics.



JASTIP Special Session, March.8-9, 2022 FLOOD & SEDIMENT MANAGEMENT



Key Research Topic Presented

- Flood Risk and Reservoir Sedimentation in **Cagayan** and **Vu Gia - Thu Bon** River Basins
- Spatial-Temporal Variations of Suspended Sediment in the **Vietnamese Mekong Delta**
- Extreme Climate Indices: Tools for Assessment of Spatio-Temporal Climate Change Risk Over **Cagayan** River Basin, Philippines

Sustainable Development (FSMaRT 2022)), and Fire Risks in Humid Tropical River Basins, Indonesia

The 1st international symposium on Integrated Flood and Sediment Management in River Basin for Sustainable Development (FSMaRT) 2022 was held in Da Nang, Vietnam on 18th – 20th December 2022. This conference aims to provide a forum for researchers, scientists, engineers and scholars from industry, academia and government to share their experience, amazing ideas and innovative research in the impacts of climate change and human interventions on reservoir sedimentation, flood inundation, agricultural practices, and river and coastal erosion. In addition, this conference was also a platform to discuss practical issues, challenges encountered as well as the solutions adopted.

This conference was attended by around 70% younger (Students/Early Career Researchers) among the more than 100 total participants (Figure 1), belongs from 37 different institutes (Table 1) in 13 different countries (Figure 2).

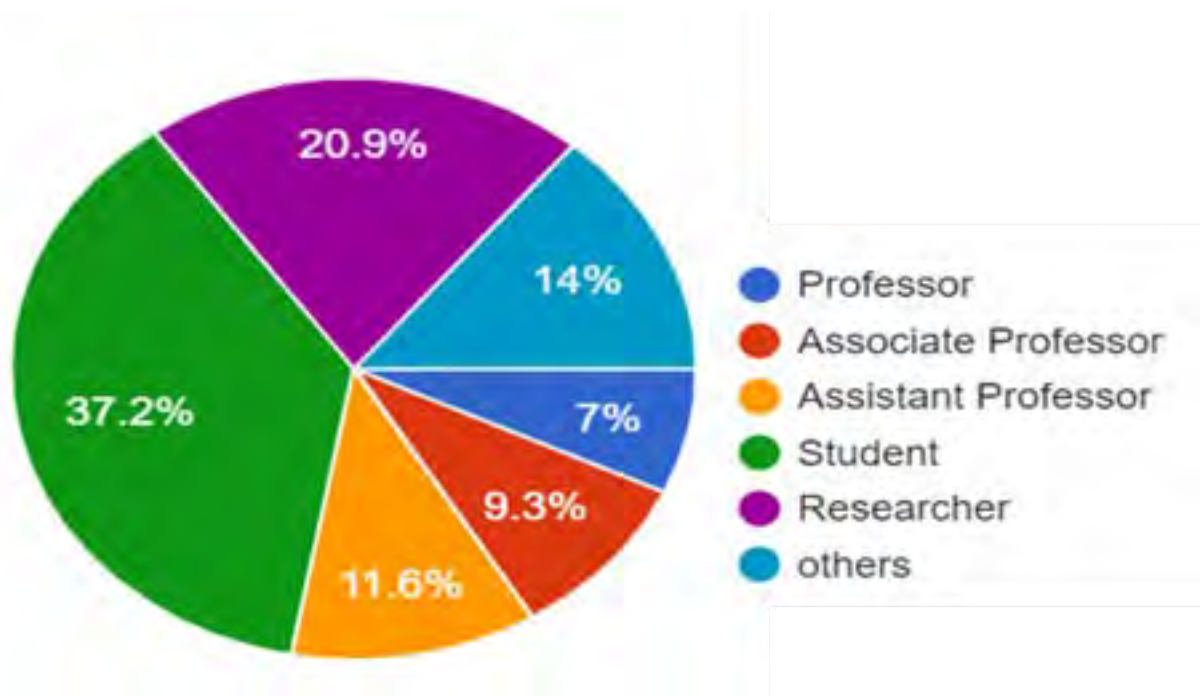


Figure 1: Participants by category

Table 1: Name of the Institutes participated in 1st FSMaRt2022, Vietnam.

| Country | Name of Institutes |
|---------------------------------------|---|
| Algeria | Badji Mokhtar-Annaba University |
| | Ghardaia University |
| | Unité de Recherche Appliquée en Energies Renouvelables |
| Canada | McGill University |
| Egypt | Cairo University |
| | Assiut University |
| France | University of Nice Sophia Antipolis |
| Germany | University of Cologne |
| Japan | Kyoto University |
| | Tokyo Metropolitan University |
| Kuwait | American University of the Middle East |
| Malaysia | Universiti Teknologi Malaysia |
| | Universiti Malaysia Sabah |
| Netherlands | Delft University of Technology |
| Philippines | Philippine Council for Industry, Energy, and Emerging Technology Research and Development |
| | Isabela State University |
| South Korea | National Irrigation Administration |
| | Korea Institute of Civil Engineering and Building Technology |
| USA | University of Houston |
| | University of Virginia |
| | University of Louisiana at Lafayette |
| Vietnam | The University of Danang - University of Science and Technology |
| | The University of Danang - University of Economic |
| | Vietnam disaster management authority |
| | Thuyloi University |
| | National Center for Water Resources Planning and Investigation (NAWAPI) |
| | Hanoi University of Natural Resources and Environment (HUNRE) |
| | Vietnamese –German University |
| | Institute of Social Sciences of Central Highland |
| | Thua Thien Hue investment and construction consultants joint stock company |
| | Southern Institute of Water Resources Research |
| | Ho Chi Minh City University of Natural Resources and Environment |
| | Southern Institute of Water Resources Planning |
| | The Alliance of Bioversity International and Centre of International Agriculture |
| | Ministry of Agriculture and Rural Development |
| Hanoi University of Civil Engineering | |
| Song Ba JSC | |

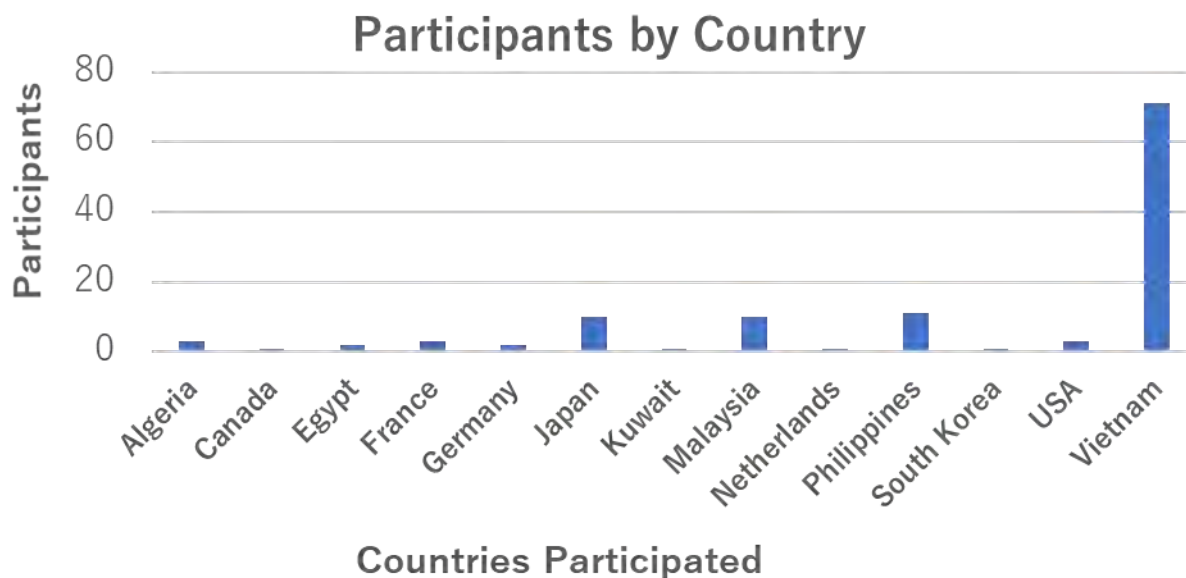


Figure 2: *Number of participants by countries in 1st FSMaRT 2022, Vietnam.*



Group Photos of participants in 1st FSMaRT 2022, Vietnam

Key Topics of 1st FSMaRT 2022

- Hydrological Modelling and Sediment Management
- Artificial Intelligence for Hydrological Application
- Flood Risk Assessment
- Remote Sensing and GIS for Flood and Water Security
- Climate Change and Sustainability



Photos of Key Presenters, and conference activities during 1st FSMaRT2022, Vietnam.

Annex 2: IO-CCA-DRRM Inauguration

The Isabela State University (ISU), Philippines, along with its partner agencies, took the lead in the inauguration of the International Organization on Climate Change Adaptation and Disaster Risk Management (IO-CCA-DRRM) Inc. Office on July 16, 2022 at 8:00 AM. To mark its official opening, the grand inauguration of the office, through a ceremonial ribbon cutting, was spearheaded by Dr. Aquino, Prof. Tetsuya Sumi, an academicians from KU and Chairman of JASTIP; and Vice Mayor Tupong.



All the dignitaries from the Japan Water Agency (JWA), Japan-ASEAN Science, Technology and Innovation Platform (JASTIP), Kyoto University (KU), Department of Science and Technology - Philippine Council for Industry, Energy, and Emerging Technology Research and Development (DOST-PCIEERD), Asia-Pacific Network (APN) for Global Change Research, and top campus officials of ISU-Echague were the part of the inauguration of IO-CCA-DRRM.



Dr. Ricmar P. Aquino simultaneously serves as the President of ISU and IO-CCA-DRRM and is one of the Board of Trustees and incorporators of the said international organization.



As the activity advances, Dr. Joe G. Lagarteja, Data Protection Officer, launched the website of IO-CCA-DRRM. Primarily, this website was developed for the wider dissemination of the University's internationalization efforts and ventures. Dr. Lagarteja also presented all the features and contents of

the website to facilitate information searching and navigation around the control system of the website.



Annex 3: Stakeholder Forum on Integrated Flood Risk Management, 14-16 July 2022, Philippines

The Stakeholders Forum on Integrated Flood Risk Management in Cagayan River Basin was commenced on July 14, 2022, at Zen Hotel, Santiago City. Numerous dignitaries from the Japan Water Agency (JWA), Japan-ASEAN Science, Technology and Innovation Platform (JASTIP), Isabela State University, Kyoto University- Disaster Prevention Research Institute (DPRI), Department of Science and Technology - Philippine Council for Industry, Energy, and Emerging Technology Research and Development (DOST-PCIEERD), Asia-Pacific Network (APN) for Global Change Research, and Water Research and Development Center, Department of Environment and Natural Resources (DENR) Region 2, National Irrigation Administration- Magat River Integrated Irrigation System (NIA-MARIIS), and Local Government Units (LGUs) of Santiago City and Isabela as well as top-level political leaders of the Province of Isabela served as resource speakers during its kickoff on July 14, 2022.



ZEN Hotel, Santiago City
Isabela, Philippines
July 14 - 16, 2022



STAKEHOLDERS FORUM ON
INTEGRATED FLOOD RISK
MANAGEMENT
IN CAGAYAN RIVER BASIN



ZEN Hotel, Santiago City
Isabela, Philippines
July 14 - 16, 2022



STAKEHOLDERS FORUM ON
INTEGRATED FLOOD RISK
MANAGEMENT
IN CAGAYAN RIVER BASIN





Prof. Tetsuya Sumi, an academican from Kyoto University and notable at JASTIP, accentuated various work plans for Japan-Philippines collaboration in the Cagayan River Basin. He highlighted several projects for 2020-2025, the challenges on dams in the 21st century, dam asset transfer to the next generation, Japan's situation of dam's flood control, pre-release operation practices, and the target basins and research groups. He even emphasized, "Japan will proactively contribute to the solution of water-related social issues faced by the Asia-Pacific region by developing "quality infrastructure" capitalizing on Japan's advanced technologies...and public-private partnerships, and fostering

digitization and innovation to solve social issues as a growth engine for sustainable development and the formation of a resilient society and economy.



Prof. Sameh Ahmed Kantoush, Leader of Asia-Pacific Network for Global Change Research Project, elucidated the topic “Flood Mitigation and Risk Communication under Successive Typhoons at Cagayan River Basin in the Philippines (DPRI International Collaborative Research Project).” Likewise, he expounded flood control dams’ scenarios as well as integrated approach for risk communication and reduction as a way forward.



To update the stakeholders regarding the case of the Philippines, Dr. Lanie A. Alejo, Director of Water Research and Development Center, ISU, expounded the topic “Integrated Flood and Water Resources Management Research and Development in the Cagayan River Basin.” She presented the CRB baseline information, various water management sectors, water-related disasters in the basin, and

numerous schematic frameworks for integrated flood, sediment, and water resources management, as well as the research projects' accomplishments.



To expand the international ventures of the stakeholders, a ceremonial MOU signing between the Japan Water Agency and Cagayan River Basin Management Council has been conducted to seal the forged partnership.



ZEN Hotel, Santiago City
Isabela, Philippines
July 14 - 18, 2022



STAKEHOLDERS FORUM ON
INTEGRATED FLOOD RISK
MANAGEMENT
IN CAGAYAN RIVER BASIN



STAKEHOLDERS FORUM ON
INTEGRATED FLOOD RISK
MANAGEMENT
IN CAGAYAN RIVER BASIN

Strengthening Knowledge Base to
Address the Impacts of Risk
Management in the Cagayan River Basin

Annex:4 Trainings and Capacity building programs

1. Training Workshop on “Flow and Sediment Transport Modelling in River Basins using TELEMAC 2D and 3D Numerical, 25-28 February 2022

A four-day online training course on “Flow and Sediment Transport Modelling in River Basins using TELEMAC 2D and 3D Numerical Codes” is being organized by **Isabela State University** in collaboration with **Kyoto University** under a capacity building programme for their working early career scientist/engineers/students from different regional centers and university from Japan and Philippines, supported by **Asia Pacific Network (APN)**.

This four-day training workshop provides an overview of the capabilities, limitations, and challenges in hydraulic modelling of flow and sediment transport in rivers. This course covers a broad range of modelling techniques for fluvial processes using the TELEMAC suite of computer models. Lectures provided both theoretical background and practical aspects of modelling flow and sediment transport processes, with hands on application using data sets acquired on real rivers.

This course was attended by more than 40 participants from collaborative institutes (viz. Kyoto University, Isabela State University, IFWaRM, Cagayan State University, Department of Science and Technology, National Irrigation Administration), from Japan and the Philippines.





2. Online Training Program – UNESCO-IHP at DPRI, Kyoto University

In December 2020, UNESCO-IHP Training was organized to train the project team from Philippines and Vietnam on climate change data analysis and hydrological modelling integrating with various types of satellite data information.



3. UNESCO-ISI Online Training Workshop on Sediment Transport Measurement and Monitoring

The UNESCO-ISI Online Training Workshop on Sediment Transport Measurement and Monitoring took place on July 5-9, 2021, focuses on "Water security: responses to local, regional, and global challenges," and addresses the wide-ranging environmental, social, and economic effects of erosion, sediment transport, and sedimentation processes. This addressed the following topics:

1. Standard measurement and monitoring techniques used to collect data on water discharge and sediment loads for rivers and reservoirs.
2. Recent advances in sediment transport measurement and monitoring: online monitoring of suspended sediment concentrations in rivers.
3. Sediment measurement and monitoring methods for mountain streams.
4. Measuring erosion and sediment yields on slopes and in small catchments for soil and water conservation; and
5. Application of sediment data in controlling sediment-related ecological problems.



Screenshots from the lecture and the certificate given by UNESCO.



Understanding the anthropogenic development impacts on long-term flow regimes in a tropical river basin, Central Vietnam

Binh Quang Nguyen, Sameh Kantoush, Doan Van Binh, Mohamed Saber, Duong Ngoc Vo & Tetsuya Sumi

To cite this article: Binh Quang Nguyen, Sameh Kantoush, Doan Van Binh, Mohamed Saber, Duong Ngoc Vo & Tetsuya Sumi (2023): Understanding the anthropogenic development impacts on long-term flow regimes in a tropical river basin, Central Vietnam, Hydrological Sciences Journal, DOI: [10.1080/02626667.2022.2153298](https://doi.org/10.1080/02626667.2022.2153298)

To link to this article: <https://doi.org/10.1080/02626667.2022.2153298>



Published online: 12 Jan 2023.



Submit your article to this journal [↗](#)



Article views: 37



View related articles [↗](#)



View Crossmark data [↗](#)

Understanding the anthropogenic development impacts on long-term flow regimes in a tropical river basin, Central Vietnam

Binh Quang Nguyen^{a,b}, Sameh Kantoush^a, Doan Van Binh^c, Mohamed Saber^a, Duong Ngoc Vo^b and Tetsuya Sumi^a

^aWater Resource Center, Disaster Prevention Research Institute (DPRI), Kyoto University, Kyoto, Japan; ^bFaculty of Water Resources Engineering, The University of Danang – University of Science and Technology, Danang, Vietnam; ^cMaster Program of Water Technology, Reuse and Management, Faculty of Engineering, Vietnamese German University, Binh Duong, Vietnam

ABSTRACT

The Vu Gia Thu Bon (VGTB) basin constitutes the primary water supply in Central Vietnam. While climate change disturbs stream discharges and affects flood extremes, upstream dam development may intensify or mitigate such impacts. Therefore, this study provides a quantitative evaluation of long-term alterations in the flow regimes of the VGTB rivers from 1977 to 2020 resulting from the impacts of upstream anthropogenic developments. The datasets are divided into two periods, pre-2000 (1977–2000) and post-2000 (2001–2020), using different indices and analytical methods. The analyses show that since 2011, reservoir operations have reduced the maximum and high-flow discharges downstream in excess of climate change and land-use effects. However, due to the impact of water transfer by the Dak Mi 4 hydropower dam from the Vu Gia River to the Thu Bon River through a diversion channel, the minimum and low-flow discharges decreased in the pre-dam period and increased in the post-dam period.

ARTICLE HISTORY

Received 27 June 2022
Accepted 31 October 2022

EDITOR

A. Castellarin

ASSOCIATE EDITOR

E. Davies

KEYWORDS

Vu Gia Thu Bon basin; hydropower dams; water transfer; flow regime

1 Introduction

Typhoons are a severe natural hazard that affects river basins worldwide. Stronger typhoons usually produce heavy rainfalls, enormous wind speeds, higher waves, and storm surges (Larson *et al.* 2014). The consequences of typhoons include damage to infrastructure, agricultural production and river-banks; coastal erosion; and the loss of human life. The Vu Gia Thu Bon (VGTB) basin (Fig. 1(a)) is located in the central coastal region of Vietnam, which is prone to a tropical monsoon climate (RETA 2011, Ribbe *et al.* 2017). According to the Japan Meteorological Agency (JMA), the area is frequently affected by typhoons and tropical depressions. In Vietnam, the majority of typhoons (70%) occur in the central parts of the country (Fig. 1(b)), according to the Vietnam General Department of Meteorology and Hydrology. Typhoons, tropical depressions, and cold air have caused heavy rain, leading to severe flooding. Wang *et al.* (2014)'s key findings indicate that increased rainfall in Central Vietnam since the beginning of the 20th century is associated with increased typhoons. Indeed, it has been revealed that there is a strong correlation between the increasing trend of stronger typhoons and the extension of the typhoon season over the last decade. Consistently, the maximum rainfall has been found to increase, along with the higher frequency of typhoons on the south coast of Vietnam (Tan and Thanh 2013). In 2020, four typhoons (i.e. Noul, Linfa, Molave, and Vam Co) affected the VGTB river basin, three of which had magnitudes higher than the long-term average (Fig. 1(d)). Due to the impacts of typhoons, the flood peak at the Ai Nghia and Giao Thuy hydrological stations recorded in the downstream basin reached 12.84 m and

8.97 m, respectively, higher than those in 1999 (Fig. 1(a)). According to the report of the Commanding Committee for Disaster Prevention and Search and Rescue in Quang Nam Province, as a consequence of typhoons in 2020, 28 people died, 19 people were reported missing, and 200 people were injured, and the typhoons resulted in total economic losses of approximately \$460 million. The increase in the frequency (Fig. 1(d)) and intensity of typhoons may be a result of climate change.

The VGTB basin ranks fourth in terms of hydropower potential in Vietnam (ICEM 2008); many hydropower plants have been built and are operating in the region. Although hydropower is essential for the country, it has significant adverse effects on river systems, such as flow regime alterations, sediment reduction, flooding, drought, water shortages, agricultural production decreases, and saline intrusion intensification (Dinh 2016, Laux *et al.* 2017, Ribbe *et al.* 2017, Firoz *et al.* 2018). The Vu Gia River is the primary source of water for Da Nang city and regional agricultural activities. A large volume of water was diverted from the Vu Gia River to the Thu Bon River (Fig. 1(a)) when the Dak Mi 4 hydropower plant began operation in 2011. This water diversion led to deficits in the water supply for agriculture and drinking water and increases in salinity intrusion in Da Nang city. Consequently, a polemic controversy between Da Nang city and Quang Nam Province (Fig. 1(a)) regarding the impact of hydropower development has begun. Da Nang city blames Quang Nam Province for a large-scale hydropower cascading system that negatively affects downstream water resources in the

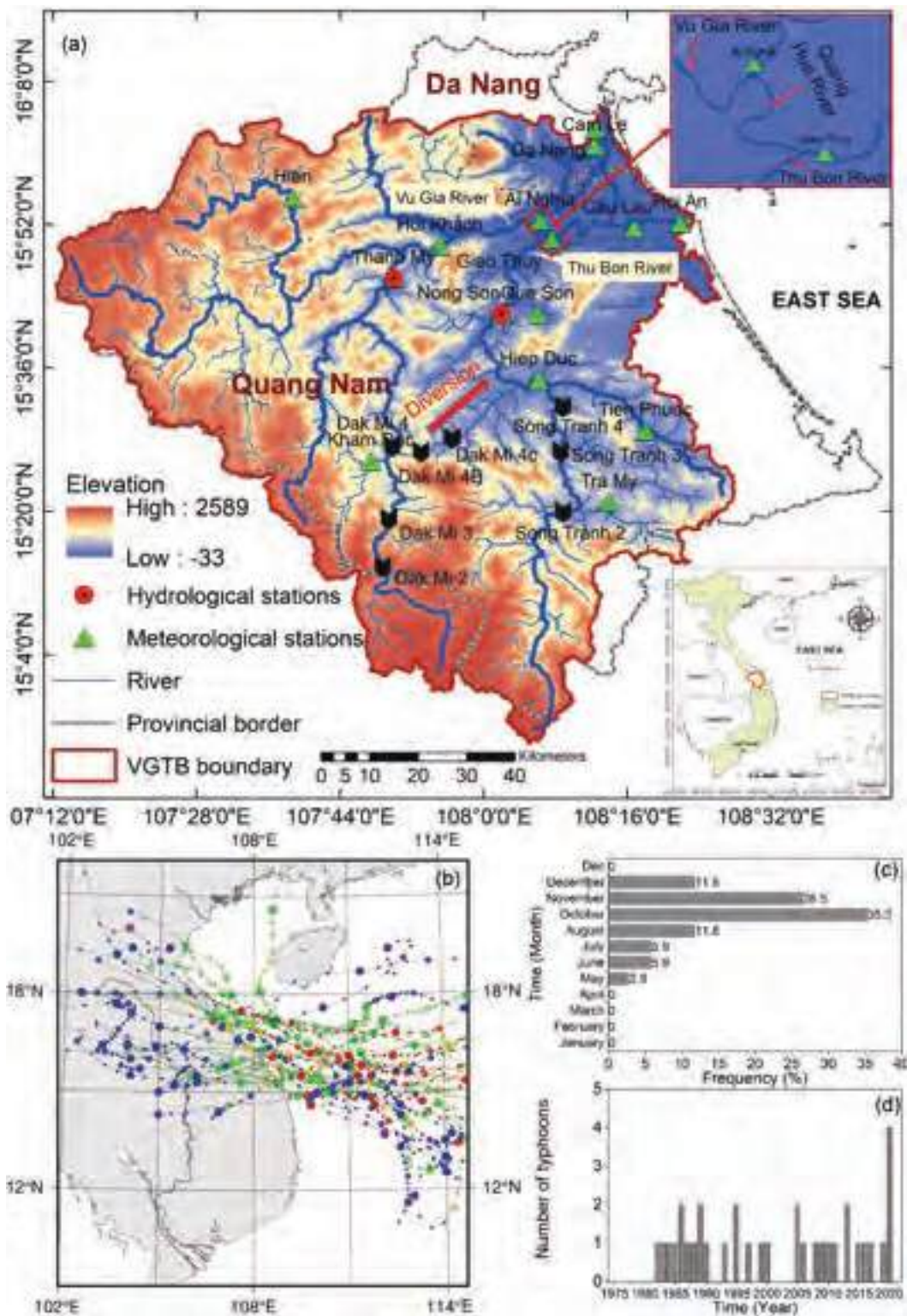


Figure 1. (a) Map of the VGTB River basin, (b) trajectories of typhoons affecting the basin, (c) frequency of typhoons by month, and (d) number of typhoons by year (Source: National Institute of Informatics, Japan. <http://agora.ex.nii.ac.jp/>) (Japan Meteorological Agency 2013).

dry season (Nauditt *et al.* 2017). Therefore, quantification of the cascading effects of hydropower dams developed in Quang Nam Province and in the entire VGTB basin on the flow regimes in Da Nang city is urgently needed to ease this conflict.

A complex series of impounding reservoirs in the VGTB basin have been built (18 reservoirs) or planned (42 reservoirs) to make the best use of elevation differences and maximize the power generated through water diversion without compensating for reductions in the water level and environmental flow.

The distribution of these dams is heavily concentrated on the Vu Gia River, with 12 small and large reservoirs, of which two diversion channels divert water to the Thu Bon River. Firoz *et al.* (2018) highlighted the impacts of eight upstream dams (six in the Vu Gia and two in the Thu Bon) over a short operational period in 2013 on drought risk and streamflow. That study concluded that the Vu Gia River has a high risk of hydrological drought, which impacts the water supplied for irrigation and drinking water in Danang city, especially in the dry season. In the rainy season, these eight dams reduced the monthly average discharge by 30% (Firoz *et al.* 2018). In contrast, the monthly average flow discharge increased in the Thu Bon River from 24 m³/s to 62 m³/s in the dry period (Firoz *et al.* 2018). Additionally, previous studies analysed the impacts of a limited number of dams following operation periods of two years or more. However, the cumulative effects of these 18 dams, plus additional dams built over an extended period ending in 2020, on flow regime alterations due to a changing climate remain unknown and constitute the root of this research.

Nauditt *et al.* (2017) examined the individual impact of a hydropower reservoir with a diversion channel from the drier Vu Gia River to the wetter Thu Bon River from 1980 to 2013. These diversion processes reduced the mean monthly discharge in Vu Gia by 13–125 m³/s. An additional individual assessment of the Song Tranh 2 reservoir in the Thu Bon River was performed to evaluate the changes in the released flow based on daily measurement data from 1996 to 2018 (Ha and Coynelb 2019). The study revealed that the average flow after the Song Tranh 2 reservoir opened decreased by 103 m³/s, from 864 m³/s to 761 m³/s. Phuong *et al.* (2020) used the classical/modified Mann-Kendall and innovative-Sen methods to evaluate the trend of hydrometeorological factors in the VGTB basin over 36 years, from 1979 to 2014. The authors used a continuous data series from 1979 to 2014 to assess the general trend, which did not accurately reflect the flow characteristics within a reservoir. The authors used only the classical/modified Mann-Kendall and innovative-Sen methods, which do not reflect all the flow regime behaviours of the basin. These studies are limited in that they do not consider the effects of all reservoirs and long-term flow alterations at all stations. The study period is relatively short, and flow indicators have not thoroughly evaluated the flow regime alterations. Therefore, in the present study, we attempt to assess flow regime alterations based on a more extended period (1977–2020) and consider all dams and flow transfer impacts.

Understanding the long-term changes in the flow regime in the VGTB basin is of vital importance for sustainable management and water resource distribution in the coming decades. However, the previous studies are limited in terms of data range (up to 2014) and thus do not assess the cascading effects of all dams (many of which were built more recently) on the flow regime alterations in the VGTB basin. Accordingly, this study aims to quantify changes in the long-term flow regimes in the VGTB basin due to climate change, reservoir cascading, and construction of water diversion structures. The contributions of this paper are (1) a

comprehensive evaluation of the long-term flow regime alterations considering a comprehensive range of hydrological alteration indicators and (2) an understanding of the impacts of reservoir operations, climate change/variability, and land-use change on the flow regimes. The results of our research provide evidence-based data regarding historical changes in the hydrology of the VGTB basin, providing stakeholders with helpful information for river basin management and solutions for informing future preparedness and sustainable development.

2 Materials and methodology

2.1 Study area

The VGTB river basin (Fig. 1(a)) is the major basin in the Central Coast region, Vietnam, with an area of 10 350 km². The basin has a tropical monsoon climate and two distinct seasons: dry summer (January–August) and heavy rain (September–December). The average annual rainfall varies significantly, from 2000 mm in the central and downstream regions to more than 4000 mm in the southern mountainous areas. There are seasonal differences, with 65% to 80% of the annual rainfall concentrated from September to December (RETA 2011). In the eight months of the dry season, rain accounts for only 20% to 35% of the annual rainfall (Nauditt *et al.* 2017). The driest period usually falls between February and April, with approximately 3% to 5% of the total annual rainfall.

The discharge of the basin is divided into three different seasons: low flow (January–April), transition flow (May–August), and high flow (September–December). Due to the difference in the rainfall distribution, the runoff in the VGTB basin varies significantly between seasons. The flow in the rainy period accounts for approximately 62.5% to 69.2% of the total annual flow. Every year, the basin is frequently hit by four to eight floods. The flood peaks usually occur in October and November due to different weather patterns, such as typhoons, tropical depressions, cold air, and northeast monsoons (Fig. 1(c)) (T. T. Vu *et al.* 2011). The frequency of cyclones ranges from one to two per year (Fig. 1(d)).

Figure 1(a) shows 18 existing dams and diversion facilities and the river gauging stations considered in this study. There are six reservoirs on the Thu Bon River, with a total storage volume of 1575 million m³ (Fig. 2(a)). There are 12 reservoirs in the Vu Gia basin, with a total storage volume of 1335 million m³ (Fig. 2(b)). Eight hydropower plants affect the flow at the Thanh My and Nong Son stations: Dak Mi 2, Dak Mi 3, Dak Mi 4, Dak Mi 4B, and Dak Mi 4C in the Vu Gia basin and Song Tranh 2, Song Tranh 3, and Song Tranh 4 in the Thu Bon basin (Fig. 1(a)). The Dak Mi 4 plant in the Vu Gia basin was constructed in 2007 and began operation in 2011. A tunnel was built in the Dak Mi 4 hydropower plant to divert water and sediment from the Vu Gia River to the Thu Bon River (Fig. 1(a)). This diversion led to a significant alteration of the basin's flow regime which is attributed to hydrological, drought and saline intrusion during the dry season in Da Nang city (Firoz *et al.* 2018).

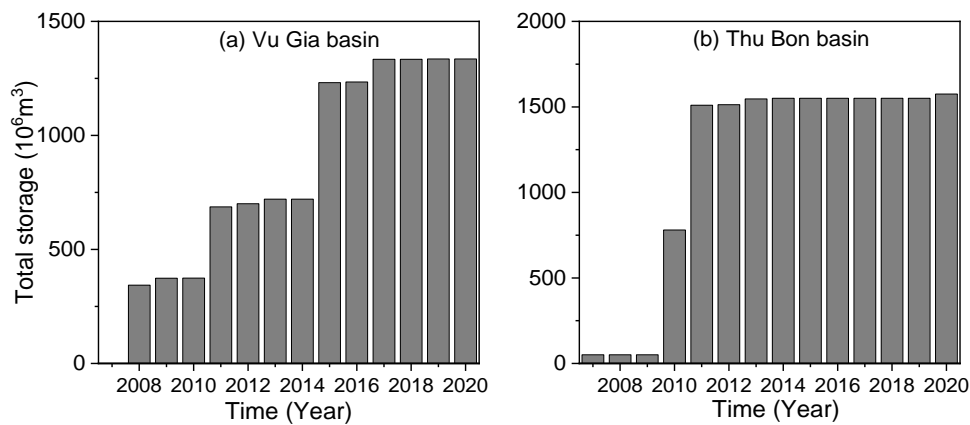


Figure 2. Total storage of hydropower dams in the (a) Vu Gia basin and (b) Thu Bon basin (ICEM 2008, MOIT 2015).

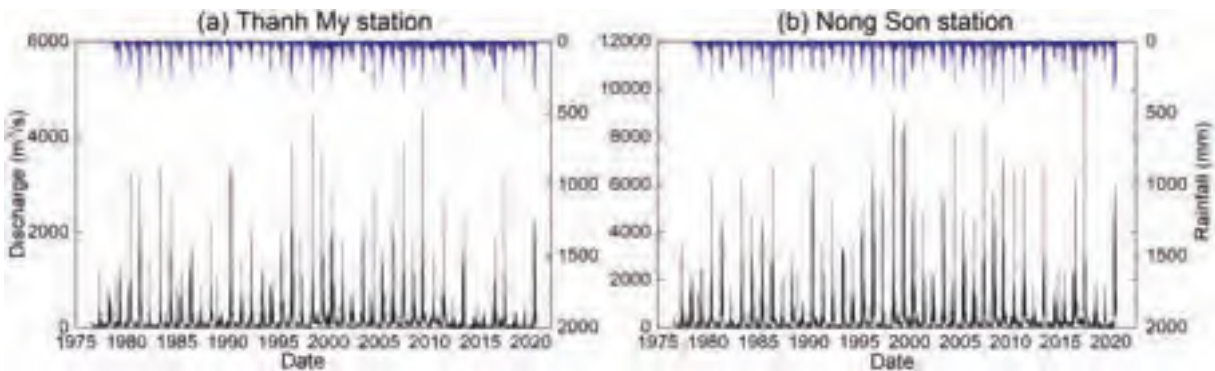


Figure 3. Daily discharge and rainfall at the (a) Thanh My station and (b) Nong Son station. The black line is the discharge, and the blue (shaded) line is the rainfall.

2.2 Data collection

In this study, rainfall data from 15 raingauges were collected from the Mid-Central Regional Hydro-Meteorological Center (Fig. 1(a)). Because of the sparse distribution of raingauges (15 gauges) in the basin, we interpolated the rainfall data from those stations to make a spatial map using the kriging method in ArcGIS 10.4 following the method of Duong and Gourbesville (2014). The discharge and water level data at the Thanh My and Nong Son stations (the only two stations monitoring discharges in the basin) were collected from 1977 to 2020, and the dataset was treated for gaps and missing data (Fig. 3). Data on the operation of the hydropower plants were obtained from the Natural Disaster Prevention and Control Department of Quang Nam Province (NDPAC). Hydraulic infrastructure data were also obtained, from Decision 1865/QD-TTg: Procedures for Operating Reservoir Systems in the VGTB River Basin (Government of Vietnam 2019). Land use in 2001, 2005, 2010, and 2020 was collected from the project “Land Use and Climate Change Interaction in Central Vietnam (LUCCI)” (www.lucci-vietnam.info) to assess the effect of land-use changes on runoff.

2.3 Methodologies

The flow regime is analysed based on the following methods: statistical trend tests (Mann-Kendall, Sen’s slope), indicators of hydrologic alteration (IHA), the index of hydrological regime

alteration (FQ), and flow regime metrics. The flood characteristic indices are analysed as a peak over threshold (POT) using the generalized Pareto distribution (GPD). We want to investigate the cumulative impacts of all dams after construction from 2001 to 2020 and prior to construction from 1977 to 2000 to be considered as climate change impacts. Therefore, the research is divided into two periods: pre-2000 (1977–2000) and post-2000 (2001–2020).

2.3.1 Statistical trend tests

The nonparametric Mann-Kendall test and the slope method of Sen are used to evaluate the long-term discharge and rainfall changes. The nonparametric Mann-Kendall test is commonly employed to detect monotonic trends (increasing or decreasing) in data collected over time. The Mann-Kendall test is used to determine the tendency of long-term data (Kendall 1938, Mann 1945), and the rate of change is estimated using the slope method of Sen (Sen 1968).

2.3.2 Indicators of hydrologic alteration (IHA)

IHA is a software program developed by scientists at the Nature Conservancy (Richter *et al.* 1996, 1998, 2003). IHA provides valuable information for those trying to understand the hydrological impacts of human activities and develop environmental flow recommendations for water managers. IHA analysis can help statistically describe how patterns have changed for a particular river or lake due to abrupt impacts

Table 1. Flow regime metrics used in the impact assessment of long-term alterations in the VGTB basin.

| Group | Regime characteristic | Hydrologic metric | Units |
|------------------------|---|--|-------------------|
| Magnitude | Average flow | Mean daily discharge of a year | m ³ /s |
| | | Mean daily discharge in each month during the low-flow period | m ³ /s |
| | | Mean daily discharge in each month during the transition-flow period | m ³ /s |
| | High flow | Mean daily discharge in each month during the high-flow period | m ³ /s |
| | | Discharges in the 40th and 60th percentiles of the FDC: Q40 and Q60 | m ³ /s |
| | | Annual one-day maximum discharge | m ³ /s |
| | | Extreme high-flow discharge Q10 (10th percentile of the FDC) | m ³ /s |
| Low flow | Annual one-day minimum discharge | m ³ /s | |
| | Extreme low-flow discharge Q90 (90th percentile of the FDC) | m ³ /s | |
| Timing | High flow | Julian date of the one-day maximum discharge | day |
| | Low flow | Julian date of the one-day minimum discharge | day |
| Duration and frequency | High flow | Index of hydrological regime alteration in high flow: FQ-high flow | % |
| | Low flow | Index of hydrological regime alteration in low flow: FQ-low flow | % |

such as dam construction or land and water use changes (Opperman 2006). This method includes 32 hydrological indicators, which are categorized into three large groups: (1) magnitude, (2) timing, and (3) duration and frequency (Table 1).

2.3.3 Index of hydrological regime alteration (FQ)

The FQ, adopted from Alcayaga *et al.*, evaluates changes in the frequency and duration of high flow and low flow.

$$FQ(\%) = \frac{NQ_{post}}{NQ_{pre}} \times 100 - 100 \quad (1)$$

where FQ (%) indicates the frequency of change, and NQ_{pre} and NQ_{post} are the number of days when the flow is higher than the high flow or lower than the low flow in the pre-2000 and post-2000 periods, respectively.

2.3.4 Impact assessment of the flow regime metrics

Reservoir operation depends mainly on operational objectives and hydrometeorological conditions and can lead to changes in flow regimes (Zhang *et al.* 2018). To see changes over the long term, flow metrics (magnitude, variability and frequency, duration, timing, and rate of change) are used (Zhang *et al.* 2018, Van Binh *et al.* 2020). Twenty-three indicators in flow mode metrics over different years are used to evaluate the effects of reservoirs, including relative and absolute values (Table 1). The equation for calculating these values is adopted from Zhang *et al.* (2018) and Van Binh *et al.* (2020).

$$AD^i = V_{post}^i - \bar{V}_{pre}^i \quad (2)$$

$$RD^i = \frac{AD^i}{\bar{V}_{pre}^i} \times 100\% \quad (3)$$

$$\bar{V}_{pre}^i = \frac{\sum_{1}^N V_{pre}^i}{N} \quad (4)$$

where AD and RD are the absolute and relative deviations of the i^{th} metric, respectively; V_{post}^i and V_{pre}^i are the values of the i^{th} metric in the post-2000 and pre-2000 periods, respectively; \bar{V}_{pre}^i is the mean value of the i^{th} metric in the pre-2000 period; and N is the number of years in the pre-2000 period. If the deviation is greater than 0, the flow regime metrics are positively impacted. If it is less than 0,

then the flow regime metrics are negatively impacted. When it is equal to 0, the flow regime metrics have no impacts. The relative difference is divided into five grades based on the percentiles adopted by Zhang *et al.* (2018): slight ($-15\% \leq RD < -5\%$ or $5\% < RD \leq 15\%$), moderate ($30\% \leq RD < -15\%$ or $15\% < RD \leq 30\%$), high ($-45\% \leq RD < -30\%$ or $30\% < RD \leq 45\%$), extreme ($RD < -45\%$ or $45\% < RD$), and no impact ($-5\% \leq RD \leq 5\%$).

2.3.5 Peak over threshold (POT) method

The POT method is used to analyse the flood frequency for the Vu Gia and Thu Bon basins. The POTs are the flood peaks that are more significant than a given threshold in each year. POT modelling provides additional flexibility and a more comprehensive description of peak floods (Lang *et al.* 1999).

The POT method depends on two factors: independent criteria and threshold selection. Therefore, how the threshold is selected is important. The first step is the consideration of the independence conditions, and the second step is the threshold selection. The distribution of the POT series can be determined by the GPD proposed by Pickands (1975).

3 Results

3.1 Alterations of the flow regime in the dry season

For the flow magnitude, the low-flow discharge of the Vu Gia (one-day minimum, Q90, May–August) was mainly positively impacted at slight to extreme grades from 2001 to 2011 and negatively affected at severe rates from 2012 to 2020 (Fig. 4(a)). The low-flow discharge of the Thu Bon was positively and negatively impacted to a significant degree before becoming positively impacted from 2012, except for 2020, in which it was negatively impacted (Fig. 4(b)). The annual impact variation in the dry season increased slightly in the Vu Gia but increased considerably in the Thu Bon in the post-2000 period (Fig. 5, Table 2). The increased rates of minimum and low-flow discharges were 1–21% for Thanh My and 20–57% for Nong Son.

For the flow variability and frequency, the impacts of the flow metrics were negative to positive in the Vu Gia starting in 2011 (Fig. 4(a)). The most impacted areas in the Thu Bon showed extremely negative grades (Fig. 4(b)). The duration of the low-flow season in the post-2000 period

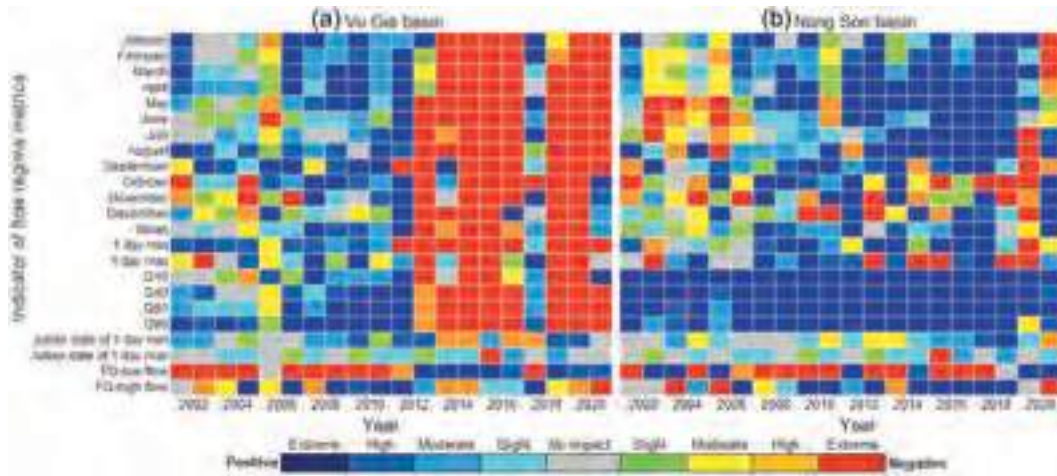


Figure 4. Heatmap quantifying the alteration of the flow regime metrics in the Vu Gia and Thu Bon basins. Blue indicates a positive impact, and red indicates a negative impact.

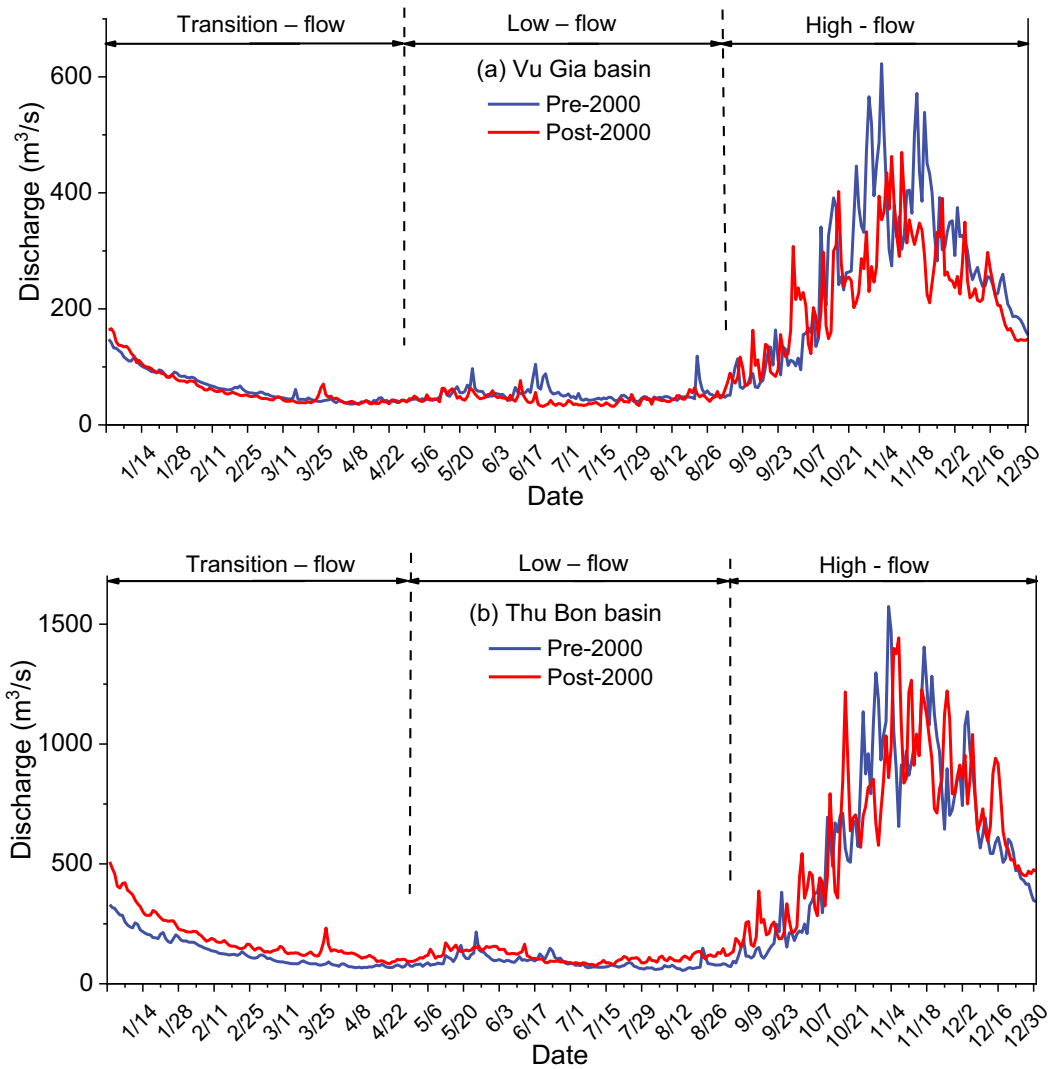


Figure 5. Differences in the discharge hydrographs between the two periods in the transition-flow, low-flow, and high-flow seasons in (a) the Vu Gia basin and (b) the Thu Bon basin. The blue line is the discharge in the pre-2000 period, and the red line is the discharge in the post-2000 period.

Table 2. Results of the IHA analysis to determine discharge alterations at the Thanh My and Nong Son stations.

| Indicator | Units | Thanh My station | | | Nong Son station | | |
|---------------------|-------------------|------------------|-----------|-------------------------|------------------|-----------|-------------------------|
| | | Pre-2000 | Post-2000 | Deviation magnitude (%) | Pre-2000 | Post-2000 | Deviation magnitude (%) |
| January | m ³ /s | 92 | 100 | 8 (9) | 194 | 234 | 40 (20) |
| February | m ³ /s | 59 | 59 | 1 (1) | 116 | 148 | 32 (27) |
| March | m ³ /s | 43 | 47 | 4 (9) | 76 | 119 | 43 (57) |
| April | m ³ /s | 34 | 38 | 5 (13) | 59 | 91 | 32 (53) |
| May | m ³ /s | 40 | 41 | 2 (4) | 80 | 130 | 50 (62) |
| June | m ³ /s | 38 | 41 | 3 (7) | 76 | 97 | 21 (27) |
| July | m ³ /s | 39 | 40 | 1 (2) | 61 | 72 | 11 (19) |
| August | m ³ /s | 39 | 42 | 3 (7) | 56 | 96 | 40 (72) |
| September | m ³ /s | 54 | 62 | 7 (14) | 88 | 139 | 50 (57) |
| October | m ³ /s | 126 | 181 | 55 (44) | 297 | 322 | 25 (8) |
| November | m ³ /s | 222 | 224 | 2 (1) | 606 | 570 | -37 (-6) |
| December | m ³ /s | 179 | 200 | 22 (12) | 427 | 482 | 55 (13) |
| Annual | m ³ /s | 80 | 90 | 10 (12) | 178 | 208 | 30 (17) |
| One-day minimum | m ³ /s | 22 | 23 | 1 (4) | 30 | 40 | 10 (34) |
| Three-day minimum | m ³ /s | 24 | 24 | 1 (3) | 31 | 43 | 12 (40) |
| Seven-day minimum | m ³ /s | 25 | 26 | 1 (4) | 33 | 47 | 14 (41) |
| 30-day minimum | m ³ /s | 30 | 33 | 4 (12) | 40 | 62 | 22 (55) |
| 90-day minimum | m ³ /s | 36 | 43 | 8 (21) | 62 | 86 | 24 (40) |
| One-day maximum | m ³ /s | 1995 | 1875 | -120 (-6) | 4635 | 5625 | 990 (21) |
| Three-day maximum | m ³ /s | 1180 | 1219 | 39 (3) | 3408 | 4527 | 1119 (33) |
| Seven-day maximum | m ³ /s | 816 | 843 | 27 (3) | 2144 | 2904 | 760 (35) |
| 30-day maximum | m ³ /s | 497 | 438 | -59 (-12) | 1247 | 1286 | 39 (3) |
| 90-day maximum | m ³ /s | 278 | 293 | 15 (5) | 748 | 801 | 53 (7) |
| Date of minimum | Day | 172 | 191 | 19 (11) | 225 | 219 | -6 (-3) |
| Date of maximum | Day | 301 | 311 | 10 (3) | 304 | 315 | 11 (4) |
| Low pulse count | Number | 13.0 | 6.5 | -7 (-50) | 10.0 | 8.5 | -2 (-15) |
| Low pulse duration | Day | 4 | 5 | 1 (27) | 5 | 2 | -3(-56) |
| High pulse count | Number | 7.5 | 7.5 | 0 (0) | 7.5 | 10.0 | 3 (33) |
| High pulse duration | Day | 3 | 2 | -1 (-33) | 3 | 3 | 0 (0) |
| Rise rate | Number | 6.8 | 6.6 | 0 (-3) | 15.4 | 20.0 | 5 (30) |
| Fall rate | Number | -4.2 | -4.2 | 0 (-2) | -8.0 | -16.1 | -8 (102) |

increased by 25% in the Vu Gia and decreased by 60% in the Thu Bon (Table 2).

For the flow timing, the Julian date of the minimum discharge was delayed from 172 to 191 days (19 days) in the post-2000 period in the Vu Gia. The appearance of the minimum release in the Thu Bon occurred six days earlier, from 225 to 219 days (Table 2).

There was a distinguishable deviation in the annual impact variations in the basins in the dry season. The low-flow discharge began changing in approximately 2011; the change became obvious in 2012. The red colour (extreme negative) extended from 2012 to 2020 for the Vu Gia. In contrast, the blue colour (extreme positive) was common from 2012 to 2019 for the Thu Bon. These changes were consistent with the operating years of the Dak Mi 4 dam in the Vu Gia basin and the Song Tranh 2 dam in the Thu Bon basin. In contrast, the regulation of Dak Mi 4 decreased the mean daily inflow annually in the Vu Gia. As a result, the regulation of the dam increased the expected flow variability and low-flow frequency.

3.2 Alterations of the flow regime in the rainy season

The results from the POT method (Fig. 6 (a) and (b)) served as a guideline for analysing the flood frequency and identifying peak floods. The thresholds from the POT method for the Vu Gia and Thu Bon basins were 850 and 2400 m³/s, respectively. This method allowed us to characterize the statistical distribution of shorter record lengths post- and pre-dam. In the Vu Gia, based on the Mann-Kendall test, the discharge increased statistically from 1977 to 2000 and decreased statistically from

2001 to 2020. In the Thu Bon, the trends in the two periods increased. In contrast to Firoz *et al.* (2018), we found that the longer period had a statistically significant frequency. Figure 7 illustrates the results of the flood frequency distribution for the Vu Gia and Thu Bon basins based on the GPD. The frequency of flood flows in the post-2000 period was smaller than that in the pre-2000 period in the Vu Gia (Fig. 7(a)). Water received from the Vu Gia combined with reservoir operations led to a higher flood frequency in the Thu Bon (Fig. 7(b)).

Due to anthropogenic intervention in the post-2000 period, the maximum discharges in the Vu Gia decreased by 6%, and those from the Thu Bon increased by 21% (Table 2). The magnitude of the high-flow discharges (one-day maximum, Q10, September–December) in the Vu Gia were positively impacted from 2001 to 2011 before becoming negatively impacted with small to severe rates from 2012 to 2020 (Fig. 4(a)). For the Bon, high-flow discharges were positively and negatively impacted and clearly negatively impacted in 2019 (Fig. 4(b)). The high-flow discharge in both basins increased during the four months of the rainy season, except for November in the Thu Bon. The largest increases in the Vu Gia and Nong Son were 44% and 57%, respectively.

The high-flow frequency (FQ-high flow) in the Vu Gia changed from a positive to a negative impact grade starting in 2011, whereas it was mostly a positive grade in the Thu Bon (Fig. 4 (a) and (b)). The duration of the high-flow discharge decreased in the Vu Gia by 33% and did not change in the Thu Bon.

For the flow timing, the patterns of discharge hydrographs in the Vu Gia and Thu Bon were also altered (Fig. 5 (a) and (b)): the peak discharge occurred 10 and 11 days later in the

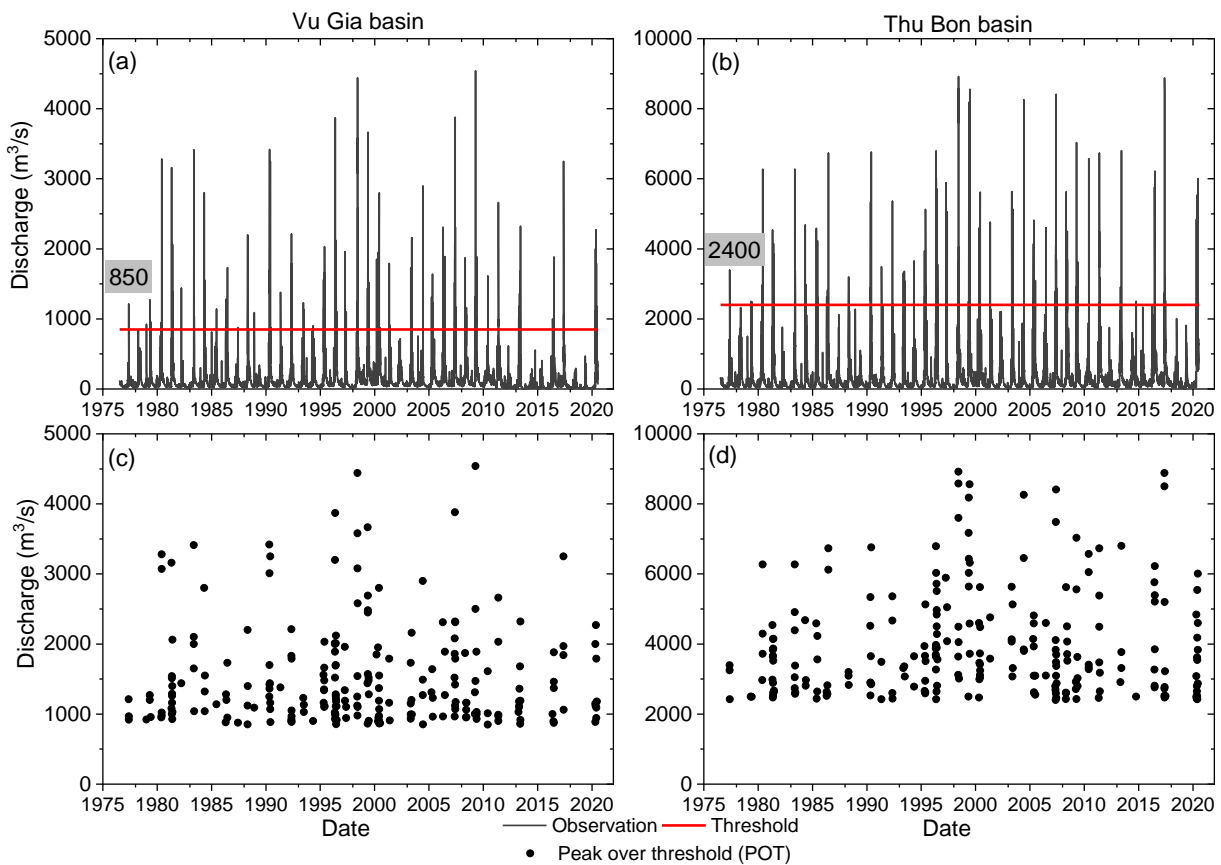


Figure 6. Threshold and POT samples selected in (a, c) the Vu Gia basin and (b, d) the Thu Bon basin. The black line is the observed discharge from 1977 to 2020, the red (horizontal) line is the threshold of the POT, and the point is the peak over the threshold.

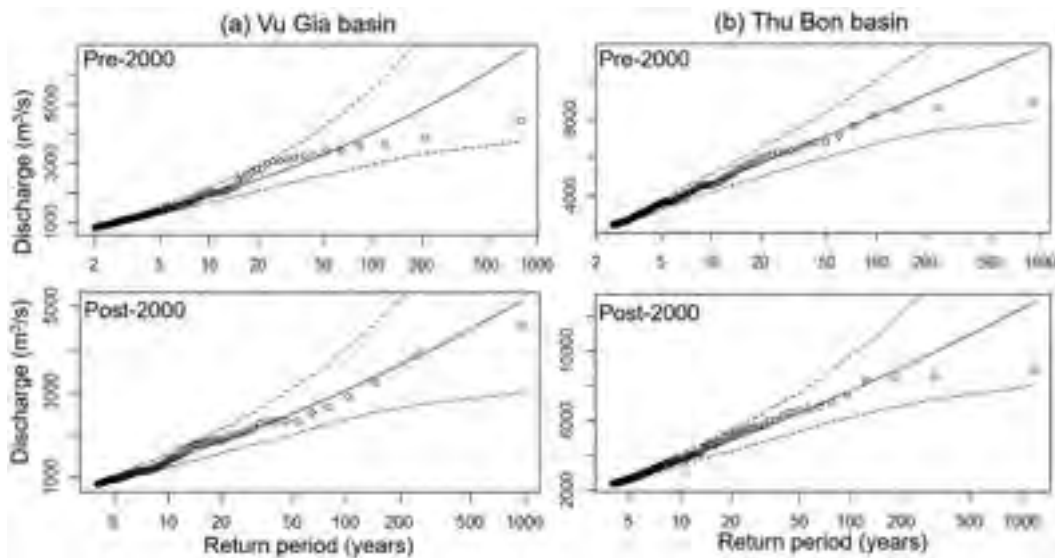


Figure 7. GPD of the POT in the pre-2000 and post-2000 periods for the (a) Vu Gia basin and (b) Thu Bon basin.

post-2000 period than in the pre-2000 period, respectively (Table 2).

3.3 Alterations of the average flow

The results of the Sen slope test show that the mean annual

discharge in the Vu Gia ($p = .012$) and Thu Bon ($p = .027$) basins significantly increased in the pre-2000 period by $0.14 \text{ m}^3/\text{s}/\text{year}$ and $0.25 \text{ m}^3/\text{s}/\text{year}$, respectively. However, during the post-2000 period, the annual discharge slightly decreased in the Vu Gia (by $0.21 \text{ m}^3/\text{s}/\text{year}$) and slightly increased in the Thu Bon (by $0.1 \text{ m}^3/\text{s}/\text{year}$) (Fig. 8).

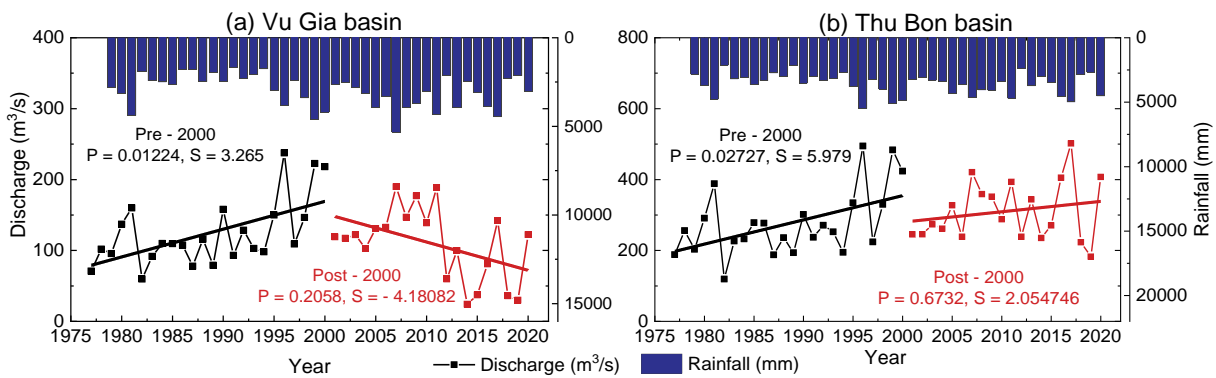


Figure 8. Long-term annual discharge and rainfall in the (a) Vu Gia basin and (b) Thu Bon basin. The black and red (shaded) lines are the discharge, and the blue bars are the rainfall.

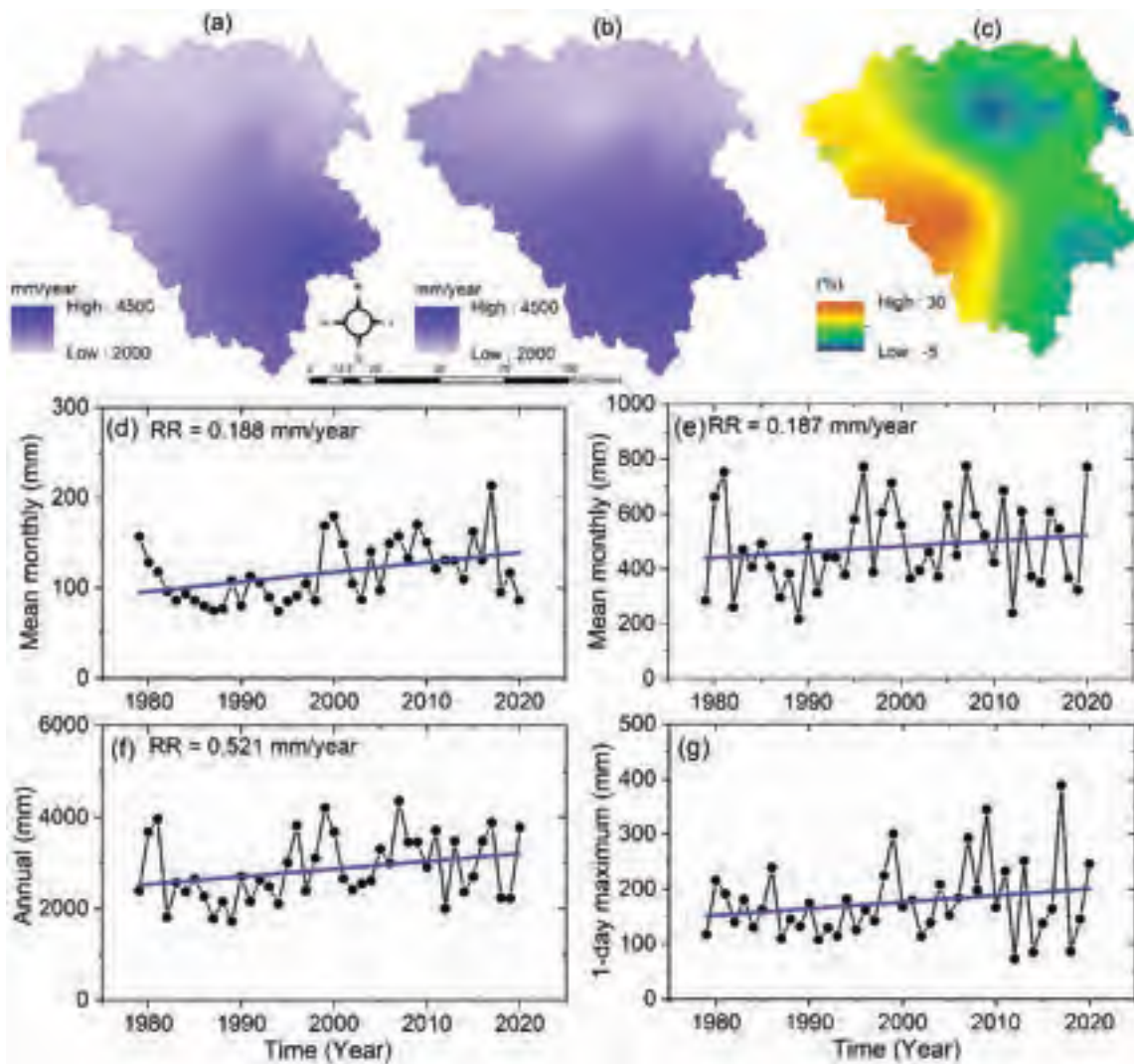


Figure 9. Temporal and spatial variations in the rainfall in the VGTB basin. (a) Mean annual rainfall in the pre-2000 period, (b) mean annual rainfall in the post-2000 period, and (c) mean annual rainfall changes in the post-2000 period relative to the pre-2000 period. (d–g) Long-term monthly means of the dry season, rainy season, annual rainfall, and one-day maximum values from 1979 to 2020.

The flow alteration in the dry and rainy seasons led to changes in the average flow in both basins. For the magnitude of the flow metrics, the average flow discharge in the Vu Gia (mean, Q40, Q60) was positively impacted from 2001 to 2011 and negatively impacted with extreme grades from 2012 to

2020 (Fig. 4(a)). The average flow discharge in the Thu Bon was mostly positively impacted (Fig. 4(b)). In the post-2000 period, the average annual flows in the Vu Gia and Thu Bon increased by 12% (from 80 to 90 m³/s) and 17% (from 178 to 208 m³/s), respectively (Table 2).

Table 3. Changes in the dry season, rainy season, and annual rainfall values in the pre-2000 and post-2000 periods.

| Time | | Pre-2000 | | Post-2000 | |
|--------------|-----------------|---------------|---------------|---------------|------------|
| | | Rainfall (mm) | Rainfall (mm) | Rainfall (mm) | Change (%) |
| Dry season | Mean | 831 | 1054 | + 26.84 | |
| | One-day maximum | 132 | 90 | - 31.85 | |
| Rainy season | Mean | 1881 | 1974 | + 4.94 | |
| | One-day maximum | 301 | 389 | + 29.35 | |
| Annual | | 2712 | 3028 | + 11.65 | |

3.4 Temporal and spatial variability in the relationships between rainfall and discharge

The impact of climate variability and the generated upstream inflow and operation of dam reservoirs are causing changes in time and space. Therefore, we wanted to investigate the climate change/variability drivers of flow alterations. Figure 9(a) and (b) show spatiotemporal variations in the rainfall in the VGTB basin. The most considerable changes in rainfall in the pre-2000 and post-2000 periods occurred mainly in the mountainous areas; smaller changes in rainfall occurred in the plains (Fig. 9(c)). The Mann-Kendall test of the rainfall showed no statistically significant trends in the dry season, rainy season, annual rainfall, and one-day maximum values in the VGTB basin. However, a slight increase was estimated from 1979 to 2020 (Fig. 9(d-g)). A comparison of the rainfall in the post-2000 period with that in the pre-2000 period shows that the rainfall increased slightly in the rainy season and annually and rose sharply in the dry season, by 4.94%, 11.65%, and 26.84%, respectively (Table 3).

In this paper, we mainly compare the pre-2000 and post-2000 periods. Therefore, we discussed these two periods first; then, we elaborated by further discussing post-2010 (2011–2020) to provide more evidence of dam impacts. Figure 10(b) shows that the correlations between the cumulative runoff and cumulative rainfall in the Thu Bon were linear in the three periods. However, in the Vu Gia, the curves were linear from 1979 to 2010 and changed suddenly starting in 2011 (Fig. 10(a)). This result shows that water transfer via the Dak Mi 4 plant reduced the flow on the Vu Gia River. Water stress on the Vu Gia resulted from the diversion of water at Dak Mi 4 to the Thu Bon.

The total rainfall in the dry season in the Vu Gia basin during the post-2010 period was 1090 mm, 47.4% higher than that in the pre-2000 period and 5.7% lower than that in the post-2000 period (Fig. 11(a)). The dry flow was 36.1% and 46.8% lower than those in the pre-2000 and post-2000 periods, respectively. The mean annual flow in the post-2010 period was 82 m³/s, 33.9% and 40.4% lower than those in the pre-2000 and post-2000 periods, respectively (Fig. 11(a)). In the Thu Bon basin, the total rainfall values in the dry seasons of the pre-2000, post-2000, and post-2010 periods were approximately 1021, 1204, and 1193 mm, respectively. Once it began to receive flow from the Vu Gia River, the flow of the Thu Bon in the post-2010 period was higher than those in the pre-2000 and post-2000 periods by 59.5% and 42.7%, respectively (Fig. 11(b)). Currently, Da Nang city often lacks water for domestic and agricultural production in the dry season. In addition, saltwater intrusion is more severe. Da Nang city and Quang Nam Province often place stress on water sources from the VGTB basin. Da Nang city requires Quang Nam to compensate for the water transferred by the Dak Mi 4.

3.5 The impact of hydropower and diversion on the alteration flow regime

3.5.1 The impact of hydropower and diversion on flood control

The most critical flood control issues for the downstream part of the VGTB basin are the reduction in the peak flood and the duration of the high-water level (Nguyen 2020).

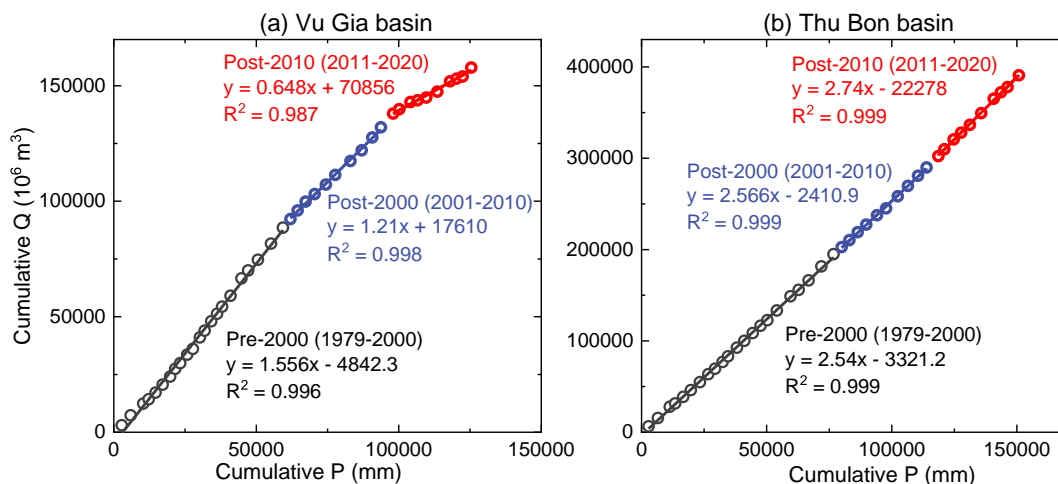


Figure 10. Curves of the cumulative rainfall and discharge in the pre-2000 (1979–2000), post-2000 (2001–2010), and post-2010 (2011–2020) periods for the (a) Vu Gia basin and (b) Thu Bon basin.

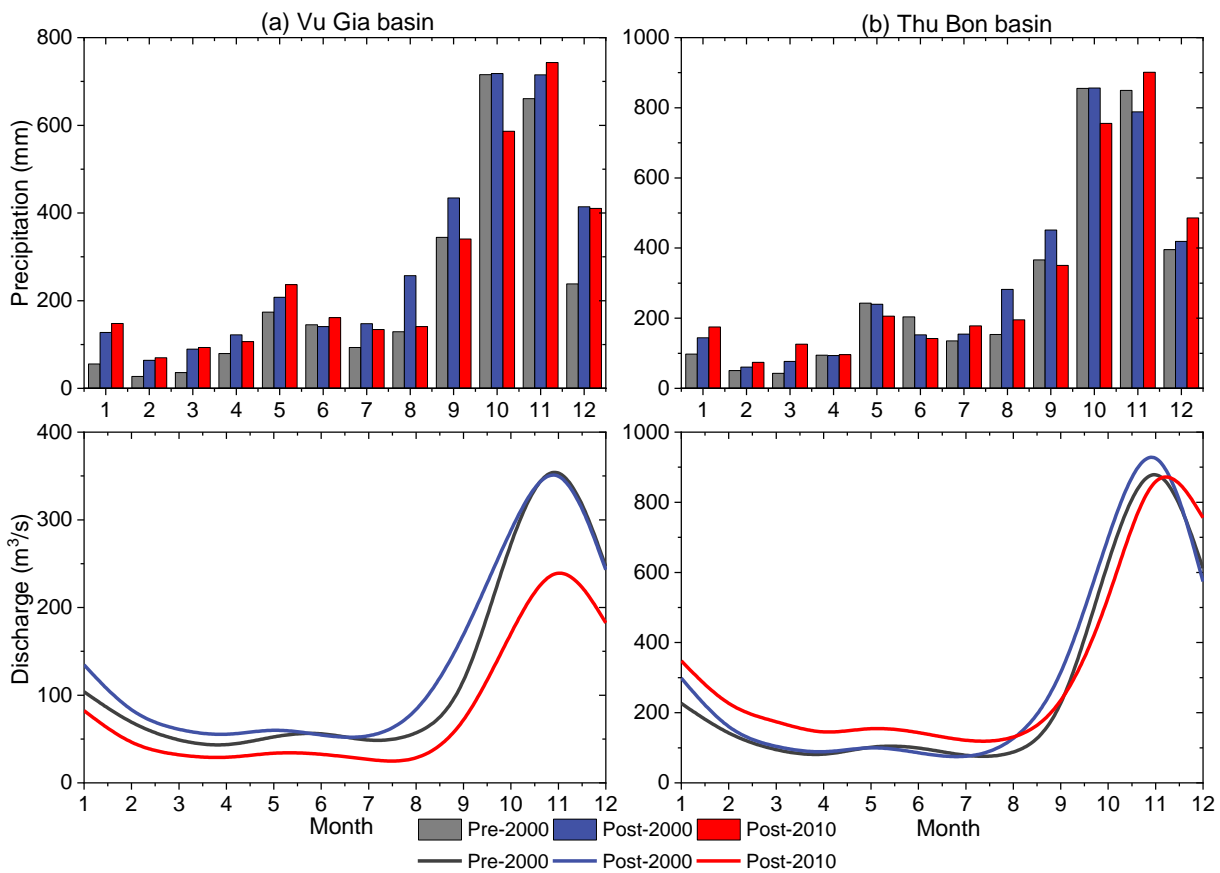


Figure 11. Monthly average rainfall and discharge of the Vu Gia and Thu Bon basins. The black line plots the pre-2000 (1979–2000) period, the blue line plots the post-2000 (2001–2010) period, and the red line plots the post-2010 (2011–2020) period.

The flood storage capacity influences the decrease in the peak flood downstream. It is important to forecast the flow to the reservoir to maintain a suitable storage capacity. Currently, there are few raingauges in the basin, which makes it challenging to accurately forecast the flow to the

reservoirs. The large flood of 2017 is a typical example; the inaccurate flow forecast of the Dak Mi 4 reservoir did not lead to a cut-off flood peak, which resulted in flooding downstream (Fig. 12). The Song Tranh 2 reservoir had better forecasts and operation.

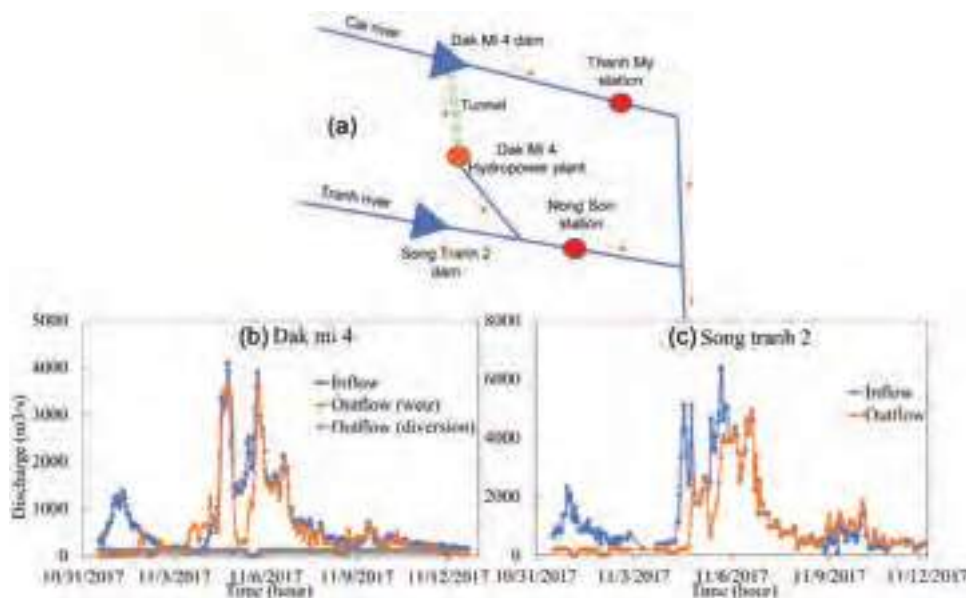


Figure 12. (a) River network and reservoirs upstream of the VGTB basin. (b) Inflow, outflow and diversion of the Dak Mi 4 reservoir. (c) Inflow and outflow of the Song Tranh 2 reservoir in the 2017 flood.

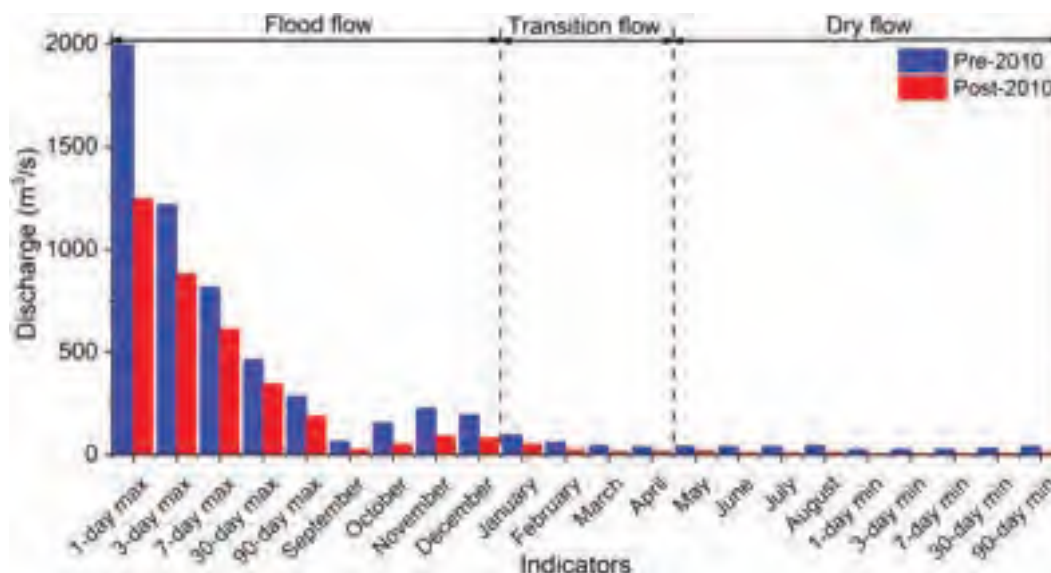


Figure 13. Changes in the extreme and monthly discharges before the Dak Mi 4 reservoir opened (pre-2010) and after the Dak Mi 4 reservoir opened (post-2010) at the Thanh My station from the IHA results.

3.5.2 The impact of water diversion structures

According to the research results of Firoz *et al.* (2018), the intensity and frequency of droughts in the entire VGTB basin mainly depend on upstream hydropower operation and water transfer from the Vu Gia basin to the Thu Bon basin by the Dak Mi 4 plant. The average annual amount of water transferred by the Dak Mi 4 plant is approximately $1.08 \times 10^9 \text{ m}^3$ (average $34.17 \text{ m}^3/\text{s}$, 26.7% of the Vu Gia River's flow). Moreover, with high energy demand in the dry season, some of the water needed for the minimum release of the Vu Gia River was used for power generation and discharge to the Thu Bon River. Part of the sediment along the flow is transferred to the Thu Bon basin, which leads to an imbalance of the natural state in the Vu Gia basin. This imbalance affects the sediment and morphology downstream.

IHA was used to analyse the periods before and after the building of the Dak Mi 4 reservoir at Thanh My: pre-2010 (1977–2010) and post-2010 (2011–2020). The flow regime alterations were considerably reduced during the dry and rainy seasons (Fig. 13). The minimum and low-flow release decreased by 53.5–76.3%. The maximum discharges significantly decreased during the post-2010 period by 37.5%. Similarly, the high-flow clearance decreased by 57.3–67.4%. As a result, the date of the minimum discharge increased from 180 to 193 days.

4 Discussion

The results of the analysis show that the flow regime changes in the dry and rainy seasons in the two basins (Figs 4–8, Table 2). The annual discharge in the Vu Gia basin decreased from 2001 to 2020 (especially from 2011 to 2020), although the corresponding rainfall increased (Figs 9–11). Therefore, we argue that these alterations in discharge are mainly due to reservoir operations and water transfer. However, another factor is land use/cover (LULC), which also has a significant impact on watershed hydrology. Therefore, we investigated whether the impacts of land-use changes act as drivers of flow alterations.

4.1 Drivers of flow alterations from land-use change

To understand the hydrological regime of the basin, it is necessary to assess the relationship between the watershed hydrological processes and LULC change (Meiyappan and Jain 2012). LULC changes may significantly affect the watershed hydrological regime and surface runoff of the basin (Jia *et al.* 2007). To clarify the effects of LULC change on the runoff in the VGTB basin, LULC maps from 2001, 2005, 2010, and 2020 were used to analyse the river section upstream of the Thanh My and Nong Son stations. The analysis shows that the land cover in the upstream area is dominated by forests, followed by mixed agricultural land, built-up areas,

Table 4. Statistics of LULC change in the VGTB basin from 2001 to 2020, from upstream to Thanh My station in the Vu Gia basin and Nong Son station in the Thu Bon basin.

| No. | Land-use types | Year 2001 | | Change in 2005 compared to 2001 | | Change in 2010 compared to 2001 | | Change in 2020 compared to 2001 | |
|-----|-------------------------|-------------------------|----------------|---------------------------------|----------------|---------------------------------|----------------|---------------------------------|----------------|
| | | Area (km ²) | Percentage (%) | Area (km ²) | Percentage (%) | Area (km ²) | Percentage (%) | Area (km ²) | Percentage (%) |
| 1 | Forest | 2710.98 | 51.89 | −31.70 | −1.17 | 100.69 | 3.71 | 59.16 | 2.18 |
| 2 | Mixed agricultural land | 2404.10 | 46.02 | 30.89 | 1.28 | −112.92 | −4.70 | −78.44 | −3.26 |
| 3 | Built-up area | 33.99 | 0.65 | 0.48 | 1.42 | 8.32 | 24.47 | 15.37 | 45.22 |
| 4 | Water | 74.91 | 1.43 | 0.32 | 0.43 | 3.91 | 5.22 | 3.91 | 5.22 |

and water (Table 4). The forest area increased by 2.18% from 2001 to 2020. The other LULCs changed minimally over time. This result is similar to the research of Nauditt *et al.* (2017). Therefore, LULC changes cannot explain the changes in flow in the VGTB basin, and thus the flow regime alterations are likely related to the operation of the reservoirs.

4.2 Challenges of water resource management in the downstream VGTB basin

The impacts of reservoir operation are particularly pronounced for the Vu Gia basin. Therefore, the Vu Gia basin is the most vulnerable. The Vu Gia basin mainly supplies water for Da Nang city and sizeable agricultural irrigation systems in Quang Nam Province (Fig. 1(a)). The flow and water level downstream during the dry season depend on the operation of the reservoirs. The flow from the reservoirs also maintains water levels to supply water for domestic use and agricultural production and to reduce salinity. The changes in flow impact the cropping pattern downstream, which is highly dependent on the water during the dry season. The reduction in flow during the rainy season is expected to reduce sediment and nutrient transport and possibly affect aquatic habitats (Pitlick and Wilcock 2001). The change in water quality due to sediment imbalance and the loss of habitats have potentially created long-term impacts for communities in the VGTB River basin.

Hydroelectric reservoirs upstream have retained significant amounts of coarse sand, gravel, and suspended sediment instead of transporting them downstream. This sediment reduction may aggravate erosion downstream from the dam. In addition, sand mining in the middle and downstream areas has removed large deposits of sediments from the riverbed. Finally, the changes in deposition have led to bed incision, which then decreases the water level. Bed incision has affected drinking water and agricultural production and increased saltwater intrusion. These issues have been detected in the Mekong and Red rivers (Kondolf *et al.* 2014, D. V. Vu *et al.* 2014, Nhan and Cao 2019, Van Binh *et al.* 2021). We anticipate that similar consequences are highly likely to occur in the VGTB basin. In recent years, saltwater intrusion hazard/risk has increased in Vu Gia River and strongly impairs socio-economic factors in Danang city, especially agricultural production and drinking water supply (Viet 2014, Nga *et al.* 2020).

5 Conclusions and outlook

We evaluated the long-term discharge changes in the VGTB river basin over 44 years (1977 to 2020) through a detailed analysis of runoff and related factors such as rainfall, land use, reservoir operation, and water diversion. We found that reservoir operation and water transfer by the Dak Mi 4 plant are the main reasons for flow alterations in the Vu Gia and Thu Bon rivers.

Based on the indicators analysed, the flow regime in the post-2000 period changed compared to that in the pre-2000 period. The Vu Gia basin changed more than the Thu Bon basin. Since 2011, reservoir operations have reduced the maximum and high-flow discharges downstream, exceeding the

climate change effect. However, in the dry season, due to the impact of water transfer, the minimum, low-flow release increased in the Thu Bon basin and decreased in the Vu Gia basin. Reducing the flow downstream of the Vu Gia River during the dry season leads to a decrease in the water level, affecting the operations of pumping stations supplying domestic and agricultural water in Da Nang city and parts of Quang Nam Province. In addition, due to the decreased flow downstream, the salinity condition in Da Nang has become more severe in recent years. Salinity penetrates farther inland and at higher levels, seriously affecting the water supply.

Reservoirs have helped to regulate flow and reduce flooding in downstream areas. However, there are still some floods with low regulatory efficiency. The cause is indicated by the few raingauging stations upstream. Therefore, maximizing the positive efficiency of reservoirs and improving the flow forecasting of reservoirs by constructing more rainfall gauging stations is necessary.

We also note that in the entire VGTB basin, there are only two stations that measure upstream streamflow. The downstream tributaries include many hydropower plants. This leads to difficulty in fully investigating the streamflow and impact of reservoirs. Therefore, in our future work we will study the entire basin using a hydrological model.

Funding

This work was funded by APN “Asia-Pacific Network for Global Change Research” under project reference number CRRP2020-09MYKantoush (Funder ID: <https://doi.org/10.13039/100005536>). Acknowledgment for the Research Unit for Realization of Sustainable Society (RURSS) at Kyoto University.

References

- Dinh, N.T., 2016. Impacts of Song Bung 4 hydropower project to biodiversity and hydrology of Vu Gia–Thu Bon basin in Quang Nam province. Vietnam.
- Duong, V.N. and Gourbesville, P., 2014. Rainfall uncertainty in distributed hydrological modelling in large catchments: an operational approach applied to the Vu Gia–Thu Bon catchment–Viet Nam. *3rd IAHR Europe Congress*, 14–16.
- Firoz, A.B.M., et al., 2018. Quantifying human impacts on hydrological drought using a combined modelling approach in a tropical river basin in central Vietnam. *Hydrology and Earth System Sciences*, 22 (1), 547–565. doi:10.5194/hess-22-547-2018.
- Government of Vietnam, 2019. *Decision 1867/QĐ-TTg: Procedures for operating reservoirs system in Vu Gia Thu Bon river basin (in Vietnamese)*.
- Ha, D.T. and Coynelb, A., 2019. Impact of tranh river 2 hydroelectric dam on sediment load on the Thu Bon river of Quang Nam province. *UED Journal of Social Sciences, Humanities and Education*, 9, 7–11.
- ICEM, 2008. Strategic environmental assessment of the Quang Nam province hydropower plan for the Vu Gia–Thu Bon River Basin. Hanoi, Vietnam: ADB, MONRE, MOITT & EVN. p. 205.
- Japan Meteorological Agency, 2013. *Digital typhoon: typhoon images and information*. Tokyo: Typhoon Center.
- Jia, N.F., Duan, J.N., and Qiao, Z.M., 2007. Analysis method of spatial distribution of land use in relation to topography. *Economic Geography*, 27 (2), 310–312.
- Kendall, M.G., 1938. A new measure of rank correlation. *Biometrika*, 30 (1/2), 81–93. doi:10.1093/biomet/30.1-2.81.

- Kondolf, G.M., Rubin, Z.K., and Minear, J.T., 2014. Dams on the Mekong: cumulative sediment starvation. *Water Resources Research*, 50 (6), 5158–5169. doi:10.1002/2013WR014651.
- Lang, M., Ouarda, T.B.M.J., and Bobée, B., 1999. Towards operational guidelines for over-threshold modeling. *Journal of Hydrology*, 225 (3–4), 103–117. doi:10.1016/S0022-1694(99)00167-5.
- Larson, M., et al., 2014. Impacts of typhoons on the Vietnamese Coastline: a case study of Hai Hau Beach and Ly Hoa Beach. In: N.D. Thao, H. Takagi and M. Esteban eds. *Coastal Disasters and Climate Change in Vietnam: Engineering and Planning Perspectives*. Elsevier, 17–42. doi:10.1016/B978-0-12-800007-6.00002-2.
- Laux, P., et al., 2017. Hydrological and agricultural impacts of climate change in the Vu Gia-Thu Bon River Basin in Central Vietnam. In: A. Nauditt and L. Ribbe, eds. *Land use and climate change interactions in Central Vietnam*. Springer Science, 123–142. doi:10.1007/978-981-10-2624-9_8.
- Mann, H.B., 1945. Nonparametric tests against trend. *Econometrica: Journal of the Econometric Society*, 13 (3), 245–259. doi:10.2307/1907187.
- Meiyappan, P. and Jain, A.K., 2012. Three distinct global estimates of historical land-cover change and land-use conversions for over 200 years. *Frontiers of Earth Science*, 6 (2), 122–139. doi:10.1007/s11707-012-0314-2.
- MOIT, 2015. Decision for hydropower plant operation: technical document, ministry of investment and trade, socialist Republic of Vietnam.
- Nauditt, A., et al., 2017. Hydrological drought risk assessment in an anthropogenically impacted tropical catchment, Central Vietnam. In: *Land use and climate change interactions in central Vietnam*. Springer, 223–239. doi:10.1007/978-981-10-2624-9_14.
- NDPAC, *Natural Disaster Prevention and Control of Quang Nam Province*. Available from: <http://pctt.quangnam.vn/> [Accessed 22 Jun 2022].
- Nga, T.T., Cong, V.H., and Hung, L., 2020. Assessing the impacts of climate change and reservoir operation on Saltwater Intrusion in the Vu Gia-Thu Bon River Basin. In: N. Trung Viet, D. Xiping and T. Thanh Tung eds. *International Conference on Asian and Pacific Coasts*. Singapore: Springer, 1207–1212. doi:10.1007/978-981-15-0291-0_165.
- Nguyen, T.H., 2020. Optimal operation of multi-reservoir system for flood control. Application to the Vu Gia Thu Bon catchment, Vietnam.
- Nhan, N.H. and Cao, N.B., 2019. Chapter 19 - Damming the Mekong: Impacts in Vietnam and Solutions. In: E. Wolanski, J.W. Day, M. Elliott and R. Ramachandran eds. *Coasts and Estuaries*. Elsevier, 321–340. doi:10.1016/B978-0-12-814003-1.00019-8.
- Opperman, J., 2006. Indicators of hydrologic alteration analysis for the Patuca River.
- Phuong, D.N.D., et al., 2020. Hydro-meteorological trend analysis using the Mann-Kendall and innovative-Şen methodologies: a case study. *International Journal of Global Warming*, 20 (2), 145–164. doi:10.1504/IJGW.2020.105385.
- Pickands, J., III, 1975. Statistical inference using extreme order statistics. *The Annals of Statistics*, 119–131.
- Pitlick, J., and Wilcock, P., 2001. Relations between streamflow, sediment transport, and aquatic habitat in regulated rivers. *Geomorphic Process. Riverine Habitat*, 4, 185–198.
- RETA, 2011. *Investment, Managing water in Asia's river basins: charting progress and facilitating - The Vu Gia-Thu Bon Basin*. Quang Nam Province, Vietnam: Department of Natural Resources and Environment.
- Ribbe, L., et al., 2017. Integrated river basin management in the Vu Gia Thu Bon Basin. In: *Land use and climate change interactions in Central Vietnam*. Springer, 153–170.
- Richter, B.D., et al., 1996. A method for assessing hydrologic alteration within ecosystems. *Conservation Biology*, 10 (4), 1163–1174. doi:10.1046/j.1523-1739.1996.10041163.x.
- Richter, B.D., et al., 1998. A spatial assessment of hydrologic alteration within a river network. *Regulated Rivers: Research & Management: An International Journal Devoted to River Research and Management*, 14 (4), 329–340.
- Richter, B.D., et al., 2003. Ecologically sustainable water management: managing river flows for ecological integrity. *Ecological Applications*, 13 (1), 206–224. doi:10.1890/1051-0761(2003)013[0206:ESWMMR]2.0.CO;2.
- Sen, P.K., 1968. Estimates of the regression coefficient based on Kendall's tau. *Journal of the American Statistical Association*, 63 (324), 1379–1389. doi:10.1080/01621459.1968.10480934.
- Tan, P.V. and Thanh, N.D., 2013. Climate change in Vietnam: some research findings, challenges and opportunities in international integration. *Vietnam National University Journal of Science*, 29, 42–55.
- Van Binh, D., et al., 2020. Long-term alterations of flow regimes of the Mekong River and adaptation strategies for the Vietnamese Mekong Delta. *Journal of Hydrology: Regional Studies*, 32, 100742.
- Van Binh, D., et al., 2021. Effects of riverbed incision on the hydrology of the Vietnamese Mekong Delta. *Hydrological Processes*, 35 (2), e14030.
- Viet, T.Q., 2014. *Estimating the impact of climate change induced saltwater intrusion on agriculture in estuaries-the case of Vu Gia Thu Bon*. Vietnam: Ruhr-Universität Bochum.
- Vu, T.T., et al., 2011. Solutions for flood and drought prevention and mitigation in Quang Nam.
- Vu, D.V., et al., 2014. Impact of the Hoa Binh Dam (Vietnam) on water and sediment budgets in the Red River basin and delta. *Hydrology & Earth System Sciences Discussions*, 11 (1).
- Wang, S.-Y.S., et al., 2014. Changes in the autumn precipitation and tropical cyclone activity over Central Vietnam and its East Sea. *Vietnam Journal of Earth Sciences*, 36 (4), 489–496.
- Zhang, Y., Zhai, X., and Zhao, T., 2018. Annual shifts of flow regime alteration: new insights from the Chaishitan Reservoir in China. *Scientific Reports*, 8 (1), 1–11. doi:10.1038/s41598-017-17765-5.



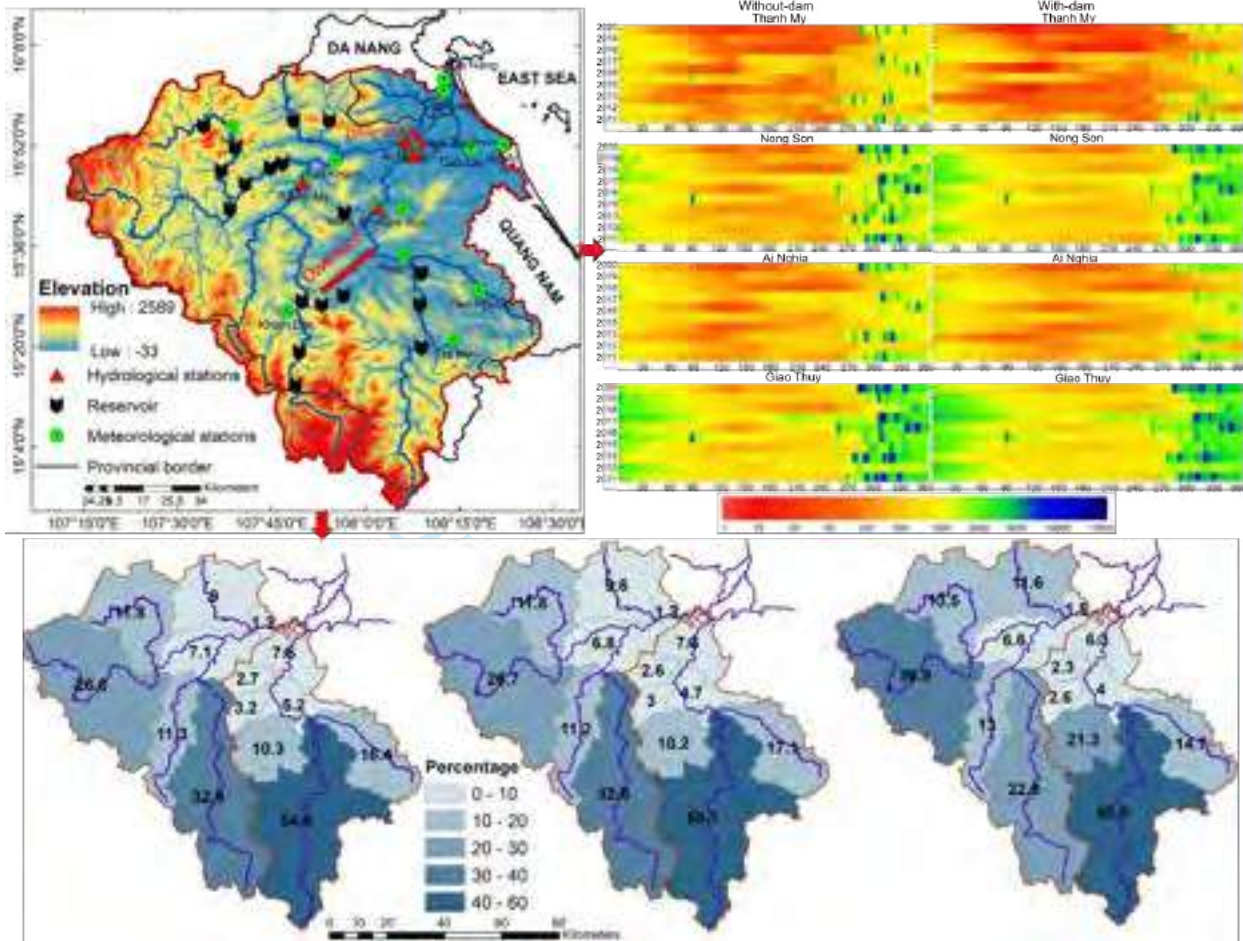
Quantifying the impacts of hydraulic infrastructures and contributions of the sub-basins on streamflow in a tropical river basin, Vietnam

| | |
|-------------------------------|--|
| Journal: | <i>Hydrological Processes</i> |
| Manuscript ID | HYP-22-0054 |
| Wiley - Manuscript type: | Special Issue Paper |
| Date Submitted by the Author: | 24-Jan-2022 |
| Complete List of Authors: | <p>Binh, Nguyen; Water Resource Center, Disaster Prevention Research Institute (DPRI), Kyoto University, Kyoto 611-0011, Japan, Water Resource Center; The University of Danang - University of Science and Technology, 54 Nguyen Luong Bang, Danang, Vietnam, Water resources engineering</p> <p>Kantoush, Sameh; Kyoto University Disaster Prevention Research Institute, Water Resources Research Center</p> <p>Saber, Mohamed ; Water Resource Center, Disaster Prevention Research Institute (DPRI), Kyoto University, Kyoto 611-0011, Japan, Water Resources Research Center</p> <p>Binh, Doan; Faculty of Engineering, Vietnamese German University, Binh Duong, Vietnam, Faculty of Engineering</p> <p>Vo, Duong; The University of Danang - University of Science and Technology, 54 Nguyen Luong Bang, Danang, Vietnam, Water resources engineering</p> <p>Sumi, Tetsuya; Kyoto University Disaster Prevention Research Institute, Water Resources Research Center</p> |
| Keywords: | Vu Gia Thu Bon River basin, Reservoir, Water diversion, Streamflow, SWAT |
| | |

SCHOLARONE™
Manuscripts

1
2
3
4
5
6
7
8
9
10
11
12
13
14
15
16
17
18
19
20
21
22
23
24
25
26
27
28
29
30
31
32
33
34
35
36
37
38
39
40
41
42
43
44
45
46
47
48
49
50
51
52
53
54
55
56
57
58
59
60

Graphical abstract



Impact of hydraulic infrastructures and contribution of the sub-basins

1
2
3 1 **Quantifying the impacts of hydraulic infrastructures and contributions of the sub-basins on**
4
5 2 **streamflow in a tropical river basin, Vietnam**

6
7 3 Nguyen Quang Binh^{1,2,*}, Sameh A. Kantoush¹, Mohamed Saber¹, Doan Van Binh³, Ngoc Duong Vo²,
8
9 4 Tetsuya Sumi¹

10
11 5 ¹Water Resource Center, Disaster Prevention Research Institute (DPRI), Kyoto University, Kyoto 611-0011,
12
13 6 Japan

14
15 7 ²The University of Danang - University of Science and Technology, 54 Nguyen Luong Bang, Danang,
16
17 8 Vietnam

18
19 9 ³Faculty of Engineering, Vietnamese German University, Binh Duong, Vietnam

20
21
22 10 **Corresponding author: Nguyen Quang Binh (nqbinh@dut.udn.vn,*
23
24 11 *nguyen.binh.27y@st.kyoto-u.ac.jp)*

25
26
27
28 13 **Highlights**

29
30 14 ➤ A semi-distributed hydrological model, SWAT (Soil and Water Assessment Tool), was developed for
31
32 15 a tropical river in Vietnam, the Vu Gia Thu Bon (VGTB) basin considering two plausible scenarios: with-
33
34 16 dam and without-dam.

35
36
37 17 ➤ The coupled impacts of reservoir operations, water transfer, and quantify variations in the multi-sub-
38
39 18 basin contributions to the water budget.

40
41 19 ➤ The cascading reservoirs decreased in the Vu Gia sub-basins and increased in the Thu Bon sub-basins.

42
43 20 ➤ The water diverted to the Thu Bon River was governed and reduced by the cascading hydropower
44
45 21 dams.

46
47 22 ➤ The operation of reservoirs has partially compensated for the lost water in the Vu Gia sub-basins.

48
49
50
51
52
53
54
55
56
57
58
59
60

Impact of hydraulic infrastructures and contribution of the sub-basins

Abstract: Hydraulic infrastructures, such as reservoirs and water diversion channels, are known to cause altered streamflow worldwide. Therefore, this study aims to assess the coupled impacts of reservoir operations and water transfer on downstream streamflow over 42 years (1979–2020) for a tropical river in Vietnam, the Vu Gia Thu Bon (VGTB). We also quantified variations in the multi-sub-basin contributions to the water budget associated with hydraulic structure development. In this regard, a semi-distributed hydrological model, SWAT (Soil and Water Assessment Tool), was developed for the entire VGTB basin considering two plausible scenarios: with-dam and without-dam. We found that the reservoirs substantially affected the streamflow during the 2011–2020 period when 12 cascading hydropower dams were constructed in the Vu Gia sub-basins. The cascading reservoirs across the Vu Gia River reduced the annual average streamflow by 28.1% during this period, whereas their influence was augmented by 13.9% at reaches further downstream. In contrast, the local reservoir and flow diversions created on the Thu Bon River resulted in a 6.5% increase in streamflow. The upstream reservoir operation significantly affected streamflow at the midstream stations by 27.8% compared with the no-dam period. The streamflow decreased in the dry season by 5.6% in the Vu Gia sub-basins and increased by 61.7% in the Thu Bon sub-basins. However, the impacts were reduced in the wet season by 41.3% due to the Dak Mi 4 reservoir operation, which is considered to be the most significant influence. It was found that the water diverted to the Thu Bon River was governed and reduced by the cascading hydropower dams. Therefore, the operation of 11 reservoirs has partially compensated for the lost water in the Vu Gia sub-basins, to which the Dak Mi 4 plant has transferred an amount of 19.7 m³/s (14%). Our findings provide a classification of the impact of cascading dams and diversion structures and their interaction with climate change.

Keywords: Vu Gia Thu Bon River basin, Reservoir, Water diversion, Streamflow, SWAT.

1. Introduction

All over the world, hydrological cycles within river basins play a key role in providing streamflow to downstream deltaic systems (Oki & Kanae, 2006). The duration and intensity of the streamflow are fundamentally dependent on climatic variables such as precipitation (Ahn & Merwade, 2014; Souvignet et al., 2014) and on the operation of basin-wide infrastructures such as hydropower dams, storage reservoirs,

Impact of hydraulic infrastructures and contribution of the sub-basins

1
2
3 50 and water diversion structures (Ribbe et al., 2017). Currently, most rivers worldwide are interrupted by
4
5 51 dammed reservoirs (Zhou et al., 2016). The boom in reservoir construction has occurred particularly in
6
7 52 regions with emerging economies, such as Southeast Asia (SEA), for irrigation, drinking water, hydropower
8
9 53 generation, and hydrological hazard control (Zarfl et al., 2015). It is undeniable that reservoirs are necessary
10
11 54 for flood control and securing water supplies for agriculture and the environment in tropical river basins
12
13 55 with complex climate characteristics, such as SEA. However, despite their benefits, reservoirs remain
14
15 56 controversial owing to their potentially negative impacts on streamflow. Reservoir operations alter the
16
17 57 natural flow regime daily and long-term (Mittal et al., 2016; Van Binh, Kantoush, & Sumi, 2020).
18
19 58 Additionally, hydrological extremes can be intensified by ineffective management of reservoir water, which
20
21 59 can sometimes have a greater impact than climate change (Di Baldassarre et al., 2018; Vu et al., 2017).
22
23 60 Therefore, there is a need to evaluate the effects of reservoir operations on streamflow in specific multi-
24
25 61 basin catchments.

26
27
28 62 The Vu Gia Thu Bon River (VGTB) basin in Central Vietnam and its water resources have been
29
30 63 developed for various purposes, including energy, agriculture, flood mitigation, water supply, and saltwater
31
32 64 intrusion control (Firoz et al., 2018; Ribbe et al., 2017; Viet, 2014). However, the basin faces challenges in
33
34 65 securing water supply and mitigating severe flooding due to climate change and the rapid development of
35
36 66 artificial hydro-structures. Since 2007, 18 hydropower dams have been built, of which 12 are on the Vu Gia
37
38 67 River, six are in the Thu Bon River, and a diversion channel carries water and sediment from the Vu Gia to
39
40 68 the Thu Bon River (Fig. 1a). Four large reservoirs, including A Vuong, Song Bung 4, Dak Mi 4, and Song
41
42 69 Tranh 2, have the greatest influence on the effectiveness of downstream flood control (T. H. Nguyen, 2020).
43
44 70 The number of dams is projected to reach 58 by 2030 (ICEM 2008). These cascaded reservoirs may alter
45
46 71 the hydrological regime of rivers by changing the seasonal flow (Ngo et al., 2018). Therefore, addressing
47
48 72 the complex interactions between reservoir operations and natural hydrological processes is essential for
49
50 73 better water resources and environmental management.

51
52
53 74 Various approaches have been used to examine and quantify the effects of hydraulic infrastructure on
54
55 75 runoff. Popular methods include streamflow time-series studies that look at monthly, seasonal, annual, and
56
57
58
59
60

Impact of hydraulic infrastructures and contribution of the sub-basins

1
2
3 76 frequency changes to determine the anthropogenic effects on streamflow (Binh et al., 2020; Y. Zhang et al.,
4
5 77 2018) and relationships between runoff and climate variables (Johnson et al., 1991; D. Wang & Hejazi,
6
7 78 2011; H. Wang et al., 2016). The fundamental analysis of hydro-climatic time series can provide the first
8
9 79 insight into hydrological systems. However, they may be incapable of capturing the nonlinear nature of
10
11 80 hydrological systems (Firoz et al., 2018). Hydrological models play an essential role in detecting and
12
13 81 explaining changes in water resource basins (Sorooshian et al., 2008). Hydrological reconstruction using
14
15 82 models is helpful for studying changes in basin hydrology. The advantage of hydrological models is that
16
17 83 they can simulate scenarios with and without dams and extract the results at various stream locations, where
18
19 84 the assessment for a group of cascading dams can be evaluated separately. The combination of hydrological
20
21 85 models, water diversion, and reservoir operation is a promising method utilised in this study. A semi-
22
23 86 distributive hydrological model, SWAT, can simulate the hydrological characteristics of the basin integrated
24
25 87 with the basic reservoir operation (Carvalho-Santos et al., 2017; Chhuon et al., 2016; Loi et al., 2019; L. H.
26
27 88 Nguyen & Fukushi, 2019; Shrestha et al., 2018; Vale & Holman, 2009; G. Wang & Xia, 2010).

28
29
30 89 Several studies have adopted numerical models to investigate the hydrological regimes of basins.
31
32 90 However, previous studies have not considered the combination of reservoir operation and diversion, and
33
34 91 have only used short study periods (Firoz et al., 2018; Loi et al., 2019; Nauditt et al., 2017; H. T. Nguyen et
35
36 92 al., 2020; Vu et al., 2017). As a result, these studies could not correctly capture the impact of reservoir
37
38 93 operation on streamflow. This study has addressed these two significant gaps. Another issue is that only two
39
40 94 stations (Thanh My on the Vu Gia sub-basins and Nong Son on the Thu Bon sub-basins) monitor streamflow
41
42 95 discharge. Previous studies that analysed historical data at these two stations could not clearly show the dam
43
44 96 impacts on streamflow (Loi et al., 2019; Vu et al., 2017), thus demanding a more advanced methodology.
45
46 97 Firoz et al. (2018) and Nauditt et al. (2017) quantified the effects of only 8 out of 18 dams for 5 years after
47
48 98 the operation commencement. This means that the impact of newly built dams has not been studied over a
49
50 99 more extended period.

51
52
53
54 100 Moreover, these studies did not combine the hydrological module with the reservoir operation module;
55
56 101 instead, they simulated them separately. Many other researchers (e.g., Loi et al., 2019; H. T. Nguyen et al.,
57
58
59
60

Impact of hydraulic infrastructures and contribution of the sub-basins

2020; Vu et al., 2017) have not considered reservoir operation in their models. Another knowledge gap to date is that previous studies have not quantified the contribution of each sub-basin and the diversion channel's role in the hydrological processes of the VGTB basin. Therefore, this study aims to fill these knowledge gaps by assessing the changes in the streamflow discharges at multiple spatial locations (i.e. upstream, midstream, and downstream) of different groups of cascading dams and quantifying the effect of the diversion channel. The advanced model incorporates a hydrological, reservoir operation, and water diversions module. Therefore, we can quantify with a high confidence level the contribution of each group of dams on downstream flow alterations and the contribution of each sub-basin to the downstream flow discharge. Finally, we discuss the implications of hydraulic structures on agriculture, water supply, saltwater intrusion, and flood control.

The main objective of the present study is to quantify the coupled impacts of reservoir operation and water transfer on streamflow and water balance in the VGTB basin at various locations. The hydrological semi-distributed model was selected to simulate the streamflow from 1979 to 2020 and the effects of cascading hydraulic structures. The principal research aims are to (1) model the basin's natural streamflow, (2) quantify the effects of hydraulic infrastructures, (3) distinguish the effects of four major reservoir operations on downstream flow, and (4) quantify the flow contribution of the sub-basins. The findings of this study will provide a detailed understanding of the effects of hydraulic infrastructures such as hydropower reservoirs and water diversion structures on downstream flow. Furthermore, the insights gained from this basin's hydraulic infrastructure effects can assist water managers in Vietnam and other tropical monsoon regions.

2. Study area

The VGTB River basin (area 10,000 km²) is located in the central region of Vietnam and accounts for approximately 2.5% of the total water volume in Vietnam (RETA, 2011) (Fig. 1a). The topography of the VGTB basin is varied. From west to east it changes from high mountains to undulating hills, with a slope of 20–30%. The altitude, steep terrain, and significant rainfall provide great potential for hydropower energy in the upstream part of the basin. The primary land use is forest (62.05%), and the predominant soil type is

Impact of hydraulic infrastructures and contribution of the sub-basins

1
2
3 128 clay and silt loam (accounting for 83.33%) (Fig. 1b, 1c). Agriculture is an important economic activity in
4
5 129 the basin. Paddy rice is the most important agricultural crop, comprising approximately 70% of irrigated
6
7 130 agriculture (Viet, 2014).
8

9 131 The characteristics of the sub-basins are shown in Figure 2a and Table 1. There are five major sub-basins
10
11 132 from the headwater to the Ai Nghia station in the Vu Gia River (i.e. Con, A Vuong, Bung, Giang, and Dak
12
13 133 Mi Rivers). From upstream to the Giao Thuy station in the Thu Bon River, there are also five major sub-
14
15 134 basins (i.e., the Khe Dien River, Que Lam River, Truong River, Tranh River, and Khang River). In the
16
17 135 VGTB basin, the inter-basin water diversion from the Vu Gia to the Thu Bon River occurs in both the
18
19 136 upstream and downstream sections through the Dak Mi 4 plant and Quang Hue River, respectively (Fig. 1a).
20
21

22 137 The data obtained over 42 years (1979–2020) show that the average annual rainfall of the entire basin is
23
24 138 2,863 mm, varying significantly from 2,184 mm in the lowlands to over 4,188 mm in the southern
25
26 139 mountainous areas (Fig. 2a). Precipitation varies by season, with 48–81% of the annual rainfall concentrated
27
28 140 between September and December. The average temperature of the basin is 25.2°C, with the lowest
29
30 141 temperatures in December or January and the highest in June and July (Fig. 2b). The streamflow varied
31
32 142 significantly between the seasons, and the flood season from October to December corresponded to the
33
34 143 heaviest rainy period. The flow in this period accounted for approximately 62.5%–69.2% of the total annual
35
36 144 flow. April is the driest month, accounting for only 2%–3% of the annual flow (RETA, 2011).
37
38

39 145 **3. Methodology and Material**

40 41 146 **3.1. SWAT model**

42
43 147 The SWAT model was developed by Arnold and Srinivasan, researchers of the United States Department
44
45 148 of Agriculture Research Service (USDA-ARS), and Texas AgriLife Research, respectively. It consists of a
46
47 149 comprehensive computer simulation tool for watershed-scale studies that integrates multiple components,
48
49 150 such as climate, hydrology, land cover, reservoir operation, and management practices (Arnold et al., 1998;
50
51 151 Keitzer et al., 2016). The model divides the watershed into sub-basins. These sub-basins are further
52
53 152 subdivided into soil characteristics, and the land use and slope units are known as hydrological response
54
55 153 units (HRUs). The SWAT model was integrated with the GIS software. The model comes in many different
56
57
58
59
60

Impact of hydraulic infrastructures and contribution of the sub-basins

154 versions, such as ArcSWAT, MWSWAT, and QSWAT. For this study, SWAT version 1.9 was used with
155 the QGIS 2.6.1.

156 **3.2. Input data**

157 Data play a crucial role in hydrological models. We collected streamflow, rainfall, temperature, relative
158 humidity, wind speed, solar radiation of stations, topography, land use, soil map, and dam data in the entire
159 VGTB basin to set up, calibrate, and validate the SWAT model.

160 *3.2.1. Streamflow*

161 Daily streamflow data at the Thanh My and Nong Son stations during 1979–2020 were used to calibrate
162 and validate the results from the SWAT model (Fig. 1a). Data were collected from the Mid-Central Regional
163 Hydro-Meteorological Center (MCRHMC n.d.). The monthly discharge released from the reservoirs from
164 2017 to 2020 was collected from the Natural Disaster Prevention and Control of Quang Nam Province
165 (NDPAC, n.d.).

166 *3.2.2. Meteorology*

167 We collected daily rainfall data from 15 stations distributed over the entire VGTB basin from 1979 to
168 2020, including nine stations in mountainous areas and seven stations in lowland areas. Daily temperature
169 data were collected at two stations, Da Nang (lowland area) and Tra My (mountainous region) (Fig. 1a).

170 *3.2.3. Topography*

171 In this study, topographic data (DEM) benefited from the ‘Land Use and Climate Change Interaction in
172 Central Vietnam’ (Lucci) project (www.lucci-vietnam.info), 30mx30m spatial resolution (Fig. 1a). The
173 DEM was created by combining Shuttle Radar Topography Mission (SRTM) data and isolines (ISO
174 19115:2003 for geographic information metadata). The DEM map has been formatted as a spatial
175 representation Type A grid and coordinate system Universal Transverse Mercator (UTM) zone 48N with a
176 reference date of 2014.

177 *3.2.4. Land use and soil map*

178 Land use and soil map data were also collected from the Lucci project with a 30mx30m resolution (Fig.
179 1b, 1c). Land use was created based on Landsat images, SPOT images, and field survey data. The soil map

Impact of hydraulic infrastructures and contribution of the sub-basins

180 was digitised using the National Institute of Agriculture Planning and Protection (NIAPP) data. The dataset
181 reference dates for land use and soil maps were obtained in 2013 and 2011, respectively.

182 3.2.5. Dams

183 Eighteen reservoirs in the SWAT model were collected from Decision 1865/QĐ-TTg: Procedures for
184 operating reservoir systems in the VGTB River basin (Government of Vietnam, 2019). The characteristics
185 of dams (volume, year of construction, water release, and operating rules) were collected from the Natural
186 Disaster Prevention and Control of Quang Nam province and are shown in Table 2 (NDPAC, n.d.).

187 3.3. Simulation scenarios

188 We evaluated the long-term alteration of streamflow in the VGTB basin over 42 years by analysing
189 observational data as well as related factors such as reservoir operation, rainfall, and land use. We found
190 that the flow alterations mainly depended on reservoir operation and water transfer. Therefore, this study
191 evaluates the reservoir operation and water transfer effects on the streamflow. The model was simulated for
192 two scenarios over the 42 years from 1979 to 2020 and focused on the period 2011–2020: (a) without-dam
193 and (b) with-dam. The model parameters were kept the same for both scenarios. The reservoir component
194 was inactivated when simulating the flow under natural conditions (without-dam).

195 All reservoirs were considered in the study, and then the impacts of the largest reservoirs (i.e. A Vuong,
196 Song Bung 4, Dak Mi 4, Song Tranh 2) were evaluated. Each reservoir was independently set up and
197 released (the other reservoirs were inactive). The flow contribution rates of the sub-basins were evaluated
198 in two cases: with and without-dam.

199 3.4. Model setup

200 The basin was divided into 153 sub-basins and 2580 HRUs. The sub-basins were divided based on slope
201 classes (0–5, 5–10, 10–20, 20–30, and > 30 degree), six land classes (Fig. 1b), six soil classes (Fig. 1c),
202 locations of hydrological stations and dams, water transfer and receiving sites, and uniform distribution of
203 size between sub-basins. The water transferred from the Vu Gia sub-basins to the Thu Bon sub-basins via
204 the Dak Mi 4 and Quang Hue rivers was also established. The water transfer via Dak Mi 4 was determined

Impact of hydraulic infrastructures and contribution of the sub-basins

for each month as the average daily value (WURES_N, the average amount of water withdrawn from the reservoir each day in the month for consumptive water 10^4 m^3). Downstream, the water transferred by the Quang Hue River was determined for each month as the average daily water (WURCH – average daily water removal from the reach for the month $10^4 \text{ m}^3/\text{day}$). From field surveys and other data, the percentage of runoff transferred to the Thu Bon River from 1979 to 2000 and from 2001 to 2020 was 13% and 43%, respectively.

3.5. Calibration and validation processes

The model was simulated during the period 1979–2020. The year 1979 was used to warm up the model. The calibration period was 1980–1995, while two periods were used to validate the model; the first validation period was 1996–2010, and the second was 2011–2020. The observed streamflow data at the Thanh My and Nong Son stations were used for model calibration and validation. The reservoir's released streamflow was calibrated in four large reservoirs (A Vuong, Song Bung 4, Dak Mi 4, Song Tranh 2) from 2017 to 2020 by monthly time steps.

The SWAT-CUP tool (SWAT Calibration and Uncertainty Procedures) with SUFI-2 algorithms was used to evaluate the sensitivity of the parameters of the SWAT model (Abbaspour, 2013). In addition, five commonly used model efficiency criteria (Moriassi et al., 2015) were used to evaluate the model performance, including the correlation coefficient (R), Nash-Sutcliffe coefficient (NSE), per cent bias (PBIAS), root mean squared error (RMSE), and the ratio of the root mean square error to the standard deviation of measured data (RSR).

4. Results

4.1. Calibration and validation of SWAT model

The simulated and observed streamflow plots for the calibration and validation performances are presented in Figures 3a and 3b, respectively. The five efficiency criteria presented in Table 3 reveal the model quality, which agrees with the observed data. The R, NSE, RSR, RMSE, and PBIAS coefficients at the Thanh My and Nong Son stations in the calibration periods were 0.82, 0.66, 0.58, $119.61 \text{ m}^3/\text{s}$, 3.76, and

Impact of hydraulic infrastructures and contribution of the sub-basins

230 0.90, 0.81, 0.44, 214.28 m³/s, 2.28, respectively. The model's results are consistent with the observations in
231 the first and second validation periods. The differences between the observed and simulated results can be
232 explained by the omission of irrigation demands on agricultural activities.

233 The calibration of the monthly streamflow released from the four reservoirs is in excellent agreement
234 with the observed data (Fig. 3c, 3d, 3e, and 3f). The NSE values of the A Vuong, Song Bung 4, Dak Mi 4,
235 and Song Tranh 2 reservoirs were 0.82, 0.70, 0.65, and 0.81, respectively. Overall, the validation results
236 indicate that the present model is suitable for further examination of the variation in streamflow under the
237 effect of the reservoirs.

238 ***4.2. Assessment results of spatial and temporal natural streamflow without dams***

239 Natural flow simulation results from 1980 to 2020 (without-dam scenarios) show that the Thu Bon sub-
240 basins have more abundant surface water resources than the Vu Gia sub-basins (Fig. 4). As a result,
241 streamflows in the dry and rainy seasons at the Thu Bon River stations are more significant than those in
242 the Vu Gia River. The average annual streamflows at Thanh My, Ai Nghia (in Vu Gia), Nong Son, and Giao
243 Thuy (in Thu Bon) are 142 m³/s, 215.5 m³/s, and 285.7 m³/s, 395.3 m³/s, respectively (Fig. 4a). The
244 respective median streamflows are 78 m³/s, 124.2 m³/s, 163.1 m³/s, and 220.2 m³/s (Fig. 4b).

245 ***4.3. Effects of cascading reservoirs operation on daily streamflow***

246 Figure 5 shows a visual comparison of the simulated daily streamflow for without-dam and with-dam
247 scenarios from 2011 to 2020. The streamflow time series presented a strong daily variation in the no-dam
248 scenario, with low dry and high peak flows during the rainy season (Fig. 5a). In the dry season of the with-
249 dam scenario, the streamflow decreased at Thanh My and Ai Nghia stations, especially at Thanh My (Fig.
250 5b). The low level (red colour) of the streamflow is prominent throughout the entire period. In contrast, the
251 streamflow increased at the Nong Son and Giao Thuy stations. During the rainy season, streamflow
252 decreased at the four stations. The ratio of difference streamflow between with-dam and without-dam
253 scenarios at Thanh My, Nong son, Ai Nghia, Giao Thuy is 0.2–1.65, 0.53–3.39, and 0.2–2.69, 0.46–2.39,
254 respectively (Fig. 5c).

Impact of hydraulic infrastructures and contribution of the sub-basins

255 **4.4. Effects of cascading reservoirs operation on the water balance**

256 Reservoir operations inverted the seasonality of the naturalised streamflow regime. The strong seasonal
257 variation and streamflow increased during the dry season and decreased during the rainy season. In contrast
258 to Fairoz et al. (2018), we found that the streamflow in the with-dam scenario was slightly changed
259 compared to the without-dam scenario (Fig. 6b, 6d, and 7, Table 4). In December, the reservoirs were
260 released to reduce storage capacity, and the streamflow was more extensive than in the without-dam scenario
261 (Fig. 6b, 6d). Water diversion led to decreased streamflow (Fig. 6a, 6c, and 7, Table 4). As a result, Thu
262 Bon's water resources became more abundant, while Vu Gia's were reduced.

263 For the Thanh My station, located upstream of the Vu Gia, the average monthly streamflow decreased
264 by approximately 42.5 m³/s, from 151.6 m³/s to 109.1 m³/s. As a result of water diversion by the Dak Mi 4
265 plant, the dry season streamflow decreased by 25.5%. In the rainy season, the streamflow decreased by 79.6
266 m³/s, from 266.7 m³/s to 187.1 m³/s (Fig. 6a, Fig. 7, Table 4). On the other hand, as a result of receiving
267 water from Vu Gia, the dry, rainy, and annual streamflow increased at Nong Son by 57.8 m³/s, 31.9 m³/s,
268 49.2 m³/s, respectively (Fig. 6b, Fig. 7, Table 4).

269 The impacts of reservoir operation, water transfer of the Dak Mi 4 plant, and Quang Hue River are most
270 obvious downstream. During the early dry season, reservoirs in the Dak Mi, Bung, A Vuong, and Con sub-
271 basins augmented the flow discharges at Ai Nghia. However, the reservoir storage volume decreased at the
272 end of the dry season (June–August), while the Dak Mi 4 plant maintained the generation capacity. As a
273 result, the streamflow decreased compared to the without-dam scenario (Fig. 6c, Fig. 7). In the dry season,
274 the streamflow decreased by 1.1% at Ai Nghia and increased by 20.6% at Giao Thuy (Table 4); the
275 streamflow in the rainy season decreased by 75.5 m³/s, 21.6 m³/s, respectively.

276 **4.5. Assessment of reservoirs operation on streamflow downstream**

277 In this study, we considered the impact and distinguished the effects of four large reservoirs (A Vuong,
278 Song Bung 4, Dak Mi 4, and Song Tranh 2) on downstream streamflow when they were operating
279 independently. The impact level depends on the location, storage capacity, and distance to hydrological

Impact of hydraulic infrastructures and contribution of the sub-basins

280 stations. In contrast to Nauditt et al. (2017), we can conclude that the operation of the Dak Mi 4 plant
281 significantly affects the downstream basins (Table 5, Fig. 8a and 8b). We also show that the reservoir
282 operation at the Vu Gia River affects the downstream reaches of the VGTB basin. In general, reservoir
283 operations are the main cause of streamflow reduction during the rainy season and increase in the dry season.

284 The Dak Mi 4 reservoir reduced the seasonal and annual streamflow at the Vu Gia River and increased
285 the flows on the Thu Bon River. The streamflow annual, dry, and rainy seasons at Ai Nghia decreased by
286 16.2%, 14.5%, and 17.4%, respectively (Table 5). In contrast, the streamflow increased at Giao Thuy by
287 6.3%, 8.1%, and 5%, respectively. A negative value for the percentage changes in the monthly streamflow
288 compared with the no-dam scenario was observed at Ai Nghia, while a positive value was observed at Giao
289 Thuy (Fig. 8c). At Ai Nghia, Dak Mi 4 releases less in March to store water for the driest month (April).
290 Therefore, the streamflow decreased by 21.9% compared to the without-dam scenario.

291 The remaining reservoirs (i.e. Song Tranh 2, Song Bung 4, and A Vuong) had a negligible influence on
292 streamflow (Table 5). In the rainy season, the reservoirs helped reduce the flood risk in the downstream
293 floodplain due to the low release of water. Flood reduction efficiency is related to the active storage of
294 reservoirs. The Song Tranh 2 reservoir has the most extensive functional capacity for storage, and is the
295 most effective reservoir in terms of flood peak cut and disaster risk reduction. The streamflow during the
296 rainy season decreased by 5.9% compared to that in the without-dam scenario (Table 5). Therefore, the
297 Song Tranh 2 hydropower operation affects only the Thu Bon sub-basins.

298 ***4.6. Contribution of streamflow of sub-basins on VGTB basin***

299 The hydrological responses and contributions of each group of cascading dams differed according to
300 sub-basin locations and periods. The Dak Mi River sub-basin contributed the most significant streamflow
301 to the Vu Gia sub-basins from 1980 to 2010 (annual flow is 97.7 m³/s) (Table 6). The Tranh River sub-basin
302 contributes the most in the Thu Bon sub-basins, with a yearly flow of 166.1 m³/s. Therefore, hydropower
303 plants have been constructed in these sub-basins (Fig. 1a).

Impact of hydraulic infrastructures and contribution of the sub-basins

304 Sub-basins without reservoirs (Giang, Que Lam, and Khang Rivers) remained the same in both scenarios
305 (Table 6, Fig. 9). In basins with reservoirs (Con River, A Vuong River, Bung River, Khe Dien River, and
306 Tranh River), the streamflow increased in the dry season and decreased in the rainy season (Table 6, Fig.
307 9). The Dak Mi 4 plant transfers water from the Dak Mi River to the Truong River. Therefore, the dry, rainy,
308 and annual streamflows decreased considerably in the Dak Mi River sub-basin and increased in the Truong
309 River sub-basin (Table 6).

310 The Dak Mi River and Tranh River sub-basins contributed the largest streamflow for the Vu Gia and
311 Thu Bon sub-basins from 1980 to 2010 by 32.9% and 54.6%, respectively (Fig. 10a). However, in the period
312 2011–2020 with dams, the contribution rate of the Dak Mi River was only 22.9%, lower than that of the
313 Bung River (30.9%) (Fig. 10c). On the other hand, the Truong River Basin increased the contribution of the
314 Thu Bon sub-basins from 10.3% to 21.3%. The results show that the Dak Mi River and Truong River basins
315 were significantly altered in both scenarios, with the remaining sub-basins slightly increasing in the Vu Gia
316 sub-basins and decreasing in the Thu Bon sub-basins (Fig. 10b, 10c).

317 5. Discussion

318 5.1. Effects of Quang Hue River on downstream streamflow

319 Flow alteration in the VGTB basin is caused by reservoir operation and water transfer from the Quang
320 Hue River (Fig. 5, 6, 7, and 8, Tables 4 and 5). Surveys and measurements from 2001 show that about 43%
321 of Vu Gia's flow is diverted to the Thu Bon River by the Quang Hue River. We found that the water diverted
322 to the Thu Bon River is governed and reduced by the cascading hydropower dams. The operation of 11
323 reservoirs partially compensates for water in the Vu Gia sub-basins that the Dak Mi 4 plant has transferred
324 (Fig. 11, Table 7). The annual flow decreased from 141 m³/s to 121.3 m³/s in the without-dam scenario
325 compared with-dam scenario. Therefore, the reservoirs partially compensate for the water in the Vu Gia
326 sub-basins that the Dak Mi 4 plant has transferred.

Impact of hydraulic infrastructures and contribution of the sub-basins

327 ***5.2. Temporal variability in the relationships between rainfall and streamflow at sub-basins***

328 Among the essential components of the basin's water budget, precipitation and runoff are closely related
329 and interrelated through the water balance equation (Rose & Stern, 1965; Shawul et al., 2013). The duration
330 and intensity of runoff are fundamentally dependent on precipitation and basin-wide infrastructure (Ahn &
331 Merwade, 2014; Ribbe et al., 2017). Most hydropower plants return water to the original river, except Dak
332 Mi 4, which diverts water from the Vu Gia River to the Thu Bon River through the Truong River to increase
333 the generated electricity efficiency. Therefore, the correlation curve of cumulative rainfall and streamflow
334 tended to decrease in the Dak Mi River and increase in the Truong River between 2011 and 2020 (Fig. 12).
335 In the other eight sub-basins, where there is no dam, rainfall is highly correlated with streamflow. However,
336 there is a weak correlation in sub-basins with dams, indicating the obvious effect of dams on streamflow.

337 We found that the rainfall in the post-2010 period in the Dak Mi River and Truong River sub-basins
338 increased compared to that in the pre-2010 period by 5.8% and 3.6%, respectively (Table 8). However, the
339 average streamflow in the Dak Mi River decreased by 34%, from 97.7 m³/s to 64.5 m³/s. On the other hand,
340 in the Truong River, average streamflow increased from 31.5 m³/s to 76.6 m³/s (143.4%). Reducing the Vu
341 Gia streamflow leads to an increasing saltwater intrusion hazard/risk and strongly impairs local socio-
342 economic factors, especially agricultural production and drinking water supply.

343 ***5.3. Managing the risk of saltwater intrusion and water shortage downstream to enable sustainable*** 344 ***development of the VGTB River basin***

345 In situations where we could quantify the sub-basin contributions on the downstream reaches at different
346 stations, we correlated the contribution of each dam group in the different sub-basins. In addition, we found
347 that reservoirs with ample active storage (A Vuong, Song Bung 4, Dak Mi 4, Song Tranh 2) have contributed
348 to the reduction of the wet season effects, which could help the government mitigate floods. Finally, we
349 discuss the implications for agriculture, drinking water supply, and the mitigation of saltwater intrusion.

350 From 2011 to 2020, the Vuong sub-basin contributed the largest streamflow (30.9%) to the Vu Gia River
351 (Fig. 10c, Table 6). During the dry season, the streamflow and water level downstream mainly depend on

Impact of hydraulic infrastructures and contribution of the sub-basins

the operation of the hydropower plants in this sub-basin. The outflow from the A Vuong and Song Bung 4 hydropower plants flow into the Song Bung 5 and 6 reservoirs. Both reservoirs are regulated daily (can store flow in one day and only generate electricity during peak hours; in the evening and early morning) (Fig. 1a, Table 2). Therefore, although the flow from the electricity generation of Song Bung 5 and 6 is substantial, it is generated in a short time, leading to a small downstream flow the rest of the time. A low water level downstream affects pumping stations and plants for agriculture and drinking water supply. Moreover, the outlet of the VGTB basin has a semi-diurnal tidal regime, up and down twice a day, with a tidal amplitude is about 0.6m. Therefore, the downstream flow is frequently affected by saline water intrusion during the dry season.

These problems require appropriate solutions, not only in the short term but also in the long term. Hydrology simulation and consultation with local experts can offer a range of measures to cope with water shortages for agriculture and drinking water supply and saltwater intrusion. The most important measures are redistributing upstream streamflow and ensuring minimal river streamflow from cascading hydropower dams in sub-basins. Specifically, coordination between reservoirs to maintain continuous downstream flow, combined with retained, upgraded water use works and reduced water transfer in the Quang Hue River, are suitable measures.

6. Conclusion and Recommendation

In this study, we used the semi-distributed hydrological model SWAT to clarify the impact of hydraulic infrastructures on the streamflow of the VGTB River basin from 1979 to 2020. The modelling results show that the Dak Mi 4 reservoir has the most significant influence on the streamflow of the Vu Gia and Thu Bon sub-basins. The overall impact of all reservoirs and water diversions on downstream flow decreased by 1.1% in the Vu Gia sub-basins and increased by 20.6% in the Thu Bon sub-basins in the dry season. On the other hand, the streamflow in the rainy season decreased in the two basins by 23% and 2.6%, respectively, compared to the scenario without-dam.

Impact of hydraulic infrastructures and contribution of the sub-basins

1
2
3 376 Owing to water transfers from the Dak Mi 4 plant, the dry season, rainy season, and annual streamflows
4
5 377 significantly decreased in the Dak Mi River sub-basin and increased in the Truong River sub-basin. We
6
7 378 found that the water diverted to the Thu Bon River is governed and decreased by the cascading hydropower
8
9 379 dams. The annual streamflow of Quang Hue River decreased from 141 m³/s to 121.3 m³/s in the without-
10
11 380 dam scenario compared with the with-dam scenario. The operation of the 11 reservoirs partially
12
13 381 compensates for water in the Vu Gia sub-basins transferred by the Dak Mi 4 plant.

14
15 382 The Dak Mi River and Tranh River sub-basins contributed the largest streamflow for the Vu Gia and
16
17 383 Thu Bon sub-basins in the 1980–2010 period by 32.9% and 54.6%, respectively. However, in the with-dam
18
19 384 period (2011–2020), the contribution rate of the Dak Mi River was only 22.9%. On the other hand, the
20
21 385 Truong River Basin increased the contribution of the Thu Bon sub-basins from 10.3% to 21.3%.

22
23
24 386 The bathymetry change caused the water transfer rate to increase. It was driven by a decrease in
25
26 387 downstream water levels of the Vu Gia sub-basins, affecting water supply and increasing the risk of
27
28 388 saltwater intrusion. Saltwater intrusion-induced water shortages during drought periods are the main
29
30 389 constraints hindering domestic water supply and agricultural production. Under the impact of climate
31
32 390 change and sea-level rise, it is predicted that saltwater intrusion in the downstream VGTB basin will worsen
33
34 391 in both frequency and magnitude during the dry season. Therefore, there should be a mechanism for
35
36 392 cooperation between institutions participating in water resource management. It is necessary to have
37
38 393 appropriate operating procedures between upstream reservoirs, water supply plants, and irrigation
39
40 394 companies, combined with maintained and upgraded water-use works.

395 **Acknowledgments**

41
42
43 396 This work was funded by APN ‘Asia-Pacific Network for Global Change Research’ under project reference
44
45 397 number CRRP2020-09MYKantoush (Funder ID: <https://doi.org/10.13039/100005536>).

398 **Conflict of Interest Statement**

399 The authors declare no conflicts of interest.

400

Impact of hydraulic infrastructures and contribution of the sub-basins

401 **Data availability statement**

402 The data that support the findings of this study are available upon reasonable request from the corresponding
403 author. The data are not publicly available due to privacy or ethical restrictions.

404 **References**

- 405 Abbaspour, K. C. (2013). Swat-cup 2012. *SWAT Calibration and Uncertainty Program—a User Manual*.
- 406 Ahn, K.-H., & Merwade, V. (2014). Quantifying the relative impact of climate and human activities on
407 streamflow. *Journal of Hydrology*, 515, 257–266.
- 408 Arnold, J. G., Srinivasan, R., Muttiah, R. S., & Williams, J. R. (1998). Large area hydrologic modeling and
409 assessment part I: model development 1. *JAWRA Journal of the American Water Resources
410 Association*, 34(1), 73–89.
- 411 Carvalho-Santos, C., Monteiro, A. T., Azevedo, J. C., Honrado, J. P., & Nunes, J. P. (2017). Climate change
412 impacts on water resources and reservoir management: uncertainty and adaptation for a mountain
413 catchment in northeast Portugal. *Water Resources Management*, 31(11), 3355–3370.
- 414 Chhuon, K., Herrera, E., & Nadaoka, K. (2016). Application of integrated hydrologic and river basin
415 management modeling for the optimal development of a multi-purpose reservoir project. *Water
416 Resources Management*, 30(9), 3143–3157.
- 417 Di Baldassarre, G., Wanders, N., AghaKouchak, A., Kuil, L., Rangelcroft, S., Veldkamp, T. I. E., Garcia,
418 M., van Oel, P. R., Breinl, K., & Van Loon, A. F. (2018). Water shortages worsened by reservoir
419 effects. *Nature Sustainability*, 1(11), 617–622.
- 420 Firoz, A. B. M., Nauditt, A., Fink, M., & Ribbe, L. (2018). Quantifying human impacts on hydrological
421 drought using a combined modelling approach in a tropical river basin in central Vietnam. *Hydrology
422 and Earth System Sciences*, 22(1), 547–565.
- 423 Government of Vietnam. (2019). *Decision 1867/QĐ-TTg: Procedures for operating reservoirs system in
424 Vu Gia Thu Bon river basin (in Vietnamese)*.
- 425 Hu, Z., Wang, L., Wang, Z., Hong, Y., & Zheng, H. (2015). Quantitative assessment of climate and human
426 impacts on surface water resources in a typical semi - arid watershed in the middle reaches of the

Impact of hydraulic infrastructures and contribution of the sub-basins

- 1
2
3 427 Yellow River from 1985 to 2006. *International Journal of Climatology*, 35(1), 97–113.
- 4
5 428 ICEM. (2008). *Strategic Environmental Assessment of the Quang Nam Province Hydropower Plan for the*
6
7 429 *Vu Gia-Thu Bon River Basin, Prepared for the ADB, MONRE, MOITT & EVN, Hanoi, Vietnam, 205*
8
9 430 *pp.*
- 10
11 431 Johnson, S. A., Stedinger, J. R., & Staschus, K. (1991). Heuristic operating policies for reservoir system
12
13 432 simulation. *Water Resources Research*, 27(5), 673–685.
- 14
15 433 Keitzer, S. C., Ludsin, S. A., Sowa, S. P., Annis, G., Arnold, J. G., Daggupati, P., Froehlich, A. M., Herbert,
16
17 434 M. E., Johnson, M.-V. V., & Sasson, A. M. (2016). Thinking outside of the lake: Can controls on
18
19 435 nutrient inputs into Lake Erie benefit stream conservation in its watershed? *Journal of Great Lakes*
20
21 436 *Research*, 42(6), 1322–1331.
- 22
23 437 Loi, N. K., Liem, N. D., Tu, L. H., Hong, N. T., Truong, C. D., Tram, V. N. Q., Nhat, T. T., Anh, T. N., &
24
25 438 Jeong, J. (2019). Automated procedure of real-time flood forecasting in Vu Gia–Thu Bon river basin,
26
27 439 Vietnam by integrating SWAT and HEC-RAS models. *Journal of Water and Climate Change*, 10(3),
28
29 440 535–545.
- 30
31 441 MCRHMC. (n.d.). *Mid-Central Regional Hydrometeorological Centre, Vietnam.*
- 32
33 442 Mittal, N., Bhave, A. G., Mishra, A., & Singh, R. (2016). Impact of human intervention and climate change
34
35 443 on natural flow regime. *Water Resources Management*, 30(2), 685–699.
- 36
37 444 MOIT. (2015). *Decision for Hydropower Plant Operation: Technical Document, Ministry of Investment*
38
39 445 *and Trade, Socialist Republic of Vietnam, 2015a.*
- 40
41 446 Nauditt, A., Firoz, A. B. M., Trinh, V. Q., Fink, M., Stolpe, H., & Ribbe, L. (2017). Hydrological drought
42
43 447 risk assessment in an anthropogenically impacted tropical catchment, Central Vietnam. In *Land use*
44
45 448 *and climate change interactions in central Vietnam* (pp. 223–239). Springer.
- 46
47 449 NDPAC. (n.d.). *Natural Disaster Prevention and Control of Quang Nam Province*. <http://pctt.quangnam.vn/>
- 48
49 450 Ngo, L. A., Masih, I., Jiang, Y., & Douven, W. (2018). Impact of reservoir operation and climate change
50
51 451 on the hydrological regime of the Sesan and Srepok Rivers in the Lower Mekong Basin. *Climatic*
52
53 452 *Change*, 149(1), 107–119.

Impact of hydraulic infrastructures and contribution of the sub-basins

- 1
2
3 453 Nguyen, H. T., Duong, T. Q., Nguyen, L. D., Vo, T. Q. N., Tran, N. T., Dang, P. D. N., Nguyen, L. D.,
4
5 454 Dang, C. K., & Nguyen, L. K. (2020). Development of a spatial decision support system for real-time
6
7 455 flood early warning in the Vu Gia-Thu Bon River Basin, Quang Nam Province, Vietnam. *Sensors*,
8
9 456 20(6), 1667.
- 11 457 Nguyen, L. H., & Fukushi, K. (2019). Addressing Climate change in the water sector: The study of Run-of-
12
13 458 river Hydropower potential in Vu Gia-Thu Bon river basin of Vietnam. *IOP Conference Series: Earth*
14
15 459 *and Environmental Science*, 266(1), 12014.
- 18 460 Nguyen, T. H. (2020). *Optimal operation of multi-reservoir system for flood control. Application to the Vu*
19
20 461 *Gia Thu Bon catchment, Vietnam*.
- 22 462 Oki, T., & Kanae, S. (2006). Global hydrological cycles and world water resources. *Science*, 313(5790),
23
24 463 1068–1072.
- 26 464 RETA. (2011). *Investment, Managing water in Asia's river basins: Charting progress and facilitating - The*
27
28 465 *Vu Gia-Thu Bon sub-basins*.
- 31 466 Ribbe, L., Trinh, V. Q., Firoz, A. B. M., Nguyen, A. T., Nguyen, U., & Nauditt, A. (2017). Integrated River
32
33 467 Basin Management in the Vu Gia Thu Bon sub-basins. In *Land Use and Climate Change Interactions*
34
35 468 *in Central Vietnam* (pp. 153–170). Springer.
- 37 469 Rose, C. W., & Stern, W. R. (1965). The drainage component of the water balance equation. *Soil Research*,
38
39 470 3(2), 95–100.
- 41 471 Shawul, A. A., Alamirew, T., & Dinka, M. O. (2013). Calibration and validation of SWAT model and
42
43 472 estimation of water balance components of Shaya mountainous watershed, Southeastern Ethiopia.
44
45 473 *Hydrology and Earth System Sciences Discussions*, 10(11), 13955–13978.
- 47 474 Shrestha, B., Maskey, S., Babel, M. S., van Griensven, A., & Uhlenbrook, S. (2018). Sediment related
48
49 475 impacts of climate change and reservoir development in the Lower Mekong River Basin: a case study
50
51 476 of the Nam Ou Basin, Lao PDR. *Climatic Change*, 149(1), 13–27.
- 53 477 Sorooshian, S., Hsu, K., Coppola, E., Tomassetti, B., Verdecchia, M., & Visconti, G. (2008). *Hydrological*
54
55 478 *modelling and the water cycle: coupling the atmospheric and hydrological models* (Vol. 63). Springer

Impact of hydraulic infrastructures and contribution of the sub-basins

479 Science & Business Media.

480 Souvignet, M., Laux, P., Freer, J., Cloke, H., Thinh, D. Q., Thuc, T., Cullmann, J., Nauditt, A., Flügel, W.,
481 & Kunstmann, H. (2014). Recent climatic trends and linkages to river discharge in Central Vietnam.
482 *Hydrological Processes*, 28(4), 1587–1601.

483 Vale, M., & Holman, I. P. (2009). Understanding the hydrological functioning of a shallow lake system
484 within a coastal karstic aquifer in Wales, UK. *Journal of Hydrology*, 376(1–2), 285–294.

485 Van Binh, D., Kantoush, S. A., Saber, M., Mai, N. P., Maskey, S., Phong, D. T., & Sumi, T. (2020). Long-
486 term alterations of flow regimes of the Mekong River and adaptation strategies for the Vietnamese
487 Mekong Delta. *Journal of Hydrology: Regional Studies*, 32, 100742.

488 Van Binh, D., Kantoush, S., & Sumi, T. (2020). Changes to long-term discharge and sediment loads in the
489 Vietnamese Mekong Delta caused by upstream dams. *Geomorphology*, 353, 107011.

490 Viet, T. Q. (2014). Estimating the impact of climate change induced saltwater intrusion on agriculture in
491 estuaries-the case of Vu Gia Thu Bon. *Ruhr-Universität Bochum, Vietnam*.

492 Vu, M. T., Vo, N. D., Gourbesville, P., Raghavan, S. V., & Liang, S.-Y. (2017). Hydro-meteorological
493 drought assessment under climate change impact over the Vu Gia–Thu Bon river basin, Vietnam.
494 *Hydrological Sciences Journal*, 62(10), 1654–1668.

495 Wang, D., & Hejazi, M. (2011). Quantifying the relative contribution of the climate and direct human
496 impacts on mean annual streamflow in the contiguous United States. *Water Resources Research*,
497 47(10).

498 Wang, G., & Xia, J. (2010). Improvement of SWAT2000 modelling to assess the impact of dams and sluices
499 on streamflow in the Huai River basin of China. *Hydrological Processes: An International Journal*,
500 24(11), 1455–1471.

501 Wang, H., Chen, L., & Yu, X. (2016). Distinguishing human and climate influences on streamflow changes
502 in Luan River basin in China. *Catena*, 136, 182–188.

503 Zarfl, C., Lumsdon, A. E., Berlekamp, J., Tydecks, L., & Tockner, K. (2015). A global boom in hydropower
504 dam construction. *Aquatic Sciences*, 77(1), 161–170.

Impact of hydraulic infrastructures and contribution of the sub-basins

- 1
2
3 505 Zhang, Y., Zhai, X., & Zhao, T. (2018). Annual shifts of flow regime alteration: new insights from the
4
5 506 Chaishitan Reservoir in China. *Scientific Reports*, 8(1), 1–11.
6
7 507 Zhou, T., Nijssen, B., Gao, H., & Lettenmaier, D. P. (2016). The contribution of reservoirs to global land
8
9 508 surface water storage variations. *Journal of Hydrometeorology*, 17(1), 309–325.
10
11 509
12
13
14
15
16
17
18
19
20
21
22
23
24
25
26
27
28
29
30
31
32
33
34
35
36
37
38
39
40
41
42
43
44
45
46
47
48
49
50
51
52
53
54
55
56
57
58
59
60

For Peer Review

Table 1. Characteristics of sub-basins on Vu Gia and Thu Bon rivers

| Basin | Sub-basin | Catchment area (Km ²) | Percentage area, compared to Ai Nghia station (%) | Percentage area, compared to Giao Thuy station (%) | Reservoir |
|---------|----------------|-----------------------------------|---|--|-----------|
| Vu Gia | Con River | 634.5 | 11.94 | | 2 |
| | A Vuong River | 769.4 | 14.48 | | 3 |
| | Bung River | 1462 | 27.52 | | 4 |
| | Giang River | 490.6 | 9.24 | | - |
| | Dak Mi River | 1394 | 26.24 | | 3 |
| Thu Bon | Khe Dien River | 135.8 | | 3.86 | 1 |
| | Que Lam River | 131.9 | | 3.75 | - |
| | Truong River | 430.9 | | 12.26 | 2 |
| | Tranh River | 1649 | | 46.90 | 3 |
| | Khang River | 584.8 | | 16.63 | - |

Table 2. Profile of 18 hydropower dams in the VGTB River basin (Government of Vietnam, 2019; ICEM, 2008; MOIT, 2015).

| Name | Catchment area | Dam high | Dead water level (DWL) | Normal water level (NWL) | Flood design water level (FWL) | Total storage | Active storage | Dead storage | Turbine discharge | Capacity | First year of operation |
|--------------|-----------------|----------|------------------------|--------------------------|--------------------------------|--------------------------------|--------------------------------|--------------------------------|-------------------|----------|-------------------------|
| Unit | km ² | m | m | m | m | 10 ⁶ m ³ | 10 ⁶ m ³ | 10 ⁶ m ³ | m ³ /s | MW | year |
| A Vuong | 682 | 80 | 340 | 380 | 382.2 | 343.55 | 266.48 | 77.07 | 78.4 | 210 | 2008 |
| A Vuong 3 | 258.4 | 22.9 | 551.6 | 552.5 | 559.45 | 2.94 | 0.44 | 2.5 | 22.7 | 1.04 | 2016 |
| Song Tranh 2 | 1100 | 96 | 140 | 175 | 178.51 | 729.2 | 521.1 | 208.1 | 245 | 190 | 2011 |
| Song Tranh 3 | 1450 | 36.5 | 70.5 | 71.5 | 75.9 | 34.1 | 3.1 | 31 | 301.6 | 62 | 2013 |
| Song Tranh 4 | 1610 | 25 | 45.5 | 46.5 | - | 24.81 | 3.32 | 21.49 | 298 | 48 | 2020 |
| Dak Mi 2 | 445 | 30 | 624 | 630 | 635.19 | 1.611 | 0.692 | 0.919 | 44.36 | 98 | 2019 |
| Dak Mi 3 | 612 | 30 | 353 | 359 | 363.96 | 5 | 2.304 | 2.696 | 76 | 63 | 2017 |
| Dak Mi 4 | 1125 | 90 | 240 | 258 | 260.33 | 312.38 | 158.26 | 154.12 | 128 | 148 | 2011 |
| Dak Mi 4B | 29 | 23.5 | 105 | 105.3 | 107.28 | 0.688 | 0.066 | 0.622 | 130 | 42 | 2012 |
| Dak Mi 4C | 82.6 | 11.5 | 66.2 | 67.2 | 68.86 | 2.67 | 0.52 | 2.15 | 140 | 18 | 2012 |
| Song Bung 4 | 1448 | 114 | 205 | 222.5 | 228.11 | 510.8 | 233.99 | 276.81 | 166 | 156 | 2015 |
| Song Bung 4A | 2276 | 46 | 95.4 | 97.4 | 99.95 | 10.6 | 1.58 | 9.02 | 166.4 | 49 | 2012 |
| Song Bung 5 | 2369 | 41.5 | 58.5 | 60 | 64 | 20.27 | 2.45 | 17.82 | 239.24 | 57 | 2013 |
| Song Bung 6 | 2386 | 39.2 | 31.8 | 31.8 | 45.89 | 3.29 | 0 | 3.29 | 239.8 | 29 | 2012 |
| Za Hung | 537 | 25 | 445 | 450 | 457.27 | 1.12 | 0.74 | 0.38 | 53.4 | 30 | 2009 |
| Khe Dien | 72 | 41 | 187.4 | 206.94 | 211.78 | 50.98 | 50.35 | 0.63 | 11.3 | 9 | 2007 |
| Song Con 2 | 81 | 48 | 319 | 340 | 345.68 | 29.19 | 25.41 | 3.78 | 9.7 | 3 | 2009 |
| An Diem 2 | 169.8 | 24.5 | 344 | 348.5 | 353.34 | 0.28 | 0.19 | 0.09 | 9 | 15.6 | 2010 |

Table 3. Statistical indices in the calibration and validation of the streamflow at Thanh My and Nong Son.

| Statistical indices | Thanh My station | | | Nong Son station | | |
|--------------------------|------------------------|-----------------------------|------------------------------|------------------------|-----------------------------|------------------------------|
| | Calibrated (1980–1995) | First Validated (1996–2010) | Second validated (2011–2020) | Calibrated (1980–1995) | First Validated (1996–2010) | Second validated (2011–2020) |
| R | 0.82 | 0.88 | 0.83 | 0.90 | 0.90 | 0.91 |
| NSE | 0.66 | 0.72 | 0.67 | 0.81 | 0.81 | 0.80 |
| RSR | 0.58 | 0.53 | 0.58 | 0.44 | 0.44 | 0.45 |
| RMSE (m ³ /s) | 119.61 | 142.12 | 105.30 | 214.28 | 305.29 | 246.79 |
| PBIAS | 3.76 | -12.38 | -32.89 | 2.28 | 1.83 | -6.29 |

Table 4. Changes of streamflow at four stations in the period (2011–2020), compared with the without-dam scenario.

| Changes | | Vu Gia sub-basins | | Thu Bon sub-basins | |
|-------------------------------------|---------------|-------------------|----------|--------------------|-----------|
| | | Thanh My | Ai Nghia | Nong Son | Giao Thuy |
| Changes in flow (m ³ /s) | Dry seasons | -24.0 | -1.2 | 57.8 | 54.9 |
| | Rainy seasons | -79.6 | -75.5 | 31.9 | -21.6 |
| | Annual | -42.5 | -26.0 | 49.2 | 29.8 |
| Changes in flow (%) | Dry seasons | -25.5 | -1.1 | 36.4 | 20.6 |
| | Rainy seasons | -29.9 | -23 | 5.8 | -2.6 |
| | Annual | -28.1 | -13.9 | 16.9 | 6.5 |

Table 5. Impact of each reservoir on seasonal and annual streamflow at Ai Nghia and Giao Thuy stations.

| Reservoir | Ai Nghia | | | Giao Thuy | | |
|--------------|----------------|------------------|--------------|----------------|------------------|------------|
| | Dry season (%) | Rainy season (%) | Annual (%) | Dry season (%) | Rainy season (%) | Annual (%) |
| A Vuong | 1 | -1.4 | -0.4 | 0.3 | -0.4 | -0.1 |
| Song Bung 4 | 2 | -4.2 | -1.5 | 0.6 | -1.4 | -0.6 |
| Dak Mi 4 | -14.5 | -17.4 | -16.2 | 8.1 | 5 | 6.3 |
| Song Tranh 2 | - | - | - | 8.1 | -5.9 | -0.6 |

Table 6. Seasonal and annual flow characteristics of main sub-basins on Vu Gia and Thu Bon rivers.

| Sub-basins | Sub-basin | Period (1980-2010) | | | Period (2011-2020) (Without-dam) | | | Period (2011-2020) (With-dam) | | |
|------------|------------------|--|--|-------------------------------|--|--|-------------------------------|--|--|-------------------------------|
| | | Dry season (January - August) (m ³ /s) | Rainy season (September - December) (m ³ /s) | Annual (m ³ /s) | Dry season (January - August) (m ³ /s) | Rainy season (September - December) (m ³ /s) | Annual (m ³ /s) | Dry season (January - August) (m ³ /s) | Rainy season (September - December) (m ³ /s) | Annual (m ³ /s) |
| Vu Gia | Con River | 12.5 | 55.4 | 26.8 | 14.9 | 64.1 | 31.3 | 18.1 | 61.8 | 32.7 |
| | A Vuong River | 15.1 | 74.9 | 35.0 | 19.7 | 76.7 | 38.7 | 22.3 | 70.0 | 38.2 |
| | Bung River | 36.1 | 166.6 | 79.6 | 49.4 | 163.8 | 87.5 | 53.7 | 154.4 | 87.3 |
| | Giang River | 15.7 | 69.1 | 33.5 | 21.9 | 66.0 | 36.6 | 21.9 | 66.0 | 36.6 |
| | Dak Mi River | 44.8 | 203.5 | 97.7 | 63.8 | 193.6 | 107.1 | 40.2 | 113.0 | 64.5 |
| | Ai Nghia | 121.6 | 431.0 | 224.7 | 116.1 | 328.5 | 186.9 | 114.9 | 253.0 | 160.9 |
| Thu Bon | Khe Dien River | 3.8 | 16.9 | 8.1 | 4.0 | 16.4 | 8.1 | 4.5 | 15.7 | 8.2 |
| | Que Lam River | 4.4 | 20.1 | 9.7 | 4.6 | 18.8 | 9.4 | 4.6 | 18.8 | 9.4 |
| | Truong River | 13.1 | 68.2 | 31.5 | 16.1 | 62.7 | 31.7 | 49.9 | 130.1 | 76.6 |
| | Tranh River | 80.9 | 336.6 | 166.1 | 89.8 | 335.2 | 171.6 | 114.4 | 298.6 | 175.8 |
| | Khang River | 23.6 | 102.9 | 50.0 | 27.5 | 104.2 | 53.1 | 27.5 | 104.2 | 53.1 |
| | Giao Thuy | 198.4 | 734.2 | 377.0 | 265.9 | 825.0 | 452.2 | 320.7 | 803.4 | 481.6 |

Table 7. Dry season, rainy season, and annual average streamflow in without-dam and with-dam scenarios.

| Scenarios | | AN1 (m ³ /s) | AN2 (m ³ /s) | GT1 (m ³ /s) | GT2 (m ³ /s) | QH | |
|-----------------|--------------|----------------------------|----------------------------|----------------------------|----------------------------|-----------------------------------|---------------------------------------|
| | | | | | | Streamflow (m ³ /s) | Percentage of Thu Bon River (%) |
| Without dams | Dry season | 203.3 | 115.9 | 177.8 | 265.2 | 87.4 | 33 |
| | Rainy season | 576.8 | 328.8 | 577.6 | 825.6 | 248.0 | 30 |
| | Annual | 328.0 | 187.0 | 311.3 | 452.3 | 141.0 | 31.2 |
| With dams | Dry season | 200.9 | 114.5 | 233.5 | 319.9 | 86.4 | 27 |
| | Rainy season | 444.3 | 253.2 | 613.4 | 804.4 | 191.0 | 23.8 |
| | Annual | 282.1 | 160.8 | 360.4 | 481.7 | 121.3 | 25.2 |

Table 8. Changes in rainfall and average streamflow on Dak Mi River, Truong River.

| River | Period | Rainfall (mm) | ΔP | Flow (m ³ /s) | ΔQ |
|--------|-----------|---------------|------------|--------------------------|----------------|
| Dak Mi | Pre-2010 | 3347 | | 97.7 | |
| | Post-2010 | 3540 | 193 (5.8%) | 64.5 | -33.23 (-34%) |
| Truong | Pre-2010 | 3493 | | 31.5 | |
| | Post-2010 | 3620 | 127 (3.6%) | 76.6 | 45.15 (143.4%) |

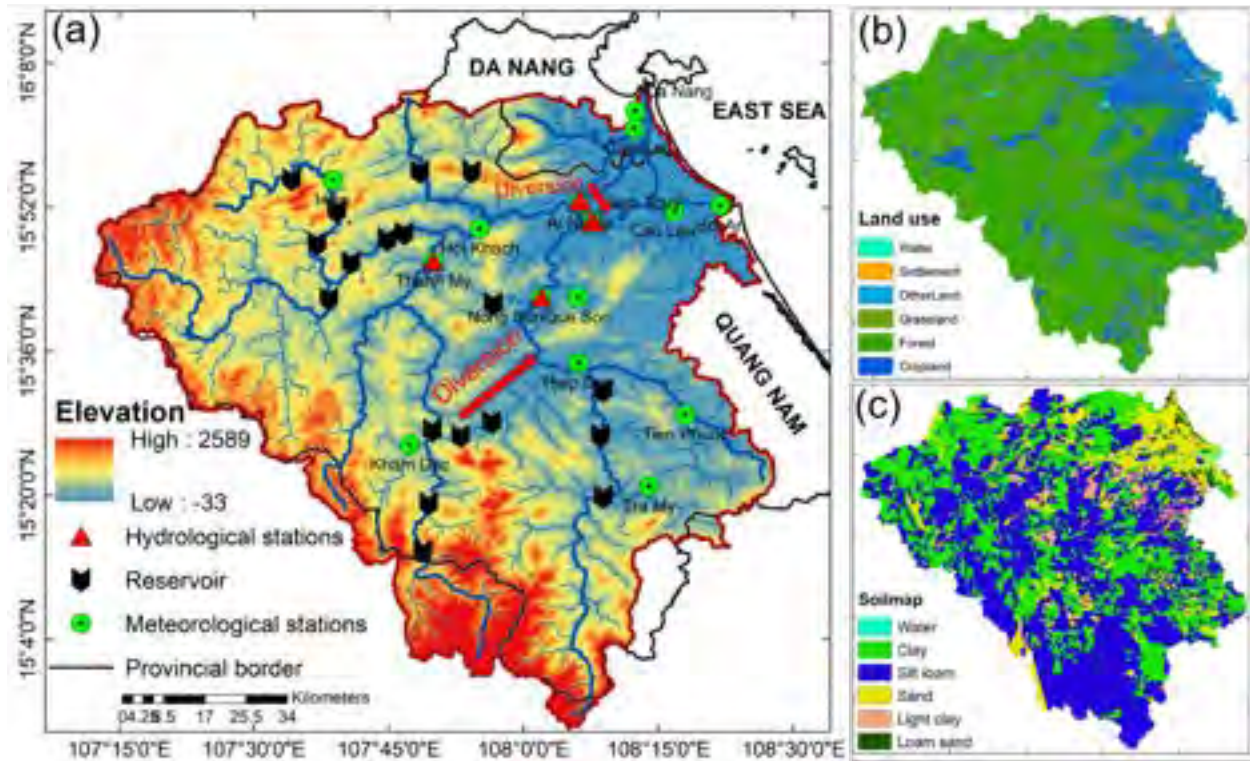


Figure 1. (a) Spatial coverage of the VGTB River basin. Locations of meteorological and hydrological stations and dams. (b) Land use map and (c) Soil map collected from the Lucci project.

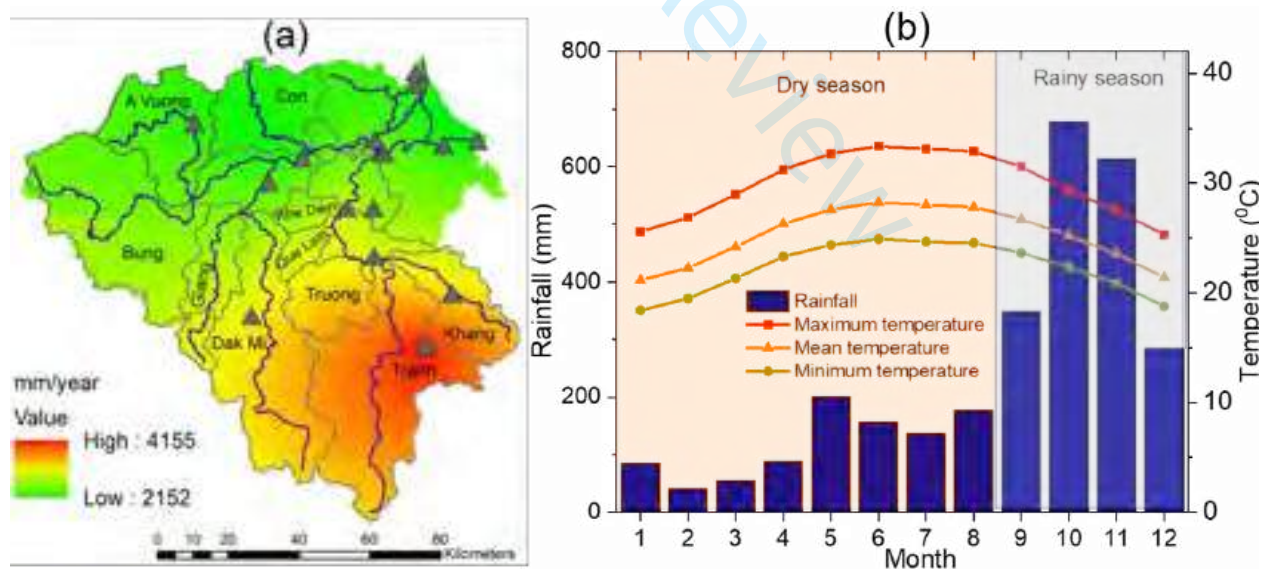


Figure 2. (a) Sub-basins and spatial variations of the rainfall from 1979 to 2020 in the VGTB basin. Data interpolated from 15 rain gauges according to the Kriging method on ArcGIS 10.4. (b) Average monthly rainfall, minimum temperature, average temperature, and maximum temperature of the VGTB basin.

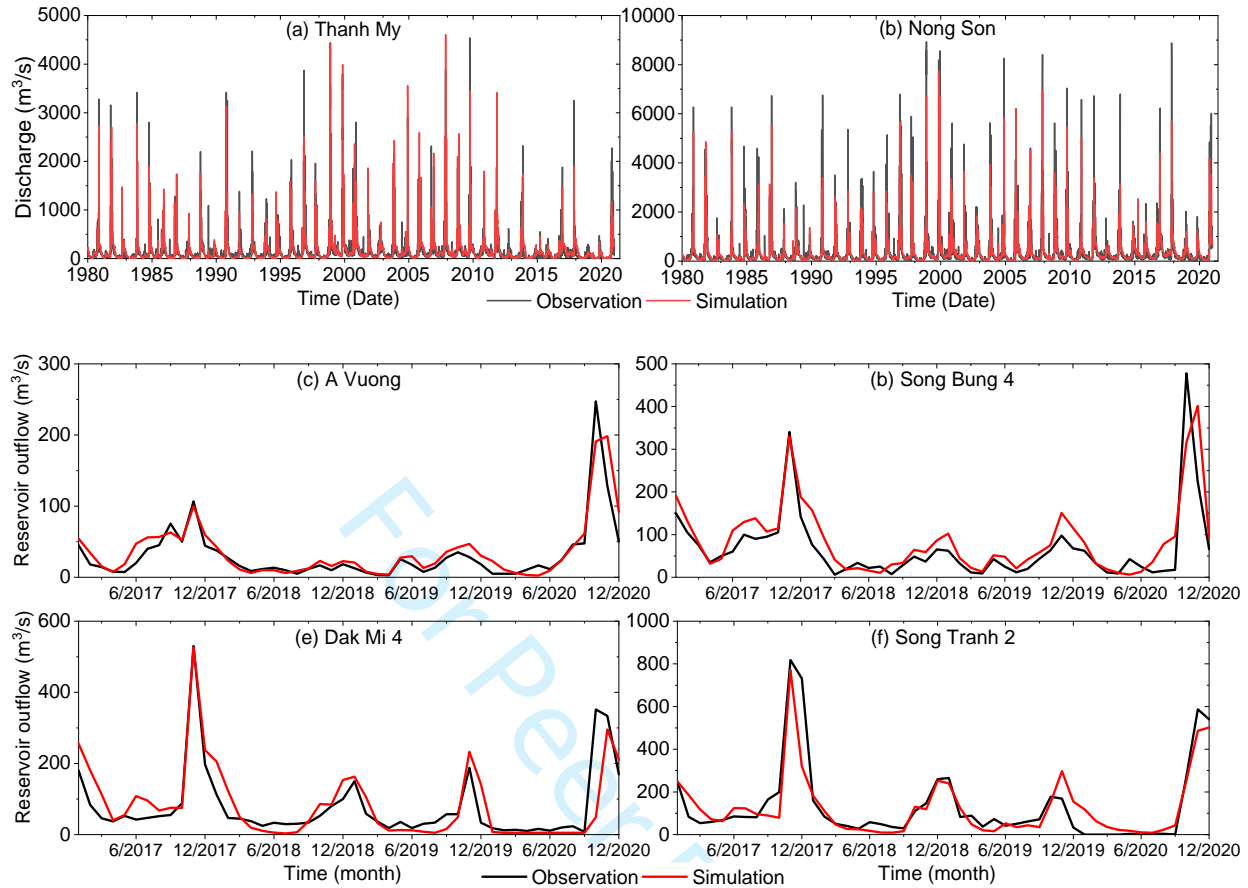


Figure 3. Calibrated and validated hydrographs of the streamflow at (a) the Thanh My station and (b) the Nong Son station; calibrated (1980–1995), first validated (1996–2010), second validated (2011–2020). Outflow calibration of reservoirs from 2017 to 2020 at (c) A Vuong, (d) Song Bung 4, (e) Dak Mi 4, (f) Song Tranh 2.

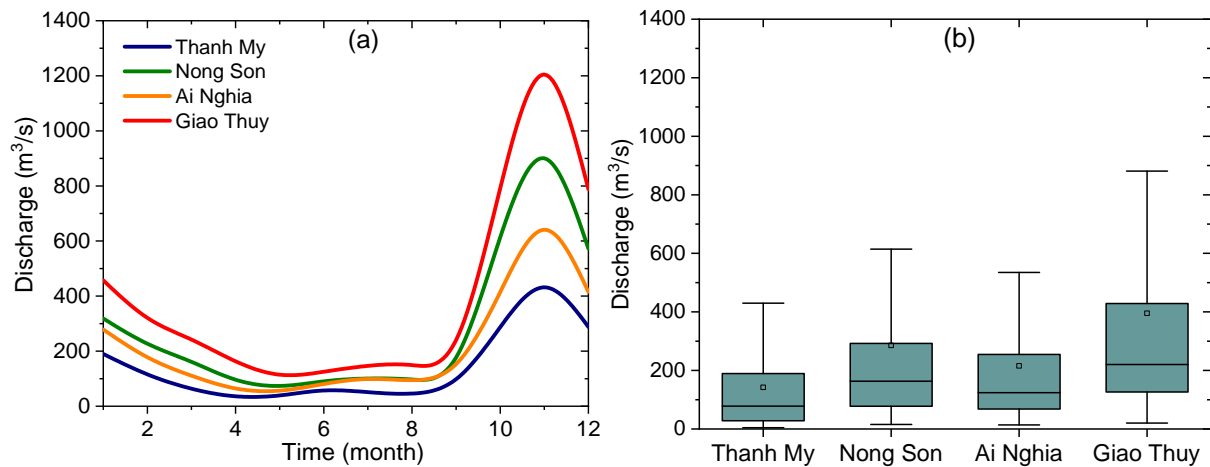


Figure 4. (a) Mean monthly streamflow at the four stations simulated with SWAT model in the period 1980–2020. (b) Box plots showing the 25th, 50th (median), and 75th percentiles of the daily streamflow time series. Thanh My and Ai Nghia are in the Vu Gia River, and Nong Son and Giao Thuy are in the Thu Bon River. The whiskers are defined as the first quartile minus $1.5 \times$ inter-quartile range (IQR), and the third quartile plus $1.5 \times$ IQR.

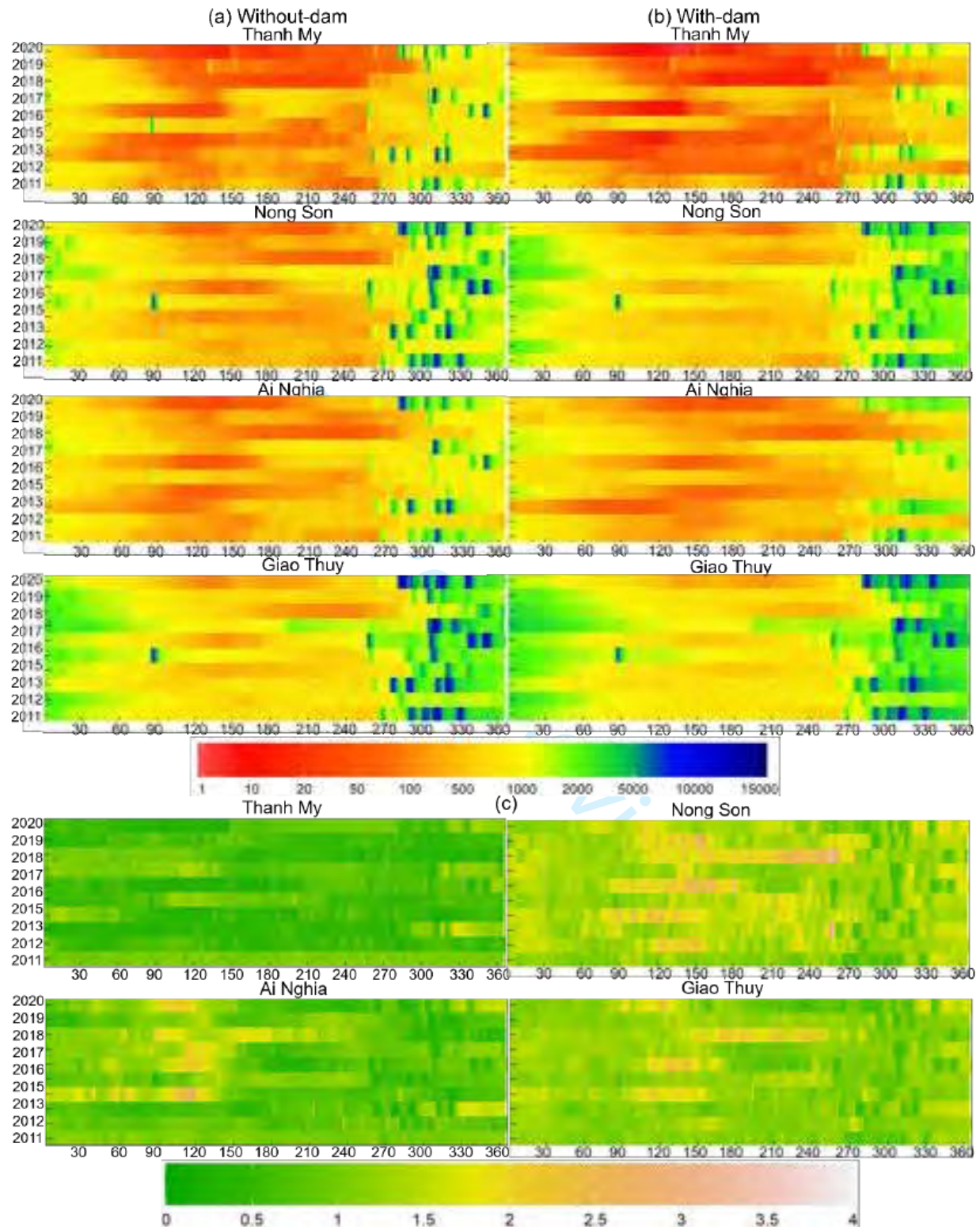


Figure 5. Daily streamflow at four stations. (a) Without-dam scenario, (b) with-dam scenario, (c) the ratio of difference in streamflow between with-dam and without-dam scenarios. The x-axis shows the Julian date, and the y-axis shows the year.

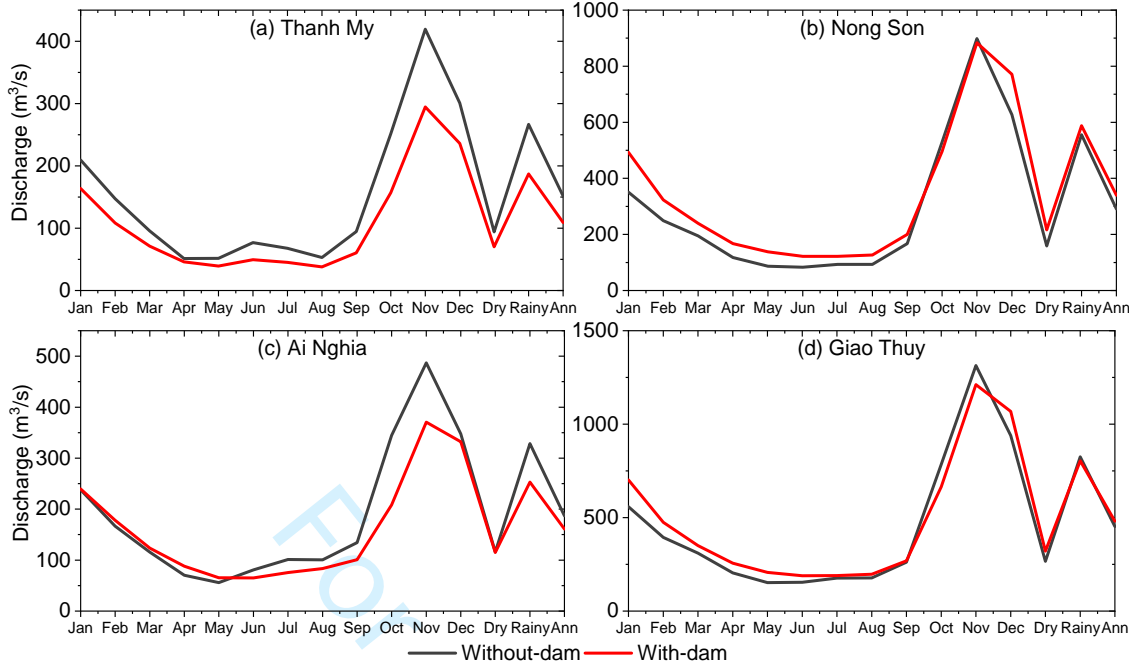
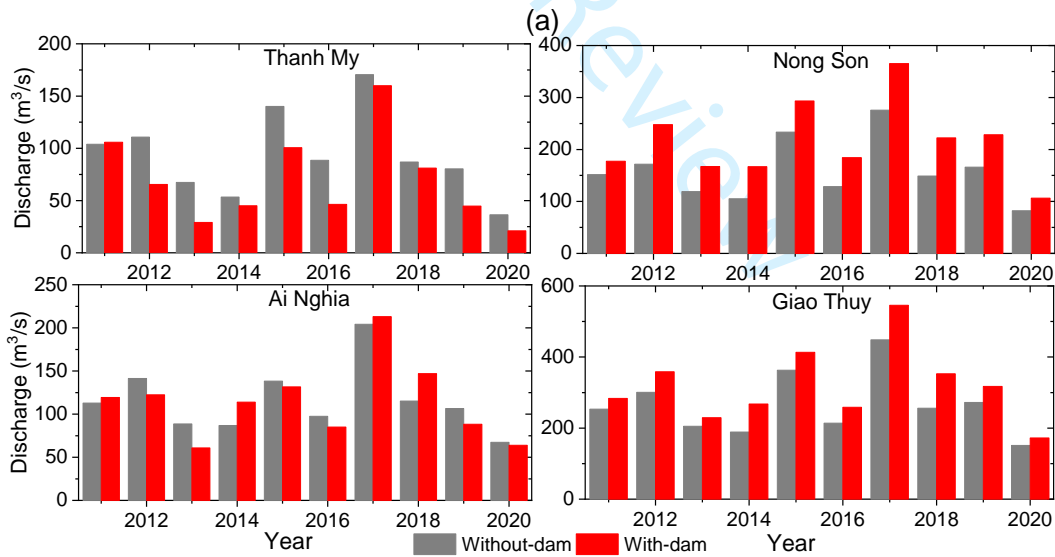


Figure 6. Average monthly streamflow at four stations in the 2011–2020 period, (a) Thanh My, (b) Nong Son, (c) Ai Nghia, and (d) Giao Thuy stations. The black line is the without-dam scenario, and the red line is the with-dam scenario.



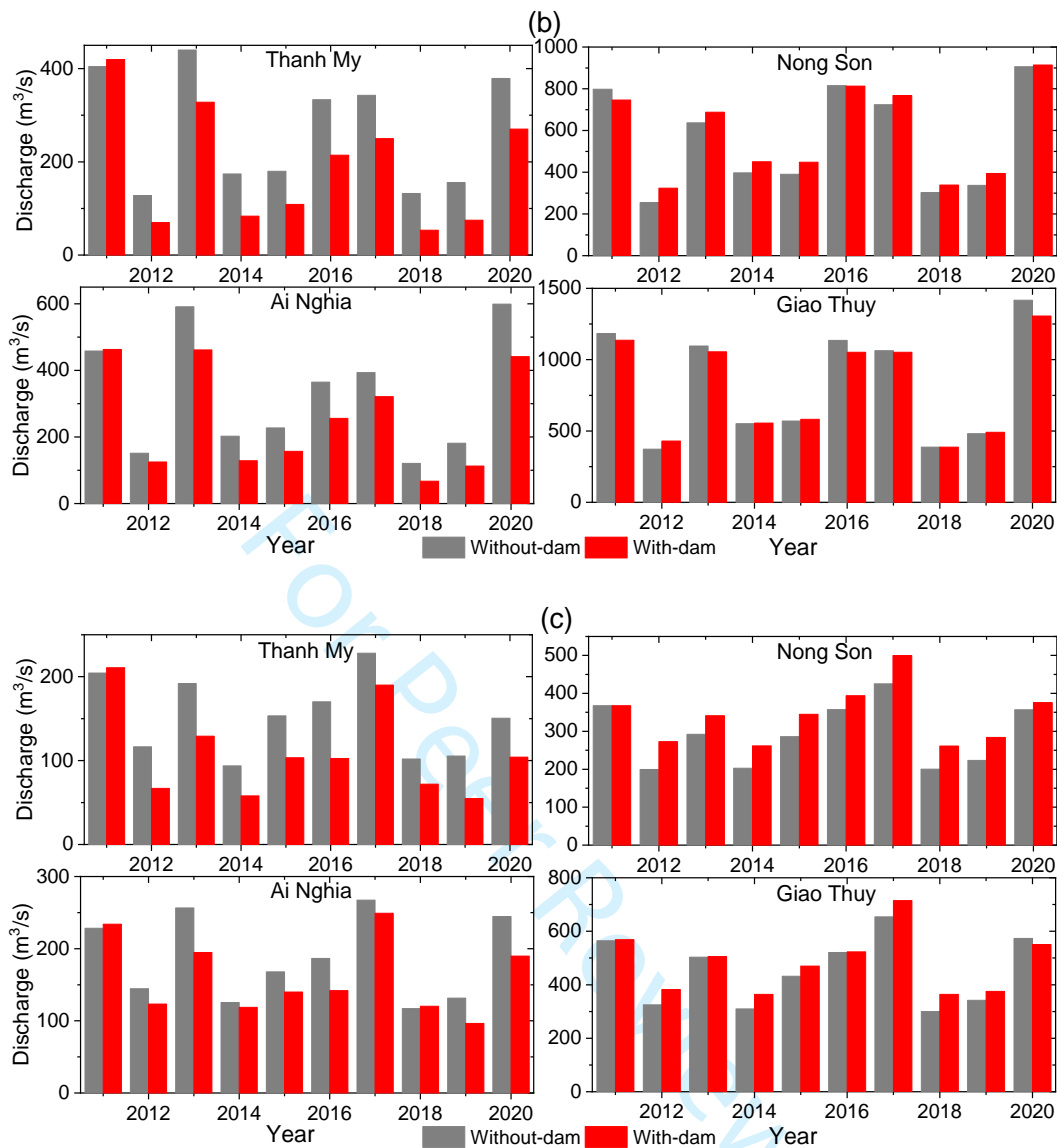


Figure 7. Comparison streamflow for the years 2011 to 2020. (a) Dry season (January to August), (b) Rainy season (September to December), (c) Annual. The grey colour is the without-dam scenario, and the red colour is the with-dam scenario.

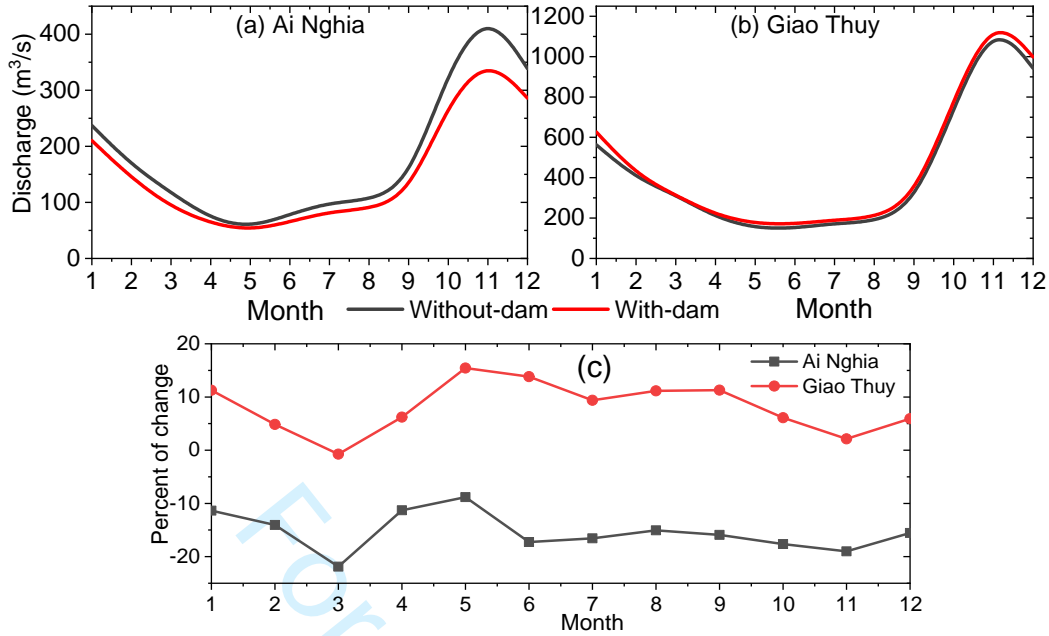


Figure 8. (a), (b) Effects of Dak Mi 4 reservoir on average monthly streamflow. (c) The percentage changes of monthly streamflow compared with the without-dam scenario at Ai Nghia and Giao Thuy stations.

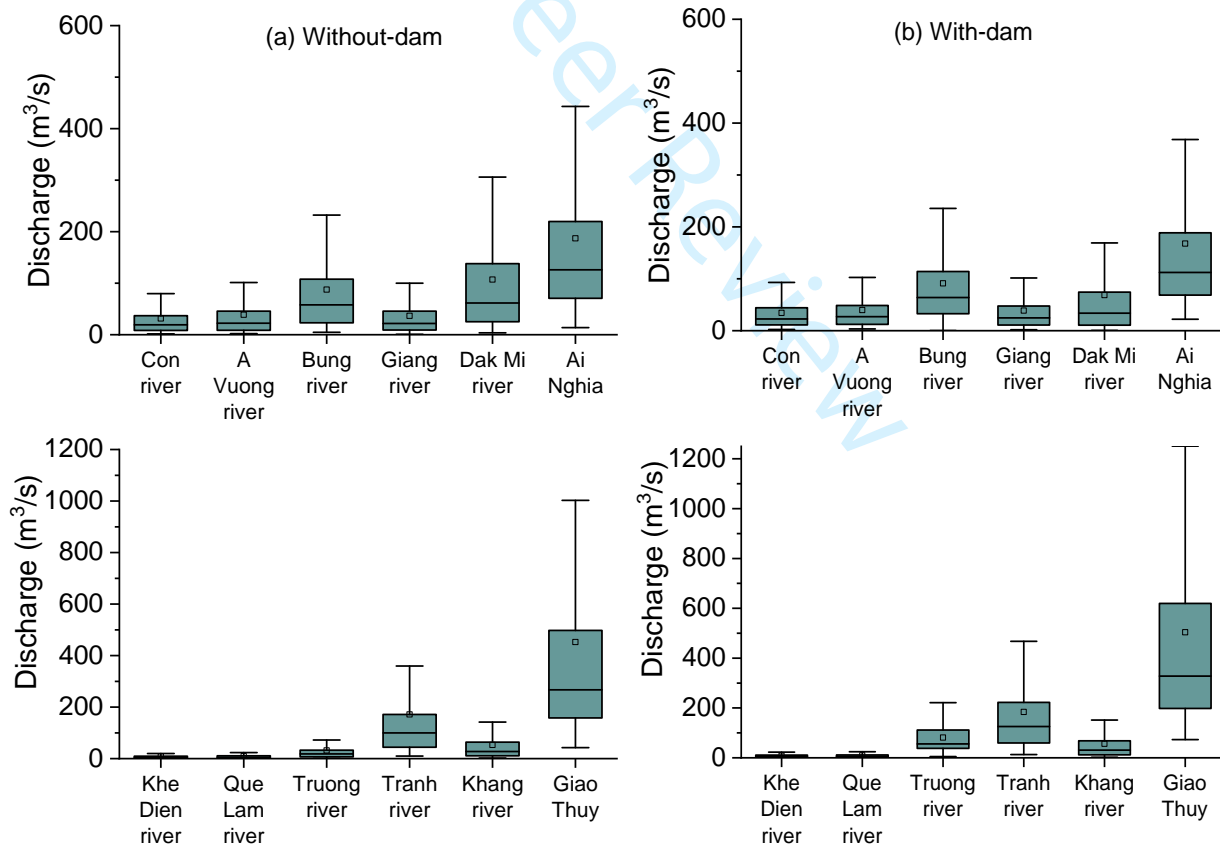


Figure 9. Box plots indicate the 25th, 50th (median), and 75th percentiles of the daily streamflow of main sub-basins in Vu Gia and Thu Bon sub-basins in the 2011–2020 period, (a) Without-dam scenario. (b) With-dam scenario.

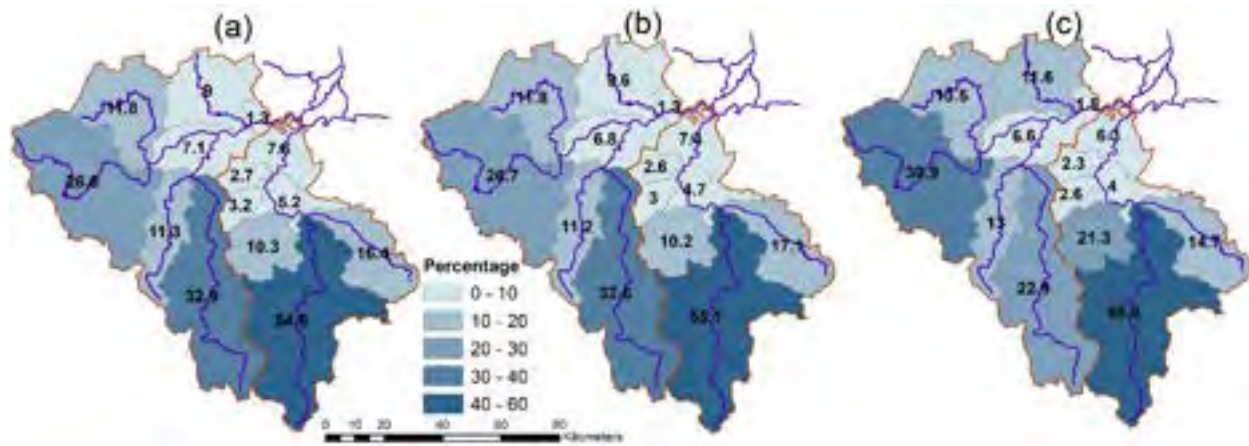


Figure 10. Percentage contribution of streamflow of sub-basins on Vu Gia and Thu Bon sub-basins, (a) 1980–2010 period, (b) 2011–2020 period without-dam, (c) 2011–2020 period with-dam. The results only consider water transfer of the Dak Mi 4 plant in the with-dam scenario and do not consider the Quang Hue River in all scenarios. The percentage contribution considers the upper Quang Hue River in Vu Gia and Thu Bon Rivers.

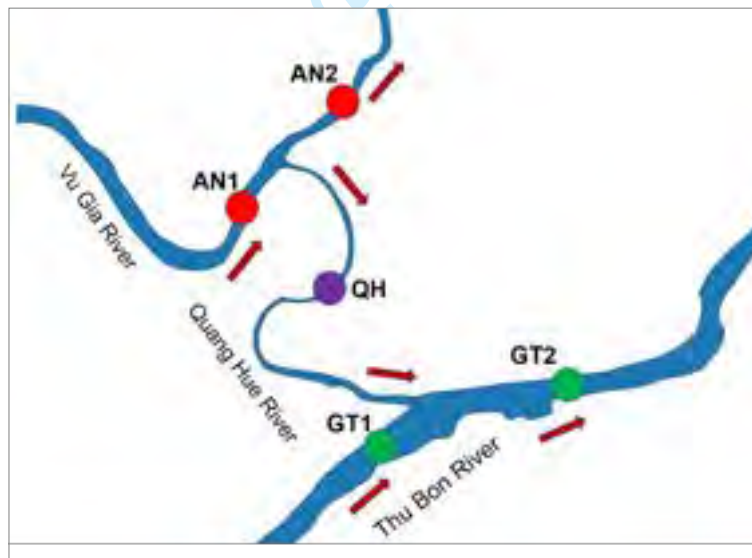


Figure 11. Five streamflow extraction locations on Vu Gia River, Thu Bon River, and Quang Hue River (AN1, AN2, GT1, GT2, QH).

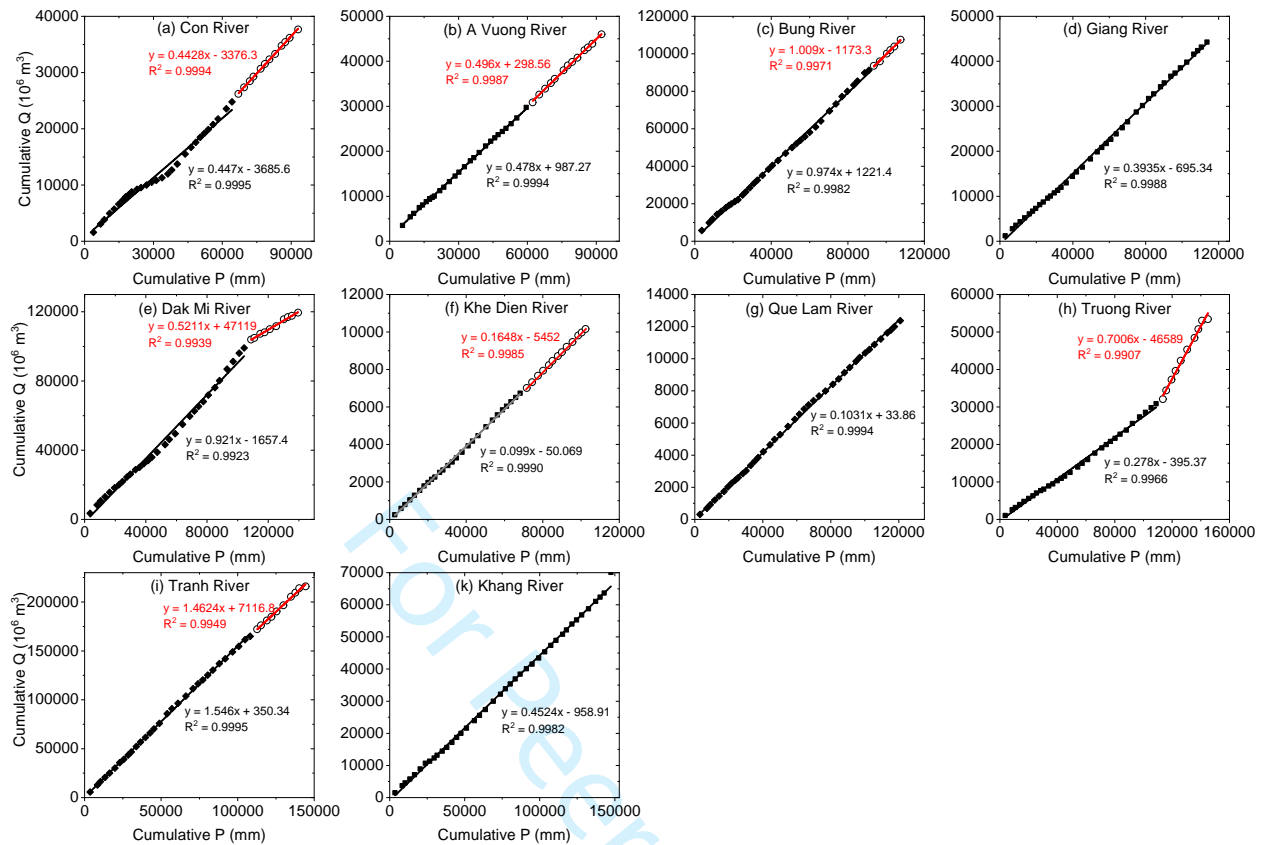


Figure 12. Correlation curves showing relationship of cumulative rainfall and streamflow at sub-basins. (a) Con River, (b) A Vuong River, (c) Bung River, (d) Giang River, (e) Dak Mi River, (f) Khe Dien River, (g) Que Lam River, (h) Truong River, (i) Tranh River, (k) Khang River.

Machine learning techniques and 2D rainfall-runoff inundation model for flood susceptibility and extent mapping

Mohamed Saber^{a*}, Tayeb Boulmaiz^b, Mawloud Guermoui^c, Karim I. Abdrabo^{d,e}, Sameh A. Kantoush^a, Tetsuya Sumi^a, Hamouda Boutaghane^f, Tomoharu Hori^a, Doan Van Binh^g, Binh Quang Nguyen^{a,h}, Thao T. P. Bui^a, Ngoc Duong Vo^h, Emad Habibⁱ, Emad Mabrouk^{j,k}

^a*Disaster Prevention Research Institute (DPRI), Kyoto University, Kyoto 611-0011, Japan.*

^b*Materials, Energy Systems Technology and Environment Laboratory, Ghardaia University, Ghardaia, Algeria*

^c*Unité de Recherche Appliquée en Energies Renouvelables, URAER, Centre de Développement des Energies Renouvelables, CDER, 47133 Ghardaïa, Algeria.*

^d*Faculty of Urban and Regional Planning, Cairo University, Giza 12613, Egypt*

^e*Department of Urban Management, Graduate School of Engineering, Kyoto University, Kyoto 615-8245 Japan.*

^f*Hydraulic Department, Badji Mokhtar-Annaba University, PO Box 12, Annaba, Algeria.*

^g*Master Program in Water Technology, Reuse, and Management, Faculty of Engineering, Vietnamese German University, 2-Le Lai Street, Hoa Phu Ward, Thu Dau Mot City, Binh Duong Province 820000, Vietnam.*

^h*The University of Danang -University of Science and Technology, 54 Nguyen Luong Bang, Danang, Vietnam.*

ⁱ*University of Louisiana at Lafayette, P.O. Box 42291, Lafayette, LA 70504, USA.*

^j*College of Engineering and Technology, American University of the Middle East, Egaila 54200, Kuwait.*

^k*Department of Mathematics, Faculty of Science, Assiut University, Assiut 71516, Egypt.*

***Corresponding:** mohamedmd.saber.3u@kyoto-u.ac.jp

Abstract

Vietnam has experienced many natural disasters, particularly typhoons. This study aims to examine three machine learning (ML) techniques random forest (RF), LightGBM, and CatBoost—for flooding susceptibility maps (FSMs) in the Vietnamese Vu Gia-Thu Bon (VGTB). The results of ML are compared with those of the rainfall-runoff model, and different training dataset sizes are utilized in the performance assessment. Ten independent factors that influence the FSMs in the study area, namely, aspect, rainfall, curvature, DEM, horizontal proximity to the river, hillshade, geology land use, slope, and stream power index, are assessed. An inventory map with approximately 850 flooding sites is based on several post-flood surveys after the typhoons in 1999, 2006, 2007, 2009, 2013, and 2020. The inventory dataset is randomly split between training (70%) and testing (30%). The AUC-ROC results are 97.9%, 99.5%, 99.5% for CatBoost, LightGBM, and RF, respectively. The FSMs developed by the ML methods show good agreement in terms of an extension with flood inundation maps developed using the rainfall-runoff model. The FSMs show that downstream areas (both urbanized and agricultural) are under high and very high levels of susceptibility. Additionally, different sizes of the input datasets (i.e., 30, 60, 90, 200, 400, 600, 800, 1000, and 1250 data points) are tested to determine the least number of data points

having acceptable reliability. The results demonstrate that the ML methods can realistically predict FSMs, regardless of the number of training samples. However, the final FSMs show some spatial differences when changes in susceptibility level are seen. Decision-makers and planners in Vietnam can use the developed FSMs for such typhoon-prone regions to propose effective mitigation measures for community resilience and development.

Keywords: Machine learning; random forest; LightGBM; CatBoost; flood susceptibility mapping; rainfall-runoff inundation model.

1. Introduction

Floods are the greatest catastrophic natural disaster on a global scale. Because of their short lag times, flash floods are more devastating than other types of flooding (Vinet 2008; Bui, Ngo, et al. 2019; Abdrabo, Kantosh, et al. 2022). Flash floods have had disastrous consequences in high and low-income countries (Bisht et al. 2018; Esmail et al. 2022). However, floods are more destructive in developing countries like Vietnam. Extreme fluctuations in storm patterns and global climate change are the main causes of the reported rise in flash floods (Hirabayashi et al. 2013; Pachauri et al. 2014; Abdrabo, Saber, et al. 2022; Saber et al. 2022). Typhoons, Tropical cyclones, extended coastal areas, and dense river networks are the primary causes of severe flooding in Vietnam. It is also highly vulnerable to floods caused by extreme storms. Vietnam is rated eighth among the top ten countries in weather events (Thao et al. 2020), where densely populated areas are more vulnerable to

floods. Consequently, continuous risk in human life and assets will always exist (Luu et al. 2021). Flash flood mitigation for risk reduction and management requires efficient monitoring measures (Arora et al. 2020). Flood susceptibility mapping is critical for scientists and governments worldwide to maintain the cities and human settlements safe, and resilient (Ali et al. 2020; Osman et al. 2021).

Several studies have been performed to forecast the likelihood of flood events. These studies can be divided into rainfall-runoff analysis, conventional analysis, and pattern categorization (Tien Bui and Hoang 2017). The traditional analysis uses time-series data for an extended period obtained from rainfall stations to produce regression models. The rainfall-runoff models (e.g., MIKE, PCSWMM 2D, HEC-RAS, etc.) concentrate on determining the correlation between runoff and rainfall to calculate temporal and spatial floods (Nguyen et al. 2015). In general, this task is complicated because of difficulties in accessing affected areas, especially in developing countries; as a result, the hydrological models' performance may be compromised, and comprehensive observational datasets are needed for calibration and validation of models (Abushandi and Merkel 2011; Abdrabo et al. 2020). Both groups have a significant deficiency: the lack of required data frequently limits their applications and incurs substantial costs for data collection (Fenicia et al. 2014). The last group, on the other hand (pattern classification), uses machine learning (ML) models that utilize historical geological, environmental, and flood data. Accordingly, flood-prone areas are defined as flood and non-flood classes (Bui, Ngo, et al. 2019). However, comparative studies and integration between these groups are lacking (Hsu et al. 1995; Demirel et al. 2009; Humphrey et al. 2016; Kratzert et al. 2019; Yang et al. 2020).

Over the last 20 years, the application of ML methods for flood susceptibility forecasting has been extensively evaluated globally. As a result, the recent advancement of ML methods has significantly improved flood modeling. Because of the ability of ML techniques to capture information without making predetermined assumptions, process complex datasets, and promptly provide high accuracy and reliable results, such practices have become widespread (Costache, Popa, et al. 2020; Arabameri et al. 2020). Several articles have been employed using GIS techniques and remote sensing to develop reliable flooding susceptibility maps (FSMs). ML models are currently associated with GIS to address various hydrological and environmental issues (Akay and Taş 2020). Logistic regression (LR), support vector machines (SVMs), Artificial neural networks (ANNs), adaptive neuro-fuzzy inference system (ANFIS), and random forest (RF) models are the most utilized in ML for FSM (Arora et al., 2020; Shahabi et al., 2020; (Hong et al. 2018; Costache, Hong, et al. 2020); Darabi et al., 2019; Shirzadi et al., 2020; Choubin et al., 2019; Dodangeh et al., 2020). Several ensemble methods to predict FFS have been used (Shahabi et al. 2020). ML methods consist of multiple stages (Arora et al. 2020), including the preparation of the inventory and influencing factors, as well as the assessment of the accuracy of the ML model. However, few studies have discussed the effect of inventory dataset size on the results' accuracy (Catal and Diri 2009; Tiwari and Chatterjee 2010; Meadows and Wilson 2021).

Ensemble and hybrid ML models have recently appeared, outperforming single models in their accuracy prediction (Zenggang et al., 2021). Several ensemble ML techniques, such as the alternating decision tree, bagging, dagging, reduced-error pruning tree, naïve Bayes tree, logistic model tree, AdaBoost, J48 decision tree, and random subspace ensembles have been

applied to enhance the predictive accuracy of the FSM (Pham, Jaafari, et al. 2021; Tuyen et al. 2021; Luu et al. 2021). Several studies have developed flooding susceptibility maps in Vietnam using ML, which can be classified into three groups. The first evaluates the utilization of new ML models and their ability to detect areas prone to floods. For instance, the AdaBoost, dagging, bagging, and random subspace ensemble learning methods were combined with the Partial Decision Tree (PART) classifier to develop new GIS-based ensemble methods for FSM in the Province of Quang Binh (Luu et al. 2021). The second group attempts to overcome the limitations in the studies number that utilize remote sensing data to generate input variables for FSM despite the merits of using such available data (Pham et al. 2019, p. 2010–2018). As such, (V.-N. Nguyen et al. 2020; Dhara et al. 2020; Nhu et al. 2020, p. 202; Ngo et al. 2021) suggested a hybrid approach using remotely sensed data with ML models for flooding susceptibility. The third group introduced a novel deep learning neural network (DLNN) algorithm for FSM (Tien Bui et al. 2020), integrating particle swarm optimization (PSO) and extreme learning machines (ELMs) (Bui, Ngo, et al. 2019; Bui et al. 2020) along with a comparison between ML and deep learning techniques (Pham, Luu, et al. 2021) for the same study area.

In the presnt study, we examined two ML models, the light gradient boosting machine (LightGBM) and categorical boosting (CatBoost) for FSM for the first time in humid regions after successful application in arid areas (Saber et al. 2021). Previously, both methods have been applied some applications. LightGBM, for example, has been employed in some previous studies due to its accuracy in predictions and short computational time, in addition to exceptional prevention of overfitting problems. Accordingly, our primary objectives are

(1) to evaluate how practical the two ML approaches (CatBoost and LightGBM) are for predicting flooding susceptibility in humid environments (Vu Gia-Thu Bon basin in Vietnam); (2) to compare the results of the used two models with that of the conventional RF method ; (3) to test the effect of the inventory datasets (number of points) on the accuracy of the results in the study area; and (4) to compare the rainfall-runoff inundation (RRI) 2D hydrological model with the proposed ML integrated models in terms of flood extent.

2. Study Area

The River Basin of Vu Gia-Thu Bon (VGTB) (Fig. 1) is one of the major river basins in Vietnam, with a surface area of 10350 km² (RETA 2011). The land use types in the basin are forest (47%), agriculture (26%), and pasture (20%) (Avitabile et al. 2016). The climate in this basin is tropical monsoon, with two seasons: dry summer (January-August) and wet (September-December). The basin's topographic features are hilly mountainous areas, with approximately 60% of the basin having an elevation of over 552 m. The average annual rainfall varies significantly, from 2000 mm in the downstream regions to more than 4000 mm in mountainous areas. There are seasonal differences, with 65% to 80% of the annual rainfall concentrated between September and December (RETA 2011). The rain in eight months of the dry season is only 20%–35% of the annual rainfall (Nauditt et al. 2017). Due to rainfall's spatial distribution, the VGTB basin's runoff varies substantially across seasons. River flow in this period accounts for around 62.5% to 69.2% of the total annual flow. The impacts of both heavy rainfall and steep terrain usually lead to flash flooding. Approximately 4–8 floods occur annually. Due to meteorological patterns such as tropical depressions,

typhoons, and cold air, the highest flood peak occurs in October and November (Vu et al. 2011). According to the Quang Nam Province Commanding Committee for Disaster Prevention, Search and Rescue report, the number of fatalities and property losses caused by floods and storms has been growing, particularly in 2020 (Fig. 2).

There are two main sub-basins in the VGTB river system: Thu Bon Basin and the Vu Gia Basin. The Quang Hue River connects both Rivers. The Vu Gia River start from the western slope of Kon Tum and flows towards the province of Quang Nam and the city of Danang. It connects with the sea at the Cua Han estuary. The length of the main river from the source to the Cua Han estuary is 204 km. At the same time, the Thu Bon River originates from a mountain of 1500 m in Kon Tum province. The river length from the source to the Cua Dai estuary is 198 km.

Fig. 1.

Fig. 2.

3. Methodology

This study's methodology comprises multiple phases, as shown in the flowchart in Fig. 3. This methodology has two main parts. First, a flood inventory map is created using 850 flooded spots. These spots were determined primarily through post-flood assessments conducted after typhoons in 1999, 2006, 2007, 2009, 2013, and 2020. Non-flooded points (850) over the catchment were randomly selected using GIS tools. Additionally, Ten

commonly used independent flood susceptibility variables (FSFs) covering hydrological, topographical, geological, and landform characteristics were considered for modeling. The flooding susceptibility influencing factors, namely elevation, aspect, slope, hillshade, horizontal flow distance, plan curvature, stream power index (SPI), geology, land use/land cover, and rainfall were used to define the linear relationship with other variables. In subsequent phases, the data was divided into two sets using a random selection scheme: (70 percent) for training and (30 percent) for testing. ArcGIS was used to create spatial maps for each flooding susceptibility factor while keeping spatial resolution consistency in mind. Following that, two approaches, the variance inflation factor (VIF) and the information gain ratio (IGR) were used to investigate the significance of the influencing factors in flooding susceptibility. The ML algorithms RF, CatBoost, and LightGBM were then implemented. The accuracy of the ML models' final results was assessed using various statistical processes, including the most dominant area under the curve (AUC). Moreover, as we have very high-quality observational flood locations, we tested the models to check the different sizes of the training datasets (Fig. 3). The final FSM developed by the ML models was then compared with the flood inundation maps from the 2D physical hydrological model regarding the flood extent.

Fig. 3.

3.1. Datasets

3.2. Flooding inventory datasets

The initial stage in flood susceptibility mapping identifies flood locations (points) based on prior flood records using several sources, such as field surveys, remote sensing data, and flood forecasting records (Tehrany et al. 2014; Wang et al. 2019; Esfandiari et al. 2020; Band et al. 2020). The locations of future hazardous events might be forecasted using previous information (Devkota et al. 2013; Tehrany and Kumar 2018). As a result, the fundamental phase of flood susceptibility study is an examination of prior historical flood occurrences and their contributing elements (Masood and Takeuchi 2012). The accuracy in selecting flood points is reflected in the model accuracy for FSM (Tehrany et al. 2013; Arora et al. 2019). In this study, 1700 ground control points (Fig. 1) were identified for flooded (850) and non-flooded points (850). Approximately 1250 were used for training and 450 for testing the models. The flooded locations were compiled from historical flood records and post-flood field surveys in 1999, 2006, 2007, 2009, 2013, and 2020 (Fig. 1). Flood and non-flood locations were assigned values 1 and 0, respectively. Using the random selection approach, the points were divided into 70% for training to create the flooding prediction model and 30% for testing the model performance and generalization abilities.

3.3. Spatial datasets (flood controlling parameters)

Identifying flood governing parameters for flooding susceptibility mapping is critical and influences model accuracy (Kia et al. 2012). Runoff in a drainage system is influenced by the watershed features, terrain, catchment area, land use types, and land cover during floods. (Hölting and Coldewey 2019). Generally, there are no uniform and standard selection criteria for FSM controlling factors. Depending on previous research and the features of the studied

area, as well as the availability of data, we were able to develop ten flood governing indicators that include topographic, geological, hydrological, and landform factors. The ten indicators are plan curvature, elevation, slope, aspect, horizontal flow distance, hillshade, SPI, rainfall, geology, and land use/land cover. Using ArcGIS, the data were developed in raster formats (Fig. 4). All topographic factors were constructed based on the spatial analysis of MERIT digital elevation model (Yamazaki et al. 2017). The terrain elevation's spatial resolution was 3 s (~90 m at the equator). It was created by removing the incorrect components from existing digital elevation models (DEMs), such as Aw3D-30m v1 and SRTM3 v2.1. These data are freely available and accessible at http://hydro.iis.u-tokyo.ac.jp/~yamadai/MERIT_DEM/. Below are the details of this study's considered flood influencing parameters.

Elevation: According to (Tehrany et al. 2013), there is a clear correlation between elevation and flooding, which makes lowland surfaces more susceptible to flooding than higher ones (Khosravi et al. 2016). This implies that the likelihood of flooding decreases with increasing topographic elevation (Youssef et al. 2016). The research area contains complicated topography characteristics, including very high elevations up to 2600 m and low altitudes ranging from 3 m to 200 m in the downstream section of the basin and the coastline area, primarily residential and agricultural areas (Fig. 4a).

Slope: This is a significant factor influencing flooding (Khosravi et al. 2016; Tien Bui et al. 2016; Meraj et al. 2018) because of its effect on water velocity and surface flow (Torabi Haghghi et al. 2018). The study area's slope varied from 0° to 70° (Fig. 4b).

Aspect: As stated by (Choubin et al. 2019), this aspect influences the hydrological parameters. There is an indirect relationship between the aspects of floods owing to their control over several geo-environmental factors, such as rainfall, vegetation, and soils (Rahmati et al. 2016). When aspects receive a low intensity of sunlight, which means more soil moisture, the moist slope will likely increase runoff, leading to increased flooding risk (Yariyan et al. 2020). The aspect raster map was categorized into ten classes from flat to northwest (Fig. 4c).

Plan Curvature: Many researchers consider this an essential flood controlling factor (Hong et al., 2018) and affects heterogeneity and hyporheic (Cardenas et al. 2004). The different values of curvatures differentiate the areas of the faster runoff from those with a slower runoff. While negative values cause an increase in runoff, the positive values decrease it. The surface runoff is affected by the shape of slope, as zero curvature (flat) and negative curvature (concave) have more potential for flooding than the convex form (positive) (Tehrany et al. 2014; Tehrany et al. 2015; Shahabi et al. 2020). Concave slopes, for instance, slow surface flow and increase filtering losses, while convex slopes do precisely the opposite of concave slopes (Cao et al., 2016). The curvature map was developed based on the DEM with three forms (concave, flat, and convex), and the flat class was more dominant in the downstream area, as shown in Fig. 4d.

Hillshade: A hill's length and shadow are intertwined with its hillshade or topshade, which may affect where the surface flow converges (Aryal et al. 2003). Prior research has shown minimal interest in topshade (Bui, Ngo, et al. 2019). Predicting flooding vulnerability

requires it after slope and elevation (Bui, Hoang, et al. 2019). Figure 4e shows that toposhade was chosen as a flood influencing factor.

Fig. 4.

Flow distance: Any area's likelihood of flooding is influenced mainly by distance from major rivers or streams (Glenn et al. 2012). Typically, nearby streams are more vulnerable to floods (Chapi et al. 2017). The farther away from rivers, the greater the chance of floods. Floods are common in places near rivers, which has been stressed as a primary influencing factor for flooding (Predick and Turner 2008); (Bui et al. 2018; Darabi et al. 2019). According to (Gigović et al. 2017; González-Arqueros et al. 2018), the distance from streams are the primary conduits for surface flow. Using ArcGIS, the horizontal flow distance was calculated for the current investigation using the flow direction, flow accumulation, and DEM (Fig. 4f.).

Rainfall: Precipitation is one of the triggering factors for flooding, as no rainfall indicates a lack of flooding. The total average rainfall was estimated between 2001 and 2019 using the PERSIANN Dynamic Infrared–Rain rate model (PDIR). Estimating precipitation was done using remotely sensed information that utilizes ANNs (P. Nguyen et al. 2020, p.). It is a real time global dataset with a high resolution of approximately $(0.04^\circ \times 0.04^\circ)$, or $4 \text{ km} \times 4 \text{ km}$, at (<https://chrdata.eng.uci.edu/>). According to the geographical maps, the average annual precipitation in the upstream and mountainous parts is 3284 mm, while 2235 mm in the downstream.

Land use/land cover: The influence of this factor was confirmed using the global cover map developed by the geospatial Japan information authority (https://www.gsi.go.jp/kankyochiri/gm_global_e.html) and mainly from this website (<https://globalmaps.github.io/glcnm.html>). Land use and land cover types were also considered as controlling factors due to their influence on filtration and runoff velocity. The study area has approximately six classes (Fig. 4h), including cropland, forest, grassland, other lands, settlement, and water. The forest is the dominant type of land cover in the mountainous area, especially upstream of the basins, and agricultural land and urban areas are located in the downstream region.

Stream Power Index: This parameter indicates the power of erosion and discharges within a specific area of the river system (Poudyal et al., 2010). Several researchers have considered the SPI a flooding contributor because it indicates surface flow. The highest values of SPI imply a fast flow of downstream water, which reveals lower flooding susceptibility, and low values imply slow flow leading to more inundation (Tehrany and Kumar 2018). SPI was calculated based on a method derived from Jebur et al. (2014). SPI was classified into five classes in the present study area (Fig. 4i).

Geology: In terms of infiltration and flow velocity, this is a critical parameter. Lithology data was given by the Land Use and Climate Change Interaction in Central Vietnam (LUCCI) (Nauditt and Ribbe 2017). In terms of geological classification, it has been subdivided into several different kinds with high variation in sedimentary, igneous, and metamorphic rock types (Fig. 4k).

3.4. Selection of flood influencing factors

The selection of controlling factors is an important stage in ML modeling for FSM. The estimated capabilities of the model may be impacted by an inaccurate selection of the hyperparameter values or redundancy (Öztürk and Akdeniz 2000). As a result, the feature selection procedure was based on Spearman's rank correlation, the IGR and the multicollinearity test to identify irrelevant features.

3.4.1. Spearman's correlation coefficient

The nonparametric Spearman rank correlation coefficient is used to show the strength of the monotonic association between two variables, X and Y. From -1 to 1, the coefficient indicates more significant and weaker correlations. As the coefficient value approaches 0, the relationship between the two variables X and Y becomes weaker. Correlation coefficient values higher than 0.7 imply considerable collinearity (Tien Bui et al. 2016). According to this formula, the correlation coefficient is calculated:

$$r(x, y) = 1 - \frac{6\sum(x - y)^2}{n(n^2 - 1)} \quad (1)$$

where r refers to the correlation coefficient, x and y are defined as the two variables, and n is the length of each variable.

3.4.2. Multicollinearity Test

Multicollinearity was examined between all contributing elements and the correlations between two characteristics using Spearman's coefficient. The VIF was used in

this study's multicollinearity analysis to identify any existing interrelatedness between variables. This element is frequently utilized in investigations of flood susceptibility (Bui et al. 2019; Khosravi et al. 2019; Rahman et al. 2019), suggesting a threshold > 5 to consider multicollinearity. The relevant predictors are, however, deemed collinear in other research if the VIF value is more than 10; hence it is advised to leave them out of the models (Dou et al. 2019; Wang et al. 2019). Thus, we considered a value of five as the threshold for selection. The independent predictors are specified as $X = \{X_1, X_2, \dots, X_n\}$ and R_j^2 , and refer to the determination coefficient when the j th independent predictor X_j is regressed on the other predictors. The following equation is used to determine VIF:

$$VIF = \frac{1}{1-R_j^2} \quad (2)$$

3.4.3. Information gain ratio

Using the IGR test, conditioning factors were assessed to determine their relative relevance in the occurrence of floods (Quinlan 1986; Xu et al. 2013). The latter is one of the feature selection techniques that considered by many previous studies (Shahabi et al. 2020). When an input has zero IGR, there is no correlation between the input and the output. This circumstance suggests that including such input in the model will not provide any information; rather, it will create noise, reducing the model's capacity for prediction. Therefore, it is strongly advised that these elements be eliminated from the inputs. Eq. (3) is used to compute the IGR.

$$IGR(x, Z) = \frac{Entropy(Z) - \sum_{i=1}^n \frac{|Z_i|}{|Z|} Entropy(Z_i)}{\sum_{i=1}^n \frac{|Z_i|}{|Z|} \log \frac{|Z_i|}{|Z|}} \quad (3)$$

3.5. Machine learning methods

ML approaches are the basic concept of employing algorithms to analyze and learn from the data to produce forecasting or classification systems. These techniques can be learned from previous experience or a given historical database. These methods can generalize the learning examples provided in the training phase to identify the main tasks that must be performed.

Several ML algorithms have been developed. These techniques can be classified according to their learning mechanisms (i.e., supervised, unsupervised, and semi-supervised learning). The choice of a suitable ML model and training method depends on the problems to be solved or the available data and its types. In the current study, we focused on using supervised ML techniques for flooding susceptibility assessment. According to previous research, various ML techniques have been proposed recently to deal with flooding susceptibility assessment (i.e., SVMs, ELMs, ANNs, Gaussian process regression (GPR), and classification and regression trees (CART)). In addition, few studies have addressed flooding susceptibility using ensemble-learning approaches based on decision trees. These algorithms are based on boosting techniques that concentrate on misclassified data during the training phase. In this respect, the goal of this study is to assess the performance of two new modeling techniques, CatBoost and LightGBM, benchmarked with the conventional RF approach.

3.5.1. Random forest

RF models have proven efficiency when dealing with prediction and classification problems (Esfandiari et al. 2020; Schoppa et al. 2020). RF is an ensemble learning approach based on a decision tree model. It was developed by Breiman (2001), who combined bagging (Breiman 2001) and random subspace (Ho 1998) techniques. This ML algorithm has proven to be reliable in many fields (Zahedi et al. 2018; Izquierdo-Verdiguier and Zurita-Milla 2020; Pourghasemi et al. 2020). In this study, we aimed to predict flood or non-flood regions according to several conditioning factors; therefore, the RF model was used as a classifier method.

The weakness of decision trees is their sensitivity to training data, which may result in very different tree structures. In the RF method, the original training set is used to randomly generate several training sets, thereby allowing the creation of different trees (bagging method). The inputs of the decision trees have the same data size as the initial training, and because the data are randomly generated, the samples may be repeated two or more times. In addition, each tree in the RF is trained with a subset of features that allows the development of diversified trees that are not correlated. The final result (classification) was obtained by performing a majority voting method on each decision tree results (Pal 2005).

Decision tree models are simple to use and easy to interpret; however, their performance is not always better than that of other classification methods (Malekipirbazari and Aksakalli 2015). On the other hand, RF outperformed other ML algorithms, such as ANNs (Bachmair et al. 2017).

3.5.2. *Light Gradient Boosting Machine*

Microsoft created the gradient boosting decision tree (GBDT) variation called LightGBM. (Ke et al. 2017). It uses a combination of weak learners to generate a robust model. The new variant includes algorithms such as histograms, leaf tree growth, gradient-based one-side sampling (GOSS), and exclusive feature bundling (EFB)).

In GBDT models, the presorted algorithm is commonly used for split operations. All possible split points are tested based on the information gain, which is a time-consuming operation to determine the optimal split. A new histogram algorithm was adopted in the LightGBM method. To reduce the time and complexity of the operation, the data are grouped into a histogram, and the split point is chosen based on it (Fig. 5).

Fig. 5.

In LightGBM, the decision tree growth strategy was changed by replacing the level-wise approach with the leafwise tree growth approach. When finding the best node to split, the former approach of the GBDT splits one level down, forming symmetric trees (Fig. 6). In LightGBM, only the leaves that reduced the maximum error were split (Fig. 6). Ge et al. (2019) recommended defining a maximum leaf-wise depth to avoid deep growth of trees and provoke overfitting of the model.

Fig. 6.

The LightGBM model also uses two algorithms (GOSS and EFB), making it faster than GBDT models while maintaining a high performance (Saber et al. 2021).

3.5.3. *Categorical boosting*

The CatBoost model is another enhanced boosting decision-tree learning technique, which was proposed by (Dorogush et al. 2018). It employs a gradient boosting scheme to construct a regression model through adjusted estimation. Furthermore, various refinements were performed to minimize overfitting of the model. The gradient boosting model is a useful ML tool that has yielded accurate results in many disciplines, including environmental parameter estimation, geospatial ecosystem factor dispersion, and meteorological forecasting. The CatBoost model operates well in terms of categorical attributes. Typically, the absence of categorical characteristics increases the accuracy of the model. It is primarily dependent on the use of gradient boosting, which employs a binary-tree classification scheme. The following points outline the differences between CatBoost and the other boosting techniques.

- A sophisticated method was incorporated to convert category characteristics into numerical information. As mentioned by (Prokhorenkova et al. 2017), target statistics are very effective for dealing with categorical attributes with minimal information errors.
- CatBoost combines categorical variables to take advantage of the existing relationship between different parameters.
- To reduce the overfitting problem and improve the classification performance, a symmetrical tree strategy is used.

Let us suppose we have a dataset:

$$D = \{(X_J, Y_J)\} \quad J = 1, \dots, m \quad (4)$$

where $X_J = (x_j^1, x_j^2, \dots, x_j^n)$ is a combination of attributes, and $Y_J \in R$, denotes the desired target. Input-output datasets are dispersed identically and independently depending on an unknown function $\rho(\cdot, \cdot)$. The target of the learning techniques is to train and examine a function $H: R^n \rightarrow R$ that can decrease information loss, that is, $L(H) := EL(y, H(X))$, where L is the smoothness error function and (X, y) denotes the testing samples from D . The gradient boosting approach builds a greedy series of approximations $H_t: R^m \rightarrow R$, $t = 0, 1, 2, \dots$, $H_t = H((t-1)) + g_t$ is the final function produced from prior approximation using an additive process $H_t = H((t-1)) + g_t$.

$$g^t = \arg \min_{g \in G} L(H^{t-1} + g) = \arg \min_{g \in G} E L(y, H^{t-1}(X)) \quad (5)$$

In general, greedy techniques, such as Newton's method, employing a second-order approach of $L(H(t-1) + g)$ at $H(t-1)$ or adopting (negative) gradient stages, are used to address the optimization issue.

3.6. *Rainfall-runoff inundation model (RRI)*

RRI model has been developed by the International Center for Water Hazard and Risk Management in Japan. It is a 2D distributed hydrological model capable of simultaneously simulating both flow discharge and flood inundation (Sayama et al., 2012). The model has been applied in many previous studies worldwide (Perera et al. 2017; Abdel-Fattah et al. 2018; Tam et al. 2019; Saber et al. 2020; Try et al. 2020). In this study, the model was

calibrated and validated based on the typhoon of 2020, showing acceptable results with the actual flood discharge and good agreement with flood inundation maps. The final flooding inundation map developed by was used for comparison with the ML FSMs for the flood extent mapping.

3.7. Evaluation of the model's performance validation

The receiver operating characteristic (ROC) curve measure is a commonly used and validated strategy for assessing the reliability of a model in geospatial research (Tehrany et al. 2013; Chen et al. 2020). The most popular method for evaluating flood vulnerability and landslide approaches is the ROC curve. The classification performance of a given technique was evaluated using the AUC in several studies (Bui et al. 2012; Youssef et al. 2016; Youssef and Hegab 2019). A high classification efficiency for a given classification model should have an AUC-ROC value of 0.5 to 1, and the model's performance is enhanced by boosting the AUC-ROC scores. When the AUC-ROC value was close to 1.0, the models offered the best rate of precision and consistency. This demonstrates the model's ability to forecast disasters without bias (Bui et al. 2012). In this study, the ROC score was determined using the following formula (Chang et al. 2018):

Other quantitative metrics (accuracy, recall, precision, and F1-score) were employed to check the model performance and compare its classification ability with that of its counterpart models in the literature. Accuracy is defined as the ratio of correctly classified data to total observations [Eq. (6)]; precision can be defined by the ratio of properly positive classified data to total positive data [Eq. (7)]. Recall, is known as sensitivity and defined by the ratio

of positive to the total observations [Eq. (8)]. F1-score uses weighted averaging for both the precision and recall [Eq. (9)].

$$\mathbf{Accuracy} = \frac{\mathbf{TP} + \mathbf{TN}}{\mathbf{TP} + \mathbf{TN} + \mathbf{FP} + \mathbf{FN}} \quad (6)$$

$$\mathbf{Precision} = \frac{\mathbf{TP}}{\mathbf{TP} + \mathbf{FP}} \quad (7)$$

$$\mathbf{Recall} = \frac{\mathbf{TP}}{\mathbf{TP} + \mathbf{FN}} \quad (8)$$

$$\mathbf{F1\ score} = \frac{2 (\mathbf{Recall} * \mathbf{Precision})}{\mathbf{Recall} + \mathbf{Precision}} \quad (9)$$

where true positive (TP) represents a properly categorized flooded pixel, true negative (TN) represents a correctly categorized non-flood pixel, false positive (FP) indicates the number of pixels miscategorized as flood pixels, and false negative (FN) refers to the number of pixels miscategorized as non-flood pixels.

4. Results and Discussion

4.1. Multicollinearity assessment and feature selection

According to (Chen et al. 2020), a value greater than 0.7 indicates a strong correlation between variables. This value was adopted in this study to detect the existence of a correlation between the flood-influencing factors. Ten conditioning factors (DEM, NDVI, flow accumulation, vertical distance from the river, and slope) were identified as correlated (Table 1). The VIF of the vertical distance from the river (= 12), DEM (= 10.5), SPI (= 7.7), and flow accumulation (= 7.4) factors were more significant than the threshold value (> 5), which indicates a problem of multicollinearity (Fig. 7a).

To formulate an opinion on the importance of influencing factors concerning flood generation, the IGR scores were computed and illustrated in Fig. 7b. According to the results, most factors had an IGR greater than 0.05. Only four had an inferior IGR, that is, flow accumulation, flow direction, rainfall, and aspect.

The selection of conditioning factors was performed as follows:

1. Based on multicollinearity analysis, the vertical distance from the river, DEM, SPI, and flow accumulation factors were removed from the selection list.
2. Using the IGR as a selection criterion, flow direction, rainfall, and aspect were removed because their IGR was almost equal to zero.
3. After removing the abovementioned factors, only the slope and the topographic wetness index (TWI) remained correlated variables. By comparing the IGR (Fig. 7), we find that the slope factor is more critical than the TWI concerning flood generation. Therefore, the slope factor was selected for flood prediction based on the

normalized difference vegetation index (NDVI), land use, curvature, geology, hillshade, and horizontal distance from the river.

Table 1

Fig. 7.

4.2. Evaluation of the models

This section offers a thorough analysis and comparison of all models created for this research concerning several categorization criteria. K-fold cross-validation was used throughout the learning phase. A learning set (60 percent) was created from the reviewed data, and the remaining data were used to gauge accuracy. The learning datasets was divided into two groups: validation data, which was used for hyperparameter tuning, and training data (80%), which was used to modify reduce classification mistakes and model weights. The relevant hyperparameters for each classification method were selected using the grid search method. A broad range of hyperparameter values was evaluated during the process. The best designs for each classifier are listed in Table 2.

The accuracy rates of all the studied models are listed in Table 3. As can be seen, all developed classification techniques achieved approximately identical results in terms of statistical metrics. The LightGBM model slightly outperformed the others regarding speed convergence and classification metrics. The ROC curve of the generated models on the test ensembles is displayed in Fig. 8, which reveals that the three suggested boosting strategies have similar qualities and provide significant accuracy. The maximum AUC was reached by

LightGBM and RF models with the same score (99.5%), and CatBoost was ranked as the worst model with an AUC of 97.9%.

Furthermore, CatBoost scored the first rank in terms of accuracy performance accuracy equal to 97.8 %, precision equal to 96%, accompanied by LightGBM classifier with an accuracy of 97.3% and precision of 95%. Finally, the RF model was ranked as the last classifier model with an accuracy equal to 95.5% and a precision of 96.2%. In comparison with previous studies, RF in this study outperformed many of the previous applications, including (e.g., AUC = 0.925, Chen et al. (2020); AUC = 0.886, Tang et al. (2020); AUC = 0.7878, Lee et al. (2017); AUC = 0.972, Achour and Pourghasemi (2020)).

The confusion matrix in Fig. 9. shows the performance of the used models in the study area, where CatBoost shows better prediction followed by LightGBM and, finally, the RF methods; however, all of them display an acceptable prediction.

This study examined two novel boosting classification models for flooding susceptibility assessment in the VGTB River Basin. From the evaluation statistics, we can conclude that the LightGBM and CatBoost models proved their performance for flooding susceptibility and can be used as essential tools for real-time application compared to their counterpart models because of their high performance and speed convergence.

Table 2.

Table 3.

This work examined two novel boosting classification approaches for predicting flood vulnerability in the VGTB. This is the first work investigating CatBoost and LightGBM for flood classification in humid environments against the frequently used RF models. The results revealed that LightGBM outperformed its counterpart ML models, especially regarding processing time and classification metrics. This agrees with the findings of Saber et al. (2021) that LightGBM has proven its efficiency in flash flood prediction and outperforms the other two methods in classification and processing time. In addition, it was stated that LightGBM outperformed other methods such as the RF, M5Tree, and empirical models for estimating daily evapotranspiration in China as a humid subtropical area (Fan et al. 2019).

Similarly, it was also found that LightGBM performed better than the others in terms of AUC (99.5%). The accuracy of CatBoost (97.9%) was also high compared to the previous studies in other fields. Among other methods, CatBoost, SVM, and RF have been applied to evapotranspiration modeling in China (Huang et al. 2019). They stated that CatBoost presented higher accuracy and lowered computational cost than the other approaches (RF and SVM).

Fig. 8.

Fig. 9.

4.3. *Flood Susceptibility Modeling*

The newly applied boosting techniques (CatBoost and LightGBM) and RF demonstrated their high performance in predicting flooding in a humid climate environment. The flood susceptibility maps for the whole VGTB river basin were thus estimated using these approaches. Then, the three FSMs developed using the three models were compared with the flood inundation map of the RRI model regarding the flood extent, as shown in Fig. 10. The flooding susceptibility values were then mapped under five levels of susceptibility classes: no flood, low, moderate, high, and very high.

The FSMs by the employed models showed that the areas of high and very high levels of susceptibility to flooding to be 13% (RF), 11% (LightGBM), and 10% (CatBoost) of the total area, which agrees with the flood inundation map developed by RRI at approximately 11%. This level of susceptibility is predominant in the coastal and plane areas along the Vu Gia and Thu Bon Rivers (Fig. 10 and 11). The spatial distributions of the high and very high levels were similar in all the maps produced by the ML and RRI models. The areas affected by a moderate level of susceptibility to flooding (Fig. 11) were estimated at 10% (RF), 0% (LightGBM), and 1% (CatBoost), indicating that both LightGBM and CatBoost are more similar to the RRI model which shows a value of approximately 1%. The areas affected by the low level of susceptibility to flooding (Fig. 11) were estimated at 36% (RF), 1% (LightGBM), and 2% (CatBoost), which also revealed that both LightGBM and CatBoost performed better, with good agreement with the RRI model showing the value of approximately 3%. It was also found that the areas that were not subjected to the flooding were approximately 42% (RF), 83% (LightGBM), and 87% (CatBoost) of the total study area (Fig. 11), showing good agreement with RRI model that shows approximately 90%.

However, the performances of the employed models are almost the same. The two new methods of LightGBM and CatBoost outperform RF in terms of the spatial coverage of the flood susceptibility levels compared with the RRI model. The RF overestimated the low flood susceptibility in the study area. The spatial distribution of FSM is consistent across utilized ML models, emphasizing that most of the residential and agricultural sectors are concentrated in coastal regions prone to flooding.

Fig. 10.

Fig. 11.

4.4. Testing different sizes of the datasets

In this section, we tested different sizes of the datasets, including flooded and non-flooded points (1250, 1000, 800, 600, 400, 90, 60, and 30) of the training model (Fig. 12). The training datasets were classified as 50% and 50% for flooded and non-flooded points, respectively; however, the testing datasets were the same during the simulation (Fig. 12). We found that accuracy scores for all the models and all the tested cases were greater than 90% (Fig. 13), except for dataset sizes of 60 and 30 points in LightGBM. The accuracy score slightly decreases with the decrease in the datasets in both the LightGBM and CatBoost models but is inconsistent in the RF model. This implies that the ML approaches employed in this study can effectively work with very limited training datasets with a slight decrease in accuracy, which will be applicable for ungauged regions with deficient monitoring and observations of flooding occurrences and impacts. The FSMs developed based on different training datasets show that most spatial maps are acceptable as overall spatial coverage;

however, there are some small spatial differences in the susceptibility flooding levels (Figs. 14 and 15). For instance, all datasets (1250, 1000, 800, 600, 400, 90, 60, and 30) except for the dataset of 200 had almost the same percentage of impacted regions (Figs. 14 and 15) in the category of extremely high flood susceptibility. On the other hand, the affected areas by the high flood susceptibility level also vary. Still, the highest percentage was 9% for the 200 and 60 datasets, and the lowest was 6% for 30, 90, 600, and 800 datasets. The variation in moderate flood occurrence ranged from 17% to 9%. The dataset size of 30 was the highest among the others, about 17%. The range of the low flood susceptibility category was highly variable, from 20% to 41%, the lowest was for the dataset of 30, and the highest was for the dataset of 800. The reasons for such variation are probably the random selection of the flooded samples, which in some cases are not representative of all the influencing factors. We noticed that the spatial coverage was not extremely different, but some differences were observed based on the categories. The areas with no flood levels are also changeable by about 42%, 42%, 38%, 45%, 44%, 45%, 42%, 44%, and 51% for the datasets of 1250, 1000, 800, 600, 400, 200, 90, 60, and 30, respectively. Interestingly, the highest percentage was recorded by the dataset of 30 points and the lowest by dataset 800. The analysis of different data sizes for ML training shows that ML can effectively predict the flood susceptibility maps in the study area regardless of the number of samples, with the condition of the used data being observational flooded sites.

Fig. 12.

Fig. 13.

Fig. 14.

Fig. 15.

4.5. *Discussion and comparison with results of the RRI model*

The flood risk assessment scientific community is endeavoring to develop much more logical and mathematical methods for FSM forecasting at different catchment scales (Arora et al. 2020). Some previous studies on flood susceptibility mapping use ML approaches and deep learning in the study area. Testing many models is therefore strongly advised, especially in areas with little data and complex hydrological models. This study applies three ML methods: LightGBM, CatBoost and RF. The LightGBM and CatBoost techniques were put to the test for the first time for mapping flood susceptibility in this humid area with a high frequency of typhoon occurrences. Compared to the commonly used RF approach, the findings of the flooding susceptibility maps show that the two methods can forecast flood-prone regions with respectable accuracy. AUC = 78 percent (Band et al. 2020), 99.3 percent (Li et al., 2019), 94.5 percent (Talukdar et al., 2020), 93.8 percent (Park and Lee, 2020), and 89.4 percent (Talukdar et al., 2020) use RFs in several additional related research with varying degrees of accuracy (Nguyen et al., 2018). Compared to earlier research, the AUC = 99 percent for RF in this study was greater.

Additionally, the newly applied methods of LightGBM and CatBoost showed almost the same accuracy of 99% and 98%, respectively, revealing better performance than most previous studies. These three methods have been tested in Hurghada, Egypt (Saber et al. 2021), stating that LightGBM has the advantage of better classification metrics and fast

processing time and outperforms other methodologies such as CatBoost and RF. In addition, their results showed that LightGBM and CatBoost had proven their efficiency in flash flood prediction in arid regions (Saber et al. 2021).

The three techniques also outperformed the 90 percent average performance of previously used methods for mapping flood susceptibility, which was based on an average of about 140 prior applications from more than 30 papers that have been analyzed. Based on AUC, the effectiveness of the prior techniques used for FSM ranges from 64 percent (Shafizadeh-Moghadam et al. 2018) to 99.3 percent (Li et al. 2019). CatBoost was also applied in Germany, with better performance than other methods, showing good accuracy with an AUC of 0.816 (Kaiser, M. H. E. (2021)).

The maps of flood susceptibility developed using ML techniques (Fig. 10) showed an acceptable fit with the generated flood inundation map by the RRI model, showing that the ML approaches are promising for flood prediction and can be used without detailed observations and challenges of model calibrations as alternative tools for hydrological models. The results of LightGBM and CatBoost are more comparable to the flood inundation map developed by the physical RRI model, indicating that they are more acceptable than RF, which overestimates the low flood susceptibility level in the study area.

Furthermore, we tested different datasets for training the three ML models, concluding that datasets more than 90 points can be sufficiently accurate for reasonable prediction of the FSM. LightGBM and CatBoost showed a slightly declining trend in the accuracy of the

results based on the dataset sizes; however, RF did not show such a trend. These results are precious for applying ML to ungauged basins with very limited datasets.

5. Conclusions

Flooding resulting from typhoons is one of the most threatening disasters in Asian countries and worldwide. Therefore, the present study introduced three ML methods to accurately predict flooding susceptibility in Vietnamese humid areas. The first method is RF, which is well known and widely applicable in many applications, including FSM, and the other methods of LightGBM and CatBoost were examined for the first time for FSM in this humid region. On the basis of a flood inventory map and ten flood-influencing factors, the models were trained and validated. Owing to the availability of high-quality observations, we also tested different datasets for the training (i.e., 30, 60, 90, 200, 400, 600, 800, 1000, and 1250 data points) to determine the minor data points that provided acceptable reliability, as well as to understand the differences in the spatial FSMs in the study area.

Interestingly, we found that the accuracy of results based on all the tested datasets was higher than 90%, indicating that a limited number of observations can be used efficiently in model accuracy. However, the final FSMs differed spatially from one susceptibility level to the others. This finding is significant to demonstrate that ML methods can work efficiently with an acceptable level of accuracy within a small number of actual training datasets. The conclusions of this study can be summarized as follows:

- We applied three ML models—RF, LightGBM, and CatBoost—to predict flood susceptibility in humid areas that experienced successive extreme typhoons.
- The LightGBM and CatBoost models were tested for the first time in this specific climatic region and showed high performance compared to the RF method.
- The results of the ML methods showed good agreement with the rainfall-runoff model for flood inundation mapping, especially the LightGBM and CatBoost models in terms of coverage areas of the flood susceptibility levels.
- Different training datasets were examined to determine ML's lowest acceptable number of observations for flooding susceptibility.
- The FSMs demonstrated that downstream areas with high residential and agricultural activity are highly susceptible to flooding.
- These results might be utilized as a guide and reference for flood risk reduction and management in this region, therefore assisting managers, decision-makers, and planners in successfully managing and reducing floods in high-risk flood zones.

The study concludes that the ML approach can effectively predict flood susceptibility with an acceptable agreement with hydrological models in flood mapping. An extension of this research is ongoing to predict the flood depth using machine learning and physical-based hydrological models.

6. Conflict of Interest

The authors declare that they have no known competing financial interests or personal relationships that could have influenced the work presented in this study.

7. Funding:

This work was funded by the Asia-Pacific Network for Global Change Research (APN) under project reference number CRRP2020-09MYKantoush (Funder ID: <https://doi.org/10.13039/100005536>).

8. Acknowledgment:

Data sources include the Geospatial Information Authority of Japan at Chiba University and collaborating organizations.

The Ministry of Higher Education of the Arab Republic of Egypt for providing a full scholarship to the author Karim Abdrabo

9. Data availability statement

The data used in this study are available from the corresponding author, Mohamed Saber, upon reasonable request.

10. References

Abdel-Fattah M, Kantoush SA, Saber M, Sumi T. 2018. Rainfall-runoff modeling for extreme flash floods in wadi samail, oman. *J Jpn Soc Civ Eng Ser B1 Hydraul Eng.* 74(5):I_691-I_696.

Abdrabo KI, Kantosh SA, Saber M, Sumi T, Elleithy D, Habiba OM, Alboshy B. 2022. The Role of Urban Planning and Landscape Tools Concerning Flash Flood Risk Reduction Within Arid and Semiarid Regions. In: *Wadi Flash Floods*. [place unknown]: Springer; p. 283–316.

Abdrabo KI, Kantoush SA, Saber M, Sumi T, Habiba OM, Elleithy D, Elboshy B. 2020. Integrated Methodology for Urban Flood Risk Mapping at the Microscale in Ungauged Regions: A Case Study of Hurgada, Egypt. *Remote Sens.* 12(21):3548. <https://doi.org/10.3390/rs12213548>

- Abdrabo KI, Saber M, Kantoush SA, ElGharbawi T, Sumi T, Elboshy B. 2022. Applications of Remote Sensing for Flood Inundation Mapping at Urban Areas in MENA Region: Case Studies of Five Egyptian Cities. In: *Appl Space Tech Nat Hazards MENA Reg.* [place unknown]: Springer; p. 307–330.
- Abushandi EH, Merkel BJ. 2011. Application of IHACRES rainfall-runoff model to the Wadi Dhuliel arid catchment, Jordan. *J Water Clim Change.* 2(1):56–71.
- Akay AE, Taş İ. 2020. Mapping the risk of winter storm damage using GIS-based fuzzy logic. *J For Res.* 31(3):729–742.
- Ali SA, Parvin F, Pham QB, Vojtek M, Vojteková J, Costache R, Linh NTT, Nguyen HQ, Ahmad A, Ghorbani MA. 2020. GIS-based comparative assessment of flood susceptibility mapping using hybrid multi-criteria decision-making approach, naïve Bayes tree, bivariate statistics and logistic regression: A case of Topľa basin, Slovakia. *Ecol Indic.* 117:106620.
- Arabameri A, Saha S, Mukherjee K, Blaschke T, Chen W, Ngo PTT, Band SS. 2020. Modeling Spatial Flood using Novel Ensemble Artificial Intelligence Approaches in Northern Iran. *Remote Sens* [Internet]. [accessed 2020 Dec 11] 12(20):3423. <https://doi.org/10.3390/rs12203423>
- Arora A, Arabameri A, Pandey M, Siddiqui MA, Shukla UK, Bui DT, Mishra VN, Bhardwaj A. 2020. Optimization of state-of-the-art fuzzy-metaheuristic ANFIS-based machine learning models for flood susceptibility prediction mapping in the Middle Ganga Plain, India. *Sci Total Environ* [Internet]. [accessed 2020 Dec 11] 750:141565. <https://doi.org/10.1016/j.scitotenv.2020.141565>
- Arora A, Pandey M, Siddiqui MA, Hong H, Mishra VN. 2019. Spatial flood susceptibility prediction in Middle Ganga Plain: comparison of frequency ratio and Shannon’s entropy models. *Geocarto Int.*:1–32.
- Aryal SK, Mein RG, O’Loughlin EM. 2003. The concept of effective length in hillslopes: assessing the influence of climate and topography on the contributing areas of catchments. *Hydrol Process.* 17(1):131–151.
- Avitabile V, Schultz M, Herold N, De Bruin S, Pratihast AK, Manh CP, Quang HV, Herold M. 2016. Carbon emissions from land cover change in Central Vietnam. *Carbon Manag.* 7(5–6):333–346.
- Bachmair S, Svensson C, Prosdocimi I, Hannaford J, Stahl K. 2017. Developing drought impact functions for drought risk management. *Nat Hazards Earth Syst Sci.* 17(11):1947–1960.
- Band SS, Janizadeh S, Chandra Pal S, Saha A, Chakraborty R, Melesse AM, Mosavi A. 2020. Flash Flood Susceptibility Modeling Using New Approaches of Hybrid and Ensemble Tree-Based Machine Learning Algorithms. *Remote Sens* [Internet]. [accessed 2020 Dec 11] 12(21):3568. <https://doi.org/10.3390/rs12213568>

- Bisht S, Chaudhry S, Sharma S, Soni S. 2018. Assessment of flash flood vulnerability zonation through Geospatial technique in high altitude Himalayan watershed, Himachal Pradesh India. *Remote Sens Appl Soc Environ.* 12:35–47.
- Breiman L. 2001. Random forests. *Mach Learn.* 45(1):5–32.
- Bui DT, Hoang N-D, Pham T-D, Ngo P-TT, Hoa PV, Minh NQ, Tran X-T, Samui P. 2019. A new intelligence approach based on GIS-based multivariate adaptive regression splines and metaheuristic optimization for predicting flash flood susceptible areas at high-frequency tropical typhoon area. *J Hydrol.* 575:314–326.
- Bui DT, Ngo P-TT, Pham TD, Jaafari A, Minh NQ, Hoa PV, Samui P. 2019. A novel hybrid approach based on a swarm intelligence optimized extreme learning machine for flash flood susceptibility mapping. *CATENA* [Internet]. [accessed 2021 Nov 24] 179:184–196. <https://doi.org/10.1016/j.catena.2019.04.009>
- Bui DT, Panahi M, Shahabi H, Singh VP, Shirzadi A, Chapi K, Khosravi K, Chen W, Panahi S, Li S. 2018. Novel hybrid evolutionary algorithms for spatial prediction of floods. *Sci Rep.* 8(1):1–14.
- Bui DT, Pradhan B, Lofman O, Revhaug I, Dick OB. 2012. Spatial prediction of landslide hazards in Hoa Binh province (Vietnam): a comparative assessment of the efficacy of evidential belief functions and fuzzy logic models. *Catena.* 96:28–40.
- Bui Q-T, Nguyen Q-H, Nguyen XL, Pham VD, Nguyen HD, Pham V-M. 2020. Verification of novel integrations of swarm intelligence algorithms into deep learning neural network for flood susceptibility mapping. *J Hydrol* [Internet]. [accessed 2021 Nov 24] 581:124379. <https://doi.org/10.1016/j.jhydrol.2019.124379>
- Cardenas MB, Wilson J, Zlotnik VA. 2004. Impact of heterogeneity, bed forms, and stream curvature on subchannel hyporheic exchange. *Water Resour Res.* 40(8).
- Catal C, Diri B. 2009. Investigating the effect of dataset size, metrics sets, and feature selection techniques on software fault prediction problem. *Inf Sci.* 179(8):1040–1058.
- Chang M-J, Chang H-K, Chen Y-C, Lin G-F, Chen P-A, Lai J-S, Tan Y-C. 2018. A support vector machine forecasting model for typhoon flood inundation mapping and early flood warning systems. *Water.* 10(12):1734.
- Chapi K, Singh VP, Shirzadi A, Shahabi H, Bui DT, Pham BT, Khosravi K. 2017. A novel hybrid artificial intelligence approach for flood susceptibility assessment. *Environ Model Softw.* 95:229–245.
- Chen T-HK, Qiu C, Schmitt M, Zhu XX, Sabel CE, Prishchepov AV. 2020. Mapping horizontal and vertical urban densification in Denmark with Landsat time-series from 1985 to 2018: A semantic segmentation solution. *Remote Sens Environ* [Internet]. [accessed 2020 Oct 21] 251:112096. <https://doi.org/10.1016/j.rse.2020.112096>

- Choubin B, Moradi E, Golshan M, Adamowski J, Sajedi-Hosseini F, Mosavi A. 2019. An ensemble prediction of flood susceptibility using multivariate discriminant analysis, classification and regression trees, and support vector machines. *Sci Total Environ.* 651:2087–2096.
- Costache R, Hong H, Pham QB. 2020. Comparative assessment of the flash-flood potential within small mountain catchments using bivariate statistics and their novel hybrid integration with machine learning models. *Sci Total Environ* [Internet]. [accessed 2020 Dec 11] 711:134514. <https://doi.org/10.1016/j.scitotenv.2019.134514>
- Costache R, Popa MC, Tien Bui D, Diaconu DC, Ciubotaru N, Minea G, Pham QB. 2020. Spatial predicting of flood potential areas using novel hybridizations of fuzzy decision-making, bivariate statistics, and machine learning. *J Hydrol* [Internet]. [accessed 2020 Dec 11] 585:124808. <https://doi.org/10.1016/j.jhydrol.2020.124808>
- Darabi H, Choubin B, Rahmati O, Haghghi AT, Pradhan B, Kløve B. 2019. Urban flood risk mapping using the GARP and QUEST models: A comparative study of machine learning techniques. *J Hydrol.* 569:142–154.
- Demirel MC, Venancio A, Kahya E. 2009. Flow forecast by SWAT model and ANN in Pracana basin, Portugal. *Adv Eng Softw.* 40(7):467–473.
- Devkota KC, Regmi AD, Pourghasemi HR, Yoshida K, Pradhan B, Ryu IC, Dhital MR, Althuwaynee OF. 2013. Landslide susceptibility mapping using certainty factor, index of entropy and logistic regression models in GIS and their comparison at Mugling–Narayanghat road section in Nepal Himalaya. *Nat Hazards.* 65(1):135–165.
- Dhara S, Dang T, Parial K, Lu XX. 2020. Accounting for Uncertainty and Reconstruction of Flooding Patterns Based on Multi-Satellite Imagery and Support Vector Machine Technique: A Case Study of Can Tho City, Vietnam. *Water* [Internet]. [accessed 2021 Nov 24] 12(6):1543. <https://doi.org/10.3390/w12061543>
- Dodangeh E, Choubin B, Eigdir AN, Nabipour N, Panahi M, Shamsirband S, Mosavi A. 2020. Integrated machine learning methods with resampling algorithms for flood susceptibility prediction. *Sci Total Environ* [Internet]. [accessed 2020 Dec 11] 705:135983. <https://doi.org/10.1016/j.scitotenv.2019.135983>
- Dorogush AV, Ershov V, Gulin A. 2018. CatBoost: gradient boosting with categorical features support. *ArXiv Prepr ArXiv181011363.*
- Dou J, Yunus AP, Bui DT, Merghadi A, Sahana M, Zhu Z, Chen C-W, Khosravi K, Yang Y, Pham BT. 2019. Assessment of advanced random forest and decision tree algorithms for modeling rainfall-induced landslide susceptibility in the Izu-Oshima Volcanic Island, Japan. *Sci Total Environ.* 662:332–346.

- Esfandiari M, Jabari S, McGrath H, Coleman D. 2020. FLOOD MAPPING USING RANDOM FOREST AND IDENTIFYING THE ESSENTIAL CONDITIONING FACTORS; A CASE STUDY IN FREDERICTON, NEW BRUNSWICK, CANADA. *ISPRS Ann Photogramm Remote Sens Spat Inf Sci.* 5(3).
- Esmail A, Abdrabo KI, Saber M, Sliuzas RV, Atun F, Kantoush SA, Sumi T. 2022. Integration of flood risk assessment and spatial planning for disaster management in Egypt. *Prog Disaster Sci [Internet].*:100245. <https://doi.org/10.1016/j.pdisas.2022.100245>
- Fenicia F, Kavetski D, Savenije HH, Clark MP, Schoups G, Pfister L, Freer J. 2014. Catchment properties, function, and conceptual model representation: is there a correspondence? *Hydrol Process.* 28(4):2451–2467.
- Gigović L, Pamučar D, Bajić Z, Drobniak S. 2017. Application of GIS-interval rough AHP methodology for flood hazard mapping in urban areas. *Water.* 9(6):360.
- Glenn EP, Morino K, Nagler PL, Murray RS, Pearlstein S, Hultine KR. 2012. Roles of saltcedar (*Tamarix* spp.) and capillary rise in salinizing a non-flooding terrace on a flow-regulated desert river. *J Arid Environ.* 79:56–65.
- González-Arqueros ML, Mendoza ME, Bocco G, Castillo BS. 2018. Flood susceptibility in rural settlements in remote zones: The case of a mountainous basin in the Sierra-Costa region of Michoacán, Mexico. *J Environ Manage.* 223:685–693.
- Hirabayashi Y, Mahendran R, Koirala S, Konoshima L, Yamazaki D, Watanabe S, Kim H, Kanae S. 2013. Global flood risk under climate change. *Nat Clim Change.* 3(9):816–821.
- Hölting B, Coldewey WG. 2019. Surface water infiltration. In: *Hydrogeology.* [place unknown]: Springer; p. 33–37.
- Hong H, Tsangaratos P, Ilia I, Liu J, Zhu A-X, Chen W. 2018. Application of fuzzy weight of evidence and data mining techniques in construction of flood susceptibility map of Poyang County, China. *Sci Total Environ.* 625:575–588.
- Hsu K, Gupta HV, Sorooshian S. 1995. Artificial neural network modeling of the rainfall-runoff process. *Water Resour Res.* 31(10):2517–2530.
- Humphrey GB, Gibbs MS, Dandy GC, Maier HR. 2016. A hybrid approach to monthly streamflow forecasting: integrating hydrological model outputs into a Bayesian artificial neural network. *J Hydrol.* 540:623–640.
- Izquierdo-Verdiguier E, Zurita-Milla R. 2020. An evaluation of Guided Regularized Random Forest for classification and regression tasks in remote sensing. *Int J Appl Earth Obs Geoinformation.* 88:102051.
- Ke G, Meng Q, Finley T, Wang T, Chen W, Ma W, Ye Q, Liu T-Y. 2017. Lightgbm: A highly efficient gradient boosting decision tree. *Adv Neural Inf Process Syst.* 30:3146–3154.

- Khosravi K, Nohani E, Maroufinia E, Pourghasemi HR. 2016. A GIS-based flood susceptibility assessment and its mapping in Iran: a comparison between frequency ratio and weights-of-evidence bivariate statistical models with multi-criteria decision-making technique. *Nat Hazards*. 83(2):947–987.
- Khosravi K, Shahabi H, Pham BT, Adamowski J, Shirzadi A, Pradhan B, Dou J, Ly H-B, Gróf G, Ho HL, et al. 2019. A comparative assessment of flood susceptibility modeling using Multi-Criteria Decision-Making Analysis and Machine Learning Methods. *J Hydrol [Internet]*. [accessed 2020 Dec 11] 573:311–323. <https://doi.org/10.1016/j.jhydrol.2019.03.073>
- Kia MB, Pirasteh S, Pradhan B, Mahmud AR, Sulaiman WNA, Moradi A. 2012. An artificial neural network model for flood simulation using GIS: Johor River Basin, Malaysia. *Environ Earth Sci*. 67(1):251–264.
- Kratzert F, Klotz D, Shalev G, Klambauer G, Hochreiter S, Nearing G. 2019. Benchmarking a catchment-aware long short-term memory network (LSTM) for large-scale hydrological modeling. *Hydrol Earth Syst Sci Discuss.*:1–32.
- Li X, Yan D, Wang K, Weng B, Qin T, Liu S. 2019. Flood Risk Assessment of Global Watersheds Based on Multiple Machine Learning Models. *Water [Internet]*. [accessed 2020 Dec 11] 11(8):1654. <https://doi.org/10.3390/w11081654>
- Luu C, Pham BT, Phong TV, Costache R, Nguyen HD, Amiri M, Bui QD, Nguyen LT, Le HV, Prakash I, Trinh PT. 2021. GIS-based ensemble computational models for flood susceptibility prediction in the Quang Binh Province, Vietnam. *J Hydrol [Internet]*. [accessed 2021 Nov 24] 599:126500. <https://doi.org/10.1016/j.jhydrol.2021.126500>
- Malekipirbazari M, Aksakalli V. 2015. Risk assessment in social lending via random forests. *Expert Syst Appl*. 42(10):4621–4631.
- Masood M, Takeuchi K. 2012. Assessment of flood hazard, vulnerability and risk of mid-eastern Dhaka using DEM and 1D hydrodynamic model. *Nat Hazards*. 61(2):757–770.
- Meadows M, Wilson M. 2021. A Comparison of Machine Learning Approaches to Improve Free Topography Data for Flood Modelling. *Remote Sens*. 13(2):275.
- Meraj G, Khan T, Romshoo SA, Farooq M, Rohitashw K, Sheikh BA. 2018. An integrated geoinformatics and hydrological modelling-based approach for effective flood management in the Jhelum Basin, NW Himalaya. *Multidiscip Digit Publ Inst Proc*. 7(1):8.
- Nauditt A, Firoz ABM, Trinh VQ, Fink M, Stolpe H, Ribbe L. 2017. Hydrological drought risk assessment in an anthropogenically impacted tropical catchment, Central Vietnam. In: *Land Use Clim Change Interact Cent Vietnam*. [place unknown]: Springer; p. 223–239.
- Nauditt A, Ribbe L. 2017. Land use and climate change interactions in central Vietnam. [place unknown]: Springer.

Ngo P-TT, Pham TD, Hoang N-D, Tran DA, Amiri M, Le TT, Hoa PV, Bui PV, Nhu V-H, Bui DT. 2021. A new hybrid equilibrium optimized SysFor based geospatial data mining for tropical storm-induced flash flood susceptible mapping. *J Environ Manage* [Internet]. [accessed 2021 Nov 24] 280:111858. <https://doi.org/10.1016/j.jenvman.2020.111858>

Nguyen HQ, Degener J, Kappas M. 2015. Flash flood prediction by coupling KINEROS2 and HEC-RAS models for tropical regions of Northern Vietnam. *Hydrology*. 2(4):242–265.

Nguyen P, Ombadi M, Gorooh VA, Shearer EJ, Sadeghi M, Sorooshian S, Hsu K, Bolvin D, Ralph MF. 2020. PERSIANN Dynamic Infrared–Rain Rate (PDIR-Now): A Near-Real-Time, Quasi-Global Satellite Precipitation Dataset. *J Hydrometeorol*. 21(12):2893–2906.

Nguyen V-N, Tien Bui D, Ngo P-TT, Nguyen Q-P, Nguyen VC, Long NQ, Revhaug I. 2018. An Integration of Least Squares Support Vector Machines and Firefly Optimization Algorithm for Flood Susceptible Modeling Using GIS. In: Tien Bui D, Ngoc Do A, Bui H-B, Hoang N-D, editors. *Adv Appl Geospatial Technol Earth Resour* [Internet]. Cham: Springer International Publishing; [accessed 2020 Dec 11]; p. 52–64. https://doi.org/10.1007/978-3-319-68240-2_4

Nguyen V-N, Yariyan P, Amiri M, Dang Tran A, Pham TD, Do MP, Thi Ngo PT, Nhu V-H, Quoc Long N, Tien Bui D. 2020. A New Modeling Approach for Spatial Prediction of Flash Flood with Biogeography Optimized CHAID Tree Ensemble and Remote Sensing Data. *Remote Sens* [Internet]. [accessed 2021 Nov 24] 12(9):1373. <https://doi.org/10.3390/rs12091373>

Nhu V-H, Thi Ngo P-T, Pham TD, Dou J, Song X, Hoang N-D, Tran DA, Cao DP, Aydilek İB, Amiri M, et al. 2020. A New Hybrid Firefly–PSO Optimized Random Subspace Tree Intelligence for Torrential Rainfall-Induced Flash Flood Susceptible Mapping. *Remote Sens* [Internet]. [accessed 2021 Nov 24] 12(17):2688. <https://doi.org/10.3390/rs12172688>

Osman T, Kenawy E, Abdrabo KI, Shaw D, Alshamndy A, Elsharif M, Salem M, Alwetaishi M, Aly RM, Elboshy B. 2021. Voluntary Local Review Framework to Monitor and Evaluate the Progress towards Achieving Sustainable Development Goals at a City Level: Buraidah City, KSA and SDG11 as A Case Study. *Sustainability*. 13(17):9555.

Öztürk F, Akdeniz F. 2000. Ill-conditioning and multicollinearity. *Linear Algebra Its Appl*. 321(1–3):295–305.

Pachauri RK, Allen MR, Barros VR, Broome J, Cramer W, Christ R, Church JA, Clarke L, Dahe Q, Dasgupta P. 2014. *Climate change 2014: synthesis report. Contribution of Working Groups I, II and III to the fifth assessment report of the Intergovernmental Panel on Climate Change*. [place unknown]: Ipcc.

Pal M. 2005. Random forest classifier for remote sensing classification. *Int J Remote Sens*. 26(1):217–222.

- Park S-J, Lee D-K. 2020. Prediction of coastal flooding risk under climate change impacts in South Korea using machine learning algorithms. *Environ Res Lett* [Internet]. [accessed 2020 Dec 11] 15(9):094052. <https://doi.org/10.1088/1748-9326/aba5b3>
- Perera EDP, Sayama T, Magome J, Hasegawa A, Iwami Y. 2017. RCP8. 5-based future flood hazard analysis for the lower Mekong river basin. *Hydrology*. 4(4):55.
- Pham BT, Jaafari A, Nguyen-Thoi T, Van Phong T, Nguyen HD, Satyam N, Masroor M, Rehman S, Sajjad H, Sahana M. 2021. Ensemble machine learning models based on Reduced Error Pruning Tree for prediction of rainfall-induced landslides. *Int J Digit Earth*. 14(5):575–596.
- Pham BT, Luu C, Phong TV, Trinh PT, Shirzadi A, Renoud S, Asadi S, Le HV, von Meding J, Clague JJ. 2021. Can deep learning algorithms outperform benchmark machine learning algorithms in flood susceptibility modeling? *J Hydrol* [Internet]. [accessed 2021 Nov 24] 592:125615. <https://doi.org/10.1016/j.jhydrol.2020.125615>
- Pham TD, Xia J, Ha NT, Bui DT, Le NN, Tekeuchi W. 2019. A review of remote sensing approaches for monitoring blue carbon ecosystems: Mangroves, seagrasses and salt marshes during 2010–2018. *Sensors*. 19(8):1933.
- Pourghasemi HR, Kariminejad N, Amiri M, Edalat M, Zarafshar M, Blaschke T, Cerda A. 2020. Assessing and mapping multi-hazard risk susceptibility using a machine learning technique. *Sci Rep*. 10(1):1–11.
- Predick KI, Turner MG. 2008. Landscape configuration and flood frequency influence invasive shrubs in floodplain forests of the Wisconsin River (USA). *J Ecol*. 96(1):91–102.
- Quinlan JR. 1986. Induction of decision trees. *Mach Learn*. 1(1):81–106.
- Rahman M, Ningsheng C, Islam MM, Dewan A, Iqbal J, Washakh RMA, Shufeng T. 2019. Flood susceptibility assessment in Bangladesh using machine learning and multi-criteria decision analysis. *Earth Syst Environ*. 3(3):585–601.
- Rahmati O, Pourghasemi HR, Zeinivand H. 2016. Flood susceptibility mapping using frequency ratio and weights-of-evidence models in the Golastan Province, Iran. *Geocarto Int*. 31(1):42–70.
- RETA. 2011. Investment, Managing water in Asia's river basins: Charting progress and facilitating - The Vu Gia-Thu Bon Basin. [place unknown].
- Saber M, Abdrabo KI, Habiba OM, Kantosh SA, Sumi T. 2020. Impacts of Triple Factors on Flash Flood Vulnerability in Egypt: Urban Growth, Extreme Climate, and Mismanagement. *Geosciences*. 10(1):24.
- Saber M, Boulmaiz T, Guermoui M, Abdrado KI, Kantoush SA, Sumi T, Boutaghane H, Nohara D, Mabrouk E. 2021. Examining LightGBM and CatBoost models for wadi flash flood susceptibility prediction. *Geocarto Int*.(just-accepted):1–27.

Saber M, Kantoush SA, Abdel-Fattah M, Sumi T, Moya JA, Abdrabo K. 2022. Flash Flood Modeling and Mitigation in Arid and Semiarid Basins: Case Studies from Oman and Brazil. In: Wadi Flash Floods. [place unknown]: Springer, Singapore; p. 355–381.

Schoppa L, Disse M, Bachmair S. 2020. Evaluating the performance of random forest for large-scale flood discharge simulation. *J Hydrol.* 590:125531.

Shafizadeh-Moghadam H, Valavi R, Shahabi H, Chapi K, Shirzadi A. 2018. Novel forecasting approaches using combination of machine learning and statistical models for flood susceptibility mapping. *J Environ Manage* [Internet]. [accessed 2020 Dec 11] 217:1–11. <https://doi.org/10.1016/j.jenvman.2018.03.089>

Shahabi H, Shirzadi A, Ronoud S, Asadi S, Pham BT, Mansouripour F, Geertsema M, Clague JJ, Bui DT. 2020. Flash flood susceptibility mapping using a novel deep learning model based on deep belief network, back propagation and genetic algorithm. *Geosci Front* [Internet]. [accessed 2020 Dec 11]:S1674987120302401. <https://doi.org/10.1016/j.gsf.2020.10.007>

Shirzadi A, Asadi S, Shahabi H, Ronoud S, Clague JJ, Khosravi K, Pham BT, Ahmad BB, Bui DT. 2020. A novel ensemble learning based on Bayesian Belief Network coupled with an extreme learning machine for flash flood susceptibility mapping. *Eng Appl Artif Intell.* 96:103971.

Talukdar S, Ghose B, Salam R, Mahato S, Pham QB, Linh NTT, Costache R, Avand M. 2020. Flood susceptibility modeling in Teesta River basin, Bangladesh using novel ensembles of bagging algorithms. *Stoch Environ Res Risk Assess.* 34(12):2277–2300.

Tam TH, Abd Rahman MZ, Harun S, Hanapi MN, Kaoje IU. 2019. Application of Satellite rainfall products for flood inundation modelling in Kelantan River Basin, Malaysia. *Hydrology.* 6(4):95.

Tehrany MS, Kumar L. 2018. The application of a Dempster–Shafer-based evidential belief function in flood susceptibility mapping and comparison with frequency ratio and logistic regression methods. *Environ Earth Sci.* 77(13):1–24.

Tehrany MS, Pradhan B, Jebur MN. 2013. Spatial prediction of flood susceptible areas using rule based decision tree (DT) and a novel ensemble bivariate and multivariate statistical models in GIS. *J Hydrol.* 504:69–79.

Tehrany MS, Pradhan B, Jebur MN. 2014. Flood susceptibility mapping using a novel ensemble weights-of-evidence and support vector machine models in GIS. *J Hydrol.* 512:332–343.

Tehrany MS, Pradhan B, Jebur MN. 2015. Flood susceptibility analysis and its verification using a novel ensemble support vector machine and frequency ratio method. *Stoch Environ Res Risk Assess.* 29(4):1149–1165.

Thao NTP, Linh TT, Ha NTT, Vinh PQ, Linh NT. 2020. Mapping flood inundation areas over the lower part of the Con River basin using Sentinel 1A imagery. *Vietnam J Earth Sci.* 42(3):288–297.

- Tien Bui D, Hoang N-D. 2017. A Bayesian framework based on a Gaussian mixture model and radial-basis-function Fisher discriminant analysis (BayGmmKda V1. 1) for spatial prediction of floods. *Geosci Model Dev.* 10(9):3391–3409.
- Tien Bui D, Hoang N-D, Martínez-Álvarez F, Ngo P-TT, Hoa PV, Pham TD, Samui P, Costache R. 2020. A novel deep learning neural network approach for predicting flash flood susceptibility: A case study at a high frequency tropical storm area. *Sci Total Environ* [Internet]. [accessed 2020 Dec 11] 701:134413. <https://doi.org/10.1016/j.scitotenv.2019.134413>
- Tien Bui D, Pradhan B, Nampak H, Bui Q-T, Tran Q-A, Nguyen Q-P. 2016. Hybrid artificial intelligence approach based on neural fuzzy inference model and metaheuristic optimization for flood susceptibility modeling in a high-frequency tropical cyclone area using GIS. *J Hydrol* [Internet]. [accessed 2020 Dec 11] 540:317–330. <https://doi.org/10.1016/j.jhydrol.2016.06.027>
- Tiwari MK, Chatterjee C. 2010. Uncertainty assessment and ensemble flood forecasting using bootstrap based artificial neural networks (BANNs). *J Hydrol.* 382(1–4):20–33.
- Torabi Haghighi A, Menberu MW, Darabi H, Akanegbu J, Kløve B. 2018. Use of remote sensing to analyse peatland changes after drainage for peat extraction. *Land Degrad Dev.* 29(10):3479–3488.
- Try S, Tanaka S, Tanaka K, Sayama T, Oeurng C, Uk S, Takara K, Hu M, Han D. 2020. Comparison of gridded precipitation datasets for rainfall-runoff and inundation modeling in the Mekong River Basin. *PLoS One.* 15(1):e0226814.
- Tuyen TT, Jaafari A, Yen HPH, Nguyen-Thoi T, Phong TV, Nguyen HD, Van Le H, Phuong TTM, Nguyen SH, Prakash I, Pham BT. 2021. Mapping forest fire susceptibility using spatially explicit ensemble models based on the locally weighted learning algorithm. *Ecol Inform* [Internet]. [accessed 2021 Nov 24] 63:101292. <https://doi.org/10.1016/j.ecoinf.2021.101292>
- Vinet F. 2008. Geographical analysis of damage due to flash floods in southern France: The cases of 12–13 November 1999 and 8–9 September 2002. *Appl Geogr.* 28(4):323–336. <https://doi.org/10.1016/j.apgeog.2008.02.007>
- Vu TTL, Nguyen LD, Hoang TS, Bui TA, Nguyen MT, Nguyen TH. 2011. Solutions for flood and drought prevention and mitigation in Quang Nam. [place unknown].
- Wang Y, Hong H, Chen W, Li S, Panahi M, Khosravi K, Shirzadi A, Shahabi H, Panahi S, Costache R. 2019. Flood susceptibility mapping in Dingnan County (China) using adaptive neuro-fuzzy inference system with biogeography based optimization and imperialistic competitive algorithm. *J Environ Manage.* 247:712–729.
- Xu Y, Dai Y, Dong ZY, Zhang R, Meng K. 2013. Extreme learning machine-based predictor for real-time frequency stability assessment of electric power systems. *Neural Comput Appl.* 22(3):501–508.

- Yamazaki D, Ikeshima D, Tawatari R, Yamaguchi T, O'Loughlin F, Neal JC, Sampson CC, Kanae S, Bates PD. 2017. A high-accuracy map of global terrain elevations. *Geophys Res Lett.* 44(11):5844–5853.
- Yang S, Yang D, Chen J, Santisirisomboon J, Lu W, Zhao B. 2020. A physical process and machine learning combined hydrological model for daily streamflow simulations of large watersheds with limited observation data. *J Hydrol.* 590:125206.
- Yariyan P, Janizadeh S, Van Phong T, Nguyen HD, Costache R, Van Le H, Pham BT, Pradhan B, Tiefenbacher JP. 2020. Improvement of best first decision trees using bagging and dagging ensembles for flood probability mapping. *Water Resour Manag.* 34(9):3037–3053.
- Youssef AM, Hegab MA. 2019. Flood-hazard assessment modeling using multicriteria analysis and GIS: a case study—Ras Gharib area, Egypt. In: *Spat Model GIS R Earth Environ Sci.* [place unknown]: Elsevier; p. 229–257.
- Youssef AM, Pradhan B, Sefry SA. 2016. Flash flood susceptibility assessment in Jeddah city (Kingdom of Saudi Arabia) using bivariate and multivariate statistical models. *Environ Earth Sci.* 75(1):12.
- Zahedi P, Parvande S, Asgharpour A, McLaury BS, Shirazi SA, McKinney BA. 2018. Random forest regression prediction of solid particle Erosion in elbows. *Powder Technol.* 338:983–992.
- Zenggang X, Zhiwen T, Xiaowen C, Xue-min Z, Kaibin Z, Conghuan Y. 2021. Research on image retrieval algorithm based on combination of color and shape features. *J Signal Process Syst.* 93(2):139–146.

List of Figures:

Fig. 1. Location of the river basin of VGTB: a) Vietnam Map, b) flood inventory dataset map for training and validation, (c) total annual precipitation of the entire basin, and (d) flooded and non-flooded locations.

Fig. 2. Number of deaths and property damage caused by storms and floods from 1997 to 2020 in the river basin of VGTB (source: Commanding Committee for Natural Disaster Prevention and Control, Search and Rescue in Quang Nam Province).

Fig. 3. Methodology flowchart for flood susceptibility mapping.

Fig. 4. Flood influencing factors: a) elevation, b) slope, c) aspect, d) plan curvature, e) hillshade, f) horizontal flow distance, g) rainfall, h) land use/land cover, i) SPI, j) geology.

Fig. 5. Split operation example based on histogram algorithm.

Fig. 6. Level-wise and leafwise tree growth strategies.

Fig. 7. Analysis of influencing factors: (a) VIF and (b) IGR for flood susceptibility.

Fig. 8. Performance of random forest, CatBoost, and LightGBM models based on AUC-ROC curves.

Fig. 9. Confusion matrix showing the performance of the used models in VGTB River Basin.

Fig. 10. Flood susceptibility maps by LightGBM (a), CatBoost (b), RF (c), and RRI (d), respectively, from top to bottom.

Fig. 11. Affected area of the flood susceptibility levels for the three applied ML methods and flood inundation map of RRI model.

Fig. 12. Datasets used in the training and testing of the ML models.

Fig. 13. Accuracy of the models based on different training datasets.

Fig. 14. Impact of data size on flood susceptibility map.

Fig. 15. Percentage of the affected areas under different flood susceptibility classes using different dataset sizes (RF method).

List of Tables:

Table 1. Spearman's correlation coefficients for flooding susceptibility mapping.

Table 2. Parameter values of random forest, CatBoost, and LightGBM models.

Table 3. Statistical parameters used for the model performance evaluation.

Figure 1

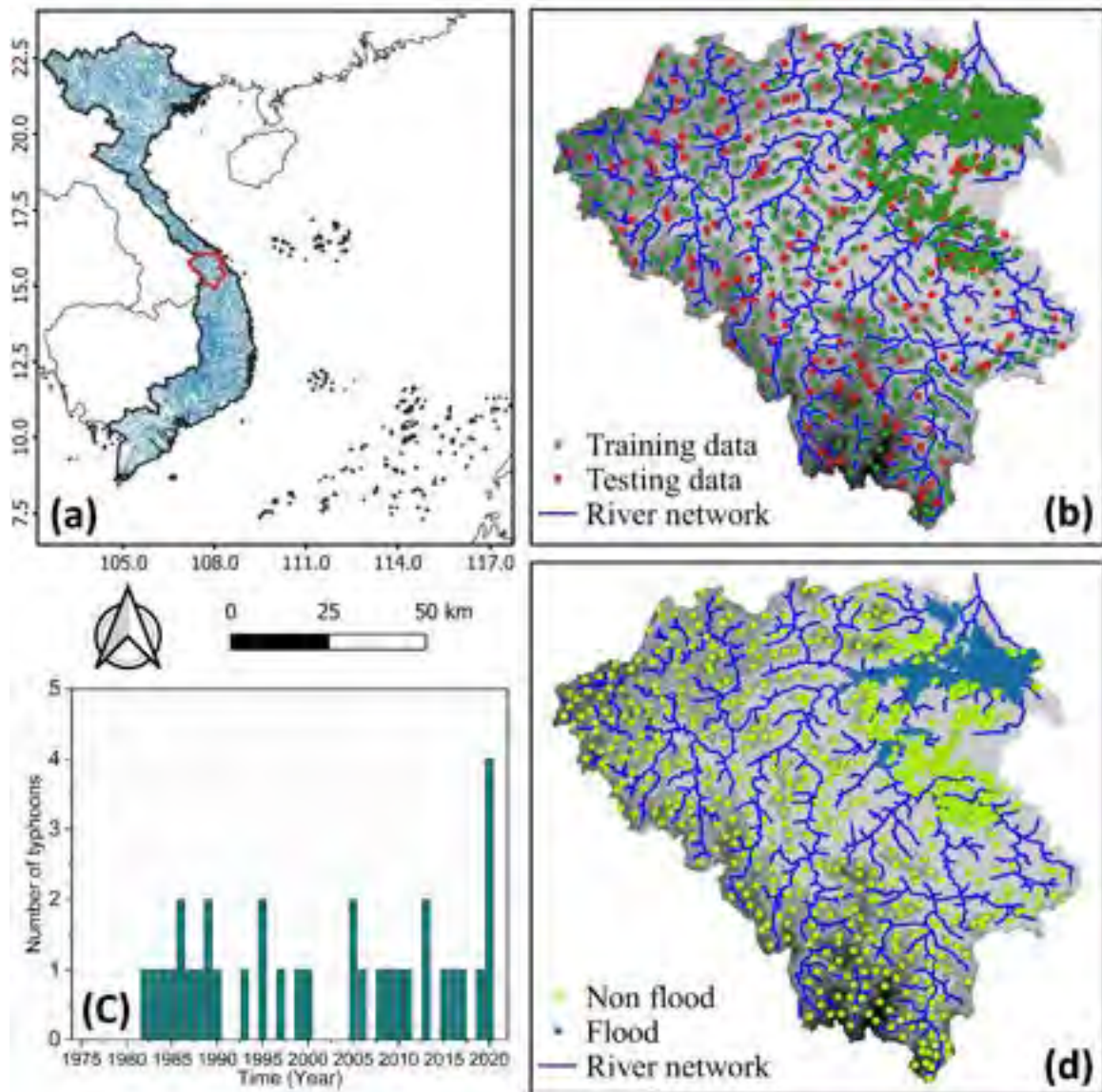


Figure 2

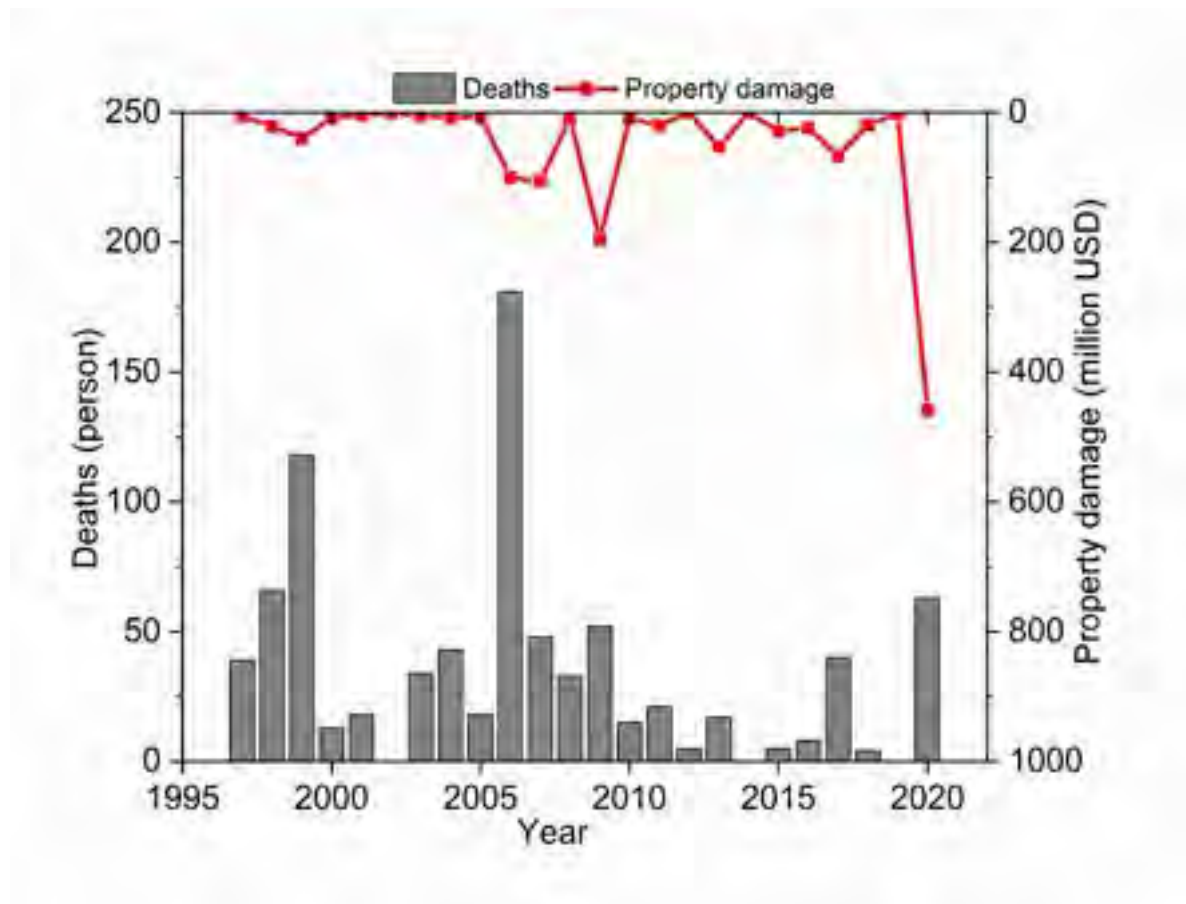


Figure 3

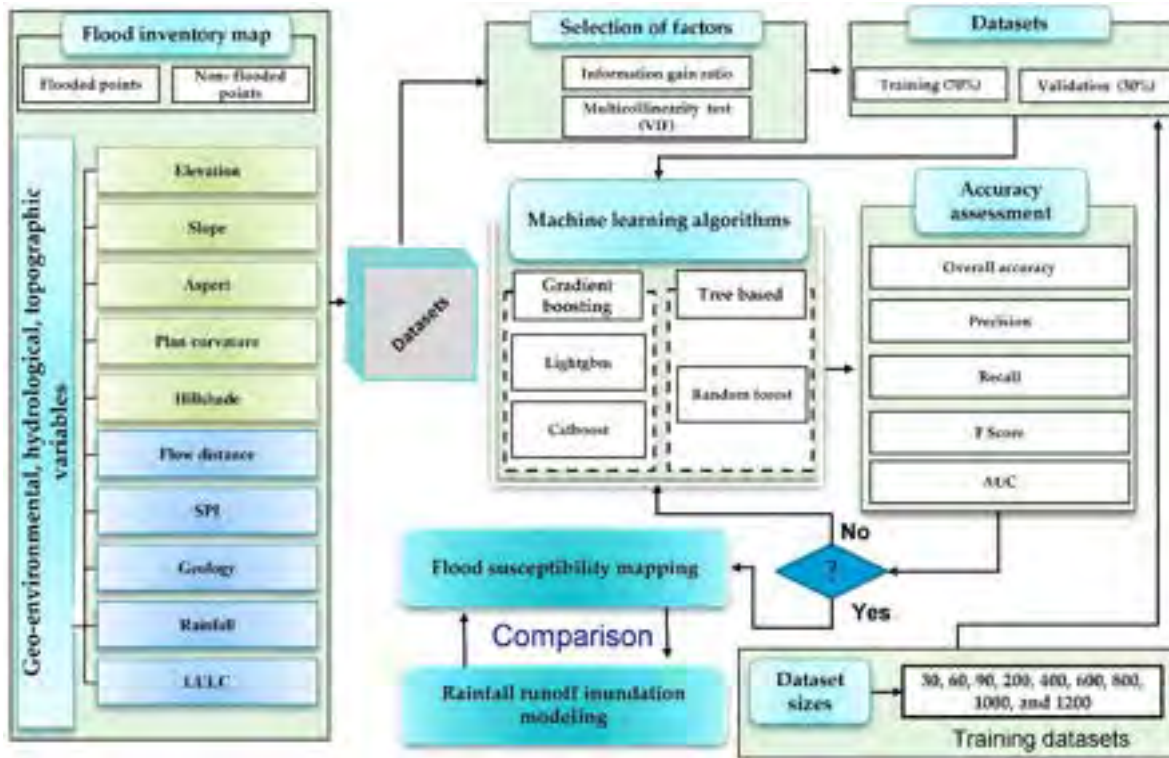


Figure 4

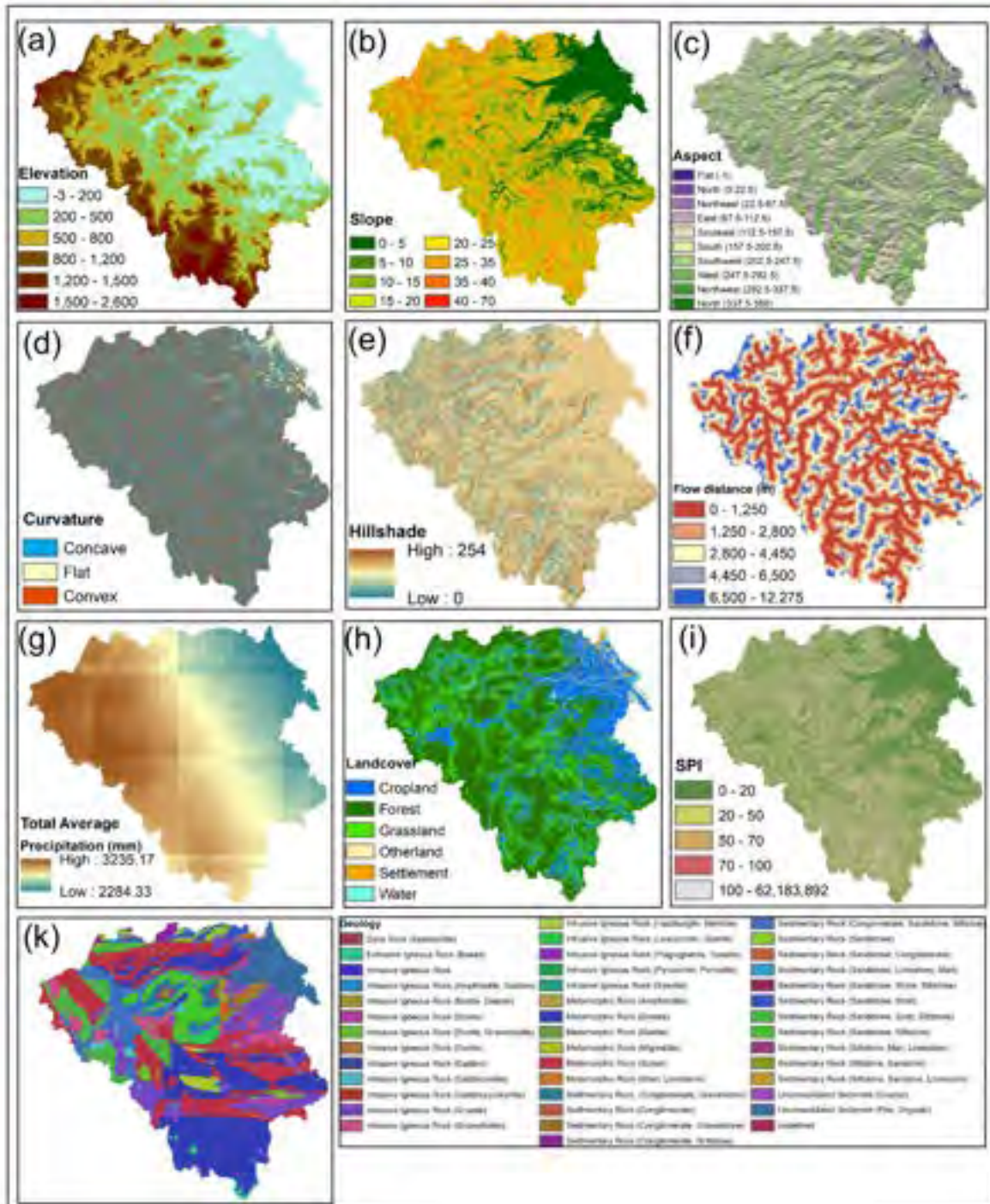
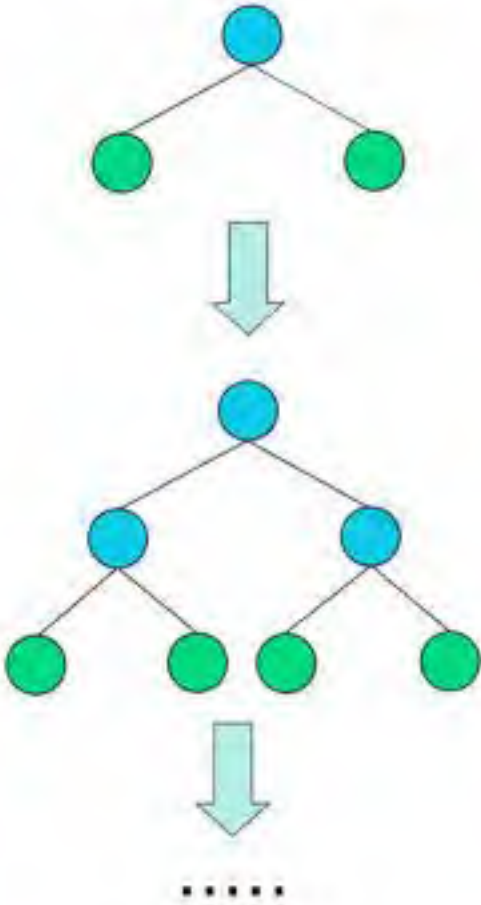


Figure 6

Level-wise tree growth



Leafwise tree growth

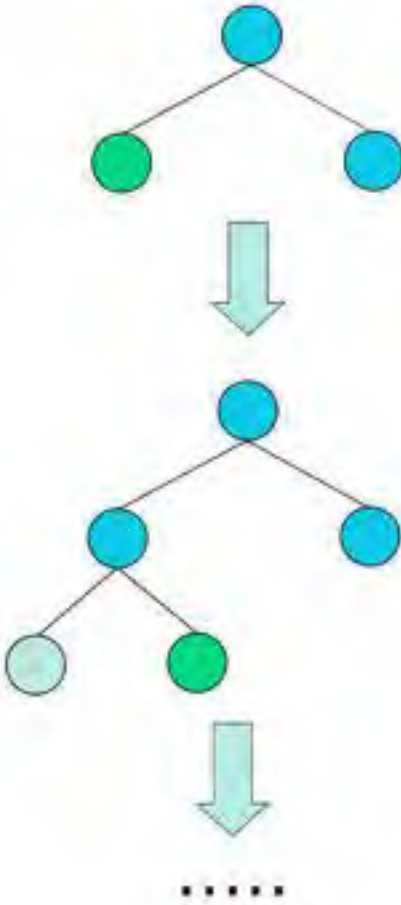


Figure 7

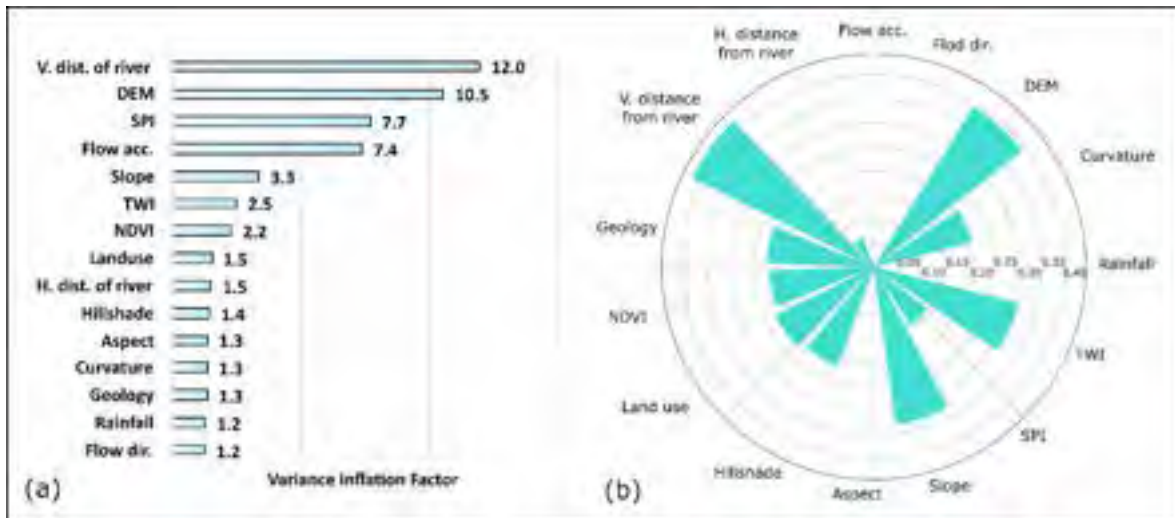


Figure 8

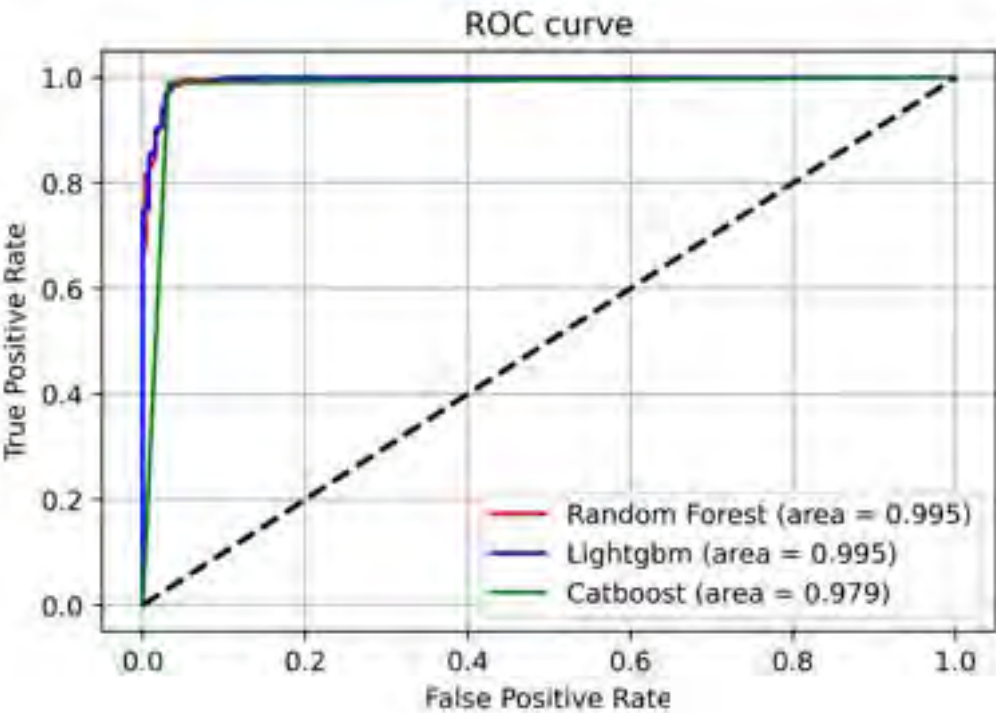


Figure 9

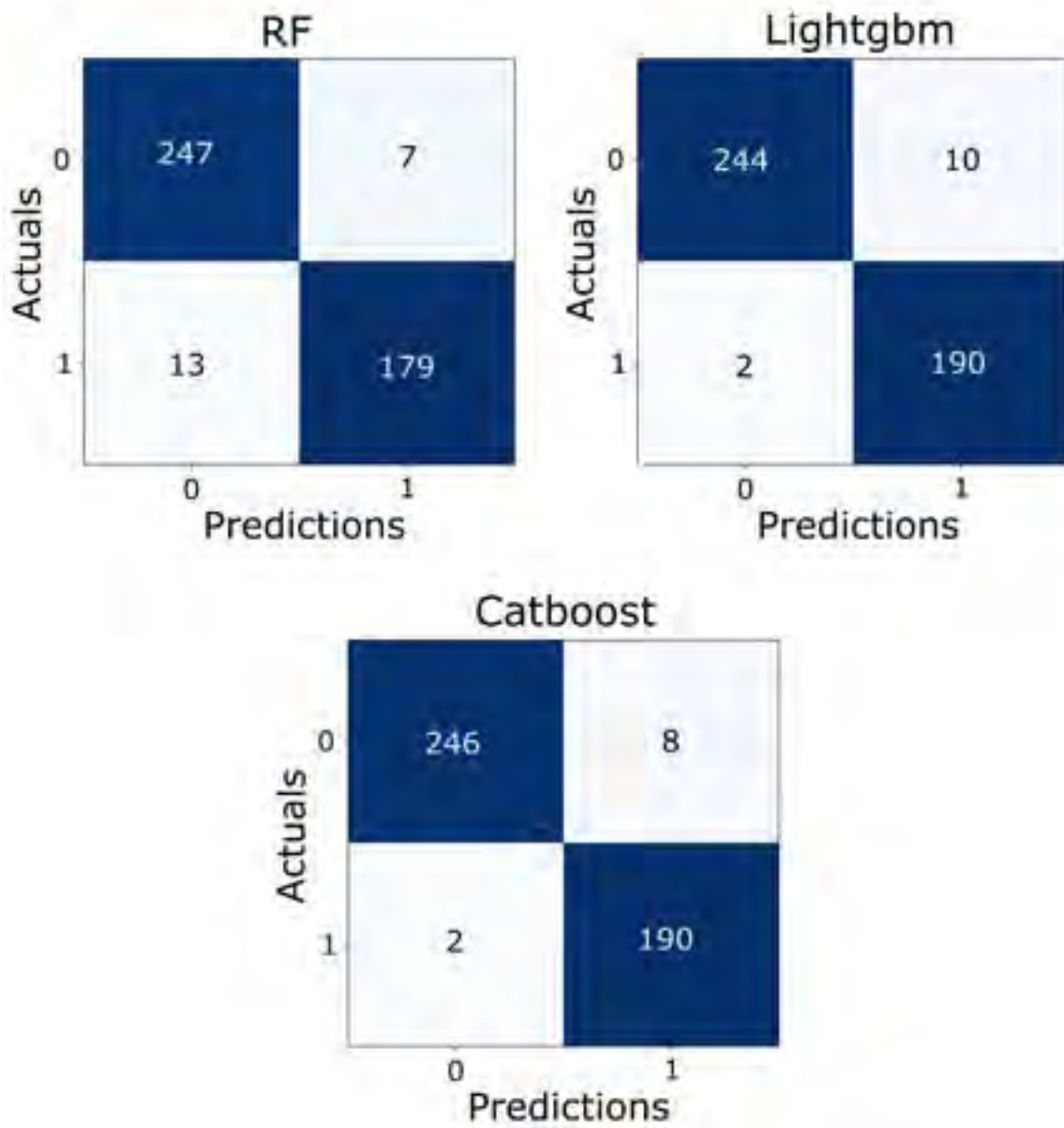


Figure 10

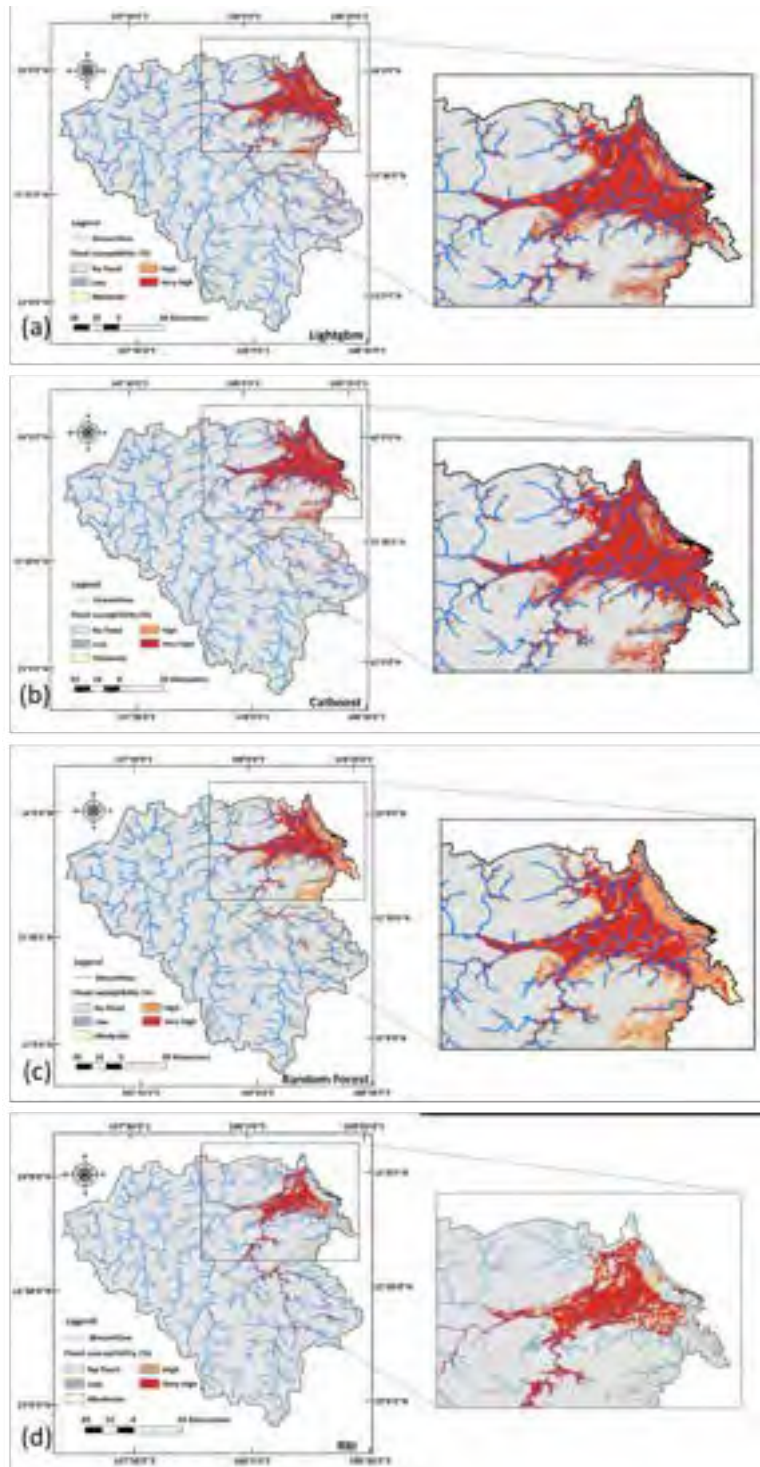


Figure 11

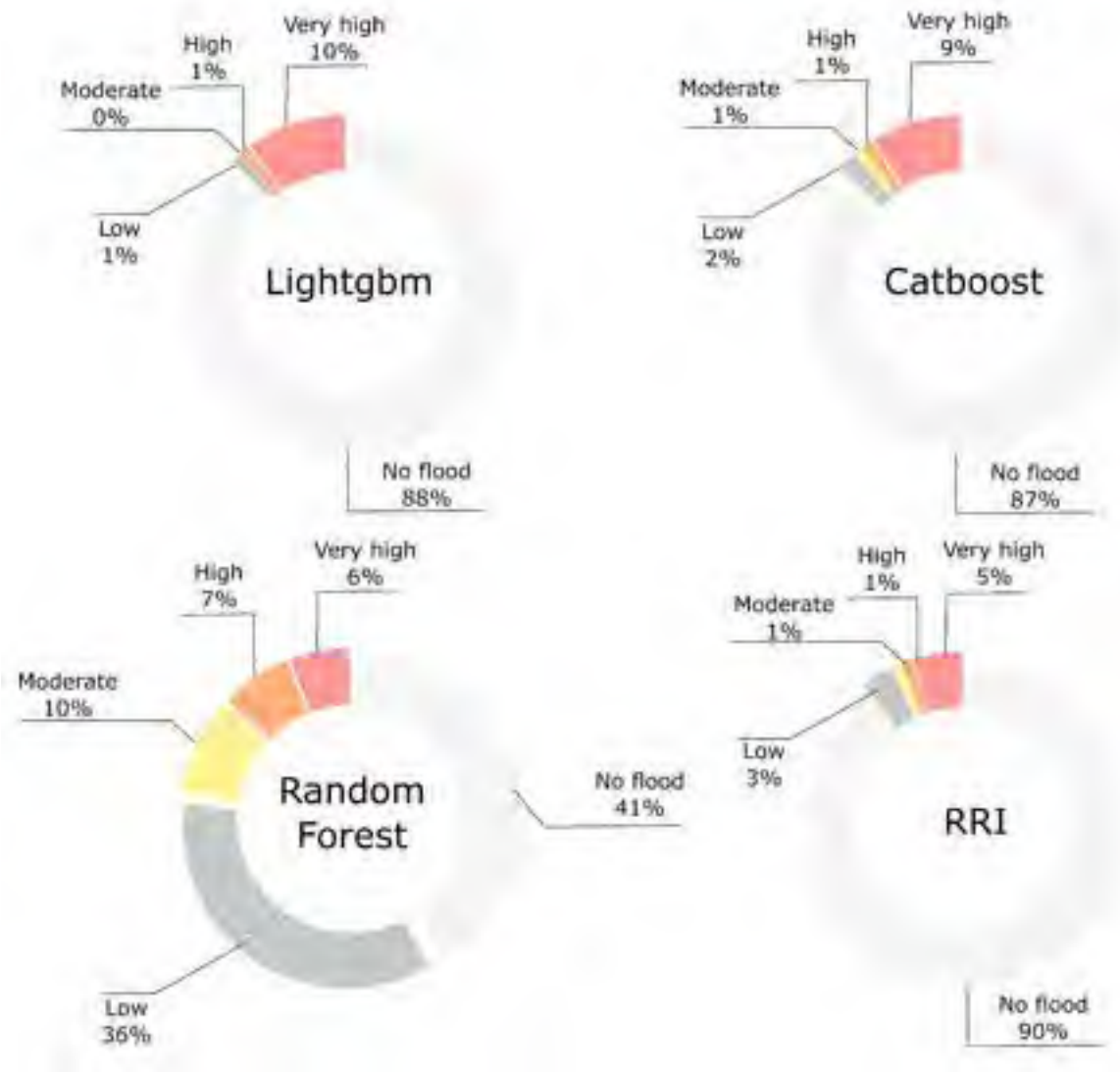


Figure 12

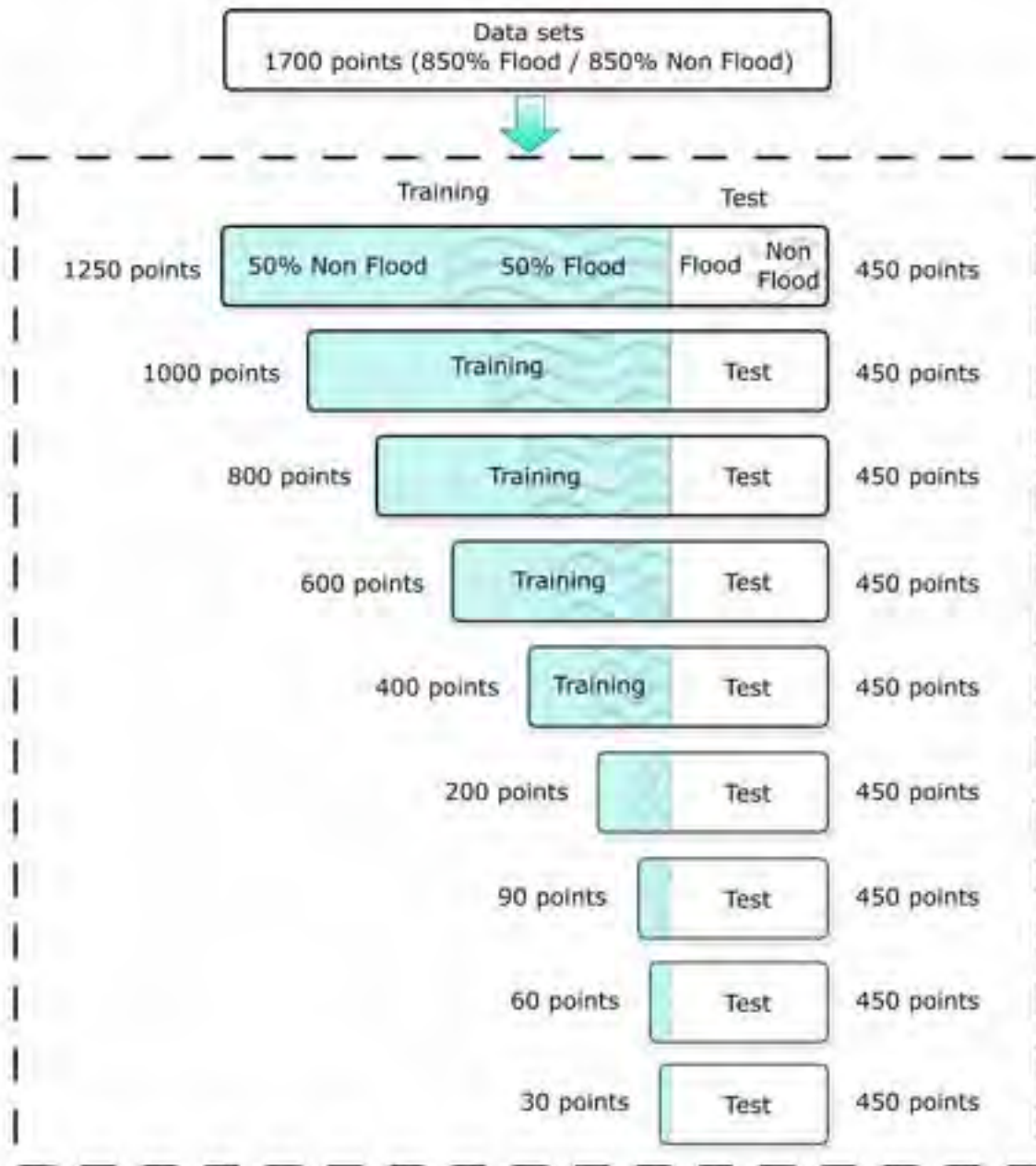


Figure 13

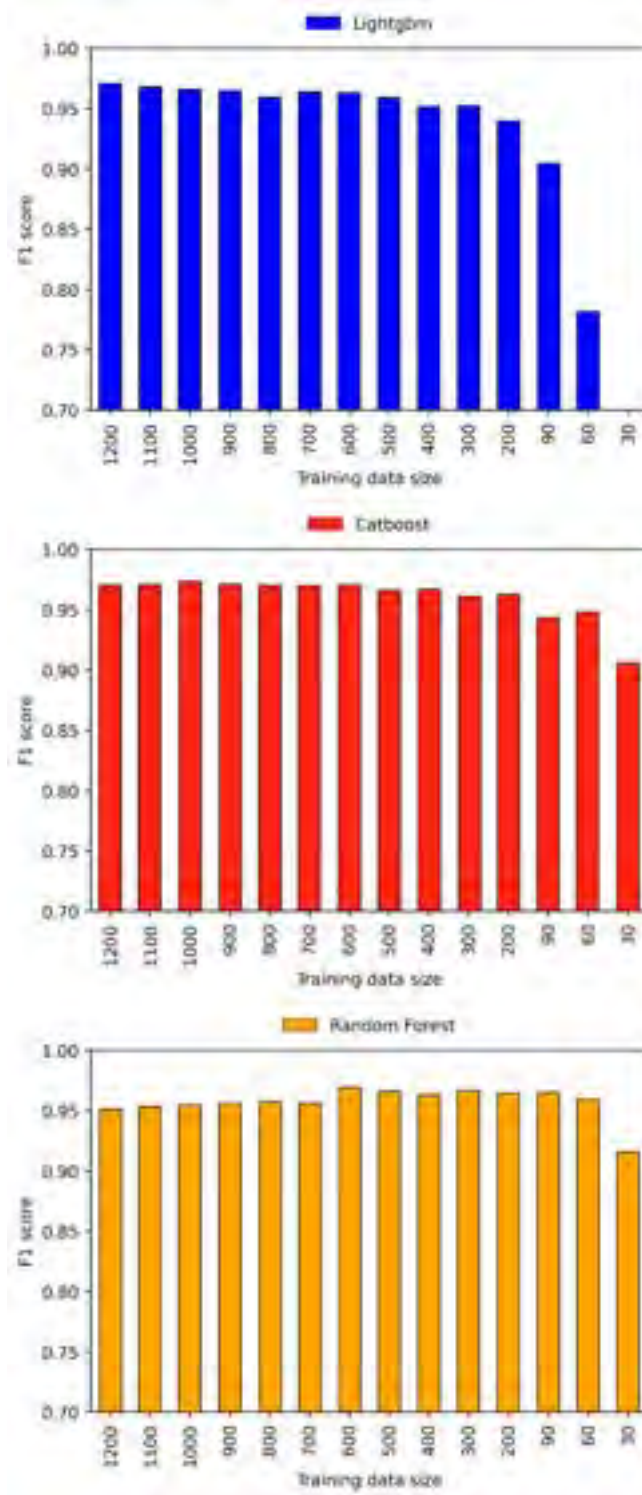


Figure 14

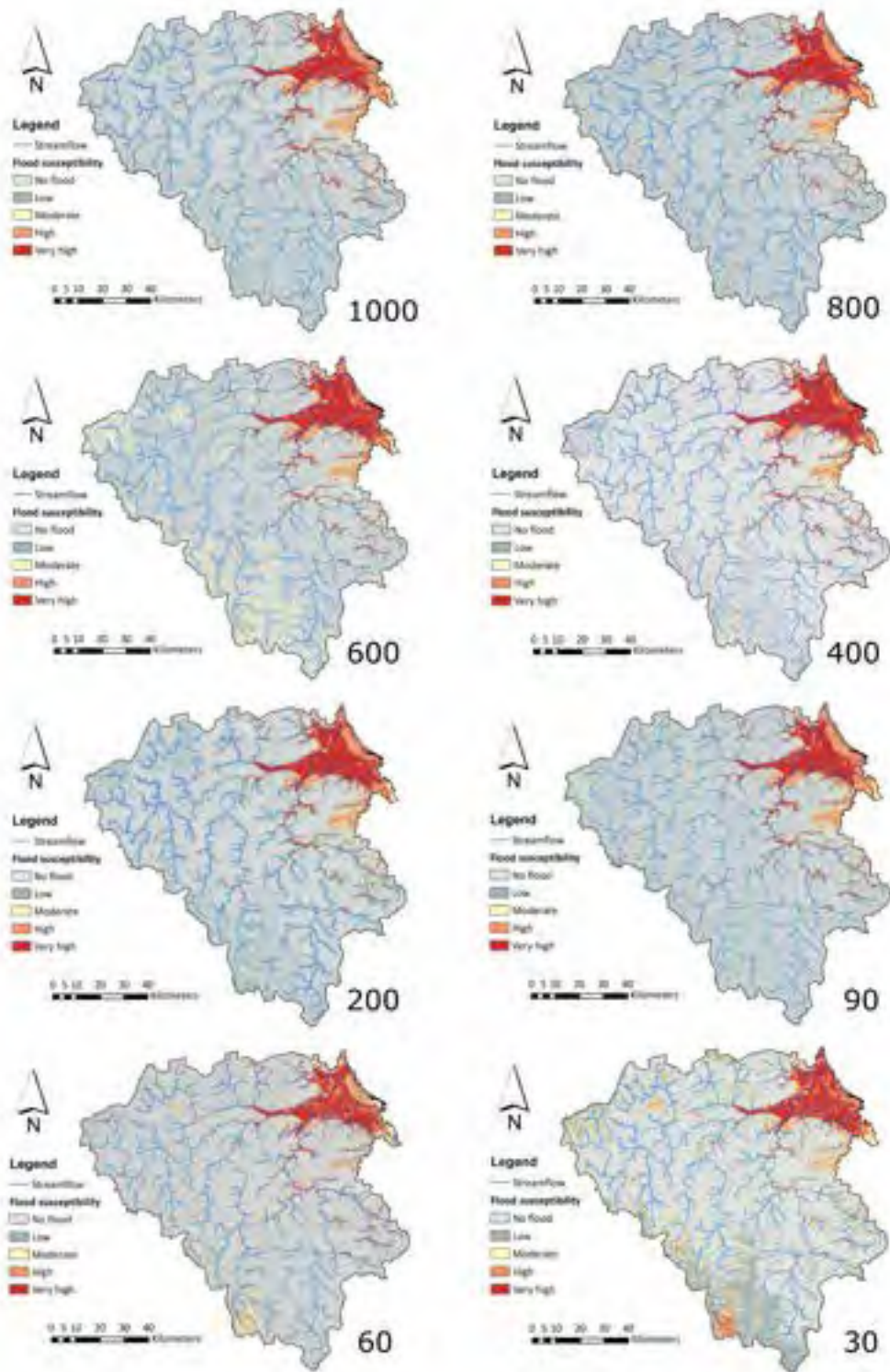
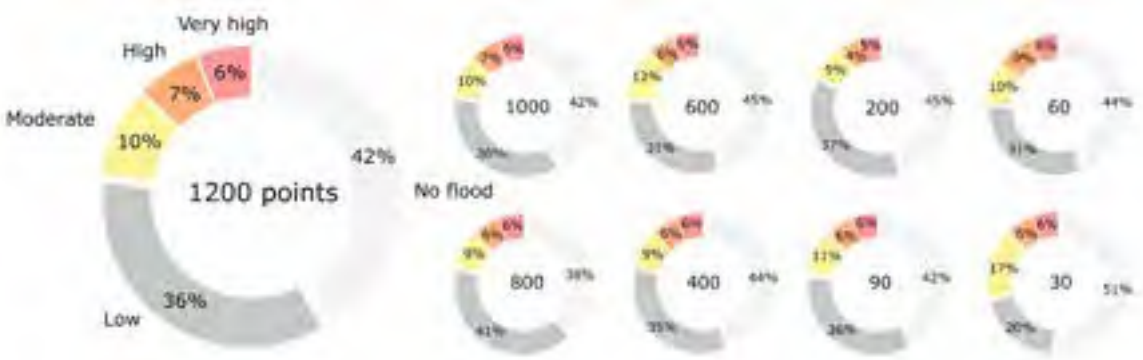


Figure 15



Water Resources Research






RESEARCH ARTICLE

10.1029/2021WR031048

Reconstructing Daily Discharge in a Megadelta Using Machine Learning Techniques

Key Points:

- Machine learning (ML) methods can reliably reconstruct missing daily discharge values
- The multivariate adaptive regression spline and random forest (RF) models outperform other ML and rating curve (RC) methods
- Data pre-processing reduces the simulation time and effort

Hung Vo Thanh¹, Doan Van Binh^{2,3} , Sameh A. Kantoush², Vahid Nourani^{4,5}, Mohamed Saber² , Kang-Kun Lee¹ , and Tetsuya Sumi²

¹School of Earth and Environmental Sciences, Seoul National University, Seoul, South Korea, ²Water Resources Research Center, Disaster Prevention Research Institute, Kyoto University, Kyoto, Japan, ³Master Program in Water Technology, Reuse and Management, Vietnamese German University, Thu Dau Mot, Vietnam, ⁴Center of Excellence in Hydroinformatics, Faculty of Civil Engineering, University of Tabriz, Tabriz, Iran, ⁵Faculty of Civil and Environmental Engineering, Near East University, Nicosia, Turkey

Correspondence to:

D. V. Binh,
binh.dv@vgu.edu.vn

Citation:

Thanh, H. V., Binh, D. V., Kantoush, S. A., Nourani, V., Saber, M., Lee, K.-K., & Sumi, T. (2022). Reconstructing daily discharge in a megadelta using machine learning techniques. *Water Resources Research*, 58, e2021WR031048. <https://doi.org/10.1029/2021WR031048>

Received 15 AUG 2021

Accepted 3 MAY 2022

Author Contributions:

Conceptualization: Doan Van Binh,

Sameh A. Kantoush, Tetsuya Sumi

Data curation: Hung Vo Thanh, Doan Van Binh

Formal analysis: Hung Vo Thanh, Doan Van Binh

Funding acquisition: Sameh A. Kantoush, Tetsuya Sumi

Investigation: Sameh A. Kantoush, Vahid Nourani, Mohamed Saber

Methodology: Hung Vo Thanh, Doan Van Binh, Sameh A. Kantoush, Vahid Nourani, Mohamed Saber

Software: Hung Vo Thanh, Vahid Nourani, Mohamed Saber

Supervision: Sameh A. Kantoush, Tetsuya Sumi

Validation: Hung Vo Thanh, Doan Van Binh

Visualization: Hung Vo Thanh, Kang-Kun Lee

Abstract In this study, six machine learning (ML) models, namely, random forest (RF), Gaussian process regression (GPR), support vector regression (SVR), decision tree (DT), least squares support vector machine (LSSVM), and multivariate adaptive regression spline (MARS) models, were employed to reconstruct the missing daily-averaged discharge in a mega-delta from 1980 to 2015 using upstream-downstream multi-station data. The performance and accuracy of each ML model were assessed and compared with the stage-discharge rating curves (RCs) using four statistical indicators, Taylor diagrams, violin plots, scatter plots, time-series plots, and heatmaps. Model input selection was performed using mutual information and correlation coefficient methods after three data pre-processing steps: normalization, Fourier series fitting, and first-order differencing. The results showed that the ML models are superior to their RC counterparts, and MARS and RF are the most reliable algorithms, although MARS achieves marginally better performance than RF. Compared to RC, MARS and RF reduced the root mean square error (RMSE) by 135% and 141% and the mean absolute error by 194% and 179%, respectively, using year-round data. However, the performance of MARS and RF developed for the climbing (wet season) and recession (dry season) limbs separately worsened slightly compared to that developed using the year-round data. Specifically, the RMSE of MARS and RF in the falling limb was 856 and 1,040 m³/s, respectively, while that obtained using the year-round data was 768 and 789 m³/s, respectively. In this study, the DT model is not recommended, while the GPR and SVR models provide acceptable results.

1. Introduction

River discharge is a crucial indicator to understand terrestrial water cycles and supplies necessary information about water resource management (Adnan et al., 2020). Direct measurement of river discharge, such as employing the acoustic Doppler current profiler, is complicated, costly, time-consuming, and labor-intensive because it requires a number of current sensors and repeated surveys performed by boats and is thus unsafe under unfavorable flow and weather conditions (Gisen & Savenije, 2015; Matte et al., 2018). Other noncontact methods, including large-scale particle image velocimetry (LSPIV) (Akbarpour et al., 2020) and remote sensing (Kebede et al., 2020), have recently begun to be used for discharge measurements. Nevertheless, the use of these methods in contiguous monitoring of river discharge is not feasible; for example, LSPIV cannot measure discharge in large rivers because of limited camera coverage, while satellite images are not always available due to cloud cover, particularly during rainy seasons. As a result, at hydrological stations situated on rivers worldwide, flow discharge is not directly measured; rather, it is indirectly estimated either from the widely used stage-discharge rating curve (RC) method or from cubature, rating-fall, tide-correction, and coaxial graphical-correction methods (Matte et al., 2018), in which the stage (water level) is recorded at specific intervals (e.g., daily, hourly, or sub-daily) depending on the goal of the measurements. Due to technical, financial, maintenance and political instability issues, long-term flow discharge datasets may have gaps, resulting in the loss of information or the misinterpretation of historical flow regime changes and hydrological processes (Tencaliec et al., 2015). Therefore, it is important to reconstruct missing discharge values to reliably provide helpful information for water resource management at the basin scale.

Several methods, including statistical methods, numerical models, and machine learning (ML) algorithms, have been employed to predict river flows. Recently, ML techniques, such as support vector regression (SVR) (Adnan et al., 2020; Luo et al., 2019), random forest (RF), Gaussian process regression (GPR) (Sun et al., 2014), M5

© 2022. The Authors.

This is an open access article under the terms of the [Creative Commons Attribution-NonCommercial-NoDerivs License](https://creativecommons.org/licenses/by/4.0/), which permits use and distribution in any medium, provided the original work is properly cited, the use is non-commercial and no modifications or adaptations are made.

Writing – original draft: Hung Vo Thanh, Doan Van Binh, Kang-Kun Lee
Writing – review & editing: Hung Vo Thanh, Doan Van Binh, Sameh A. Kantoush, Vahid Nourani, Mohamed Saber, Kang-Kun Lee, Tetsuya Sumi

model tree (Nourani et al., 2019), decision tree (DT) (Choi et al., 2019), least squares support vector machine (LSSVM) (Rezaali et al., 2021), multivariate adaptive regression spline (MARS) (Jei’houni et al., 2020), and adaptive neuro-fuzzy inference system (Hadi & Tombul, 2018a) models, have been increasingly used because they are powerful, robust and efficient algorithms for streamflow prediction given their advantages compared to traditional approaches (Khan et al., 2016; Liu et al., 2020; Mispan et al., 2015).

SVR is easily adaptable for use in multiple engineering disciplines and, in many cases, outperforms other methods, such as artificial neural networks and DTs (Raghavendra & Deka, 2014). Luo et al. (2019) developed 14 ML techniques to predict the monthly discharge of the Jinsha River in Iran, revealing that a hybrid SVR method performed better than a generalized regression neural network (GRNN). In modeling the monthly discharge in the Swat River basin in Pakistan, Adman et al. (2020) found that least squares SVR was superior to other ML models and was recommended for monthly streamflow forecasting without local data. The RF nonparametric algorithm is a type of DT algorithm that includes an ensemble collection of unrelated trees for classification and regression purposes (Breiman, 2001). The advantage of using an RF over a single DT is the reduction in variance achieved by creating several trees, in which each tree is constructed based on a leverage sample of the training database (James et al., 2013). In an attempt to predict the water level in an urban reservoir in Atlanta, Georgia, Obringer and Nateghi (2018) demonstrated that an RF was the most accurate predictive model among the nonparametric ML algorithms considered, and the proposed method is highly transferable to other reservoirs. RF algorithms have been used to reliably predict the outflows of nine reservoirs in California, given reliable input parameters related to precipitation, reservoir inflows, reservoir storage, and downstream conditions (Yang et al., 2016). GPR is a Bayesian learning technique for model approximation, multivariate regression, and experimental design (Rasmussen & Williams, 2006). The power of GPR compared to other ML models is that it simplifies the integration of several ML functions, including hyperparameter evaluation, model training, and uncertainty quantification (Rasmussen & Williams, 2006; Sun et al., 2014). Thus, GPR is relatively uninfluenced by subjectivity, and the results can easily be interpreted (Sun et al., 2014). Zhu et al. (2018) used a GPR model to estimate the streamflow in the Jinsha River; they reported that GPR performed better than a GRNN but was not good at predicting extreme flows. Sun et al. (2014) established a GPR model to simulate monthly streamflow in 438 river basins in the U.S. (MOPEX database); they revealed that the GPR model outperformed regression methods in most basins.

Most recently, advanced ML techniques, including LSSVM and MARS, have received intense attention in hydrological studies. Wang et al. (2020) proposed a new method to predict the evaporation of arid areas in China by applying the MARS method. In a digital application, Jei’houni et al. (2020) employed the MARS model to map soil moisture retention parameters using only satellite data with less prediction uncertainty and high accuracy results. Additionally, Safari (2020) employed MARS and multi non-linear regression (MNLr) to improve the precision of predicting sediment accumulation in open channel flow areas.

Regarding the prospects for the application of the LSSVM model, Rezaali et al. (2021) used this advanced model for highly accurate forecasting of the urban water demand in Qom, Iran. In addition, the LSSVM model was used for water resource management by enhancing the accuracy of the prediction of mid-to long-term streamflow (Zhao et al., 2021). In methane transport modeling, Taherdangkoo et al. (2021) employed the LSSVM model to estimate methane solubility in aquatic environments for a variety of temperatures and pressures. Moreover, the LSSVM model was demonstrated to be effective for forecasting the quality of the air in the Yangtze River Delta of China (Zhou et al., 2020). Because numerous ML models are available, researchers may struggle to determine which ML model is appropriate for a particular problem. Unfortunately, no ML algorithm provides a satisfactory result for all problems involving hydrological processes, and many methods remain in the development stage. Although the SVM, RF, DT, LSSVM, MARS, and GPR models have been widely employed in various research fields (e.g., Jei’houni et al., 2020; Granata et al., 2017; Kisi & Parmar, 2016; Panahi et al., 2020; Rezaali et al., 2021), their application in estimating river discharge has been limited (e.g., Tongal & Booi, 2018; Yaghoubi et al., 2019). Therefore, this study employs these techniques to explore their power/applicability in reconstructing the daily discharge in the Mekong River.

Hydrological data are highly nonstationary (Yarar, 2014), and ML models, or artificial intelligence models in general, have demonstrated limitations in coping with nonstationary phenomena (Nourani et al., 2017). Moreover, hydrological data often contain seasonal effects driven by hydrologic cycles. It is therefore necessary to

perform data pre-processing before applying ML models, and Fourier series fitting can decompose complex original hydrological data into sub-signals with a variety of valuable features to interpret the time series structure and clarify spectral and temporal information (Nourani et al., 2019). Another challenging task in simulating hydrological processes using ML models is model input selection. Too many or too few model inputs may introduce noise, increase model complexity and increase the model run time; both instances can lead to poor model performance (Tran et al., 2015). A traditional approach in model input selection involves the use of a rank-based correlation coefficient, such as the Pearson correlation coefficient, to reflect the linear relations among variables (Zhu et al., 2018). Another more advanced metric is mutual information (MI), which can help reduce the number of model inputs (Nourani et al., 2017). Although MI, as a nonlinear measure used to explain one variable based on another random variable, is useful in reducing simulation effort, its application in the field of hydrology remains limited. This study used both MI and the Pearson correlation coefficient to derive the dominant model inputs after data pre-processing by standardization to remove trends related to the variance and mean; additionally, Fourier series fitting was performed to remove seasonal effects, and first-order differencing was used to convert a nonstationary data set to a stationary data set.

Most previous studies reconstructed/predicted monthly and annual averaged discharge series (Adnan et al., 2020; Hadi & Tombul, 2018b; Khalil et al., 2001; Liu et al., 2020; Sun et al., 2014; Yarar, 2014; Zhu et al., 2016), and studies that have reconstructed daily-averaged series are scarce. This scarcity is likely due to data availability and the complex non-stationarity and nonlinearity of daily averaged data. Notably, the complexity of hydrological data is increased by the effects of tides in the major deltas worldwide, such as the Vietnamese Mekong Delta (VMD), which is the study area considered in this paper. In tidal deltas, flow discharge is seasonally variable, with riverine and marine dominance in the flood and dry seasons, respectively. River tides are largely nonstationary and nonlinear because tides are governed by the effects of hundreds of major and minor astronomical factors (Moftakhari et al., 2013); thus, analyses of flows in tidally affected rivers are complicated by the appearance of a large number of frequencies (Hoitink & Jay, 2016). Spatial acceleration, friction, and discharge gradients also control river-tide interactions, making the direct estimation of fluvial discharge challenging (Hoitink & Jay, 2016). Being nonstationary, water levels in tidally affected rivers are continuously variable during spring-neap tidal cycles, which has led to a consensus that water levels at tidal stations are not the same under different tidal conditions (Hoitink & Jay, 2016). Moreover, tides may increase the water surface gradient and river slope (Jay et al., 2011) to transport more river water during spring tides than during neap tides. Such an increase in the water surface gradient is necessary to enhance the transport capacity of rivers against the increased river friction generated by high discharge amplitudes during spring tides (Buschman et al., 2009).

Moftakhari et al. (2013) proposed a conceptual modeling tool for tidal discharge estimation (TDE) based on sets of governing equations by combining theories of astronomical forcing, tidal constituents, and friction to hindcast the monthly averaged tidal discharges in the San Francisco Bay. Although the estimation was promising, the use of the TDE model is complicated, and many hindcast parameters and extended periods of data observations are required (Gisen & Savenije, 2015); because these are system specific, their application to other tidally affected rivers, particularly in developing countries, where river systems are largely ungauged, is difficult. Gisen and Savenije (2015) developed a semi-empirical approach to compute bankfull discharge in ungauged estuaries by combining hydraulic geometry and hydrodynamic theories. The methodology developed included five main components, namely, estuary geometry, freshwater discharge upscaling, tidal dynamics, regime relations, and estuarine flood number estimation. The derived discharges are estimated with high confidence; however, the application of this method is relatively challenging due to the introduction of several restriction criteria. Moftakhari et al. (2016) developed the multiple-gauge tidal discharge estimate (MTDE) method to estimate the discharge in tidal rivers in North America using tidally observed data at multiple stations near estuaries. The MTDE method can estimate the discharge with a temporal resolution of less than a week; this resolution is finer than that of the TDE method. However, the major shortcoming of the MTDE method is the need for at least three tide gauges, one of which must be near the ocean. This is not applicable in most of the world's tidal rivers because hydrological stations are relatively far from the river mouths (Gisen & Savenije, 2015).

RC has been widely used to reconstruct missing data in deltas, although a special focus must be placed on various tasks, such as establishing RCs for the rising and falling limbs separately (Binh, Kantoush, et al., 2021).

Moftakhari et al. (2015) employed the RC method to reconstruct daily discharge and sediment delivered to San Francisco Bay by dividing the water level data into two subsets (i.e., <6.2 and >6.2 m) according to the effect of flooding. However, the RC method involves several limitations and uncertainties induced by dynamic changes in river geometry and roughness or the effects of backwater and tides (Matte et al., 2018). Uncertainties also arise from the difficulty in measuring the discharge during extreme floods for updating the RCs. Studies reported in the literature have shown that conventional approaches such as the RC and TDE methods have their own limitations and uncertainties under the effects of reversing tidal flow, tidal Stokes drift, spring-neap tidal cycle, lateral circulation, estuarine dynamics, and the occurrence of multiple branches in estuaries (Moftakhari et al., 2016). Therefore, the use of ML models in discharge estimation is expected to overcome the shortcomings of their conventional counterparts. Although ML models have been proven to be an efficient and promising tool, their application for daily-averaged discharge prediction in tidally affected rivers remains uncommon worldwide. In the VMD and Mekong River, no study has used ML algorithms to reconstruct daily-averaged discharge. One of the advantages of using ML models is that they are highly transferable to other river systems with little effort in acquiring a variety of datasets required compared to conceptual, statistical, and numerical models, making them time-saving and cost-effective.

This study developed a robust methodology to reconstruct missing daily-averaged discharge values in a tidally affected river in the VMD using ML techniques. First, the model inputs using multi-station data with respect to upstream-downstream relations were optimized by employing MI and Pearson correlation coefficients after three-step data pre-processing. SVR, GPR, RF, DT, LSSVM, and MARS models were then used and compared to determine the most reliable model. Finally, the best model(s) was further evaluated considering the seasonal patterns of the input data. The purpose of this analysis was to answer the following question: can ML approaches increase the daily-averaged discharge reconstruction accuracy considering seasonal patterns? In this study, we employed ML models using multi-station input data to reconstruct daily-averaged discharges in a tidally affected river. The use of only the water levels at multiple upstream stations as inputs into the ML models has two major advantages. First, the water level is directly, easily, and cheaply monitored in river systems, whereas direct discharge measurement is time-consuming, expensive, and impractical. Second, during extreme events, it is impossible to measure the discharge due to safety concerns (i.e., having to operate a boat in a flooded river), whereas measurements of the water level can be obtained anywhere, at any time, and under all conditions, although river gauges can fail or become compromised (Helaire et al., 2020). Finally, the method developed in this paper can easily be adopted for any river system even though ML models contain black box algorithms.

2. Case Study and Used Data Set

The Mekong River is the eighth largest river globally in terms of the annual discharge of 475 km^3 (Grumbine et al., 2012), and it flows through six countries from the watercourse in China to the ocean in Vietnam. The VMD (Figure 1a) has been formed and propagated over the last 6,000 years (Ta et al., 2002) by water and sediment transported by the Mekong River (Binh, Kantoush, & Sumi, 2020). The flow regime in the VMD is seasonally variable, with two distinct flood and dry seasons (Binh, Kantoush, Saber, et al., 2020). August-October (flood months) is when approximately half of the annual discharge occurs, and approximately 8% occurs in February-April (dry months). The VMD faces many hydrological problems, such as floods, droughts, and salinity intrusion (Eslami et al., 2019; Hoa et al., 2007; Kantoush et al., 2017; Loc et al., 2021; Triet et al., 2017). La Niña and El Niño have caused periodic occurrences of extreme floods (e.g., 1996, 2000, and 2011) and droughts (e.g., 1993, 1998, 2005, 2010, 2015, and 2020), resulting in tremendous damage to the delta. The flow regime in the delta is influenced by tides, with strong tidal effects in the dry season (peak in dry months) and fewer tidal effects in the flood season (Gugliotta et al., 2017). In dry seasons, tidal effects are observable at Phnom Penh, Cambodia, which is approximately 320 km from the river mouth (Gugliotta et al., 2017). The semidiurnal tide in the East Vietnam Sea (Figure 1a) causes the discharge hydrograph to have two peaks and two troughs daily.

Tan Chau and Chau Doc (in the Tien and Hau Rivers, respectively) are the first two major hydrological gauges (tidally affected) at the entrances of the VMD, and the historical data series obtained at these stations are longer

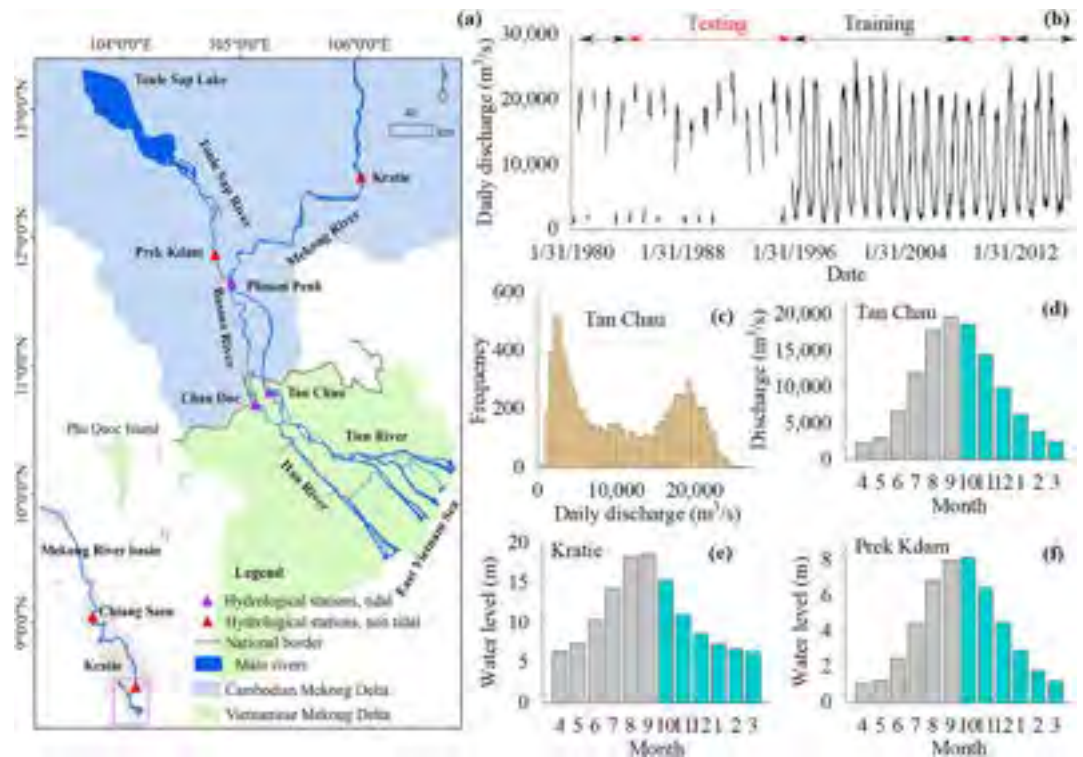


Figure 1. (a) The Mekong River basin and the Vietnamese Mekong Delta (VMD): the main rivers and hydrological stations. The tidally affected and non-tidally affected hydrological stations are distinguished by different colors. (b) Observed daily-averaged discharge values at Tan Chau (1980–2015) with the periods of training and testing in the machine learning (ML) models indicated. (c) Histogram showing the frequency of the daily-averaged discharge at Tan Chau from 1980 to 2015. Mean monthly discharge values at (d) Tan Chau and the water levels at (e) Kratie and (f) Prek Kdam from 1996 to 2015 show similar seasonality for flow regimes. The data in (d–f) were sorted to clearly illustrate the rising (gray bars) and falling limbs (green bars).

than those obtained at newer hydrological gauges. Tan Chau conveys approximately four times more water than Chau Doc (Binh, Kantoush, et al., 2021). Hourly discharge at Tan Chau was persistently monitored from 1996 to 2015, whereas daily-averaged discharge (from 1980 to 1995) was available several months per year (Figure 1b). The hourly discharge from 1996 to 2015 was averaged over a day to create the daily-averaged discharge, which is equivalent to the de-tided discharge (Binh, Kantoush, et al., 2021); however, the tidal effect does not disappear completely (Hoitink & Jay, 2016). A frequency analysis of the observed daily-averaged discharge at Tan Chau from 1980 to 2015 (Figure 1c) shows that the majority of the discharge values are less than $6,500 \text{ m}^3/\text{s}$ (39%) and vary from 16,250 to $22,250 \text{ m}^3/\text{s}$ (31%); only 2% of the daily-averaged discharge values exceed $22,500 \text{ m}^3/\text{s}$. Given the importance of understanding long-term flow variations when assessing the corresponding causes, consequences, and appropriate actions, it is important to fill the gaps in the historical records. In this study, ML algorithms were used to reconstruct the missing daily-averaged discharge values at Tan Chau and to establish a framework for the other stations in the VMD.

The VMD receives water directly from the Mekong River, and Kratie is a gauging station at the apex of the Mekong Delta (from the Cambodian Mekong Delta) (Figure 1a). Tonle Sap Lake in Cambodia is of utmost importance in naturally regulating the flow in the VMD to the extent that the lake retards flood water and reverses the flow back to the VMD in the dry season (Park et al., 2022; Pokhrel et al., 2018). Tonle Sap Lake is connected with the Mekong River by the Tonle Sap River, and Prek Kdam is an important gauging station that records the exchanged flow regimes (Figure 1a). Figures 1d–1f show that the flow pattern at Tan Chau is physically consistent with those at Kratie and Prek Kdam, with similar rising (April–September) and falling (October–March) limbs.

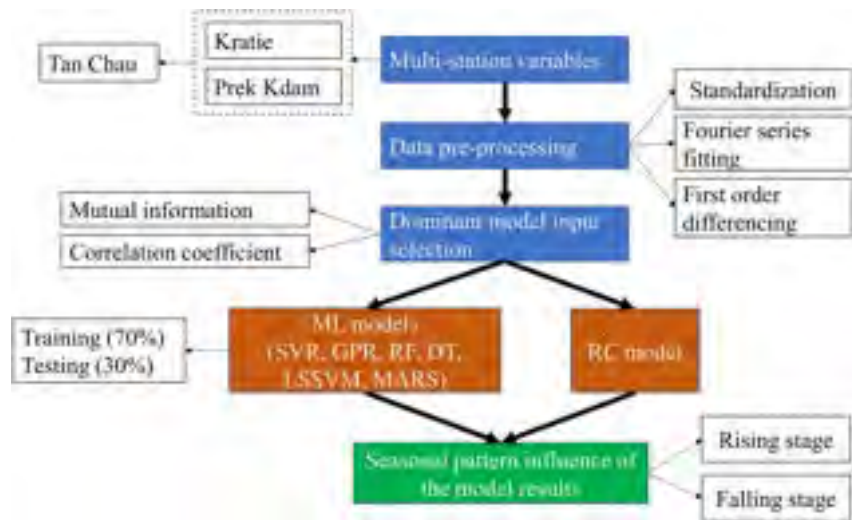


Figure 2. Flowchart of the study showing the research steps.

In reconstructing the daily-averaged discharge at Tan Chau using the ML models, data from multiple upstream stations, that is, the daily-averaged water levels at Kratie and Prek Kdam, were used. The Mekong River Commission provided water level data at Kratie and Prek Kdam from 1980 to 2015 (<https://portal.mrcmekong.org/time-series>). Using water levels as the input data is practically feasible because these values, rather than discharge values, are directly monitored at all hydrological stations on the Mekong River. Researchers can request such data from the Mekong River Commission. The daily-averaged discharge data at Tan Chau collected from 1980 to 2015 (38.8% of the data are missing) were obtained from the Vietnam National Centre for Hydrometeorological Forecasting. The outcomes from the ML models were compared to those from the conventional RC to assess the applicability of ML in the VMD and tidally affected river systems in general.

3. Proposed Method and Materials Used

3.1. Data Pre-Processing and Model Input Selection

Figure 2 shows the methodology proposed in this study. Six ML models were built considering the input data at multiple upstream stations (i.e., water levels at Kratie and Prek Kdam) to assess the trends at individual stations and the combined contributions to the results. In the ML models, the tidal effect is implicitly considered in the target model (output) because the input water levels are not affected by tides. The results from the ML models were compared with those obtained from linear stage-discharge RCs at the station examined (Tan Chau). These RCs were separately established based on both year-round data and data for the rising and falling limbs, following the work of Binh, Kantoush, et al. (2021). One of the purposes of this approach was to understand the advantages of nonlinear models with ML versus linear regression models based on RCs.

In this study, we applied three data pre-processing steps for the raw normalized datasets. The first step was standardization to remove trends related to the variance and mean from the datasets; the second step was the removal of seasonal effects through Fourier series fitting because the data were influenced by seasonality (Figure 1b); the third step was first-order differencing to convert a nonstationary data set to a stationary data set. Then, MI and correlation coefficient methods were applied to determine the dominant model inputs, accounting for time lags. The correlation coefficient was used in the analysis because it defines the dependence of two independent variables in time and space; therefore, it is a kind of temporal correlation for time series with different time lags.

To remove the seasonal influence from time series data, a fitting Fourier series model was used. The basic concept of this Fourier series model for time series decomposition was proposed by Delurgio (1998) as follows:

$$X_t = a + bt + \sum_{j=1}^k (a_j \cos jwt + b_j \sin wt) \quad (1)$$

where X_t is the fitted value at time t ; a is a constant related to the series level; b is the trend estimate of the series; a_j and b_j ($j = 1, 2, 3, \dots, k$) are Fourier coefficients; w is the Fourier frequency; and k is the highest harmonic of w .

The first-order differencing method has been widely used as a simple procedure to convert nonstationary time series to stationary time series, as proposed by Anderson (1976). In other words, a new data set of a variable can be obtained from a measured data set by subtracting the value of that variable at time $t - 1$ (X_{t-1}) from its value at time t (X_t). This method can be expressed as follows:

$$Y_t = X_t + X_{t-1} \quad (2)$$

MI is a quantitative metric based on information entropy, and it expresses the dependence or cooperation among random variables (Akca & Yozgatligil, 2020). Unlike traditional correlation metrics, MI does not require an assumption based on dependence, and the provided mutual information encompasses both linear and nonlinear relationships. MI stems from Shannon entropy in information theory (Shannon, 1948). The discontinuous random variable x (from x_1 to x_n) and probabilities (from P_1 to P_N) are expressed by the following equation:

$$H(x) = \sum_{i=1}^N P(x_i) \text{Log}[P(x_i)] \quad (3)$$

The MI criterion is the amount of information shared among discontinuous variables X and Y (Yang et al., 2000). It is assumed that the two variables x and y correspond to probabilities m and n , and the ranges of these probabilities are indicated by i and j , respectively. Accordingly, MI is defined as $MI(X, Y)$, where A and B share MI.

$$MI(X, Y) = \sum_{i=1}^K \sum_{j=1}^L P_{XY}(x_i, y_j) \log \left(\frac{P_{XY}(x_i, y_j)}{P_1(X = x_i)P_2(X = y_j)} \right) \quad (4)$$

In this equation, P_i is the probability of i ; $P(i, j)$ is the joint probability of i and j .

Based on the results of the MI and correlation coefficient analyses, five dominant model inputs were used: the water levels at Kratie at $t-1$ (WK_{t-1}) and $t-2$ (WK_{t-2}) and the water levels at Prek Kdam at t (WP_t), $t-1$ (WP_{t-1}), and $t-2$ (WP_{t-2}). In this case, t is the selected time, and $t-1$ and $t-2$ are the 1- and 2-day lagged times, respectively. Notably, the flow at Prek Kdam changes sooner than the flow at Kratie because Prek Kdam is closer to Tan Chau than is Kratie. The time lag concept is not considered in the RC model.

3.2. ML Models: Theoretical Background and Optimization

In the ML models, we considered three periods for the training data set (70% of the data), namely, 1980–1983, 1996–2007, and 2012–2015, and two periods in the testing data set (30% of the data), namely, 1984–1995 and 2008–2011. The training data set was selected to represent all kinds of flow events, ranging from flood years (e.g., in 2000) to drought years (e.g., in 2015). Similarly, the testing data set covered both flood years (e.g., in 2011) and drought years (e.g., in 2010). For each ML method, we established the theoretical background and adjusted hyperparameters for model optimization.

3.2.1. Decision Tree

DT is an ML method used for prediction and classification (Quinlan, 1986). This method has been employed in various studies due to its simplicity and high predictive accuracy (Choi et al., 2019).

A DT could predict responses by converting the observed values of features in ML models. These models are based on the relationship between the predictor and the response for a given data set. A DT defines each parameter and determines distinct values based on the impurities observed at roots. Therefore, the DT approach is straightforward to implement; nevertheless, its reliability is sometimes inadequate because it is prone to overfitting and linear regression loss (Ragetti et al., 2017). Therefore, to limit the likelihood of overfitting and inaccuracy, the tree size should be determined via cross-validation (Choi et al., 2020).

This study used fine tree regression and ensemble boosting regression to train the ML model. The corresponding DTs were compared with other models to find a suitable DT for reconstructing missing data at the analyzed

station. Each DT is composed of an initial point (root) and an ultimate point (leaf) in tree form (Saghafi & Arabloo, 2017). The main tuning hyperparameter in DTs is the minimum leaf size. Leaf size was used to train the DT-based ML model, while trees were used to search for the optimal result (Krzywinski & Altman, 2017).

3.2.2. Gaussian Process Regression

The GPR paradigm is a probabilistic non-parametric kernel model (Rasmussen & Williams, 2006). The GP is a potential algorithm for calculating the ideal distribution of flexible and malleable regression and classification modeling techniques that are not restricted to basic parametric forms (Weir et al., 2019). Furthermore, one of the GPR's advantages is its wide range of covariance coefficients. Notably, functions with varying degrees of smoothness or other kinds of contiguous structures may be employed. This enables the user to make an acceptable choice (Rasmussen & Nickisch, 2010). Furthermore, GPR models may determine the distributions of functions using one or more input parameters (Rasmussen & Williams, 2006). When such functions are used to calculate the average response of the regression model with Gaussian error, the related matrix computations may be modified for inference; this technique is useful for training datasets with a large number of samples (Neal, 1997; Weir et al., 2019).

In detail, GPR analyses the training database $\{(x_i, y_i); i = 1, 2, \dots, n\}$, in which $x_i \in R^d$ and $y_i \in R$; both factors were selected from an undefined population. GPR models estimate values of the response parameter y_{new} based on the new input variable x_{new} and the training database. The corresponding linear equation is expressed as follows (Rasmussen & Williams, 2006):

$$y = x^T \beta + \varepsilon, \quad (5)$$

where the error term $\varepsilon \sim N(0, \sigma^2)$, the predictor observation N , the error variance σ^2 , and the coefficient β are determined from the database.

Moreover, the GPR model's building blocks include a GP that uses a random variable to convert objective functions (Rasmussen & Williams, 2006). Therefore, a Gaussian second-order statistic is established, and the new form of the GP is as follows:

$$f(x) \sim GP[m(x), k(x, x')] \quad (6)$$

in which $m(x)$ and $k(x, x')$ are the mean and covariance functions, respectively.

The predicted observation values are the same as those obtained with Equation 5, but the corresponding variances depend on the noise in the observation set (Weir et al., 2019). To convert GPR to a covariance function, Equation 6 is implemented for all plausible compositions of points, and the result is rewritten in three matrices (Rasmussen & Williams, 2006):

$$K(X, X) = \begin{pmatrix} k(x_1, x_1) & k(x_1, x_2) \cdots & k(x_1, x_n) \\ k(x_2, x_1) & k(x_2, x_2) \cdots & k(x_2, x_n) \\ \vdots & \vdots & \vdots \\ k(x_n, x_1) & k(x_n, x_2) \cdots & k(x_n, x_n) \end{pmatrix} \quad (7)$$

To optimize the GPR training models, $k(x, x')$ is normally parameterized using a group of kernel parameters (θ), known as tuning hyperparameters. $k(x, x')$ is denoted as $k(x, x'|\theta)$ to explicitly specify the dependence on θ (Sun et al., 2014). Hence, θ and ε in Equation 5 are the major tuning hyper-parameters in this paper.

3.2.3. Support Vector Regression

SVR, first developed by Vapnik (2013), has been extensively applied for classification and prediction in many research domains. The basic equation in SVR is as follows:

$$\hat{f}(x) = \omega^T \phi(x) + b, \quad (8)$$

in which ϕ is a mapping function with a weight of ω and b is a scalar. T is the inner product/dot product parameter of the hyperplane equation. The widely used regression form of SVR, ϵ -SVR, was applied in this paper. Considering N_s training samples, the ordinary formula for ϵ -SVR is provided by Vapnik (2013):

$$\min_{\omega, b, \xi, \xi^*} \frac{1}{2} \omega^T \omega + C \sum_{i=1}^{N_s} (\xi_i + \xi_i^*) \quad (9)$$

Subject to $\omega^T \phi(x_i) + b - y_i \leq \epsilon + \xi_i$,

$$y_i - \omega^T \phi(x_i) - b \leq \epsilon + \xi_i^*,$$

$$\xi_i, \xi_i^* \geq 0, i = 1, 2, \dots, N_s,$$

where C is used to signify the penalized variable, and ξ_i and ξ_i^* are the slack variables, which specify the upper and lower bounds, respectively, of the training errors, considering the error tolerance ϵ (Chen & Pawar, 2019). The optimization problem in Equation 9 can be handled with the aid of a collection of Lagrange multipliers: α_i and α_i^* (Chen & Pawar, 2019; Schölkopf & Smola, 2002). By adopting a typical quadratic programming technique, this process allows the optimization issues to be addressed quickly in dual format (Shevade et al., 2000). As a consequence, the second equation utilized to solve the SVR optimization problem is as follows (Chen & Pawar, 2019; Schölkopf & Smola, 2002; Shevade et al., 2000):

$$\min_{\alpha_i, \alpha_i^*} \frac{1}{2} \sum_{i,j=1}^{N_s} (\alpha_i - \alpha_i^*) (\alpha_j - \alpha_j^*) K(x_i, x_j) + \epsilon \sum_{i=1}^{N_s} (\alpha_i + \alpha_i^*) + \sum_{i=1}^{N_s} y_i (\alpha_i - \alpha_i^*) \quad (10)$$

subject to $\sum_{i=1}^{N_s} (\alpha_i - \alpha_i^*) = 0$,

$$0 \leq \alpha_i, \alpha_i^* \leq C, i = 1, 2, \dots, N_s,$$

where $K(x_i, x_j)$, the kernel function, is the inner product of $\phi(x_i)$ and $\phi(x_j)$. The linear kernel, the polynomial kernel, the radial basis function (RBF) kernel, and the hyperbolic tangent kernel are all frequently used kernel functions. In this research, the SVR model was trained using the RBF kernel, as follows (Chen & Pawar, 2019; Schölkopf & Smola, 2002):

$$K(x_i, x_j) = \exp(-\gamma \|x_i - x_j\|^2), \gamma > 0 \quad (11)$$

By using α_i and α_i^* , the predictive model is expressed as follows (Chen & Pawar, 2019):

$$\hat{f}(x) = \sum_{i=1}^{N_s} (-\alpha_i + \alpha_i^*) K(x_i, x) + b \quad (12)$$

The matrix for the nonnegative module of $(-\alpha_i + \alpha_i^*)$, where $i = 1, 2, \dots, N_s$, is referred to as the linear kernel. The SVR model can output all the support vectors if an input x is given. In this study, the three tuning hyperparameters C , γ , and ϵ were used to optimize the predictive models, and default values were used for all the variables.

3.2.4. Random Forest

RF is a classification and regression technique based on DT (Breiman, 2001). RF regression is also characterized as an ensemble-based ML technique that generates a set of input variables (known as training datasets and predictions) to create numerous regression trees. These trees can be merged to provide more precise and reliable results (Liaw & Wiener, 2002). Moreover, each DT regression in the ensemble is trained utilizing bootstrap samples or a sampling bag from the training data set to ensure that it performs well. Ultimately, each tree node is divided using binary splits based on a selection of randomly chosen predictors, with each split resulting in a different outcome (Liaw & Wiener, 2002). The RF method generates various independent DTs, which are described as follows (Breiman, 2001):

$$h_N(x) = \frac{1}{N_{DT}} \sum_{i=1}^N h_i(x) \quad (13)$$

where $h_i(x)$ is a DT and N_{DT} is defined as the total number of DTs.

The number of DTs in the forest ($N_{E_{st}}$) serves as one of the tuning hyperparameters in the optimum RF model, while the maximum depth of DTs (Max_D) and number of features are used to search for the best split (Max_F) (Kim & Shin, 2020).

3.2.5. Least Square Support Vector Machine

The LSSVM model is regarded as a more straightforward variant of the SVM regression model (Suykens & Vandewalle, 1999) and is more flexible than the original SVM method. Moreover, instead of utilizing quadratic programming to tackle regression problems, it is beneficial to determine a linear set of equations using a support vector to solve them more rapidly (Suykens et al., 2002).

A target training data set is determined as $\{x_k, y_k\}$, $k = 1, 2, \dots, N$, in which $x_k \in R$ stands for the k th input data; $y_k \in R$ is the output parameter for the given input parameter; and N is the amount of data trained (Ahmadi & Ahmadi, 2016). By considering the nonlinear function $\varphi(\cdot)$, the following regressed equation is generated (Suykens & Vandewalle, 1999):

$$y = \omega^T \varphi(x) + b \quad (14)$$

in which ω is a weight vector; $\varphi(x)$ is the nonlinear function; T depicts the transpose of the matrix; and b denotes the bias parameter. According to Equation 14, this nonlinear function plots the input data set x into the n -infinite feature space (Vong et al., 2006). When the LSSVM is used, it introduces a unique optimizing case. The approach adopted tackles the following optimization issue:

$$\frac{\min}{\omega, b, e} J(\omega, e) = \frac{1}{2} \omega^T \omega + \frac{1}{2} \gamma \sum_{k=1}^N e_k^2 \quad (15)$$

Equation 15 considers the following equality constraint:

$$y = \omega^T \varphi(x_k) + b + e_k \quad k = 1, 2, \dots, N \quad (16)$$

in which v represents the model parameters and takes into account the model's complexity and the training error (Mehdizadeh & Movagharnejad, 2011); e_k indicates the error in the regression. The Lagrangian is constructed in the following manner to seek a resolution to the unbounded optimization problem:

$$L(\omega, b, e, \alpha) = J(\omega, e) - \sum_{k=1}^N \alpha_k \{ \omega^T \varphi(x_k) + b + e_k - y_k \} \quad (17)$$

in which α_k denotes the Lagrange multiplier or supporting value. In obtaining a solution for Equation 17, the transformation of the equation in terms of ω, b, e_k, α_k is described as follows:

$$\frac{\partial L(\omega, b, e, \alpha)}{\partial \omega} = 0 \rightarrow \omega = \sum_{k=1}^N \alpha_k \varphi(x_k) \quad (18)$$

$$\frac{\partial L(\omega, b, e, \alpha)}{\partial b} = 0 \rightarrow \sum_{k=1}^N \alpha_k = 0 \quad (19)$$

$$\frac{\partial L(\omega, b, e, \alpha)}{\partial e_k} = 0 \rightarrow \alpha_k = \gamma e_k, \quad k = 1, 2, \dots, N \quad (20)$$

$$\frac{\partial L(\omega, b, e, \alpha)}{\partial \alpha_k} = 0 \rightarrow y_k = \varphi(x_k) \omega^T + b + e_k, \quad k = 1, 2, \dots, N \quad (21)$$

When the parameters ω and e are removed, the Karush–Kuhn–Tucker system can be obtained as follows:

$$\begin{bmatrix} 0 \\ 1_b \end{bmatrix} - \frac{1_b^T}{\Omega + \gamma^{-1}I} \begin{bmatrix} b \\ \alpha \end{bmatrix} = \begin{bmatrix} 0 \\ y \end{bmatrix} \quad (22)$$

In Equation 22, $y = [y_1, \dots, y_N]^T$; $1_N = [1, \dots, 1]^T$; $\alpha = [\alpha_1, \dots, \alpha_N]^T$; I is the identity matrix.

$\Omega_k = \varphi(x_k)^T \cdot \varphi(x_l) = K(x_k, x_l) \forall k, l = 1, 2, \dots, N$; $K(x_k, x_l)$ is the kernel function that must satisfy Mercer's condition (Li et al., 2008). Three options are available for the kernel function:

$$K(x, x_k) = x_k^T x \quad (23)$$

$$K(x, x_k) = (\tau + x_k^T x)^d \quad (24)$$

$$K(x, x_k) = \exp(-x - x_k^2/\sigma^2) \quad (25)$$

Based on the above three options, the following is a description of the latest part of the LSSVM algorithm for parameter estimation:

$$y(x) = \sum_{k=1}^N \alpha_k K(x, x_k) + b \quad (26)$$

where τ denotes the slope; d represents the degree of the polynomial; σ^2 denotes the kernel sample variance; (b, α) stands for the answer to the equations' linear system illustrated in Equation 22. In this study, σ^2 and γ were considered to be the two main hyperparameters for tuning the LSSVM model. These two parameters are vital for obtaining the optimal prediction performance for daily discharge in mega deltas.

3.2.6. Multivariate Adaptive Regression Splines

MARS is defined as non-parametric regression technique proposed by Friedman (1991). It can map nonlinearities and interactions between parameters. MARS creates a predictive model (\hat{f}) via the following equation:

$$\hat{f}(x) = \sum_{i=1}^k \alpha_i B_i(x) \quad (27)$$

where x represents the vector that includes all the input variables; B_i represents the basis functions; k denotes the number of basis functions defined by the regression function; and α_i denotes the i_{th} constant coefficient. Additionally, each basis function $B_i(x)$ considers one of the following constraints: (a) a single basis function has a constant value approximately equal to 1; (b) a hinge function; (c) at least two or multiple hinge functions. A hinge function is illustrated by $\max(0, x - c)$ or $\max(0, c - x)$, in which c is a constant, namely, a knot (Chen & Pawar, 2019).

The utilization of hinge functions supports MARS by splitting the response surface into different continuous areas. MARS constructs a model in two stages with forward and backward processes. MARS begins with a model that comprises the single basis function of 1. Then, MARS frequently includes paired basis functions for the available basis functions. In each iteration step, it searches for the pair of basis functions that minimizes the sum-of-squares residual error (SSRE), which is defined as follows (Friedman, 1991):

$$SSRE = \sum_{i=1}^{N_s} (y_i - \hat{f}(x_i))^2 \quad (28)$$

in which N_s denotes the number of training points; y_i is the i_{th} output achieved from training datasets; and x_i are the i_{th} input variables of training points. The added terms repeat until the change in the residual error is less than a target value or the maximum allowable term value is obtained. The forward process often creates an overfit model. To prevent overfitting, a backwards process is implemented to shape the ML model. The model extracts one less effective term in a paired basis function at each step until the best sub-model is obtained. The term choice to be removed is based on the minimum value of the generalized cross validation (GCV). The GCV is defined as follows:

$$GCV = \frac{SSRE}{N_s * (1 - N_e/N_s)} \quad (29)$$

where N_e indicates the number of effective terms. The backwards process permits the MARS method to build a model that integrates the good fit and model parsimony criteria. According to Friedman (1991), if MARS is given an input x , it can produce all the basis functions, $B_i(x)$, and their corresponding coefficients, α_i . In this study, the maximum number of terms and max_degree was the two main tuning hyperparameters, and all the remaining parameters were set to the default values.

3.2.7. K-Fold Cross Validation and Grid Search Process for Hyperparameter Tuning

The data set was separated into two subsets (training [70%] and testing [30%]) to develop the DT, GPR, SVR, RF, LSSVM, and MARS models. These ML models can be adjusted by varying the hyperparameters that control model performance. First, the training data were subjected to k-fold cross-validation (k-FCV) to determine the optimal hyperparameters (Markatou & Hripcsak, 2005). The training samples were subdivided into k subsets: $k-1$ sets were used to train the models. The k th parameter was employed to assess the performance of the hyperparameters based on the validation data. For each candidate hyperparameter, the procedure was repeated k times. Then, the goodness of fit of the ML models was estimated based on four statistical indicators for the training and validation datasets, namely, the root mean square error (RMSE), correlation coefficient (r), Nash-Sutcliffe number (NSE), and mean absolute error (MAE).

The grid search (GS) process creates groups for all compositions of values based on the prescribed search extent of hyperparameters and assesses each group using k-FCV (Kanin et al., 2019). The lowest RMSE and MAE or the highest r and NSE help to decide the optimum hyperparameter values. The RMSE, r , NSE, and MAE were computed as follows:

$$RMSE = \sqrt{\frac{1}{n} \sum_{i=1}^n (Y_{i,m} - Y_{i,e})^2} \quad (30)$$

$$r = \frac{n \sum_{i=1}^n (Y_{i,m} \times Y_{i,e}) - \sum_{i=1}^n Y_{i,m} \sum_{i=1}^n Y_{i,e}}{\sqrt{\left(n \sum_{i=1}^n Y_{i,m}^2 - \left(\sum_{i=1}^n Y_{i,m} \right)^2 \right) \left(n \sum_{i=1}^n Y_{i,e}^2 - \left(\sum_{i=1}^n Y_{i,e} \right)^2 \right)}} \quad (31)$$

$$NSE = 1 - \frac{\sum_{i=1}^n (Y_{i,m} - Y_{i,e})^2}{\sum_{i=1}^n (Y_{i,m} - \bar{Y}_{i,m})^2} \quad (32)$$

$$MAE = \frac{\sum_{i=1}^n |Y_{i,m} - Y_{i,e}|}{n} \quad (33)$$

In these equations, $Y_{i,m}$, $Y_{i,e}$, and n are the observed discharge, predicted discharge, and total number of observations, respectively. RMSE is the difference between the simulated and measured values. r expresses the agreement between the simulated and observed values. NSE represents how well the simulated data match the corresponding observed values. MAE measures the errors between the predictions and the observations.

4. Results and Discussion

4.1. Selection of the Optimization Models

The proposed ML models require many tuning hyperparameters to train the data set. Some of these variables are important for achieving satisfactory model performance; therefore, they must be defined appropriately. To evaluate the ML model performance in reconstructing the daily-averaged discharge, k-FCV and GS processes were applied to achieve the optimal hyperparameter values for the DT, GPR, SVR, RF, LSSVM, and MARS models. In the GS process, the search range was divided into 30 grid divisions, and each grid division was then assessed using k-FCV. In this work, 10-fold cross-validation was selected for ML model optimization. Then,

Table 1
The Variables Used in the ML Models

| Model | Adjusted hyperparameters | Specific search range | Optimal values of hyperparameters | Input | Output |
|-------|--------------------------|-----------------------|-----------------------------------|--|-----------------------------|
| DT | Leaf Size | 1–3,115 | 40 | WK_{t-1} | Daily discharge at Tan Chau |
| GPR | θ | 57–57,000 | 12,100 | WK_{t-2} | |
| | ϵ | 0.001–69,055 | 68,500 | WP_t WP_{t-1} WP_{t-2} | |
| SVR | C | 0.001–1,000 | 930 | WK_{t-2} | |
| | γ | 0.01–2,000 | 960 | *WK: water level at | |
| | ϵ | 10–9,000 | 2,300 | Kratie | |
| RF | N_Est | 100–500 | 310 | *WP: water level at | |
| | Max_D | 10–100 | 60 | Prek Kdam | |
| LSSVM | Max_F | 0.5–1.0 | 0.96 | * t is the time, and $t-1$ and $t-2$ are the 1- and 2-day lagged times | |
| | σ^2 | 0.1–10 | 0.5 | | |
| | γ | 5–100 | 10 | | |
| MARS | Max-terms | 500–2,000 | 1,000 | | |
| | Max_degree | 100–1,000 | 300 | | |

the GS process was used to determine the minimum MSE for all six ML models based on the specific ranges of parameters. Table 1 provides detailed descriptions of the variables employed in training the six ML models.

The DT model was first examined by the GS process. Leaf size was used as the key tuning parameter. As shown in Table 1, the optimal leaf size was 40, and the DT model achieved the best prediction performance at this leaf size. Next, the GPR model was employed to evaluate the prediction ability for the daily discharge. This study used θ and ϵ to achieve the best estimating outcome of the GPR scheme. The best values of θ and ϵ were 12,100 and 68,500, respectively. The computational time to achieve the optimal tuning parameter of the GPR model was quite long because of the complex mathematical functions. Regarding the SVR model, three tuning parameters were used to achieve the desired predictive performance. Table 1 highlights the optimal values for various hyper-parameters. As previously mentioned, SVR can produce quick predictions to obtain the optimal tuning parameters. Following SVR, the RF model was applied to predict daily discharge at the Tan Chau station. N_Est , Max_D , and Max_F were used for the tuning process of the RF. The optimum values for the parameters were 310, 60, and 0.96, respectively. The computational time of the GS process for RF to achieve the optimal values for the three tuning parameters was also relatively short.

Furthermore, this study adopted advanced LSSVM and MARS approaches to validate the most robust ML models and reconstruct the daily-averaged discharge in the mega delta. According to the LSSVM model, σ^2 and γ are the two key parameters for the tuning process. The computational cost of the LSSVM model was high compared to that of the prior four evaluated ML models. In addition, the MARS model was also used for the comparison. As mentioned earlier in ML theory, max-terms and max_degree were employed to determine the best prediction performance of the MARS model. By tuning these two parameters using the GS process, the optimal outcome of the MARS method to predict daily-averaged discharge at the Tan Chau station was achieved.

4.2. What Models Are Recommended?

Here, we present a comparison of the results estimated by the ML and RC models in reconstructing the missing values of the daily-averaged discharge. Generally, all ML models were superior to the RC model, as indicated by the time series comparison, statistical indicators (r , $RMSE$, NSE , MAE , and percentile values in the violin plots), and percentage differences in the peak discharge (Figures 3–5; Table 2). These results suggest that ML models are applicable for simulating the hydrology of the VMD. On the basis of the MI and correlation coefficients in the

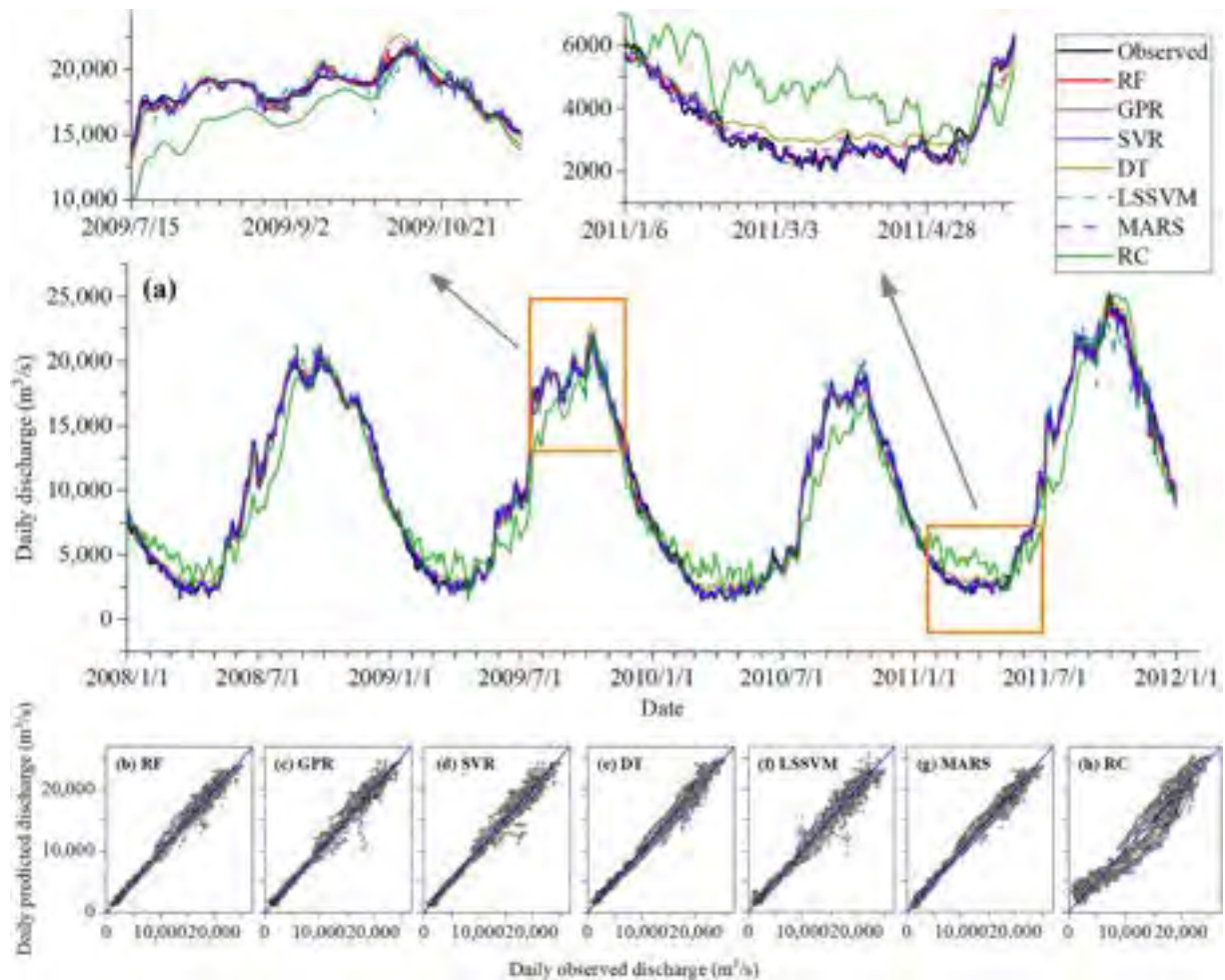


Figure 3. Results of the six machine learning (ML) and rating curve (RC) models for the testing data set. (a) Time series comparison between the predicted and measured values. (b–f) Scatter plots of the predicted versus measured values of individual ML and RC models, with the bisector line (1:1) shown.

data pre-processing, the effect of the flow at Prek Kdam on the flow at Tan Chau was found to be faster than the corresponding effect at Kratie by 1 day; in other words, the flow at Prek Kdam influenced the flow at Tan Chau sooner than the flow at Kratie. This difference is physically explained by the distance from Tan Chau to Prek Kdam (~144 km), which is much shorter than that from Tan Chau to Kratie (~316 km). This result confirms the importance of Tonle Sap Lake in regulating flows in the VMD, as also noted in previous research (e.g., Pokhrel et al., 2018).

The RC method produced the worst values of the statistical indicators (e.g., *RMSE* up to 2,438 m³/s in the training period) and the lowest accuracy in flood peak simulation (e.g., the flood peak was underestimated by –31% and –11.1% for the training and test datasets, respectively) (Table 2; Figures 3–5). A time series plot (Figure 3a) shows that the RC significantly underestimates the flood flow and overestimates the dry flow relative to the observed data. The underestimation of the flood peak is remarkably large in dry years, for instance, in 2010 (by –11.1%) and 1993 (by –7%) (Figure 5a). In flood months, the *NSE* values are very low (0.154 in the training and 0.523 in the testing periods) and are much lower than the respective values acquired from all the ML models (Table 2). The goodness of the predictions in the dry months from the RC is even lower than that in flood months (*NSE* = –0.77 and –2.64; *r* = 0.691 and 0.655; *RMSE* = 1,599 and 1,744 m³/s in the training and testing periods, respectively). Furthermore, Figures 4 and 5a clearly show the poor performance of the RC model compared to all six ML models.

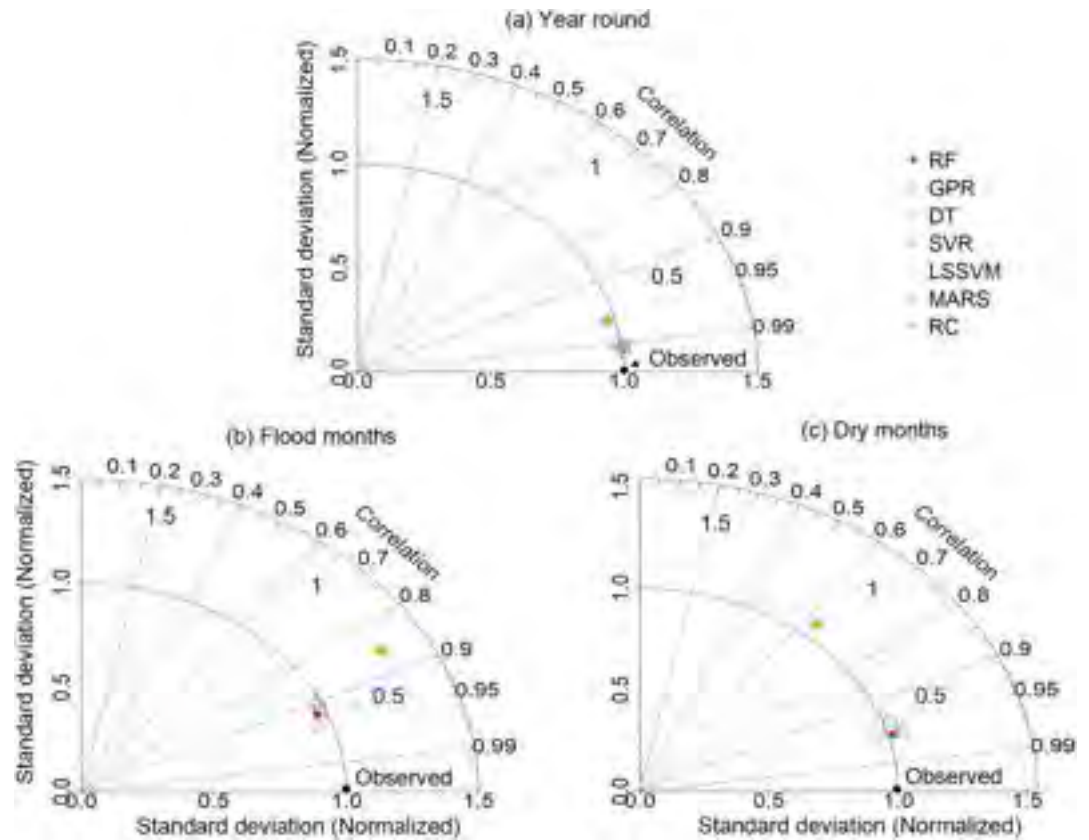


Figure 4. Taylor diagrams indicating the performance of six machine learning (ML) and rating curve (RC) models using the data from (a) year-round, (b) flood months, and (c) dry months.

These results indicate that the RC model based on year-round data alone cannot provide accurate reconstructions because of seasonal effects, which result in different hydrological behavior. To enhance the goodness of fit of the RC method, Moftakhari et al. (2015) established two RCs to predict the discharge of the Sacramento River by dividing the water level data into two subsets (i.e., <6.2 and >6.2 m) to account for seasonal effects. Binh, Kantoush, et al. (2021) revealed a clockwise hysteresis relation between the discharge and water level in the VMD, suggesting that RCs for rising and falling limbs should be developed differently. In the VMD, the flow characteristics in the rising and falling limbs are completely different: the former is controlled by riverine flood waves from upstream and the latter is strongly influenced by tides. RC is strongly influenced by the evolution of river geometry (i.e., erosion and deposition) and roughness (e.g., vegetation, infrastructure) and the effects of backwater and tides (Matte et al., 2018). Under the fluctuational tidal influence induced by oceanic and astronomical forcing (Jay et al., 2011; Moftakhari et al., 2013), a discharge magnitude does not yield a unique water level; rather, different water level values can be recorded (Hoitink & Jay, 2016). Specifically, because of the interactions among the reversing tidal flow, the tidal Stokes drift, spring-neap tidal cycle, lateral and estuarine circulations, the occurrence of multiple branches, and nonlinear frictional interactions between riverine flow and oceanic tides (Moftakhari et al., 2016), a hysteresis phenomenon is typically involved in the tidal process, in addition to many other hydrologic processes, as reported by Nourani, Parhizkar, et al. (2014). Due to this hysteresis behavior and loop, different outputs are possible for the same input; therefore, the RC method, which uses an injective function and a linear regression model, is not sufficiently robust to handle such nonlinear and complex problems. The above-mentioned phenomena are the root causes of the low prediction accuracy of the RC. To handle such issues, in the ML models established in this study, we used the data from multiple upstream gauges, as suggested by Moftakhari et al. (2016). We also used time-series data in the ML models to account for the temporal sequences involved in the data. This inclusion improved the modeling performance compared to that of RCs, which do not consider temporal data as an input. The complex hysteresis phenomenon involved in the tidal flow process can be robustly handled by the nonlinear artificial intelligence-based methods used in this study, as noted by Nourani,

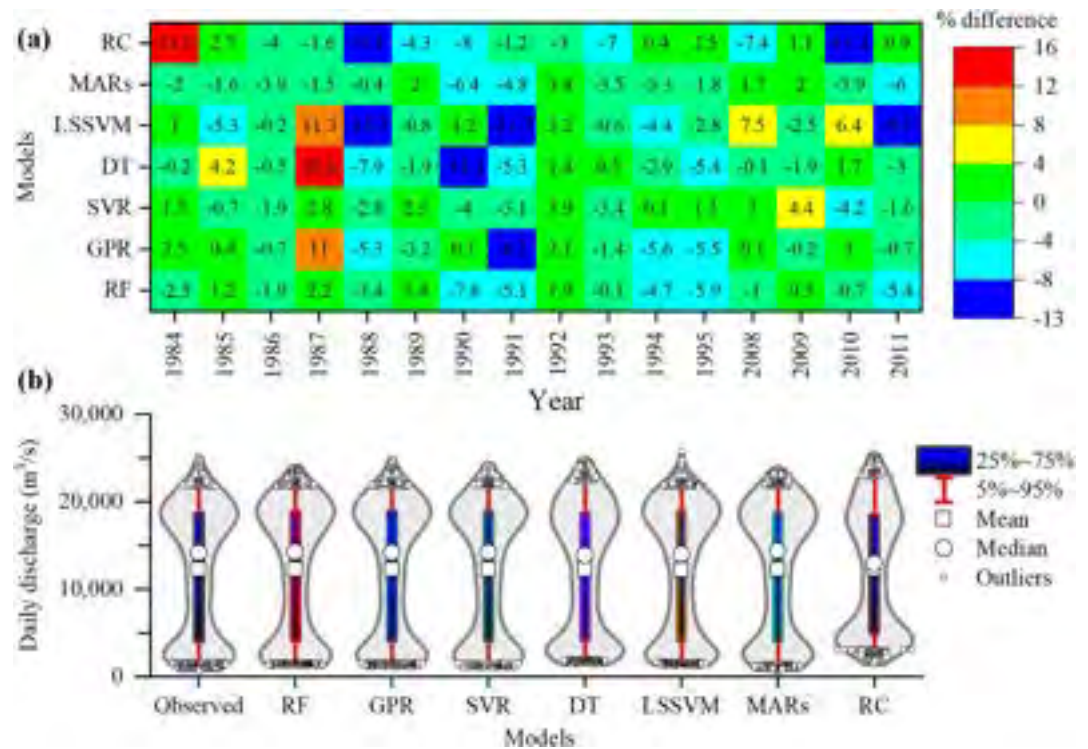


Figure 5. (a) Heatmap showing the percentage differences in the flood peaks predicted by the machine learning (ML) and rating curve (RC) models relative to the observed data. (b) Violin plots showing the goodness of fit of the predicted discharges versus the observed values. These plots are based on the data from the testing period.

Parhizkar, et al. (2014). Moreover, the use of RCs requires an extensive understanding of flow behavior and input data because both discharge and water level information from the same station are used; any misuse of the input data could directly lead to large discrepancies in the output. This influence is negligible in ML methods. Additionally, lag time must be considered in the ML models when water flows in the river from upstream to downstream, while this lag is ignored in the RC model. Moreover, ML models account for upstream-downstream relations and consider physical relations in addition to hydrological processes.

Among the ML models considered for the training data set, GPR and SVR perform better than the RF, DT, LSSVM, and MARS models in terms of statistical indicators (Table 2). For instance, the *RMSE* of GPR and SVR using year-round data is 389 and 476 m³/s, respectively, compared to 1,037 and 973 m³/s for the DT and MARS models, respectively. However, the MARS and RF models showed the best performance in the testing period, with the highest *r* and *NSE* values (e.g., *r* = 0.994 for both the MARS and RF models compared to 0.988 for the LSSVM model and 0.992 for the DT model using year-round data) and the lowest *RMSE* and *MAE* values (e.g., *RMSE* = 768 m³/s for the MARS model and 789 m³/s for the RF model compared to 943 m³/s for the SVR model and 1,098 for the LSSVM model considering the year-round data). Table 2 also shows the superior operation of the MARS and RF methods in both flood and dry months over the remaining four ML models with regard to all four statistical metrics.

The outstanding performance of the MARS and RF models over the other ML models can be clearly seen in the scatter plots (Figures 3b and 3g), Taylor diagrams (Figures 4b and 4c), and violin plots (Figure 5b). The scatter plots show that a majority of the scatter points using MARS and RF are concentrated around the bisector 1:1 line. Likewise, the Taylor diagrams point to the superior performance of the MARS and RF models because their results were the closest to the observed values. Based on the Taylor diagram, the LSSVM showed the worst performance, followed by the DT model because their results are the farthest from the observed points. This finding is confirmed by the *NSE* indicator shown in Table 2; for instance, the *NSE* values of the LSSVM and DT models were 0.528 and 0.676 in the dry months, respectively. Regarding the time series comparison (Figure 3a), the MARS and RF results effectively agree with the observed data. The SVR model produced unreasonable

Table 2
Statistical Indicators for the Six ML and RC Models

| Model | Year round | | | | Flood months | | | | Dry months | | | |
|----------|------------|-------------|------------|------------|--------------|-------------|------------|------------|------------|-------------|------------|------------|
| | <i>r</i> | <i>RMSE</i> | <i>NSE</i> | <i>MAE</i> | <i>r</i> | <i>RMSE</i> | <i>NSE</i> | <i>MAE</i> | <i>r</i> | <i>RMSE</i> | <i>NSE</i> | <i>MAE</i> |
| Training | | | | | | | | | | | | |
| RF | 0.996 | 602 | 0.992 | 412 | 0.965 | 695 | 0.931 | 528 | 0.978 | 251 | 0.956 | 193 |
| GPR | 0.998 | 389 | 0.997 | 273 | 0.988 | 399 | 0.977 | 286 | 0.976 | 263 | 0.952 | 202 |
| DT | 0.989 | 1,037 | 0.977 | 802 | 0.914 | 1,209 | 0.792 | 1,008 | 0.934 | 625 | 0.729 | 538 |
| SVR | 0.997 | 476 | 0.995 | 315 | 0.977 | 573 | 0.953 | 410 | 0.984 | 210 | 0.969 | 158 |
| LSSVM | 0.996 | 560 | 0.993 | 399 | 0.975 | 583 | 0.951 | 432 | 0.981 | 229 | 0.963 | 172 |
| MARS | 0.99 | 973 | 0.980 | 708 | 0.936 | 928 | 0.877 | 754 | 0.959 | 341 | 0.919 | 264 |
| RC | 0.954 | 2,087 | 0.91 | 1,629 | 0.841 | 2,438 | 0.154 | 2,026 | 0.691 | 1,599 | -0.77 | 1,405 |
| Testing | | | | | | | | | | | | |
| RF | 0.994 | 789 | 0.988 | 517 | 0.928 | 978 | 0.86 | 722 | 0.961 | 264 | 0.917 | 200 |
| GPR | 0.992 | 878 | 0.985 | 533 | 0.919 | 1,056 | 0.837 | 748 | 0.944 | 313 | 0.884 | 234 |
| DT | 0.992 | 886 | 0.985 | 659 | 0.929 | 1,082 | 0.829 | 815 | 0.939 | 522 | 0.676 | 454 |
| SVR | 0.991 | 943 | 0.983 | 588 | 0.901 | 1,160 | 0.804 | 845 | 0.961 | 274 | 0.911 | 206 |
| LSSVM | 0.988 | 1,098 | 0.977 | 747 | 0.826 | 1,497 | 0.673 | 1,059 | 0.818 | 631 | 0.528 | 426 |
| MARS | 0.994 | 768 | 0.989 | 544 | 0.942 | 872 | 0.889 | 646 | 0.96 | 257 | 0.921 | 198 |
| RC | 0.968 | 1,851 | 0.937 | 1,517 | 0.858 | 1,807 | 0.523 | 1,469 | 0.655 | 1,744 | -2.64 | 1,578 |

Note. The models were built using year-round data; however, statistical indicators are also shown for the flood and dry months to highlight the performance of the individual models. The flood months are from August to October, and the dry months are from February to April. Time lag was not considered in the RC model. The unit of the *RMSE* and *MAE* is m³/s.

fluctuations in the discharge in the flood months; moreover, the DT model was unable to reliably reconstruct the discharge in the dry months. Another important indicator of discharge reconstruction is the flood peak, which has significant implications for flood management. All six ML models generally underestimated the flood peak, for instance, by -12.5% in 1990 using the LSSVM model; additionally, the GPR and SVR models overestimated the flood peak by up to 11% and 15.6% in 1987, respectively (Figure 5a). In flood years (e.g., 1996, 2000, and 2011), the RF and GPR models performed better than the SVR and DT models for the training data set, while the GPR and DT models performed better than the RF and SVR models for the testing data set. However, in drought years (i.e., 1993, 1998, 2005, and 2015), RF outperformed the other five ML models. For instance, the RF model underestimated the flood peak in 2010 by only -0.7%, while the DT model underestimated it by -4.2% (Figure 5a). The underestimation of the flood peaks, particularly in the extreme flood (e.g., 2000) and drought years (e.g., 2015), by the ML models was attributed to the limited data used to train the models. Underestimation of predicted flood peaks is common in hydrological modeling for both types of hydrological models (Tegegne et al., 2017; Vansteenkiste et al., 2014) and ML algorithms (Adnan et al., 2020; Tencaliec et al., 2015).

A comparison of the predicted and observed values using the time series plots, scatter plots, Taylor diagram, violin plots, heatmap, and statistical indicators reveals that the MARS and RF models most reliably reconstructed the daily-averaged discharge at Tan Chau (Figures 3-5; Table 2), although the performance of MARS was slightly better than that of RF. Thus, the MARS and RF models are recommended for daily-averaged discharge reconstruction in tidally affected river systems such as that in the VMD. This finding agrees with those of previous research that used ML models to assess hydrological processes (e.g., Hussain & Khan, 2020; Jekhouni et al., 2020; Li et al., 2016; Obringer & Nateghi, 2018). For instance, Obringer and Nateghi (2018) verified that the RF model was the best model among nonparametric ML algorithms in predicting riverine water levels. The GPR model is also trustworthy for reconstructing the discharge in tidally affected rivers. Notably, the DT model is not recommended in this study based on the abnormal and unreasonable fluctuations in the time series results, especially in dry months, compared to the measured data. In this study, we used individual ML models to reconstruct the missing discharge values. However, using a hybrid model by combining an ML model with an analytical, empirical or numerical model may improve the performance, and this research direction will be examined in future work.

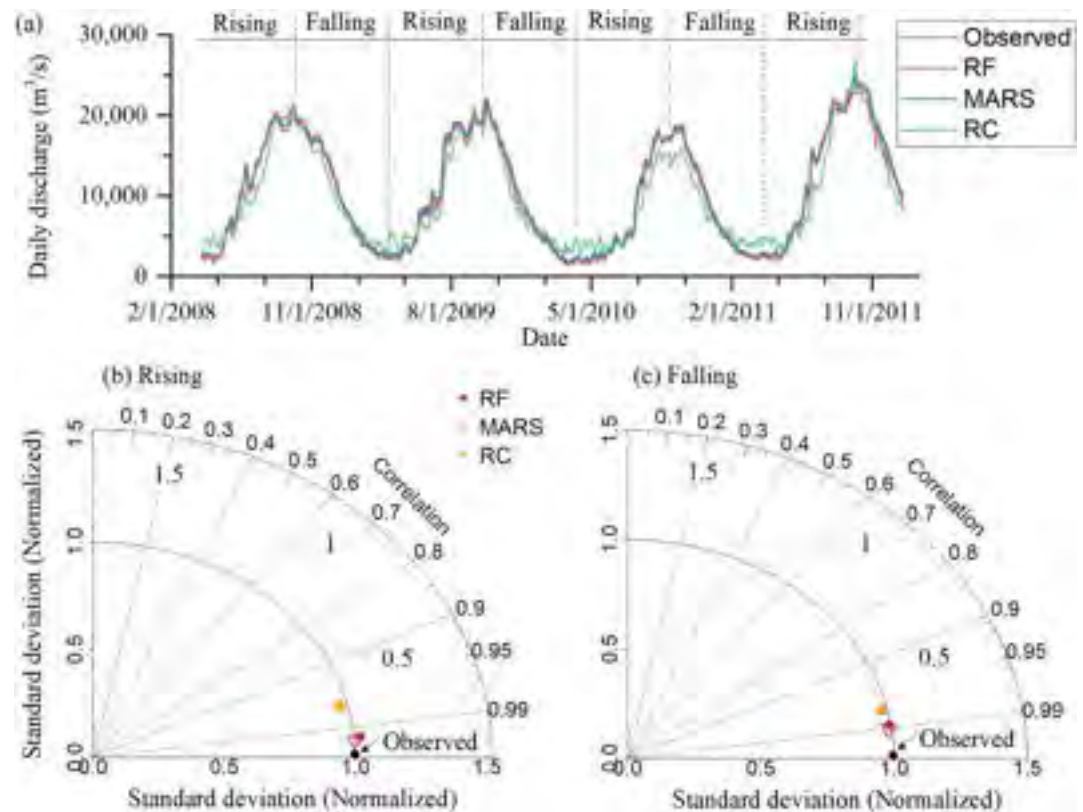


Figure 6. (a) Time series plot comparing the predicted discharge from multivariate adaptive regression spline (MARS), random forest (RF), and rating curve (RC) models with the observed data. (b, c) Taylor diagrams showing the performance of the three models in the rising and falling phases.

For instance, Safari (2020) found that the hybridization of the MARS and RF models with the empirical MNL model provides better predictions of incipient sediment deposition compared to the individual MARS and RF models.

4.3. Is Prediction Accuracy Increased by Considering Seasonal Patterns?

Binh, Kantoush, et al. (2021) found that separately constructing stage-discharge RCs for the rising and falling limbs can improve the reconstruction of the missing daily-averaged discharge in the VMD. Therefore, in this section, we attempt to apply the MARS and RF models in assessments of these two limbs to determine whether the prediction accuracy is enhanced. This approach also reduces the computational time and the effort required to collect data if the research focus is in flood or drought seasons.

Comparison of Figures 6 and 7 with Figures 3–5 along with statistical indicators (Table 2) reveals that the MARS and RF models established for the rising and falling limbs separately do not improve the prediction accuracy compared to the results obtained using the year-round data; in fact, the accuracy decreases slightly. Specifically, the statistical indicators of the RF model from the falling phase in the testing period ($r = 0.987$, $RMSE = 1,040 \text{ m}^3/\text{s}$, $NSE = 0.973$, $MAE = 742 \text{ m}^3/\text{s}$) are lower than those obtained using the year-round data ($r = 0.994$, $RMSE = 789 \text{ m}^3/\text{s}$, $NSE = 0.988$, $MAE = 517 \text{ m}^3/\text{s}$). Similarly, the corresponding values of the MARS model are $r = 0.991$, $RMSE = 856 \text{ m}^3/\text{s}$, $NSE = 0.982$, $MAE = 485 \text{ m}^3/\text{s}$, while those from the year-round data are $r = 0.994$, $RMSE = 768 \text{ m}^3/\text{s}$, $NSE = 0.989$, $MAE = 544 \text{ m}^3/\text{s}$. In flood peak prediction, however, the accuracy of the MARS and RF models considering seasonal patterns improves slightly compared to that in the original case. For instance, relative to the measured data, the mean predicted flood peaks in the test period of MARS and RF are underestimated by -1.4% and -1.1% , respectively, when seasonal patterns are considered and by -1.9% and -2% , respectively, when year-round data are used. The unexpected lack of improvements in the MARS and RF models for the rising and falling limbs is likely because of the reduction in the number of data points used ($\sim 50\%$ reduction). The above results, together with the Taylor diagrams (Figures 6b and 6c) and the scatter and violin

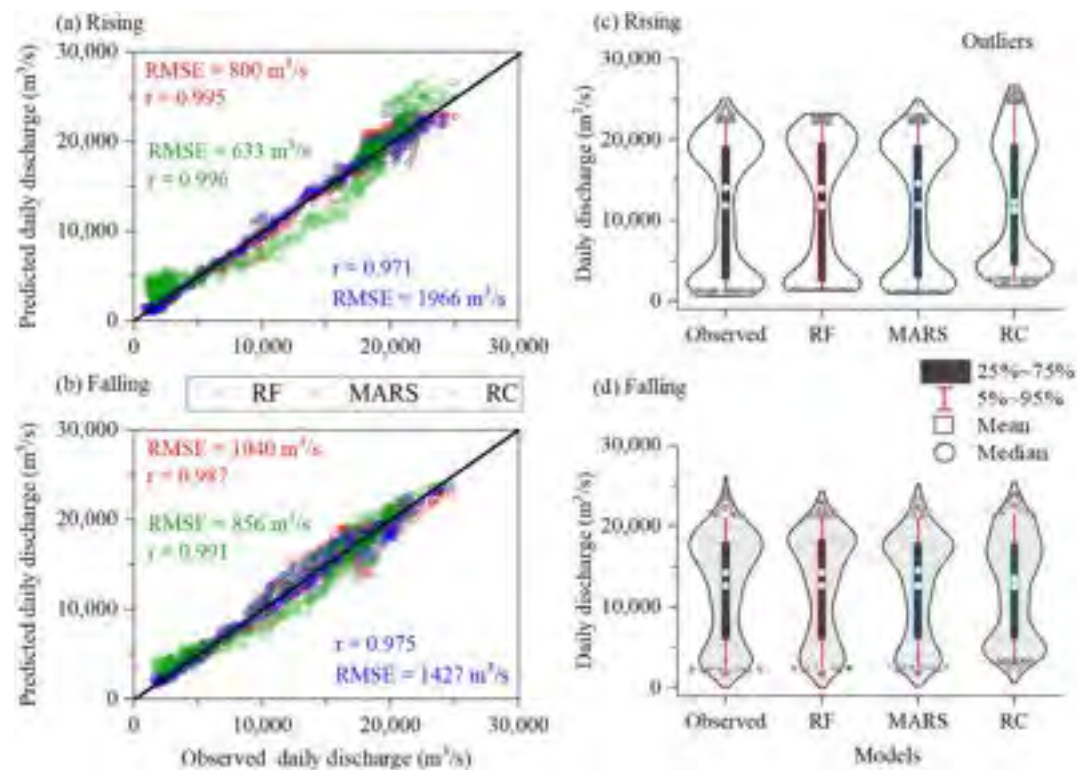


Figure 7. Predicted versus observed discharge values using the multivariate adaptive regression spline (MARS), random forest (RF), and rating curve (RC) models for the rising and falling phases. (a, b) Scatter plots with statistical indicators. (c, d) Violin plots comparing the results of the MARS, RF, and RC models with their observed counterparts for the rising and falling phases. All data plotted are from the test period. The MARS and RF models outperform the RC model.

plots (Figure 7), demonstrate that MARS is marginally better than RF. We also observed that the accuracy of MARS and RF in predicting the discharge in the rising phase was greater than that in the falling phase.

In contrast, the RCs that were separately developed for the rising and falling limbs enhanced the prediction accuracy substantially compared to those based on the year-round data. For example, in the test period, the performance of the RC model considering seasonal patterns (e.g., $r = 0.975$, $RMSE = 1,427 \text{ m}^3/\text{s}$ in the falling limb) was improved relative to that of the model using the year-round data (e.g., $r = 0.968$, $RMSE = 1,851 \text{ m}^3/\text{s}$). Although improved, the results of the RC model are still inferior to those of the MARS and RF models, particularly for the rising limb (Figures 6 and 7).

In short, there are two main implications drawn from the above results. First, although using separate RCs for the rising and falling limbs can improve the prediction accuracy compared to those based on year-round data, the MARS and RF models still outperformed the RC model. However, if only the water level at a station at which the discharge needs to be reconstructed is available, RCs considering seasonal patterns can produce acceptable results. Second, the MARS and RF models that were separately established for the rising and falling limbs should be used with care, especially for the falling limb, if the research interest is the flood or drought period alone.

4.4. Prospects of Using ML in Hydrological Assessment in the Mekong River Basin

ML has been used by hydrologists to assess hydrological processes in many rivers worldwide, and its applications include rainfall (Alizadeh et al., 2017; Tikhmarine et al., 2020), streamflow (Luo et al., 2019; Zia et al., 2015), salinity (Tran et al., 2021), water quality (Elkiran et al., 2019; Imani et al., 2021), and sediment (Huang et al., 2019; Zounemat-Kermani et al., 2020) assessments. In tidally affected river systems, such as the Mekong River basin, the use of ML to explore hydrology and hydrological processes is limited. Notably, the use of ML to study hydrology is especially limited in the VMD, where data availability is a constraint for scientific research and resource management. Therefore, the use of ML in the VMD is recommended for (a) data reconstruction,

such as for tide, sediment, and salinity concentration data, and (b) hydrological and water quality prediction. We acknowledge that reconstructing salinity and sediment data is even more challenging than reconstructing river flows; thus, the latter is vital for the former and will be the focus of our future research. Such predictions have been made using statistical models (Apel et al., 2020). However, most predictions are medium-term estimates (up to 9 months), and appropriate and proactive water resource planning and management tasks require long-term predictions, especially considering variations in upstream inflows because of changes in dam management and climate change, downstream rising sea level and saline water intrusion, and the increasing water demand within the delta (e.g., Binh, Kantoush, Saber, et al., 2020; Park et al., 2021, 2022). Therefore, ML methods are promising tools for gaining insight into hydrological processes and improving water resource management.

Flooding is an annual event in the VMD; however, extreme floods, such as the historical floods in 1996, 2000, and 2011, have appeared periodically and may cause disastrous damage to society (Triet et al., 2018). Therefore, flood prediction has an important role in flood preparedness. In the study of floods, it is crucial to predict flood water levels because it is the water level, not the discharge, that causes flood problems. In the tidally affected rivers in the VMD, the water level fluctuates remarkably under tidal effects within a day. Given the rapid evolution of flood water, it is necessary to predict hourly water levels instead of daily-averaged values, as was done in this study for the discharge reconstruction. Collectively, predicting the hourly flood water levels is even more challenging than predicting the daily-averaged discharge. As such, ML and RC models may yield undesirable predictions. Although challenging, we intend to develop a robust methodology using deep learning models to predict hourly flood water levels in the VMD in future studies, with the goal of helping the delta to prepare to cope with future flood disasters.

5. Concluding Remarks

Six ML-based methods were employed in the present research to reconstruct the missing daily-averaged discharge in a tidal river system, the VMD. The missing historical data have limited studies of long-term flow regime variations under the effects of climate change and intensifying anthropogenic intervention, such as the construction of hydropower dams and irrigation expansion. We used multi-station data considering upstream-downstream relations, and the water level at two upstream stations in different geographical settings was used to reconstruct the discharge at a downstream station. While many studies have ignored data pre-processing when completing similar tasks, we performed it in three steps: first, the raw data were normalized to remove trends in variance and mean; second, the Fourier series were fitted to remove seasonal effects; and third, first-order differencing was conducted. Additionally, MI and correlation coefficient methods were applied to optimize the model inputs and avoid the use of too many simulation parameters; moreover, lagged data were considered, thereby reducing the simulation time and effort. The results of our study are important for long-term water resource management in the delta, and the methodology developed can easily be adopted for other river systems.

Unlike the traditional stage-discharge RC method using linear regression, ML models can provide reliable reconstructions of the missing daily-averaged discharge. The water levels, with lagged time considerations, at Kratie and Prek Kdam are appropriate to input into the ML models. The present study provides a basis for hydrologists and researchers who plan to employ ML models for future water resource management in the VMD in the context of global warming. Our next step is to use ML to predict the discharge in the Mekong River from the short to the long term for optimal water resource allocation, particularly to enhance flood and drought preparedness.

The MARS and RF models are the two most suitable algorithms for reconstructing the missing daily-averaged discharge, although the MARS model performs slightly better than the RF model. These approaches can reliably predict flood peak, flood flow, and drought flow discharges and are therefore suitable for flood, drought and salinity intrusion studies. Compared to the RC method, the RF model reduces the *RMSE* and *MAE* by 135% and 194% (year-round data), 85% and 104% (flood-month data), and 561% and 691% (dry-month data), respectively. The respective values for the MARS and RC models are 141% and 179% (year-round data), 107% and 127% (flood-month data), and 578% and 696% (dry-month data). Establishing MARS and RF models for the rising and falling limbs separately did not improve the prediction accuracy; however, acceptable results could be obtained for a specific flood or drought period. MARS and RF reconstruct the daily-averaged discharge in the rising phase better than in the falling phase. The GPR and SVR models are also appropriate for daily-averaged discharge

reconstruction in the delta. The DT model, however, is not recommended because it produces abnormal, unreasonable fluctuations in the predicted discharge.

Since this paper is our first attempt to use ML models to estimate hydrological parameters in the VMD, we applied simple techniques to pre-process the input data. In future works, more advanced de-noising methods, such as the wavelet de-noising approach (Nourani, Baghanam, et al., 2014) or ensemble empirical mode decomposition (EEMD) (Gaci, 2016), are recommended for obtaining better performance in the application of ML models. Moreover, more advanced artificial intelligence models, such as deep learning neural networks (Ha et al., 2021), should be considered in the next attempt to forecast the discharge, sediment, and salinity in the VMD to support strategic decision making. The hybridization of ML models with other empirical, analytical or numerical models is also a good strategy to improve the prediction power of ML. Finally, our future work will focus on estimating the tidal water level and discharge on an hourly interval to quantify the net riverine and tidal flux exchange between rivers and seas.

Conflict of Interest

The authors declare no conflicts of interest relevant to this study.

Data Availability Statement

Daily-averaged water levels at Kratie and Prek Kdam are available at <https://portal.mrcmekong.org/time-series> (the station names and type of data requested must be typed into the search boxes), and daily-averaged discharges at Tan Chau can be downloaded from Binh, Thanh, et al. (2021).

Acknowledgments

The authors would like to acknowledge the Mekong River Commission and the Vietnam National Center for Hydrometeorological Forecasting for providing the data. We thank the Japan-ASEAN Science, Technology and Innovation Platform (JASTIP), the Supporting Program for Interaction-Based Initiative Team Studies (SPIRITS) 2016 of Kyoto University, the Asia-Pacific Network for Global Change Research under project reference number CRRP2020-09MY-Kantoush, and BrainKorea21 FOUR Postdoctoral Fellowship of Seoul National University for funding this research. This work was supported by the Korea Institute of Energy Technology Evaluation and Planning (KETEP) grant funded by the Korean government (MOTIE) (20212010200010, Technical development of enhancing CO₂ injection efficiency and increasing storage capacity).

References

- Adman, R. M., Liang, Z., Heddam, S., Zounemat-Kermani, M., Kisi, O., & Li, B. (2020). Least square support vector machine and multivariate adaptive regression splines for streamflow prediction in mountainous basin using hydro-meteorological data as inputs. *Journal of Hydrology*, 586, 124371. <https://doi.org/10.1016/j.jhydrol.2019.124371>
- Ahmadi, M. A., & Ahmadi, A. (2016). Applying a sophisticated approach to predict CO₂ solubility in brines: Application to CO₂ sequestration. *International Journal of Low Carbon Technologies*, 11(3), 325–332. <https://doi.org/10.1093/ijlct/ctu034>
- Akbarpour, F., Fathi-Moghadam, M., & Schneider, J. (2020). Application of LSPIV to measure supercritical flow in steep channels with low relative submergence. *Flow Measurement and Instrumentation*, 72, 101718. <https://doi.org/10.1016/j.flowmeasinst.2020.101718>
- Akca, E., & Yozgatgil, C. (2020). Mutual information model selection algorithm for time series. *Journal of Applied Statistics*, 47(12), 2192–2207. <https://doi.org/10.1080/02664763.2019.1707516>
- Alizadeh, M. J., Kavianpour, M. R., Kisi, O., & Nourani, V. (2017). A new approach for simulating and forecasting the rainfall-runoff process within the next two months. *Journal of Hydrology*, 548, 588–597. <https://doi.org/10.1016/j.jhydrol.2017.03.032>
- Anderson, O. (1976). *Time series analysis and forecasting: The box-Jenkins approach*. Butterworth.
- Apel, H., Khiem, M., Quan, N. H., & Toan, T. Q. (2020). Brief communication: Seasonal prediction of salinity intrusion in the Mekong Delta. *Natural Hazards and Earth System Sciences*, 20(6), 1609–1616. <https://doi.org/10.5194/nhess-20-1609-2020>
- Binh, D. V., Kantoush, S., & Sumi, T. (2020). Changes to long-term discharge and sediment loads in the Vietnamese Mekong Delta caused by upstream dams. *Geomorphology*, 353, 107011. <https://doi.org/10.1016/j.geomorph.2019.107011>
- Binh, D. V., Kantoush, S. A., Saber, M., Mai, N. P., Maskey, S., Phong, D. T., & Sumi, T. (2020). Long-term alterations of flow regimes of the Mekong River and adaption strategies for the Vietnamese Mekong Delta. *Journal of Hydrology: Regional Studies*, 32, 100742. <https://doi.org/10.1016/j.ejrh.2020.100742>
- Binh, D. V., Kantoush, S. A., Sumi, T., Mai, N. P., Ngoc, T. A., Trung, L. V., & An, T. D. (2021). Effects of riverbed incision on the hydrology of the Vietnamese Mekong Delta. *Hydrological Processes*, 35(2), e14030. <https://doi.org/10.1002/hyp.14030>
- Binh, D. V., Thanh, H. V., Kantoush, S. A., Nourani, V., Saber, M., Lee, K. K., & Sumi, T. (2021). Long-term daily-averaged discharge time series in a megadelta. *Mendeley Data*. V1. <https://doi.org/10.17632/xnzvfcyy68.1>
- Breiman, L. (2001). Random forests. *Machine Learning*, 45(1), 5–32. <https://doi.org/10.1023/a:1010933404324>
- Buschman, F. A., Hoitink, A. J. F., van der Veet, M., & Hoekstra, P. (2009). Subtidal water level variation controlled by river flow and tides. *Water Resources Research*, 45(10), W10420. <https://doi.org/10.1029/2009WR008167>
- Chen, B., & Pawar, R. J. (2019). Characterization of CO₂ storage and enhanced oil recovery in residual oil zones. *Energy*, 183, 291–304. <https://doi.org/10.1016/j.energy.2019.06.142>
- Choi, C., Kim, J., Han, H., Han, D., & Kim, H. S. (2020). Development of water level prediction models using machine learning in wetlands: A case study of Upo wetland in South Korea. *Water (Switzerland)*, 12(1), 93. <https://doi.org/10.3390/w12010093>
- Choi, C., Kim, J., Kim, J., & Kim, H. S. (2019). Development of combined heavy rain damage prediction models with machine learning. *Water (Switzerland)*, 11(12), 2516. <https://doi.org/10.3390/w11122516>
- Delurgio, S. A. (1998). *Forecasting principles and applications*. Mc Graw-Hill.
- Elkiran, G., Nourani, V., & Abba, S. I. (2019). Multi-step ahead modelling of river water quality parameters using ensemble artificial intelligence-based approach. *Journal of Hydrology*, 577, 123962. <https://doi.org/10.1016/j.jhydrol.2019.123962>
- Eslami, S., Hoekstra, P., Trung, N. N., Kantoush, S. A., Binh, D. V., Dung, D. D., et al. (2019). Tidal amplification and salt intrusion in the Mekong Delta driven by anthropogenic sediment starvation. *Scientific Reports*, 9(18746). <https://doi.org/10.1038/s41598-019-55018-9>
- Friedman, J. H. (1991). Multivariate adaptive regression splines. *Annals of Statistics*, 19(1), 1–67. <https://doi.org/10.1214/aos/1176347963>

- Gaci, S. (2016). A new ensemble empirical mode decomposition (EEMD) denoising method for seismic signals. *Energy Procedia*, 97, 84–91. <https://doi.org/10.1016/j.egypro.2016.10.026>
- Gisen, J. I. A., & Savenije, H. H. G. (2015). Estimating bankfull discharge and depth in ungauged estuaries. *Water Resources Research*, 51(4), 2298–2316. <https://doi.org/10.1002/2014WR016227>
- Granata, F., Papirio, S., Esposito, G., Gargano, R., & de Marinis, G. (2017). Machine learning algorithms for the forecasting of wastewater quality indicators. *Water (Switzerland)*, 9(2), 105. <https://doi.org/10.3390/w9020105>
- Grumbine, R. E., Dore, J., & Xu, J. (2012). Mekong hydropower: Drivers of change and governance challenges. *Frontiers in Ecology and the Environment*, 10(2), 91–98. <https://doi.org/10.1890/110146>
- Gugliotta, M., Saito, Y., Nguyen, V. L., Ta, T. K. O., Nakashima, R., Tamura, T., et al. (2017). Process regime, salinity, morphological and sedimentary trends along the fluvial marine transition zone of the mixed-energy Mekong River Delta, Vietnam. *Continental Shelf Research*, 147, 7–26. <https://doi.org/10.1016/j.csr.2017.03.001>
- Ha, S., Liu, D., & Mu, L. (2021). Prediction of Yangtze River streamflow based on deep learning neural network with El Niño-Southern Oscillation. *Scientific Reports*, 11(1), 11738. <https://doi.org/10.1038/s41598-021-90964-3>
- Hadi, S. J., & Tombul, M. (2018a). Forecasting daily streamflow for basins with different physical characteristics through data-driven methods. *Water Resources Management*, 32(10), 3405–3422. <https://doi.org/10.1007/s11269-018-1998-1>
- Hadi, S. J., & Tombul, M. (2018b). Monthly streamflow forecasting using continuous wavelet and multi-gene genetic programming combination. *Journal of Hydrology*, 561, 674–687. <https://doi.org/10.1016/j.jhydrol.2018.04.036>
- Helaire, L. T., Talke, S. A., Jay, D. A., & Chang, H. (2020). Present and future flood hazard in the lower Columbia river estuary: Changing flood hazards in the Portland-Vancouver metropolitan area. *Journal of Geophysical Research: Oceans*, 125(7), e2019JC015928. <https://doi.org/10.1029/2019JC015928>
- Hoa, L. T. V., Nhan, N. H., Wolanski, E., Cong, T. T., & Shigeko, H. (2007). The combined impact on the flooding in Vietnam's Mekong River delta of local man-made structures, sea level rise, and dams upstream in the river catchment. *Estuarine, Coastal and Shelf Science*, 71(1–2), 110–116. <https://doi.org/10.1016/j.ecss.2006.08.021>
- Hoitink, A. J. F., & Jay, D. A. (2016). Tidal river dynamics: Implications for deltas. Reviews of. *Geophysics*, 54(1), 240–272. <https://doi.org/10.1002/2015RG000507>
- Huang, C. C., Fang, H. T., Ho, H. C., & Jong, B. C. (2019). Interdisciplinary application of numerical and machine-learning-based models to predict half-hourly suspended sediment concentrations during typhoons. *Journal of Hydrology*, 573, 661–675. <https://doi.org/10.1016/j.jhydrol.2019.04.001>
- Hussain, D., & Khan, A. A. (2020). Machine learning techniques for monthly river flow forecasting of Hunza River, Pakistan. *Earth Science Informatics*, 13(3), 939–949. <https://doi.org/10.1007/s12145-020-00450-z>
- Imani, M., Hasan, M. M., Bittencourt, L. F., McClymont, K., & Kapelan, Z. (2021). A novel machine learning application: Water quality resilience prediction model. *The Science of the Total Environment*, 768, 144459. <https://doi.org/10.1016/j.scitotenv.2020.144459>
- James, G., Witten, D., Hastie, T., & Tibshirani, R. (2013). *An introduction to statistical learning with applications in R* (pp. 303–335). Springer Texts in Statistics Book Series.
- Jay, D. A., Leffler, K., & Degens, S. (2011). Long-term evolution of Columbia river tides. *Journal of Waterway, Port, Coastal, and Ocean Engineering*, 137(4), 182–191. [https://doi.org/10.1061/\(ASCE\)WW.1943-5460.0000082](https://doi.org/10.1061/(ASCE)WW.1943-5460.0000082)
- Jeihouni, M., Alavipanah, S. K., Toomanian, A., & Jafarzadeh, A. A. (2020). Digital mapping of soil moisture retention properties using solely satellite-based data and data mining techniques. *Journal of Hydrology*, 585, 124786. <https://doi.org/10.1016/j.jhydrol.2020.124786>
- Kanin, E. A., Osipov, A. A., Vainshtein, A. L., & Burnaev, E. V. (2019). A predictive model for steady-state multiphase pipe flow : Machine learning on lab data. *Journal of Petroleum Science and Engineering*, 180, 727–746. <https://doi.org/10.1016/j.petrol.2019.05.055>
- Kantouh, S., Binh, D. V., Sumi, T., & Trung, L. V. (2017). Impact of upstream hydropower dams and climate change on hydrodynamics of Vietnamese Mekong Delta. *Journal of Japan Society of Civil Engineers, Series B1 (Hydraulic Engineering)*, 73(4), I_109–I_114. https://doi.org/10.2208/jscje.73.i_109
- Kebede, M. G., Wang, L., Li, X., & Hu, Z. (2020). Remote sensing-based river discharge estimation for a small river flowing over the high mountain regions of the Tibetan Plateau. *International Journal of Remote Sensing*, 41(9), 3322–3345. <https://doi.org/10.1080/01431161.2019.1701213>
- Khalil, M., Panu, U. S., & Lennox, W. C. (2001). Groups and neural networks-based streamflow data infilling procedures. *Journal of Hydrology*, 241(3–4), 153–176. [https://doi.org/10.1016/S0022-1694\(00\)00332-2](https://doi.org/10.1016/S0022-1694(00)00332-2)
- Khan, M. Y. A., Hasan, F., Panwar, S., & Chakrapani, G. J. (2016). Neural network model for discharge and water level prediction for Ramganga River catchment of Ganga Basin, India. *Hydrological Sciences Journal*, 61(11), 2084–2095. <https://doi.org/10.1080/02626667.2015.1083650>
- Kim, M., & Shin, H. (2020). Machine learning-based prediction of the shale barrier size and spatial location using key features of SAGD production curves. *Journal of Petroleum Science and Engineering*, 191, 107205. <https://doi.org/10.1016/j.petrol.2020.107205>
- Kisi, O., & Parmar, K. S. (2016). Application of least square support vector machine and multivariate adaptive regression spline models in long term prediction of river water pollution. *Journal of Hydrology*, 534, 104–112. <https://doi.org/10.1016/j.jhydrol.2015.12.014>
- Krzywinski, M., & Altman, N. (2017). Classification and regression trees. *Nature Methods*, 14(8), 757–759. <https://doi.org/10.1038/nmeth.4370>
- Li, B., Yang, G., Wan, R., Dai, X., & Zhang, Y. (2016). Comparison of random forests and other statistical methods for the prediction of lake water level: A case study of the Poyang Lake in China. *Hydrology Research*, 47(S1), 69–83. <https://doi.org/10.2166/nh.2016.264>
- Li, C. H., Zhu, X. J., Cao, G. Y., Sui, S., & Hu, M. R. (2008). Identification of the Hammerstein model of a PEMFC stack based on least squares support vector machines. *Journal of Power Sources*, 175(1), 303–316. <https://doi.org/10.1016/j.jpowsour.2007.09.049>
- Liaw, A., & Wiener, M. (2002). Classification and regression by random forest. *R News*, 2, 18–22.
- Liu, D., Jiang, W., Mu, L., & Wang, S. (2020). Streamflow prediction using deep learning neural network: Case study of Yangtze River. *IEEE Access*, 8, 90069–90086. <https://doi.org/10.1109/ACCESS.2020.2993874>
- Loc, H. H., Binh, D. V., Park, E., Shrestha, S., Dung, T. D., Son, V. H., et al. (2021). Intensifying saline water intrusion and drought in the Mekong Delta: From physical evidence to policy outlooks. *The Science of the Total Environment*, 757, 143919. <https://doi.org/10.1016/j.scitotenv.2020.143919>
- Luo, X., Yuan, X., Zhu, S., Xu, Z., Meng, L., & Peng, Z. (2019). A hybrid support vector regression framework for streamflow forecast. *Journal of Hydrology*, 568, 184–193. <https://doi.org/10.1016/j.jhydrol.2018.10.064>
- Markatou, M., & Hripcsak, G. (2005). Analysis of variance of cross-validation estimators of the generalization error. *Journal of Machine Learning Research*, 6, 1127–1168.
- Matte, P., Secretan, Y., & Morin, J. (2018). Reconstruction of tidal discharges in the St. Lawrence fluvial estuary: The method of cubature revisited. *Geophysical Research: Oceans*, 123(8), 5500–5524. <https://doi.org/10.1029/2018JC013834>

- Mehdizadeh, B., & Movagharnajad, K. A. (2011). Comparative study between LS-SVM method and semi empirical equations for modeling the solubility of different solutes in supercritical carbon dioxide. *Chemical Engineering Research and Design*, 89(11), 2420–2427. <https://doi.org/10.1016/j.cherd.2011.03.017>
- Mispan, M. R., Rahman, N. F. A., Ali, M. F., KHalid, K., Bakar, M. H. A., & Haron, S. H. (2015). Missing river discharge data imputation approach using artificial neural network. *ARPN Journal of Engineering and Applied Sciences*, 10(22), 10480–10485.
- Moftakhari, H. R., Jay, D. A., & Talke, S. A. (2016). Estimating river discharge using multiple-tide gauges distributed along a channel. *Journal of Geophysical Research: Oceans*, 121(4), 2078–2097. <https://doi.org/10.1002/2015JC010983>
- Moftakhari, H. R., Jay, D. A., Talke, S. A., Kukulka, T., & Bromirski, P. D. (2013). A novel approach to flow estimation in tidal rivers. *Water Resources Research*, 49(8), 4817–4832. <https://doi.org/10.1002/wrcr.20363>
- Moftakhari, H. R., Jay, D. A., Talke, S. A., & Schoellhamer, D. H. (2015). Estimation of historic flows and sediment loads to San Francisco Bay, 1849–2011. *Journal of Hydrology*, 529, 1247–1261. <https://doi.org/10.1016/j.jhydrol.2015.08.043>
- Neal, R. M. (1997). Monte Carlo implementation of Gaussian process models for Bayesian regression and classification. *Preparation Physics* (Technical Report No. 9702, pp. 1–24). Department of Statistics, University of Toronto.
- Nourani, V., Andalib, G., & Dabrowska, D. (2017). Conjunction of wavelet transform and SOM-mutual information data pre-processing approach for AI-based multi-station nitrate modeling of watersheds. *Journal of Hydrology*, 548, 170–183. <https://doi.org/10.1016/j.jhydrol.2017.03.002>
- Nourani, V., Baghanam, A. H., Rahimi, A. Y., & Nejad, F. H. (2014). Evaluation of Wavelet-based de-noising approach in hydrological models linked to artificial neural networks. In I. Islam, P. K. Srivastava, M. Gupta, X. Zhu, & S. Mukherjee (Eds.), *Computational intelligence techniques in Earth and environmental sciences*. Springer.
- Nourani, V., Parhizkar, M., Vousoughi, F. D., & Amini, B. (2014). Capability of artificial neural network for detecting hysteresis phenomenon involved in hydrological processes. *Journal of Hydrologic Engineering*, 19(5), 896–906. [https://doi.org/10.1061/\(asce\)jhe.1943-5584.0000870](https://doi.org/10.1061/(asce)jhe.1943-5584.0000870)
- Nourani, V., Tajbakhsh, A. D., Moladjou, A., & Gokcekus, H. (2019). Hybrid wavelet-M5 model tree for rainfall-runoff modeling. *Journal of Hydrologic Engineering*, 24(5), 04019012. [https://doi.org/10.1061/\(ASCE\)JHE.1943-5584.0001777](https://doi.org/10.1061/(ASCE)JHE.1943-5584.0001777)
- Obringer, R., & Nateghi, R. (2018). Predicting urban reservoir levels using statistical learning techniques. *Scientific Reports*, 8(1), 5164. <https://doi.org/10.1038/s41598-018-23509-w>
- Panahi, M., Sadhasivam, N., Pourghasemi, H. R., Rezaie, F., & Lee, S. (2020). Spatial prediction of groundwater potential mapping based on convolutional neural network (CNN) and support vector regression (SVR). *Journal of Hydrology*, 588, 125033. <https://doi.org/10.1016/j.jhydrol.2020.125033>
- Park, E., Ho, H. L., Binh, D. V., Kantoush, S., Poh, D., Alcantara, E., et al. (2022). Impacts of agricultural expansion on floodplain water and sediment budgets in the Mekong River. *Journal of Hydrology*, 605, 127296. <https://doi.org/10.1016/j.jhydrol.2021.127296>
- Park, E., Loc, H. H., Binh, D. V., & Kantoush, S. (2021). The worst 2020 saline water intrusion disaster of the past century in the Mekong Delta: Impacts, causes, and management implications. *Ambio*, 51(3), 691–699. <https://doi.org/10.1007/s13280-021-01577-z>
- Pokhrel, Y., Burbano, M., Roush, J., Kang, H., Sridhar, V., & Hyndman, D. W. (2018). A review of the integrated effects of changing climate, land use, and dams on Mekong River hydrology. *Water*, 10(3), 266. <https://doi.org/10.3390/w10030266>
- Quinlan, J. R. (1986). Induction of decision trees. *Machine Learning*, 1, 81–106. <https://doi.org/10.1007/bf00116251>
- Ragetti, S., Zhou, J., Wang, H., Liu, C., & Guo, L. (2017). Modeling flash floods in ungauged mountain catchments of China: A decision tree learning approach for parameter regionalization. *Journal of Hydrology*, 555, 330–346. <https://doi.org/10.1016/j.jhydrol.2017.10.031>
- Raghavendra, S., & Deka, P. C. (2014). Support vector machine applications in the field of hydrology: A review. *Applied Soft Computing*, 19, 372–386. <https://doi.org/10.1016/j.asoc.2014.02.002>
- Rasmussen, C. E., & Nickisch, H. (2010). Gaussian processes for machine learning (GPML) toolbox. *Journal of Machine Learning Research*, 11, 3011–3015.
- Rasmussen, C. E., & Williams, C. K. I. (2006). Gaussian processes in machine learning. In *Adaptive computation and machine learning* (p. 48). MIT Press.
- Rezaali, M., Quilty, J., & Karimi, A. (2021). Probabilistic urban water demand forecasting using wavelet-based machine learning models. *Journal of Hydrology*, 600, 126358. <https://doi.org/10.1016/j.jhydrol.2021.126358>
- Safari, M. J. S. (2020). Hybridization of multivariate adaptive regression splines and random forest models with an empirical equation for sediment deposition prediction in open channel flow. *Journal of Hydrology*, 590, 125392. <https://doi.org/10.1016/j.jhydrol.2020.125392>
- Saghafi, H., & Arabloo, M. (2017). Modeling of CO₂ solubility in MEA, DEA, TEA, and MDEA aqueous solutions using AdaBoost-decision tree and artificial neural network. *International Journal of Greenhouse Gas Control*, 58, 256–265. <https://doi.org/10.1016/j.ijggc.2016.12.014>
- Schölkopf, B., & Smola, A. J. (2002). *Learning with Kernels: Support vector machines, regularization, optimization, and beyond*. MIT Press.
- Shannon, C. E. (1948). A mathematical theory of communication. *The Bell System Technical Journal*, 27(3), 379–423. <https://doi.org/10.1002/j.1538-7305.1948.tb01338.x>
- Shevade, S. K., Keerthi, S. S., Bhattacharyya, C., & Murthy, K. R. K. (2000). Improvements to the SMO algorithm for SVM regression. *IEEE Transactions on Neural Networks*, 11(5), 1188–1193. <https://doi.org/10.1109/72.870050>
- Sun, A. Y., Wang, D., & Xu, X. (2014). Monthly streamflow forecasting using Gaussian process regression. *Journal of Hydrology*, 511, 72–81. <https://doi.org/10.1016/j.jhydrol.2014.01.023>
- Suykens, J. A., & Vandewalle, J. (1999). Least squares support vector machine classifiers. *Neural Processing Letter*, 9(3), 293–300. <https://doi.org/10.1023/A:1018628609742>
- Suykens, J. A., Van Gestel, T., De Brabanter, J., & Van Moor, B. (2002). *Least squares support vector machines*. World Scientific. <https://doi.org/10.1142/5089>
- Ta, T. K. O., Nguyen, V. L., Tateishi, M., Kobayashi, I., Tanabe, S., & Saito, Y. (2002). Holocene delta evolution and sediment discharge of the Mekong River, southern Vietnam. *Quaternary Science Review*, 21(16–17), 1807–1819. [https://doi.org/10.1016/S0277-3791\(02\)00007-0](https://doi.org/10.1016/S0277-3791(02)00007-0)
- Taherdangkoo, R., Liu, Q., Xing, Y., Yang, H., Cao, V., Sauter, M., & Butscher, C. (2021). Predicting methane solubility in water and seawater by machine learning algorithms: Application to methane transport modeling. *Journal of Contaminant Hydrology*, 242, 103844. <https://doi.org/10.1016/j.jconhyd.2021.103844>
- Teegne, G., Park, D. K., & Kim, Y. O. (2017). Comparison of hydrological models for the assessment of water resources in a data-scarce region, the Upper Blue Nile River Basin. *Journal of Hydrology: Regional Studies*, 14, 49–66. <https://doi.org/10.1016/j.ejrh.2017.10.002>
- Tencaliec, P., Favre, A. C., Prieur, C., & Mathevet, T. (2015). Reconstruction of missing daily streamflow data using dynamic regression models. *Water Resources Research*, 51(12), 9447–9463. <https://doi.org/10.1002/2015WR017399>
- Tikhmarine, Y., Souag-Gamane, D., Ahmed, A. N., Sammen, S. S., Kisi, O., Huang, Y. F., & El-Shafie, A. (2020). Rainfall-runoff modelling using improved machine learning methods: Harris hawks optimizer vs. particle swarm optimization. *Journal of Hydrology*, 589, 125133. <https://doi.org/10.1016/j.jhydrol.2020.125133>

- Tongal, H., & Booij, M. J. (2018). Simulation and forecasting of stream flows using machine learning models coupled with base flow separation. *Journal of Hydrology*, *564*, 266–282. <https://doi.org/10.1016/j.jhydrol.2018.07.004>
- Tran, D. A., Tsujimura, M., Ha, N. T., Nguyen, V. T., Binh, D. V., Dang, T. D., et al. (2021). Evaluating the predictive power of different machine learning algorithms for groundwater salinity prediction of multi-layer coastal aquifers in the Mekong Delta, Vietnam. *Ecological Indicators*, *127*, 107790. <https://doi.org/10.1016/j.ecolind.2021.107790>
- Tran, H. D., Muttill, N., & Perera, B. J. C. (2015). Selection of significant input variables for time series forecasting. *Environmental Modelling & Software*, *64*, 156–163. <https://doi.org/10.1016/j.envsoft.2014.11.018>
- Triet, N. V. K., Dung, N. V., Fujii, H., Kummu, M., Merz, B., & Apel, H. (2017). Has dyke development in the Vietnamese Mekong Delta shifted flood hazard downstream? *Hydrology and Earth System Sciences*, *21*(8), 3991–4010. <https://doi.org/10.5194/hess-21-3991-2017>
- Triet, N. V. K., Dung, N. V., Merz, B., & Apel, H. (2018). Towards risk-based flood management in highly productive paddy rice cultivation—Concept development and application to the Mekong delta. *Natural Hazards and Earth System Sciences*, *18*(11), 2859–2876. <https://doi.org/10.5194/nhess-18-2859-2018>
- Vansteenkiste, T., Tavakoli, M., Steenbergen, N. V., Smedt, F. D., Batelaan, O., Pereira, F., & Willems, P. (2014). Intercomparison of five lumped and distributed models for catchment runoff and extreme flow simulation. *Journal of Hydrology*, *511*, 335–349. <https://doi.org/10.1016/j.jhydrol.2014.01.050>
- Vapnik, V. N. (2013). *The nature of statistical learning theory*. Springer.
- Vong, C. M., Wong, P. K., & Li, Y. P. (2006). Prediction of automotive engine power and torque using least squares support vector machines and Bayesian inference. *Engineering Application of Artificial Intelligence*, *19*(3), 277–287. <https://doi.org/10.1016/j.engappai.2005.09.001>
- Wang, H., Yan, H., Zeng, W., Lei, G., Ao, C., & Zha, Y. (2020). A novel nonlinear Arps decline model with salp swarm algorithm for predicting pan evaporation in the arid and semi-arid regions of China. *Journal of Hydrology*, *582*, 124545. <https://doi.org/10.1016/j.jhydrol.2020.124545>
- Weir, K., Salmasi, F., Arvanaghi, H., Karbasi, M., & Farsadizadeh, D. (2019). Application of Gaussian process regression model to predict discharge coefficient of gated Piano. *Water Resources Management*, *33*(11), 3929–3947. <https://doi.org/10.1007/s11269-019-02343-3>
- Yaghoubi, B., Hosseini, S. A., & Nazif, S. (2019). Monthly prediction of streamflow using data-driven models. *Journal of Earth System Science*, *128*(6), 141. <https://doi.org/10.1007/s12040-019-1170-1>
- Yang, H. H., Van Vuuren, S., Sharma, S., & Hermansky, H. (2000). Relevance of time–frequency features for phonetic and speaker-channel classification. *Speech Communication*, *31*(1), 35–50. [https://doi.org/10.1016/S0167-6393\(00\)00007-8](https://doi.org/10.1016/S0167-6393(00)00007-8)
- Yang, T., Gao, X., Sorooshian, S., & Li, X. (2016). Simulating California reservoir operation using the classification and regression-tree algorithm combined with a shuffled cross-validation scheme. *Water Resources Research*, *52*(3), 1626–1651. <https://doi.org/10.1002/2015WR017394>
- Yarar, A. (2014). A hybrid wavelet and neuro-fuzzy model for forecasting the monthly streamflow data. *Water Resources Management*, *28*(2), 553–565. <https://doi.org/10.1007/s11269-013-0502-1>
- Zhao, X., Lv, H., Lv, S., Sang, Y., Wei, Y., & Zhu, X. (2021). Enhancing robustness of monthly streamflow forecasting model using gated recurrent unit based on improved grey wolf optimizer. *Journal of Hydrology*, *601*, 126607. <https://doi.org/10.1016/j.jhydrol.2021.126607>
- Zhou, W., Wu, X., Ding, S., & Cheng, Y. (2020). Predictive analysis of the air quality indicators in the Yangtze River Delta in China : An application of a novel seasonal grey model. *The Science of the Total Environment*, *748*, 141428. <https://doi.org/10.1016/j.scitotenv.2020.141428>
- Zhu, S., Luo, X., Xu, Z., & Ye, L. (2018). Seasonal streamflow forecasts using mixture-kernel GPR and advanced methods of input variable selection. *Hydrology Research*, *50*(1), 200–214. <https://doi.org/10.2166/nh.2018.023>
- Zhu, S., Zhou, J., Ye, L., & Meng, C. (2016). Streamflow estimation by support vector machine coupled with different methods of time series decomposition in the upper reaches of Yangtze River, China. *Environmental Earth Sciences*, *75*(6), 531. <https://doi.org/10.1007/s12665-016-5337-7>
- Zia, H., Harris, N., Merrett, G., & Rivers, M. (2015). Predicting discharge using a low complexity machine learning model. *Computers and Electronics in Agriculture*, *118*, 350–360. <https://doi.org/10.1016/j.compag.2015.09.012>
- Zounemat-Kermani, M., Mahdavi-Meymand, A., Alizamir, M., Adarsh, S., & Yaseen, Z. M. (2020). On the complexities of sediment load modeling using integrative machine learning: Application of the great river of Loiza in Puerto Rico. *Journal of Hydrology*, *585*, 124759. <https://doi.org/10.1016/j.jhydrol.2020.124759>



Hydrodynamics, sediment transport, and morphodynamics in the Vietnamese Mekong Delta: Field study and numerical modelling

Doan Van Binh^{a,b,*}, Sameh A. Kantoush^b, Riadh Ata^c, Pablo Tassi^d, Tam V. Nguyen^e,
Jérémy Lepesqueur^{f,g}, Kamal El Kadi Abderrezzak^d, Sébastien E. Bourban^d,
Quoc Hung Nguyen^a, Doan Nguyen Luyen Phuong^a, La Vinh Trung^h, Dang An Tranⁱ,
Thanh Le Trungⁱ, Tetsuya Sumi^b

^a Faculty of Engineering, Vietnamese-German University, Binh Duong Province, Viet Nam

^b Water Resources Research Center, Disaster Prevention Research Institute, Kyoto University, Goka-sho, Uji City, Kyoto, Japan

^c Flow Science, Santa Fe, NM, USA

^d National Laboratory for Hydraulics and Environment, Research & Development Division, Electricité de France and Saint-Venant Hydraulics Laboratory, Chatou, France

^e Department of Hydrogeology, Helmholtz Centre for Environmental Research, Leipzig, Germany

^f Environmental Research and Innovation Department, Luxembourg Institute of Science and Technology, Belvaux, Luxembourg

^g Météo-France DIRAG/EC-MPF, DESAIX, BP Fort-de-France, France

^h Research Management Department, Vietnamese-German University, Binh Duong Province, Viet Nam

ⁱ Thuyloi University, Dong Da, Hanoi, Viet Nam

ARTICLE INFO

Keywords:

Morphological change
Diversion channel
Riverbed incision
Scour hole
Sediment reduction
2D numerical modelling

ABSTRACT

Flow, suspended sediment transport and associated morphological changes in the Vietnamese Mekong Delta (VMD) are studied using field survey data and a two-dimensional (2D) depth-averaged hydromorphodynamic numerical model. The results show that approximately 61–81 % of the suspended sediment load in the Hau River during the flood seasons is diverted from the Tien River by a water and suspended sediment diversion channel. Tidal effects on flow and suspended sediment load are more pronounced in the Hau River than in the Tien River. The results show the formation of nine scour holes in the Tien River and seven scour holes in the Hau River from 2014 to 2017. Additional six scour holes are likely to form by the end of 2026 if the suspended sediment supply is reduced by 85 % due to damming. Notably, the scour holes are likely to form at locations of severe riverbank erosion. In the entire study area, the simulated total net incision volume in 2014–2017 is approximately 196 Mm³ (equivalent to 65.3 Mm³/yr). The predicted total net incision volumes from 2017 to 2026 are approximately 2472 and 3316 Mm³ under the 18 % and 85 % suspended sediment reduction scenarios, respectively, thereby likely threatening the delta sustainability. The methodology developed in this study is helpful in providing researchers and decision-makers with one way to predict numerically the scour hole formation and its association with riverbank stability in river deltas. Of equal importance, this research serves as a useful reference on the role of water and suspended sediment diversion channels in balancing landforms in river-delta systems, particularly where artificial diversion channels are planned.

1. Introduction

Sediments transported by rivers are the major sources of materials for protecting deltas from the natural processes of subsidence. However, sediment loads worldwide have been significantly reduced by climate change and anthropogenic activities (e.g., damming, mining, urbanization) (Maeda et al., 2008; Lu et al., 2015; Darby et al., 2016; Binh et al.,

2020b; Hackney et al., 2020; Park et al., 2022), causing detrimental impacts on landforms, aquatic environments, and salinity intrusion in river-delta systems (Kondolf et al., 2014a; Best, 2019; Eslami et al., 2019; Binh et al., 2021; Loc et al., 2021). The Vietnamese Mekong Delta (VMD) is not an exception.

The flow regime of the Mekong River, which is one of the largest river systems worldwide and most important food-producing regions in

* Corresponding author at: Faculty of Engineering, Vietnamese-German University, Binh Duong, Viet Nam.

E-mail address: binh.dv@vgu.edu.vn (D.V. Binh).

<https://doi.org/10.1016/j.geomorph.2022.108368>

Received 10 January 2022; Received in revised form 30 June 2022; Accepted 2 July 2022

Available online 8 July 2022

0169-555X/© 2022 Elsevier B.V. All rights reserved.

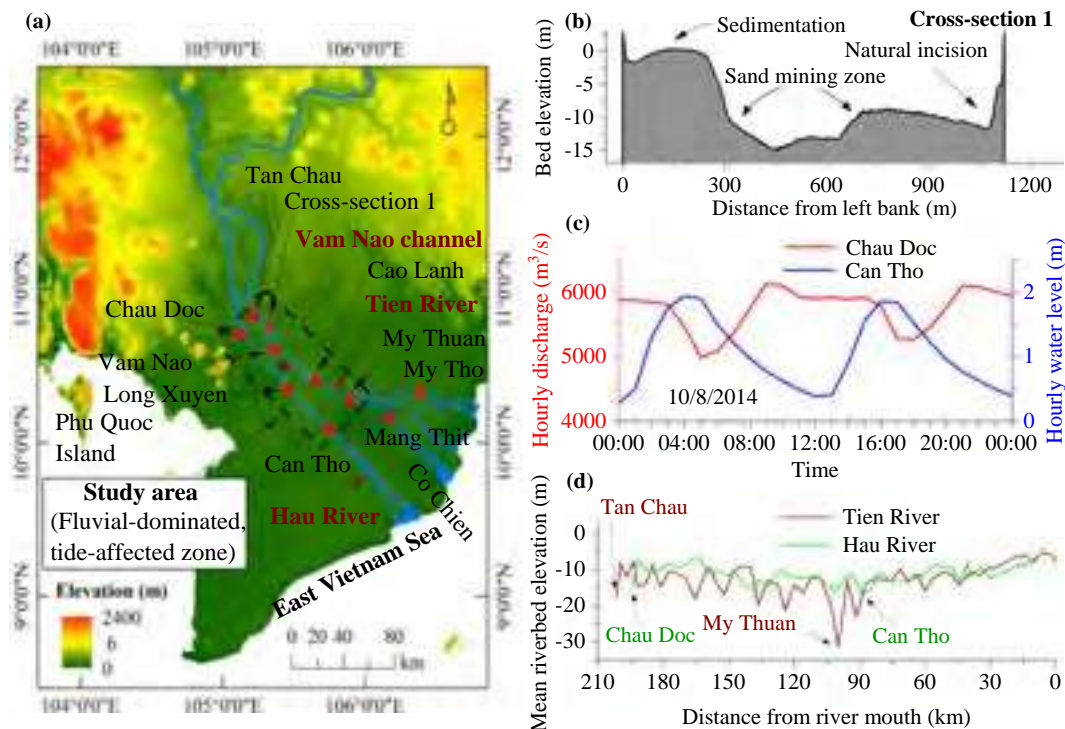


Fig. 1. Vietnamese Mekong Delta: (a) major rivers and hydrological stations (red triangle symbols); (b) a typical cross-section where sand mining causes riverbed incision; (c) the hourly flow discharge and water level at Chau Doc and Can Tho during the flood season; and (d) longitudinal riverbed profiles along the Tien and Hau Rivers. The digital elevation map shown in panel (a) is from the Shuttle Radar Topography Mission (SRTM) with a 30-m spatial resolution downloaded from <https://dwtkns.com/srtm30m/>. Among the eight gauging stations indicated in panel (a), Tan Chau, Chau Doc, Vam Nao, My Thuan, and Can Tho monitor water level, discharge, and SSC; Long Xuyen, Cao Lanh, and My Tho monitor water level.

Southeast Asia (Boretti, 2020), has been significantly altered (Lauri et al., 2012; Lu et al., 2014; Binh et al., 2018; Hecht et al., 2019; Binh et al., 2020a, 2020c), with the suspended sediment load (SSL) being substantially reduced (Kummu and Varis, 2007; Kondolf et al., 2014b; Binh et al., 2020b). Six mainstream dams in the Lancang cascade (upper Mekong basin) have reduced the SSL by 50–94 % along the lower Mekong River (Kummu et al., 2010; Kondolf et al., 2014b; Manh et al., 2015), and sixty-four completed dams in the Mekong basin were responsible for a 74 % SSL reduction in the VMD (Binh et al., 2020b). Additionally, sand mining activities have accelerated in the VMD, jumping from 7.75 Mm³/yr in 2012 (Bravard et al., 2013) to 29.3 Mm³/yr in 2018 (Jordan et al., 2019); these values are likely underestimated compared to an average volume of 42 Mm³/yr during 2015–2020 (Gruel et al., 2022) considering illegal mining activities. Overall, damming and sand mining have caused severe morphological degradation and salinity intrusion in the VMD (Anthony et al., 2015; Li et al., 2017; Mai et al., 2018, 2019a, 2019b; Eslami et al., 2019; Jordan et al., 2019; Binh et al., 2020d).

Flow, suspended sediment transport, and morphodynamic processes in the VMD are not fully understood due to the hydrological and hydraulic complexity of the system (i.e., seasonal interactions between fluvial flows and tidal currents) and scarcity of field data. While the delta covers an area of 39,000 km², there are only five gauging stations that monitor flow and suspended sediments. Some studies analysed the flow and SSL at these stations (e.g., Dang et al., 2016; Ha et al., 2018; Binh et al., 2020a, 2020b, 2021), while other studies dealt with suspended sediment dynamics in some floodplain and coastal areas only (e.g., Wolanski et al., 1996; Hung et al., 2014a, 2014b). Large parts of the VMD is mostly unknown and its morphodynamics remains unexplored because the bathymetry has not been monitored regularly.

Scour holes in tidal channels are formed at confluences (Rice et al., 2008), outer banks of meandering channels or sand mining locations (Jordan et al., 2019; Hackney et al., 2020), under complex

hydro-sedimentary processes caused by the alternating flood/ebb of tidal currents (Ferrarin et al., 2018). Bedload is trapped in scour holes (Anh et al., 2022), which induces progressive (regressive) erosion far downstream (upstream). Scour hole formation and evolution in the VMD are unexplored. Moreover, quantifying water and suspended sediment interchange between the two main rivers (Tien and Hau Rivers) via the Vam Nao diversion channel has not been adequately assessed at the monthly or seasonal scales.

To overcome the scarcity of measurements, remotely sensed satellite data have been employed (Loisel et al., 2014; Dang et al., 2018) and numerical models have been applied to simulate hydrodynamics (Wassmann et al., 2004; Van et al., 2012) and suspended sediment dynamics (Xue et al., 2012; Hein et al., 2013; Manh et al., 2014, 2015; Vinh et al., 2016; Thanh et al., 2017; Xing et al., 2017; Tu et al., 2019; Le, 2020). Xing et al. (2017) found numerically that sand is exported from and imported into the lower Hau River in the high-flow and low-flow seasons, respectively. According to Tu et al. (2019), erosion and deposition occurred alternately along the coast, whereas the preliminary results by Thuy et al. (2019) showed that erosion is more dominant and severe in the upper part (upstream of My Thuan) of the Tien River, but is relatively low in the estuaries. Jordan et al. (2020) found that hydro-power dams have the strongest impact on riverbed incision, amplified by sand mining, whereas relative sea level rise has the lowest effect. Recently, Anh et al. (2022) estimated, for the first time, the effect of sand mining and dredging on morphological dynamics in the Soai Rap River using the Telemac modelling suite of codes. Although the model, which was neither calibrated nor validated, encompassed the lower VMD main rivers, Anh et al. (2022) focused only on the Sai Gon–Dong Nai River system. Overall, the existing studies have focused either on the lower part of the VMD and coastal zone (Xing et al., 2017; Tu et al., 2019) or on a small region in the upper VMD (Jordan et al., 2020), while the suspended sediment transport and morphodynamics in the whole upper VMD have been largely ignored. The studies did not provide sufficient

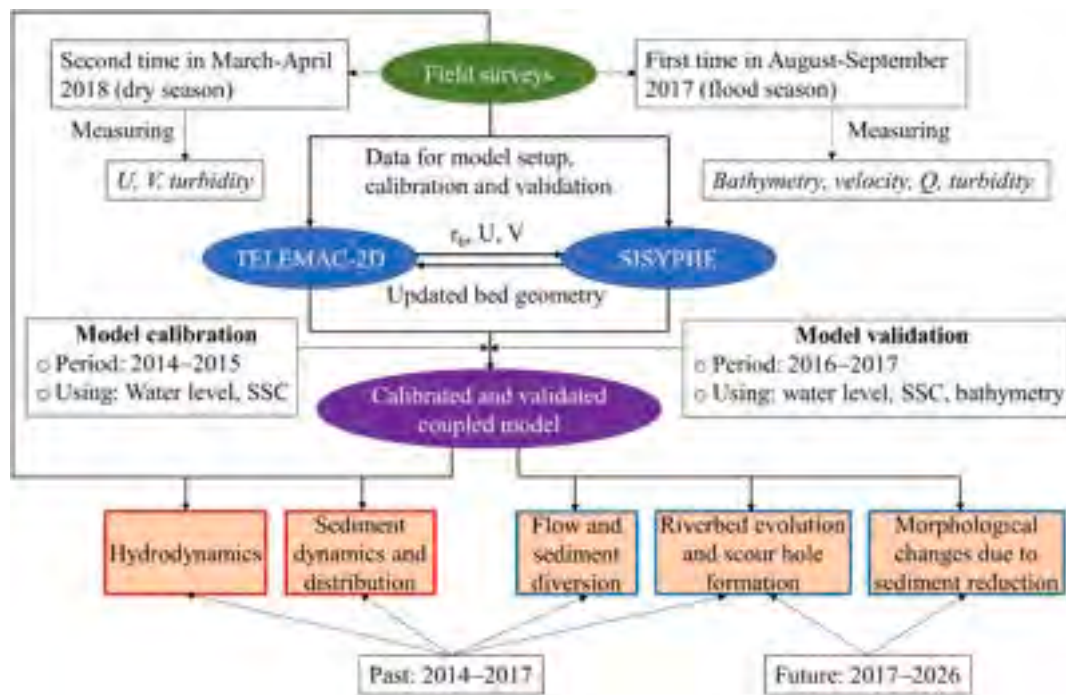


Fig. 2. Methodological framework adopted in this study. U , V : velocities in the x - and y -direction. τ_b : critical bed shear stress. Q : discharge.

understanding of either the inter- or intra-annual variations in the morphodynamics in the VMD or the formation of scour holes that cause riverbank instability (Hackney et al., 2020). Although authorities and researchers know well about the hydrological role of the Vam Nao diversion channel, but quantitative estimates of inter-intra-sediment diversion remain unknown.

Using field data and numerical modelling, this study aims therefore at addressing quantitatively the formation of scour holes in the VMD, and the role of the diversion channel in diverting suspended sediment between the river systems is comprehensively evaluated. The present work provides a crucial reference for other deltas where the construction of artificial diversion structures may be planned or constructed (e.g., in Mississippi and Yellow River deltas) (Guan et al., 2019; Pahl et al., 2020). Moreover, this research is among the pioneering works applying the *open-source* Telemac package (www.opentelemac.org) for modelling flow, suspended sediment transport and morphodynamics in the VMD rather than using commercial numerical codes.

The paper is organized as follows: Section 2 describes the study area. Section 3 presents the methodology, including the field measurements, numerical model set-up and simulated scenarios. Results and discussions are given in Section 4, followed by conclusion in Section 5.

2. Study area

The VMD is located in the estuary of the Mekong River (Fig. 1a), which discharges approximately 300–550 km³/yr of water (Milliman and Farnsworth, 2011; Darby et al., 2016) and 40–167 Mt/yr of suspended sediment (Kondolf et al., 2014b; Nowacki et al., 2015; Binh et al., 2020b) into the East Vietnam Sea via two main distributaries, namely, the Tien and Hau Rivers. Upstream of the Vam Nao diversion channel (Fig. 1a), the Tien River transports approximately 80 % of the flow and suspended sediment from the Mekong River. Due to redistribution of the flow and suspended sediment by the Vam Nao diversion channel, the Tien and Hau Rivers transport similar amounts of water downstream of the diversion channel.

The flow regime in the VMD is characterized by strong seasonality, with two distinct seasons driven by a monsoonal climate: flood season (July–December) and dry season (January–June). The SSL of the VMD

has been reduced by 74 % due to the sixty-four existing dams in the Mekong basin (Binh et al., 2020b), and is expected to decrease by 96 % if all one hundred thirty-three planned dams are completed (Kondolf et al., 2014b). Sand mining increased from 7.75 Mm³/yr in 2012 to 29.3 Mm³/yr in 2018 (Bravard et al., 2013; Jordan et al., 2019). Fig. 1b shows a typical cross-section where sand mining occurs.

The VMD is located in the fluvial-to-marine transition zone, which is divided into two distinctive zones: the upstream, fluvial-dominated zone and the downstream, tide-dominated zone (Gugliotta et al., 2017). The boundary between these zones is at the My Thuan and Can Tho gauging stations (Fig. 1a). The river areas considered in this study are located in the fluvial-dominated, tide-affected zone (Fig. 1a). During the flood season, tidal influence is limited to the upper VMD (e.g., at Chau Doc) compared to the lower VMD (e.g., at Can Tho) (Fig. 1c) due to high riverine fluvial discharges. However, tide-driven water level fluctuations are significant during the dry season (e.g., approximately 1 m at Tan Chau and Chau Doc and 2 m at My Thuan and Can Tho) (Gugliotta et al., 2017). The flow is bidirectional during the dry season because of the interaction between the semidiurnal tide from the East Vietnam Sea and the riverine discharge from the Mekong River. The rivers are deep and narrow, with bed elevations decreasing seaward (Fig. 1d). The SSL is dominated by silt and clay, accounting for 95 to 98 % of the total load (Koehnken, 2014; Binh et al., 2020b). Bedload, composed of fine sand, constitutes only 1 to 3 % of the total annual load (Gugliotta et al., 2017; Jordan et al., 2019; Hackney et al., 2020).

3. Materials and Methods

3.1. Methodological framework

Fig. 2 shows a methodological flowchart. We conducted two field surveys along VMD main rivers to measure bathymetry, velocity, discharge and turbidity. These data were combined with the monitored data at gauging stations for analysing flow and suspended sediment dynamics and distribution in the river-delta system. The data were also used to establish a 2D morphodynamic numerical model. The numerical model together with the field data were used to estimate flow and suspended sediment diverted through the Vam Nao diversion channel, to

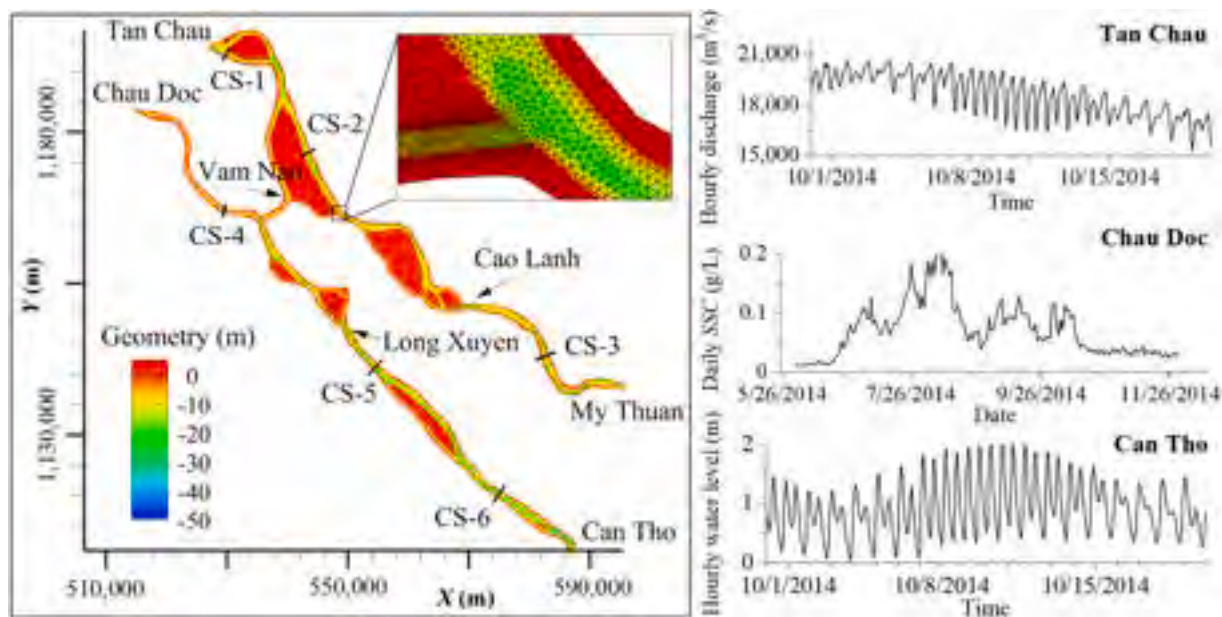


Fig. 3. Geometry and mesh discretization of the computational domain, including locations used for calibrating and validating the model. Representative data of the hourly discharge and daily SSC at upstream boundaries and the hourly water level at downstream boundaries are given.

predict (for the past and future) riverbed evolution and scour hole formation, and to forecast morphological changes under some likely scenarios of reduced suspended load at the upstream end.

3.2. Field measurements

Two field surveys were conducted from August to September 2017 (flood season) and from March to April 2018 (dry season) along 570 km of the Tien and Hau Rivers and the Vam Nao channel (Fig. 1a). In the first survey, we measured the river bathymetry (i.e., eighty-two cross-sections), velocity, discharge, and turbidity using an acoustic Doppler current profiler (aDcp) and an Infinity-ATU75W2-USB turbidity meter. Vertical flow velocities were measured every 0.4–1.5 m depending on the water depth. Data processing is given by Binh et al. (2020b). In the second survey, infinity velocity and turbidity meters were used to measure velocity and turbidity longitudinally and vertically. Three to six vertical profiles were recorded at each cross-section depending on the river width. Positions of the profiles were recorded by a handheld Garmin GPS, and the interval of turbidity measurements was 60 s. Turbidity measurements were converted to suspended sediment concentrations (SSCs) using specific equations (see Supplementary Material).

In the first survey, the measured suspended sediment samples at My Thuan and Mang Thit stations in the Tien River (Fig. 1a) yield median diameters d_{50} of 12.6 μm and 6.1 μm , respectively. The associated settling velocities are 0.052 and 0.012 mm/s, respectively, estimated by Stokes' (1851) law. These values may be underestimated because flocs can be formed for cohesive particles. However, this underestimation does not affect our numerical results because the settling velocity is one of the tuning parameters in the numerical model. Our estimated settling velocity combined with the values published in previous papers (see Section 3.5) serve as a reference for the initial selection of the settling velocity in our model.

3.3. Numerical modelling framework

We used the widely known and well-tested Telemac-Mascaret modelling system (Hervouet, 2007, www.opentelemac.org) to simulate flow, suspended sediment transport, and morphodynamics in the upper VMD. Hydrodynamics was modelled using the 2D depth-averaged

TELEMAC-2D module, and sediment transport and riverbed evolution were simulated using the SISYPHE module (Villaret et al., 2013; Langendoen et al., 2016). Both the TELEMAC-2D and SISYPHE modules are internally coupled (El Kadi Abderrezak et al., 2016; Sisyph, 2018) and are solved using the finite element method of an unstructured mesh. Telemac-Mascaret can be run in parallel mode, substantially reducing the computational time.

Bedload is negligible in the VMD (Jordan et al., 2019; Hackney et al., 2020). Suspended sediment consists of both cohesive ($d_{50} < 63 \mu\text{m}$) and noncohesive ($d_{50} > 63 \mu\text{m}$) particles (Wolanski et al., 1996; Xing et al., 2017). The suspended sediment transport of the sand-mud mixture is simulated by solving a 2D advection-diffusion equation for the k th size class ($k = 1$ for cohesive and $k = 2$ for noncohesive):

$$\frac{\partial(hC_k)}{\partial t} + \frac{\partial(huC_k)}{\partial x} + \frac{\partial(hvC_k)}{\partial y} = \frac{\partial}{\partial x} \left(h\epsilon_s \frac{\partial C_k}{\partial x} \right) + \frac{\partial}{\partial y} \left(h\epsilon_s \frac{\partial C_k}{\partial y} \right) + E^k - D^k \quad (1)$$

where t is time; h is the flow depth; u and v are depth-averaged flow velocities in the x - and y -Cartesian directions, respectively; C_k is the depth-averaged concentration of the k th size class (in % volume); ϵ_s is the sediment turbulent diffusivity, usually related to the eddy viscosity by $\epsilon_s = \nu_t / \sigma_c$ with σ_c as the Schmidt number (set at 1.0 in SISYPHE); and E^k and D^k are erosion and deposition rates of the k th size class, respectively. SISYPHE computes the bed evolution using the following Exner (1925) equation:

$$(1 - \lambda) \frac{\partial z_b}{\partial t} + (E - D) = 0 \quad (2)$$

in which λ is the bed porosity and z_b the bed level (m). In Eq. (2), the updated bed elevations are used in TELEMAC-2D to estimate the hydrodynamic variables, which are sent back into SISYPHE to continue the simulation. Governing equations of TELEMAC-2D and erosion and deposition estimation in SISYPHE are described in the Supplementary material.

3.4. Model setup and boundary conditions

We simulated the flow and suspended sediment transport in the upper Tien and Hau Rivers (Figs. 1 and 3). The computational domain included a 200–300 m wide floodplain extending from both banks of the

Table 1

Physical parameters of cohesive suspended sediment in previous publications that were used to tune our coupled model.

| Parameters | | | | References |
|---|---|--|------------------------------------|----------------------|
| ω_s (m/s) | u_{*cr} (m/s) | M kg/(s·m ²) | τ_{ce} (N/m ²) | |
| 10^{-4} – 3×10^{-4} | 8.9×10^{-3} – 1.1×10^{-2} | 5×10^{-6} – 1×10^{-4} | 0.15–1.5 | Letrung et al., 2013 |
| 2.16×10^{-4} – 1.85×10^{-3} | 4.5×10^{-3} – 5.3×10^{-3} | 5.13×10^{-6} – 8×10^{-6} | 0.028–0.044 | Hung et al., 2014b |
| 10^{-4} – 1.3×10^{-3} | 4.4×10^{-3} – 5×10^{-3} | | | Manh et al., 2014 |
| 5×10^{-5} – 3.3×10^{-4} | 1.0 | 2×10^{-5} | 0.2 | Thanh et al., 2017 |

ivers and all islands. The unstructured finite element triangle mesh was generated with a typical element size equal to 80 m in the main rivers, islands and floodplains and 30–40 m in the narrow channels. The domain consisted of 106,413 nodes and 206,455 elements. A time step of 10 s was selected to keep the Courant number <0.78 for model stability.

There were four boundaries: two upstream boundaries (i.e., Tan Chau and Chau Doc) used hourly flow discharges and daily SSCs, and two downstream boundaries (i.e., My Thuan and Can Tho) used hourly water levels (Fig. 3). The hourly discharge and water level were used because of the tidal effect. The initial riverbed material fractions were 95 % noncohesive sediment (fine sand) and 5 % cohesive sediment (Gugliotta et al., 2017). Uniform diameters of $d_{50} = 12.6 \mu\text{m}$ (from our first field survey in 2017) and $d_{50} = 214 \mu\text{m}$ (Gugliotta et al., 2017) were used for the cohesive and noncohesive sediments, respectively. The initial geometry was the 2014 river bathymetric data (we also used the 2010 and 2012 bathymetric data in the Hau River because of data availability) collected from the Southern Institute of Water Resources Research, Vietnam, and the 2013 SRTM floodplain topography. The model performance was evaluated using coefficient of determination (R^2), Nash-Sutcliffe efficiency (NSE), and root mean square error (RMSE) (see Supplementary material).

3.5. Model calibration and validation

The VMD model was calibrated and validated using the data from 2014 to 2015 and 2016–2017, respectively. For each year, the model simulated seven months in the flood season from June to December to reduce the simulation time because >90 % of the suspended sediment was conveyed during the flood season (Binh et al., 2020b). In fact, June and December have relatively low discharges that are compatible with the dry season discharges, indicating that our model partially covered the dry season flow. Manning coefficients ranging from 0.016 to 0.034 were used initially, as recommended by Manh et al. (2014). Initial selections of other parameters were based on various publications, as shown in Table 1. We used water levels at Vam Nao, Cao Lanh, and Long Xuyen (as the discharges were not available), SSCs at Vam Nao, and riverbed elevations at six cross-sections (i.e., CS-1–CS-6) (Fig. 3a) to calibrate and validate the model.

We first calibrated the single hydrodynamic module TELEMAC-2D by adjusting the Manning coefficients and velocity diffusivity. We then recalibrated the coupled TELEMAC-2D/SISYPHE model by further tuning the reference near-bed concentration (z_{ref}), the critical bed shear stress for erosion (τ_{ce}), the critical shear velocity for mud deposition (u_{*cr}), the settling velocity of the cohesive material (ω_s), and the Krone-Partheniades erosion constant (M), together with a slight modification of the hydrodynamic tuning parameters. Manning coefficients were set by zones, namely, $0.15 \text{ m}^{1/3}/\text{s}$ in the floodplains and islands based on the suggestion of Mtamba et al. (2015) and 0.015 – $0.04 \text{ m}^{1/3}/\text{s}$ in the river channels. In the sediment transport module, $\tau_{ce} = 0.15 \text{ N/m}^2$, $u_{*cr} = 0.03 \text{ m/s}$, $\omega_s = 6.6 \times 10^{-5} \text{ m/s}$, and $M = 10^{-6} \text{ kg/(s·m}^2\text{)}$. The selected ω_s was slightly larger than the value we measured at My Thuan because the sediment grain sizes were coarser in the upstream areas of this site (Hung et al., 2014b). The reference elevation z_{ref} was 2.5 times the median diameter of the noncohesive sediment. Values of RMSE, NSE,

Table 2

Evaluation of the model performance.

| Stations | Water levels | | | SSCs | | |
|-------------------|--------------|------|-------|------------|------|-------|
| | RMSE (m) | NSE | R^2 | RMSE (g/L) | NSE | R^2 |
| Model calibration | | | | | | |
| Vam Nao | 0.10 | 0.83 | 0.90 | 0.02 | 0.72 | 0.87 |
| Cao Lanh | 0.09 | 0.94 | 0.94 | | | |
| Long Xuyen | 0.07 | 0.95 | 0.97 | | | |
| Model validation | | | | | | |
| Vam Nao | 0.12 | 0.80 | 0.88 | 0.05 | 0.68 | 0.78 |
| Cao Lanh | 0.08 | 0.93 | 0.93 | | | |
| Long Xuyen | 0.06 | 0.97 | 0.98 | | | |

and R^2 (Table 2) indicate that the coupled model was reliably calibrated and validated. Moreover, the simulated water levels, SSCs and riverbed elevations were in good agreement with the corresponding measured data (Fig. 4).

3.6. Simulated scenarios

Hydropower dams are the dominant driver of suspended sediment reduction and riverbed incision along the Mekong River (e.g., Lu and Siew, 2006; Kummur and Varis, 2007; Kummur et al., 2010; Kondolf et al., 2014b; Manh et al., 2015; Jordan et al., 2020; Binh et al., 2020b, 2021; Schmitt et al., 2021), together with sand mining (Brunier et al., 2014; Park et al., 2020; Gruel et al., 2022) and shifting in tropical cyclones (Darby et al., 2016). In this study, we did not focus on the drivers of morphological changes (see the work by Jordan et al. (2020)). Instead, we focused more on the morphodynamic processes and the quantification of the effects of the suspended sediment supply reductions by dams under three likely scenarios (Table 3). We simulated morphological changes for a ten-year period from 2017 to 2026 by considering the tradeoff between the model simulation time and morphological responses after upstream dam construction (15 years after Nuozhadu—the last largest mega dam in the Mekong basin). Scenario 1 (S1) used the flow and suspended sediment data of 2017, which were assumed to be unchanged until 2026. S1 was used as a baseline scenario. Scenarios 2 (S2) and 3 (S3) used the same flow conditions of 2017 until 2026, while the imposed inflow SSCs were reduced. Based on the long-term monthly suspended sediment reduction at Tan Chau plus Chau Doc analysed by Binh et al. (2020b), daily SSCs from 2017 to 2026 at the upstream boundaries at these two stations in S2 were estimated. Kondolf et al. (2014b) estimated that the SSL of the Mekong Delta would be only 4 % of that in the predam period (pre-1992) if all 133 planned dams in the Mekong Basin were built. This means that the post-133-dam SSL will be 6.7 Mt/yr (Binh et al., 2021). Compared to the 2017 SSL of 43.9 Mt, the 2026 SSL in S2 and S3 is reduced by 17.5 % and 84.8 %, respectively.

4. Results and discussions

4.1. Observed and simulated river flow dynamics

The flow regimes of the Tien and Hau Rivers show strong seasonality: high flows during July–December and low flows during January–June

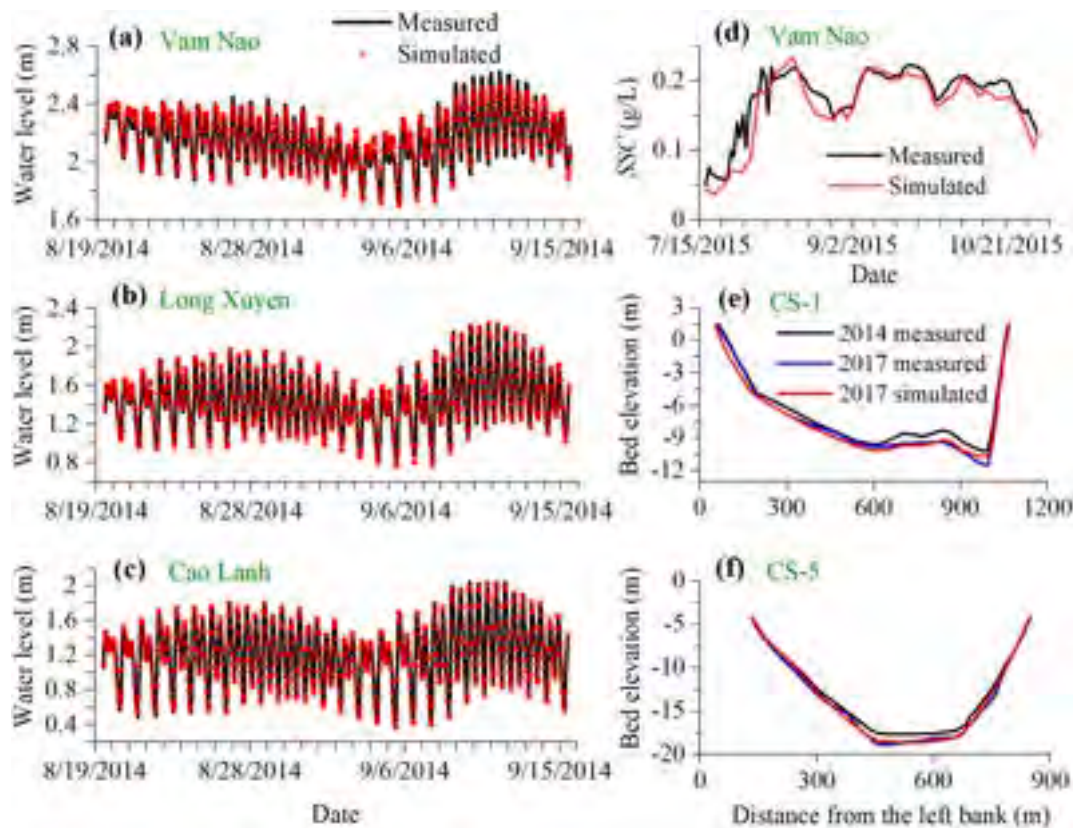


Fig. 4. Measured versus simulated water levels, SSCs, and riverbed elevations at various locations for (a–d) model calibration and (e–f) model validation. The locations indicated in the figure are shown in Fig. 3.

Table 3

Simulated scenarios in the coupled model to forecast morphological changes from 2017 to 2026 caused by suspended sediment reductions due to river damming.

| Scenario | Discharge (m ³ /s) | Water level (m) | SSC (g/L) | SSL change (%) (2026 vs. 2017) |
|----------|-------------------------------|-----------------|---|--------------------------------|
| S1 | Same as 2017 | Same as 2017 | Same as 2017 | – |
| S2 | Same as 2017 | Same as 2017 | Based on long-term monthly suspended sediment reduction in Binh et al. (2020b) 2017 | –17.5 % |
| S3 | Same as 2017 | Same as 2017 | Based on Kondolf et al. (2014b) 2017 → 2019 ↓ 2020 → 2026 | –84.8 % |

(Figs. 5a–b and 6). The observed daily flood peaks at Tan Chau and Chau Doc were large in 2014, corresponding to maximum daily discharges of 24,350 and 6620 m³/s (water levels of 3.71 m and 2.95 m), respectively. However, due to (mainly) the redistribution of flow by the Vam Nao diversion channel, the simulated daily flood peaks at Long Xuyen and Cao Lanh in 2014 were 18,930 and 16,230 m³/s, respectively. During the period from 2014 to 2017, the observed data show that the mean annual flow ratio between the Tien and Hau Rivers upstream of the Vam Nao channel (i.e., at Tan Chau and Chau Doc) was 83:17, while that downstream of the Vam Nao channel (from simulated results at Cao Lanh and Long Xuyen) was 52:48. This analysis indicates that the Vam Nao diversion channel may have a significant impact on the flow dynamics of the Tien and Hau Rivers.

The observed and simulated discharges from 2014 to 2017 during the dry season (March–April) show that the flow direction was reversed (Figs. 5a and 7), with maximum hourly rates of –4780 m³/s and –1850 m³/s (in 2016) at Tan Chau and Chau Doc, respectively (Fig. 5a). This is because of the tidal effect, which causes the tidal discharge to exceed the

low riverine flow. In the dry year (i.e., 2016), the observed mean annual discharge at My Thuan was lower than that at Can Tho, with a ratio of 48:52. This indicates that the tidal effect may be stronger in the Hau River than in the Tien River (Fig. 5b). Both observed and simulated data show that the tidal regime may have had a clear effect on the water levels of the two rivers (Figs. 4a–c and 5b). This is illustrated by a sinusoidal oscillation of the water levels in these rivers, which mimics changes in the tidal regime.

The observed data show that the vertical distribution of the flow velocity largely depended on the shape of the cross-section (Fig. 5c–d). In asymmetric cross-sections (Fig. 5c), the flow was faster on the steeper bank, whereas in symmetric cross-sections (Fig. 5d), the velocity was symmetric. The velocity was generally larger in the upper zone than in the lower zone in a cross-section. During the flood peak, the simulated maximum flow velocity exceeded 2 m/s in some areas, especially in narrow and meandering sections (Fig. 6c), resulting from high unit discharges (Fig. 6a). On the other hand, the simulated dry season flow velocities were mostly smaller than 1.5 m/s (Fig. 6f). However, the

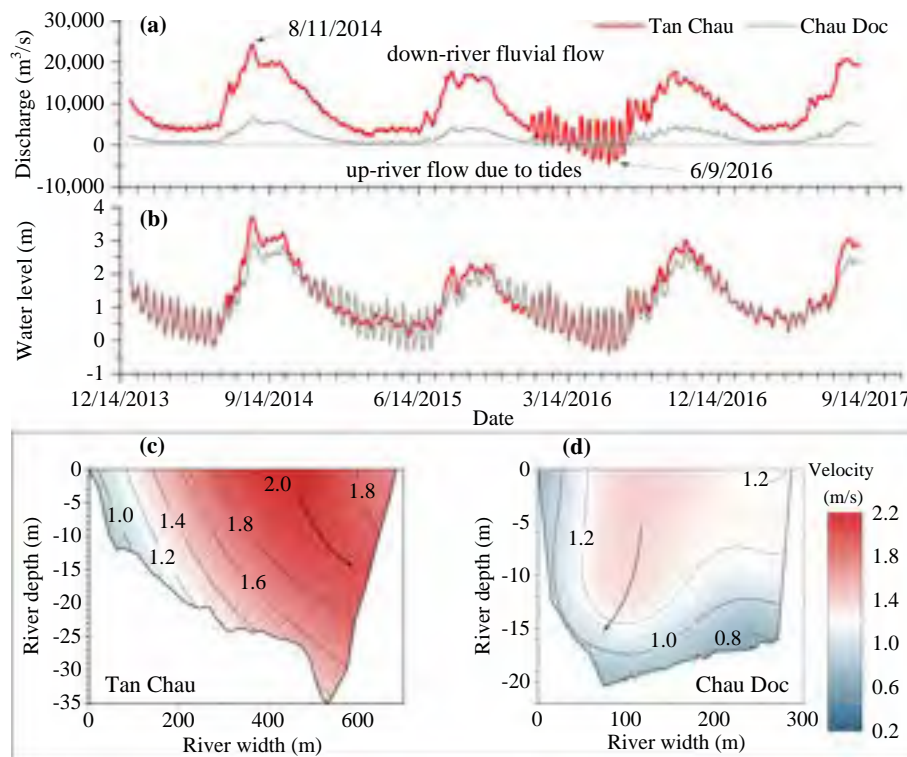


Fig. 5. Observed hydraulic conditions at Tan Chau and Chau Doc: a) daily discharge and b) water level from 2014 to 2017. Vertical velocity distribution at c) Tan Chau and d) Chau Doc measured in August 2017 (flood season) during the first field survey.

pattern of the simulated water depth in the dry season was similar to that in the flood season (Fig. 6b, e).

4.2. Suspended sediment dynamics and distribution

Suspended sediment in the VMD varies inter- and intra-annually (Figs. 8–9). The observed and simulated maximum daily SSC (from the gauging stations at Tan Chau to Vam Nao) during the flood season (i.e., August–September) reached 0.47 g/L (equivalent to almost 1 Mt), while the minimum value during the dry season (i.e., March–April) was negligible. Most of the suspended sediment was transported during the flood season: 90–98 % at Tan Chau, 91–96 % at Chau Doc, 89–93 % at My Thuan, and 86–94 % at Can Tho during 2014–2017 (Fig. 8b–e). Although the maximum SSL of the VMD during 2014–2017 was 66 Mt/yr (in 2014), this value was lower than the predam SSL (pre-1992) of 166.7 Mt/yr (Binh et al., 2020b). On average, the mean annual SSL of the VMD in 2014–2017 (42 Mt/yr) decreased by approximately 75 % compared to the predam amount. Because hydropower dams are likely to contribute to a significant reduction in the SSL in the VMD (Binh et al., 2020b), a sustainable reservoir sediment management plan should be implemented for current and planned dams in the Mekong basin. For existing dams, prompt measures (i.e., excavation) can be considered to urgently dredge the accumulated sediment in reservoirs for delivery downstream. For planned dams, alternative locations and designed configurations of dams should be revised to minimize reservoir sedimentation. Then, conventional sediment management measures (e.g., drawdown flushing, bypassing, and sluicing) to route sediment through or bypass reservoirs should be considered at the design stage. Furthermore, advanced sediment management techniques, such as hydro-suction, dam asset management, and dam rehabilitation and retrofitting, can be employed. Schmitt et al. (2021) found that it is very important to consider strategic placement of hydropower dams to maintain sediment supply from the Mekong basin rather than trying to increase sediment yields or improve sediment management for individual dams.

There are substantial differences in the spatial variations in the suspended sediment between the flood and dry seasons (Figs. 8–9). In dry seasons, the simulated SSLs along the rivers were relatively similar because of the low supply of suspended sediment from the Mekong River (Fig. 9a) and the high SSC induced by tides and wind (Thanh et al., 2017; Xing et al., 2017; Eslami et al., 2019). However, during flood seasons, the simulated results show that the SSC decreased in the downstream direction because of the high suspended sediment supplied from the Mekong River (Fig. 9b). In the Hau River, the observed mean suspended sediment ratios between Can Tho and Chau Doc from 2014 to 2017 were 3.2–5.6 and 1.6–3.1 during the dry and flood seasons, respectively. The mean ratio in 2009 estimated by Manh et al. (2014) was 2.8. These results imply that the sediment flux of the Mekong River in the flood season may play a key role in stabilizing landforms in the VMD estuaries, especially in compacting with the shrinkage of the delta due to rapid coastal and riverbank erosion (Li et al., 2017; Khoi et al., 2020). The newly deposited suspended sediment in the floodplains carried by the Mekong's flood flows may also help counteract the delta's sinking resulting from relative land subsidence (i.e., absolute land subsidence plus rising sea level) due to groundwater overexploitation (Minderhoud et al., 2020; Tran et al., 2021). However, the sediment load of the Mekong River has been reducing due to human activities (Kondolf et al., 2014b) and tropical cyclone shifts (Darby et al., 2016). To address this issue, Schmitt et al. (2021) suggested maintaining the sediment supply from the Mekong basin in enhancing climate resilience and maintaining lands in the delta.

Both the observed and simulated SSC and SSL in the Tien River were significantly greater than those in the Hau River (Figs. 8–9). The observed mean annual suspended sediment ratios between the Tien and Hau Rivers during 2014–2017 were 84:16 and 61:39 upstream (i.e., Tan Chau and Chau Doc) and downstream (i.e., My Thuan and Can Tho) of the Vam Nao diversion channel, respectively. This difference between the upstream and the downstream is likely because of the Vam Nao channel, which diverts large amounts of water and suspended sediment

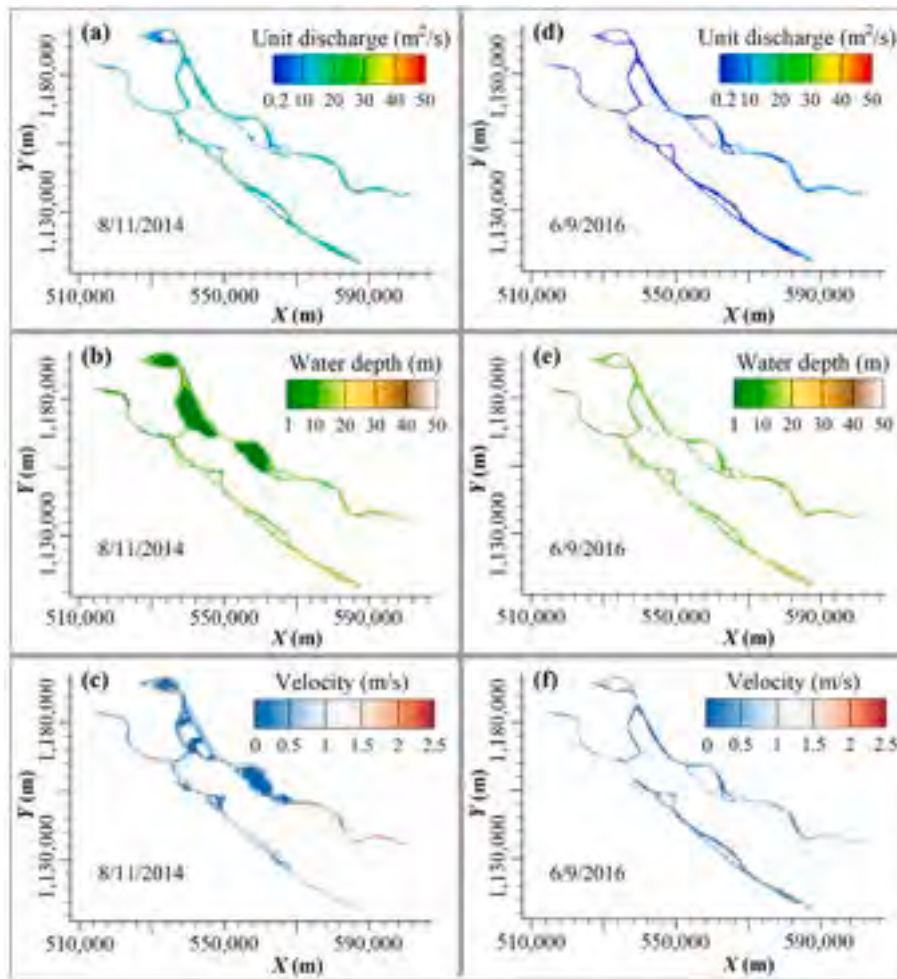


Fig. 6. Simulated unit discharge, water depth, and velocity magnitude (a–c) during the annual flood peak on 8/11/2014 and (d–f) during the nonflood period on 6/9/2016. For clarity, we applied cut-offs of 0.2 m²/s, 1 m, and 0.02 m/s to the maps showing the unit discharge, water depth, and flow velocity, respectively.

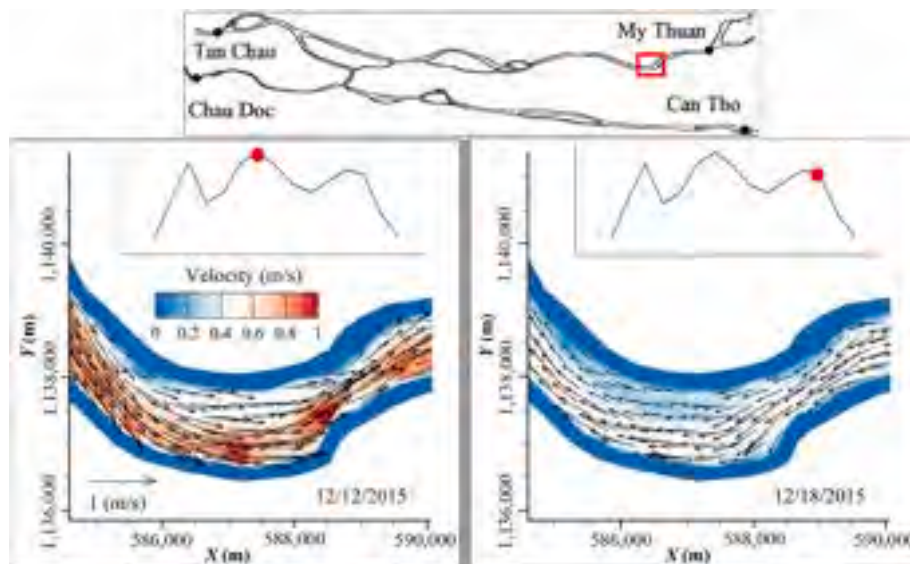


Fig. 7. Simulated magnitude and direction of flow velocity, showing reversed flow caused by tidal effects under low riverine fluvial discharge. The sketch on the top indicates the study area.

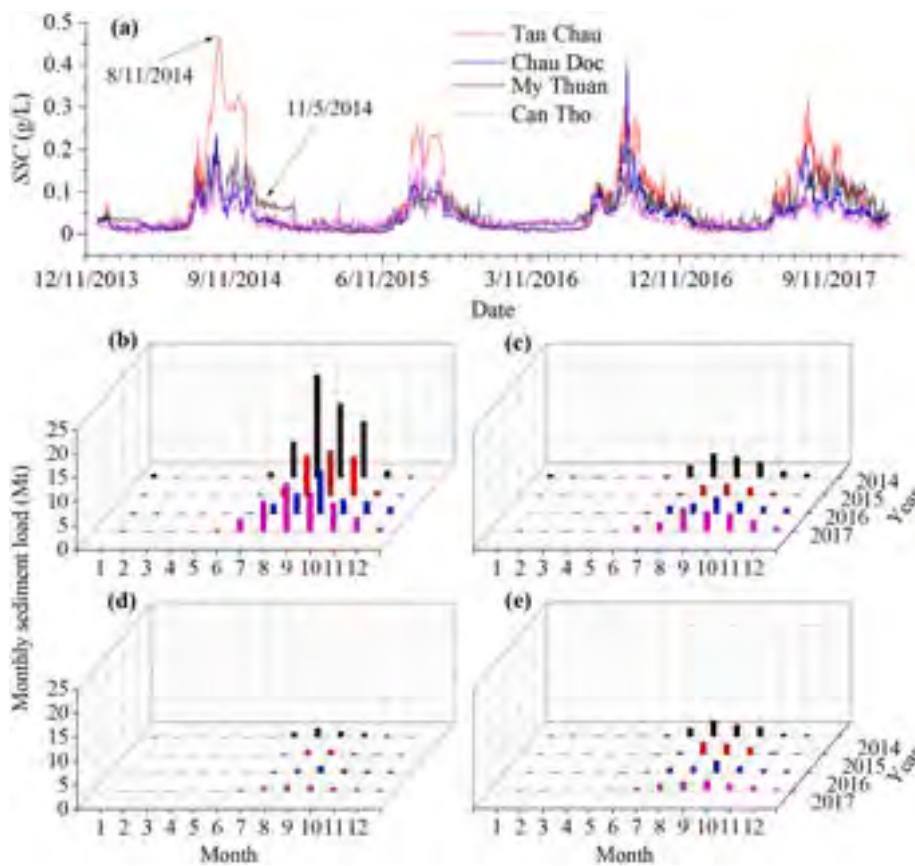


Fig. 8. Observed (a) daily SSC in the VMD and monthly SSL at (b) Tan Chau, (c) Chau Doc, (d) My Thuan, and (e) Can Tho.

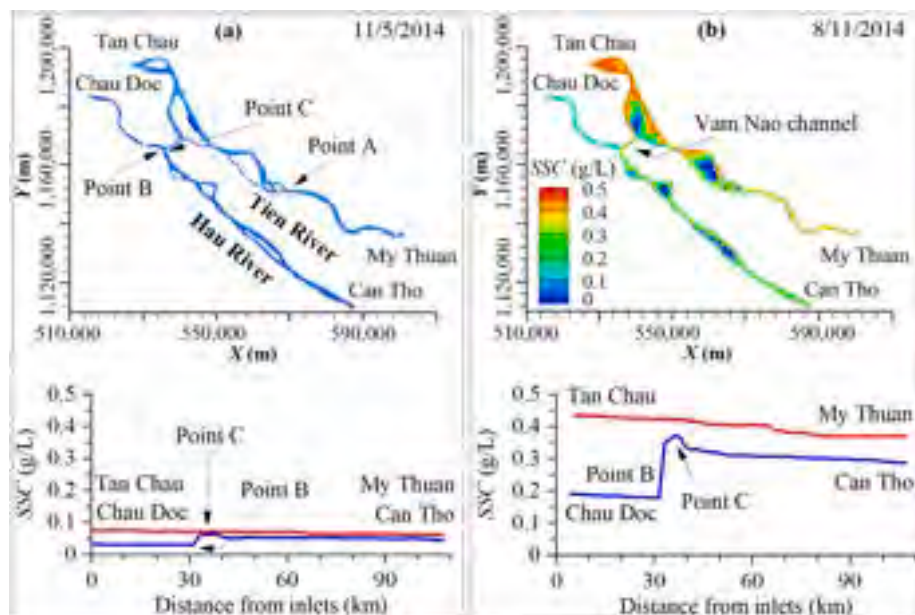


Fig. 9. Spatial and longitudinal distribution of the simulated SSC in (a) nonflood conditions on 11/5/2014 and (b) flood conditions on 8/11/2014. Longitudinal SSCs are extracted along the main branches of the Tien and Hau Rivers.

from the Tien River to the Hau River. Suspended sediment diverted from the Tien River to the Hau River via the Vam Nao channel (mainly in the flood season) can be attributed to a significant discharge difference between the two rivers upstream of this diversion channel (i.e., 83 % in the Tien River and 17 % in the Hau River, see Section 4.1). Such a large

discharge difference may create a hydraulic gradient from the Tien River towards the Hau River, leading to a sharing of suspended sediment from the former to the latter that balances the suspended sediment budget and geomorphological conditions in the VMD's river network. Fig. 9 clearly shows that the simulated SSC in the Hau River above Point B was very

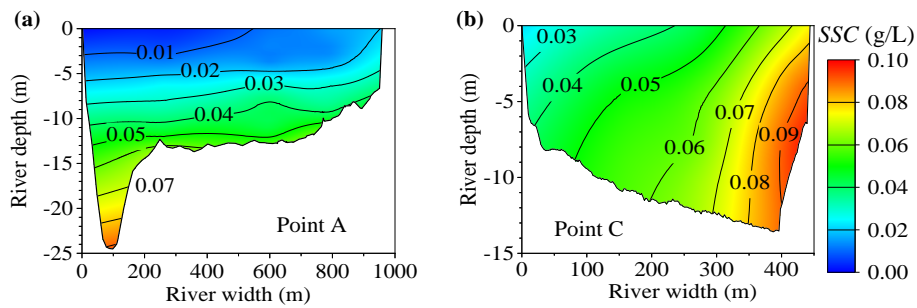


Fig. 10. Observed vertical distribution of SSC at (a) the cross-section at Point A (35 km from My Thuan) in which a scour hole appeared on the left bank and (b) the cross-section at Point C (located at the Vam Nao channel-Hau River confluence, 1 km downstream from Point B) in April 2018 (dry season) during our field survey. The locations of Points A and C are shown in Fig. 9.

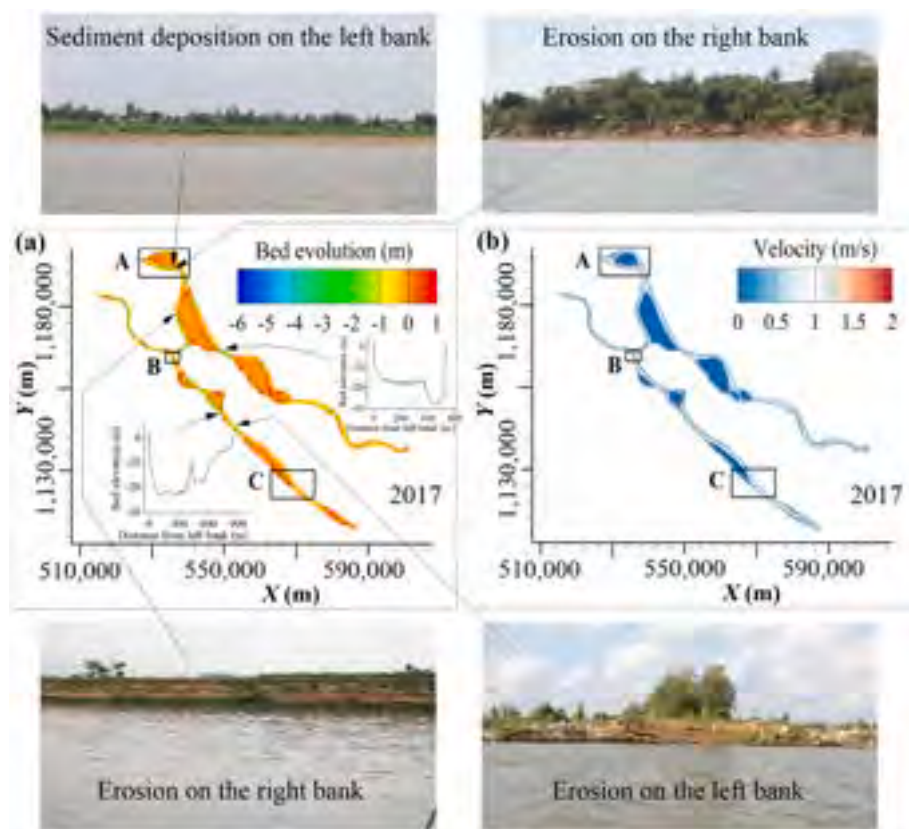


Fig. 11. Simulated riverbed evolution in 2017 compared to the 2014 riverbed level: (a) spatial evolution depth and (b) velocity magnitude. The modelled scour holes are typically compared with the scour holes in cross-sections measured in September 2017 during the first field survey (Fig. a) to illustrate the prediction reliability. Some typical locations of riverbank erosion and deposition are shown by photos taken during the second field trip in April 2018. Details of Zones A–C are shown in Fig. 12.

low and suddenly increased from Point B to Point C. In particular, approximately 61–81 % of the monthly SSL during flood seasons from 2014 to 2017 at Point C was from the Vam Nao channel. These percentages are in line with the estimate of 76 % in 2009 by Manh et al. (2014). This indicates that the Vam Nao channel is very important in balancing water and suspended sediment in the VMD river system. Any changes in the morphology of the Vam Nao channel (discussed in Section 4.3) may cause changes in the total water and suspended sediment budgets in the delta. Therefore, maintaining the geomorphological stability of the Vam Nao channel may favour the sustainable development of the VMD.

Fig. 10 shows the vertical distribution of the observed SSC, which depended on the shape of the cross-section and flow pattern. The SSC was always higher in the lower layer than in the upper layer, on the order of 2 or 3 times. The sediment tends to be trapped in the scour holes, resulting in higher SSCs in cross-sections at such locations (Fig. 10a). The SSC in the scour hole was approximately 8 times greater

than that at the surface. In an asymmetric cross-section, the SSC was higher on the steeper-slope bank than on the opposite bank. For instance, the SSC on the right bank in Fig. 10b was more than double that on the left bank. This is likely because of the higher flow velocity, which has a larger capacity to transport and erode sediment from the bank.

4.3. Riverbed evolution and scour hole formation

Fig. 11 shows the simulated riverbed changes from 2014 to 2017. Generally, the riverbed of the Vam Nao channel was highly incised compared to those of the Tien and Hau Rivers. Riverbed incision mainly occurred on the outer banks of meanders, at confluences, and in the middle of the narrowing (contracted) channels (Figs. 11a and 12a–b), where the flow velocity was high (Fig. 11b). On the other hand, deposition mostly appeared on the inner banks of meanders, on the tail of islands, and in secondary channels (Figs. 11a and 12c), where the

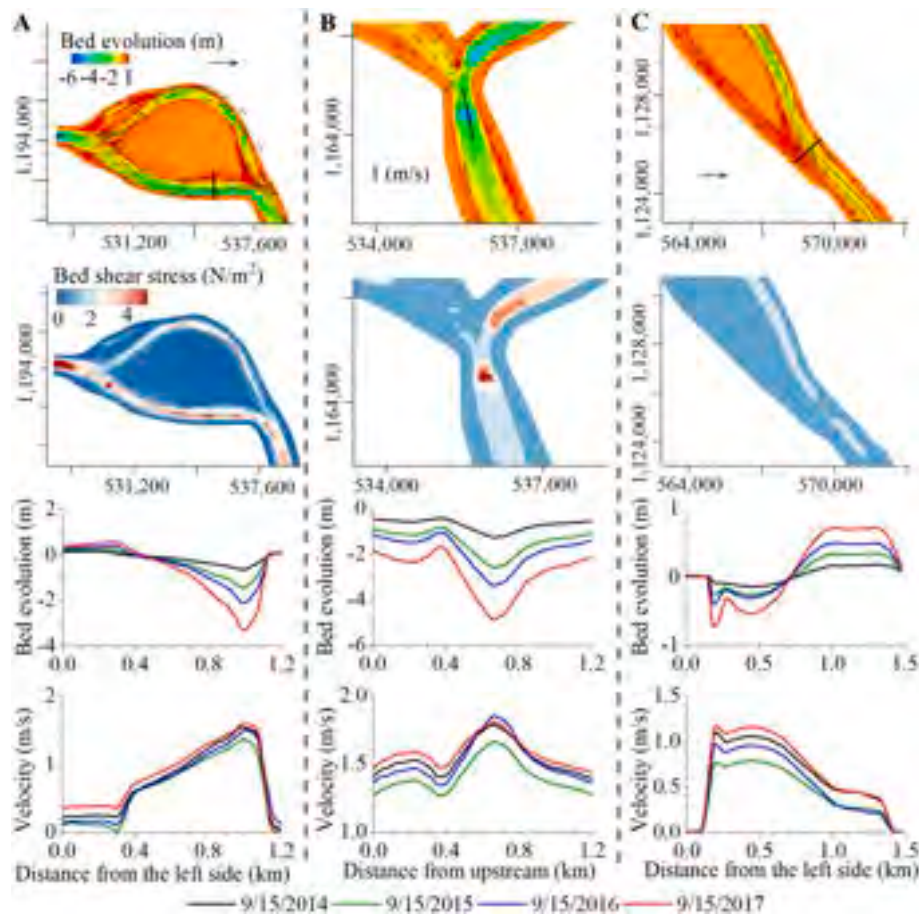


Fig. 12. Typical locations of riverbed evolution (e.g., at scour holes) during the simulated 2014–2017 period and associated bed shear stress (average over 2014–2017 period) and flow velocity distributions. The locations of Zones A–D are shown in Fig. 11.

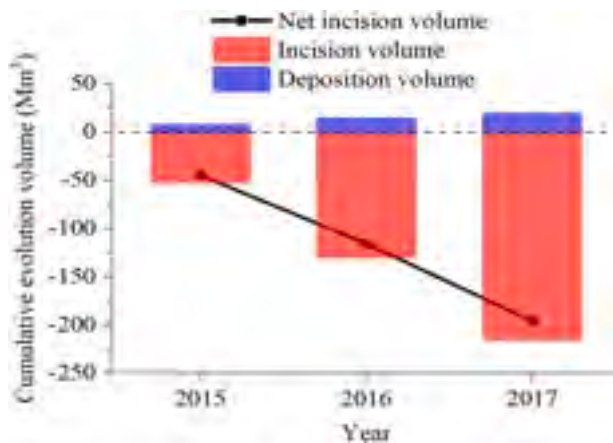


Fig. 13. Simulated cumulative riverbed erosion and deposition volume of the entire study area. The riverbed experiences annual net erosion.

velocity was low. In the Tien River, most of the riverbed incision sections were from Tan Chau to Vam Nao and from Cao Lanh to My Thuan. These most significant incision sections were also reported by Binh et al. (2020b) and Jordan et al. (2019) based on measured bathymetric data. In the Hau River, the riverbed was more incised from Chau Doc to Long Xuyen.

The simulated mean net riverbed incision depths of the Vam Nao, Tien, and Hau Rivers were -2.38 , -1.12 , and -0.68 m, respectively, from 2014 to 2017. These values corresponded to incision rates of 0.79,

0.37, and 0.23 m/yr, respectively. The simulated results show that the mean cumulative incision volume of the entire study area from 2014 to 2017 was -65.3 Mm^3/yr (Fig. 13), which was underestimated by 22.4 % compared to the measured volume of -84.1 Mm^3/yr in the same period. The model underestimates the incision volume and depth because the sand mining effect was not accounted for in our model. Sand mining accounted for 25.6 % of the total incision volume (Binh et al., 2021). Moreover, model uncertainty may partially contribute to such an underestimation. Conversely, riverbed incision in 2017 was the most significant (85.2 Mm^3 incision compared to only 5.1 Mm^3 deposition) (Fig. 13) because of its high flood flow (Fig. 5a) and relatively low SSC (Fig. 8a). Additionally, the total net simulated incision volume of the entire study area was -196 Mm^3 from 2014 to 2017, which was on the same order as -200 Mm^3 over the ten-year period of 1998–2008 in the entire VMD estimated by Brunier et al. (2014).

According to Fig. 14a–b, the model predicted the formation of nine scour holes in the Tien River and seven scour holes in the Hau River. The riverbed will be identified as a scour hole if the slope of the riverbed at the scour zone is suddenly steeper than the slope of the surrounding areas; the mean ratio of the slopes between the scour holes and the surrounding areas was, on average, approximately 15 times. The modelled scour hole locations were verified by comparing them with those measured during the first field survey in September 2017 (Fig. 11a). We classified scour holes into three categories according to the scour depths (i.e., at the deepest point), namely, shallow (scour depths <5 m), medium (scour depths from 5 m to 10 m), and deep (scour depths >10 m), based on percentiles of approximately 33 %. Under this consideration, two scour holes in the Tien River and one scour hole in the Hau River were classified as medium, whereas the remaining scours

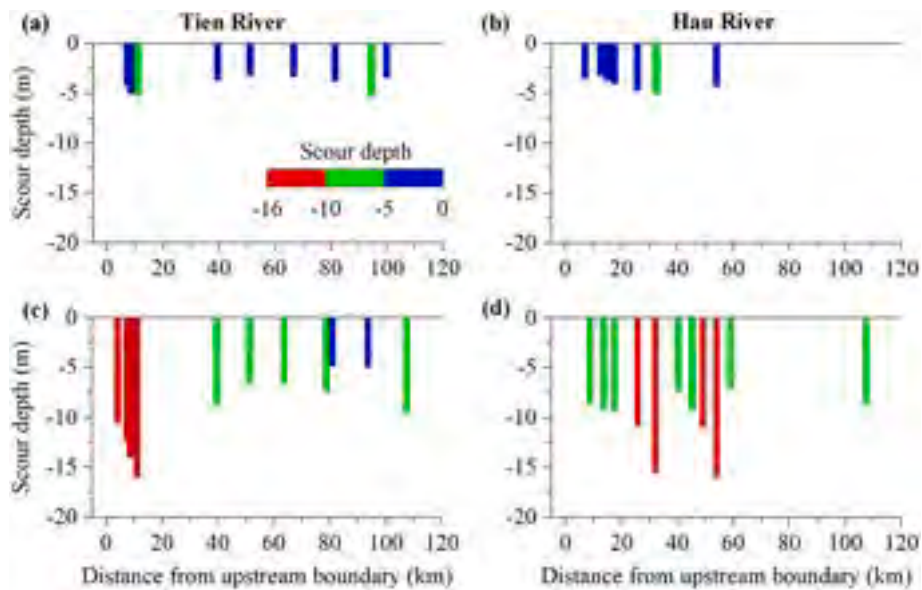


Fig. 14. Classifications of scour holes based on the scour depth (the bar charts) and geomorphological settings (pie charts) during 2014–2017 (a–b) and in scenario 3 during 2017–2026 (c–d).

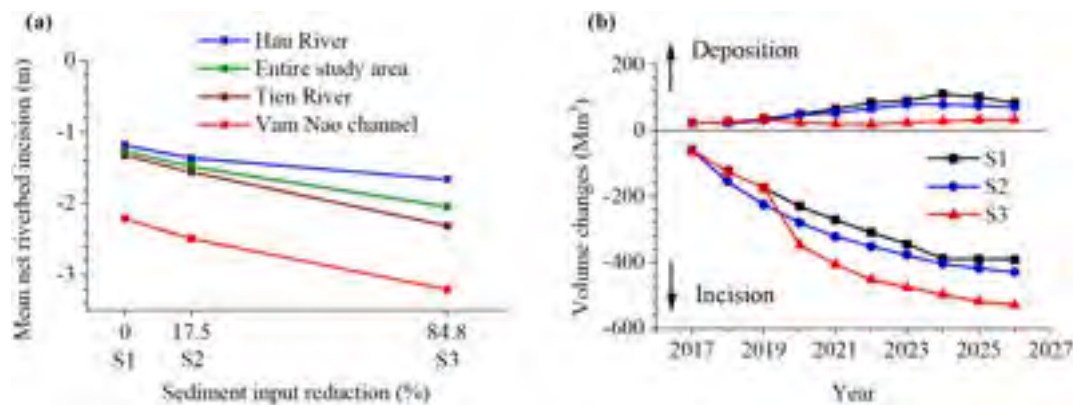


Fig. 15. Predicted morphological changes in the three scenarios: (a) mean net riverbed incision depth and (b) annual total volume changes in the entire study area.

were shallow.

We found that most of the scour holes were formed at river confluences and meandering segments. Although the processes of scour hole formation were different in these geomorphological settings (Rice et al., 2008; Ferrarin et al., 2018), the common mechanism was that the erosive capacity of the flow was very high in the scour holes because of the high flow velocity, which induced high bed shear stresses. In this study, we neglected the small-scale processes in scour holes. Representative simulated scour holes at Zones A and B are illustrated in Fig. 12a–b. In these scour holes, the incision rate was largest in 2017 when high flood flow was combined with low SSC (Figs. 5a and 8a). Notably, the scour hole at Zone B was at the location of a severe riverbank collapse that occurred on 22 April 2017 (Binh et al., 2020b). Therefore, we speculate that scour holes are likely one of the main causes of riverbank erosion in the VMD that local authorities should consider in their protective actions against riverbank collapse.

4.4. Forecasted morphological changes between 2017 and 2026 due to sediment reductions

Riverbeds in the VMD were forecasted to be significantly incised by 2026 (Fig. 15). The mean net riverbed incision depths of the Tien, Hau, and Vam Nao Rivers in S1 were -1.32 , -1.18 , and -2.21 m,

respectively. The respective values were -1.56 , -1.36 , and -2.49 m in S2 and -2.31 , -1.66 , and -3.2 m in S3. We found that the forecasted riverbed incision in the Vam Nao channel was higher than that in the Tien and Hau Rivers (Fig. 15a). Upstream of the Vam Nao channel, the riverbed of the Tien River was more incised than that of the Hau River, but the opposite was true downstream of the Vam Nao channel. The forecasted riverbed incision of both the Tien and Hau Rivers was more severe upstream than downstream of the Vam Nao channel. We estimated that the total net bed sediment losses from 2017 to 2026 in the entire study area were -2472 and -3316 Mm³ in scenarios S2 and S3, respectively, which were increased by 23 % and 65 % compared to S1 (-2011 Mm³) (Fig. 15b). On average, the forecasted mean net riverbed incision by 2026 of the entire study area was increased by 17 % and 61 % in S2 (-1.48 m) and S3 (-2.04 m), respectively, compared to S1 (-1.27 m) (Fig. 15a). The projected increasing riverbed incision may in turn cause some resulting environmental changes in the VMD. First, it may intensify salinity intrusion, causing difficulties in people's livelihoods (Loc et al., 2021). This may require a large-scale economic transformation (i.e., plants and animals that can survive under high salinity concentrations) for the system to adapt to changing conditions. Second, the incised riverbed may also reduce water levels during dry seasons, causing difficulty for irrigation because of river–floodplain disconnection (Park et al., 2020; Binh et al., 2021).

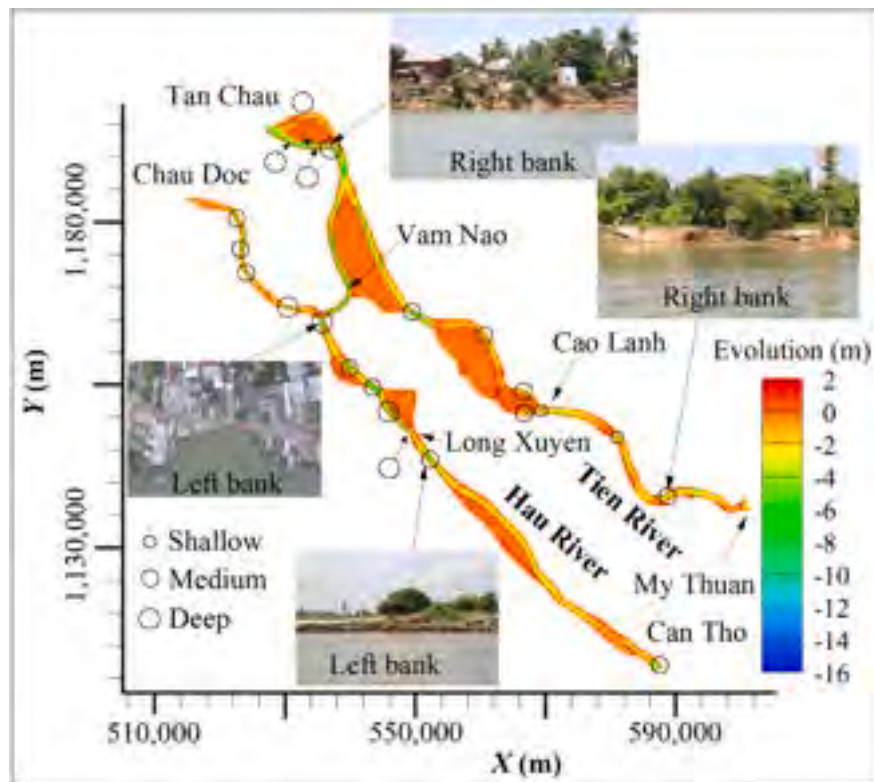


Fig. 16. Forecasted riverbed evolution in 2026 relative to 2017 in S3 under an 84.8 % suspended sediment reduction. Twenty-two scour holes (indicated by black circles) are formed. Some of the scour holes are at the locations of riverbank erosion observed during the 2018 field survey. A drone photo of a severe bank collapse at the Hau River-Vam Nao channel confluence was retrieved from [Vnextpress.net](https://vnextpress.net) accessed on 1/18/2021.

During 2017–2026, twenty-two large-scale scour holes were forecasted to form in the Tien and Hau Rivers in S3, 11 in each (Fig. 16). The scour depths in S3 became deeper than those in 2014–2017. In the Tien River, four scour holes were classified as deep and five as medium (Fig. 14c). In the Hau River, four scour holes were classified as deep and seven as medium (Fig. 14d). The most severe scour hole was likely at the Hau River-Vam Nao channel confluence (Figs. 14d and 16). The maximum scour depth at this location in S3 was forecasted to be up to -16 m by 2026. In the Tien River, the most severe scour hole was likely at a location 11 km downstream from Tan Chau, at which the riverbank was eroded (Figs. 14c and 16). Notably, our forecasted riverbed incision at this location was likely underestimated because we did not account for the sand mining effect in our model, while sand mining was very active there (Fig. 1b). Generally, the forecasted severe scour holes were around the locations of severe riverbank erosion observed during our field surveys in 2018 (Fig. 16). Therefore, it is likely that scour holes will continue to cause the increasing collapse of the riverbank in the near future.

Although not included in the model, sand mining remains one of the key causes of riverbed incision in the VMD (Brunier et al., 2014; Gruel et al., 2022). Scour holes formed by sand mining are likely to trap the bedload, which may result in a deficit in the bedload supply to the downstream reaches, likely causing migration/expansion of riverbed incision in both upstream and downstream directions (Anh et al., 2022). Moreover, scour holes created by sand mining can be a root cause of riverbank instability (Hackney et al., 2020). This can explain why the scour holes predicted by our model were near the locations of severe riverbank erosion (Figs. 11 and 16). To alleviate/decelerate the likely consequences of riverbed incision and scour holes on river system stability, in addition to considering integrated sediment management at the basin scale, including sustainable reservoir sedimentation management, sand mining should be strictly prohibited in the VMD with stronger regulations to prevent illegal mining activities, both from licensed

operators and from local citizens. Decision makers are recommended to take actions to limit sand mining activities (i.e., considering not relicensing the expired mining sites while not approving new licenses) to save our delta in the long run.

4.5. Model uncertainties and outlook

The developed model may encounter some uncertainties. First, the 2014 bathymetric data are not fully available for the entire Hau River. Therefore, the bathymetric data measured in 2010 and 2012 were also used to create the input geometry. However, these data are up-to-date. Second, the model did not include sand mining effects on morphological changes. Thus, the simulated mean net riverbed incision volume in the entire study area from 2014 to 2017 ($-65.3 \text{ Mm}^3/\text{yr}$) was underestimated by 22.4 % compared to the measured data ($-84.1 \text{ Mm}^3/\text{yr}$). This value is within the range of 14.8–25.6 % under sand mining effects on riverbed incision (Binh et al., 2020b, 2021). The underestimation can be attributed partially to sand mining (i.e., it is present in reality but was not considered by the model) and partially to model uncertainty. Third, bedload transport was not considered, which may lead to unavoidable uncertainty in bed evolution. However, this is acceptable because the bedload contributes a negligible amount (1–3 %) to the total load (Jordan et al., 2019; Hackney et al., 2020). Fourth, to reduce the simulation time, we simulated only seven months during the flood season in each simulated year. This may have uncertainties in the erosion and deposition processes. However, this consideration is appropriate because up to 98 % of the suspended sediment in the VMD is transported within the flood season (Fig. 8b–e). Fifth, the model used a sediment mixture of only two sediment classes (cohesive and non-cohesive), while the natural sediment is usually composed of different grain sizes (Lepesqueur et al., 2019). This simplification may result in under- or overestimation of bed evolution because the model neglects the effects of sediment densities and grain size distributions, which have

been proven to substantially enhance the performance of the model (Lepesqueur et al., 2019). Sixth, longer projected time scales (e.g., spanning several decades) should be forecasted to provide better information for holistic river management. Finally, drivers of riverbed incision are not only dams but also sand mining/dredging (Anh et al., 2022; Gruel et al., 2022) and climate variability/change (Darby et al., 2016). Therefore, future studies are expected to quantify the role of each driver on riverbed incision in the large-scale VMD, which can provide important indications for the government to sustainably develop the delta while effectively minimizing the negative impacts.

5. Conclusions

Hydrodynamics, suspended sediment transport, and morphodynamics in fluvial-dominated, tide-affected rivers in the VMD from 2014 to 2017 were investigated using field survey data and a coupled hydrodynamic and sediment transport model. The morphological evolution under three scenarios of suspended sediment supply reductions was forecasted for the decade ending in 2026. The main findings of this study are as follows:

- The Vam Nao channel has a significant impact on the flow and suspended sediment dynamics of the Tien and Hau Rivers. We estimated that approximately 61–81 % of the mean SSL of the Hau River was diverted from the Tien River via the Vam Nao channel in the flood season from 2014 to 2017.
- We found that the tidal effect was stronger in the Hau River than in the Tien River. Both observed and simulated data from 2014 to 2017 show that the tidal regime has a clear effect on the water level.
- In the Tien River during the dry season from 2014 to 2017, the SSL was longitudinally higher upstream than downstream of the Vam Nao channel due to tidal effects. However, the opposite relationship was observed during the flood season because of the dominance of the riverine fluvial flow from the Mekong River. In the Hau River, the SSL was always higher downstream than upstream of the Vam Nao channel because of suspended sediment diverted from the Tien River.
- The simulated results from 2014 to 2026 show that riverbed incision is higher in the Vam Nao channel than in the Tien and Hau Rivers. In the Tien River, the sections with the most riverbed incision are from Tan Chau to Vam Nao and from Cao Lanh to My Thuan. In the Hau River, the riverbed is more incised from Chau Doc to Long Xuyen.
- Simulated results show that 16 scour holes were formed in the Tien and Hau Rivers during 2014–2017. We forecasted that 22 scour holes are likely to appear in these rivers by 2026 if the suspended sediment supply from the Mekong River is reduced by 84.8 % due to river damming. Scour holes are predicted to be formed at locations of severe riverbank erosion observed during our field surveys in 2018. We anticipate that scour holes are likely to continue to cause increasing collapse of the riverbank in the near future. Therefore, the predicted results can provide useful information for local authorities to actively propose appropriate countermeasures against riverbank erosion.

Declaration of competing interest

None.

Acknowledgements

The authors would like to acknowledge the Mekong River Commission and the Vietnam National Center for Hydrometeorological Forecasting for providing the data. The data from the Mekong River Commission can be obtained from <https://www.mrcmekong.org/>. The Telemac-Mascaret modelling system can be freely downloaded at <http://www.opentelemac.org/>. The authors would like to acknowledge

Dr. Nguyen Thi Phuong Mai from Thuyloi University, Vietnam, for supporting us in conducting the field surveys and in collecting the flow data in the Vietnamese Mekong Delta. We are thankful to Mr. Nguyen Hoang Long, director of Hai Au Technology Joint Stock Company, and Mr. Take Toshiaki, adviser of JFE Advantech Co., Ltd., for supporting us with the Infinity turbidity and velocity meters and accompanying us in the 2018 field survey. This work was funded by the Japan-ASEAN Science, Technology and Innovation Platform (JASTIP), the Supporting Program for Interaction-Based Initiative Team Studies (SPIRITS) 2016 of Kyoto University, and the Asia-Pacific Network for Global Change Research under project reference number CRRP2020-09MY-Kantoush. This paper is based on a part of Doan Van Binh's doctoral thesis.

Appendix A. Supplementary data

Supplementary data to this article can be found online at <https://doi.org/10.1016/j.geomorph.2022.108368>.

References

- Anh, L.N., Tran, D.D., Thong, N., Van, C.T., Vinh, D.H., Au, N.H., Park, E., 2022. Drastic variations in estuarine morphodynamics in Southern Vietnam: investigating riverbed sand mining impact through hydrodynamic modelling and field controls. *J. Hydrol.* 608, 127572.
- Anthony, E.J., Brunier, G., Besset, M., Goichot, M., Dussouillez, P., Nguyen, V.L., 2015. Linking rapid erosion of the Mekong River Delta to human activities. *Sci. Rep.* 5, 14745.
- Best, J., 2019. Anthropogenic stresses on the world's big rivers. *Nat. Geosci.* 12, 7–21.
- Binh, D.V., Kantoush, S., Sumi, T., Mai, N.P., 2018. Impact of Lancang cascade dams on flow regimes of Vietnamese Mekong Delta. *Annu. J. Hydraul. Eng.* 74, 487–492.
- Binh, D.V., Kantoush, S.A., Saber, M., Mai, N.P., Maskey, S., Phong, D.T., Sumi, T., 2020a. Long-term alterations of flow regimes of the Mekong River and adaptation strategies for the Vietnamese Mekong Delta. *J. Hydrol. Reg. Stud.* 32, 100742.
- Binh, D.V., Kantoush, S., Sumi, T., 2020b. Changes to long-term discharge and sediment loads in the Vietnamese Mekong Delta caused by upstream dams. *Geomorphology* 353, 107011.
- Binh, D.V., Kantoush, S., Sumi, T., Mai, N.P., Trung, L.V., 2020. Dam-induced riverbed incision and saltwater intrusion in the Mekong Delta. In: Uijttewaai, W.S.J., Crosato, A., Schielen, R. (Eds.), *River Flow*. Taylor & Francis Group, London, UK.
- Binh, D.V., Wietlisbac, B., Kantoush, S., Loc, H.H., Park, E., de Cesare, G., Cuong, D.H., Tung, N.X., Sumi, T., 2020d. A novel method for river bank detection from Landsat satellite data: a case study in the Vietnamese Mekong Delta. *Remote Sens.* 12, 3298.
- Binh, D.V., Kantoush, A.A., Sumi, T., Mai, N.P., Ngoc, T.A., Trung, L.V., An, T.D., 2021. Effects of riverbed incision on the hydrology of the Vietnamese Mekong Delta. *Hydrol. Process.* 35, e14030.
- Boretti, A., 2020. Implications on food production of the changing water cycle in the Vietnamese Mekong Delta. *Glob. Ecol. Conserv.* 22, e00989.
- Bravard, J.-P., Goichot, M., Gaillot, S., 2013. Geography of sand and gravel mining in the lower Mekong River: first survey and impact assessment. *EchoGéo* 26, 1–18.
- Brunier, G., Anthony, E.J., Goichot, M., Provansal, M., Dussouillez, P., 2014. Recent morphological changes in the Mekong and Bassac River channels, Mekong Delta: the marked impact of river-bed mining and implications for delta destabilisation. *Geomorphology* 224, 177–191.
- Dang, T.D., Cochrane, T.A., Arias, M.E., Van, P.D.T., Vries, T.T.D., 2016. Hydrological alterations from water infrastructure development in the Mekong floodplains. *Hydrol. Process.* 30, 3824–3838.
- Dang, T.D., Cochrane, T.A., Arias, M.E., 2018. Quantifying suspended sediment dynamics in mega deltas using remote sensing data: a case study of the Mekong floodplains. *Int. J. Appl. Earth Obs. Geoinf.* 68, 105–115.
- Darby, S.E., Hackney, C.R., Leyland, J., Kumm, M., Lauri, H., Parsons, D.R., Best, J.L., Nicholas, A.P., Aalto, R., 2016. Fluvial sediment supply to a mega-delta reduced by shifting tropical-cyclone activity. *Nature* 539, 276–279.
- El kadi Abderrezzak, K., Die Moran, A., Tassi, P., Ata, R., Herouvet, J.M., 2016. Modelling river bank erosion using a 2D depth-averaged numerical model of flow and non-cohesive, non-uniform sediment transport. *Adv. Water Res.* 93, 75–88.
- Eslami, S., Hoekstra, P., Trung, N.N., Kantoush, S.A., Binh, D.V., Dung, D.D., Quang, T.T., van der Vegt, M., 2019. Tidal amplification and salt intrusion in the Mekong delta driven by anthropogenic sediment starvation. *Sci. Rep.* 9, 18746.
- Exner, F.M., 1925. Über die Wechselwirkung zwischen Wasser und Geschiebe in Flüssen. *Akad. Wiss. Wien Math. Naturwiss. Klasse* 134, 165–204.
- Ferrarin, C., Madricardo, F., Rizzetto, F., Kiver, W.M., Dellafiore, D., Umgieser, G., Kruss, A., Zaggia, L., Fogliani, F., Ceregato, A., Sarretta, A., Trincardi, F., 2018. Geomorphology of scour holes at tidal channel influences. *J. Geophys. Res. Earth Surf.* 123, 1386–1406.
- Gruel, C.R., Park, E., Switzer, A.D., Kumar, S., Ho, H.L., Kantoush, S., Binh, D.V., Feng, L., 2022. New systematically measured sand mining budget for the Mekong Delta reveals rising trends and significant volume underestimations. *Int. J. Appl. Earth Obs. Geoinf.* 108, 102736.

- Guan, B., Chen, M., Elseiy-Quirk, T., Yang, S., Shang, W., Li, Y., Tian, X., Han, G., 2019. Soil seed bank and vegetation differences following channel diversion in the Yellow River Delta. *Sci. Total Environ.* 693, 133600.
- Gugliotta, M., Saito, Y., Nguyen, V.L., Ta, T.K.O., Nakashima, R., Tamura, T., Uehara, K., Katsuki, K., Yamamoto, S., 2017. Process regime, salinity, morphological, and sedimentary trends along the fluvial to marine transition zone of the mixed-energy Mekong River delta, Vietnam. *Cont. Shelf Res.* 147, 7–26.
- Ha, D.T., Ouilion, S., Vinh, G.V., 2018. Water and suspended sediment budgets in the lower Mekong from high-frequency measurements (2009–2016). *Water* 10, 846.
- Hackney, C.R., Darby, S.E., Parsons, D.R., Leyland, J., Best, J.L., Aalto, R., Nicholas, A.P., Houseago, R.C., 2020. River bank instability from unsustainable sand mining in the lower Mekong River. *Nat. Sustain.* 3, 217–225.
- Hecht, J.S., Lacombe, G., Arias, M.E., Dang, T.D., 2019. Hydropower dams of the Mekong River basin: a review of their hydrological impacts. *J. Hydrol.* 568, 285–300.
- Hein, H., Hein, B., Pohlmann, T., 2013. Recent sediment dynamics in the region of Mekong water influence. *Glob. Planet. Chang.* 110, 183–194.
- Hervouet, J.M., 2007. *Hydrodynamics of Free Surface Flows*. John Wiley and Sons, USA.
- Hung, N.N., Delgado, J.M., Güntner, A., Merz, B., Bárdossy, A., Apel, H., 2014a. Sedimentation in the floodplains of the Mekong Delta, Vietnam. Part I: suspended sediment dynamics. *Hydrol. Process.* 28, 3132–3144.
- Hung, N.N., Delgado, J.M., Güntner, A., Merz, B., Bárdossy, A., Apel, H., 2014b. Sedimentation in the floodplains of the Mekong Delta, Vietnam. Part II: deposition and erosion. *Hydrol. Process.* 28, 3145–3160.
- Jordan, C., Tiede, J., Lojek, O., Visscher, J., Apel, H., Nguyen, H.Q., Quang, C.N.X., Schlurmann, T., 2019. Sand mining in the Mekong Delta revisited – current scales of local sediment deficits. *Sci. Rep.* 9, 17823.
- Jordan, C., Visscher, J., Dung, N.V., Apel, H., Schlurmann, T., 2020. Impacts of human activity and global changes on future morphodynamics within the Tien River, Vietnamese Mekong Delta. *Water* 12 (8), 2204.
- Khoi, D.N., Dang, T.D., Pham, L.T.H., Loi, P.T., Thuy, N.T.D., Phung, N.K., Bay, N.T., 2020. Morphological change assessment from intertidal to river-dominated zones using multiple-satellite imagery: a case study of the Vietnamese Mekong Delta. *Reg. Stud. Mar. Sci.* 34, 101087.
- Koehnken, L., 2014. Discharge Sediment Monitoring Project (DSMP) 2009–2013 Summary & Analysis of Results. Final Report. Mekong River Commission/ Gesellschaft für Internationale Zusammenarbeit, Phnom Penh, Cambodia.
- Kondolf, G.M., Gao, Y., Annadale, G.W., Morris, G.L., Jiang, E., Zhang, J., Cao, Y., Carling, P., Fu, K., Guo, Q., Hotchkiss, R., Peteuil, C., Sumi, T., Wang, H.W., Wang, Z., Wei, Z., Wu, B., Wu, C., Yang, C.T., 2014a. Sustainable sediment management in reservoirs and regulated rivers: experiences from five continents. *Earth's Future* 2, 256–280.
- Kondolf, G.M., Rubin, Z.K., Minear, J.T., 2014b. Dams on the Mekong: cumulative sediment starvation. *Water Resour. Res.* 50, 5158–5169.
- Kummu, M., Varis, O., 2007. Sediment-related impacts due to upstream reservoir trapping, the lower Mekong River. *Geomorphology* 85, 275–293.
- Kummu, M., Lu, X.X., Wang, J.J., Varis, O., 2010. Basin-wide sediment trapping efficiency of emerging reservoirs along the Mekong. *Geomorphology* 119, 181–197.
- Langendoen, E.J., Mendoza, A., Abad, J.D., Tassi, P., Wang, D., Ata, R., El kadi Abderrezak, K., Hervouet, J.M., 2016. Improved numerical modelling of morphodynamics of rivers with steep banks. *Adv. Water Res.* 93, 4–14.
- Lauri, H., De-Moel, H., Ward, P.J., Räsänen, T.A., Keskinen, M., Kummu, M., 2012. Future changes in Mekong River hydrology: impact of climate change and reservoir operation on discharge. *Hydrol. Earth Syst. Sci.* 16 (12), 4603–4619.
- Le, H.A., 2020. Field And Model Investigation of Flow And Sediment Transport in the Lower Mekong River. Doctoral dissertation. Louvain-la-Neuve, 151 pp.
- Lepesqueur, J., Hostache, R., Martínez-Carreras, N., Montargès-Pelletier, E., Hissler, C., 2019. Sediment transport modelling in riverine environments: on the importance of grain-size distribution, sediment density and boundary conditions. *Hydrol. Earth Syst. Sci.* 23, 3901–3915.
- Letrung, T., Li, Q., Li, Y., Vukien, T., Nguenhtai, Q., 2013. Morphology evolution of Cuadaí estuary, Mekong River, southern Vietnam. *J. Hydraul. Eng.* 18, 1122–1132.
- Li, X., Liu, J.P., Saito, Y., Nguyen, V.L., 2017. Recent evolution of the Mekong Delta and the impacts of dams. *Earth Sci. Rev.* 175, 1–17.
- Loc, H.H., Binh, D.V., Park, E., Shrestha, S., Dung, T.D., Son, V.H., Truc, N.H.T., Mai, N. P., Seijger, C., 2021. Intensifying saline water intrusion and drought in the Mekong Delta: from physical evidence to policy outlooks. *Sci. Total Environ.* 757, 143919.
- Loisel, H., Mangin, A., Vantrepotte, V., Dessailly, D., Dinh, D.N., Garnesson, P., Ouilion, S., Lefebvre, X.P., Meriaux, X., Phan, T.M., 2014. Remote sensing of environment variability of suspended particulate matter concentration in coastal waters under the Mekong's influence from ocean color (MERIS) remote sensing over the last decade. *Remote Sens. Environ.* 150, 218–230.
- Lu, X.X., Siew, R.Y., 2006. Water discharge and sediment flux changes over the past decades in the lower Mekong River: possible impacts of the Chinese dams. *Hydrol. Earth Syst. Sci.* 10, 181–195.
- Lu, X.X., Li, S., Kummu, M., Padawangi, R., Wang, J.J., 2014. Observed changes in the water flow at Chiang Saen in the lower Mekong: impacts of Chinese dams? *Quat. Int.* 336, 145–157.
- Lu, X.X., Oeurng, C., Le, T.P.Q., Thuy, D.T., 2015. Sediment budget as affected by construction of a sequence of dams in the lower Red River, Vietnam. *Geomorphology* 248, 125–133.
- Mai, N.P., Kantoush, S., Sumi, T., Thang, T.D., Trung, L.V., Binh, D.V., 2018. Assessing and adapting the impacts of dams operation and sea level rising on saltwater intrusion into the Vietnamese Mekong Delta. *J. Jpn. Soc. Civ. Eng. Ser. B1 (Hydraul. Eng.)* 74, 373–378.
- Mai, N.P., Kantoush, S., Sumi, T., Thang, T.D., Binh, D.V., Trung, L.V., 2019. The influences of tidal regime and morphology change on salinity intrusion in Hau River. In: *E-proceedings of the 38th IAHR World Congress*, Panama City, Panama.
- Mai, N.P., Kantoush, S., Sumi, T., Thang, T.D., Binh, D.V., Trung, L.V., 2019b. Study on salinity intrusion processes into Hau River of Vietnamese Mekong Delta. *J. Jpn. Soc. Civ. Eng. Ser. B1 (Hydraul. Eng.)* 75 (2), 751–756.
- Manh, N.V., Dung, N.V., Hung, N.N., Kummu, M., Merz, B., Apel, H., 2015. Future sediment dynamics in the Mekong Delta floodplains: impacts of hydropower development, climate change and sea level rise. *Glob. Planet. Chang.* 127, 22–33.
- Manh, N.V., Dung, N.V., Hung, N.N., Merz, B., Apel, H., 2014. Large-scale suspended sediment transport and sediment deposition in the Mekong Delta. *Hydrol. Earth Syst. Sci.* 18, 3033–3053.
- Maeda, E.E., Formaggio, A.R., Shimabukuro, Y.E., 2008. Impacts of land use and land cover changes on sediment yield in a Brazilian Amazon drainage basin. *GI Sci. Remote Sens.* 45 (4), 443–453.
- Milliman, J.D., Farnsworth, K.L., 2011. *River Discharge to the Coastal Ocean: A Global Synthesis*. Cambridge University Press.
- Minderhoud, P.S.J., Middelkoop, H., Erkens, G., Stouthamer, E., 2020. Groundwater extraction may drown mega-delta: projections of extraction-induced subsidence and elevation of the Mekong delta for the 21st century. *Environ. Res. Commun.* 2, 011005.
- Mtamba, J., Velde, T.V.D., Ndomba, P., Zoltán, V., Mtaló, F., 2015. Use of radarsat-2 and Landsat TM images for spatial parameterization of Manning's roughness coefficient in hydraulic modeling. *Remote Sens.* 7, 836–864.
- Nowacki, D.J., Ogston, A.S., Nittrouer, C.A., Fricke, A.T., Van, P.D.T., 2015. Sediment dynamics in the lower Mekong River: transition from tidal river to estuary. *J. Geophys. Res. Oceans* 120, 6363–6383.
- Sisyph, 2018. *Sisyph User Manual*, Version v7p3, 70 pp.
- Pahl, J.W., Freeman, A.M., Raynie, R.C., Day, J., 2020. Response of the coastal systems to freshwater input with emphasis on Mississippi River deltaic plain river diversions: Synthesis of the state of the science. *Estuar. Coast. Shelf Sci.* 243, 106866.
- Park, E., Ho, H.L., Tran, D.D., Yang, X., Alcantara, E., Merino, E., Son, V.H., 2020. Dramatic decrease of flood frequency in the Mekong Delta due to river-bed mining and dyke construction. *Sci. Total Environ.* 723, 138066.
- Park, E., Ho, H.L., Binh, D.V., Kantoush, S., Poh, D., Alcantara, E., Try, S., Lin, Y.N., 2022. Impacts of agricultural expansion on floodplain water and sediment budgets in the Mekong River. *J. Hydrol.* 605, 127296.
- Rice, S.P., Roy, A.G., Rhoads, B.L., 2008. *River Confluences, Tributaries And the Fluvial Network*. John Wiley, Chichester, UK.
- Schmitt, R.J.P., Giuliani, M., Bizzi, S., Kondolf, G.M., Daily, G.C., Castelletti, A., 2021. Strategic basin and delta planning increases the resilience of the Mekong Delta under future uncertainty. *PNAS* 118 (36), e2026127118.
- Stokes, G., 1851. *On the Effect of the Internal Friction of Fluids on the Motion of Pendulums*. Cambridge Pitt Press, Cambridge.
- Thanh, V.Q., Reynolds, J., Wackerman, C., Eidam, E.F., Roelvink, D., 2017. Modelling suspended sediment dynamics on the subaqueous delta of the Mekong River. *Cont. Shelf Res.* 147, 213–230.
- Thuy, N.T.D., Khoi, D.N., Nhan, D.T., Nga, T.N.Q., Bay, N.T., Phung, N.K., 2019. Modelling accretion and erosion processes in the Bassac and Mekong Rivers of the Vietnamese Mekong Delta. In: Viet, N.T., Xiping, D., Tung, T.T. (Eds.), *Proceeding of the 10th International Conference on Asian and Pacific Coasts*, 2019, Hanoi, Vietnam. Springer, Hanoi, pp. 1431–1437.
- Tran, D.A., Tsujimura, M., Pham, H.V., Nguyen, T.V., Ho, L.H., Vo, P.L., Ha, K.Q., Dang, T.D., Binh, D.V., Doan, Q.V., 2021. Intensified salinity intrusion in coastal aquifers due to groundwater overextraction: a case study in the Mekong Delta, Vietnam. *Environ. Sci. Pollut. Res.* 29, 8996–9010.
- Tu, L.X., Thanh, V.Q., Reynolds, J., Van, S.P., Anh, D.T., Dang, T.D., Roelvink, D., 2019. Sediment transport and morphodynamical modeling on the estuaries and coastal zone of the Vietnamese Mekong Delta. *Cont. Shelf Res.* 186, 64–76.
- Van, P.D.T., Popescu, I., Van Griensven, A., Solomatine, D.P., Trung, N.H., Green, A., 2012. A study of the climate change impacts on fluvial flood propagation in the Vietnamese Mekong Delta. *Hydrol. Earth Syst. Sci.* 16, 4637–4649.
- Villaret, C., Hervouet, J.M., Kopmann, R., Merkel, U., Davies, A.G., 2013. Morphodynamic modelling using the Telemac finite element system. *Comput. Geosci.* 53 (105–113), 2013.
- Vinh, V.D., Ouilion, S., Van Thao, N., Ngoc Tien, N., 2016. Numerical simulations of suspended sediment dynamics due to seasonal forcing in the Mekong coastal area. *Water* 8, 255.
- Wassmann, R., Hien, N.X., Hoanh, C.T., Tuong, T.P., 2004. Sea level rise affecting the Vietnamese Mekong Delta: water elevation in the flood season and implications for rice production. *Clim. Chang.* 66, 89–107.
- Wolanski, E., Huan, N.N., Dao, L.T., Nhan, N.H., Thuy, N.N., 1996. Fine-sediment dynamics in the Mekong River Estuary, Viet Nam. *Estuar. Coast. Shelf Sci.* 43, 565–582.
- Xing, F., Meselhe, E.A., Allison, M.A., Weathers III, H.D., 2017. Analysis and numerical modeling of the flow and sand dynamics in the lower Song Hau channel, Mekong Delta. *Cont. Shelf Res.* 147, 62–77.
- Xue, Z., He, R., Liu, J.P., Warner, J.C., 2012. Modeling transport and deposition of the Mekong River sediment. *Cont. Shelf Res.* 37, 66–78.

Satellite-Based Flood Inundation and Damage Assessment

C B Mata^{1*}, O F Balderama² L A Alejo³ JL R Bareng⁴ S A Kantoush⁵

¹ Water Research and Development Center, Isabela State University, Isabela, Philippines

^{2, 3, 4} College of Engineering, Isabela State University, Isabela, Philippines

⁵ Water Resources Research Center – Disaster Prevention Research Institute Kyoto University, Kyoto, Japan

*Corresponding author

Christine B Mata, Water Research and Development Center, Isabela State University, Isabela, Philippines.

Submitted: 29 Jun 2022; Accepted: 11 Jul 2022; Published: 21 Jul 2022

Citation: Mata, C.B., Balderama, O.F., Alejo, L.A., Bareng, J.L.R., Kantoush, S.A. (2022). Satellite-based flood inundation and damage assessment. *J Robot Auto Res*, 3(2), 209-219.

Abstract

Because recurring floods in the Philippines have become more damaging throughout time, risk assessments, quantifying, and visualizing flood damages as accurately as possible become imperative. To deal with an up-to-date database and a practical assessment tool, a satellite imagery-based method was used which aimed to map flood inundation and estimate damages brought by the flood during Typhoon Ulysses. This paper presents a framework for an integrated flood risk management in a river basin context with the following components as follows: 1) collection of the comprehensive database containing information relevant for flood analysis; 2) use of a satellite-imagery based method for flood inundation map using Google Earth engine; 3) validation of map accuracy through quick post-flood participatory approach. Analysis of the recent flood inundation event in November 2020 in Cagayan Valley, Philippines showed the inundation of an extensive area of 620.88 km² affecting the Cagayan province at 55.91% and Isabela province at 44% share of inundation. The flood severely affected approximately 614.05 km² of the total croplands. Using a participatory validation approach, the overall accuracy of datasets used is 97.78% while flood extent is 95%. Through this study, the framework, approach, and methodology can be replicated in other locations in the Philippines and in other countries which recurrently experience flooding.

Keywords: Google Earth Engine, Sentinel-1, flood mapping, flood damage assessment

Introduction

Floods are one of the most destructive natural disasters in terms of socio-economic damages, both globally and in the Philippines. Due to geographic location and diverse topography, many countries especially in Asia including China, Bangladesh, Japan, India, and Philippines have been severely affected and suffered from floods. Over the last half-century, more than 80% of natural catastrophes in the Philippines are accounted for typhoons and floods.

The recent flooding in the Philippines 2020 was brought about by the succeeding occurrences of six (6) tropical cyclones in the country, the last of which is Typhoon Ulysses, bringing unprecedented rains to the Cagayan Valley region resulting in unexpected floods heights and extensive inundation to the provinces of Isabela and Cagayan. Flood risk assessment and decision-making necessitate the most precise quantification of flood risk damages feasible [2-4]. The availability of a detailed spatial database for damage assessment can potentially improve the ability to generate high-resolution flood damage maps. However, just extracting and mapping these resources alone is laborious while the adoption of the traditional approach is time-consuming and expensive. Flood

damage estimate using GIS and RS has become a useful instrument for developing a near real-time flood mapping and effective flood risk mitigation policy [5-6].

Many attempts have been made in the past to map flood vulnerability in the Philippines using LiDAR but unfortunately, the coverage for a sufficiently high accurate Digital Terrain Model (DTM) is not complete, especially in the river basin context [7-8]. Flood management based on water level forecasting is ineffective in providing a spatial flood region for mapping flood events [9-10]. The limitations of the hydrological model-based method are addressed by satellite-based flood extent monitoring [11]. In the Philippines, suggest the use of Google Earth Engine (GEE) in post-disaster recovery monitoring in Leyte brought by Typhoon Haiyan in 2013 [12]. GEE also offers a rapid and direct flood damage estimation with the default embedded data and script in GEE [3,13,14].

One of the satellite data in GEE is the Sentinel-1. Apart from multiple applications of Sentinel-1, it uses a wide area coverage with near real-time data acquisition making it a more feasible tool allowing for more efficient and cost-effective use. Over the last few

decades, a considerable number of studies have been through on the SAR flood mapping method in combination with other Remote Sensing (RS) imageries whereas other researchers suggest the use of Sentinel-1 radar image to calibrate or validate the extent derived using other models [1, 15,16].

All flood mapping-related research in the Philippines is useful in giving a geographic representation of the distribution of flooded regions however, no studies have yet been conducted to evaluate and map the actual flooding of the entire Cagayan River Basin using different datasets. GEE can offer an estimation of flood damages but in very low-resolution datasets (MODIS land cover 500m, JRC Population 250m) thereby affecting the accuracy of reports. With the readily available, free, up-to-date, and high-resolution data accessible in OpenStreetMap (OSM) and obtainable from National Mapping and Resource Information (NAMRIA), a comprehensive database containing information relevant for flood analysis was collected and analyzed in this study. Since GIS and RS have proven their capability in flood mapping, the study is very timely and significant, especially in the case of the Philippines.

Hence, this paper aimed to 1) collect the comprehensive database containing information relevant for flood analysis; 2) use a satellite-imagery-based method for flood inundation map using GEE; 3) validate map accuracy through a quick post-flood participatory approach. This resolution will exhort the Disaster Risk Management Council and the Cagayan Valley Regional Disaster Management Council in the Philippines to expedite the restoration of typhoon-damaged regions and provide basic needs to significantly affected people. The study's findings will be beneficial in developing flood risk reduction policies and preventive measures for future flood events.

Materials and Methods

Figure 1 depicts the overall methodological framework used in the study. Two validations were performed: for datasets and flood extent. A post-flood survey was conducted to determine the threshold for estimating flood extent in GEE. Flood maps and flood-risked resources were quantified and tabulated. Validation of map accuracy through a quick post-flood participatory approach was done. A step-by-step procedure was presented for future replication of the study.

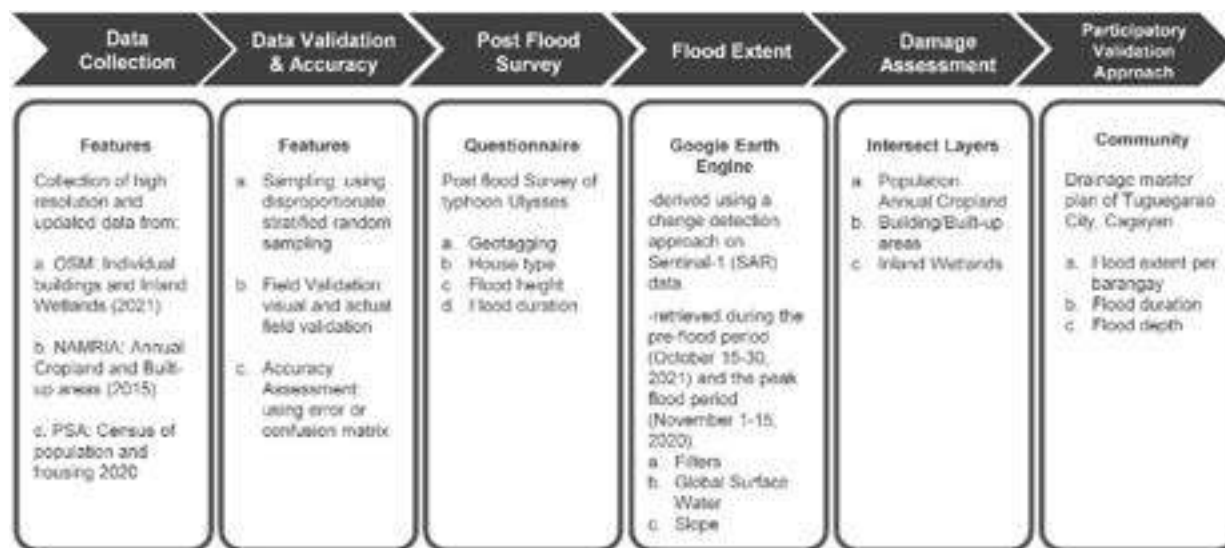


Figure 1: A summary of the overall methodological framework used in the study

Data Collection, validation, and accuracy

A comprehensive and up-to-date database containing information relevant to flood analysis was collected. Data is characterized by

different sources and dates depending on the latest and finest data there is. Flood damages were evaluated in the following features (Table 1).

Table 1: Definition of features and sources of data where damages were evaluated

| Class Feature | Definition | Data Reference |
|----------------|---|--|
| Population | The number of people living in a place | Philippine Statistics Authority (PSA). 2020. |
| Annual Crop | Cultivated with crops with a growing cycle under one year, which must be newly sown or planted for further production after harvesting. | National Mapping and Resource Information Technology (NAMRIA). 2015. |
| Built-up | Composed of areas of intensive use with much of the land covered with structures. Individual buildings or groups of connected buildings | NAMRIA 2015 OpenStreetMap (OSM). 2020. |
| Inland Wetland | Aquatic influence environments are sometimes referred to as freshwater and inland water/water bodies but also include brackish water located within land boundaries | NAMRIA. 2015. |

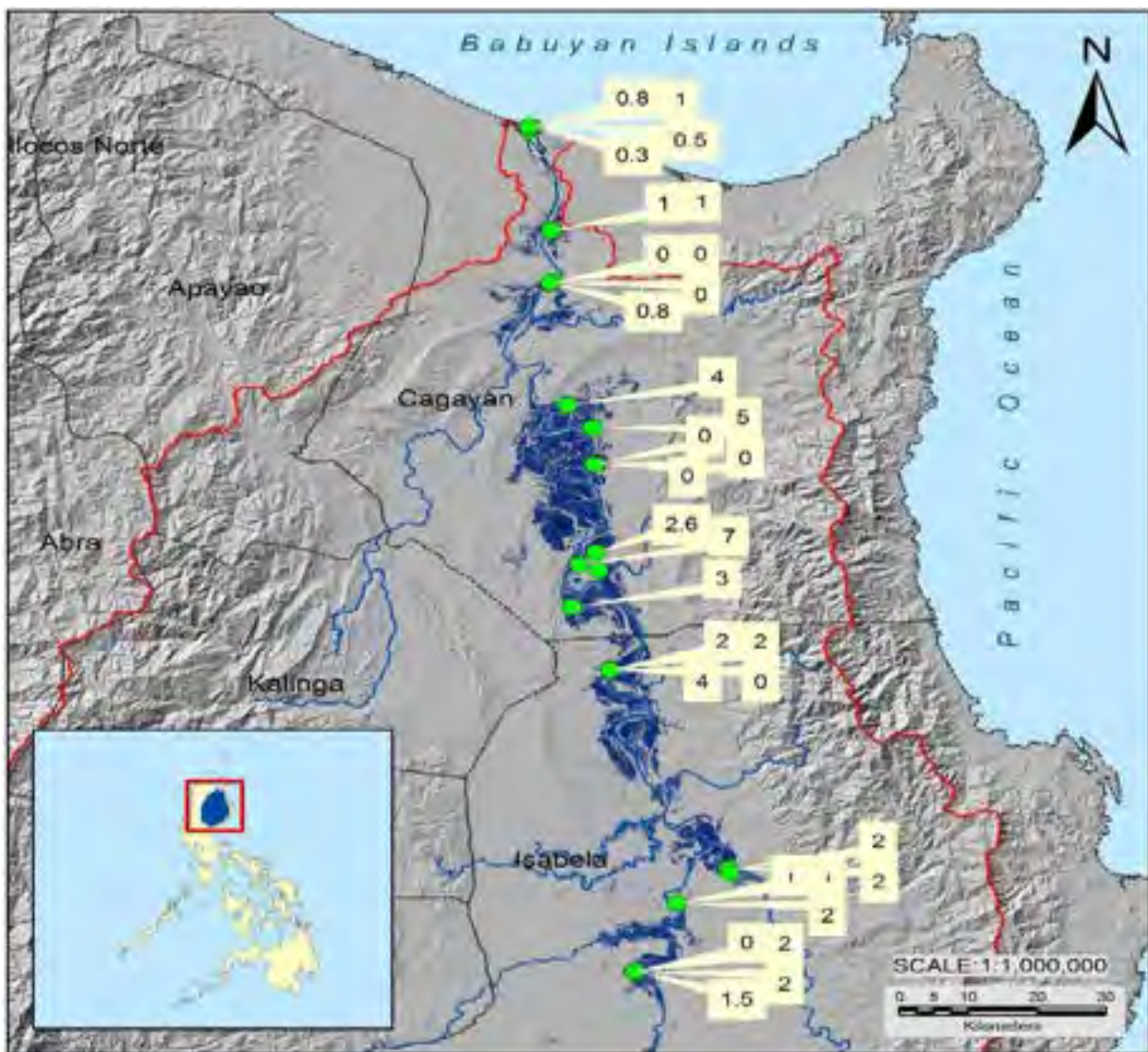


Figure 2: Locations of households (green dots) interviewed during the post-flood survey of typhoon Ulysses showing the flood depths. Those with a zero value indicate that no flooding happened in that specific location.



Figure 3: Ground photographs of sites where households were asked information such as flood duration and flood height to indicate water levels during flooding.

Flood inundation using GEE and damage assessment

Detailed workflow of flood extent derivation using GEE is shown in Figure 4. The workflow was based on the recommended practice developed by [13]. Flood inundation was derived using a change detection approach on Sentinel-1 (SAR) data. The Sentinel 1AVH polarization images were retrieved during the pre-flood period (October 20, 2021) and during the flood period (November 13-

16, 2020). The various pre-processing techniques including radiometric calibration, removal of noise, and orthorectification were performed. The threshold of 1.10 was applied to deduce the flood hazard in the lower basin. The Global Surface Water dataset (2018, 30m resolution) was used to mask areas covered by water for more than 10 months.

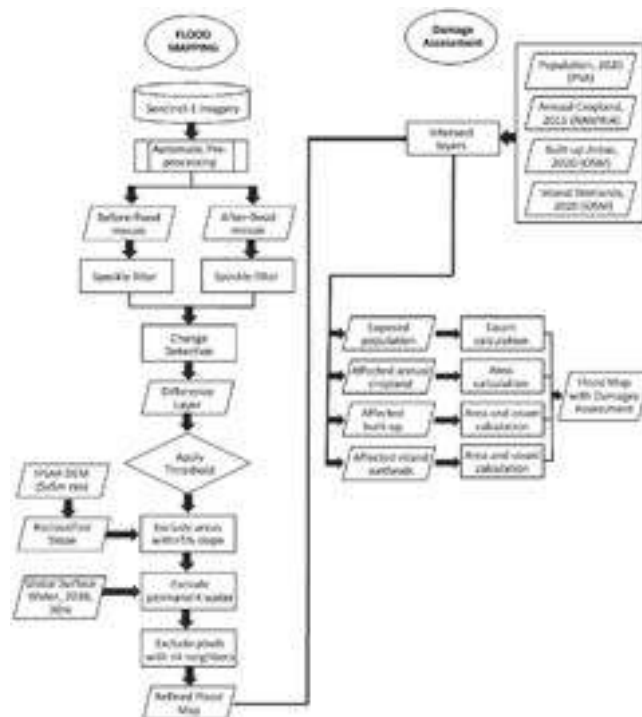


Figure 4: Workflow of flood inundation using GEE and damage assessment in ArcGIS. The high-resolution datasets like DTM for slope and land cover maps were the two main inputs altered from the default dataset used by GEE.

In this study, IFSAR DTM of 5-m resolution was used to derive slope instead of World Wildlife Fund WWF HydroSHEDS hydrologically conditioned DTM which is based on Shuttle Radar Topography Mission (SRTM) and has a spatial resolution of 3 arc-seconds. To estimate the damage that occurred due to flood, elements discussed earlier like population, built-up, croplands, and inland wetland were intersected. The area and/or count of each inundated land cover was calculated and tabulated. This was done for all barangays affected. It should be noted that the damages were evaluated in a river basin context.

Quick post-flood participatory approach

Department of Public Works and Highways Region 2 in collab-

oration with Hdronet Consultancy, Inc. and barangay officials, mapped flood extents where they were instructed to assign appropriate colors to each region of their barangay-based on Typhoon Ulysses' results. Important areas wherein floodwater originates (Cagayan River, Pinacanan River, and open drainage system) were explained to the participants for easier mapping. When they finished assigning colors and identifying important facilities and routes in their respective barangays, they were then tasked to list the priority areas which are usually flooded. Figure 5 shows the barangay personnel identifying the extent and time concentration of flood during typhoon Ulysses.



(a)



(b)



(c)



(d)

Figure 5: Representatives from barangays (a), (b), (c) identify the subsidence and duration time in their area, and a sample color-coded flood depth map (d)

Source: Department of Public Works and Highways (2021) Consulting Services for the Drainage Master Plan of Tuguegarao City

The consulting agency carefully digitized the output maps in Google Earth producing laid-out maps in JPEG format, which were then georeferenced by our group for flood extent validation us-

ing GEE. Figure 6 shows the georeferenced photos and sampling points for validation of flood extent using GEE.

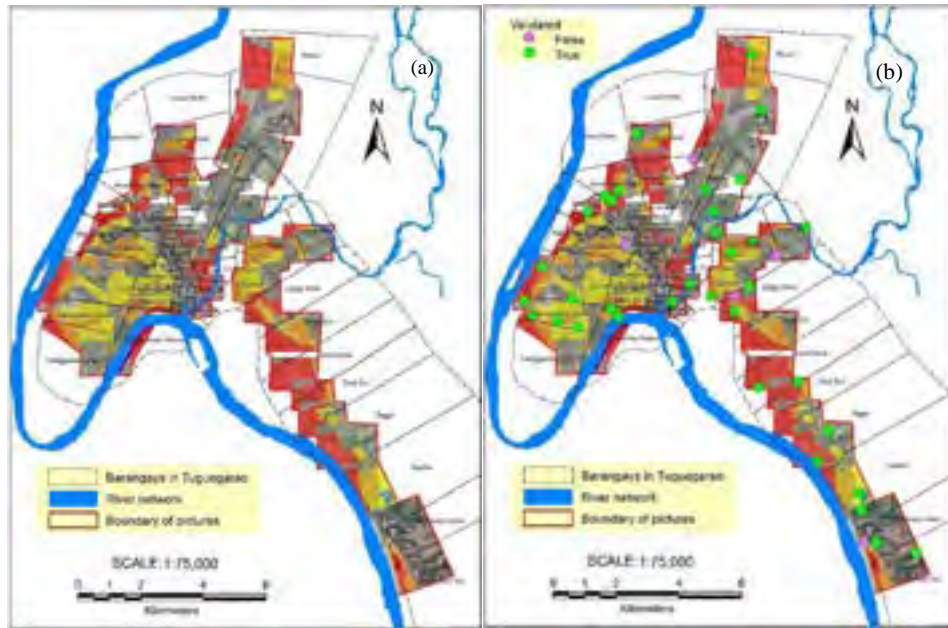


Figure 6: Tuguegarao City featuring the (a) georeferenced flood maps and (b) sampling points (circle dots) for validation of flood extent (light blue) using GEE.

Results and Discussion

The flood was caused by continuous and excessive rainfall in November from 1 to 13, 2020. The pre and postflood datasets were determined based on rainfall data. As a result, an inundation map

(Figure 7) dented by blue overlaid on the administrative boundaries of the region and the affected land cover map (Figure 8) were created with a total area of 620.88 km². The flood was most densely distributed along the low-lying stretch of the Cagayan River.

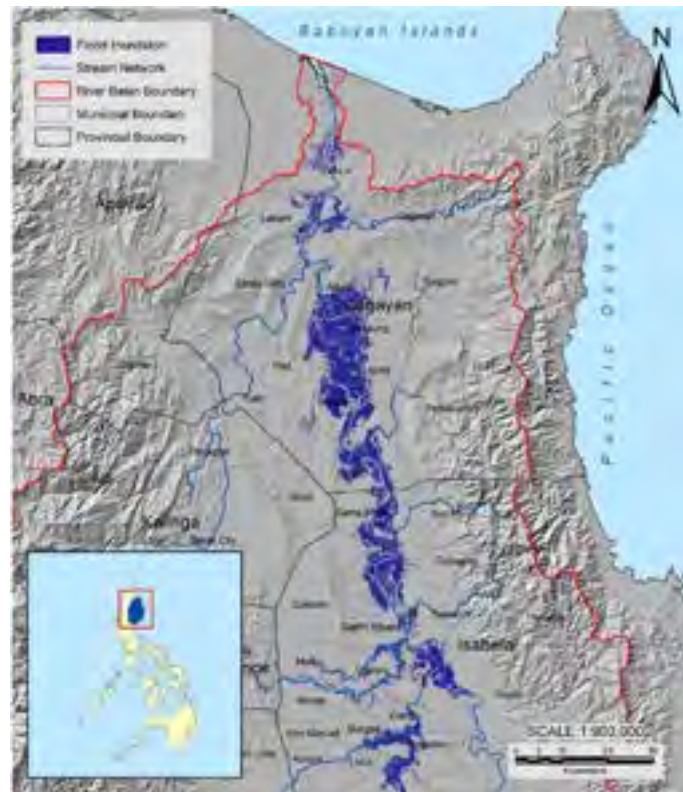


Figure 7: Final flood inundation map of typhoon Ulysses using GEE showing the terrain and provinces affected



Figure 8: Affected land cover in Cagayan River Basin during the flood due to Typhoon Ulysses

To estimate flooded area and damages per province, the final flood inundation (slope and GSW deducted) was used. As shown in Table 2, two provinces in the region were greatly affected by a series of typhoons in November 2020. Cagayan was the most affected (347.128 km²) with about 11.98% of its area flooded, followed by Isabela (273.162; 3.10%). On the other hand, Kalinga (0.545 km²), Ifugao (0.043 km²), and Apayao (0.0002 km²) had minimal damage of less than a square kilometer flooded area due to their

safer site and situation. The use of satellite-based flood inundation analysis like GEE will aid in the identification of the worst-affected districts in terms of submerged areas. Of the land classes listed, annual cropland was the most affected (98.90% of the total inundation), followed by built-up (1%) which affected a large population (~ 225,634). Therefore, it is critical to focus on lowering damage in annual croplands.

Table 2: Area and percentage distribution of inundation per province and affected land cover in Cagayan River Basin after intersecting inundation map using GEE

| Province | Provincial Area (km ²) | Flooded Area (km ²) | % Area wrt province | % Area of inundation | Annual Crop (km ²) | Built-up | | Inland Wetland (km ²) | Population Affected | % Affected Population |
|--------------|------------------------------------|---------------------------------|---------------------|----------------------|--------------------------------|--------------|-------------------------|-----------------------------------|---------------------|-----------------------|
| | | | | | | Count | Area (km ²) | | | |
| Cagayan | 2,897.67 | 347.128 | 11.98% | 55.91% | 344.36 | 4,355 | 2.19 | 0.55 | 113,636 | 50.36% |
| Isabela | 8,813.95 | 273.162 | 3.10% | 44.00% | 269.10 | 2,981 | 4.03 | 0.03 | 111,959 | 49.62% |
| Kalinga | 10,276.73 | 0.545 | 0.01% | 0.09% | 0.55 | 36 | | | 37 | 0.02% |
| Ifugao | 2,503.45 | 0.043 | 0.00% | 0.01% | 0.04 | 4 | | | 3 | 0.00% |
| Apayao | 3,913.88 | 0.0002 | 0.00% | 0.00% | 0.00 | 2 | | | 1 | 0.00% |
| TOTAL | 28,405.68 | 620.879 | 2.19% | 100.00% | 614.05 | 7,378 | 6.22 | 0.58 | 225,634 | 100.00% |

Two provinces are most affected: Cagayan (Table 3) and Isabela (Table 4). In Cagayan, Amulung has the largest total area affected in Cagayan Province and has the most population affected by the flood. Tuguegarao, the capital 139 city is the 5th most affected

with a total area of 24.91 km² flooded and 29,041 estimated affected population. There are 140 18 out of 28 municipalities affected in Cagayan Province.

Table 3: Summary of flooded areas and damages per municipality in Cagayan

| Province | Annual Crop (km ²) | Built-up | | Inland Wetland (km ²) | Population | Total (km ²) |
|-----------------|--------------------------------|----------|-------------------------|-----------------------------------|------------|--------------------------|
| | | Count | Area (km ²) | | | |
| Amulung | 81.40 | 702 | 0.29 | 0.00 | 17,101 | 81.70 |
| Solana | 71.32 | 745 | 0.11 | | 3 | 71.44 |
| Alcala | 44.84 | 755 | 0.79 | 0.43 | 10,505 | 46.07 |
| Enrile | 38.19 | 401 | 0.07 | | 10,248 | 38.26 |
| Tuguegarao City | 24.75 | 366 | 0.15 | | 29,041 | 24.91 |
| Gattaran | 17.97 | 266 | 0.19 | 0.00 | 3,725 | 18.16 |
| Iguig | 17.97 | 131 | 0.15 | | 5,285 | 18.11 |
| Lasam | 17.12 | 230 | 0.18 | | 3,763 | 17.30 |
| Lal-Lo | 16.30 | 236 | 0.09 | | 3,271 | 16.43 |
| Baggao | 6.18 | 153 | 0.06 | | 2,337 | 6.24 |
| Santo Niño | 4.64 | 114 | 0.04 | | 1,126 | 4.68 |
| Piat | 1.13 | 47 | 0.00 | | 42 | 1.13 |
| Tuao | 1.08 | 85 | 0.01 | | 448 | 1.09 |
| Camalaniugan | 0.59 | 36 | 0.02 | | 190 | 0.61 |
| Aparri | 0.57 | 47 | 0.01 | 0.08 | 619 | 0.66 |
| Peñablanca | 0.28 | 32 | 0.01 | | 114 | 0.29 |
| Rizal | 0.03 | 4 | | | 3 | 0.03 |
| Allacapan | 0.02 | 5 | | | 3 | 0.02 |
| Cagayan | 344.36 | 4355 | 2.19 | 0.55 | 111,959 | 347.13 |

Table 4: Summary of flooded area and damages per municipality in Isabela

| Province | Annual Crop (km ²) | Built-up | | Inland Wetland (km ²) | Population | Total (km ²) |
|----------------|--------------------------------|----------|-------------------------|-----------------------------------|------------|--------------------------|
| | | Count | Area (km ²) | | | |
| Ilagan | 44.48 | 590 | 0.77 | 0.02 | 20,734 | 45.27 |
| | 44.48 | 590 | 0.77 | 0.02 | 20,734 | 45.27 |
| Santo Tomas | 26.94 | 124 | 0.20 | | 10,666 | 27.14 |
| Delfin Albano | 26.21 | 243 | 0.53 | | 5,738 | 26.73 |
| Santa Maria | 24.50 | 166 | 0.12 | | 8,724 | 24.62 |
| Tumauini | 23.78 | 189 | 0.58 | | 10,963 | 24.36 |
| Cabagan | 23.31 | 146 | 0.25 | | 14,655 | 23.56 |
| Cauayan City | 21.66 | 215 | 1.04 | | 11,126 | 22.70 |
| Reina Mercedes | 14.70 | 61 | 0.23 | | 7,452 | 14.93 |
| Quirino | 12.18 | 208 | 0.02 | | 2,020 | 12.20 |
| Gamu | 10.23 | 142 | 0.05 | | 3,968 | 10.27 |
| Naguilian | 9.14 | 72 | 0.03 | | 4,372 | 9.16 |
| Angadanan | 6.28 | 134 | 0.02 | | 1,984 | 6.31 |
| Burgos | 5.42 | 85 | 0.00 | | 1,819 | 5.42 |
| San Pablo | 4.84 | 44 | 0.12 | | 3,355 | 4.96 |
| Luna | 4.57 | 40 | 0.00 | | 1,128 | 4.58 |
| Alicia | 4.01 | 185 | 0.04 | | 986 | 4.05 |
| San Isidro | 2.40 | 110 | 0.00 | | 1,169 | 2.41 |

| | | | | | | |
|----------------|--------|-------|------|------|---------|--------|
| Santiago City | 1.42 | 60 | 0.01 | | 1,405 | 1.44 |
| Echague | 0.78 | 34 | 0.01 | | 766 | 0.79 |
| Benito Soliven | 0.45 | 14 | | | 49 | 0.45 |
| Roxas | 0.39 | 29 | 0.00 | | 79 | 0.39 |
| San Mateo | 0.31 | 24 | 0.00 | | 130 | 0.31 |
| Cabatuan | 0.23 | 12 | | | 155 | 0.23 |
| Ramon | 0.20 | 14 | 0.00 | 0.01 | 36 | 0.21 |
| Quezon | 0.19 | 8 | 0.00 | | 17 | 0.19 |
| San Manuel | 0.16 | 6 | | | 47 | 0.16 |
| Mallig | 0.15 | 13 | | | 45 | 0.15 |
| Aurora | 0.10 | 8 | | | 28 | 0.10 |
| Cordon | 0.07 | 5 | 0.00 | | 17 | 0.07 |
| Isabela | 269.10 | 2,981 | 4.03 | 0.03 | 113,633 | 273.16 |

Isabela province, on the other hand, has a total flooded area of 269.1 km² and more than 100 thousand people affected. Ilagan as the capital city is the most affected with an area of 43.27 km² and a 20,734 estimated population affected. There are 30 of 34 municipalities of Isabela affected by the flood.

Tuguegarao City and Ilagan City, two of the most populated riverine towns in the region are located approximately 50-600 m away from the Cagayan River. Cagayan River Basin (CRB) is the largest river basin in the Philippines but is densely populated along the flood-hit areas resulting in a high number of casualties. The spatial variation in the extent of floods can be attributed to many factors such as the precipitation, land cover types, and topographic conditions. Since Cagayan province is surrounded by the Sierra Madre mountain range to the east while the western boundaries are generally hilly and the central area is dominated by a wide valley, the province forms the lower basin of the Cagayan River therefore receiving a higher volume of floodwater. In the Philippines, from June to October, the southwest monsoon brings heavy rainfall. This heavy rainfall extends up to the early part of November. The successive days of rain exacerbated by typhoons led to flooding.

Validation of flood extent using the data from the survey reveals 95% accuracy. In many studies, Sentinel 1 (SAR) was demonstrated suitable for mapping flood areas due to its ability to penetrate cloud forms among others. This result are in line and supports the findings of previously conducted researches [3,17]. concluded that GEE algorithm performs well with an optimum accuracy of 96.44%. monitored flood events using multi-temporal Sentinel 1 images [17]. The accuracy ranges from 92.8%-96.2% with an overall accuracy higher than 90%. Sentinel 1 perfectly separates the distinction of submerged areas to non-flooded areas allowing an accurate flood mapping possible. GEE that uses Sentinel 1 with medium-high resolution can therefore be used for rapid mapping of events with high accuracy. The assurance of high accuracy and more specific information embedded in local data is the primary benefit. The damage estimates provide useful information, not only in the form of numerical statistics but also in multi-boundary

maps that can assist the decision-makers in visualizing areas that need the most help. This advantage of utilizing more detailed geospatial data and readily available for processing makes it appropriate for a rapid source of information.

Conclusion and Recommendation

This study has developed a methodology to determine the extent of damages not only in the area but also in number by integrating high-resolution datasets that are readily available in the Philippines. The use of these data instead of the default materials used by GEE may be utilized by local flood mappers without difficulty. The flood inundation and damage maps created using ArcGIS provide improved visualization of disaster severity across communities. The concurrent flood study imposes adopting an integrated approach with an emphasis on disaster risk mitigation, preparedness, and streamlining of the relief distribution system, with an emphasis on self-reliance on Local Government Units and Non-Governmental Organizations. Future work will be aimed to use the workflow applied in assessing flood damages for other typhoon events in the Philippines. A set of technical and institutional recommendations are to be firmed up in consultation with the Cagayan River Basin Management Council and the Cagayan Valley Regional Disaster Management Council. Through this study, the framework, approach, and methodology can be replicated across a range of geographical case studies arising due to floods. Further validations and comparisons against future similar studies are encouraged. The framework is also recommended to be applied in diverse catastrophic scenarios, i.e. storm surges, tsunamis, and flash floods. The framework could assist local authorities in estimating disaster impacted land features in a practical means.

Acknowledgment

The authors would like to express their appreciation for the support of the Department of Science and Technology-Philippines Council and the Industry, Energy, and Emerging Technology Research and Development (DOST-PCIEERD), the project Integrated Flood and Water Resources Management (IFWaRM) in the ASEAN Basins for Sustainable Development in collaboration with Thuy Loi University of Vietnam and Kyoto University of Japan.

Statements and Declarations

Funding

This work was funded by the Department of Science and Technology (DOST) with the support of DOST-Philippines Council and the Industry, Energy, and Emerging Technology Research and Development (DOST-PCIEERD).

Author information

Authors and Affiliations

Water Research and Development Center, Isabela State University, Isabela, Philippines Christine Mata

College of Engineering, Isabela State University, Isabela, Philippines

Orlando Balderama, Lanie Alejo, & Jeffrey Lloyd Bareng

Water Resources Research Center – Disaster Prevention Research Institute Kyoto University, Kyoto, Japan

Sameh Ahmed Kantoush

Corresponding Author
Correspondence to Christine Mata

Contributions

All authors contributed to the study, conception, and design. OB, LA, and JL B helped in conceptualization and data collection; LA and SA K contributed to software, reviewing and editing; CM helped in conceptualization, writing and analysis.

Conflicts of Interest

The authors have no relevant financial or non-financial interests to disclose.

References

1. Elkharchy, I., Pham, Q. B., Costache, R., Mohajane, M., Rahman, K. U., Shahabi, H., ... & Anh, D. T. (2021). Sentinel-1 remote sensing data and Hydrologic Engineering Centres River Analysis System two-dimensional integration for flash flood detection and modelling in New Cairo City, Egypt. *Journal of Flood Risk Management*, 14(2), e12692.
2. National Research Council. (2015). *Tying flood insurance to flood risk for low-lying structures in the floodplain*. National Academies Press. Accessed 6 February 2022.
3. Uddin, K., Matin, M. A., & Meyer, F. J. (2019). Operational flood mapping using multi-temporal Sentinel-1 SAR images: A case study from Bangladesh. *Remote Sensing*, 11(13), 1581.
4. Meyer, V., Haase, D., & Scheuer, S. (2007). GIS-based multi-criteria analysis as decision support in flood risk management (No. 6/2007). UFZ Discussion Paper.
5. Shrestha, B. B., Okazumi, T., Miyamoto, M., Nabesaka, S., Tanaka, S., & Sugiura, A. (2014). Fundamental analysis for flood risk management in the selected river basins of South-east Asia. *Journal of Disaster Research*, 9(5), 858-869.
6. Manfré, L. A., Hirata, E., Silva, J. B., Shinohara, E. J., Giannotti, M. A., Larocca, A. P. C., & Quintanilha, J. A. (2012). An analysis of geospatial technologies for risk and natural disaster management. *ISPRS International Journal of Geo-Information*, 1(2), 166-185.
7. Rodriguez M., Ong R., Baluyut R, Aying JA., Epino E. (2017). Lidar-based flood hazard and exposure mapping of a critical river system in the Zamboanga Peninsula, Mindanao, Philippines. *Asian Conference on Remote Sensing 2017*. New Delhi, India.
8. Puno, G. R., & Amper, R. A. L. (2016). Flood modeling of Musimusi river in Balingasag, Misamis Oriental. *CMUJS*, 20(3), 150-165.
9. Lin, L., Di, L., Tang, J., Yu, E., Zhang, C., Rahman, M. S., ... & Kang, L. (2019). Improvement and validation of NASA/MODIS NRT global flood mapping. *Remote Sensing*, 11(2), 205.
10. Jung, Y., Kim, D., Kim, D., Kim, M., & Lee, S. O. (2014). Simplified flood inundation mapping based on flood elevation-discharge rating curves using satellite images in gauged watersheds. *Water*, 6(5), 1280-1299.
11. Rahman, M., & Di, L. (2017). The state of the art of space-borne remote sensing in flood management. *Natural Hazards*, 85(2), 1223-1248.
12. Ghaffarian, S., Rezaie Farhadabad, A., & Kerle, N. (2020). Post-disaster recovery monitoring with google earth engine. *Applied Sciences*, 10(13), 4574.
13. UN-SPIDER (2019) Step-by-Step: Recommended Practice: Flood Mapping and Damage Assessment Using Sentinel-1 SAR Data in Google Earth Engine. Advisory Support, Recommended Practices, Retrieved September 25, 2021, from <https://www.un-spider.org/advisorysupport/recommendedpractices/recommended-practice-google-earth-engine-flood-mapping/step-by-step>
14. Lal, P., Prakash, A., & Kumar, A. (2020). Google Earth Engine for concurrent flood monitoring in the lower basin of Indo-Gangetic-Brahmaputra plains. *Natural Hazards*, 104(2), 1947-1952.
15. Jokar, M., López-Bernal, Á., & Kamkar, B. (2022). The effect of spring flooding on management and distribution of cotton bollworm (*Helicoverpa armigera*) by flood mapping using SAR sentinel-1 and optical imagery landsat-8; a case study in golestan province, Iran. *International Journal of Pest Management*, 1-11.
16. Ezzine, A., Saidi, S., Hermassi, T., Kammessi, I., Darragi, F., & Rajhi, H. (2020). Flood mapping using hydraulic modeling and Sentinel-1 image: Case study of Medjerda Basin, northern Tunisia. *The Egyptian Journal of Remote Sensing and Space Science*, 23(3), 303-310.
17. Moharrami, M., Javanbakht, M., & Attarchi, S. (2021). Automatic flood detection using sentinel-1 images on the google earth engine. *Environmental monitoring and assessment*, 193(5), 1-17.

-
18. Benzougagh, B., Frison, P. L., Meshram, S. G., Boudad, L., Dridri, A., Sadkaoui, D., ... & Khedher, K. M. (2021). Flood Mapping Using Multi-temporal Sentinel-1 SAR Images: A Case Study—Inaouene Watershed from Northeast of Morocco. *Iranian Journal of Science and Technology, Transactions of Civil Engineering*, 46(2), 1481-1490.

Copyright: ©2022: Christine B Mata, et al. This is an open-access article distributed under the terms of the Creative Commons Attribution License, which permits unrestricted use, distribution, and reproduction in any medium, provided the original author and source are credited.

MODELLING CLIMATE CHANGE IMPACT ON THE INFLOW OF MAGAT RESERVOIR USING THE SOIL AND WATER ASSESSMENT TOOL (SWAT) MODEL FOR DAM MANAGEMENT

C.L. Singson^{1^}, L.A. Alejo², O.F. Balderama³, J.L.B. Bareng⁴

¹ Science Research Specialist II, Isabela State University, Echague, Isabela, Philippines
(E-mail: czarimah.l.singson@isu.edu.ph)

² Assistant Professor III, College of Engineering, Isabela State University, Echague, Isabela, Philippines
(E-mail: ghan_1023@yahoo.com)

³ Professor VI, College of Engineering, Isabela State University, Echague, Isabela, Philippines
(E-mail: orly_isu@yahoo.com)

⁴ Professor III, College of Engineering, Isabela State University, Echague, Isabela, Philippines
(E-mail: jlloydbareng@gmail.com)

[^] Corresponding author
(E-mail: czarimah.l.singson@isu.edu.ph)
(Postal Address: *Purok 06, San Fabian, Echague, Isabela, Philippines, 3309*)

Abstract

Understanding the impact of climate change on watersheds using hydrologic models is timely and vital to dam management. The study predicts changes in the inflow of the Magat reservoir using the Soil and Water Assessment Tool (SWAT) under the two Representative Concentration Pathways (RCP) Scenario for future centuries. The monthly calibration process (18 years) and validation process (10 years) of the model resulted in an NSE of 0.73, R^2 of 0.74, RSR of 0.52, PBIAS of 8.38, and NSE of 0.56, R^2 of 0.62, RSR of 0.66, and a PBIAS of 17.3 respectively. Under RCP 4.5 and RCP 8.5 scenarios, the model predicted that during the dry and normal years, there will be an average decrease of inflow by 18.56% and 5.41% but an increase of 19.25% during the wet years. Peak flow will likely occur in September for all the scenarios with a maximum discharge of up to 342.46 m³/s. The study recommends the integration of the model results to update the dam discharge protocol on the forecasting of monthly and annual inflow of the Magat Dam to aid the dam management in observing long-term changes in the flow of water going into the reservoir.

Keywords

Climate Change, framework, inflow, Magat reservoir, SWAT, watershed

1. Introduction

The Philippines is extremely vulnerable to climate change. Climate change threatens the country by increasing the intensity and frequency of storms and droughts (Principe 2012). CAD-PAGASA (2004) reported that the country is likely to be adversely affected by climate change since its economy is heavily dependent on agriculture and natural resources. Furthermore, Tolentino *et al.* (2016) stated in their modeling study that the consequences of climate change on Visayas and

55 Mindanao are projected to be relatively mild in comparison to Luzon, where a major rise in return
56 intervals for maximum river flow rates is forecasted. In Cagayan Valley, Luzon alone, precipitation
57 is anticipated to increase. In terms of seasonality, the dry months (March-April-May) will remain dry,
58 while during the rainy season, July and November will likely become more noticeable wet months.
59 There are also signs that the frequency of heavy rainfall events, protracted dry spells, and extreme
60 daytime temperatures is increasing (especially in Aparri) (Basconcillo *et al.* 2016). In the year 2020,
61 the Philippines observed five consecutive typhoons from the end of October to early November.
62 These disastrous events happened in less than a month causing damage in different regions of the
63 Philippines – parts of Manila were shut down, the Bicol region was buried in mud, and Cagayan
64 Valley was extremely flooded. From the recent typhoons, in Cagayan Valley alone, almost 151,600
65 families were affected by the flood caused by the rising of the Cagayan River. The residents were
66 also very eager to point out that the reason for flooding was the release of water from the Magat Dam
67 although the Dam and Reservoir Management reiterated that the cause of massive flooding was the
68 extreme continuous rainfall and deforestation in the whole basin. With incoming typhoons, protocols
69 of the Dam Management include the release of water from the dam. Hence, people from downstream
70 of the dam and the riverine area had a high chance of being flooded especially with the excessive
71 amount of rain over the past months.

72 One main impact area of climate change is on the hydrology of watersheds, where alterations
73 in temperature and rainfall directly influence the dynamics and supply of water resources, and in the
74 long run the present Stakeholders will struggle to meet their water requests (Arnell 1999). Different
75 analysts have considered the possible impact of climate change on water quality and quantity in river
76 basins. Thanh Nguyen *et al.* (2020) observed that extreme rainfall and severe river flooding events
77 are anticipated to increase considerably in the future, ranging from 29 to 35% and 37 to 56% increase
78 in rainfall and streamflow, respectively. Azari *et al.* (2016) found out that in the Gorganroud River
79 Basin of Iran, climate change led to a 9.5 percent increase in annual streamflow and that sediment
80 yield could increase by up to 83.9 percent. In the Philippines, there have been very few studies
81 examining the threat of climate change. For instance, Panondi & Izumi (2021) found that observed
82 changes in maximum mean annual rainfall, and maximum and minimum temperature correspond to
83 increases in runoff (44.58–76.80%) and sediment yield (1.33–26.28%).

84 With climate change, man-made and land-cover changes, the inevitable effects of this
85 phenomenon on the hydrology of these watersheds will be evident in the following years. Hydrologic
86 modeling has long been used by researchers to track these changes as they occur along these basins.
87 To evaluate the impact of climate change on water resources, climate model data is integrated into
88 hydrologic models (Naumann *et al.* 2019). The Soil and Water Assessment Tool (SWAT) is one of
89 the most commonly used modeling software for assessing hydrologic impacts (Oo 2020). It has been
90 recognized worldwide as an effective tool in water resource management for assessing the impact of
91 the climate on water supplies and nonpoint sources of pollution in watersheds (Guiamel and Lee
92 2020). In the case of the Magat watershed and its reservoir, it is important to understand the impact
93 of climate change on the inflow of the dam using hydrologic models. However, no current studies are
94 being undertaken and there are no model-based forecasts for long-term or seasonal flow.

95 Taking into account the probability of streamflow changes might help water resource
96 stakeholders make better decisions (Sivakumar 2011; Ouyang *et al.* 2015). Better decisions in this
97 context can be outcomes of a strong impact assessment towards reducing climate change risks through
98 adaptation strategies, perhaps, for the agriculture sector (Abbasi *et al.* 2020). One of the most difficult
99 aspects of reservoir operations management is estimating inflow parameters accurately (Fourcade &
100 Quentin 1994). Reservoir managers in the Philippines base their inflow estimates on water level
101 information (Sarmiento *et al.* 2010). For instance, the Magat Dam reservoir is presently operated by
102 an Operation Rule Curve jointly developed in 1985 to optimize the utilization of the water stored in
103 the Magat reservoir. The 37-year discharge protocol of dam management needs updating using
104 current science-based tools.

105 With the absence of alternative estimation and forecasting techniques, the Magat reservoir
106 managers adapt their management policies to the present measurements and rainfall statistics.
107 Moreover, the temporal distribution of river discharge, especially the extreme value, brings water-
108 related disasters. Thus, the operation of reservoirs has been a great concern in the field of operational

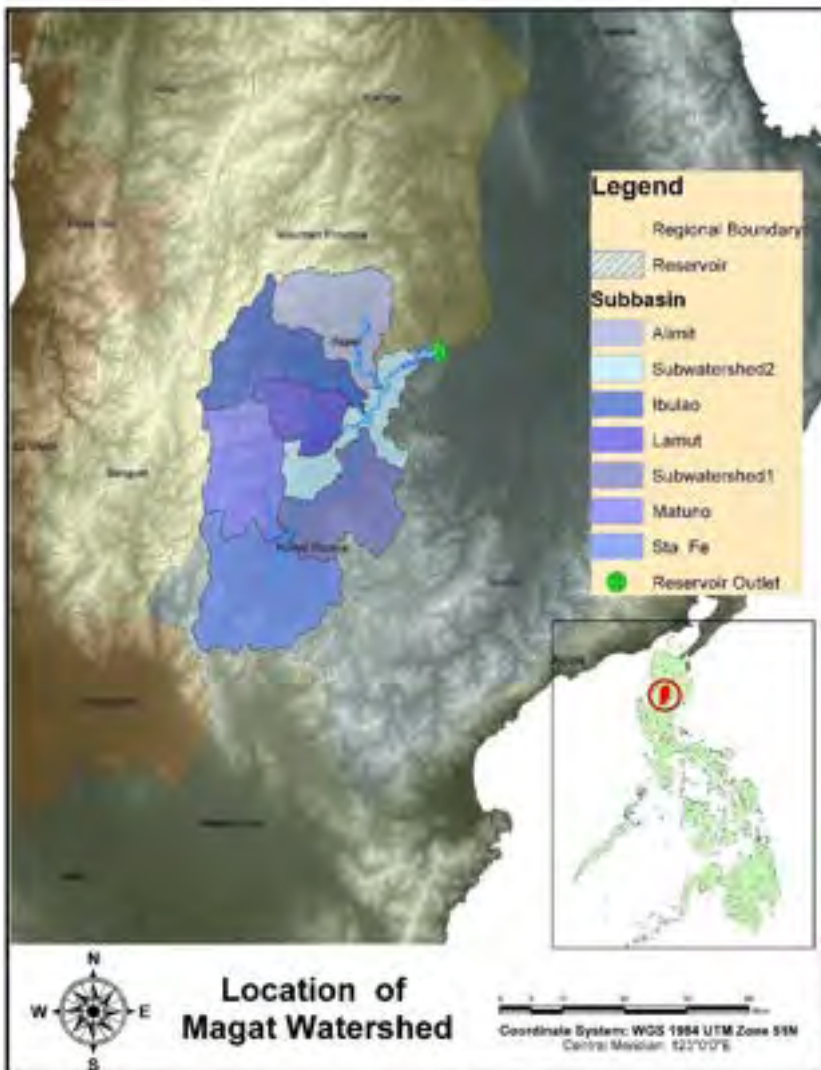
109 hydrology. It is not easy, however, to construct new facilities to cope with the situation, yet the
 110 nonfacility-based countermeasures like the effective utilization of dam reservoirs are getting more
 111 important.

112 The main objective of this study is to assess the impacts of climate change on the inflow of the
 113 Magat reservoir using the SWAT Model towards the development of a dam discharge protocol
 114 framework. Climate forecasts from Representative Concentration Pathways (RCP) Scenario were
 115 used to project inflow changes in the watershed during the Mid and Late 21st Centuries. The
 116 Methodology of the study is presented in Section 2. The result and discussion are presented in Section
 117 3 followed by the conclusion of the study in Section 4.

118 **2. Materials and Methods**

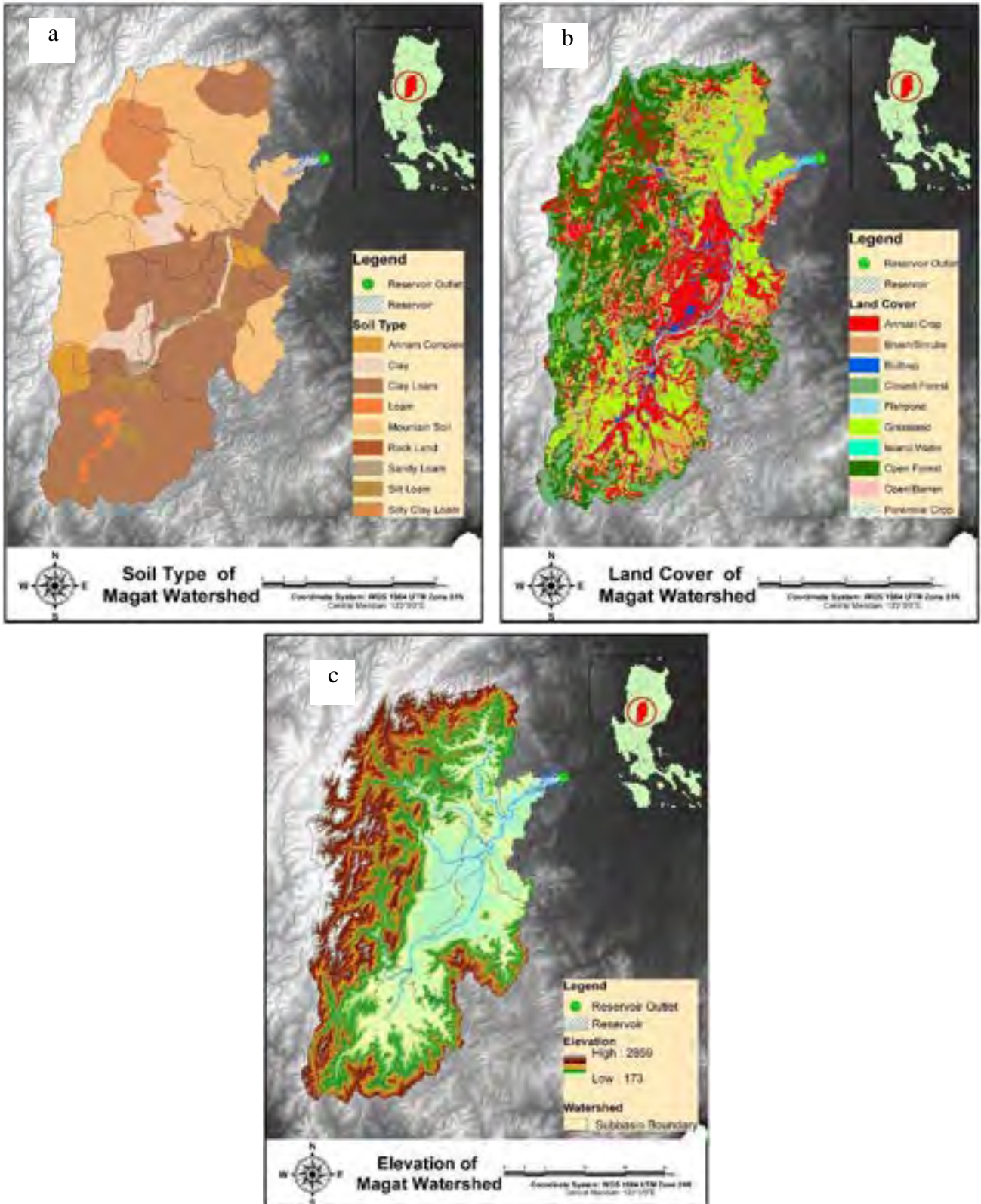
119
 120 **2.1 The Study Area**

121
 122 The Magat watershed and its reservoir are located in the northern part of the Philippines
 123 covering major portions of Ifugao, Nueva Vizcaya, and parts of Isabela provinces. Magat Watershed
 124 with its 7 subbasins, is highly forested with a predominant soil classification of clay loam and highly
 125 steep slopes (see Figure 1). Located within the watershed, the Magat Dam and its reservoir are one
 126 of the largest dams in the Philippines. It is a multipurpose dam that is used primarily for irrigating
 127 86,887 hectares of agricultural lands, flood control, and power generation through the Magat
 128 Hydroelectric Power Plant. The dam was constructed in 1978 and completed on October 27, 1982.



129
 130 Figure 1. Location of Magat Watershed and its Subbasin.

131



132 Figure 2. Soil Type (a), Land Cover (b), and Elevation (c) of Magat Watershed.

133 2.2. Data used

134

135 The spatial data that were used in the study included a 5x5 m resolution Digital Elevation
 136 Model (DEM), 2015 land use/cover, soil classification, and 31-year historical climatic/weather data.
 137 The input parameters for reservoir and dam operation were obtained from the National Irrigation
 138 Administration Magat River Integrated Irrigation System Dam and Reservoir Division (NIA-MARIIS
 139 DRD). The DEM of the Magat watershed which was extracted from the Digital Terrain Model (DTM)
 140 issued by the National Mapping and Resource Information Authority (NAMRIA) was subjected to

141 watershed delineation. Moreover, the weather data were taken from the meteorological station of
 142 PAG-ASA, while the daily rainfall data were provided by the NIA-MARIIS DRD specifically from
 143 the two rain gauge stations inside the basin. On the other hand, the land cover map was obtained from
 144 NAMRIA, while the soil map was from the Bureau of Soil and Water Management (BSWM). Some
 145 of the soil and land cover data were validated and gathered from the field survey per sub-basin.

146 The monthly inflow data (1993-2020) that were used as a baseline in the study were gathered
 147 from NIA-MARIIS DRD.

148

149 2.3 SWAT Model

150

151 2.3.1. Description of SWAT Model

152

153 In several watersheds, the Soil and Water Assessment Tool (SWAT) Model has been used to
 154 model the effects of climatic change on hydrologic and biogeochemical cycles (Arnold *et al.* 1998).
 155 SWAT employs hydrologic response units (HRUs) to explain spatial variation in land cover and soil
 156 types within a watershed as a physically based model. For each HRU, the model calculates essential
 157 hydrologic components such as surface runoff, baseflow, ET, and soil moisture change. According to
 158 Neitsch *et al.* (2011), the simulation of the hydrological cycle in SWAT is separated into a land phase
 159 and a water phase. The land phase is based on the water balance equation which is calculated
 160 separately in each sub-watershed using the following formula:

$$161 \quad SW_t = SW_0 + \sum_{i=1}^t (R_{day} - Q_{surf} - E_a - w_{seep} - Q_{gw}) \quad (1)$$

162 where:

163 SW_t = final soil water content at time t (mm),

164 SW_0 = the initial soil water content (mm),

165 t = time (days),

166 R_{day} = total precipitation on day i (mm),

167 E_a = total evapotranspiration on day i (mm),

168 Q_{surf} = total surface runoff on day i (mm),

169 w_{seep} = seepage from the bottom soil layer on day i (mm), and

170 Q_{gw} = total groundwater flow on day i (mm).

171

172 On the other hand, the water phase of the hydrologic cycle depicts the routing of runoff in the
 173 stream channel using either a variable storage coefficient method or the Muskingum routing method.
 174 The concentration time in the watershed is estimated using Manning's formula which considers both
 175 the overland and channel flow. Meanwhile, surface runoff occurs whenever the rate of precipitation
 176 exceeds the rate of infiltration. Using the daily rainfall data, SWAT simulated the surface runoff using
 177 the Soil Conservation Service Curve Number (SCS CN) method (USDA-SCS 1972) with the
 178 following formula:

179

$$180 \quad Q_{surf} = \frac{(R_{day} - I_a)^2}{(R_{day} - I_a + S)} \quad (2)$$

181 where:

182 Q_{surf} = accumulated runoff or rainfall excess (mm),

183 R_{day} = rainfall depth for the day (mm),

184 I_a = initial abstractions including surface storage, interception and infiltration prior to runoff (mm),

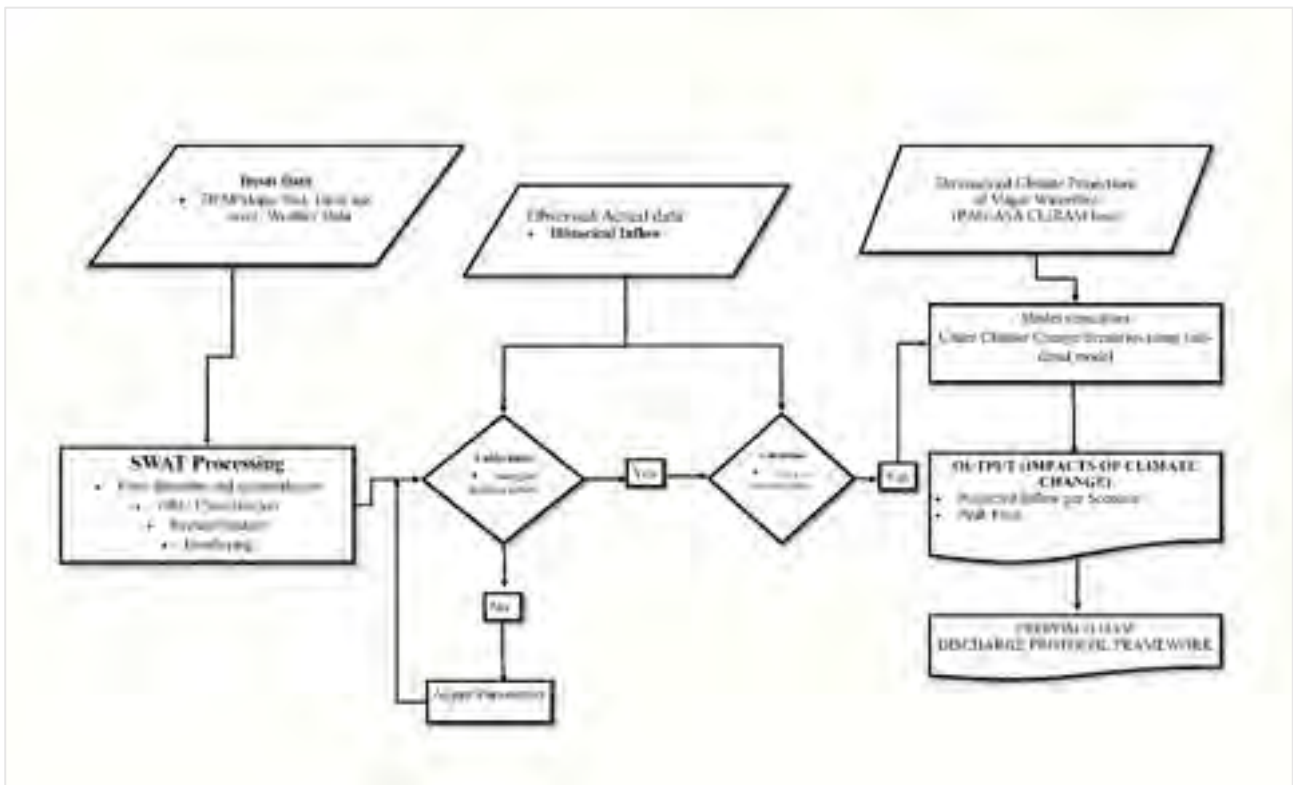
185 and

186 S = retention parameter (mm).

187

188

189 This study applied the following procedure to predict the inflow of the Magat reservoir using SWAT.
 190 The method throughout the model simulation was clearly required for each phase. A clear overview
 191 of the approaches used with the SWAT model is also provided in Figure 3, which summarizes the
 192 analytical process.



193
194 Figure 3. Methodological Framework of the SWAT Model used in the study.
195

196 First, input weather datasets were prepared to match the required input formats. The processed
197 weather dataset was loaded and utilized for the entire modeling process. The Magat Watershed
198 underwent processing and unmasking of the geospatial information, including the DEM, land use,
199 and land cover. The watershed is then delineated in order to establish the direction of the flow and
200 the accumulation. The HRUs were produced by ArcSWAT using the processed land use and land
201 cover. Then, initial values of the parameters were set up and adjusted after calibrating simulation
202 results using the SWAT-CUP SUFI2 and manual calibration. Actual inflow data were divided to be
203 used during the calibration and validation processes. Once the model is deemed acceptable, further
204 simulations incorporating the climate projections by PAG-ASA were done to determine the impacts
205 of climate change on the inflow of the reservoir. Based on this, a proposed dam discharge protocol
206 framework was recommended.

207
208 **2.3.2. SWAT Model Set-up**

209
210 Simulation, calibration, and validation were done using long-term inflow data gauged along
211 the Magat River. Also, 31-year (1990-2020) historical data was simulated with a 3-year warm-up
212 period (1990-1992). Moreover, 18 years (1993-2010) of the monthly simulated historical data were
213 used in calibration.

214 In this study, calibration was done both ways, manually using the trial-and-error method and
215 SWAT CUP SUFI2. The initial calibration was performed manually by means of adjusting the most
216 influential parameters. The trial-and-error approach was done until the model was already statistically
217 acceptable. The result was imported to SWAT CUP SUFI2, a software used for further calibration.

218 On the other hand, evaluation statistics were used to determine the reliability of the calibrated
219 model. The Coefficient of Determination (R^2), Nash-Sutcliffe Model Efficiency (NSE), Root Mean
220 Square Error-observations standard deviation ratio (RSR), and percent bias (PBIAS) were used to
221 measure the acceptability of the SWAT model to imitate temporal trends of the observed data (Table
222 1).
223

Table 1. Model Performance Evaluation Indices

| Indices | Statistically accepted value |
|--|------------------------------|
| Coefficient of determination (R^2) | > 0.5 (50%) |
| Nash–Sutcliffe efficiency (NSE) | > 0.5 (50%) |
| RMSE-observations standard deviation ratio (RSR) | Low RSR, <0.70 (70%) |
| Percent Bias (PBIAS) | +/-25% |

224

225

2.4 Climate Change Scenarios

226

227

228

229

230

231

232

233

234

235

236

237

238

239

240

241

242

243

244

245

246

247

248

249

2.5. Dam Discharge Protocol Framework Development

251

252

253

254

255

The framework was developed to include the results of the model and the study as a basis for long-term forecasting of dam management. The localized SWAT model developed can be used as the engine to a decision support system to estimate the seasonal and monthly changes in reservoir inflow. They can modify their monthly operational rule curve depending on the changes in climate using the local SWAT model.

256

3. Results

257

3.1. Climate Projections in the Magat Watershed

258

259

260

261

262

263

264

265

- a) Projected Rainfall for the Mid-21st Century. During these years, up to 48.4% increase in rainfall can be noted under RCP 4.5 while up to 39.9% increase in precipitation can be seen under RCP 8.5. These increases in rainfall will likely happen during the Wettest years. A decrease in rainfall up to 35.8% can also be noted under RCP 4.5 while for RCP 8.5, a notable decrease of 27.8% can happen. These descending changes will likely happen during the Driest years.
- b) Projected Mean Temperature for the Mid-21st Century. An increase in temperature in the Watershed under both scenarios can be observed from the tables below. Under RCP 4.5's

266 driest, normal and wettest years, the increases in temperature were noted to go up to 1°C,
 267 1.3°C, and 2.0°C respectively. Furthermore, under RCP 8.5, an increase in temperature by
 268 1.4°C, 1.7°C, and 2.5°C can be observed for its driest, normal and wettest years, respectively.
 269 c) Projected Rainfall for the Late-21st Century. During the 21st century, a projected increase of
 270 rainfall under RCP 4.5 can go up to 49.6% while for RCP 8.5, it can go as high as 51.1 %.
 271 These events will likely happen during the wettest years. On the other hand, projected rainfall
 272 can decline up to 26.8% under RCP 4.5 while for RCP 8.5, it can go down to a 36% decrease
 273 in rainfall. These declines in rainfall will likely happen during the driest years.
 274 d) Projected Mean Temperature for Late 21st Century. Similar to the Mid-21st Century, there
 275 will be a notable increase in temperature for both scenarios. During RCP 4.5's driest year, the
 276 temperature can increase up to 1.4°C while during the normal years, it can go as high as a
 277 1.8°C increase of temperature. Meanwhile, in the wettest years, the temperature can increase
 278 up to 2. 7°C. Furthermore, RCP 8.5's driest, normal and wettest years noted an increase in
 279 temperature by 2.8°C, 3.4°C, and 4.5°C respectively.

280 **3.2. Simulation, Calibration, and Validation Results of SWAT Model**

281 3.2.1. Model Parameters

282 Table 2 shows the 17 most influential parameters that were calibrated in the model using
 283 manual and SWAT-CUP Calibration. These parameters directly influence the inflow along the Magat
 284 Watershed into the reservoir. These parameters were related to groundwater (ALPHA_BF,
 285 GW_DELAY, GWQMN, GW_REVAP, RCHRG_DP), soil properties (SOL_AWC, SOL_K,
 286 SOL_BD), HRU factors (HRU_SLP, LAT_TIME, ESCO, EPCO), routing (CH_K2, ALPHA_BNK),
 287 watershed management (CN2) and basin management (SURLAG).
 288

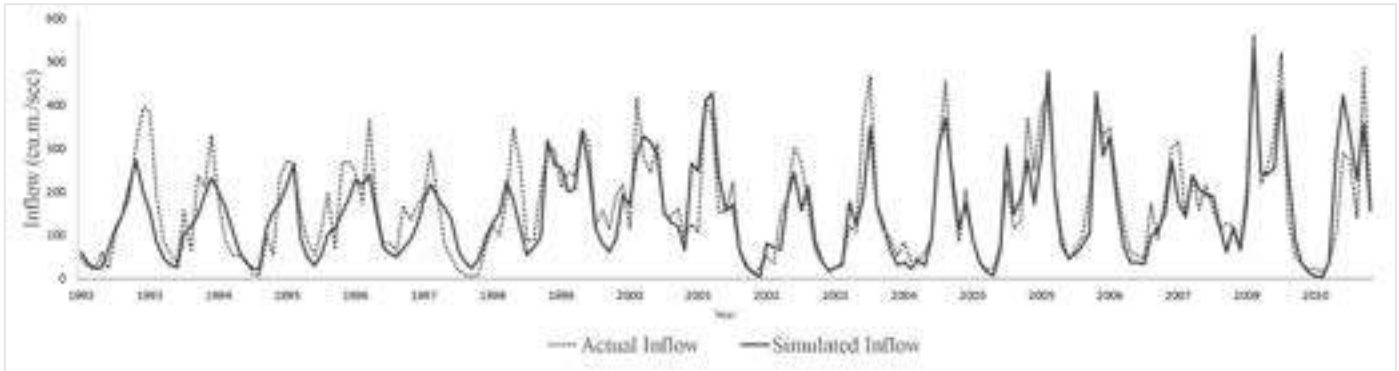
Table 2. Calibrated Parameters in the SWAT Model

| Parameter | Description | Calibrated Value |
|--------------------|---|------------------|
| 1. CN2.mgt | Initial SCS curve number for moisture condition II | 0.157 |
| 2. ALPHA_BF.gw | Baseflow Alpha Factor | 0.98 |
| 3. GW_DELAY.gw | groundwater delay | 0.1 |
| 4. GWQMN.gw | Threshold depth of water in the shallow aquifer required for return flow to occur | 600 |
| 5. GW_REVAP.gw | Groundwater "revap" coefficient | 0.02 |
| 6. ESCO.hru | Soil Evaporation compensation factor | 1 |
| 7. EPCO.hru | Plant uptake compensation factor | 1 |
| 8. CH_K2.rte | Effective Hydraulic Conductivity in the main channel alluvium | 142.31 |
| 9. ALPHA_BNK.rte | Baseflow Alpha Factor for bank storage | 0.98 |
| 10. SOL_AWC (.sol) | Available Water Capacity of the soil Layer | 0.01 |
| 11. SOL_K (.sol) | Saturated Hydraulic Conductivity | 193.69 |
| 12. SOL_BD (.sol) | Moist Bulk Density | 1.2 |
| 13. OV_N.hru | Manning's value for overland flow | 0.01 |
| 14. RCHRG_DP.gw | Deep Aquifer percolation factor | 0.01 |
| 15. HRU_SLP.hru | Average Slope Steepness | 0.6 |
| 16. SURLAG.bsn | Surface runoff lag coefficient | 4 |
| 17. LAT_TIME.hru | Lateral flow travel time | 30 |

289 **3.2.2. Calibration and Validation Results**

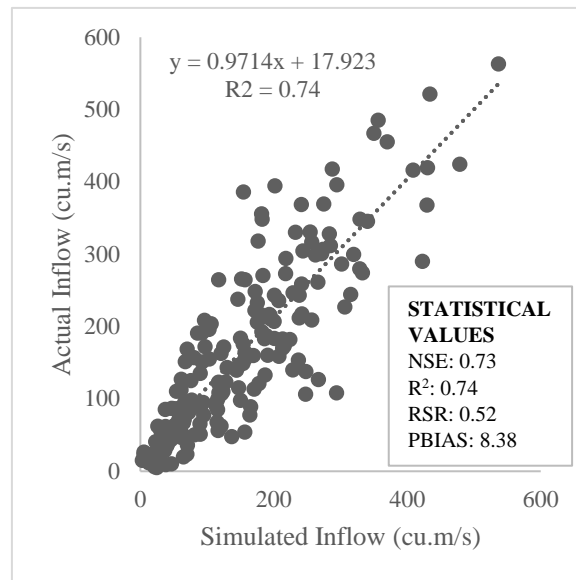
290 The calibration and validation resulted in a satisfactorily acceptable model. Calibration
 291 showed that the model had an NSE of 0.73, R² of 0.74, RSR of 0.52, and PBIAS of 8.38 which were
 292 all considered statistically acceptable when compared to the indices that were set. From Figure 4a,
 293
 294

295 the graph shows that the model generally underestimated the peak flows. This is one of the known
 296 limitations of the SWAT model. Although studies pertaining to the modeling of the inflow of a
 297 reservoir is very limited in the country, studies regarding streamflow, which is mostly associated with
 298 and similar to inflow, are conducted. For instance, Alejo (2019) satisfactorily calibrated and validated
 299 a SWAT Model in Maasin River Watershed in Laguna, the Philippines using actual streamflow. The
 300 calibration process resulted in 0.82 R^2 , 82% NSE, 0.024 RSR and PBIAS of -3.7%. This suggests
 301 that SWAT can be locally applied in river basin conditions in the country.
 302



303
 304

(a)



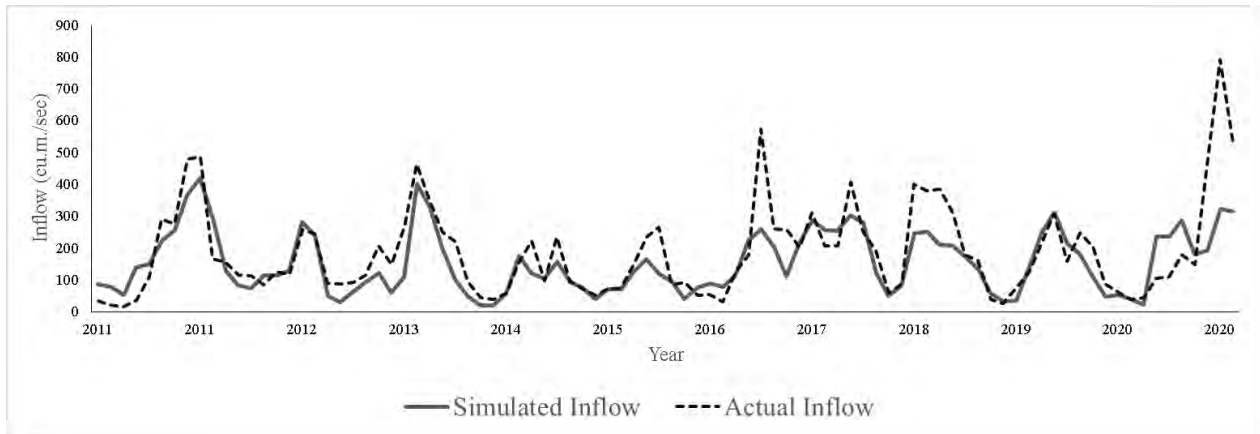
305

(b)

306 Figure 4. Monthly Simulated and Actual Inflow for Calibration Period (a) and the Scatter Diagram
 307 of the Simulated Inflow and Actual Inflow (b)
 308

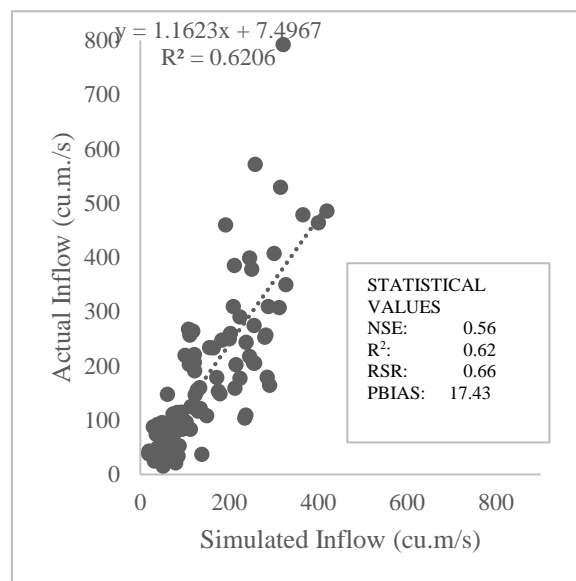
309 Moreover, the validated SWAT Model yielded satisfactory results. The model had an NSE of
 310 0.56, R^2 of 0.62, RSR of 0.66, and a PBIAS of 17.3. This means that the model satisfactorily predicted
 311 the inflow of water to the Magat Reservoir based on the validation results. However, like the
 312 calibration results, the model underestimated most of the peak flows as seen in Figure 5a. Validation
 313 results showed model accuracy values on NSE, R^2 , PBIAS, and RSR of 0.41, 0.57, 25.09%, and 0.71,
 314 respectively. Although the model was considered satisfactory, it can be observed that there was a
 315 drop in the performance of the validation results compared to the calibration results.
 316

317



318

(a)



319

(b)

320 Figure 5. Monthly Simulated and Actual Inflow for Validation Period (a) and the Scatter Diagram of
 321 the Simulated Inflow and Actual Inflow (b).
 322

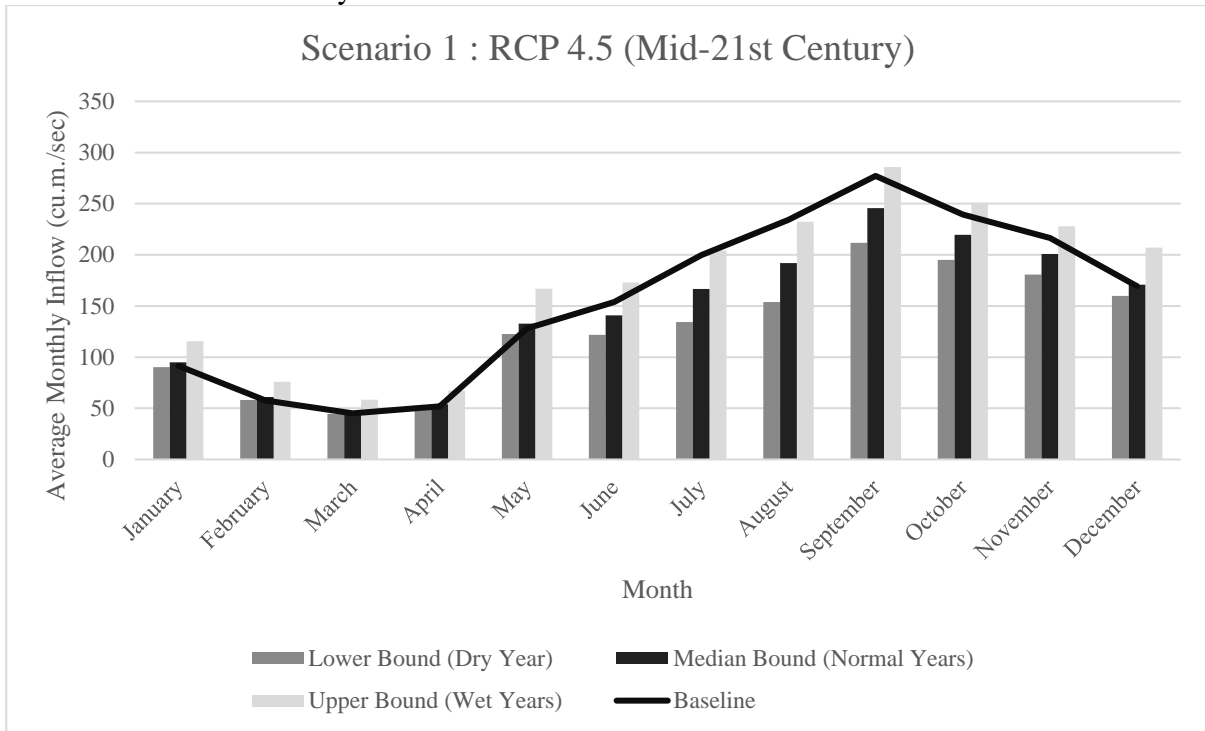
323 **3.3. Impact of Climate Change on the Inflow of Water to the Reservoir**

324 To understand the impact of increasing temperature and rainfall changes on the water balance of
 325 the watershed, the calibrated SWAT model was used. The downscaled climate projection provided
 326 by PAG-ASA was used as the future scenario for both changes in rainfall and temperature. There are
 327 no current studies observing the impacts of climate change on the inflow of the Magat reservoir or
 328 any river basin in the country in particular.

329 However, numerous analyses of the effects of climate change on the streamflow of these basins
 330 exist. An assessment of climate change impacts on the streamflow of the Mun River in the Mekong
 331 Basin, Southeast Asia using the SWAT model was conducted by Li and Fang (2021). Using the
 332 SWAT Model, they predicted that under scenarios RCP4.5, and RCP8.5, the mean annual streamflow
 333 of the basin decreased by 11.1%, and 7.6%, respectively, during the 2030s and increased by 40.9%,
 334 and 43.3% during the 2060s. Streamflow was projected to increase by 3.1% and 5.3% in the 2080s
 335 under the RCP4.5 and RCP8.5 scenarios. However, during the wet years, the streamflow was
 336 projected to increase by 45.7%, and 48.9% under RCP4.5, and RCP8.5, respectively. Notably, the
 337 streamflow in the dry season was projected to decrease in all future decades under these RCP
 338 scenarios—especially at the end of the century. From this example study, the impact of climate
 339 change on the flow of water is shown below corresponding to Scenarios 1,2,3, and 4.

340
 341 **3.3.1. Scenario 1: RCP 4.5 (Mid-21st Century)**

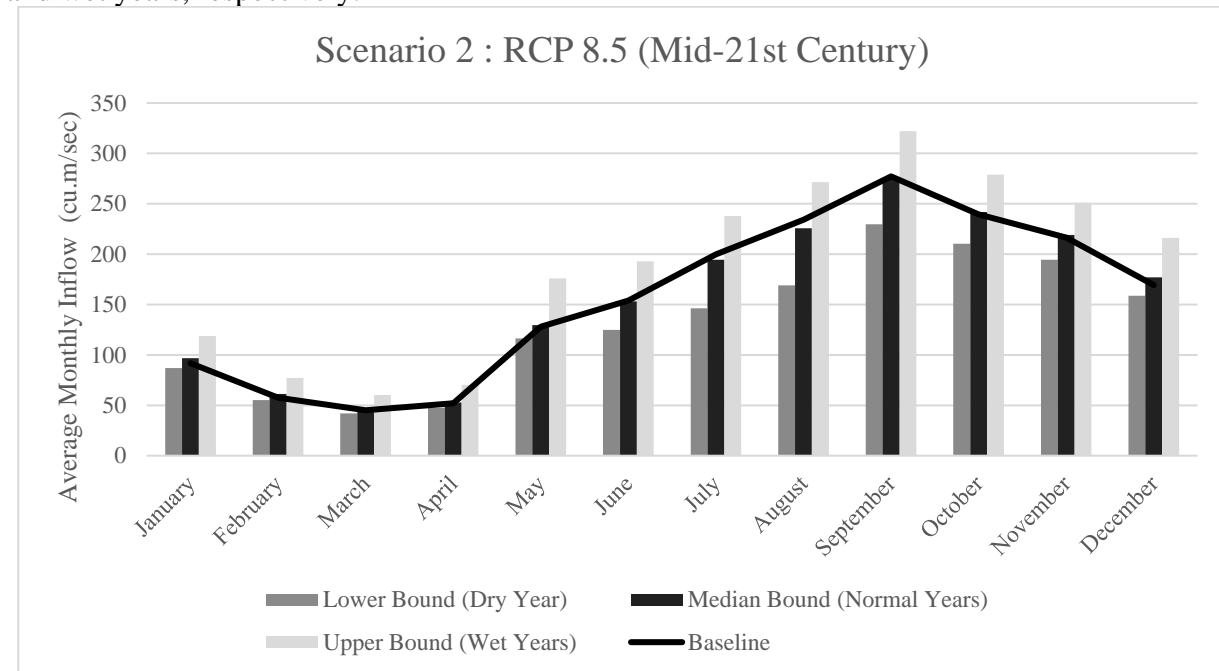
342 For the RCP 4.5 scenario for the Mid-21st Century, the model predicted that there will be a
 343 decrease of inflow by 18.27% for dry years and 7.42% for normal years, but for wet years, there will
 344 be an increase of inflow by 10.79%.



345
 346 Figure 6. Monthly Estimation of Future Inflow under RCP 4.5 Scenario during the Mid-21st Century.
 347

348 3.3.2. Scenario 2: RCP 8.5 (Mid-21st Century)

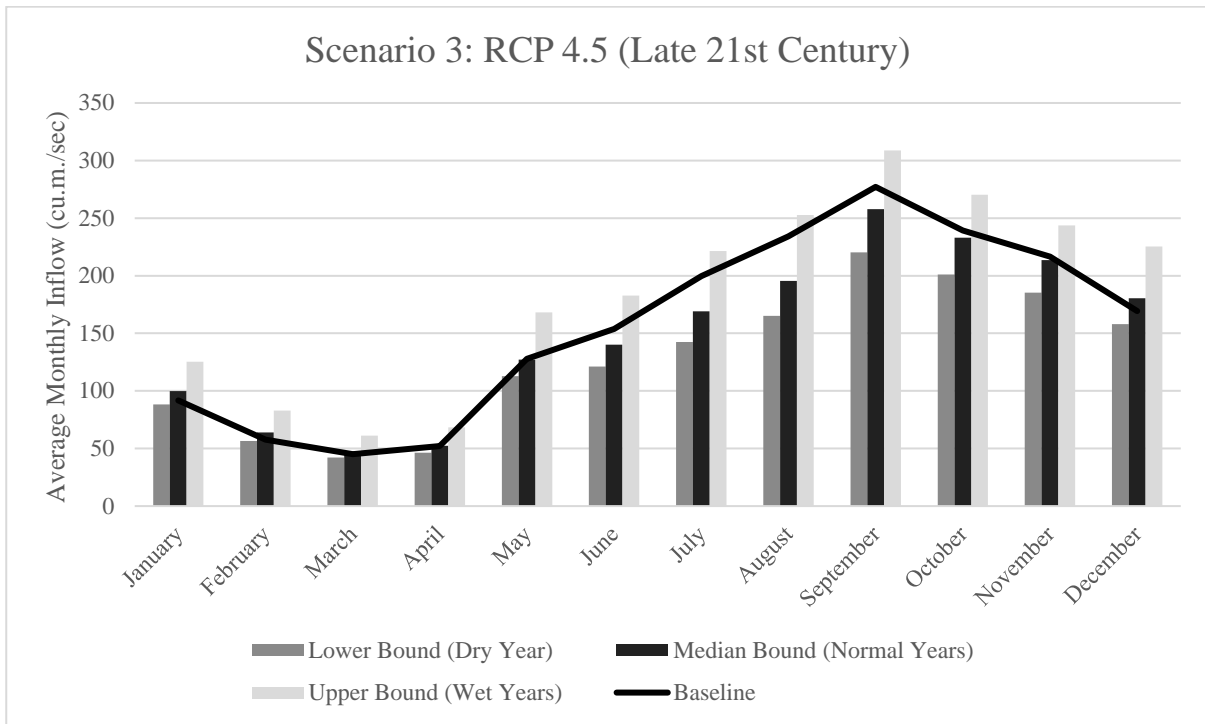
349 The model estimated a 15.21% decline in inflow during the dry years for the RCP 8.5 scenario
 350 in the mid-21st Century. However, there will be a 0.53% and 21.88% increase in inflow during normal
 351 and wet years, respectively.



352
 353 Figure 7. Monthly Estimation of Future Inflow under RCP 8.5 Scenario during the Mid-21st Century.
 354

355 3.3.3. Scenario 3: RCP 4.5 (Late 21st Century)

356 Under this scenario, the model projected that the inflow would reduce by 17.41% and 4.51%, in
 357 the dry and normal years respectively but during the wet years, there will be an 18.57% increment of
 358 inflow.

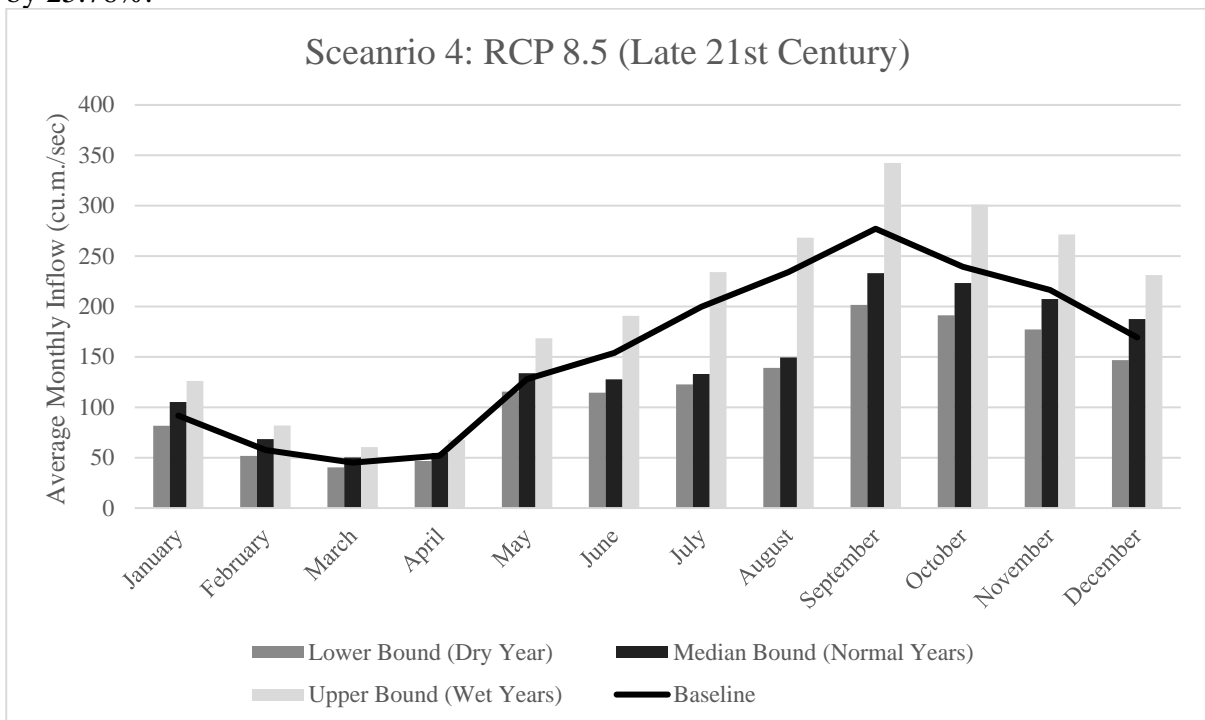


359
360
361
362
363
364
365

Figure 8. Monthly Estimation of Future Inflow under RCP 4.5 Scenario during the Late 21st Century.

3.3.4. Scenario 4: RCP 8.5 (Late 21st Century)

Both normal and dry years were estimated to decline by 23.33% and 10.21% under the RCP 8.5 Scenario for the late 21st century. However, the wet years for this century were estimated to increase by 25.76%.



366
367
368
369
370
371
372
373
374

Figure 9. Monthly Estimation of Future Inflow under RCP 8.5 Scenario during the Late 21st Century.

Future Peak Flow

3.3.5. Scenario 1: RCP 4.5 (Mid-21st Century)

For the RCP 4.5 scenario for the mid-21st century, the predicted peak flow for dry, normal, and wet years will most likely occur in the month of September with an average of at least 187.08 m³/s.,

375 227.09 m³/s, and 264.77 m³/s, respectively (see Table 3).

376

Table 3. Peak Flow for RCP 4.5 Scenario for Mid-21st Century

| Scenario | Peak Flow | Q (m ³ /s) |
|-----------------------|-----------|-----------------------|
| Dry (Lower Bound) | September | 211.88 |
| Normal (Median Bound) | September | 245.76 |
| Wet (Upper Bound) | September | 285.88 |

377

378 3.3.6. Scenario 2: RCP 8.5 (Mid-21st Century)

379 The estimated peak flow will take place in the month of September for dry, normal, and wet
 380 years respectively. The Magat reservoir is expected to have an average peak flow of at least 229.72
 381 m³/s for the dry years, 275.69 m³/s for the normal years, and 321.98 m³/s for the wet year as shown
 382 in Table 4.

383

Table 4. Peak Flow for RCP 8.5 Scenario for Mid-21st Century.

| Scenario | Peak Flow | Q (m ³ /s) |
|-----------------------|-----------|-----------------------|
| Dry (Lower Bound) | September | 229.72 |
| Normal (Median Bound) | September | 275.69 |
| Wet (Upper Bound) | September | 321.98 |

384

385 3.3.7. Scenario 3: RCP 4.5 (Late 21st Century)

386 The predicted peak flow will most likely happen during the month of September. For the Dry
 387 Years, the average peak flow is expected to have at least 220.36 m³/s. During the Normal and Wet
 388 years, the average peak flow is expected to have at least 257.84 m³/s and 308.73 m³/s (see Table 5).

389

Table 5. Peak Flow for RCP 4.5 Scenario for Late-21st Century.

| Scenario | Peak Flow | Q (m ³ /s) |
|-----------------------|-----------|-----------------------|
| Dry (Lower Bound) | September | 220.36 |
| Normal (Median Bound) | September | 257.84 |
| Wet (Upper Bound) | September | 308.73 |

390

391 3.3.8. Scenario 4: RCP 8.5 (Late 21st Century)

392 Under the RCP 8.5 Scenario during the late 21st century, the peak flow will most likely happen
 393 during the month of September for the dry years with at least 201.70 m³/s. Similarly, during the wet
 394 years and normal years, the peak flow will likely happen during the month of September with 342.46
 395 m³/s and 233.14 m³/s respectively as shown in Table 6.

396

Table 6. Peak Flow for RCP 8.5 Scenario for Late-21st Century

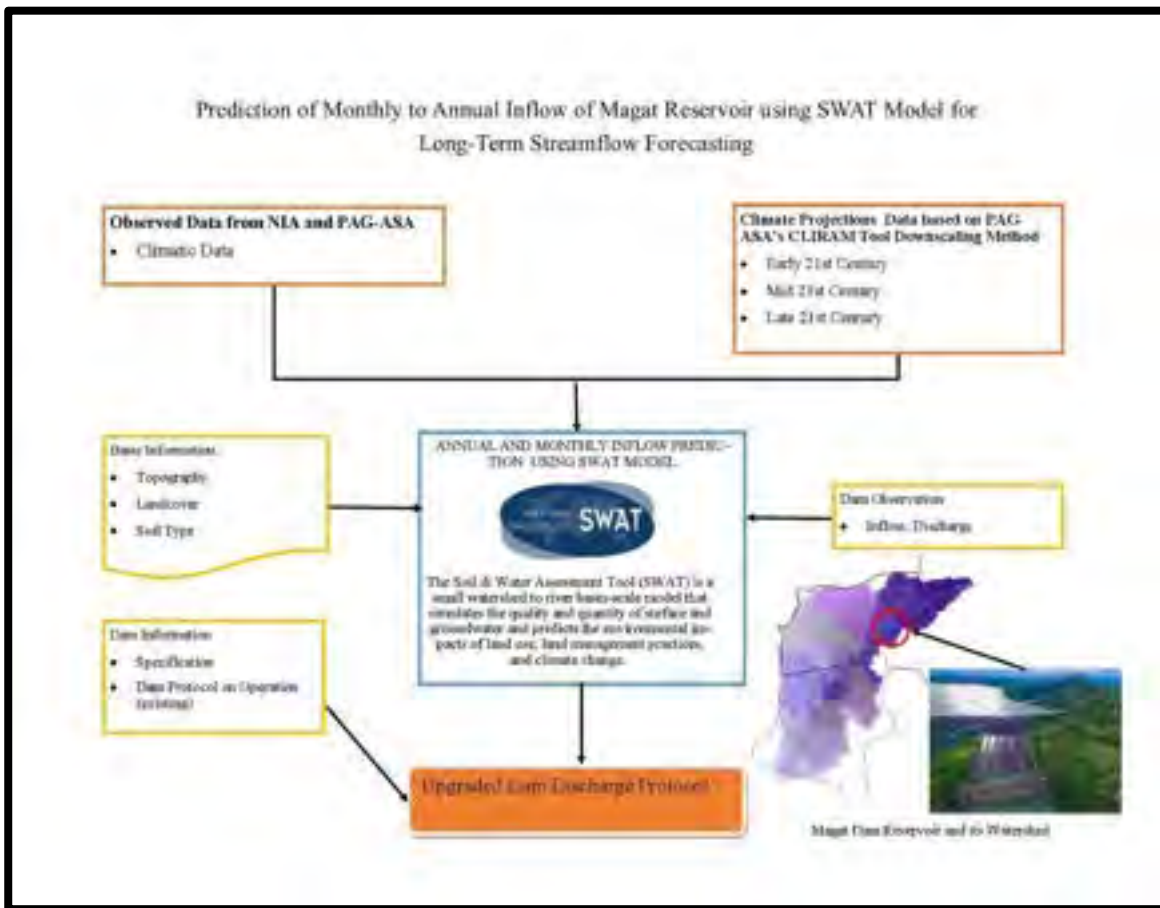
| Scenario | Peak Flow | Q (m ³ /s) |
|-----------------------|-----------|-----------------------|
| Dry (Lower Bound) | September | 201.70 |
| Normal (Median Bound) | October | 233.14 |
| Wet (Upper Bound) | September | 342.46 |

397

398 3.4 Recommendation of Framework towards the Development of Dam Discharge Protocol

399

400 Figure 10 shows the recommended framework for the upgrading of the Dam Discharge Protocol
 401 of Magat reservoir incorporating the developed SWAT Model emphasizing the predictions for annual
 402 and monthly streamflow forecasting.



403

404 Figure 10. Framework for Upgrading the Dam Discharge Protocol Using SWAT Model.

405 The amount of rainfall that will trigger pre-release in the dam depends on the current elevation
 406 of water in the dam. For example, the dam management decided to release about 189 m³/s during
 407 Typhoon Ulysses (International name Vamco) in 2020 when the current dam elevation was 190.92.
 408 The typhoon brought almost 300 mm of rainfall in the Magat watershed which brought about 7,200
 409 m³/s per second of dam inflow.

410 Rule curves for reservoirs are based on desired end-of-month storage; as a result, the key choice
 411 to be made each month is how much storage to provide for the reservoir. Once the monthly inflows
 412 are known, the monthly outflows through the turbines and gates are determined. The end-of-month
 413 storage targets depend on many factors that require inputs, especially on the water demands from
 414 irrigation, hydropower, and domestic water supply. This study, however, is limited to providing the
 415 monthly inflows and proposing a framework for dam management use.

416 The proposed framework is focused on the forecasting of monthly and annual inflow of the
 417 Magat Dam. For particular cases, it can also be used for seasonal forecasting along the river basin.
 418 This will help the dam management to observe long-term changes in the flow of water going into the
 419 reservoir. This will contribute to the awareness of the availability of water to be stored. With PAG-
 420 ASA's latest initiative in climate projections, the impacts of any changes in the climate will also be
 421 anticipated. The Upgraded Dam Discharge Protocol should be used by the NIA-MARIIS DRD to aid
 422 decision-making on seasonal scenarios, particularly on the inflow of the Magat reservoir.

423

424 **4. Discussion**

425

426 Climate change will lead to increased reservoir inflow during wet years largely due to a
 427 substantial increase in rainfall input to the watershed. It will also lead to a significant reduction in
 428 reservoir inflow during dry years due to decreased rainfall. Hydrological models provide a helpful
 429 platform for reliable estimates of water supply under many drivers of changes in watersheds which
 430 include climate changes. The SWAT model has been continuously supporting many water resources
 431 research in this avenue. The majority of these researchers in the Philippines have studied the ability

432 of the SWAT model for streamflow estimates. For example, Alejo & Ella (2019), used SWAT for
 433 streamflow estimates for irrigable area determination, Araza *et al.* (2021) for river flow analysis.
 434 Other local SWAT studies focused solely on land use change impact assessments and streamflow
 435 changes (Araza *et al.* 2021). Similarly, Alejo (2019) satisfactorily calibrated and validated a SWAT
 436 Model in Maasin River Watershed in Laguna, Philippines using actual streamflow. Reyes (2017) also
 437 applied the SWAT Model to predict streamflow and sedimentation in Wahig-Inabanga Watershed,
 438 Bohol, Philippines. This study focused on the calibration and validation of reservoir inflow using the
 439 SWAT model as support to dam management actions and plans.

440 The most sensitive parameters for reservoir inflow were ALPHA_BF, GW_DELAY, GWQMN,
 441 GW_REVAP, RCHRG_DP (groundwater), SOL_AWC, SOL_K, SOL_BD (soil properties),
 442 HRU_SLP, LAT_TIME, ESCO, EPCO (HRU factors), CH_K2, ALPHA_BNK (routing), CN2
 443 (watershed management) and SURLAG (basin management). The parameters calibrated in this study
 444 can also be seen in a SWAT study conducted by Panondi ~~&~~ Izumi (2021) in the Pulangi River
 445 Basin (PRB), which is located on the Mindanao Island of the Philippines. They pointed out that CN2,
 446 SOL_AWC, HRU_SLP, GW_DELAY, and CNCOEFF are the most sensitive parameters in the
 447 combined simulation analysis of streamflow and sediment yield. A reservoir modeling study by
 448 Beharry *et al.* (2021) found 16 sensitive parameters (ALPHA_BNK, CH_K2, GW_DELAY,
 449 ALPHA_BF, CH_N2, CN2, EPCO, OV_N, REVAPMN, SURLAG, SOL_K, SOL_BD, GWQMN,
 450 SOL_AWC, and GW_REVA) in their study. Almost the same parameters were deemed sensitive in
 451 this study.

452 Meanwhile, a study conducted by Araza *et al.* (2021) in the Abuan Watershed found that
 453 parameters directly influencing its peak and low flows were the coefficients on runoff (CN2 and
 454 SURLAG), baseflow (ALPHA BF), soil evaporation (ESCO), and soil depth for baseflow (GWQN).
 455 The model underestimated the peak flows in the study area which has been common in many SWAT
 456 studies (Le & Principe 2017; Tolentino & Ella 2016). According to research by Gassman *et al.* (2007),
 457 SWAT overestimated streamflow during dry years when low flows occurred and underestimated
 458 streamflow during wet years when big flows are presumably anticipated. In a separate USDA study,
 459 it was shown that SWAT underestimated river flows in the summer but underestimated them in the
 460 winter.

461 The SWAT performance was better during calibration which has been commonly observed in
 462 other SWAT studies. This was also seen in the SWAT model study by Briones *et al.* (2016). Their
 463 validation also yielded acceptable simulation results although NSE and R² dropped to 0.61 and 0.68
 464 from calibrated results of 0.85 and 0.86. They also stated that this marked decrease in the model's
 465 performance can be attributed to several factors and one of the factors can be associated with LULC
 466 change between the calibration period and validation period. In order to estimate streamflow, Reyes
 467 (2017) also successfully calibrated and verified the SWAT model. However, it should be emphasized
 468 that the calibration and validation periods for these researches are shorter (4 to 6 years), and they are
 469 almost the same duration. In comparison, the SWAT model used in the current study for the Magat
 470 watershed is significantly longer, lasting 18 and 10 years, respectively. It is crucial to use longer
 471 calibration and validation periods since they tend to produce better model results than shorter ones,
 472 mostly because of making effects. Additionally, there is a significant difference in simulation length
 473 between calibration and validation, which might justify the impact of simulation length on the model
 474 results of the present study.

475 It has been crucially shown that there would be projected shifts in the months where the peak
 476 reservoir inflow occurs. Furthermore, because of the significant increase in rainfall input to the Magat
 477 watershed brought on by climate change, there will be an increase in reservoir inflow during rainy
 478 years. Less rainfall during dry years will also result in a large decrease in reservoir inflow. Moreover,
 479 it has also been importantly shown that there will be projected shifts in months where peak inflow
 480 occurs. Various studies have shown the adverse varied impacts of climate changes on water resources
 481 in the Philippines. Climate change has been shown to decrease water availability in reservoirs as a
 482 result of decreased water supply and increased water demand which will eventually lead to reduced
 483 irrigable areas, especially in dry years (Alejo & Alejandro 2022). The threat of severe flooding and
 484 excessive soil loss due to increased runoff and sediment yield are threats to the sustainability of
 485 ecosystems due to climate change (Panondi & Izumi 2021). Croplands are at risk when this happens

486 and would lead to huge economic losses as estimated by Araza *et al.* (2020). It is then important that
487 the cropping calendar in the vast service area of the reservoir be made dynamic or retrofitted to future
488 changes in climate to make the irrigation system climate resilient. The fully calibrated and validated
489 SWAT model for the Magat watershed provided adequate estimates of reservoir inflow. The
490 increased peak inflow during wet years might lead to potential flooding downstream of the reservoir
491 when the dam management is not appropriately planned. The significantly reduced inflow during dry
492 years will lead to reduced water supply for irrigation and hydropower capacity of the dam. These
493 reductions in inflow in the reservoir during dry seasons convey a strong indication that the reservoir
494 may become dry in the near future (Joshi & Makhasana 2020). An increase in the inflow, however,
495 may require a change of the operation rules of the reservoir in order to adapt to the new changing
496 reality (Muhammad *et al.* 2020). However, Rule curves for reservoirs are based on desired end-of-
497 month storage; as a result, the key choice to be made each month is how much storage to provide for
498 the reservoir. Once the monthly inflows are known, the monthly outflows through the turbines and
499 gates are determined. The end-of-month storage targets depend on many factors that require inputs,
500 especially on the water demands from irrigation, hydropower, and domestic water supply. This study,
501 however, is limited to providing the monthly inflows and proposing a framework for dam
502 management use. The SWAT model developed can provide a basis for predicting monthly to annual
503 reservoir inflow trends for long-term projections.

504 5. Conclusion

505
506 The impact of climate change on water resources is inevitable, however, through hydrologic
507 models, it is quantifiable. This study using the SWAT model implies that this method can adequately
508 predict the monthly inflow of the Magat reservoir under different climate change scenarios for the
509 Mid-21st Century and Late 21st century. The latest and most accurate data from different agencies
510 were used as inputs in the model as well as the downscaled climate projection from PAG-ASA.
511 Model performance was deemed satisfactory as the model attained an NSE of 0.73, R² of 0.74, RSR
512 of 0.52, PBIAS of 8.38, and NSE of 0.56, R² of 0.62, RSR of 0.66, and a PBIAS of 17.3 respectively.
513 However, the model tends to underestimate the peak flows which is a known limitation of the SWAT
514 Model. The study found that if the climate change would worsen and reach the RCP 4.5 and RCP 8.5
515 scenario in the basin level, there will be a significant decrease in inflow during their dry and normal
516 years, but a substantial increase will occur during the wet years. These decreases in reservoir inflow
517 during dry seasons serve as a clear warning that the reservoir may soon become dry. However, a rise
518 in the inflow might necessitate modifying the reservoir's operating guidelines in order to
519 accommodate the new, shifting reality. In addition, the highest inflow of water to the reservoir is
520 anticipated from the month of September followed by October to December since this is already the
521 rainy season in the country.

522 Climate change impact studies have been widely explored for streamflow estimations using
523 SWAT to quantify available river flows and their fluctuations. This study focused on the estimation
524 of reservoir inflow to support dam management actions, decisions, and plans. Given the importance
525 of the dam specifically to the agriculture sector, it is necessary to take steps to review the existing
526 Dam and Reservoir policy and adopt mitigation strategies for climate change problems.
527 Consequently, this study will contribute to the development of the framework for the upgrading of
528 the Dam Discharge Protocol and Dam Management focusing on seasonal forecasting along river
529 basins. This will help the dam management to observe long-term changes in the flow of water going
530 into the reservoir. Also, the results could pave the way toward the design of various interventions to
531 take care of the watershed and its river networks and reduce the negative impacts of climate change
532 on the Magat reservoir in the future. Additionally, the study demonstrated a scientifically sound
533 methodology to quantify the impacts of climate change and its potential as a decision support system
534 for dam management in river basins in the Philippines and other countries.

535 6. Acknowledgment

536
537 The research presented in this article was a part of the Project titled “Integrated Flood and Water

538 Resources Management in the ASEAN Basins for Sustainable Development” funded by the
 539 Department of Science and Technology with additional funding from Isabela State University. The
 540 Project is in collaboration with the National Irrigation Administration Magat River Integrated
 541 Irrigation System (NIA-MARIIS), which provided the majority of the data used in the SWAT
 542 modeling. The authors would also like to thank the Kyoto University Water Resources Research
 543 Center - Disaster Prevention Research Institute through the APN Project for the technical assistance
 544 during the conduct of the study. The authors would like to acknowledge all the agencies, locally and
 545 internationally, which provided the needed data and support leading to the accomplishment of this
 546 study. The authors wish to thank all researchers, staff, and critics who helped them complete this
 547 research.

548 **References**

- 549
- 550 Abbasi H., Delavar M., Nalbandan RB, Shahdany MH. (2020) Robust Strategies for Climate Change
 551 Adaptation in the Agricultural Sector Under Deep Climate Uncertainty. *Stochastic Environmental*
 552 *Research and Risk Assessment*, 1–20
 553
- 554 Alejo, L.A., Alejandro, A.S. (2022) Changes in Irrigation Planning and Development Parameters Due
 555 to Climate Change. *Water Resources Management* 36, 1711–1726. [https://doi.org/10.1007/s11269-](https://doi.org/10.1007/s11269-022-03105-4)
 556 [022-03105-4](https://doi.org/10.1007/s11269-022-03105-4)
 557
- 558 Alejo, L.A., Ella V.B. (2019) Assessing the impacts of climate change on dependable flow and
 559 potential irrigable area using the SWAT model. The case of Maasin River watershed in Laguna,
 560 Philippines. *Journal of Agricultural Engineering* 2019; volume L:94.
 561
- 562 Araza, A. & Perez, M. & Cruz, R. & Aggabao, LF & Soyosa, E. (2021) Probable streamflow changes
 563 and its associated risk to the water resources of Abuan watershed, Philippines caused by climate
 564 change and land use changes. *Stochastic Environmental Research and Risk Assessment*. 35. 1-16.
 565 10.1007/s00477-020-01953-3.
 566
- 567 Arnell NW. (1999) Climate change and global water resources. *Glob Environ Change* 9:S31–S49
 568
- 569 Arnold, J. G., Srinivasan, R., Muttiah, S., and Williams, J. R. (1998) Large-area hydrologic modeling
 570 and assessment: Part I. Model development. *J. American Water Resour. Assoc.*, 34(1), 73-89.
 571
- 572 Azari, M., Moradi, H.R., Saghafian, B., Faramarzi, M. (2016) Climate change impacts on streamflow
 573 and sediment yield in the North of Iran. *Hydrological Sciences Journal*. 61:1, 123-133. DOI:
 574 10.1080/02626667.2014.967695
 575
- 576 Basconcillo, J., Lucero, A., Solis, A., Sandoval, Jr, Bautista, E, Koizumo, T., Kanamaru, H. (2016)
 577 Statistically Downscaled Projected Changes in Seasonal Mean Temperature and Rainfall in Cagayan
 578 Valley, Philippines. *Journal of the Meteorological Society of Japan*. Ser. II. 94A. 151-164.
 579 10.2151/jmsj.2015-058.
 580
- 581 Beharry, S.L., Gabriels, D., Lobo, D. et al. (2021) Use of the SWAT model for estimating reservoir
 582 volume in the Upper Navet watershed in Trinidad. *SN Appl. Sci.* 3, 163
 583 <https://doi.org/10.1007/s42452-021-04201-7>
 584
- 585 Briones R., Ella V., Bantayan N. (2016) Hydrologic Impact Evaluation of Land Use and Land Cover
 586 Change in Palico Watershed, Batangas, Philippines Using the SWAT model. *J. Environ. Sci. Manag.*
 587 19:96-107
 588
- 589 CAD-PAGASA. (2004) DOST Service Institutes “Climate Change Scenario for the Philippines”.
 590 <http://kidlat.pagasa.dost.gov.ph/cab/scenario.htm>. (27 October 2011).

- 591 DOST-PAGASA. (2018) Observed and Projected Climate Change in the Philippines. Philippine
592 Atmospheric, Geophysical and Astronomical Services Administration, Quezon City, Philippines.
- 593 Fourcade, F. and F. Quentin. (1994) Balancing Reservoir Management and Water Conservation:
594 Application of Hydropower and Irrigation”. *NATO ASI Series E Applied Sciences*. 275, pp. 455-464
595
- 596 Gassman, P.W., Reyes, M.R., Green, C.H., and Arnold, J.G. (2007) The soil and water assessment
597 tool: historical development, applications, and future research directions. *Trans. ASAE*. vol. 50, pp.
598 1211–1250. <https://doi.org/10.1.1.88.6554>
599
- 600 Guiamel, Ismail & Lee, Han Soo. (2020) Watershed Modelling of the Mindanao River Basin in the
601 Philippines Using the SWAT for Water Resource Management. *Civil Engineering Journal*. 6. 626-
602 648. 10.28991/cej-2020-03091496.
- 603
- 604 Joshi, G. S., & Makhasana, P. (2020) Impact of Climate Change on Hydrological Parameters in
605 Dharoi Dam Reservoir Basin, India. *International Journal of Climate Change: Impacts & Responses*,
606 12(1).
- 607
- 608 Le, A.M. and Pricope, N.G. (2017) Increasing the accuracy of runoff and streamflow simulation in
609 the Nzoia Basin, Western Kenya, through the incorporation of satellite-derived CHIRPS data, *Water*.
610 vol. 9. <https://doi.org/10.3390/w9020114>
611
- 612 Li, C., & Fang, H. (2021) Assessment of climate change impacts on the streamflow for the Mun River
613 in the Mekong Basin, Southeast Asia: Using SWAT model. *CATENA*, 201, 105199. doi:
614 10.1016/j.catena.2021.105199
615
- 616 Lv, M.,Hu, T.,Dan, L.,and Lv, M. (2014) Daily Streamflow simulation in a small-scale farmland
617 catchment using modified SWAT Model. *Trans. ASABE*. vol. 57, pp. 31–41.
618 <https://doi.org/10.13031/trans.57.10134>
619
- 620 Muhammad, A., Evenson, G. R., Unduche, F., & Stadnyk, T. A. (2020). Climate Change Impacts on
621 Reservoir Inflow in the Prairie Pothole Region: A Watershed Model Analysis. *Water*, 12(1), 271.
622 <https://doi.org/10.3390/w12010271>
623
- 624 Nauman, S., Zulkafli, Z., Bin Ghazali, A.H., Yusuf, B. (2019). “Impact Assessment of Future Climate
625 Change on Streamflows Upstream of Khanpur Dam, Pakistan using Soil and Water Assessment
626 Tool”. *Water 11*, no. 5: 1090. <https://doi.org/10.3390/w11051090>
627
- 628 Neitsch, S.L., et al. (2011). “Soil and Water Assessment Tool theoretical documentation version
629 2009”. *Texas Water Resources Institute Technical Report No. 406*. Texas A&M University System,
630 College Station, Texas
631
- 632 Oo, H.T.; Zin, W.W.; Kyi, C.T. (2020) Analysis of Streamflow Response to Changing Climate
633 Conditions Using SWAT Model. *Civ. Eng. J.*, 6, 194–209.
634
- 635 Ouyang F, Zhu Y, Fu G, Lü H, Zhang A, Yu Z, Chen X (2015) Impacts of climate change under
636 CMIP5 RCP scenarios on streamflow in the Huangnizhuang catchment. *Stoch Env Res Risk Assess*
637 29(7):1781–1795
638
- 639 Panondi, W., Izumi, N. (2021) Climate Change Impact on the Hydrologic Regimes and Sediment
640 Yield of Pulangi River Basin (PRB) for Watershed Sustainability. *Sustainability*, 13, 9041
641
- 642 Principe, Jeark (2012) Exploring Climate Change Effects on Watershed Sediment Yield and Land
643 Cover-Based Mitigation Measures Using Swat Model, Rs, and Gis: Case of Cagayan River Basin,

- 644 Philippines. *ISPRS - International Archives of the Photogrammetry, Remote Sensing and Spatial*
645 *Information Sciences*. XXXIX-B8. 193-198. 10.5194/isprsarchives-XXXIX-B8-193-2012.
- 646
- 647 Reyes, T. (2017). Application of Soil and Water Assessment Tool (SWAT) Model to Predict
648 Streamflow and Sediment Yield in Wahig-Inabanga Watershed, Bohol, Philippines. *International*
649 *Journal of Environmental and Rural Development*. Volume 8, Issue 1, Pages 104-110,
650 https://doi.org/10.32115/ijerd.8.1_104, [https://www.jstage.jst.go.jp/article/ijerd/8/1/8_104/_article/-](https://www.jstage.jst.go.jp/article/ijerd/8/1/8_104/_article/-char/en)
651 [char/en](https://www.jstage.jst.go.jp/article/ijerd/8/1/8_104/_article/-char/en)
- 652
- 653 Sarmiento, C., Ayson, R., Gonzalez, R., Castro P. (2010) Remote Sensing and GIS in Inflow
654 Estimation: The Magat Reservoir, Philippines Experience. Vol. Xxxviii, Part 7a. P. 227.
- 655
- 656 Sivakumar B. (2011) Global climate change and its impacts on water resources planning and
657 management: assessment and challenges. *Stoch Env Res Risk Assess* 25(4):583–600
- 658
- 659 Thanh Nguyen, T., Nakatsugawa, M., J. Yamada, T., & Hoshino, T. (2020) Assessing climate change
660 impacts on extreme rainfall and severe flooding during the summer monsoon season in the Ishikari
661 River basin, Japan. *Hydrological Research Letters*, 14, 155-161.
- 662 Tolentino, A.B. and Ella, V.B., Assessment of SWAT model applicability and performance for
663 predicting surface runoff in an ungauged watershed in the Philippines. (2016) *IAMURE Int. J. Ecol.*
664 *Conserv.* vol. 17, pp. 142–159. <https://doi.org/10.7718/ijec.v17i1.1067>
- 665
- 666 Tolentino PLM, Poortinga A, Kanamaru H, Keesstra S, Maroulis J, et al. (2016) Projected Impact
667 of Climate Change on Hydrological Regimes in the Philippines. *PLOS ONE* 11(10): e0163941.
668 <https://doi.org/10.1371/journal.pone.0163941>

Journal of Water and Climate Change

Climate Change Intensifies the Drought Vulnerability of River Basins

--Manuscript Draft--

| | |
|---|---|
| Manuscript Number: | |
| Article Type: | Research Paper OA |
| Section/Category: | Extreme events (droughts/temperature) |
| Corresponding Author: | Alvin John B. Felipe, MSci (Ongoing) Isabela State University Echague, Region 2 PHILIPPINES |
| First Author: | Alvin John Bague Felipe, MS in Agricultural Engineering |
| Order of Authors: | Alvin John Bague Felipe, MS in Agricultural Engineering Lanie Alejandro Alejo, PhD in Agricultural Engineering Orlando F. Balderama, PhD in Agricultural Engineering Elmer A. Rosete, MS in Agricultural Engineering |
| Abstract: | River Basins are highly significant resources that contribute to agro-industrial and domestic development. This study was conducted to assess the socio-economic impacts of climate change on the vulnerability of a significant river basin in the Philippines, the Magat River Basin, to drought by considering agriculture as the major sector of focus. The results imply that the current drought susceptibility of Magat Watershed is at 1.9 – 3.39 min-max scale or from low to above moderate, where the basin's Sensitivity and Exposure, account for 57% and 31% of the total vulnerability, respectively. And that the resulting adaptive capacity has a mitigating factor of only 12%, thereby construed to be very low. Averagely, the Santa Fe and Subbasin 2 sub-watersheds were identified to be moderately susceptible to drought with an average rating of 3.1 and 3.25 respectively. Meanwhile, the average drought vulnerability rating of other subbasins is between 2.08 and 2.91 which is from a low to an approximately moderate level. The overall drought susceptibility of the basin is projected to increase future climate scenarios up to 30% (High) of the current level. Catalyzing effective policies and climate change governance are highly encouraged to inhibit further improve mitigation and adaptation measures. |
| Full Title: | Climate Change Intensifies the Drought Vulnerability of River Basins |
| Additional Information: | |
| Question | Response |
| Please explain why this paper is of interest to readers of <i>Journal of Water and Climate Change</i> . | The Journal of Water Science and Climate Change is one of the most respected and reputable journals for water resources and climate science which tackles a wide variety of areas. This paper will suite the interest of the journal's readers since it offers a comprehensive overview and methodology mainstreaming climate change effect on drought vulnerability of a river basin. This study can generate readers from policy making professionals, and researchers that focuses on climate change remediation and mitigation. In this paper, it is of high interest to contribute and to serve as a basis for future drought studies for Magat Rive Basin as there are no other studies that exist just yet. This research paper also aims to give a holistic approach in looking on both sides of the spectrum by looking at the level of vulnerability with regards to effect on human and related dimensions associated in agriculture. This is a timely issue as climate change tends to bend towards influencing future water resources that can threaten food production and security. |
| Has your manuscript been submitted to a conference? | No |
| HIGHLIGHTS: Please list up to 5 | 1. GIS-based socioeconomic assessment and benchmarking of the impacts of drought |

| | |
|--|--|
| <p>numbered points that briefly describe the significance (in terms of innovation and contribution to the knowledge base) of this research.</p> <p>Note that the highlights should help increase the discoverability of your article. Ensure the highlights are concise, easy to read, and include key search terms (you should not simply rewrite the abstract). When listing the highlights of your research, please bear in mind (for example) novelty, scope, and international relevance.</p> | <p>on Magat River Basin.</p> <p>2. The Entropy and AHP techniques of multi-criteria decision-making were used to appraise the corresponding weight of drought indicators.</p> <p>3. Based on the future changes in rainfall and temperature, the vulnerability of MRB for mid and late-21st Century was projected to increase at about 30% under RCP 4.5 and 8.5 Scenarios</p> |
| <p>IWA Publishing is committed to ensuring complete transparency regarding conflicts of interest. Please complete the Conflict of Interest Statement to certify that the authors are not affiliated with or involved with any organization or entity with any financial interest or non-financial interest in the subject matter or materials discussed in this paper. Please address queries about Conflicts of Interest to the journal office: editorial@iwap.co.uk</p> | <p>The authors declare there is no conflict.</p> |
| <p>Suggested Reviewers:</p> | <p>Rey C. Naval, PhD Agricultural Engineering Associate Professor, Quirino State University reyn_qsc@yahoo.com He has great background in soil and water resources management and socio economic researches related to agriculture.</p> <p>Virgil Bello Bilaro, PhD major in Water Resources Professor, Bicol University virgil_bilaro@yahoo.com He has a PhD from University of the Philippines Diliman and he has a strong academic and research experience in the field of water resources.</p> <p>Vyas Pandey, PhD in Agricultural Meteorology Professor and Head, Anand Agricultural University pandey04@yahoo.com He is an internationally-known expert in Agrometeorology and climatic science application in agriculture. He has been a part of numerous scientific articles and considered to be one of the most respected figures in agrometeorology, and now serves as the President of the Association of Agrometeorologists.</p> |

Climate Change Intensifies the Drought Vulnerability of River Basins

Short title: GIS-based Drought Vulnerability Assessment using AHP-Entropy Method

A.J. B. Felipe^{1*}, L. A. Alejo^{1,2}, O. F. Balderama^{1,2}, and E.A. Rosete³

¹ Water Research and Development Center, Isabela State University, 3309 San Fabian, Echague, Isabela, PH.
(E-mail: alvinjohn316felipe@gmail.com)

² Department of Agricultural and Biosystems Engineering, College of Engineering, 3309 San Fabian Isabela State University, Echague, Isabela
(E-mail: lhan_1023@yahoo.com; orly_isu@yahoo.com)

³ University Research Department, Isabela State University, San Fabian, Echague, Isabela
(E-mail: rosete_elmer@yahoo.com)

* Corresponding author

Abstract

River Basins are highly significant resources that contribute to agro-industrial and domestic development. This study was conducted to assess the socio-economic impacts of climate change on the vulnerability of a significant river basin in the Philippines, the Magat River Basin, to drought by considering agriculture as the major sector of focus. The results of this study imply that the current drought susceptibility of Magat Watershed is at 1.9 – 3.39 min-max scale or from low to above moderate, where the basin's Sensitivity and Exposure, account for 57% and 31% of the total vulnerability, respectively. And that the resulting adaptive capacity has a mitigating factor of only 12%, thereby construed to be very low. Averagely, the Santa Fe and Subbasin 2 sub-watersheds are identified to be moderately susceptible to drought with an average rating of 3.1 and 3.25 respectively. Meanwhile, the average drought vulnerability rating of other subbasins is between 2.08 and 2.91 which is from a low to an approximately moderate level. The overall drought susceptibility of the basin is projected to increase due to climate change under future climate scenarios up to 30% (High) of the current level. Catalyzing effective policies and climate change governance are highly encouraged to inhibit further improve mitigation and adaptation measures.

Keywords

climate change, drought vulnerability, GIS, indicator, magat river basin, MCDA

Introduction:

In the recent past, climate scientists have observed an increasing trend in temperature and have forewarned us that as we move forward, it has become imperative for us to witness the natural catastrophes precipitated from climatic variations induced by unprecedented global warming which reflects anthropogenic activities in terms of increment carbon footprint and greenhouse gas emissions (Houghton, et al., 2001). In our contemporary world, the frequency of emerging climatic extremes disrupts environmental and societal processes caused by deleterious impacts of such disasters that tend to play havoc with human well-being, and engender severe consequences on ecosystems, communities, and the economy. Calamities induced by national extremes worldwide have caused

billions of dollars-worth of destruction, damage, and injury where about 20% of it is attributed to drought occurrences (Salvacion, 2021).

Drought is a commonly recurring element related to climate, it is a natural peril affecting millions of households as it demands a difficult and sophisticated approach to scientifically address its inherent characteristics (Wu, et al., 2011). For the past decades, interdisciplinary measures have been applied globally to mitigate drought-related jeopardies around the world in terms of famine due to reduced production-causing food insecurity, economic losses, natural resources, and environmental systems degradation. There has been a huge collection of research and sustainability efforts that have been established to address the need for a more serious undertaking in drought studies. For detailed information, the reader is referred to (Wilhite, 2012) and (Sheffield, 2012). The Intergovernmental Panel on Climate Change Framework on Vulnerability assessment has become one of the most used tools in assessing the impacts of natural hazards. In his working paper (Brooks, 2003), introduced a preliminary conceptual framework for vulnerability and adaptation that adapts to a variety of applications, systems, and hazards concerning climate change. Vulnerability is either perceived as a consignment of damage as an outcome of a specific climatic hazard or a superimposed aspect that thrives within the system to be stimulated when a climatic risk occurs. It is much broader in the real sense when it comes to the system's response to drought. It is an indicative measure of the susceptibility of an area, with respect to the main focus of evaluation may it be more in an economic, environmental, social, or physical aspect (Dabanli, 2018).

Drought vulnerability assessment is contingent on the target sector to be evaluated and the geographical features of the area. Understanding the susceptibility to drought may require an in-depth consideration of several factors that can make the situation worse or on the other hand manageable. In other words, drought vulnerability is always related to the way a certain system under a climatic hazard responds in terms of its capacity to prepare for the possible occurrence of drought using diversification options in reducing the possible damage not only in an economic sense but may also be evident in the condition of their lives being affected by drought hazards. While drought can be correlated with the decrease in rainfall over an area, the real vulnerability might lay in how farmers incur an equivalent loss by not using a drought-resistant crop variety, or how much help a water-impounding reservoir could make if it is available. There are complex approaches in mainstreaming drought mitigation efforts through vulnerability assessment that in a way, compliment each. It is now a globally-recognized agenda to weaken the social, environmental, and economical impact of drought by promulgating progressive routes in making societies more resilient to drought risk and vulnerability (Naumann et al., 2014).

Agriculture is often regarded as the backbone of the Philippine economy as more than 30% of its land area is being cultivated. The country where the total production has been observed to rise in the past decade. Improved agro-methodologies and farming techniques as a by-product of productive research and development agenda have resulted in an almost 500% increase in rice production from 1961 to 2018 However, the Philippines is identified to be at the fore-front as to experiencing climatic extremes and disasters. Up to 327 million dollars-worth of agricultural damages have been estimated inherent to the El Nino incident from 2015 to 2019. The frequency and intensity of climate-related disasters always deter this positive course of development. (Perez, at al., 2022). In the Philippines, a handful of different vulnerability studies and methodologies have been performed to impose awareness and mainstream multi-calamity impacts of climate-related disasters. Following the IPCC model, to address the consequences of numerous disasters on society, the development of a thorough method for evaluating vulnerability was done in the Philippines as part of disaster risk reduction efforts conducted by (Robielos, et. al. 2020). Also, (Perez, et al., 2022) investigated the evolution of drought in the Philippines based on an El Niño event using strategically selected drought indices driven by satellite-sourced data. Watershed-specific climate change vulnerability studies were also conducted, as well as crop-oriented susceptibility assessment to climate-risk crop-based climate risk vulnerability assessment and climate change impact investigation under different climatic hazards but do not specifically focus on droughts, rather more concerned with exhibiting multi-disaster vulnerability analysis.

The Cagayan Valley Region where the MRB is situated is identified to be one of the highly vulnerable regions in the Philippines (Yusuf & Francisco, 2009) where the Magat River Basin (MRB)

1 has been considered to be one of the 142 critical watersheds in the Philippines by the Department of
2 Environment and Natural Resources (DENR) and the majority of its area is under the protective
3 custody of the government to secure the health of the watershed. The DENR has been mandated to
4 steward the basin's 4,143,000,000 m² as a forest reserve and the National Irrigation Administration
5 has been given the authority to develop some 15,000 ha. for irrigation and agricultural purposes
6 (DENR, 2016). MRB harbors the infamous Magat Multi-Purpose Dam which plays a role in the
7 economic development of the communities inside the watershed. To put into perspective, the Magat
8 River Integrated Irrigation System (MARIIS) alone is servicing more than 86,000 ha. of rice fields
9 and farm-based aquaculture ponds. The vast extent of land is being cultivated, ergo, providing
10 opportunities for livelihood to farmers and fisherfolks and hence, making agriculture the primary
11 endeavor, catapulting the basin as a prominent contributor in making the Province of Isabela the 2nd
12 top rice-producing province in the Philippines.

13 As climate change-induced anomalies keep on getting worse, thus putting the agriculture
14 sector and dependent people at risk, the MRB is no stranger to such climatic hazards that affects all
15 the sectors and industry that benefits from its resources. and one of the most devastating climate-related
16 calamities is the occurrence of drought, a commonly occurring meteorological hazard in the
17 Philippines (Warren, 2018). Climate change transmutes the occurrence, duration, intensity, and extent
18 of drought. The slow-pacing onset of droughts can be observed and ranges from a considerable extent
19 of time from a few months to even a couple of years. Drought impact is location specific and it
20 challenges the stability of the basin to provide for its stakeholders. Drought is considered to be a real
21 problem in irrigated agriculture, especially rice which at the same time threatens the agricultural
22 capacity to support food security (Manalo et al., 2020). It is an emerging concern to reduce the
23 corresponding social and economic cost of drought and assessing the corresponding economic
24 damage should be made in evaluating the severity of drought impacts (Neri & Magaña, 2016).
25 However, there is no distinct way to address drought vulnerability. Studies on drought vulnerability
26 are quite diverse, and there is a lack of standardized methodology, consistent vulnerability
27 measurements, and a shared conceptual understanding of susceptibility. Many of these highlighted
28 the potential of merging the vulnerability and socio-economic hazard of a certain place in order to
29 satisfactorily assess the corresponding drought risk. The socio-economic factor is concerned with the
30 population of the area of interest, the cost of damage, the extent of lands affected, and the availability
31 of adequate water supply (Jia et al., 2015).

32 GIS-based methods are widely accepted and established to be a great tool not only in real-
33 time monitoring and detection capabilities but also in terms of data processing and calculation. GIS
34 handles input data, its storage, management, processing, and analysis up to the production of output
35 to be used in strategic frameworks and planning for risk and hazard mitigation and preparation. It fills
36 in a huge part in the development of highly essential maps, necessary for promoting social security
37 and emergency responses of the concerned agencies for the benefit of the stakeholders. (Karmakar,
38 2010). This study was conducted to benchmark and assess the impacts of climate change on the
39 vulnerability of the Magat River Basin to drought by considering agriculture as the major sector of
40 focus by employing a quantitative analysis of data available from concerned agencies and reports,
41 and by applying a site-specific an expert-judgment approach for agriculture derived from
42 (Hagenlocher et al., 2019; Macawile, et. al., 2018) but have been tailor-made to tackle the genuine
43 concern of the stakeholders and the real impact of drought branching from the decrease in the water
44 supply to the way it affects every individual in many ways. As there are no current drought analyses
45 specifically conducted for MRB, this study serves to be a pioneering approach in quantifying drought
46 impacts concerning the basin's vulnerability concerning agricultural socio-economic aspects. This
47 study uses the principles of the Analytic Hierarchy Process (AHP) and Entropy method of multi-
48 criteria decision-making to reliably appraise the corresponding weight of indicators in both subjective
49 and objective dimensions to appropriately assess the basin's sensitivity, exposure, and adaptive
50 capacity to drought. It was done using Geographic Information System (GIS) tools and techniques in
51 calculating and formulating vulnerability maps. For the benefit of catalyzing appropriate policy,
52 governance, and decisions, and to enhance the monitoring efforts for suitable site-mitigation measures
53 to be employed. This study will also include vulnerability projection which is explicitly affected by
54 the future changes in the rainfall regime which is estimated utilizing the RCP-based projection in the
55 Philippines that was generated using the Climate Information Risk Analysis Matrix (CLIRAM) tool
56
57
58
59
60
61
62
63
64
65

which was obtained from the Philippine Atmospheric, Geophysical and Astronomical Services Administration (PAGASA) that have been explicitly reporting the future changes in rainfall, temperature, sea level rise, and changes in tropical cyclone under different scenarios. (PAGASA, 2018).

Methods:

A. Site of the Study

The Magat River Basin (MRB) is located N 16° 09' – 17° 01'; E 120° 52' – 121° 48' and is situated south of the Cagayan River Basin, which is the main watershed in Luzon Island, Philippines. It is under the Type II category in terms of climate. MRB has an area of 4,306,820,000 m² of which 97% is situated in the province of Nueva Vizcaya, while parts of the province of Isabela and Ifugao encompass the remaining area. As a tributary of the great Cagayan River (Fig. 1.), the Magat River flows north-east from the Caraballo Mountain Ranges at about 135 km before converging with the Cagayan Main River at Naguillan Isabela. The major tributaries of the Magat River basin define its 7 sub-watersheds (Fig. 2) namely Ibulao, Alimit, and Lamut sub-watersheds in Ifugao province; Matuno, and Sta. Fe sub-watersheds in Nueva Vizcaya; and two unnamed watersheds which cover the Isabela Area where the Magat Dam is located, and adjacent is another unnamed watershed on the part of Nueva Vizcaya (UNESCO-IHP, 1995).

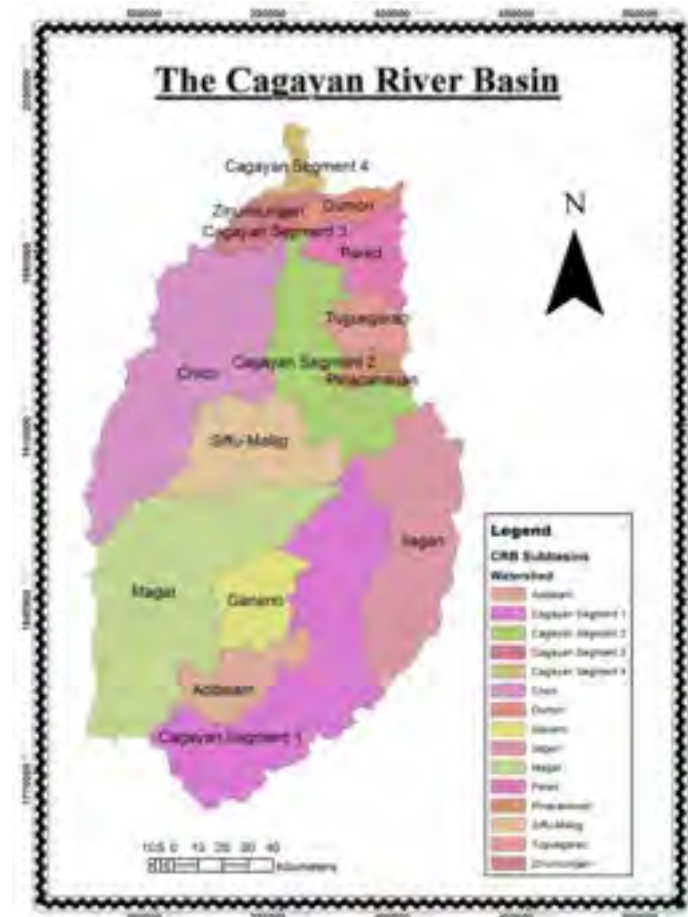


Fig. 1. Cagayan River Basin Sub-watersheds.



Fig. 2. Magat River Basin Sub-watersheds.

B. Data Acquisition and Analysis

The success of all drought vulnerability studies is dependent on the availability and quality of data. Data gathering might be the most difficult aspect or part of such studies but the adequacy of data determines the study output which will, later on, affect future policies that will be patterned based on the results generated from this research.

The vulnerability in this study was generally assessed per subbasin level. The data were gathered using survey questionnaires and readily available information from concerned agencies and published information from credible sources.

Rainfall

The rainfall data has been acquired thru collaboration with the Dam and Reservoir Division of the National Irrigation Administration. Further evaluation of the available data shows that there are 5 rainfall stations over the watershed that has an available precipitation record for the past 9 years which covers the 2014-2016 drought years (Official Gazette of the Republic of the Philippines, 2015) The other stations available were newly installed, while many stations considerably lack precipitation data for a long period making it unsuitable for the study.

The annual rainfall data were interpolated in terms of a geostatistical approach using GIS 10.8.1 where the kriging method was used to approximate the amount of rainfall per subbasin and the basis for the annual continuous dry days. It was done to approximate the unavailable climatic data over an area.

In order to set a baseline year where the average number of dry days and the duration of drought will be patterned, a 9-year Standardized Precipitation Index was used. SPI is one of the most common indices that is being employed in detecting meteorological drought from historical precipitation anomalies in a specific location. It can be utilized using as low as 1 month to a couple

of years of precipitation data. As with other climatic indicators, the time series of data used to calculate SPI does not need to be of a specific length. SPI fits historical precipitation data to a probability distribution to be transformed into a normal distribution. While other researchers identify an SPI value of less than -1 to indicate drought, no standard is imposed. Some can venture by choosing a threshold value less than zero to indicate relative drought occurrence (Svoboda & Fuchs, 2016) (WMO, 2012).

$$SPI = \frac{X_{ij} - \bar{x}_i}{\sigma_i} \tag{1}$$

where: X_{ij} is the rainfall for the i th and j th station observations, \bar{x}_i is the mean rainfall for the i th station and σ is the standard deviation for the i th station.

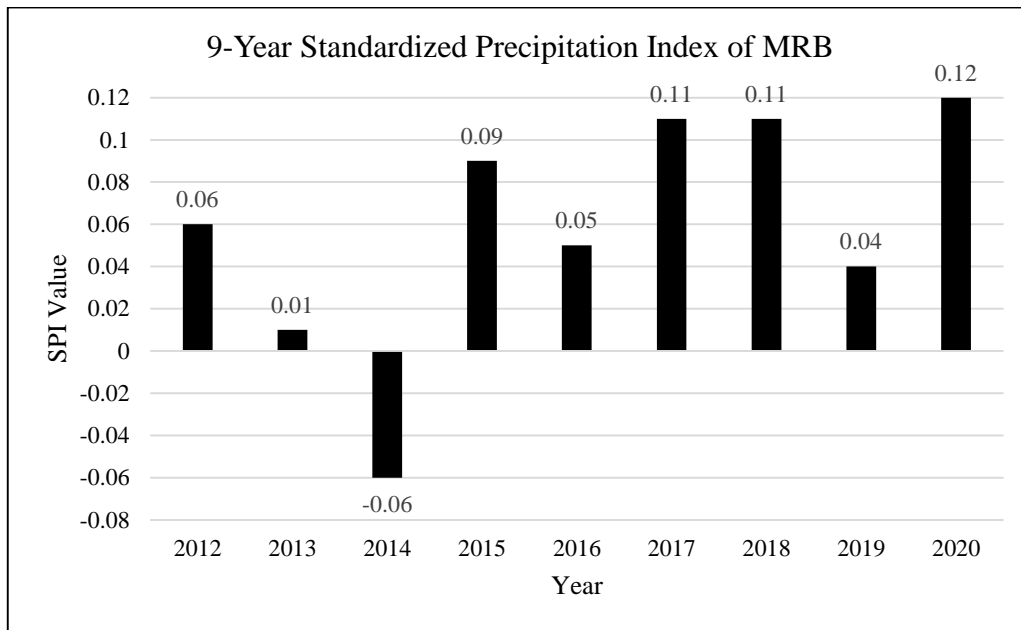


Fig. 3. 9-Year Standardized Precipitation Index of Magat River Basin

Land Cover and Stream Data

In order to assess the Land Use and Forest Cover Indicators, the latest up-to-date, 2015 Land Cover Dataset obtained from the National Mapping and Resources Information Authority (NAMRIA) where Landsat8 digital and visual image interpretation was used for land cover mapping, acquired from Earth Observing System's LandViewer (EOS). The stream data has been identified thru ocular field inspection and dialogue with the locals. The spatial data has been subjected to geoprocessing using GIS.

Planting Calendar and Service area of Irrigation System

In order to determine the plant growth stage at the onset of a drought, the general cropping calendar with respect to the type of climate, type 3 or in the case of MRB, and the quantity of agricultural land that is irrigation dependent. Data were gathered from the Department of Agriculture, the National Irrigation Administration where analysis was performed to consolidate and arrive at the required set of data requirements.

Field Data

While the climatic and farming aspect datasets are obtained thru coordination with concerned agencies and are available for public access online which includes several auxiliary data that support the main information. The majority of datasets that will be needed to qualify the indicators of corresponding components of vulnerability i.e. sensitivity, exposure, and adaptive capacity, were gathered thru field surveys where the farming households, as the primary stakeholders of the basin,

were the clientele of focus.

To gather the necessary information, the researchers conducted a survey in chosen localities per Subbasin from the 7th to the 8th of February, 2022. The survey was carried out to collect key drought risk information, such as economic losses caused by protracted drought, as well as existing interventions and adaptive measures that assist farmers in fulfilling crop and water demands, such as irrigation infrastructure and crop types. Furthermore, the survey represents the socioeconomic metrics employed in this study's analysis. Such information was employed to quantify the adaptation measures that are being undertaken, as well as to entice proper accounting of the basin's susceptibility and exposure to drought from an agro-economic standpoint.

C. Vulnerability Assessment Work Flow

The purpose of this study is to generate a solid and meaningful output that will aid in the creation of effective policies and actions to manage drought risk and avert human, socioeconomic, and environmental harm. To assist individuals and technical authorities in performing related investigations in mitigating possible dangers by offering benchmarking methodology and findings to supplement their efforts.

Figure 3. shows the workflow of the study in generating the vulnerability map of the Magat River Basin using Geographic Information System (GIS) tools and procedures.

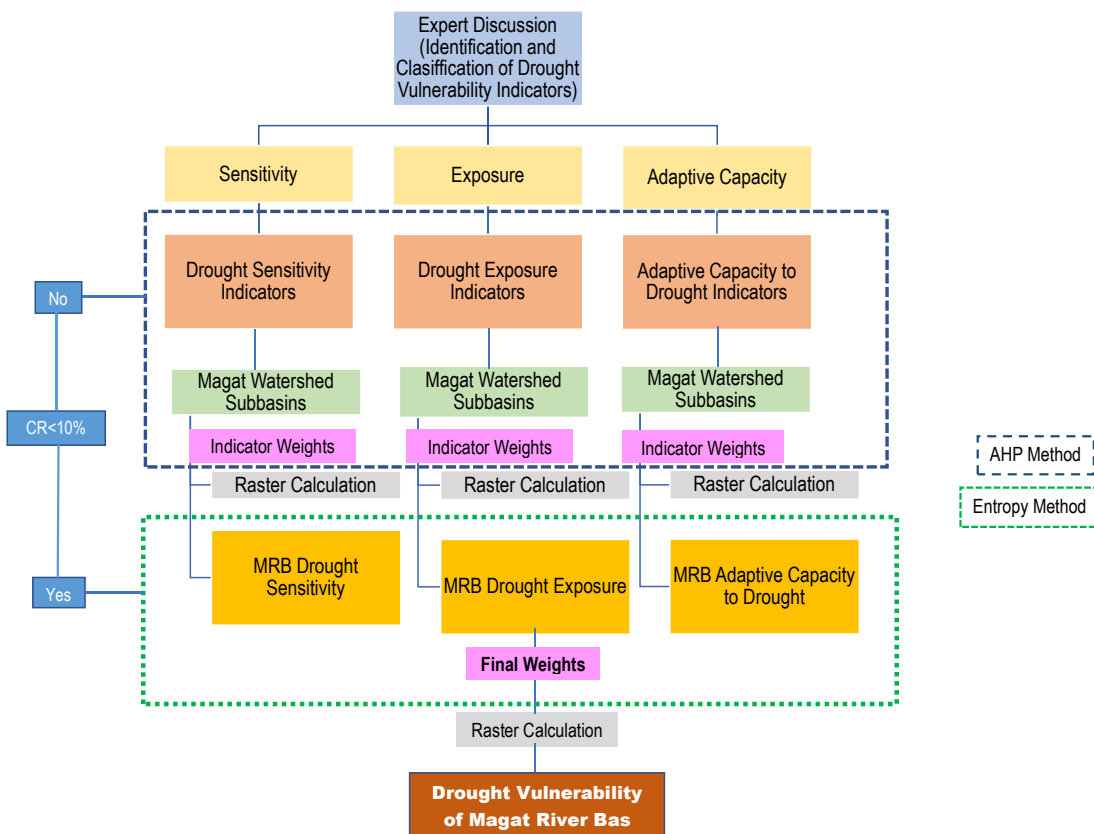


Fig. 4. Drought Vulnerability Flow Chart

C.1. Calculation of the Weight of Indicators

The weight of each component of vulnerability was subjected to both subjective and objective Multi-Criteria Decision Analysis (MCDA) in order to carefully account for the respective contributory factor of indicators in the total vulnerability of MRB. For hazard and disaster-related studies (Li, et.al., 2022; Sahana, et. al., 2021; Liu, et. al., 2019; Zeng and Huang, 2018) involving multi-criteria analysis, two of the most frequently employed methods for weight estimation are the analytic hierarchy process (AHP) (Saaty, 1980), to and Entropy Weighting Method (Zhu, et. al., 2020).

Palchaudhuri and Biswas (2016) coupled AHP and GIS in assessing the drought risk in India.

Similarly, AHP was employed in this study to establish pairwise comparison matrices among the indicators of drought dimensions to synthesize the vehemence of indicators against each other based on Saaty's scale of relative importance (Table 1). Separate analyses were conducted for each of the dimensions of vulnerability (Sensitivity, Exposure, and Adaptive Capacity) to determine the respective weight of indicators based on pairwise comparisons. Here, the idea is to determine the level of sensitivity, exposure, and adaptive capacity of the MRB subbasins using the indicators of the dimensions of vulnerability. In generating the sensitivity, exposure, and adaptive capacity maps of MRB, a reliable weighting coefficient for each indicator is needed to how an indicator is more important or of lesser importance than the other indicators.

Table 1. Saaty's Scale of Relative Importance (Saaty, 2008).

| Intensity of Importance | Definition | Explanation |
|-------------------------|---|---|
| 1 | Equal Importance | Two activities contribute equally to the objective |
| 2 | Weak or Slight | |
| 3 | Moderate Importance | Experience and judgment slightly favor one activity over another |
| 4 | Moderate Plus | |
| 5 | Strong Importance | Experience and judgment strongly favor one activity over another |
| 6 | Strong Plus | |
| 7 | Very Strong or Demonstrated Importance | An activity is favored very strongly over another; its dominance demonstrated in practice |
| 8 | Very, very strong | |
| 9 | Extreme Importance | The evidence favoring one activity over another is of the highest possible order of affirmation A reasonable assumption |
| Reciprocals of above | If activity <i>i</i> has one of the above non-zero numbers assigned to it when compared with activity <i>j</i> , then <i>j</i> has the reciprocal value when compared with <i>i</i> | |
| 1.1-1.9 | If the activities are very close | May be difficult to assign the best value but when compared with other contrasting activities the size of the small numbers would not be too noticeable, yet they can still indicate the relative importance of the activities. |

Table 2. Resulting Weight of Indicators Based on Pairwise Comparisons. a.) Sensitivity b.) Exposure c.) Adaptive Capacity

a.)

| Category | Weight | Rank |
|--------------------------------|--------|------|
| 1 Number of dry days | 24.60% | 2 |
| 2 Percent Forest Cover | 10.00% | 5 |
| 3 Type of River | 2.90% | 7 |
| 4 Continuous Dry Days | 30.90% | 1 |
| 5 Land Use/ Land Cover | 13.60% | 3 |
| 6 Plant Growth Stage | 12.70% | 4 |
| 7 Land Dependent on Irrigation | 5.30% | 6 |

b.)

| Category | Weight | Rank |
|--|--------|------|
| 1 Rainfall | 16.50% | 3 |
| 2 Average max temperature | 7.00% | 6 |
| 3 Income Loss | 28.20% | 1 |
| 4 Extent of production area 2 droughts | 3.70% | 7 |
| 5 Yield loss | 25.70% | 2 |
| 6 Agriculture Dependent Families | 8.30% | 5 |
| 7 Drought Duration | 10.60% | 4 |

c.)

| Category | Weight | Rank |
|---|--------|------|
| 1 Availability of irrigation program | 30.80% | 1 |
| 2 Available Maps of drought-prone area | 3.00% | 9 |
| 3 Total farmers doing crop diversification. | 9.10% | 4 |
| 4 Access to crop insurance, loans, or subsidies | 7.70% | 6 |
| 5 Access to drought forecasting information | 4.70% | 7 |
| 6 Cloud seeding program (Coverage) | 2.40% | 10 |
| 7 Farmers with diversified livelihood | 17.30% | 2 |
| 8 Access planting calendar and other info. | 4.00% | 8 |
| 9 Average expenditure for agriculture programs | 13.30% | 3 |
| 10 Farmers using drought-resistant varieties | 7.70% | 5 |

AHP was employed to evaluate the significance of the indicators in influencing the respective dimensions of drought vulnerability. The weight coefficients will be determined using a pairwise comparison matrix which will be normalized. The weight vector (\mathbf{w}) is calculated using the formula (Ahamed, et.al., 2000; Liang and Yang, 2022)

$$A = [a_{ij}], i, j = 1, 2, 3, \dots, n. \quad (2)$$

where \mathbf{A} is the pairwise comparison matrix and a_{ij} is the ratio w_i/w_j which shows the degree to which the w_i indicator is greater than w_j indicator.

The weighting coefficient vector (\mathbf{w}) is determined by the formula;

$$A\mathbf{w} = \lambda_{\max} \mathbf{w} \quad (3)$$

λ_{\max} is the maximum eigenvalue of, matrix \mathbf{A} .

In determining the reliability of the pairwise comparison matrix, the Consistency Ratio (CR) is calculated using the formula;

$$CR = CI/RI \quad (4)$$

where CI is the consistency Index and is given by the formula, $\frac{(\lambda_{max} - n)}{(n-1)}$; n = number of the compared indicators. And RI is the Random Index that is based on the structure of matrix **A** (Saaty, 1980)

The computed CR of the respective drought vulnerability dimensions is less than the acceptable CR value of less than 0.1 (10%). Resultingly, the Sensitivity Dimension has a CR percentage value of 6.3%. And 7.3% and 8.1% for Exposure and Adaptive Capacity, respectively. This implies that the weights are reliable and can be considered in the analysis. The generated weight assigned to the different indicators was then incorporated into the raster calculation formula in GIS to quantify the final Sensitivity, Exposure, and Adaptive Capacity rating of MRB to drought. For a more comprehensive understanding of the AHP process, the reader is referred to (Saaty, 1980; Vargas, 1990; Saaty, 2008)

In obtaining the final weights for the dimensions of vulnerability, this study employs the Entropy method, an objective, comprehensive, and widely used method of weighting the components of vulnerability by circumventing human influence. This measures the degree of variance in order to assess value. The greater the deviation of the measured value, the higher the level of differentiation of the indicator and the more information that may be extracted. (Taheriyoun, et al., 2010)

The method starts by standardizing the measured values of each vulnerability dimension with respect to each subbasin obtained using the AHP method. Here, the categories of vulnerability are Sensitivity (S), Exposure (E), and Adaptive Capacity (AC).

$$R_{ij} = \frac{X_{ij}}{\sum_{i=1}^m X_{ij}} \quad (6)$$

where: X_{ij} is the measured value of the i^{th} indicator in the j^{th} sample and R_{ij} denotes the standardized value of the i^{th} value in the j^{th} sample.

The entropy index formula is given by:

$$E_i = -k \sum_{i=1}^n f_{i,j} \log f_{i,j} \quad (7)$$

Where k is $\frac{1}{\ln n}$, and n is the number of alternatives. $f_{i,j} = \frac{R_{ij}}{\sum_{i=1}^m R_{ij}}$

The weight calculation (W_i) is represented by: \

$$W_i = \frac{1 - E_i}{\sum_{i=1}^m (1 - E_i)} \quad (8)$$

where: W_i is the weight of the evaluated category and $(1 - W_i)$ is the degree of diversity.

Here, $0 < W_i < 1$. And the $\sum_{i=1}^m W_i = 1$.

C.2. Calculation of Vulnerability

Vulnerability is determined by the kind, amount, and pace of climatic change and fluctuation to which a system is subjected or exposed, as well as the sensitivity and adaptive capacity of the system. Exposure and Sensitivity are identified to be the implicit impact or corresponding influence of drought and adaptive capacity serves as an opposing dimension that covers the coping mechanism and defense mechanism of the system.

And the overall value of Sensitivity, Exposure, and Adaptive Capacity components was also calculated using Raster Calculator in GIS. Since the respective drought indicators have corresponding ranks and scales, the respective value of the drought vulnerability component is equal to the mean of the rating/rank of its corresponding indicators.

$$\text{Sensitivity; Exposure; AdaptiveCapacity} = \frac{\sum_{i=1}^n I_i}{n} \quad (9)$$

where: I_i is the indicator with respect to the drought vulnerability component and n is the number of indicators under each drought vulnerability component.

For this study, the vulnerability of the MRB was computed using the Raster Calculator Spatial Analysis tool in GIS by employing the formula that was used by (Shim, et al., 2021; Liu. et. al., 2013)

$$V = S (W_S) + E (W_E) - AC (W_{AC}) \quad (10)$$

where V is the vulnerability, S is the sensitivity, E is the exposure, AC is the adaptive capacity, and W_S ; W_E ; W_{AC} is the computed weight of the dimensions of vulnerability.

D. Assessment of Drought Indicators

From local to global dimensions, indicator-based techniques have been pushed as valuable tools for assessing, comparing, and monitoring the complexity of drought risk (Hagenlocher, et al., 2019).

The basin's vulnerability has been carefully attributed to three categories: Sensitivity, Exposure, and Adaptive Capacity (Cui, et al., 2010) which is adapted to the concept of vulnerability of the Intergovernmental Panel on Climate Change. Each category has taken into account the best indicators that will succinctly represent each category. The agriculture sector has been the main sector of focus since a considerable number of studies in developing frameworks, methods, and the selection of indicators have been conducted considering agricultural aspects (Shim, et al., 2021) There is no standard for identifying hazard vulnerability indicators, it is always affected by the specific characteristics that govern the local system (Zarafshani. Et al., 2016). Hence, the indicators were formulated based on an expert-judgment approach from the global expert survey results report by (Meza, et al., 2019) of the European Commission which includes relevant indicators for agricultural systems, which have been modified to select the indicators that are uniquely applicable to Magat River Basin.

D.1. Sensitivity

Sensitivity is consistently defined as the factor by which a certain system is positively or negatively affected by drought. Or in simple terms, sensitivity pertains to the environment since it includes social, economic, and ecological conditions driven by drought hazards. A higher sensitivity value of a system is equivalent to a higher exposure it will be subjected leading to a higher vulnerability.

For MRB, the sensitivity indicators were analyzed according to class and given a rating or rank, where the highest sensitivity rating is five (5) and one (1) as the lowest. Table 3 shows the different sensitivity indicators used in this study.

Table 3. Drought sensitivity Indicators.

| Sensitivity | | | |
|---|------------|--------|-----------|
| Indicator | Class | Rating | Scale |
| a. Number of continuous dry days (Annual Average) | >72 days | 5 | Very High |
| | 48-72 days | 4 | High |
| | 30-48 days | 3 | Moderate |
| | 6-30 days | 2 | Low |
| | <6 day | 1 | Very Low |
| b. Percent forest cover (%) | ≤ 20 | 5 | Very High |
| | 21-40 | 4 | High |
| | 41-60 | 3 | Moderate |
| | 61-80 | 2 | Low |

| | | | | |
|----|------------------------|-----------------------|---|-----------|
| | | >80 | 1 | Very Low |
| 1 | | Upland agriculture | | |
| 2 | | and settlements | 5 | Very High |
| 3 | b. Landuse | Pasture and grazing | | |
| 4 | | lands | 4 | High |
| 5 | | Agroforestry | 3 | Moderate |
| 6 | | Plantation forest | 2 | Low |
| 7 | | Natural forest | 1 | Very Low |
| 8 | | | | |
| 9 | | | | |
| 10 | | None | 5 | Very High |
| 11 | e. Type of rivers or | Ephemeral | 4 | High |
| 12 | streams | Intermittent | 3 | Moderate |
| 13 | | Perennial (1 only) | 2 | Low |
| 14 | | Perennial (2 or more) | 1 | Very Low |
| 15 | | | | |
| 16 | | | | |
| 17 | | Seedling stage | 5 | Very High |
| 18 | f. Plant growth stage | Maturing stage | 4 | High |
| 19 | at the time of drought | Flowering stage | 3 | Moderate |
| 20 | | Fruiting stage | 2 | Low |
| 21 | | | | |
| 22 | | | | |
| 23 | | Harvesting stage | 1 | Very Low |
| 24 | | | | |
| 25 | | | | |
| 26 | | | | |
| 27 | g. Dependence on | >80 | 5 | Very High |
| 28 | irrigation (% of | 61-80 | 4 | High |
| 29 | agricultural lands | 41-60 | 3 | Moderate |
| 30 | dependent on | 21-40 | 2 | Low |
| 31 | irrigation) | <20 | 1 | Very Low |
| 32 | | | | |
| 33 | | | | |
| 34 | | | | |
| 35 | h. Duration of | >2 | 5 | Very High |
| 36 | drought, No. of | 1-2 | 3 | Moderate |
| 37 | Months | <1 | 2 | Low |

D.2. Exposure

The inclusion of Exposure to previous and recent drought studies is always being done. The intensity, duration, or frequency of stress on a system is measured by exposure. From the term alone, exposure pertains to the state to which a certain system is exposed or remains in a condition to be affected by consequential drought.

This study utilizes drought exposure indicators (Table 4) in order to evaluate the exposure category of vulnerability in MRB.

Table 4. Drought Exposure Indicators

| Exposure | | | | |
|-----------------|---------------|--------|---------------------|--|
| Indicator | Class | Rating | Scale | |
| | <1,500 | 5 | Very High | |
| a. Rainfall, mm | 1,501 – 2,000 | 4 | High | |
| | 2,001 – 2,500 | 3 | Moderate | |
| | 2,501 – 3,000 | 2 | Low | |
| | >3,000 | 1 | Very Low | |
| | | | | |
| b. Temperature | >35 | 5 | Very high | |
| | 25-35 | 2 | Low (Most Suitable) | |

| | | | | |
|----|------------------------|-------|---|------------------------------------|
| | | <25 | 3 | Moderate (Secondarily Suitable) |
| 1 | | | | |
| 2 | | >80% | 5 | Very High |
| 3 | c. Extent of | 61-80 | 4 | High |
| 4 | production areas | 41-60 | 3 | Moderate |
| 5 | affected, (%) | 21-40 | 2 | Low |
| 6 | | | | Y7Very Lowu4 |
| 7 | | ≤20 | 1 | |
| 8 | | | | |
| 9 | | | | |
| 10 | | >40 | 5 | Very High |
| 11 | d. Yield losses due | 31-40 | 4 | High |
| 12 | to drought (%) | 21-30 | 3 | Moderate |
| 13 | | 11-20 | 2 | Low |
| 14 | | ≤10 | 1 | Very Low |
| 15 | | | | |
| 16 | | >40 | 5 | Very High |
| 17 | e. Income loss from | 31-40 | 4 | High |
| 18 | production, (%) | 21-30 | 3 | Moderate |
| 19 | | 11-20 | 2 | Low |
| 20 | | ≤10 | 1 | Very Low |
| 21 | | | | |
| 22 | | >40 | 5 | Very High |
| 23 | f. Number of | 31-40 | 4 | High |
| 24 | agriculture-dependent | 21-30 | 3 | Moderate |
| 25 | families affected, (%) | 11-20 | 2 | Low |
| 26 | | ≤10 | 1 | Very Low |
| 27 | | | | |
| 28 | | >2 | 5 | Very High |
| 29 | g. Duration of | 1-2 | 3 | Moderate |
| 30 | drought, No. of | <1 | 2 | Low |
| 31 | Months | | | |

D.3. Adaptive Capacity

Vulnerability is composed of positive and negative dimensions. Positive is the Sensitivity and Exposure factor since they are the positive effects of drought on the vulnerability of the system, and negative is the adaptive capacity since it is the counter measure in mitigating possible drought consequences. Or in other words, adaptive capacity pertains to the coping mechanism and response of the system to lower or lessen the potential impacts of drought. It includes the construction or irrigation facilities, the introduction of crop-resistant varieties, cloud seeding, etc. whose ultimate aim is to alleviate drought implications.

Modern vulnerability studies consider the concept of adaptive capacity as the most important factor that separates it from earlier studies concerning climate-related vulnerability. It is said to be mainly defined by social, economic, and biophysical processes. The Adaptive Capacity Indicators in this study are shown in Table 5

Table 5. Adaptive Capacity Indicators.

| Adaptive Capacity | | | |
|-------------------|-------|--------|--|
| Indicator | Class | Rating | Scale (Against Potential Drought Impact) |

| | | | | |
|----|---|----------------------|---|-----------|
| 1 | a. Availability of small-scale irrigation program | Available | 1 | Very High |
| 2 | | Partially Available | 3 | Moderate |
| 3 | | Not Available | 5 | Very Low |
| 4 | | | | |
| 5 | | Available | 1 | Very High |
| 6 | b. Maps of drought Prone Areas | Partially Available | 3 | Moderate |
| 7 | | Not Available | 5 | Very Low |
| 8 | | | | |
| 9 | | | | |
| 10 | | >40 | 1 | Very High |
| 11 | c. Percentage of | 31-40 | 2 | High |
| 12 | the total number of farmers doing | 21-30 | 3 | Moderate |
| 13 | crop diversification practices | 11-20 | 4 | Low |
| 14 | | <10 | 5 | Very Low |
| 15 | | >40 | 1 | Very High |
| 16 | | | | |
| 17 | | | | |
| 18 | | | | |
| 19 | d. Access to crop insurance, loans, or subsidies | 31-40 | 2 | High |
| 20 | | 21-30 | 3 | Moderate |
| 21 | | 11-20 | 4 | Low |
| 22 | | <10 | 5 | Very Low |
| 23 | | | | |
| 24 | | | | |
| 25 | e. Access to drought forecasting information and early warning system, AWS or AGROMET station | Accessible | 1 | Very High |
| 26 | | Partially Accessible | 3 | Moderate |
| 27 | | Not Accessible | 5 | Very Low |
| 28 | | | | |
| 29 | | | | |
| 30 | | | | |
| 31 | f. Cloud seeding program (Coverage) | Covered | 1 | Very High |
| 32 | | Partially Covered | 3 | Moderate |
| 33 | | Not Covered | 5 | Very Low |
| 34 | | | | |
| 35 | | | | |
| 36 | | >40 | 1 | Very High |
| 37 | g. Percentage of the total farmers with diversified livelihood practices | 31-40 | 2 | High |
| 38 | | 21-30 | 3 | Moderate |
| 39 | | 11-20 | 4 | Low |
| 40 | | <10 | 5 | Very Low |
| 41 | | | | |
| 42 | | | | |
| 43 | | >40 | 1 | Very High |
| 44 | h. Access planting calendar bulletins and other relevant information | 31-40 | 2 | High |
| 45 | | 21-30 | 3 | Moderate |
| 46 | | 11-20 | 4 | Low |
| 47 | | <10 | 5 | Very Low |
| 48 | | | | |
| 49 | | | | |
| 50 | | | | |
| 51 | i. Average expenditure (% of the total budget) for agricultural programs for drought-prone areas for the past 5 years | >40 | 1 | Very High |
| 52 | | 31-40 | 2 | High |
| 53 | | 21-30 | 3 | Moderate |
| 54 | | 11-20 | 4 | Low |
| 55 | | <10a | 5 | Very Low |
| 56 | | | | |
| 57 | | | | |
| 58 | | >40 | 1 | Very High |
| 59 | j. Use of drought-resistant crop varieties (% of total farmers) | 31-40 | 2 | High |
| 60 | | 21-30 | 3 | Moderate |
| 61 | | 11-20 | 4 | Low |
| 62 | | <10 | 5 | Very Low |
| 63 | | | | |
| 64 | | | | |
| 65 | | | | |

Projected Changes in Exposure

In order to make projections on the future climatic trend in the basin, the RCP-based projections that were requested from DOST-PAGASA were used. The projections available in the Philippines that were generated using the Climate Information Risk Analysis Matrix (CLIRAM) tool that has been explicitly included in the report are changes in rainfall, temperature, sea level rise, and changes in tropical cyclone (DOST-PAGASA, 2018). It was based on the IPCC AR5 where climate scientists, modelers, and experts collaboratively catalyzed resolution-based datasets that have been downscaled on a 0.5x0.5 grid resolution (including land use data, air pollutants, etc.). The IPCC Expert Panel has chosen four scenarios based on radiative forcing level as influenced by greenhouse gasses emissions and other contributory agents. For this study, we considered the RCP 4.5, a scenario that reaches a peak radiative forcing of 4.5 W/m² (2040) which declines and stabilizes in the year 2100 since it is the scenario that is most likely to happen considering the trajectory of climatic and emission trend that is observed in the Philippines and the adaptive measures that are being promulgated. Also, the RCP 8.5 where the radiative forcing exceeds 8.5 W/m² by 2100 and will progressively increase with the same amount of time (van Vuuren, et al., 2011).

The location of rainfall gauging stations over the Magat Watershed are strategically located in different provinces. The downscaled (provincial-level) seasonal projections as provided by the CLIRAM tool was used to estimate the projected rainfall in the year 2036-2065 Mid-21st century and 2070 to 2099 Late-21st Century.

Results

From the survey conducted, the response of the farmers ranging from ages 33-75 years old has been gathered to further establish the sensitivity, exposure, and adaptive capacity of the study area. The farmer respondents, of which 26% are female, all registered an additional source of income mainly backyard livestock farming (e.g. native chicken, pigs, duck, small ruminants, cattle). 1/3 of the farmers said that they have a secondary income that supports them aside from farming.

The farmer respondents that we have considered are using 3 main commodities e.g. rice, corn, tobacco, and a considerable number of them venture into high-value vegetable crops. For corn, the average yield loss is tallied at 20% to as much as 60% in highly exposed areas. For rice, an average of 35% yield loss was also estimated based on the response of the farmers and the comparison of crop yield during normal cropping season to drought season. Tobacco farmers, however, incur some significant 30% to 60% yield and income loss when facing severe droughts even if they use drought-resistant varieties. For vegetable/High-Value Crop farmers, it was estimated that 20% of their normal income is being reduced during drought season, or in some isolated cases, damage crop does not do well under stressed conditions that they abort farming for that particular season, rendering them a 100% loss of income.

From the results of the survey conducted, it has also been found that only 21% of the farmer-respondents have confirmed that they have crop insurance and only 42% are using drought-resistant varieties. All of the farmers positively affirmed that they have access to forecasting and AGROMET stations and more than 95% of them undergo crop diversification practices.

Most of the farmers (95%) have access to irrigation facilities where a considerable number of such irrigation sources are privately owned e.g. deep well for tobacco, vegetable, and some rice farmers.

Sensitivity

The raster data from NAMRIA has been subjected to GIS processing in order to acquire the needed land cover information in assessing the land use of the MRB. The rating of every respective subbasin is not far from the basin's sensitivity rating of 3.6 which takes place from Moderate to High on the Sensitivity Scale. This is due to the fact that the primary endeavor in the basin is agriculture

with the corresponding settlements of communities (Very High) and which also engage in livestock and pastures (High) that raise the sensitivity in terms of land use into such scale but however countered by the vast extent of forest areas.

In terms of the Percentage of Forest Cover, the MRB's rating is 2.85 or between the Low to Moderate Sensitivity Scale. Subbasin 2 has a High sensitivity since it only has 21-40% of forest cover, it is true since part of the land area is developed for agricultural purposes as part of the 86,000 ha of the irrigated service area of the Magat River Integrated Irrigation System (MARIIS). Ibulao and Matuno subbasins, however, have a very low sensitivity to drought which is attributed to more than 80% of its area being covered by forest and in the mountainous zone of Ifugao. Alimit is under some 41-60% of forest lands (Moderate), and Lamut Subbasin has very low drought sensitivity having a 61-80% of forest overlain its terrain.

The MRB has a very low sensitivity to drought in terms of the type of streams available. The presence of a perennial type of stream has been identified by field visits and ocular inspection supported by the responses of the locals verifying a year-long stream flow which has a corresponding rating of sensitivity rating of 1 (very low).

The plant growth stage during the occurrence of drought was evaluated using 2014 as the year of basis. For ease of assessment, the crop growth stages of major commodities per province have been considered. The general cropping calendar of the provinces with respect to its crop commodities i.e. Rice, Yellow Corn, and High-Value Crops like Cabbage and Potato. Alimit, Ibulao, and Lamut Subbasins have been identified to be subjected to a High Sensitivity rating based on our data gathering and assessment, since the majority of the crops have been affected by drought during its maturity stage, while the Subbasin 2, Matuno, Sta. Fe, and Subbasin 1 were rated at 5 (Very High).

The percentage of agricultural lands dependent on agriculture has been evaluated using the readily available online data of irrigation systems and facilities and their service area access thru the respective websites of NIA Irrigation Management Offices. The assessment indicates that 80% of the agricultural areas are dependent on irrigation. This is true since rice fields are prevalent over the basin where irrigation supply relies on conventional surface irrigation and pumping wells. Subbasin 2 alone has over 860,000,000 m² of rice fields supplied by water diverted from the Magat Dam, excluding those crop varieties that are being supplied from other sources. The Ifugao and Nueva Vizcaya areas also have newly built and improved irrigation facilities making about 80% of the agricultural areas to be dependent on irrigation.

The corresponding rating of each subbasin with respect to the given indicator was used in generating a raster map of all drought sensitivity indicators. The sensitivity to the drought of MRB Basin has been computed using the Raster Calculator, a spatial analyst tool, in GIS

The overall drought sensitivity rating of Magat River Basin is calculated to be in a range of 2.597 to 4.757 (Moderately low to Very High) as shown in Fig.5. Subbasin 2 is the most sensitive to drought having a sensitivity rating of 4.68, followed by Sta. Fe with a 4.26 rating. Ibulao Subbasin is the least susceptible to drought having a rating of 2.81 (Low-Moderately Vulnerable). While the other Subbasins are above the moderate and concurrently approaching the High Drought Vulnerability Scale of 4.

1
2
3
4
5
6
7
8
9
10
11
12
13
14
15
16
17
18
19
20
21
22
23
24
25
26
27
28
29
30
31
32
33
34
35
36
37
38
39
40
41
42
43
44
45
46
47
48
49
50
51
52
53
54
55
56
57
58
59
60
61
62
63
64
65

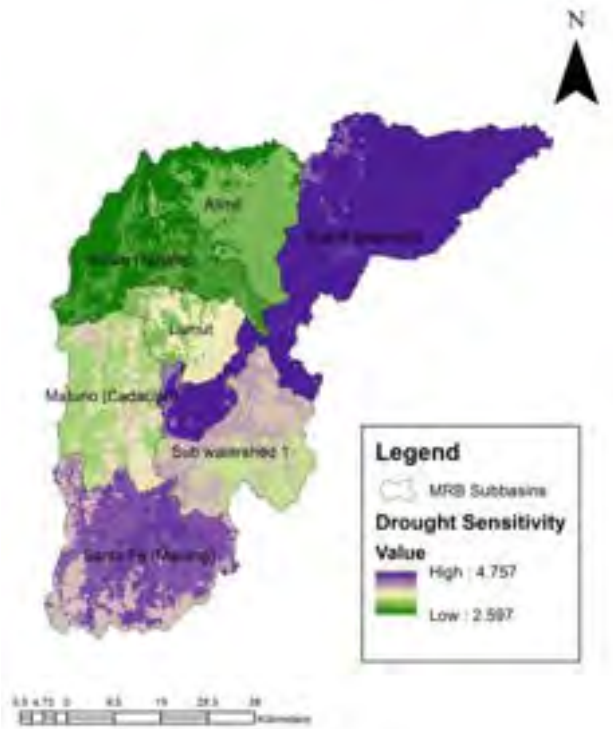


Fig. 5. Drought Sensitivity Map of Magat River Basin.

Exposure

In calculating the current sensitivity of the Basin, the 9-year Standardized Precipitation Index (Fig.4) implies that 2014 was relatively dry in comparison to the other years. The mean annual rainfall harnessed from the Rainfall Stations over the Magat River Basin has a rating of 3.71 or less than 2000 mm whereas Santa Fe and Subbasin 2 have an annual rainfall of less than 1500 mm which in Drought Sensitivity Scale is Moderate to High. The continuous dry days for the entire MRB having the 2014 drought as a baseline has lasted for 42-72 days which is classified to be in a High where Subbasin 2 and Santa Fe Subbasin recorded more than 72 days without rainfall (Very High); Ibulao and Alimit Subbasin sustained 30-48 days of no rainfall (Moderate), and Lamut and Subbasin 1 falls on a High Sensitivity Scale having been experience a 42-72 days of no rainfall.

Table 6. Monthly Cumulative Rainfall Data of MRB.

| 2014 | BANAUE (mm) | DUPAX (mm) | HALONG (mm) | IMUGAN (mm) | MAGAT (mm) |
|------|----------------|---------------|----------------|----------------|---------------|
| Jan | 0.0 | 0.0 | 0.0 | 0.0 | 91.0 |
| Feb | 67.8 | 1.2 | 176.6 | 2.0 | 0.0 |
| Mar | 74.8 | 0.8 | 111.4 | 0.6 | 29.0 |
| Apr | 283.2 | 1.8 | 236.2 | 109.0 | 33.0 |
| May | 363.0 | 4.2 | 170.2 | 124.4 | 275.0 |
| Jun | 197.4 | 0.6 | 206.4 | 297.6 | 35.0 |
| Jul | 311.4 | 129.2 | 240.6 | 268.0 | 137.0 |
| Aug | 338.8 | 5.4 | 209.8 | 370.4 | 109.0 |
| Sep | 367.4 | 0.0 | 454.0 | 509.2 | 109.0 |
| Oct | 383.8 | 356.8 | 403.6 | 161.8 | 109.0 |
| Nov | 227.0 | 53.0 | 244.0 | 68.8 | 60.0 |
| Dec | 0.0 | 0.0 | 0.0 | 0.0 | 91.0 |

1 The survey implies that the basin's exposure to drought has a mean value of 3.4 for the entire MRB
2 or up to 40% of the total area. Results of analyses also imply that about 70% of the agricultural
3 production areas have been affected by drought occurrences where Alimit, Ibulao, Ibulao, Lamut, and
4 Matuno Subbasins have 41-60% (moderately exposed to drought) of the respective production areas
5 affected by drought while Subbasin 1 and 2, and Sta. Fe Subbasins have a high drought exposure of
6 61-80% in terms of production areas affected.

7 Yield and income losses for the whole MRB were estimated at about 30%. The Santa Fe and
8 Subbasin 1, from consolidating farmer response, lose 31-40% of yield and income compared to
9 production years without drought. Subbasin 2 however, having the Magat Dam as their main source
10 of irrigation support, accounted for 11-20% losses (very low). The remaining subbasins have an
11 estimated 21-30% loss which is considered to be moderately exposed to drought.

12 The number of agriculture-dependent families or families having agriculture as their main
13 source of livelihood and income is quite high. Lamut, Subbasin 2, and Subbasin 1, from the results
14 of the survey, house 40% of families that are highly depended on agriculture. And respected 15-30%
15 of agriculture-dependent families for each of the other subbasins which are in the scale of low to
16 moderated exposure to drought in terms of a number of agriculture-dependent families indicators.

17 The corresponding rating of each subbasin with respect to the given indicator was used in
18 generating a raster map of all drought exposure indicators. The exposure to the drought of the Magat
19 River Basin has been computed using the Raster Calculator, a spatial analyst tool, in GIS.

20 In terms of the duration of drought, the Magat River Basin as a whole experienced drought
21 for 1-2 months making it moderately sensitive to drought in terms of drought duration indicator.

22 Subbasin 1, Subbasin 2, Matuno, and Santa Fe have an average drought exposure value of
23 3.75, 3.38, 3.46, and 3.67, respectively which is more than the moderate scale while the other
24 subbasins are found to be in between low and moderate drought exposure merits. The overall drought
25 exposure value of MRB is ranging from 2.76 – 3.75 (Fig. 6) which identifies the basin to be
26 moderately exposed to drought events.



56 Fig. 6. Drought Exposure Map of Magat River Basin.

57 **Adaptive Capacity**

58 From the conducted survey and data gathering, it was determined that each subbasin has an
59 available irrigation system or water-impounding reservoir, making the MRB relatively low in terms
60 of potential impact. Some published reports from the respective NIA IMOs also show the
61
62
63
64
65

rehabilitation and newly installed irrigation projects which can be found inside the zone of each subbasin.

1 Crop diversification practices are also in a way being observed but not quite radical in
2 comparison to the conventional practice of cropping patterns. 21-30% of the farmers from Alimit,
3 Ibulao, and Lamut Subbasins are doing some diversification and planting new crop varieties to
4 explore opportunities of having a bigger profit. While there are 15% of farmers in Subbasin 1,
5 Matuno, and Sta. Fe subbasins that are doing crop diversification practices. Subbasin 2 only has less
6 than 10% of farmers doing crop diversification practice since the cropping patten of planting a legume
7 crop after 2 cropping of rice is the conventional practice that is being observed since most of the
8 agricultural production areas are rice fields. And in terms of maps of drought-prone areas, the
9 available maps are not area specific but presented to be in general as part of a wider regional basis so
10 a “partially available” classification has been expertly assigned to it.

11 Moreover, from the survey, in terms of farmers' access to crop insurance and subsidies, there
12 is a relatively low risk of the potential impact of drought since about 40% of the farmers confirmed
13 that they are eligible for subsidies and are registered for crop insurance programs where subbasin 2
14 have more than 45% of farmers having their rice fields insured and have access to previous and future
15 subsidies. And the other subbasins have about 25-40% of farmers with access to crop loans, insurance,
16 and subsidies. It is also manifested in the results of the data gathering from available sources (47-48)
17 and survey that more than 40% of the total budget of agriculture are being utilized for drought
18 response programs in order to alleviate the suffering of the farmers in terms of severely dry climate.

19 The majority of the farmers also claim that they have access to weather information from
20 AGROMET stations being broadcast and circulated locally. Also, in the case of those that are being
21 supplied by the National Irrigation System are observing a proper cropping calendar and since the
22 MRB has a type 2 climate the farmers follow a traditional cropping calendar for high-value crops. It
23 also included the service of the concerned agencies by providing cloud seeding programs and from
24 the study, the MRB was partially covered with cloud seeding programs. Moreover, the majority of
25 the farmers said that they are planting drought-resistant crop varieties especially, rice. From the
26 response of the farmers from Alimit, Ibulao, Subbasin 2, Matuno, and Subbasin 1, analysis shows
27 that more than 40% of the total farmers for each respective subbasin are using crop-resistant varieties.
28 About 35% of the farmers from the other subbasins say that they are using drought-resistant varieties,
29 classifying it to be in a low potential impact scale due to high adaptive capacity value.

30 The analysis of survey data suggests that in Alimit, Lamut, Subbasin 2, Matuno, and Subbasin
31 1, the number of farmers with diverse livelihoods has a range of 50-70%, which implies that the latter
32 indicator has a scale of 5 (Very High) against potential impacts. Setting the overall adaptive capacity
33 to alleviate the potential impact of drought on MRB to 4.6

34 The corresponding rating of each subbasin with respect to the given indicator was used in
35 generating a raster map of all adaptive capacity indicators. The potential impact of drought on the
36 MRB that is traying to be alleviated by the Adaptive Capacity measures on the basin has been
37 computed using the Raster Calculator, a spatial analyst tool, in GIS.

38 The Adaptive Capacity of the MRB is ranging from 3.17 to 3.99, implying that the indicators
39 are said to be on a moderate to high scale in terms of their effect in fortifying the Basin's response to
40 drought hazards (Fig. 7).

1
2
3
4
5
6
7
8
9
10
11
12
13
14
15
16
17
18
19
20
21
22
23
24
25
26
27
28
29
30
31
32
33
34
35
36
37
38
39
40
41
42
43
44
45
46
47
48
49
50
51
52
53
54
55
56
57
58
59
60
61
62
63
64
65

1
2
3
4
5
6
7
8
9
10
11
12
13
14
15
16
17
18
19
20
21
22
23
24
25
26
27
28
29
30
31
32
33
34
35
36
37
38
39
40
41
42
43
44
45
46
47
48
49
50
51
52
53
54
55
56
57
58
59
60
61
62
63
64
65



Fig. 7. Adaptive Capacity to Drought Map of Magat River Basin.

Overall Vulnerability

The MRB's drought vulnerability was calculated using the weighted categories of Sensitivity, Exposure, and Adaptive Capacity and was classified to be in the range of low to moderate (1.94 to 2.98) having the upstream section (Santa Fe, Sub-watershed 1) to be the moderately susceptible (Fig.8.)

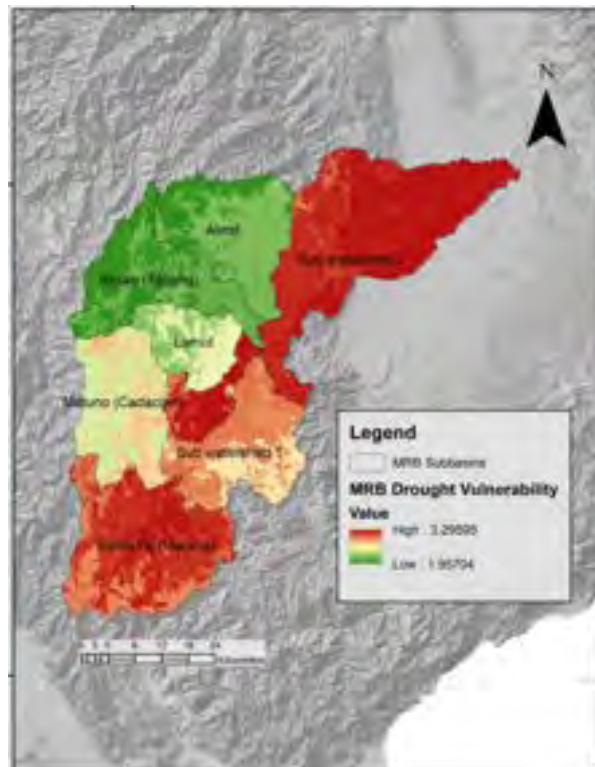


Fig.8. Overall Drought Vulnerability Map of Magat River Basin.

The contemporary condition of MRB in terms of its level of Sensitivity, Exposure, and

Adaptive Capacity to drought, and its overall drought vulnerability serves as the baseline for future projection.

Projected Changes in MRB’s Drought Exposure and Vulnerability

Using the CLIRAM Tool of PAGASA, the observed climate trends in the Philippines is only contingent on rainfall, temperature, sea level rise, and tropical cyclone. For this study, rainfall and temperature were defined as drought exposure indicators. Given the projected percentage change of rainfall and temperature parameters, the projected Drought Exposure of Magat River Basin under RCP 4.5 and RCP 8.5 Scenarios for both Mid (2036 – 2065) and Late (2070-2099) 21st Century. The current drought exposure level of MRB is at 2.76 – 3.75 and is projected to have a minute increase to a value of 2.77 for RCP 4.5 Mid-Century (Normal), RCP 4.5 Late Century (Lower-bound and Normal), RCP 8.5 Mid-Century (Lower-bound), and RCP 8.5 Late Century (Lower-bound and Normal). But is projected to have a minimum value decrease at 2.16 for RCP 4.5 Mid-Century (Lower-bound) and a 2.61 projected minimum exposure rating of 2.61 for RCP 4.5 Mid-Century (Upper-bound), RCP 4.5 Late Century (Upper-bound), RCP 8.5 Mid-Century (Normal and Upper-bound), and RCP 8.5 Late Century (Upper-bound). However, the maximum exposure rating of MRB in all future scenarios is projected to subside to as low as 2.4 (a decrease of 36%) for RCP 4.5 Mid-Century Scenario (Lower-bound) and at considerable decrease at 3.27, 3.44, and 3.45 exposure rating under all other scenarios (Table 7).

Table 7. Projected Exposure Values of Magat River Basin

| Contemporary Exposure of Magat River Basin | Drought Exposure Under RCP 4.5 Scenario | Drought Exposure Under RCP 8.5 Scenario |
|---|---|---|
| | <i>Mid Century</i> | |
| | Lower bound | 2.16 - 2.40 |
| | Normal | 2.77 - 3.4 |
| | Upper bound | 2.61 - 3.27 |
| 2.76 - 3.75 | | 2.77 - 3.44 |
| | <i>Late Century</i> | |
| | Lower bound | 2.77 - 3.44 |
| | Normal | 2.77 - 3.45 |
| | Upper bound | 2.61 - 3.27 |

The vulnerability rating of the Magat River has observed a dramatic increase up to a maximum of about 30% beyond the baseline or the current vulnerability rating, for both RCP 4.5 and 8.5 Climate Change Scenarios. The current vulnerability range of 1.9 -3.29 is seen to have a minimum value of 2.62 under RCP 4.5 (Mid-21st Century Scenario Lower bound) up to a maximum value of 4.33 (Mid-21st Century Scenario Lower bound). For the RCP 8.5 Scenario, the least projected minimum is at 2.67 (Mid-21st Century Upper bound and Late 21st Century Upper bound) to up to a maximum value of 4.3 (Mid-21st Century Lower bound) (Table 8).

Table 8. Projected Vulnerability Values of Magat River Basin

| Contemporary Vulnerability of Magat River Basin | Drought Vulnerability Under RCP 4.5 Scenario | Drought Vulnerability Under RCP 8.5 Scenario |
|---|--|--|
| | <i>Mid Century</i> | |
| | Lower bound | 2.62 - 4.29 |
| | Normal | 2.71 - 4.33 |
| | Upper bound | 2.68 - 4.25 |
| 1.9 - 3.29 | | |
| | <i>Late Century</i> | |
| | Lower bound | 2.71 - 4.28 |
| | Normal | 2.71 - 4.30 |
| | Upper bound | 2.68 - 4.27 |

Discussion:

This study was conducted to assess the impacts of climate change on the drought vulnerability of Magat Watershed in terms of the social and economic features of agriculture-dependent communities. The results of the projection imply that due to the future changes in rainfall and temperature as attributed to climate change, the basin’s overall vulnerability is projected to increase to up to 30% beyond the baseline. The potential impact of the drought that was assessed in the study is the combined effect of the Basin’s Sensitivity and Exposure to Drought. The AHP-Entropy Method of Multi-Criteria Decision Making was used to calculate the baseline value of the Sensitivity and Exposure of the basin accounts for 57% and 31% of the basin's overall vulnerability to drought, respectively, This may be attributed to the reason that MRB is subjected to type 3 climate where rice (lowland) cropping season usually starts from October; corn (dry season) starts on March; and another high-value commodity like cabbage being planted from January to March. All months were under subsequent drought stress having the cumulative monthly rainfall value of 2014 as the basis where relatively below-average rainfall has been recorded distinctly from January to June and the last quarter of the year. On the other side, the extent of drought areas is a difficult indicator to satisfy, since there is no specific local data per municipality in each subbasin that summarizes the extent of drought-affected production. In the study conducted (Macawile, et. al. 2018) where they applied a focus group discussion approach (FGD) by coming down to the site and connecting and interviewing the farmers. To satisfy this, the indicator was assessed by consulting the farmers inside the concerned areas. Hence, there has been an established interrelationship since Sensitivity Indicators mainly depend on the meteorology of the area, and the resulting exposure is highly dependent upon these indicators e.g. the yield and income losses are two inseparable indicators since the latter is dependent on the sensitivity indicators. High-intensity droughts for that matter, induce lesser yield, and lower-income secured. (Tongson et. al., 2017)

In hindsight, the vulnerability of the MRB is on a high scale as plausibly indicated by the corresponding values of the Basin’s Sensitivity and Exposure to Drought. However, the Adaptive Capacity values of 3.17 to 3.99 indicates a high effect of adaptive interventions against drought which makes the Adaptive Capacity a negative dimension of vulnerability. Farming is the most prominent livelihood of the communities inside the basin, while most of the farmers are also engaging in other activities like operating a small-grocery store business, tricycle transport service, construction works, and handiworks like word carving and fiber-weaving for an additional source of income. Farmers are considered to be the poorest of the poor, (Philippine Statistics Authority, 2017), and the ability to adapt is higher for wealthy societies or those who can afford climate protection than for less fortunate ones (Fankhauser & McDermott, 2014). Based on the results of the AHP-Entropy Method, the Adaptive Capacity component has a constituted weight of only 12% of the total vulnerability value of MRB which is the least of all the vulnerability components, implying that as of the moment, existing policies and practices may still be improved. The Entropy Weighting Method was applied for this matter because it is an objective weighting method and it can eliminate human bias in

1 assigning the corresponding weight to the categories of vulnerability, which is perceived to be highly
2 reliant on the quantity of essential available information (Li, et al., 2011). Adaptive capacity in this
3 context is the constituted counter measure of the basin to the potential impacts that is the combination
4 of drought sensitivity and exposure. The corresponding value of Adaptive Capacity indicators reflects
5 the quality and effectivity of the mitigation and in battling the potential impact of drought i.e.
6 Sensitivity and Exposure.

7 The IPCC Framework (Sharma & Ravindranath, 2019) and principles are at the core of this
8 research. The drought Vulnerability of MRB is from 1.96 to 3.29 (Fig. 9 and 10). Subbasin 2 is
9 detected to be in a moderate drought vulnerability. While the subbasin houses one of the biggest
10 irrigation systems (Magat River Integrated Irrigation System) that supplies an enormous extent of
11 rice fields, it is also the watershed that incurs considerable losses during climatic extremes. The basin
12 is also at the forefront of receiving capacity programs as it is considered an agro-economic asset for
13 rice and high-value crop production.

14 The MRB's overall vulnerability is can be exacerbated to a higher extent by just the changes
15 in rainfall, approaching the Mid-21st Century. The potential increment in rainfall in this study is in
16 lieu of the findings of (Supharatid & Nafung, 2021) who projected an increase in annual precipitation
17 by Mid 21st Century (2050) and Late 21st Century (2100) under both SSP5-8.5 and SSP2-4.5
18 Scenarios. The projected sensitivity under the RCP 4.5 and RCP 8.5 Scenario is observed to be lower
19 than the estimated sensitivity of the basin. It may seem to be peculiar in the sense that a lower
20 sensitivity range has catapulted the vulnerability value to 2.8-3.8 (moderate to high), which means
21 that in the future, different areas will be highly vulnerable to drought. In closer inspection, the
22 projected change in rainfall using the CLIRAM tool has designated a negative percentage change in
23 rainfall concerning the location of the rain gauges. And while it is true that the overall range of
24 sensitivity has been projected to be reduced under future climate scenarios, the predetermined high
25 rainfall areas were observed to get an additional amount of rainfall towards the end of the century,
26 and areas with seemingly lower rainfall events were even more stressed to the projected future
27 decrease in annual rainfall. This remark follows the trend that dry areas will get drier and wet areas
28 will become wetter (Byrne & O'Gorman, 2015), and it is occurring on a longer time scale as climate
29 change's effects, directly and indirectly, manifest in altering the global and local water cycle due to
30 the ever-increasing global temperature as a result of global warming.

31 This can be very alarming since as of the moment, communities seem to be unaware of the
32 related impacts of climate change and how rainfall variation alone can potentially alter their state of
33 living and traditional practices. Cultural norms and other related factors not only limit the
34 communities to adjust but the lack of proper promulgation of knowledge through systematic and
35 policy enforcement. Initial adaptive measures should not only be employed momentarily but should
36 be sustainable in the sense that, scientific-based practices should be downscaled to the farmers and
37 related constituents. In their study, Manalo IV, et. al. (2022) found out that the inability of farmers to
38 adapt to climate change is also due to some non-climatic stressors. They stated that there are variables
39 that do not appear to have anything to do with climate change mitigation and adaptation yet have a
40 significant influence on how well coping-mechanisms function, and non-climatic variables that
41 directly inhibit the efforts in climate change adaptation. Human activities and interventions that may
42 be perceived as non-climate change related may in the end cause stringent social and economic
43 limitations that can alter the aptness of adaptive capacity involvement of the communities affected.

44 The vulnerability value that was estimated by this study denotes that, parts of MRB are highly
45 sensitive and exposed to drought hazards, and that Adaptive Capacity interventions being rendered
46 that contribute to counteracting drought-related hazards are still pre-mature and will be continuously
47 challenged by changing climate. It only suggests that in order to lower the Basin's vulnerability, more
48 adaptive measures and accompanying policies should be imposed. Other factors such as population
49 growth that increases industrial, agricultural, and domestic water demand can also increase
50 vulnerability (Sehgal & Sridhar, 2019). Also, future development may impede natural processes that
51 can reshape the system's operations and activity.

52 For future research endeavors, systematic consideration of factors to be assessed in drought
53 and related studies may also try to look for other opportunities such as using different multi-criteria
54 decision-making methods in weighting relative matrices for more transparent discrimination between
55 variables intrinsic to vulnerability.

1
2
3
4
5
6
7
8
9
10
11
12
13
14
15
16
17
18
19
20
21
22
23
24
25
26
27
28
29
30
31
32
33
34
35
36
37
38
39
40
41
42
43
44
45
46
47
48
49
50
51
52
53
54
55
56
57
58
59
60
61
62
63
64
65

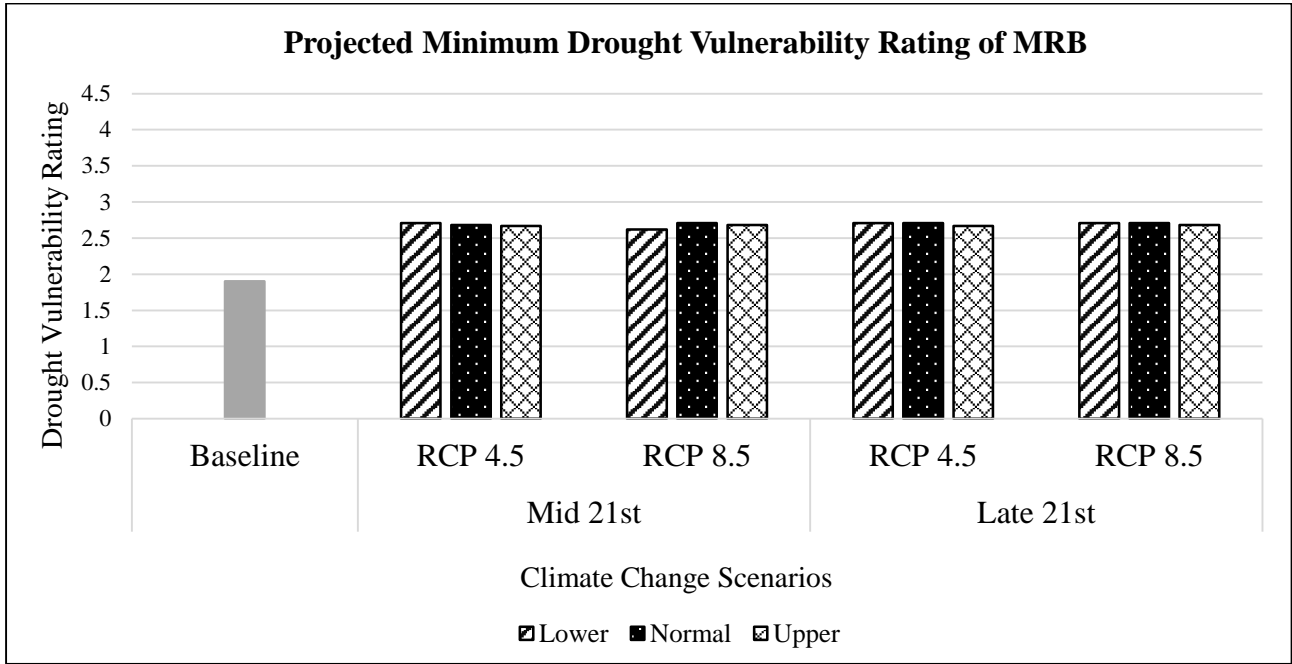


Fig. 9. Projected Minimum Drought Vulnerability Rating of MRB.

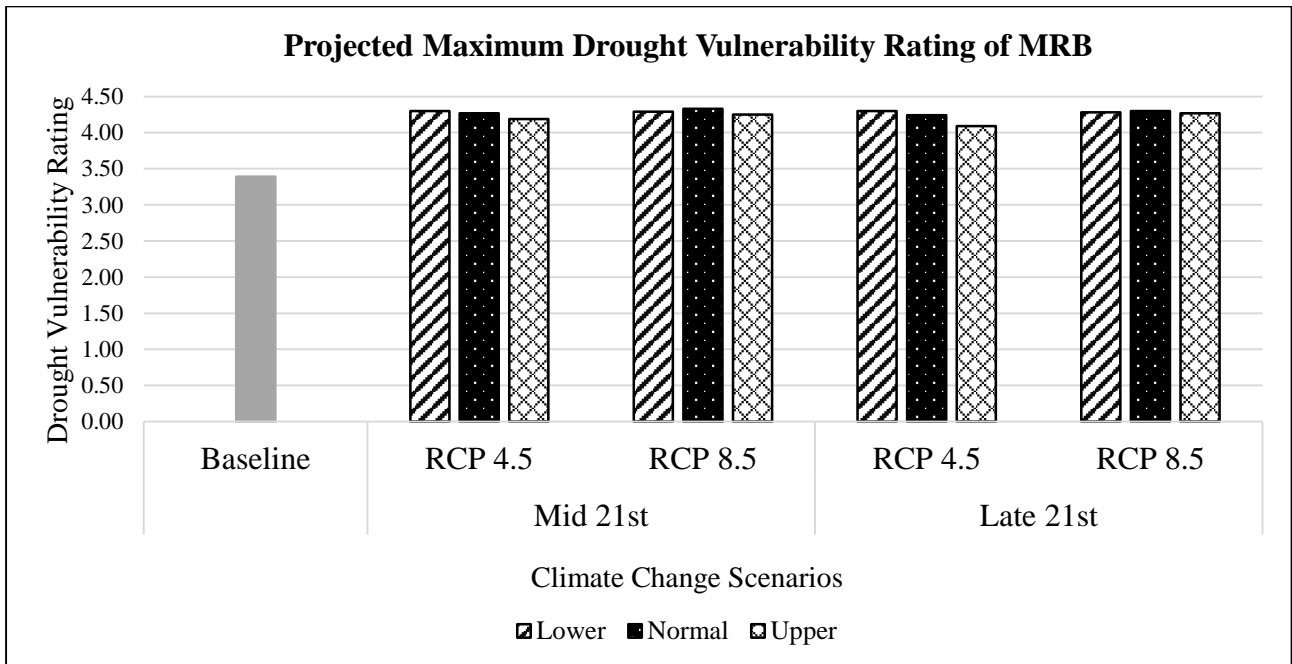


Fig. 10. Projected Maximum Drought Vulnerability Rating of MRB.

Conclusions:

This paper gives emphasis refeon agriculture as the main sector in the Magat River Basin and the farmers as its major stakeholders through intelligent selection and consolidation of the indicators of the respective drought vulnerability components on the agricultural systems of the basin.

Using AHP-Entropy Weighting Method, GIS-based calculation was employed and deduced that the MRB’s Sensitivity and Exposure to drought are highly identical and at the same time correlated with a given magnitude of 57% and 31%, respectively. The weight factor of the corresponding countermeasure in terms of Adaptive Capacity at 12% was also deduced.

The overall current Vulnerability value of the basin was estimated to be at a low to moderate level. However, considering the future impact ascribed by climate change using RCP 4.5 Mid-21st

1 Century normal scenario, it is projected to increase to a moderate to a high level, implying that with
2 the currently promulgated and observed mitigation and adaptive measures will become less
3 significant in the future, let alone a scenario where communities will not practice proper conservation
4 routines. If there will be no changes in the current state of the basin, i.e. the socio-economic aspect
5 of agriculture-based communities, Fig. 9 & 10 show that the basin will experience a noticeable
6 increase in vulnerability level as we go towards the Mid-21st century, and somehow stabilizes towards
7 to end of the 21st century. This projection however is only based on the change in the exposure
8 dimension due to the projected change in rainfall and temperature. The other factors were not included
9 such as the expected increase of losses in yield and in income is not included, the future extent of
10 production areas to be affected by drought occurrences, the future agriculture-dependent households
11 to be affected by droughts, etc. still as vital as the currently included indicators. In a broader sense,
12 the projected vulnerability tells us one thing. Climate change intensively stimulates the drought
13 vulnerability of river basins from a socio-economic perspective. And that there are still other related
14 factors that are involved which may add up to worsen the situation, even more than the projected
15 level.

16 This study can guide policymakers in conceptualizing management measures and devising
17 plans to mitigate the impacts of drought extremes by carefully assimilating science-based studies in
18 developing intervention programs in invigorating former adaptive capacity measures and creating
19 new schemes in withstanding the effect of climatic anomalies and extremes. In addition, in order to
20 establish a more accurate future drought study, the need for adequate meteorological data on the
21 ground is of high importance. Vulnerability studies greatly rely on the quality and quantity of data.
22 This study shows that MRB's response to climate disturbances and extremes is can be enhanced thru
23 proper collaboration of stakeholders. Furthermore, a locally-based drought assessment and analysis
24 using ensemble techniques can give better and more reliable results, such studies can be undertaken
25 having this study as baseline data. The topic of climate change can not be contained in a box. It must
26 be addressed differently as it can be site specific as influenced by microclimate, or be a part of the
27 general system. Hence, quantifying the major aspects of drought vulnerability and integrating climate
28 change effects can reduce drought impacts and improve mitigation measures to further benefit the
29 stakeholders under climatic-induced threats and stresses.
30
31
32
33
34
35
36
37
38
39
40
41
42
43
44
45
46
47
48
49
50
51
52
53
54
55
56
57
58
59
60
61
62
63
64
65

REFERENCES:

- 1 Ahamed, T. N., Rao, K. G., & Murthy, J. S. R. (2000). GIS-based fuzzy membership model for crop-
2 land suitability analysis. *Agricultural systems*, 63(2), 75-95.
3
- 4 Brooks, N., & Adger, N. W. (2003). Country level risk measures of climate-related natural disasters
5 and implications for adaptation to climate change.
6
- 7 Byrne, M. P., & O’Gorman, P. A. (2015). The Response of Precipitation Minus Evapotranspiration
8 to Climate Warming: Why the “Wet-Get-Wetter, Dry-Get-Drier” Scaling Does Not Hold over Land,
9 *Journal of Climate*, 28(20), 8078-8092.
10
- 11 Cui, G., Lee, W.-K., & Chung, J. (2010). Vulnerability Assessment of Water Resources to Climate
12 Change Using GIS. 2010 ESRI International User Conference. San Diego, CA.
13
- 14 Dabanli, I. (2018). Drought hazard, vulnerability, and risk assessment in Turkey. *Arabian Journal of*
15 *Geosciences*, 11(18), 1-12.
16
- 17 Department of Natural Resources, (2016). Convergence for Magat Watershed. Retrieved from
18 Department of Environment and Natural Resources Region 2 Cagayan Valley:
19 [https://r2.denr.gov.ph/index.php/news-events/photo-releases/1387-convergence-for-magat-](https://r2.denr.gov.ph/index.php/news-events/photo-releases/1387-convergence-for-magat)
20
- 21 DOST-PAGASA, (2018). Observed and Projected Climate Change in the Philippines. Philippine
22 Atmospheric, Geophysical and Astronomical Services Administration, Quezon City, Philippines, 36
23 pp.
24
- 25 Fankhauser, S., & McDermott, T. K. J. (2014). Understanding the adaptation deficit: Why are poor
26 countries more vulnerable to climate events than rich countries? *Global Environmental Change*, 27
27 (Supplement C), 9–18.
28
- 29 Hagenlocher, M., Meza, I., Anderson, C. C., Min, A., Renaud, F. G., Walz, Y., ... & Sebesvari, Z.
30 (2019). Drought vulnerability and risk assessments: state of the art, persistent gaps, and research
31 agenda. *Environmental Research Letters*, 14(8), 083002.
32
- 33 Hibbard, K., Hurtt, G. C., Kram, T., Krey, V., Lamarque, J.-F., Masui, T., Meinshausen, M.,
34 Nakicenovic, N., Smith, S. J., & Rose, S. K. (2011). The Representative Concentration Pathways: An
35 overview. *Climatic Change*, 109(1-2), 5–31.
36
- 37 Houghton, J. T., Ding, Y. D. J. G., Griggs, D. J., Noguer, M., van der Linden, P. J., Dai, X., ... &
38 Johnson, C. A. (Eds.). (2001). *Climate change 2001: the scientific basis: contribution of Working*
39 *Group I to the third assessment report of the Intergovernmental Panel on Climate Change*.
40 Cambridge university press.
41
- 42 Jia, H., Pan, D., Wang, J. A., & Zhang, W. C. (2016). Risk mapping of integrated natural disasters in
43 China. *Natural Hazards*, 80(3), 2023-2035.
44
- 45 Karmakar, S., Simonovic, S. P., Peck, A., & Black, J. (2010). An information system for risk-
46 vulnerability assessment to flood. *Journal of Geographic Information System*, 2(03), 129.
47
- 48 Li, J., Chou, J., Zhao, W., Xu, Y., Hao, Y., & Li, Y. (2022). Future Drought and Flood Vulnerability
49 and Risk Prediction of China’s Agroecosystem under Climate Change. *Sustainability*, 14(16), 10069.
50
- 51 Li, X., Wang, K., Liu, L., Xin, J., Yang, H., & Gao, C. (2011). Application of the entropy weight and
52 TOPSIS method in safety evaluation of coal mines. *Procedia engineering*, 26, 2085-2091.
53
54
55
56
57
58
59
60
61
62
63
64
65

Liang, J., & Yang, J. (2022). Application of the AHP method on the optimization with undesirable priorities. *Engineering with Computers*, 38(3), 2137-2153.

Liu, X., Wang, Y., Peng, J., Braimoh, A. K., & Yin, H. (2013). Assessing vulnerability to drought based on exposure, sensitivity and adaptive capacity: a case study in middle Inner Mongolia of China. *Chinese Geographical Science*, 23(1), 13-25.

Liu, Y., You, M., Zhu, J., Wang, F., & Ran, R. (2019). Integrated risk assessment for agricultural drought and flood disasters based on entropy information diffusion theory in the middle and lower reaches of the Yangtze River, China. *International Journal of Disaster Risk Reduction*, 38, 101194.

Macawile, M. J. P., Sarte, S. M., Ballado, A. H., & Bentir, S. A. P. (2018). Assessment of Indicators for Agricultural Vulnerability to Drought in the Municipality of Taal. In *2018 IEEE 10th International Conference on Humanoid, Nanotechnology, Information Technology, Communication and Control, Environment and Management (HNICEM)* (pp. 1-5). IEEE.

Manalo IV, J. A., van de Fliert, E., & Fielding, K. (2020). Rice farmers adapting to drought in the Philippines. *International Journal of Agricultural Sustainability*, 18(6), 594-605.

Meza, I., Hagenlocher, M., Naumann, G., Vogt, J. and Frischen, J., Drought vulnerability indicators for global-scale drought risk assessments, EUR 29824 EN, Publications Office of the European Union, Luxembourg.

Naumann, G., Barbosa, P., Garrote, L., Iglesias, A., & Vogt, J. (2014). Exploring drought vulnerability in Africa: an indicator based analysis to be used in early warning systems. *Hydrology and Earth System Sciences*, 18(5), 1591-1604.

Neri, C., & Magaña, V. (2016). Estimation of vulnerability and risk to meteorological drought in Mexico. *Weather, Climate, and Society*, 8(2), 95-110.

Official Gazette of the Republic of the Philippines. (2015). *El Niño Advisory no. 2: Drought assessment as of April 23, 2015: GOVPH*. Retrieved February 11, 2022, from <https://www.officialgazette.gov.ph/2015/04/23/el-nino-advisory-no-2-drought-assessment-as-of-april-23-2015/>

Palchadhuri, M., & Biswas, S. (2016). Application of AHP with GIS in drought risk assessment for Puruliya district, India. *Natural Hazards*, 84(3), 1905-1920.

Perez, G. J., Enricuso, O., Manuis, K., & Valet, M. A. (2022). CHARACTERIZING THE DROUGHT DEVELOPMENT IN THE PHILIPPINES USING MULTIPLE DROUGHT INDICES DURING THE 2019 EL NIÑO. *ISPRS Annals of the Photogrammetry, Remote Sensing and Spatial Information Sciences*, 3, 463-470.

Philippine Statistics Authority. (2017). Farmers, fishermen, and children consistently posted the highest poverty incidence among basic sectors – PSA. <https://psa.gov.ph/poverty-press-releases/nid/120251>

Robielos, R. A. C., Lin, C. J., Senoro, D. B., & Ney, F. P. (2020). Development of vulnerability assessment framework for disaster risk reduction at three levels of geopolitical units in the Philippines. *Sustainability*, 12(21), 8815.

Saaty, T.L., 1980. *The Analytical Hierarchy Process*. McGraw Hill, New York.

Saaty, T. L. (2008). Decision making with the analytic hierarchy process. *International journal of*

services sciences, 1(1), 83-98.

1 Sahana, V., Mondal, A., & Sreekumar, P. (2021). Drought vulnerability and risk assessment in India:
2 Sensitivity analysis and comparison of aggregation techniques. *Journal of Environmental*
3 *Management*, 299, 113689.

4
5 Salvacion, A. R. (2021). Mapping meteorological drought hazard in the Philippines using SPI and
6 SPEI. *Spatial Information Research*, 29(6), 949-960.

7
8
9 Sehgal, V., & Sridhar, V. (2019). Watershed-scale retrospective drought analysis and seasonal
10 forecasting using multi-layer, high-resolution simulated soil moisture for Southeastern US. *Weather*
11 *and Climate Extremes*, 23, 100191

12
13 Sharma, J., & Ravindranath, N. H. (2019). Applying IPCC 2014 framework for hazard-specific
14 vulnerability assessment under climate change. *Environmental Research Communications*, 1(5),
15 051004.

16
17
18 Sheffield, J., & Wood, E. F. (2012). *Drought: past problems and future scenarios*. Routledge.

19
20
21 Shim, I., Kim, H., Hong, B., An, J., & Hwang, T. (2021). Drought vulnerability assessment and cluster
22 analysis of island areas taking Korean Island areas at eup (town) and myeon (subcounty) levels as
23 study targets. *Water*, 13(24), 3657.

24
25
26 Supharatid, S., & Nafung, J. (2021). Projected drought conditions by CMIP6 multimodel ensemble
27 over Southeast Asia. *Journal of Water and Climate Change*, 12(7), 3330-3354.

28
29
30 Svoboda, M. D., & Fuchs, B. A. (2016). *Handbook of drought indicators and indices* (pp. 1-44).
31 Geneva, Switzerland: World Meteorological Organization.

32
33 Taheriyoun, M., Karamouz, M., & Baghvand, A. (2010). Development of an entropy-based fuzzy
34 eutrophication index for reservoir water quality evaluation. *Journal of Environmental Health Science*
35 *& Engineering*, 7(1), 1-14.

36
37
38 Tongson, E. E., Alejo, L. A., & Balderama, O. F. (2017). Simulating impacts of El Niño and climate
39 change on corn yield in Isabela, Philippines. *Clim. Disaster Dev. J*, 2(1), 29-39.

40
41
42 UNESCO-IHP, (1995). *Ilog Magat. CATALOGUE OF RIVERS FOR*
43 *SOUTHEAST ASIA AND THE PACIFIC*-Volume I. Hywr.kuciv.kyoto. (October, 1995). Retrieved
44 from http://hywr.kuciv.kyoto-u.ac.jp/ihp/riverCatalogue/Vol_01/

45
46
47 van Vuuren, D. P., Edmonds, J., Kainuma, M., Riahi, K., Thomson, A., Hibbard, K., Hurtt, G. C.,
48 Kram, T., Krey, V., Lamarque, J., Masui, T., Meinhausen, M., Nakicenovic, N., Smith, S. J., & Rose,
49 S. K. (2011). The representative concentration pathways: an overview. *Climatic change*, 109(1), 5-
50 31.

51
52
53 Vargas, L. G. (1990). An overview of the analytic hierarchy process and its applications. *European*
54 *journal of operational research*, 48(1), 2-8.

55
56
57 Warren, J. F. (2018). Typhoons and droughts: Food shortages and famine in the Philippines since the
58 seventeenth century. *International Review of Environmental History*, 4(2), 27-44

59
60 Wilhite, D. A. (Ed.). (2012). *Drought assessment, management, and planning: theory and case*
61 *studies: theory and case studies* (Vol. 2). Springer Science & Business Media.

62
63
64
65

World Meteorological Organization. (2012). *Standardized precipitation index user guide*.

1 Wu, J., He, B., Lü, A., Zhou, L., Liu, M., & Zhao, L. (2011). Quantitative assessment and spatial
2 characteristics analysis of agricultural drought vulnerability in China. *Natural Hazards*, 56(3), 785-
3 801.

4
5 Yusuf, A. A., & Francisco, H. (2009). Climate change vulnerability mapping for Southeast Asia.

6
7
8 Zarafshani, K., Sharafi, L., Azadi, H., & Van Passel, S. (2016). Vulnerability assessment models to
9 drought: Toward a conceptual framework. *Sustainability*, 8(6), 588.

10
11 Zeng, J., & Huang, G. (2018). Set pair analysis for karst waterlogging risk assessment based on AHP
12 and entropy weight. *Hydrology research*, 49(4), 1143-1155.

13
14
15 Zhu, Y., Tian, D., & Yan, F. (2020). Effectiveness of entropy weight method in decision-
16 making. *Mathematical Problems in Engineering*, 2020.

17
18
19
20
21
22
23
24
25
26
27
28
29
30
31
32
33
34
35
36
37
38
39
40
41
42
43
44
45
46
47
48
49
50
51
52
53
54
55
56
57
58
59
60
61
62
63
64
65

Supplementary Material:

Annual Rainfall Under RCP 4.5 for Mid-21st Century (2036-2060). a.) Lower bound b.) Normal c.) Upper bound

a.)

| SEASON | BANAUE (mm) | DUPAX (mm) | HALONG (mm) | IMUGAN (mm) | MAGAT (mm) |
|------------|-----------------|-----------------|-----------------|-----------------|-----------------|
| DJF | 476.4973 | 209.998 | 783.7293 | 153.4972 | 220.9495 |
| MAM | 579.9517 | 197.3547 | 647.7667 | 197.6932 | 296.8296 |
| JJA | 844.6776 | 439.6011 | 651.3019 | 567.3632 | 331.1501 |
| SON | 277.5192 | 2488.899 | 997.9401 | 480.8214 | 390.1028 |
| Sum | 2178.646 | 3335.853 | 3080.738 | 1399.375 | 1239.032 |

b.)

| SEASON | BANAUE (mm) | DUPAX (mm) | HALONG (mm) | IMUGAN (mm) | MAGAT (mm) |
|------------|-----------------|-----------------|-----------------|-----------------|-----------------|
| DJF | 488.3188 | 216.1222 | 803.173 | 157.9736 | 238.0277 |
| MAM | 621.8232 | 208.6152 | 694.5343 | 208.973 | 323.8408 |
| JJA | 1099.923 | 509.8404 | 848.1127 | 658.0163 | 379.2424 |
| SON | 298.6419 | 2763.819 | 1073.896 | 533.9321 | 472.1573 |
| Sum | 2508.707 | 3698.396 | 3419.716 | 1558.895 | 1413.268 |

c.)

| SEASON | BANAUE (mm) | DUPAX (mm) | HALONG (mm) | IMUGAN (mm) | MAGAT (mm) |
|------------|-----------------|-----------------|-----------------|----------------|-----------------|
| DJF | 590.1655 | 276.9683 | 970.6877 | 202.4488 | 316.801 |
| MAM | 739.3135 | 255.04 | 825.7629 | 255.4774 | 362.596 |
| JJA | 1347.274 | 580.6852 | 1038.837 | 749.4508 | 459.3963 |
| SON | 331.1383 | 3126.479 | 1190.751 | 603.9931 | 512.9554 |
| Sum | 3007.891 | 4239.172 | 4026.038 | 1811.37 | 1651.749 |

Annual Rainfall Under RCP 4.5 for Late-21st Century (2070-2099). a.) Lower bound b.) Normal c.) Upper bound

a.)

| SEASON | BANAUE (mm) | DUPAX (mm) | HALONG (mm) | IMUGAN (mm) | MAGAT (mm) |
|------------|-----------------|-----------------|-----------------|----------------|-----------------|
| DJF | 459.6744 | 201.5033 | 763.5378 | 147.288 | 215.826 |
| MAM | 633.0723 | 175.4264 | 715.4751 | 175.7273 | 297.1232 |
| JJA | 1334.117 | 449.8948 | 1041.88 | 580.6486 | 464.4345 |
| SON | 329.1885 | 2550.317 | 1198.93 | 492.6866 | 464.3645 |
| Sum | 2756.052 | 3377.142 | 3719.823 | 1396.35 | 1441.748 |

b.)

| SEASON | BANAUE (mm) | DUPAX (mm) | HALONG (mm) | IMUGAN (mm) | MAGAT (mm) |
|------------|-----------------|-----------------|-----------------|-----------------|-----------------|
| DJF | 462.4024 | 225.6047 | 770.2683 | 164.9048 | 216.6799 |
| MAM | 636.197 | 197.5523 | 719.6632 | 197.8911 | 298.5912 |
| JJA | 1336.748 | 518.923 | 1048.982 | 669.7386 | 465.3506 |
| SON | 329.8384 | 2907.128 | 1205.942 | 561.6175 | 465.2813 |
| Sum | 2765.186 | 3849.208 | 3744.855 | 1594.152 | 1445.903 |

c.)

| SEASON | BANAUE (mm) | DUPAX (mm) | HALONG (mm) | IMUGAN (mm) | MAGAT (mm) |
|------------|-----------------|-----------------|-----------------|-----------------|-----------------|
| DJF | 465.1305 | 295.5382 | 774.7553 | 216.0224 | 218.1743 |
| MAM | 641.1966 | 246.9403 | 727.3415 | 247.3639 | 301.2336 |
| JJA | 1349.905 | 650.9244 | 1059.126 | 840.1039 | 470.3888 |
| SON | 333.413 | 3296.11 | 1218.796 | 636.7635 | 470.7821 |
| Sum | 2789.645 | 4489.513 | 3780.019 | 1940.254 | 1460.579 |

Annual Rainfall Under RCP 8.5 for Mid-21st Century (2036-2060). a.) Lower bound b.) Normal c.) Upper bound

a.)

| SEASON | BANAUE (mm) | DUPAX (mm) | HALONG (mm) | IMUGAN (mm) | MAGAT (mm) |
|------------|-----------------|-----------------|-----------------|-----------------|-----------------|
| DJF | 431.03 | 193.0086 | 708.946 | 141.0788 | 210.2756 |
| MAM | 574.3272 | 184.7114 | 641.4845 | 185.0282 | 296.8296 |
| JJA | 949.9333 | 471.0876 | 732.461 | 608.0008 | 347.1808 |
| SON | 296.0422 | 2673.154 | 1064.547 | 516.4169 | 447.8619 |
| Sum | 2251.333 | 3521.961 | 3147.439 | 1450.525 | 1302.148 |

b.)

| SEASON | BANAUE (mm) | DUPAX (mm) | HALONG (mm) | IMUGAN (mm) | MAGAT (mm) |
|------------|-----------------|-----------------|-----------------|-----------------|-----------------|
| DJF | 490.5921 | 214.5417 | 806.9122 | 156.8184 | 239.949 |
| MAM | 633.0723 | 200.318 | 707.0988 | 200.6616 | 314.152 |
| JJA | 1289.383 | 587.9513 | 994.1991 | 758.8287 | 446.1136 |
| SON | 324.964 | 2971.471 | 1168.548 | 574.0477 | 508.8298 |
| Sum | 2738.012 | 3974.282 | 3676.758 | 1690.356 | 1509.044 |

c.)

| SEASON | BANAUE (mm) | DUPAX (mm) | HALONG (mm) | IMUGAN (mm) | MAGAT (mm) |
|------------|-----------------|-----------------|-----------------|----------------|-----------------|
| DJF | 606.9884 | 276.3756 | 998.3575 | 202.0156 | 295.4532 |
| MAM | 815.5571 | 258.5959 | 910.9219 | 259.0395 | 344.3928 |
| JJA | 1494.632 | 682.411 | 1152.459 | 880.7415 | 575.7339 |
| SON | 362.6598 | 3442.343 | 1304.1 | 665.0139 | 532.6668 |
| Sum | 3279.837 | 4659.726 | 4365.839 | 2006.81 | 1748.247 |

Annual Rainfall Under RCP 8.5 for Late-21st Century (2070-2099). a.) Lower bound b.) Normal c.) Upper bound

a.)

| SEASON | BANAUE (mm) | DUPAX (mm) | HALONG (mm) | IMUGAN (mm) | MAGAT (mm) |
|------------|-----------------|-----------------|-----------------|-----------------|-----------------|
| DJF | 464.2211 | 186.0942 | 756.0595 | 136.0248 | 217.5339 |
| MAM | 640.5717 | 184.7114 | 707.0988 | 185.0282 | 300.6464 |
| JJA | 1351.221 | 387.5271 | 1028.692 | 500.1549 | 470.8468 |
| SON | 333.413 | 2468.426 | 1183.739 | 476.8664 | 470.3237 |
| Sum | 2789.427 | 3226.759 | 3675.589 | 1298.074 | 1459.351 |

b.)

| SEASON | BANAUE (mm) | DUPAX (mm) | HALONG (mm) | IMUGAN (mm) | MAGAT (mm) |
|------------|-----------------|-----------------|-----------------|-----------------|-----------------|
| DJF | 468.3132 | 245.3599 | 760.5465 | 179.3448 | 219.6686 |
| MAM | 644.3214 | 205.6519 | 710.5889 | 206.0046 | 302.1144 |
| JJA | 1360.431 | 408.1145 | 1030.721 | 526.7256 | 473.137 |
| SON | 335.3628 | 2883.73 | 1186.076 | 557.0974 | 472.6157 |
| Sum | 2808.428 | 3742.856 | 3687.932 | 1469.172 | 1467.536 |

c.)

| SEASON | BANAUE (mm) | DUPAX (mm) | HALONG (mm) | IMUGAN (mm) | MAGAT (mm) |
|------------|-----------------|-----------------|-----------------|-----------------|-----------------|
| DJF | 471.0412 | 285.8581 | 765.0335 | 208.9468 | 220.9495 |
| MAM | 651.1958 | 248.1256 | 716.1731 | 248.5512 | 305.344 |
| JJA | 1373.588 | 690.2827 | 1040.866 | 890.9009 | 478.6332 |
| SON | 338.9374 | 3673.393 | 1198.93 | 709.6495 | 478.1166 |
| Sum | 2834.762 | 4897.659 | 3721.003 | 2058.048 | 1483.043 |

Projected Changes (%) in Seasonal Mean Temperature in the Mid-21st Century (2036-2065)

| RCP 4.5 | | | | RCP 8.5 | | | |
|----------------|---------------|---------------|---------------|---------|---------------|---------------|---------------|
| Month | lower bound | Normal | Upper bound | Month | lower bound | Normal | Upper bound |
| DJF | 32.495 | 32.563 | 32.676 | DJF | 32.537 | 32.692 | 32.772 |
| MAM | 32.482 | 32.573 | 32.737 | MAM | 32.595 | 32.730 | 32.914 |
| JJA | 32.505 | 32.598 | 32.811 | JJA | 32.621 | 32.698 | 32.988 |
| SON | 32.495 | 32.534 | 32.791 | SON | 32.608 | 32.688 | 32.920 |
| Average | 32.495 | 32.567 | 32.754 | | 32.590 | 32.702 | 32.898 |

Projected Changes (%) in Seasonal Mean Temperature in the Mid-21st Century (2070-2099)

| RCP 4.5 | | | | RCP 8.5 | | | |
|----------------|--------------------|---------------|--------------------|----------------|--------------------|---------------|--------------------|
| Month | lower bound | Normal | Upper bound | Month | lower bound | Normal | Upper bound |
| DJF | 32.537 | 32.705 | 32.910 | DJF | 32.827 | 33.129 | 33.322 |
| MAM | 32.598 | 32.737 | 33.023 | MAM | 32.978 | 33.149 | 33.499 |
| JJA | 32.634 | 32.695 | 33.036 | JJA | 33.049 | 33.258 | 33.612 |
| SON | 32.598 | 32.669 | 33.017 | SON | 33.026 | 33.194 | 33.557 |
| Average | 32.592 | 32.701 | 32.997 | | 32.970 | 33.182 | 33.498 |

1
2
3
4
5
6
7
8
9
10
11
12
13
14
15
16
17
18
19
20
21
22
23
24
25
26
27
28
29
30
31
32
33
34
35
36
37
38
39
40
41
42
43
44
45
46
47
48
49
50
51
52
53
54
55
56
57
58
59
60
61
62
63
64
65

FORECASTING DAM INFLOW AND FLOOD INUNDATIONS UNDER EXTREME RAINFALL EVENTS USING THE RAINFALL-RUNOFF-INUNDATION MODEL

A S Alejandro^{1*}, L A Alejo², O F Balderama³, J L Bareng⁴ and S A Kantoush⁵

¹ National Irrigation Administration, Magat River Integrated Irrigation System, Dam and Reservoir Division, Ramon, Isabela, Philippines, arlenalejandro001@gmail.com

^{2,3,4} College of Engineering, Isabela State University, Echague, Isabela, Philippines,

⁵Water Resources Research Center - Disaster Prevention Research Institute Kyoto University, Kyoto, Japan,

Abstract. The downstream of river basins are prone to flash floods during rainy seasons. Flood forecasting is vital in preventing and mitigating flood damages. Flood inundation can be simulated to forewarn the affected areas on the possible effect of flood brought by the heavy rainfall events. In this study, the dam inflow and river water level were simulated using a successfully calibrated and validated Rainfall-Runoff-Inundation (RRI) Model during a strong typhoon. This was done in the Cagayan River Basin (CRB), the largest river basin in the Philippines, with a significant dam, which is the Magat Dam during Typhoon Ulysses with international name Vamco. The model satisfactorily estimated the inflow in the Dam with RSR, NSE, PBIAS, and R^2 equal to 0.36, 0.87, 6.90 & 0.88, respectively. Also, the RSR, NSE, PBIAS, and R^2 with 0.50, 0.75, -0.39, and 0.75, respectively, showed good agreement with the measured river water level data. The RRI calibrated parameters were also tested and validated on Typhoon Tisoy in December 2019 and Monsoon Rains in December 2020. Results gave a satisfactory statistical index for both Magat Inflow and Buntun Bridge river water levels. The RRI model estimated flood heights ranged from ≥ 0 meters at locations relatively far from the riverbanks and ≥ 6 meters along the Cagayan riverbanks which is almost the same as the gathered actual data ranged from 0.3 to 7 meters. The calibrated parameter of RRI could be used to forecast the inflow of Magat Dam and flood inundation in CRB during extreme weather events for effective protective planning, decision-making, and flood early warnings.

Keywords: forecasting; inflow; validation; simulated; calibrated; parameters

1. Introduction

Flooding was responsible for nearly half of all-natural catastrophe-related losses in 2013, with floods in Europe, Asia, Canada, the United States, and Australia causing over \$20 billion (U.S. dollars) in losses (Coffman, 2013). According to World Risk Report, 2015, the Philippines is a country frequently ravaged by natural disasters, ranking third in the World Risk Index with a risk percentage of 27.98%. It is also the third most exposed country to natural disasters. Flooding is one of the prominent water-based natural hazards (about 50%) across the globe, which accounts to 15% of all deaths related to natural disasters. Tropical cyclones and flash floods are the two worst disasters in the country, affecting a total of around 132 million citizens (Philippine Disaster Situation, 2014). Extreme storms are one of the most prominent climate-related hazards in the Philippines. The torrential rainfall intensity and frequency have both escalated since the mid-20th century in the country and in the last decade, the tropical storms and cyclones are frequently accompanied by storm surges, high winds, flooding, and landslides (Hilly et al., 2016). Typhoon-related damages and monsoonal rains have contributed to the highest damages to agriculture. Typhoon Yolanda caused more than P28 billions of damages in agriculture in 2013. In 2014, more than P21 billion in damages to coconut areas were dealt with by Typhoon Glenda. Rice production worth P9 billion was lost due to Typhoons Karen and Lawin in 2016 (Department of Agriculture, 2017). By 2050, losses due to floods are expected to intensify which causes the number of individuals susceptible to flooding around the globe to rise to 2 billion because of climate change, denuded watersheds, landuse change, sea levels rise, and increase in population in flood plain areas (Bogardi, 2004; ICHARM, 2009; Vogel, et al., 2011)

Flood Forecasting with sufficient lead time and accuracy has great significance for effective flood warning and emergency response. It is one among the few practical options to cope with floods in many parts of the world. There have been observed increase in the trustworthiness of forecasts due to rise in meteorological and hydrological expertise, better data collection mechanisms and improved knowledge and models for simulations and uncertainty analyses (Jain et al., 2018). Forecasters commonly rely on in situ measurements of precipitation and river stage (height of the water above a fixed reference point). Stream gauges often only measure river stage, and this must be converted to flow volume using information about the riverbed cross section (which itself often

changes). Lack of hydro-meteorological data for model calibration has always been an issue for predicting floods in ungauged basins (Pagano et al., 2014). The Philippines, being a developing country, is constrained with lack of permanent ground-based weather monitoring stations due to factors like lack of funding which leads to insufficient institutional setup and inadequate road infrastructures, among others (Ferraris et al., 2002). Another problem that arises when predicting floods in fast-response basins is that peak discharges tend to occur as a result of a localized rainfall event and times to peak may be too short for raising adequate warnings based on real time rainfall observations (Alejo, 2018).

A basin-wide flood monitoring and warning systems is being implemented sequentially in river basins of the Philippines, which suffer from severe floods (Miyamoto et al., 2014). The Cagayan River Basin is one of the 18 major river basins in the Philippines. It is a large basin comprising 27,281 km². The Cagayan River Basin in the Philippines was used as a case area for the present study. Flooding is one of the perennial problems existing in the basin and about 14% of the river basin is susceptible to flooding. Areas near the river systems have high to very high susceptibility to flooding of which cover mostly parts of Isabela and Cagayan (Climate-Responsive Integrated Master Plan for Cagayan River Basin, nd). All the rainfall coming from the 18 tributaries is being discharged in the Cagayan River down to the Babuyan channel at Aparri. It was observed that CRB had problems with inundation around main rivers. Riverside municipalities, especially those located on river mouths, experience the heaviest inundation (Alfonso et al., 2019). Magat Dam has always been solely blamed to cause floods in Cagayan. The inflow coming to Magat reservoir comes from Vizcaya and Ifugao province. Cagayan River Basin has 15 sub-basins, one of these is the Magat River Basin. Of all tributaries of the Cagayan River, Magat Dam is the only one that has hydrological data closely monitored. Among 18 tributaries of CRB, only the Magat dam can regulate the volume of water coming from upstream areas. Magat Dam is the only dam with control gates among 4 dams (Addalam, Magat, Siffu, and Chico) within CRB, others are already runoff-the-river type dams wherein water is continuously flowing. Miyamoto et. Al 2014 also stated that the Cagayan River basin is suffering from frequent severe floods as well as other river basin in the Philippines. Although real-time flood monitoring system has been installed, floods remain as a serious menace due to torrential rainfall by typhoon and insufficient accumulation of reliable hydrological data (Miyamoto et al., 2014). Complex models, such as those physically based and distributed, usually require large amounts of hydro-meteorological data, which are commonly not available in data-scarce conditions. The main issue for predicting flood hydrograph in data-scarce basins is the lack of observational discharge data for the selection and calibration of an adequate model for prediction (Eduardo & Puga, n.d.).

Flood forecasting and warning is a prerequisite for flood strategy that should cover the entire river basin area and promote the coordinated development and management of actions regarding water, land and related resources. successful mitigation of flood damage. If models can be used to identify the extent of flooded areas on a near real-time basis, the information can be useful for disaster managers to estimate the severity of the damage and to prioritize regions for effective rescue work (Water Directors of the European Union, 2003). Flood forecasting modelling in small basins is primarily made using rainfall-runoff models, together with radar rainfall, telemetering rainfall data or rainfall forecasts, whereas in large basins, this usually involves rainfall-runoff and hydraulic models. Predicting floods in data-scarce basins is limited by the availability of good and sufficiently long time series of sub-daily rainfall and discharge observations for model calibration (Eduardo & Puga, n.d.). The catchment models applied for flood forecasting are categorized based on criteria which is either deterministic or data driven depending on how the processes on the catchment basin are characterized; or how the watershed is spatially distributed. Integrated equations in deterministic models are being solved which represents the different processes in watershed creating results for a certain set of parameters. On the other hand, models that are data-driven have the ability to mimic the random characteristics and processes that controls streamflow. Data-driven models are those that are stochastic in nature (i.e. regression, timeseries and Bayesian) and those timeseries that are nonlinear (i.e. Artificial Neural Networks, and Fuzzy) that require big volume and high-resolution hydrological data (Water Directors of the European Union, 2003).

The Artificial Neural Networks (ANNs) model has the potential to be used on rainfall-runoff modelling for flood forecasting (ASCE Task Committee, 2000a & 2000b). The ANNs, however, are not yet used in flood early warning systems operation, (Kneale & Smith, 2001). This is possibly due to several practical issues such as the need for huge volume of data, possibilities of model overfitting to datasets, errors in trend-shift, and not enough expertise on parameters (Dawson et al., 2006). Frequently, the reliability of the ANN model-based forecast is observed only at small lead times that leads to uncertainty flood event management applications (Prakash & Srinivasan, 2014). RR models combines the watershed's physical characteristics and its hydro-meteorological conditions to calculate river discharge and inundation depths. For RR models to adequately perform, it needs appropriate representation of the catchment and enough volume of good quality data. Typical distributed rainfall-runoff models define flow directions from topography, and track water flows along the defined flow directions;

therefore, the models are not capable of stimulating flood inundations, with a few exceptions (Yamazaki, D. et al., 2011).

For more effective and efficient flood forecasting in the insufficiently-gauged river basin, ICHARM has developed Integrated Flood Analysis System called “IFAS” [25]. The Indus-IFAS developed under a UNESCO Pakistan project also uses the RRI model for flood simulation over the lower Indus River. Thus, the Indus-IFAS becomes a coupling model taking advantages of the two powerful components: IFAS for high-speed simulation of runoff in upstream mountains and RRI for flood inundation simulation in downstream rivers. To further expand and disseminate the RRI model, ICHARM started the development of GUI in 2014 for easy input and output, and released it with an execution program on its website in 2016 [26].

The Rainfall-Runoff-Inundation model is a 2D grid cell-based hydrodynamic model capable of simulating both rainfall-runoff and flood inundation processes (Sayama et al., 2012). The RRI model has been successfully applied to several regions in the world to simulate flooding events with good performances in all cases (Sayama et al., 2012, Sayama et al., 2010, Nastiti et al., 2015). Ferrer et al., 2014 conducted flood hazard assessment under climate change using a rainfall-runoff-inundation (RRI) model in the Pampanga River basin, Philippines. However, it was not used for flood forecasting purposes which is imperative to reduce flood damages. To date, there are still no model-based flood forecasting system being used in the country. The RRI could use forecasted rainfall data to estimate the inflow that might cause flooding river basins. Simulated hourly runoff results can be used as an input to forecast Dam water levels that could be helpful for water managers and operators of Dams for decision making during extreme rainy events. Flood inundation in the River basins can be simulated to forewarn affected areas on the possible effect of flood brought by the heavy rainfall events. The RRI is a helpful tool in forecasting flood events because it only requires simple data input, calibrations and does not take a lot of time to produce simulated results. The RRI quantifies the surface runoff based on the rainfall amount of a certain extreme rain event. To predict flood risk and flood scenarios through the RRI model, it is essential to issue flood warnings and to complete evacuation processes in flash flood-prone river catchment areas.

2. Methods

2.1 Description of RRI Model. The Rainfall-Runoff-Inundation (RRI) model is a two-dimensional model capable of simulating rainfall-runoff and flood inundation simultaneously (Sayama et al., 2012; Sayama et al., 2015a; Sayama et al., 2015b). The model deals with slopes and river channels separately. At a grid cell in which a river channel is located, the model assumes that both slope and river are positioned within the same grid cell. The channel is discretized as a single line along its centerline of the overlying slope grid cell. The flow on the slope grid cells is calculated with the 2D diffusive wave model, while the channel flow is calculated with the 1D diffusive wave model. For better representations of rainfall-runoff-inundation processes, the RRI model simulates also lateral subsurface flow, vertical infiltration flow, and surface flow. The lateral subsurface flow, which is typically more important in mountainous regions, is treated in terms of the discharge-hydraulic gradient relationship, which takes into account both saturated subsurface and surface flows. On the other hand, the vertical infiltration flow is estimated by using the Green-Amp model. The flow interaction between the river channel and slope is estimated based on the different overflowing formulae, depending on water-level and levee-height conditions (Sayama,2017).

2.2 Brief description of the Case Study Area. The CRB is located in the northeastern part of Luzon Island. It lies between 15° 52' and 18° 25' north latitude and between 120° 51' and 122° 18' east longitude. The total basin area and river length of the Cagayan River is 27,281 km² and 520 km, respectively. The major tributaries of the Cagayan River are the Chico (basin area: 4,550 km²), Siffu-Mallig (2,015 km²), Magat (5,110 km²) on the left side, and Pared (970 km²), Tuguegarao (660 km²), Tumauini (960 km²) and Ilagan (3,130 km²) (Fig. 1).

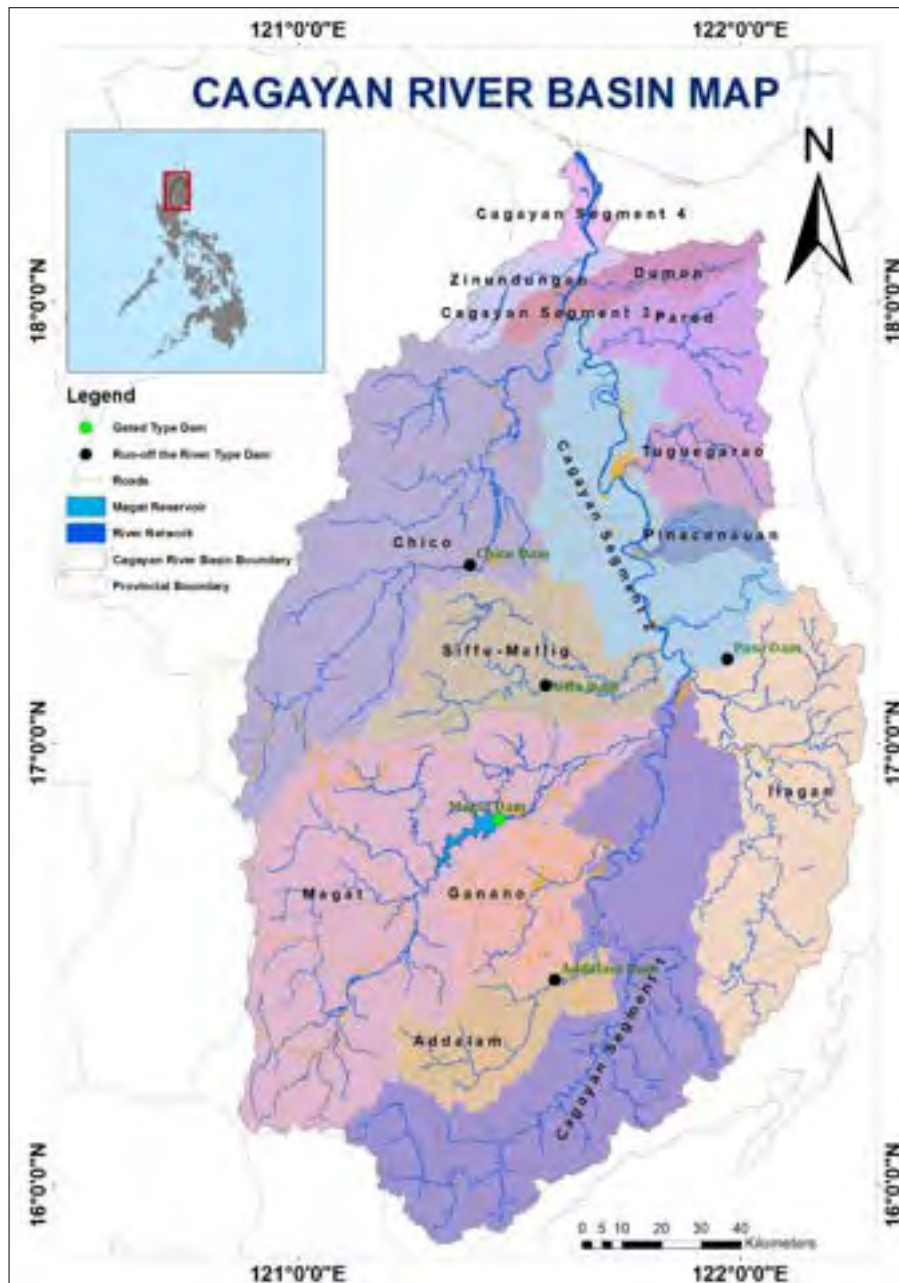


Figure 1. Cagayan River Basin Map

2.3 RRI Calibration, validation, and performance assessment of the Cagayan River Basin RRI model. The RRI parameters were adjusted manually based on the largest parameter map unit the RRI model built. These units are the dominant combination of soil, elevation, and landcover in the Basin. Inflow data from Magat dam was used for the RRI performance assessment. Inundations were validated based on flood stages in flooded areas in Isabela and Cagayan. The RRI model for the Cagayan River Basin was assessed based on statistical indices. Statistical indicators for model performance evaluation that were used are selected based on the recommendations of Moriasi et al. (2007).

The coefficient of determination (R^2), Nash–Sutcliffe model efficiency (NSE), RMSE-observations standard deviation ratio (RSR), and percent bias (PBIAS) are the most widely used indicators for hydrological studies and assessments. The R^2 describes the ratio of the variance in observed data explained by the model. R^2 ranges from zero to one, with higher values indicating less error of variance, and typically values greater than 0.5 are considered acceptable (Santhi et al., 2001; Van Liew et al., 2003). The Nash-Sutcliffe efficiency (NSE) is a normalized statistic that defines the relative magnitude of the residual variance compared to the observed data variance (Nash and Sutcliffe, 1970). NSE of greater than 0.5 is widely considered satisfactory. RSR is the ratio between the root mean square error (RMSE) and the standard deviation of the observed values. Zero RSR means

there is no error and the model is perfect for simulations. A lower RSR value generally means better simulation results and a value <0.7 implies a satisfactory model rating. Percent bias (PBIAS) measures the average tendency of the simulated data to be larger or smaller than their observed counterparts [33]. A PBIAS of $\pm 25\%$ is considered satisfactory.

2.4 Data Input. Input needed in RRI are the Digital Elevation Model (DEM), Flow Accumulation, Flow Direction, Actual rainfall from Magat Rain gauge instruments, PAG-ASA AWS, and Forecasted Rainfall data. For simulation and validation, actual hourly inflow data from Magat Dam was used. Landuse and Soil Maps integrated with the RRI model were validated on the ground.

The hourly rainfall data from NIA-MARIIS DRD Flood Forecasting and Instrumentation Section and PAGASA AWS (<https://philsensors.asti.dost.gov.ph/site/data>) was used for the calibration of the model during Typhoon Ulysses and rainfall for two (2) other extreme events (Typhoon Tisoy and Northeast monsoon) for validation were also collected. All the weather stations with available rainfall data were extracted particularly from the Province of Isabela, Quirino, Nueva Vizcaya, Mountain Province, Aurora, Kalinga, Apayao, and Cagayan. There were 69 weather stations with available rainfall data for Typhoon Ulysses (Nov 8-13, 2020), 49 for Monsoon Rains (Dec 15-21, 2020) & 92 for Typhoon Tisoy (Dec 1-10, 2019) (Figure 2).

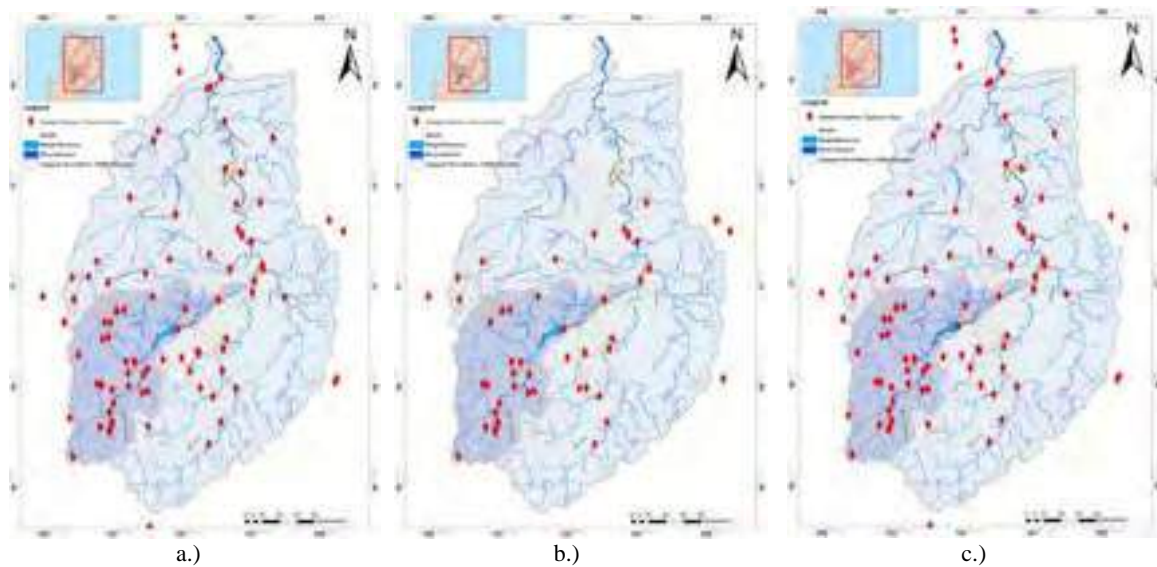


Figure 2. Available Weather Stations during Typhoon Ulysses (a), Monsoon Rains (b), and Typhoon Tisoy (c)

3. Results and Discussion

3.1 Characterization of Soil Properties in Cagayan River Basin. Soil Type from RRI default was used in the calibration of the model (Figure 3a). As shown in Figure 3b, the Soil type from BSWM was reclassified and was validated on the part of Magat Watershed. Sandy clay loam, clay loam, and clay were very visible from the default soil type data of RRI. The resolution of the two soil maps is one of the apparent differences. Figure 3b shows a detailed soil type map within Cagayan River Basin while the default soil map in the RRI model is 30 meters by 30 meters resolution. It is also apparent that the soils in the BSWM map are more variable than the soils in the default RRI map. Notably, it can be observed that there are relatively consistent similarities in the majority of the spatial locations of clay loam over the two soil map datasets. Also, the mountain soils in the BSWM soil map were almost consistently classified as Clay in the RRI model default soil map. These differences in soil could be a source of variance between the modeled and actual inflow, water level, and flood inundations.

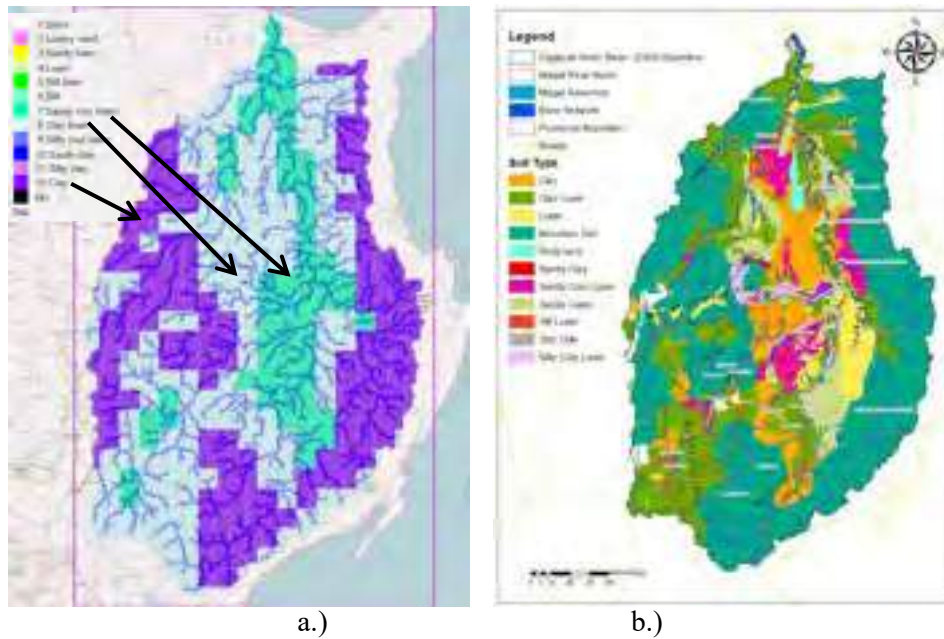


Figure 3. The default soil type in RRI (a) and the reclassified BSWM soil type (b)

Lack of actual data for the soil property in the parameter calibration of RRI that includes porosity, hydraulic conductivity, and soil depth was also one of the limitations of the model to accurately mimic the actual soil properties of the study area. However, most of the said soil parameters were set to zero in the calibration to further increase the simulated values of inflow and water level heights.

3.2 Land Cover in Cagayan River Basin. The landcover input used in the model was the default in the RRI model (Figure 4a) where the dominated landcover data was broadleaf deciduous forest along the east and west borders of the basin, and cropland in the middle part. Figure 4b reveals the 2015 landcover map obtained from NAMRIA which is the latest landcover map released to date. It can be observed that the dominant land cover of NAMRIA in the middle part of the basin was also crops particularly annual crops and the east and west borders are mainly closed and open forests. Figure 5 shows the landcover data validated by ISU-Echague under Project IFWARM for the Magat River watershed where the west borders are primarily closed and open forest. The Magat River Watershed is located in the Southeastern part of the Cagayan River Basin.

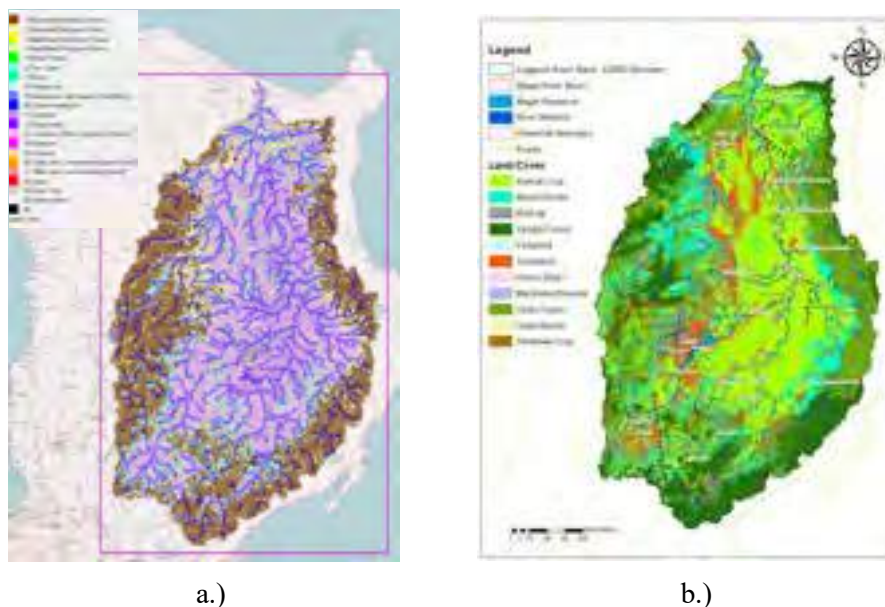


Figure 4. The default landcover map in RRI (a) and the reclassified NAMRIA

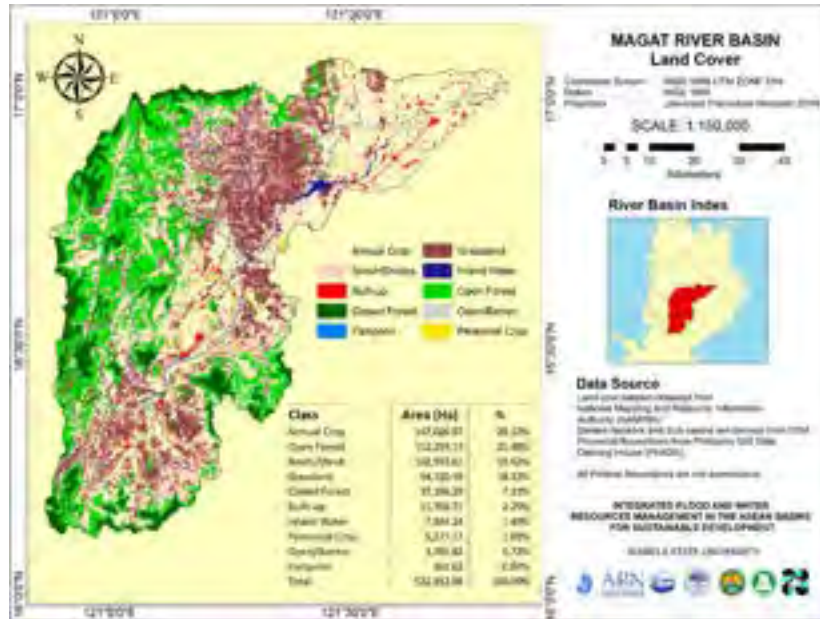


Figure 5. Validated Landcover Map (ISUE-PROJECT IFWARM)

Comparing these maps, it can be observed that there are not much differences in the dominant landcover. They only differ in nomenclatures which are completely explained by the difference in map data sources. On the other hand, it can be observed that there are more grasslands in the NAMRIA landcover map than the bare soils in the RRI default landcover map. These differences in land cover could be a source of variance in modeled and actual inflow, water level, and flood inundations on top of the differences in soils.

3.3 Calibration and Performance Validation of Rainfall-Runoff-Inundation Model

3.3.1 The RRI Model Calibrated Parameters. The table shows the parameters that were calibrated in the model. During the process of calibration, the parameters that has the most significant effect in the simulated results were the Manning's roughness coefficient for river and land (n_s river, and n_s slope), followed by the vertical and lateral hydraulic conductivity (k_{sv} , & k_a) which is both set to zero where saturated subsurface + saturation excess overland flow are considered and soil depth. Just like the study of Abdel-Fattah et al., (2018) wherein the sensitivity analysis for the RRI model was conducted in W. Samail. According to results from sensitivity analysis, the most significant parameters in all flow cases are channel roughness coefficient (n_{river}) and hillslope roughness coefficient (n_{slope}). The soil depth and soil porosity (ϕ) are the second most significant parameters after the roughness coefficients. While vertical saturated hydraulic conductivity (k_v), lateral saturated hydraulic conductivity (k), and unsaturation effective porosity (ϕ_u) have a medium impact on the generated hydrographs. The suction at the vertical wetting front (S_f) and the lateral unsaturated hydraulic conductivity have a minor impact on the model results.

Table 1. RRI Calibrated Parameter Values

| Parameter | Definition | Parameter Set | | | | | | | | |
|----------------|---------------------------------|---------------|--------|--------|--------|----------|--------|--------|--------|--------|
| | | 1 | 2 | 3 | 4 | 5 | 6 | 7 | 8 | 9 |
| n_{s_river} | channel roughness coefficient | | | | | 6.500d-3 | | | | |
| | hillslope roughness coefficient | 3.000d | 2.000d | 2.500d | 9.000d | 6.000d | 6.000d | 6.000d | 9.000d | 9.000d |
| n_{s_slope} | soil depth | -1 | -1 | -1 | -1 | -1 | -1 | -1 | -1 | -1 |
| | soil porosity | 2.000d | 2.000d | 5.000d | 1.000d | 1.000d | 4.000d | 5.000d | 6.000d | 5.000d |
| γ_{maa} | soil depth | 0 | 0 | -1 | -1 | -1 | -1 | -1 | -1 | -1 |
| | soil porosity | 4.640d | 1.670d | 1.670d | 4.640d | 3.980d | 4.630d | 4.750d | 3.980d | 3.980d |
| k_{sv} | vertical saturated | -1 | -1 | -1 | -1 | -1 | -1 | -1 | -1 | -1 |
| | soil depth | 0.000d | 0.000d | 0.000d | 0.000d | 0.000d | 0.000d | 0.000d | 0.000d | 0.000d |
| k_{sv} | soil depth | 0 | 0 | 0 | 0 | 0 | 0 | 0 | 0 | 0 |
| | soil porosity | 0 | 0 | 0 | 0 | 0 | 0 | 0 | 0 | 0 |

| | | | | | | | | | | |
|-----------|---------------------------------------|--------|--------|--------|--------|--------|--------|--------|--------|--------|
| | hydraulic conductivity | | | | | | | | | |
| | suction at the vertical wetting front | 2.185d | 2.185d | 2.185d | 2.088d | 2.088d | 2.088d | 3.163d | 3.163d | 3.163d |
| faif / Sf | | -1 | -1 | -1 | -1 | -1 | -1 | -1 | -1 | -1 |
| | lateral hydraulic conductivity | 0.000d | 0.000d | 0.000d | 0.000d | 0.000d | 0.000d | 0.000d | 0.000d | 0.000d |
| ka | | 0 | 0 | 0 | 0 | 0 | 0 | 0 | 0 | 0 |
| | unsaturation effective porosity | 4.000d | 4.800d | 3.800d | 4.500d | 2.500d | 2.500d | 2.000d | 1.000d | 5.000d |
| gammam | | -2 | -2 | -2 | -2 | -2 | -2 | -2 | -2 | -2 |

3.3.2 The RRI calibration results using the Magat Inflow and Buntun Water Level. The most severe typhoon in 2020, Typhoon Ulysses caused flash floods in many places in Cagayan Valley particularly in Tuguegarao, Cagayan was used for the calibration of the RRI model. The result shows the actual and simulated Magat Inflow during Typhoon Vamco/Ulysses on November 8-13, 2020 (Figure 6a). The observed maximum inflow was recorded on November 12, 2020, at 7:00 pm with 7,128 m³/s while the peak inflow simulated from the Rainfall-Runoff-Inundation model was 6933.2 m³/s that was also on November 12, 2020, at 7:00 pm. The RRI model underestimated the peak flow inflow by only 2.7%. Also, the RRI model was able to estimate the date and time of the peak inflow correctly relative to the observed peak inflow date and time.

The statistical indicators in evaluating the RRI performance in estimating hourly discharge are based on the recommendations of Moriasi et al. (2007). The coefficient of determination (R^2), Nash–Sutcliffe model efficiency (NSE), RMSE-observations standard deviation ratio (RSR), and percent bias (PBIAS) are the most widely used indicators for assessments base on the literature reviewed. Based on the statistical indices, the model satisfactorily estimated the inflow in Magat with R^2 , RSR, NSE, and PBIAS equal to 0.88, 0.36, 0.87, 6.90, respectively (Figure 6c). The simulated peak inflow was estimated by RRI at almost the same time as the actual peak inflow. This is particularly important as it is very crucial for flood forecasting in Magat Dam to estimate the peak inflow during extreme weather events, especially typhoons. As shown in the computed statistical indices, the coefficient of determination (R^2) with a value of 0.88 revealed that the estimated inflow shows good agreement with the observed inflow data. The coefficient of determination or squared correlation coefficient R^2 describes the degree of collinearity between simulated and measured data. Percent bias or PBIAS measures the average tendency of the simulated data to be larger or smaller than their observed counterparts. The optimal value for PBIAS is zero (0). A positive PBIAS value of 6.90 indicates that the simulated discharge underestimated the actual data. Though the peak was underestimated, a difference of 195 cms is considered insignificant. The simulated peak value was in close agreement with the actual maximum recorded inflow of Magat during the typhoon. Nash-Sutcliffe efficiency indicates how well the plot of observed versus simulated data fits the 1:1 line. The NSE value of 0.87 is considered satisfactory because the optimal value of Nash-Sutcliffe Efficiency is one (1). The RMSE-Observation Standard Deviation Ratio, RSR with a value equal to 0.36 determines the accuracy of the model concentration of data in the line of best fit. And the value of RSR with 0.36 shows good model simulation performance. The lower the RSR, the lower the RMSE, and the better the model simulation performance.

The calibrated RRI model was validated using the water level data at Buntun bridge located in Tuguegarao City, Cagayan. Figure 6b shows the actual and simulated Buntun Water Level located in Tuguegarao City, along the Cagayan River. The Cagayan River water level in Buntun bridge reached its maximum critical level with 13.3 meters on November 13, 2020, at 10:00 PM. As observed from the graph, the RRI model simulated river depth peaked on November 13 at 13.6 meters at 9:00 AM. The RRI model simulated the peak river height 8 hours earlier than the actual. Simulating earlier could be better relative to later peak flow simulations to enable earlier flood warning alarms. This way, damages and loss of lives could be prevented. Statistically, the R^2 , RSR, NSE, and PBIAS with 0.75, 0.50, 0.75, -0.39, respectively, showed good agreement with the measured river water level data (Figure 6d). A negative PBIAS value of -0.39 indicates an overestimation of the measured data.

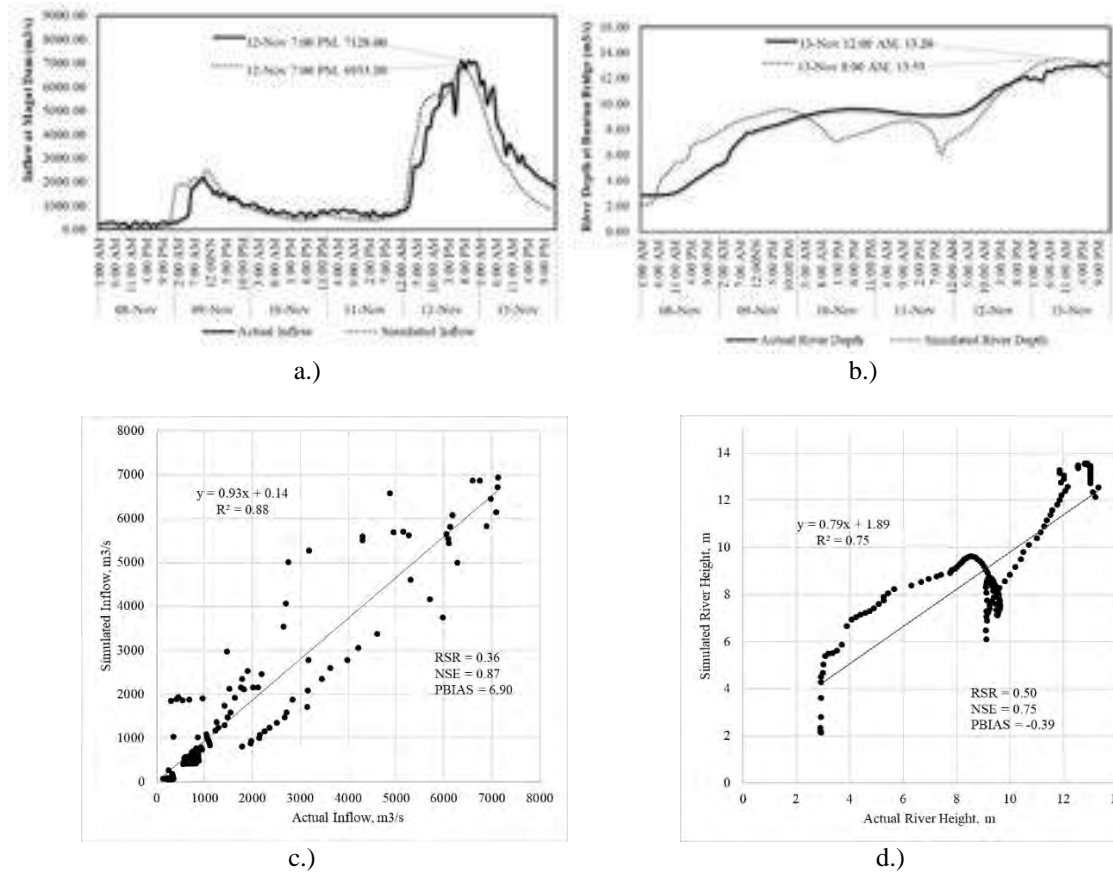


Figure 6. RRI Model Calibration on Typhoon Ulysses at Magat Dam (Left) (a) (c) and Buntun Bridge (Right) (b) (d)

3.4 Validation of RRI Model Calibrated Parameters. The calibrated parameters from Typhoon Ulysses were tested and validated on other extreme weather events during Typhoon Tisoy (December 1-10, 2019) and Northeast Monsoon (December 15-21, 2020). Results showed that the RRI model has better performance during the Monsoon rains in December 2020. Uncertainties on the model can be attributed to the input data used, just like Bhagabati S. & Kawasaki A., 2017 mentioned in their study that several other factors may help improve the RRI model: (1) more precipitation data, (2) a consideration of dam operations, and (3) higher-resolution elevation data (Jain et al., 2018). Accurate precipitation data are the most important in implementing the model.

3.4.1 RRI Model Validation on Typhoon Tisoy (December 1-10, 2019). It can be seen that the RRI simulations statistically agreed with the observed data during typhoon Tisoy with a value of R^2 , RSR, NSE, and PBIAS of 0.77, 0.83, 0.30, and 34.81 which is considered satisfactory (Figure 7c). The statistical indices were lower during typhoon Tisoy but in terms of simulating the peak flow, the model can get the maximum inflow on December 4 at 5:00 AM with 1,276.26 m³/s compared to the actual with 1,231 m³/s peaked on the same day at 9:00 AM (Figure 7a). The PBIAS 34.81 shows an underestimation of the actual data. The underestimation bias was due to the capability of the model to simulate lower inflow values. This can be attributed to the groundwater parameter which affects the water on the streams. Abdel-Fattah M. et al. (2018) mentioned that the main source of the bias error is the absence of a stable groundwater module in the RRI model (under development), to represent the active groundwater processes in W. Samail such as groundwater recharge and seepage to the channel. Even the hydrological model has good generation for the hydrograph main peak in terms of value and time to peak, still, the model cannot generate some small and minor peaks in the measured data.

The model is also verified in another validation point located in Buntun Bridge wherein the simulated river height of 11.75 meters on December 6 at 2:00 AM was closed to the maximum actual data of 12.22 meters on December 6 at 4:00 AM (Figure 7b). Statistical indices of R^2 , RSR, NSE, and PBIAS of 0.77, 0.88, 0.23, and 31.86 respectively are already satisfactory. As revealed in the graph there are simulated data that do not agree with the actual (Figure 7d). Based on Jain et al. 2018, in flood forecasting, a model with constant parameters may not be able to completely represent the complex processes in a basin. As a result, the simulated hydrograph can differ from the observed hydrograph, mainly due to uncertainties in input data, differences between basin physics and model structure, model calibration, and changes in catchment characteristics over time. Serban and Askew (1991)

categorized these errors as (i) volumetric or amplitude errors, (ii) timing or phase errors, and (iii) shape errors. The volumetric errors are mainly attributed to inadequate model structure and basin representation, input/output data error, or a combination of these errors. Timing errors may be introduced by the routing component of the model or by spatial and temporal discretization, whereas the shape errors are induced mainly in the conversion of rainfall to runoff by the model. These three types of errors can occur in different combinations in hydrologic models.

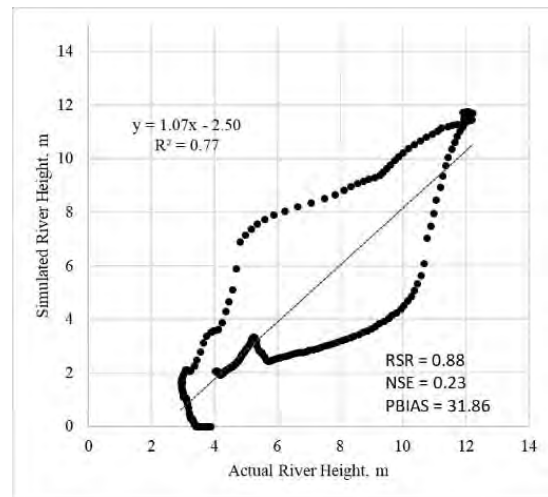
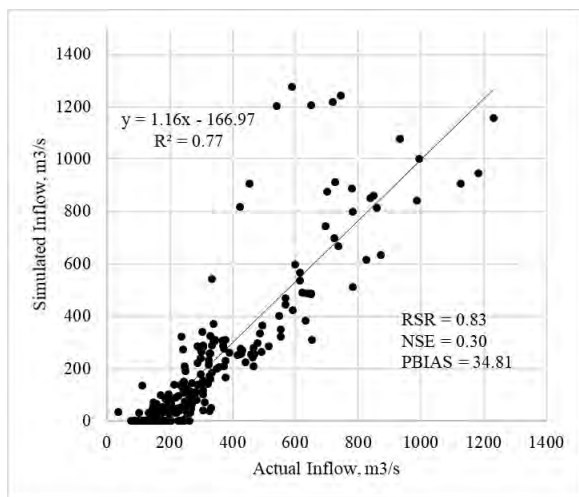
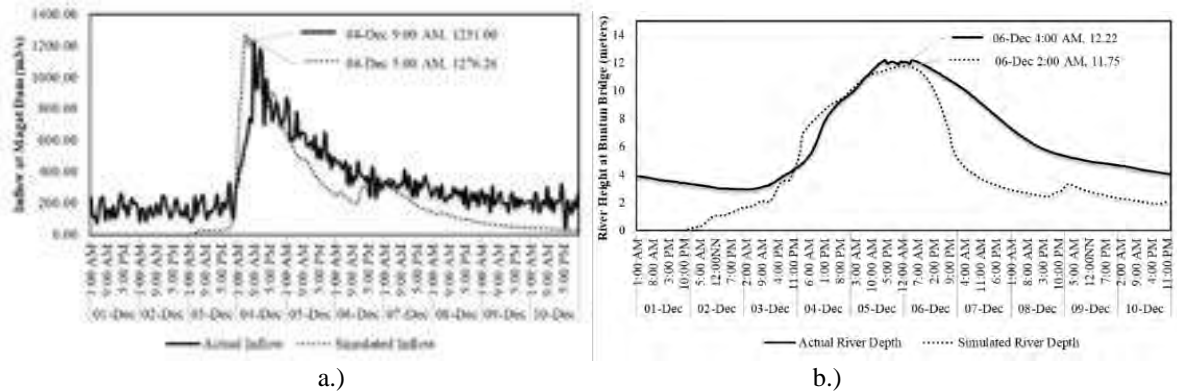


Figure 7. RRI Model Validation on Typhoon Tisoy at Magat Dam (Left) (a) (c) and Buntun Bridge (Right) (b) (d)

3.4.2 RRI Model Validation on Northeast Monsoon (December 15-21, 2020). The model was also tested in one extreme event on December 15-21, 2020 wherein the Northeast monsoon was experienced. Statistical indices of R2, RSR, NSE, and PBIAS showed satisfactory values with 0.85, 0.50, 0.75, and 22.36 respectively (Figure 8c). The simulated peak was higher with 22.85 percent compared to the actual maximum inflow of 2,755 m³/s on December 19, 2020, at 7:00 PM (Figure 8a). The underestimation bias was also due to the lower simulated values seen before and after the peak discharge. The amplification of the data was mimicked by the model though it occurred earlier than the actual time. Validation on the Northeast Monsoon which affects the Buntun water level had better R2, RSR, NSE, and PBIAS of 0.88, 0.35, 0.87, and -1.30, respectively (Figure 8d). The maximum simulated river height of 11.98 meters that occurred on December 20, 2020, at 8:00 AM was close to the peak river height on the same day at 10:00 PM with 11.68 meters (Figure 8b). A negative PBIAS of -1.30 shows an overestimation bias on the actual data which is better than an underestimation bias.

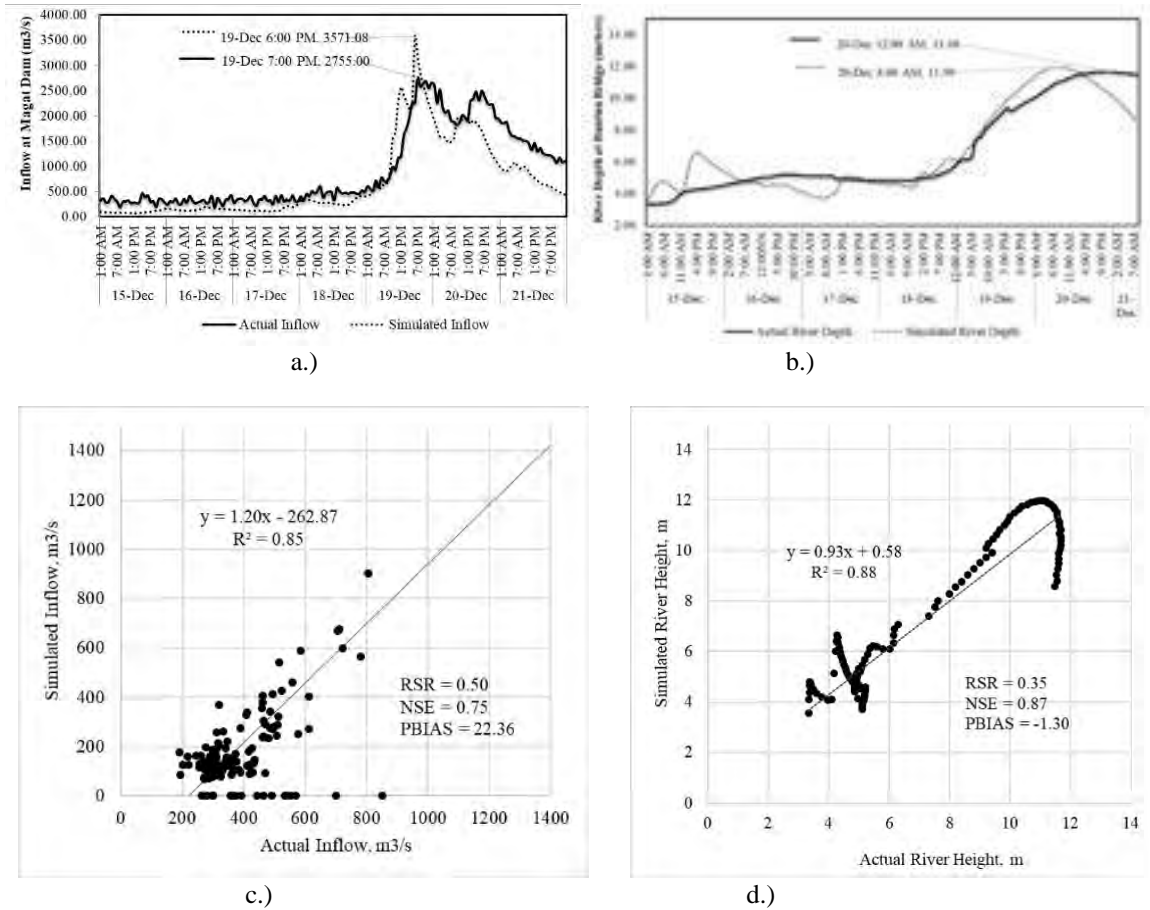


Figure 8. RRI Model Validation on Monsoon Rains (Left) (a) (c) and Buntun Bridge (Right) (b) (d)

3.5 Flood Inundation in Cagayan River Basin. Figure 9 reveals the gathered actual flood heights caused by Typhoon Ulysses in Cagayan. These flood residents' interviews the said data show that the maximum height was located in Annafunan, Tuguegarao City, Cagayan that reached the flood height of 7 meters followed by Baculud, Amulung with 5.0 meters. This place is near the Buntun Bridge. The spatial location of these data is mapped out in Figure 10 which shows the minimum and maximum flood height in Isabela and Cagayan. The actual flood height varies from 0.5 meters in Gattaran, Cagayan to 2.6 meters in Santa Maria, Isabela. The actual data gathered however is limited only to places where the validation interview was conducted.

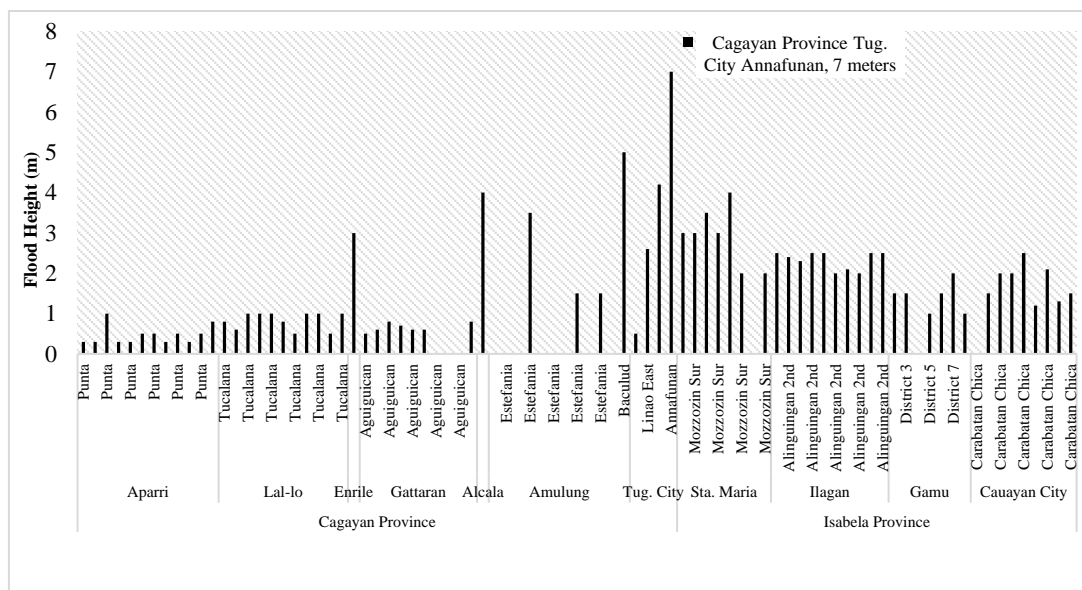


Figure 9. Flood Inundation Height during Ulysses

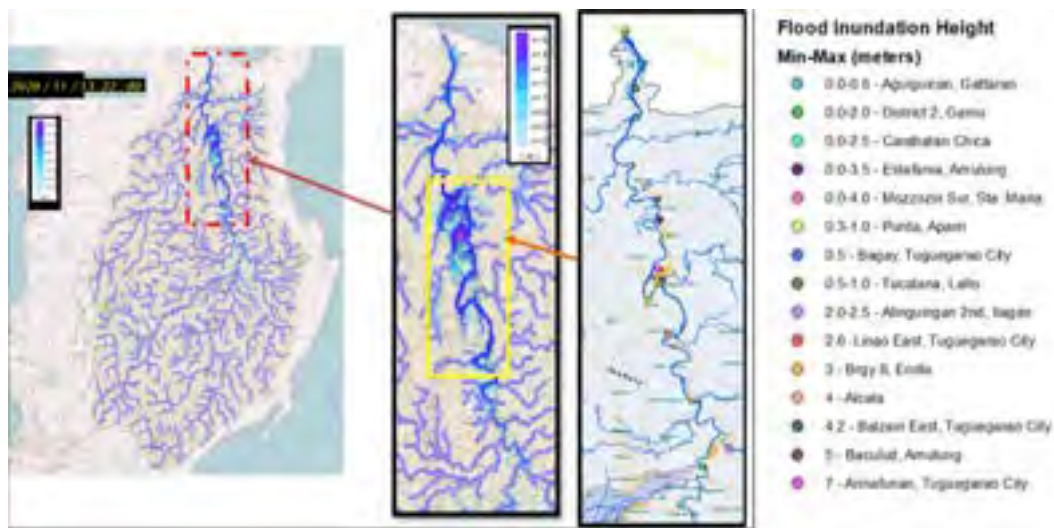


Figure 10. The actual minimum and maximum flood height map (point symbols) along the Cagayan River Basin.

The Inundation Map from RRI in Figure 10 showed the depth of flooding caused by Typhoon Ulysses on November 13 at 10 PM. From the actual surveyed data that was gathered on the barangays of each municipality located near the Cagayan River, as observed from both Maps, the RRI result is almost the same as the gathered actual data with flood height reached during the event. From the RRI map, the concentration of the flood water was found to be in the parts of Amulung and Alcalá. The maximum flood height in Cagayan was found to be in Annafunan, Tuguegarao City. Followed by Baculud, Amulung with 5 meters, and Alcalá with 4-meter-high flood water. Mozzozin Sur has a 0-4.0 meters flood height. The location of the 4 meters is located in the lowest part of the barangay. Reports and social media posts, however, showed that flood heights reached up to the second-storey of houses particularly in Tuguegarao City, Cagayan which rendered residents to stay at the roofs of their houses during the peak floods brought by Typhoon Ulysses. This could be estimated to be about 6 meters in height. The RRI model estimated maximum flood heights to be ≥ 6 meters. This implies that the RRI model was able to capture the flood inundations spatial range and variability in the Cagayan River Basin.

3.6 Cagayan River Subwatershed Discharge to Buntun Bridge During Typhoon Ulysses



Figure 11. Cagayan River Subwatershed Upstream of Buntun Map.

Table 2. Percent RRI Simulated Discharge (Q) per Subwatershed relative to Buntun Q.

| Subwatershed Outlet | Basin Area (ha) | RRI Simulated Maximum Peak Inflow (m ³ /s) | % Discharge (Q) Relative to Buntun Q | Time to Peak (dd/mm/yyyy hh:mm) |
|---------------------------|-----------------|---|--------------------------------------|---------------------------------|
| Buntun Bridge | | 23,180 | | 13/11/2020 22:00 |
| Magat Watershed (Gamau) | 522,812.08 | 7306 | 31.52 | 12/11/2020 22:00 |
| Upper Cagayan (Naguillan) | 665,090.10 | 15866 | 68.44 | 12/11/2020 18:00 |
| Siffu-Mallig | 194,087.41 | 3578 | 15.43 | 09/11/2020 12:00 |
| Pinacanauan De Ilaguen | 311,716.17 | 7591 | 32.75 | 11/11/2020 0:00 |
| Pinacanauan De Tumauni | 21,114.76 | 323 | 1.39 | 08/11/2020 22:00 |
| Pinacanauan De San Pablo | 34,183.98 | 564 | 2.43 | 08/11/2020 9:00 |
| Pinacanauan De Tuguegarao | 45,090.10 | 1244 | 5.37 | 12/11/2020 12:00 |

The subwatersheds of upstream of Buntun were mapped out (Figure 11). The simulated discharge was extracted on RRI which is located on the outlet of each subbasin. These are the Upper Cagayan wherein the outlet discharge that was collected on the part of Naguillan along Cagayan River, the Magat Watershed in Gamau, Siffu-Mallig, Pinacanauan de Ilaguen, Pinacanauan de Tumauni, Pinacanauan De San Pablo, and Pinacanauan De Tuguegarao. The Percentage inflow relative to Buntun discharge was computed (Table 3). The result shows that the Upper Cagayan had the largest peak inflow of 15,866 m³/s which is 68.44% of Buntun Simulated Discharge on November 13 at 10:00 PM, Buntun reached its actual maximum critical level of 13.3 meters. The peak time of the discharge extracted in subwatersheds' outlet was shown in Table 3, the RRI simulated discharge in Buntun with 23, 180 m³/s has peaked on November 13 at 8 AM. It also revealed that the Pinacanauan San Pablo and De Tumauni has a peak discharge of 564 and 323 m³/s on November 8, 2020, at 9 PM and 10 PM, respectively followed by Siffu-Mallig with a peak of 3,578 m³/s November 9 at 12:00 NN, Pinacanauan De Ilaguen with 7,591 m³/s on November 11 at 12:00 AM while in the Upper Cagayan (the discharge data was extracted in Naguillan) with 15,866 m³/s which appears to be the subwatershed with the largest amount of discharge contribution peaked on November 11 at 6 PM. The last to reach the maximum discharge was the Magat Watershed (at Gamau outlet) with 7,306 m³/s on November 12 at 10 PM. The simulated discharge implies that the other subwatershed had already contributed to the flood height in low-lying areas in Isabela and Cagayan during Typhoon Ulysses.

4. Conclusion

This study assessed the performance of the Rainfall-Runoff-Inundation model to estimate the Magat dam inflow, river water level, and flood inundations in Cagayan River Basin. The results revealed that the RRI model could be used for estimating the Magat dam peak inflow as well as the peak's time and date. This could be a good basis for the conduct of pre-emptive water release in the Magat dam. Furthermore, it will provide necessary decision support for early flood warning alarms in the frequently flooded areas along the Cagayan River. Hence, the RRI model was able to satisfactorily estimate the river water level in the Buntun bridge located in Tuguegarao City, Cagayan. Moreover, the simulated time of peak flow was 8 hours early which could already be used as a good basis for early evacuation advisories. The flood inundations variability in the Cagayan River Basin was also captured by the RRI model. Based on the simulated discharge of Cagayan River tributaries during Typhoon Ulysses, the Magat dam and Magat River is not the sole contributor to the floods downstream. Results showed the potential of the Rainfall-Runoff-Inundation model as a science-based decision-making tool during extreme rainfall conditions. It can be used for flood forecasting, early flood warning systems, evacuation implementations, and emergency response. It could also be used as inputs to flood risk mapping and flood risk mitigations and adaptations plans and projects.

Acknowledgment: The authors would like to thank the agencies and projects mentioned in this article, which generously shared their data. This work was supported by the Department of Science and Technology – Philippine Council for Industry, Energy, and Emerging Technology Research and Development in collaboration with Thuy Loi University of Vietnam and Kyoto University of Japan.

Author contribution Engr. Alejandro collected the data, conceived the analysis, performed the analysis, and wrote the paper. Dr. Alejo conceived, designed the analysis, supervised the analysis and proofread the paper. Dr. Balderama, Dr. Bareng & Dr. Kantoush supervised the analysis.

Code availability Not applicable

Declarations

Ethics approval Not applicable

Consent to participate The authors participated in the publication process voluntarily

Consent for publication The authors understand and adhere to all the submission and publication policies of the journal.

Conflict of interest The authors declare no competing interests.

References

- Abdel-Fattah, M., Kantoush, S. A., Saber, M., & Sumi, T. (2018). Rainfall-Runoff Modeling For Extreme Flash Floods In Wadi Samail, Oman. *Journal of Japan Society of Civil Engineers, Ser. B1 (Hydraulic Engineering)*, 74(5), I_691-I_696. https://doi.org/10.2208/jscejhe.74.5_i_691.
- Alejo, L. 2018. Suitability analysis for optimum network of agrometeorological stations: A case study of Visayas region, Philippines. *Journal of Agrometeorology*. Vol. 20 No. 4. 269-274. <https://doi.org/10.54386/jam.v20i4.564>
- Alfonso, C. D. Q., Sundo, M. B., Zafra, R. G., Velasco, P. P., Aguirre, J. J. C., & Madlangbayan, M. S. (2019). Flood risk assessment of major river basins in the philippines. *International Journal of GEOMATE*, 17(64), 201–208. <https://doi.org/10.2166/0/2019.64.17155>
- ASCE Task Committee on Application of Artificial Neural Networks in Hydrology, 2000a. Artificial neural networks in hydrology I: preliminary concepts. *Journal of Hydrological Engineering*, 5 (2), 115–123. doi:10.1061/(ASCE)1084-0699(2000)5:2(115).
- ASCE Task Committee on Application of Artificial Neural Networks in Hydrology, 2000b. Artificial neural networks in hydrology II: hydrologic applications. *Journal of Hydrological Engineering*, 5 (2), 124–137. doi:10.1061/(ASCE)1084-0699(2000)5:2(124).
- Bhagabati, S. S., & Kawasaki, A. (2017). Consideration of the rainfall-runoff-inundation (RRI) model for flood mapping in a deltaic area of Myanmar. *Hydrological Research Letters*, 11(3), 155–160. <https://doi.org/10.3178/hrl.11.155>
- Bogardi J. 2004. Update.unu.edu. The newsletter of the United Nations University and its international network of research and training centres/programmes. Issue 32. (available online at <http://update.unu.edu/archive/issue32.htm>).
- Climate-Responsive Integrated Master Plan for Cagayan River Basin VOLUME I-EXECUTIVE SUMMARY. (n.d.).
- Coffman, K., 2013: Property losses from Colorado flood projected at about \$2 billion. Reuters, 19 September. [Available online at www.reuters.com/article/2013/09/19/us-usa-colorado-flooding-idUSBRE98H1BA20130919.]
- Dawson, C. W. et al., 2006. Flood estimation at ungauged sites using artificial neural networks. *Journal of Hydrology*, 319 (1), 391–409. doi:10.1016/j.jhydrol.2005.07.032.
- Department of Agriculture [DA] (2017). Damages to agriculture\ sector. Quezon City, PH: Department of Agriculture – Field Programs Operational Planning Division.
- Eduardo, J., & Puga, R. (n.d.). Flood Prediction in data-scarce basins Maximising the value of limited hydro-meteorological data. <http://urn.kb.se/resolve?urn=urn:nbn:se:uu:diva-368532>
- Ferraris, L., Rudari, R. & Siccardi, F. (2002) The Uncertainty in the Prediction of Flash Floods in the Northern Mediterranean Environment. *J. Hydrometeorology*. 3, 714–727.
- Ferrer S.B., Gusyev, M., & Husiev, A. (2014). ASSESING CURRENT AND FUTURE FLOOD IMPACTS IN THE PAMPANGA RIVER BASIN , PHILIPPINES. 22–32.
- Gupta, H. V., S. Sorooshian, and P. O. Yapo. 1999. Status of automatic calibration for hydrologic models: Comparison with multilevel expert calibration. *J. Hydrologic Eng.* 4(2): 135-143.
- Hilly, B. F., Roa-Quiaoit, A., Lo, D., & Narisma, G. (2016). Climate Disasters in the Philippines: A Case Study of Immediate Causes and Root Drivers from Cagayan de Oro, Mindanao and Tropical Storm Sendong/Washi. www.belfercenter.org/ENRP
- ICHARM Report, 2009. Global trends in water related disasters: an insight for policymakers. International Centre for Water Hazard and Risk Management (UNESCO), Tsukuba, Japan, <http://www.icharm.pwri.go.jp>
- Jain, S. K., Mani, P., Jain, S. K., Prakash, P., Singh, V. P., Tullios, D., Kumar, S., Agarwal, S. P., & Dimri, A. P. (2018). A Brief review of flood forecasting techniques and their applications. *International Journal of River Basin Management*, 16(3), 329–344. <https://doi.org/10.1080/15715124.2017.1411920>

- Jain, S. K., Mani, P., Jain, S. K., Prakash, P., Singh, V. P., Tullos, D., Kumar, S., Agarwal, S. P., & Dimri, A. P. (2018). A Brief review of flood forecasting techniques and their applications. *International Journal of River Basin Management*, 16(3), 329–344. <https://doi.org/10.1080/15715124.2017.1411920>
- Jain, S. K., Mani, P., Jain, S. K., Prakash, P., Singh, V. P., Tullos, D., Kumar, S., Agarwal, S. P., & Dimri, A. P. (2018). A Brief review of flood forecasting techniques and their applications. *International Journal of River Basin Management*, 16(3), 329–344. <https://doi.org/10.1080/15715124.2017.1411920>
- Kneale, P.E., See, L., and Smith, A., 2001. Towards defining evaluation measures for neural network forecasting models. *Proceedings of the Sixth International Conference on GeoComputation*, University of Queensland, Australia.
- Miyamoto, M., Ono, M., Nabesaka, S., Okazumi, T., & Iwami, Y. (2014). Applicability of a flood forecasting method utilizing global satellite information to an insufficiently-gauged river basin: a case of a river basin in the Philippines. *11th International Conference on Hydroinformatics*.
- Moriassi, D.N., Arnold, J.G., Van Liew, M.W., Bingner, R.L., Harmel, R.D., Veith, T.L., 2007. Model evaluation guidelines for systematic quantification of accuracy in watershed simulations. *Trans. ASABE* 50, 885–900.
- Nastiti, K. D., Kim, Y., Jung, K., & An, H. (2015). The application of Rainfall-Runoff-Inundation (RRI) model for inundation case in upper Citarum Watershed, West Java-Indonesia. *Procedia Engineering*, 125, 166–172. <https://doi.org/10.1016/j.proeng.2015.11.024>
- Pagano, T. C., Wood, A. W., Ramos, M.-H., Cloke, H. L., Pappenberger, F., Clark, M. P., Cranston, M., Kavetski, D., Mathevet, T., Sorooshian, S., & Verkade, J. S. (2014). Challenges of Operational River Forecasting. *Journal of Hydrometeorology*, 15(4), 1692–1707. <https://doi.org/10.1175/jhm-d-13-0188.1>
- Philippine Disaster Situation (2014). Citizen’s disaster response center. Retrieved from: <http://www.cdrc-phil.com/2014-philippine-disaster-report/>, 2014.
- Prakash, O., Sudheer, K.P., and Srinivasan, K., 2014. Improved higher lead time river flow forecasts using sequential neural network with error updating. *Journal of Hydrology and Hydromechanics*, 62 (1), 60–74.
- Sayama T, Fukami K, Tanaka S, Takeuchi K. (2010). Rainfall- runoff-inundation analysis for flood risk assessment at the regional scale. *Proceedings of the Fifth Conference of Asia Pacific Association of Hydrology and Water Resources (APHW)*, November 8–10, 2010 Hanoi, Vietnam; 568–576.
- Sayama T., Ozawa G., Kawakami T., Nabesaka S., and Fukami K. (2012). Rainfall–runoff–inundation analysis of the 2010 Pakistan flood in the Kabul River basin *International Centre for Water Hazard and Risk Management*, Public Works Research Institute, Minamihara 1-6, Tsukuba, 305-8516, Japan
- Sayama T., Tatebe Y. and Tanaka S. (2015b). An emergency response-type rainfallrunoff-inundation simulation for 2011 Thailand floods, *Journal of Flood Risk Management*, 2015b (in print).
- Sayama T., Tatebe Y., Iwami Y., and Tanaka, S. (2015a). Hydrologic sensitivity of flood runoff and inundation: 2011 Thailand floods in the Chao Phraya River basin, *Nat. Hazards Earth Syst. Sci.*, 15, pp. 1617-1630, doi:10.5194/nhess-15-1617-2015, 2015a
- Sayama, T. (2017). *Rainfall-Runoff-Inundation (RRI) Model User’s Manual ver. 1.4.2*.
- Serban, P., and Askew, A.J., 1991. Hydrological forecasting and updating procedures. *20th General Assembly of the International Union of Geodesy and Geophysics*, Vienna, Austria, 08/11-24/91, 357–369.
- T. Sugiura, T. Kawakami, G. Ozawa, K. Fukami, J. Magome and S. Nabesaka, “Experimental application of flood forecasting system (IFAS) using satellite-based rainfall”, *9th International Conference on Hydroinformatics*, China, (2010).
- Vogel, R.M., Yaindl, C., and Walter, M., 2011. Nonstationarity: flood magnification and recurrence reduction factors in the United States. *Journal of the American Water Resources Association*, 47 (3), 464–474. doi:10.1111/j.1752-1688.2011.00541.x
- Water Directors of the European Union. (2003). *Best Practices on Flood Prevention , Protection*. Ec.Europa.Eu, 1–29. http://ec.europa.eu/environment/water/flood_risk/pdf/flooding_bestpractice.pdf
- World Risk Report (2015). *United Nations University Institute for Environment and Human Safety*. Stuttgart, Germany: Universität Stuttgart, 2015.
- Yamazaki, D. et al., 2011. A physically based description of floodplain inundation dynamics in a global river routing model. *Water Resources Research*, 47, W04501, doi:10.1029/2010WR009726.



FORECASTING INFLOW IN MAGAT DAM AND FLOOD INUNDATIONS IN CAGAYAN RIVER BASIN UNDER EXTREME RAINFALL EVENTS USING THE RAINFALL-RUNOFF-INUNDATION MODEL

Arlen Alejandro¹, Lanie Alejo², Orlando Balderama³, Jeffrey Lloyd Bareng⁴, Sameh Kantoush⁵

¹National Irrigation Administration, Magat River Integrated Irrigation System, Dam, and Reservoir Division,
Ramon, Isabela, Philippines
arlenalejandro001@gmail.com

^{2,3,4}College of Engineering, Isabela State University, Echague, Isabela, Philippines

⁵Water Resources Research Center - Disaster Prevention Research Institute Kyoto University, Kyoto, Japan

ABSTRACT

The downstream of Cagayan River Basin (CRB) has been experiencing flash floods yearly during the rainy season. Flood forecasting is vital in preventing and mitigating flood damages. Flood inundation can be simulated to forewarn the affected areas on the possible effect of flood brought by the heavy rainfall events. In this study, the inflow in Magat Dam and water level in Buntun Bridge located in Tuguegarao City was simulated using the successfully calibrated Rainfall-Runoff-Inundation (RRI) Model using Typhoon Ulysses. The model satisfactorily estimated the inflow in Magat with RSR, NSE, PBIAS, and R^2 equal to 0.36, 0.87, 6.90 & 0.88, respectively. Also, the RSR, NSE, PBIAS, and R^2 with 0.50, 0.75, -0.39, and 0.75, respectively, showed good agreement with the measured river water level data. The RRI calibrated parameters were also tested and validated on Typhoon Tisoy in December 2019 and Monsoon Rains in December 2020. Results gave a satisfactory statistical index for both Magat Inflow and Buntun water levels. The RRI model was able to capture the flood inundations spatial range and variability in the Cagayan River Basin. The calibrated parameter of RRI could be used to forecast the inflow of Magat Dam and flood inundation in CRB during extreme weather events for effective protective planning, decision-making, and flood early warnings.

Keywords: forecasting; inflow; validation; simulated; calibrated; satisfactory

INTRODUCTION

Flood Forecasting with sufficient lead time and accuracy has great significance for effective flood warning and emergency response. The Rainfall-Runoff-Inundation model is a 2D grid cell-based hydrodynamic model capable of simulating both rainfall-runoff and flood inundation processes. The RRI model has been successfully applied to several regions in the world to simulate flooding events with good performances in all cases (Sayama et al., 2012; Nastiti et al., 2015). Thus, this study was conducted to assess the performance of the Rainfall-Runoff-Inundation Model and simulate runoff and flood inundation during heavy rain events in Cagayan River Basin.

The RRI parameters were adjusted manually based on the largest parameter map unit the RRI model built. These units are the dominant combination of soil, elevation, and landcover in the Basin. Inflow data from Magat dam was used for the RRI performance assessment. Inundations were validated based on flood stages in flooded areas in Isabela and Cagayan. The hourly rainfall data from NIA-MARIIS DRD and PAGASA online website was used for the calibration of the model during Typhoon Ulysses and rainfall for two (2) other extreme events (Typhoon Tisoy and Northeast monsoon) for validation were also collected. Statistical indicators for model performance evaluation that were used are the coefficient of determination (R^2), Nash-Sutcliffe model efficiency (NSE), RMSE-observations standard deviation ratio (RSR), and percent bias (PBIAS).

Affiliation

¹Engineer A, National Irrigation Administration, Magat River Integrated Irrigation System, Dam and Reservoir Division, ^{3,4}Professor, Isabela State University, ⁵Associate Professor, Kyoto University



MAIN RESULTS

Typhoon Ulysses was used for the calibration of the RRI model. Based on the statistical indices, the model satisfactorily estimated the inflow in Magat with RSR, NSE, PBIAS, and R^2 equal to 0.36, 0.87, 6.90 & 0.88, respectively. The observed maximum inflow was recorded on November 12, 2020, at 7:00 PM with 7,128.00 m^3/s while the peak inflow simulated from the RRI model was 6933.20 m^3/s that was also on Nov. 12, 2020, at 7:00 pm. The RRI model was able to estimate the date and time of the peak inflow correctly relative to the observed peak inflow date and time. This is very important for flood forecasting in Magat Dam to estimate the peak inflow during extreme weather. Also, the simulated river depth that peaked on Nov. 13 at 13.6 meters at 9:00 AM was 8 hours earlier than the actual maximum critical level of 13.3 meters on Nov. 13, 2020, at 10:00 PM. Simulating earlier could be better relative to later peak flow simulations to enable earlier flood warning alarms. Statistically, the RSR, NSE, PBIAS, and R^2 with 0.50, 0.75, -0.39, and 0.75, respectively, showed good agreement with the measured river water level data.

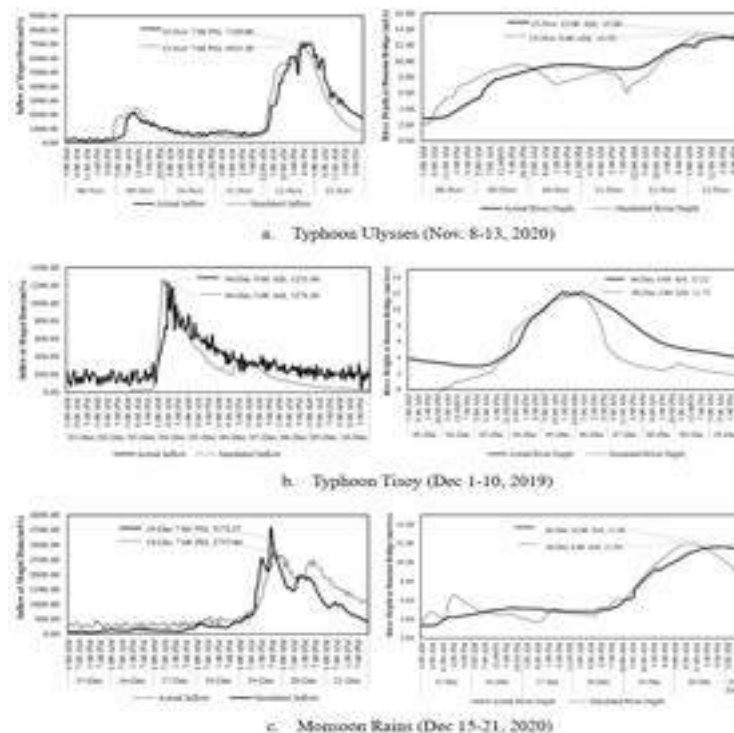


Figure 1. RRI Model Calibration on Typhoon Ulysses (a) and Validation on Typhoon Ulysses (b) and Monsoon Rains (c) at Magat Dam (Left) and Buntun Bridge (Right)

The calibrated parameters from Typhoon Ulysses were tested and validated on other extreme weather events during Typhoon Tisoy (December 1-10, 2019) and Northeast Monsoon (December 15-21, 2020). The RRI simulations in Magat inflow statistically agreed with the observed data during typhoon Tisoy with a value of R^2 , RSR, NSE, and PBIAS of 0.77, 0.83, 0.30, and 34.81 which is considered satisfactory. In terms of simulating the peak flow, the model can get the maximum inflow on Dec. 4 at 5:00 AM with 1,276.26 m^3/s compared to the actual with 1,231 m^3/s peaked on the same day at 9:00 AM. The PBIAS value of 34.81 indicated underestimation of the actual data. This can be attributed to the groundwater parameter which affects the water flow on the streams. Abdel-Fattah M. et al. (2018) mentioned in their study that the main source of the bias error is the absence of a stable groundwater module in the RRI model which is under development. Also, the simulated river height of 11.75 meters on December 6 at 2:00 AM was closed to the maximum actual data of 12.22 meters on December 6 at

Affiliation

¹Engineer A, National Irrigation Administration, Magat River Integrated Irrigation System, Dam and Reservoir Division, ^{3,4}Professor, Isabela State University, ⁵Associate Professor, Kyoto University



4:00 AM. Statistical indices of R^2 , RSR, NSE, and PBIAS of 0.77, 0.88, 0.23, and 31.86, respectively, are already satisfactory. Validation on Northeast Monsoon on December 15-21, 2020 also showed satisfactory statistical indices of R^2 , RSR, NSE, and PBIAS with 0.85, 0.50, 0.75, and 22.36, respectively. The simulated peak was higher with 22.85 percent compared to the actual maximum inflow of 2,755 m³/s on December 19, 2020, at 7:00 PM. Buntun water levels had satisfactory R^2 , RSR, NSE, and PBIAS of 0.88, 0.35, 0.87, and -1.30, respectively. The maximum simulated river height of 11.98 meters that occurred on December 20, 2020, at 8:00 AM was close to the peak river height on the same day at 10:00 PM with 11.68 meters. Uncertainties on the model can be attributed to the input data used, just like Bhagabati S. & Kawasaki A., 2017 said that more precipitation data, consideration of dam operations, and higher-resolution elevation data can improve the RRI model. Moreover, flood inundations were validated based on the residents' interview on the actual flood heights during typhoon Ulysses which shows the maximum height of 7 meters located in Annafunan, Tuguegarao City, Cagayan. The model estimated flood height in Amulung, Cagayan that ranged from ≥ 0 meters at locations relatively far from the riverbanks and ≥ 6 meters along the Cagayan riverbanks. Based on actual flood height data gathered, the actual flood height in Amulung ranged from 0 meters to 5 meters which were within the range of RRI simulated flood height. Also, reports and social media posts showed that flood heights reached up to the second-storey of houses mostly in Tuguegarao City during the peak floods. The model's estimated flood heights to be ≥ 6 meters. The RRI model was able to capture the flood inundations spatial range and variability in the Cagayan River Basin.

CONCLUSION

This study could be a good basis for the conduct of pre-emptive water release in the Magat dam. It will provide decision support for early flood warning alarms in the frequently flooded areas along the Cagayan River. Results showed the potentials of the RRI model as a science-based decision-making tool during extreme rainfall conditions. It can be used for flood forecasting, early flood warning systems, evacuation implementations, emergency response, inputs to flood risk mapping, flood risk mitigations, adaptations plans, and projects.

Acknowledgment: The authors would like to thank the agencies and projects mentioned in this article, which generously shared their data. This work was supported by the Department of Science and Technology – Philippine Council for Industry, Energy, and Emerging Technology Research and Development in collaboration with Thuy Loi University of Vietnam and Kyoto University of Japan.

REFERENCES

- Abdel-Fattah, M., Kantoush, S. A., Saber, M., & Sumi, T. (2018). Rainfall-Runoff Modeling For Extreme Flash Floods In Wadi Samail, Oman. *Journal of Japan Society of Civil Engineers, Ser. B1 (Hydraulic Engineering)*, 74(5), 1_691-1_696. https://doi.org/10.2208/jscejhe.74.5_i_691
- Bhagabati, S. S., & Kawasaki, A. (2017). Consideration of the rainfall-runoff-inundation (RRI) model for flood mapping in a deltaic area of Myanmar. *Hydrological Research Letters*, 11(3), 155–160. <https://doi.org/10.3178/hrl.11.155>
- Nastiti, K. D., Kim, Y., Jung, K., & An, H. (2015). The application of Rainfall-Runoff-Inundation (RRI) model for inundation case in upper Citarum Watershed, West Java-Indonesia. *Procedia Engineering*, 125, 166–172. <https://doi.org/10.1016/j.proeng.2015.11.024>
- Sayama T., Ozawa G., Kawakami T., Nabesaka S., and Fukami K. (2012). Rainfall-runoff-inundation analysis of the 2010 Pakistan flood in the Kabul River basin International Centre for Water Hazard and Risk Management, Public Works Research Institute, Minamihara 1-6, Tsukuba, 305-8516, Japan.

Affiliation

¹Engineer A, National Irrigation Administration, Magat River Integrated Irrigation System, Dam and Reservoir Division, ^{3,4}Professor, Isabela State University, ⁵Associate Professor, Kyoto University



IMPACTS OF FLOODS DUE TO EXTREME RAINFALL DURING TYPHOON ULYSSES IN THE CAGAYAN RIVER BASIN

Christine Mata¹, Orlando Balderama², Lanie Alejo³, Jeffrey Lloyd Bareng⁴, Sameh Kantoush⁵, Czarimah Singson¹, Elmer Rosete⁶, Alvin John Felipe⁷, Jeremy Balderama⁷, Janyzelle Ventura⁷, Genesis Querubin⁷

^{1, 6, 8} *Water Research and Development Center, Isabela State University, Isabela, Philippines*

^{2, 3, 4} *College of Engineering, Isabela State University, Isabela, Philippines*

⁵ *Water Resources Research Center – Disaster Prevention Research Institute*

Kyoto University, Kyoto, Japan

ifwarm@isu.edu.ph

ABSTRACT

Because recurring floods in the Philippines have become more damaging throughout time, risk assessments, quantifying, and visualizing flood damages as accurately as possible becomes imperative. To deal with an up-to-date database containing information and a practical assessment tool, a satellite imagery-based method was used which aimed to map flood inundation using the Google Earth Engine and estimate damages brought by the flood during Typhoon Ulysses. Analysis of the recent flood inundation event in November 2020 in Cagayan Valley showed the inundation of an extensive area of 502.86 km² affecting the Cagayan province at 53.96% and Isabela province at 45.93% share of inundation. The flood severely affected approximately 477.44 km² of the total croplands. Using a participatory validation approach, the overall accuracy of datasets used is 97.78% while flood extent is 95%. Through this study, the framework, approach, and methodology can be replicated in other locations in the country.

Keywords: flood mapping; synthetic aperture radar; flood risk assessment; Google Earth Engine; damage

1. INTRODUCTION

The recent flooding in 2020 was brought by the succeeding occurrences of six (6) tropical cyclones in the country, the last of which is Typhoon Ulysses, bringing unprecedented rains to the Cagayan Valley region resulting in unexpected floods heights and extensive inundation to the provinces of Isabela and Cagayan. Flood risk assessment requires quantifying flood risk damages as accurately as possible (Meyer et al, 2009). An up-to-date database containing information on hazard-prone regions is critical for supporting hazard preparedness and response operations, particularly in the case of recurring floods. However, just extracting and mapping these resources alone is laborious (Hermann et al., 2007) while the adoption of the traditional approach is time-consuming and expensive. Flood damage estimate using GIS and RS has become a useful instrument for developing a near real-time flood mapping and effective flood risk mitigation policy (Shrestha et al., 2013; Manfre et al., 2012). Hence, this paper aimed to 1) map flood inundation using Google Earth Engine (GEE), and 2) estimate the damages brought by the flood during Typhoon Ulysses.

In the Philippines, Ghaffarian et al. (2020) suggest the use of GEE in post-disaster recovery monitoring in Leyte brought by Typhoon Haiyan in 2013. Flood mapping using GEE and damage assessment of different datasets to identify flood-risked resources will be the foremost in the country. GEE can offer an estimation of flood damages but in very low-resolution datasets (MODIS land cover 500m, JRC Population 250m) thereby affecting the accuracy of reports. With the readily available, free, up-to-date, and high-resolution data accessible in OpenStreetMap (OSM) and obtainable from National Mapping and Resource Information (NAMRIA), a comprehensive database containing information relevant for

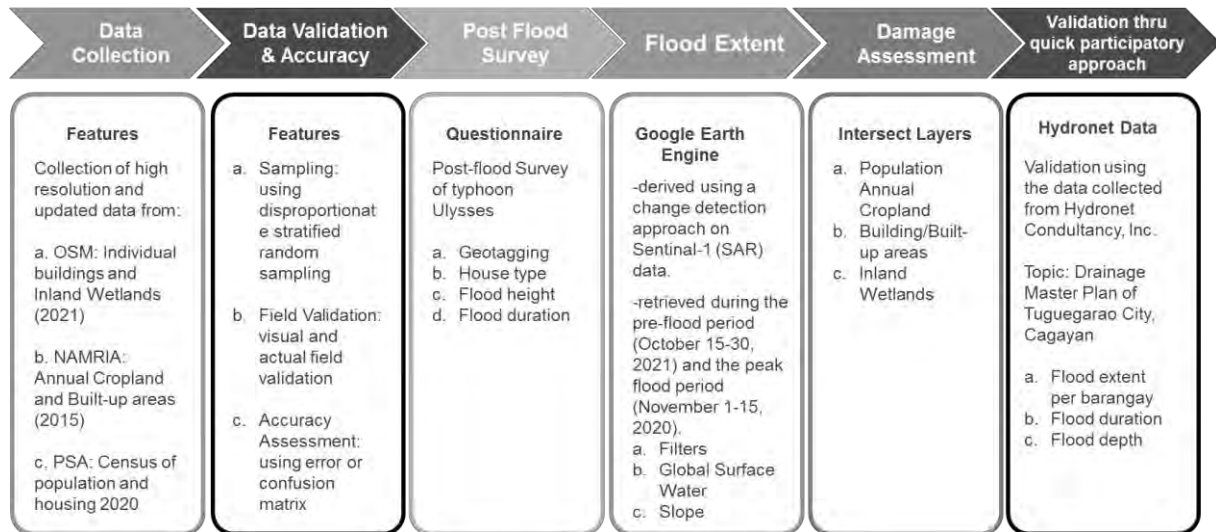
Affiliation

¹ Science Research Specialist, Isabela State University; ^{2,4} Professor, Isabela State University; ³ Assistant Professor, Isabela State University; ⁵ Associate Professor, Kyoto University; ⁶ University Research Associate, Isabela State University; ⁷ Science Research Assistant, Isabela State University



flood analysis were collected and analyzed in this study. Since GIS and RS have proven their capability in flood mapping, the study is very timely and significant especially in the case of the Philippines.

Below summarizes the overall methodological framework used in the study. Two validations were performed: for datasets and flood extent. A post-flood survey was conducted to determine the threshold for estimating flood extent in GEE. Flood maps and flood-risked resources were quantified and tabulated. Validation of map accuracy through a quick post-flood participatory approach was done.



2. MAIN RESULTS

Figure 1 displays the resulting inundation map using GEE. As shown in Table 1, two provinces in the region were greatly affected by a series of typhoons in November 2020. Cagayan was the most affected (271.35km²) of about 9.36% of its area flooded, followed by Isabela (230.98; 2.62%). On the other hand, Kalinga (0.5 km²), Ifugao (0.02 km²), and Apayao (0.01 km²) had minimal damages of less than a square kilometer flooded area. Approximately 7,378 built-up and 225,633 people were affected.

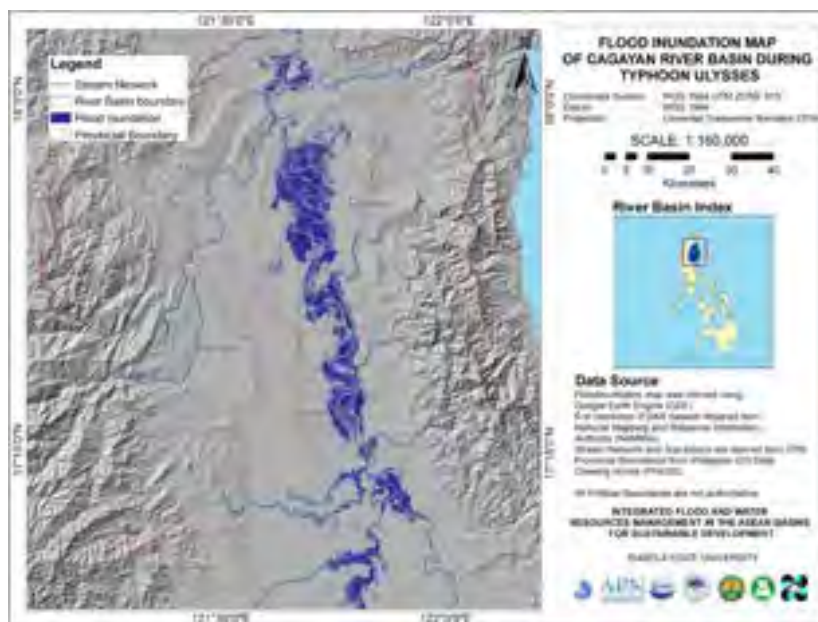


Figure 1. Final flood inundation map of Typhoon Ulysses in November 2020

Affiliation

¹ Science Research Specialist, Isabela State University; ^{2,4} Professor, Isabela State University; ³ Assistant Professor, Isabela State University; ⁵ Associate Professor, Kyoto University; ⁶ University Research Associate, Isabela State University; ⁷ Science Research Assistant, Isabela State University



Table 1. Summary of flooded area and damages per affected province in Cagayan River Basin

| Province | Area (km ²) | Flooded Area (km ²) | % Area of Province | % Area of Inundation | Annual Crop (km ²) | Built-up | | Inland Wetland (km ²) | Population | % Affected Population |
|----------|-------------------------|---------------------------------|--------------------|----------------------|--------------------------------|----------|-------------------------|-----------------------------------|------------|-----------------------|
| | | | | | | Count | Area (km ²) | | | |
| Cagayan | 2,897.67 | 271.35 | 9.3645 | 53.96 | 344.36 | 4,355 | 2.19 | 0.55 | 111,959 | 50.36 |
| Isabela | 8,813.95 | 230.98 | 2.6206 | 45.93 | 269.10 | 2,981 | 4.03 | 0.03 | 113,633 | 49.62 |
| Kalinga | 10,276.73 | 0.50 | 0.0048 | 0.10 | 0.55 | 36 | 0.00 | 0.00 | 37 | 0.02 |
| Ifugao | 2,503.45 | 0.02 | 0.0009 | 0.00 | 0.04 | 4 | 0.00 | 0.00 | 3 | 0.00 |
| Apayao | 3,913.88 | 0.01 | 0.0002 | 0.00 | 0.00 | 2 | 0.00 | 0.00 | 1 | 0.00 |
| TOTAL | 28,405.68 | 502.86 | 11.991 | 100 | 614.05 | 7,378 | 6.22 | 0.58 | 225,633 | 100 |

3. CONCLUSION

The high-resolution datasets that are readily available in the Philippines were used instead of the default materials used by GEE and may be utilized by flood mappers without difficulty. The concurrent flood study imposes adopting an integrated, multi-hazard, multi-stakeholder, approach with an emphasis on disaster risk mitigation, preparedness, streamlining of the relief distribution system, with an emphasis of self-reliance on LGUs and NGOs for sustenance with local resources and practices. Future work will be aimed to use the workflow applied in assessing flood damages for other typhoon events in the Philippines. A set of technical and institutional recommendations are to be firmed up in consultation with the Cagayan River Basin Management Council and the Cagayan Valley Regional Disaster Management Council.

Acknowledgment: The authors would like to express their appreciation for the support of the Department of Science and Technology-Philippines Council and the Industry, Energy, and Emerging Technology Research and Development (DOST-PCIEERD), the project Integrated Flood and Water Resources Management (IFWaRM) in the ASEAN Basins for Sustainable Development in collaboration with Thuy Loi University of Vietnam and Kyoto University of Japan.

4. REFERENCES

- Ghaffarian, S. Farhadabad, A.R, Kerle, N. (2020). Post-disaster recovery monitoring with google earth engine. *Applied Sciences* 10 (13): 4574. 1-4. <https://doi.org/10.3390/app10134574>
- Manfre, L., Hirata, E., Silva, J. B., Shinohara, E., Giannotti, M., Larocca, A., Quintanilha, J., (2012). An analysis of geospatial technologies for risk and natural disaster management. *ISPRS Int. J. Geo-Inf* 312, 1(2), 166-185, <https://doi.org/10.3390/ijgi1020166>
- Meyer V., Haase D., Scheuer S. (2009). GIS-based multicriteria analysis as decision support in flood risk management. *Helmholtz Centre for Environmental Research (UFZ) Discussion Paper No. 6/2007*. Corpus IF: 128321410. p.4 <http://hdl.handle.net/10419/45237>
- Shrestha, B., Okazumi, T., Miyamoto, M., Nabesaka, S., Tanaka, S., Sugiura, A. (2014). Fundamental Analysis for Flood Risk Management in the Selected River Basins of Southeast Asia. *Journal of Disaster Research*. 9. 858-869. 10.20965/jdr.2014.p0858. 1-2 <https://www.fujipress.jp/jdr/dr/dsstr000900050858/>

Affiliation

¹ Science Research Specialist, Isabela State University; ^{2,4} Professor, Isabela State University; ³ Assistant Professor, Isabela State University; ⁵ Associate Professor, Kyoto University; ⁶ University Research Associate, Isabela State University; ⁷ Science Research Assistant, Isabela State University



ANALYSIS OF THE IMPACTS OF CLIMATE CHANGE ON THE HYDROLOGIC INFLOW OF MAGAT RESERVOIR USING THE SWAT MODEL

Czarimah Singson¹, Orlando Balderama², Lanie Alejo³, Jeffrey Lloyd Bareng⁴, Sameh Kantoush⁵,
Christine Mata¹, Elmer Rosete⁶, Alvin Felipe⁷, Jeremy Balderama⁷, Jayzelle Ventura⁷, Genesis Querubin⁷

^{1,6,7}Water Research and Development Center, Isabela State University, Echague, Isabela, Philippines

^{2,3,4}College of Engineering, Isabela State University, Echague, Isabela, Philippines

⁵Water Resources Research Center - Disaster Prevention Research Institute

Kyoto University, Kyoto, Japan

czarimah.l.singson@isu.edu.ph

ABSTRACT

This study was conducted to assess the impacts of climate change on the inflow of Magat Reservoir using the Soil and Water Assessment Tool (SWAT) Model. The knowledge of inflow is essential in scheduling dam discharges, estimating current and future power production, and preventing floods. The SWAT calibration results showed an NSE of 0.73, R² of 0.74, RSR of 0.52, and PBIAS of 8.24 while the validation resulted in an NSE of 0.57, R² of 0.62, RSR of 0.47, and PBIAS of 9.90. The model showed that there would be at most a 20.42% increase and 27.08% decrease in inflow for wet and dry years, respectively. Peak inflows were observed during September and October. The results of the model can be used as a basis for long-term strategic plans of the Magat Dam Management to prepare and respond to future climate risks in the reservoir.

Keywords: Climate Change; Inflow; Peak; SWAT

INTRODUCTION

The Philippines is highly vulnerable to the impacts of climate change, including sea-level rise, increased frequency of extreme weather events, rising temperatures, and extreme rainfall. With the impact of climate change, both man-made and land-cover changes, watersheds as well as water resources have been constantly affected. To assess the impact of climate change on water resources, the Soil and Water Assessment Tool (SWAT) model has been used as an effective tool to illustrate the impacts of climatic change on hydrologic and biogeochemical cycles in a variety of watersheds (Arnold et al., 1998). Consequently, this study was conducted to parameterize, calibrate, validate and simulate the SWAT model; quantify the effects of future climate change on the inflow of Magat Reservoir, and determine the peak flow.

Climatic and spatial data were gathered from different agencies. Monthly simulation, calibration, and validation were done using a 31-year (1990-2020) historical data with the 3-year warm-up period (1990-1992). Moreover, 18 year-data (1993-2010) was used for calibration while 10-year data (2011-2020) were used for validation. Calibration was done using a trial-and-error method and SWATCUP SUFI2. The Coefficient of Determination (R²), Nash-Sutcliffe Model Efficiency (NSE) and Root Mean Square Error (RMSE), and percent bias (PBIAS) were used to measure the acceptability of the SWAT model. Scenario analysis was also used to evaluate the impacts of climate variability on the inflow of the reservoir. These scenarios were based on the recent climate projections published by the Philippine Atmospheric, Geophysical, and Astronomical Services Administration (PAGASA). The climate scenarios considered were medium-range and high-range emissions for two-time frames: mid-21st century (2036-2065) and late 21st century (2070-2099). The mid and high-range scenarios were then further categorized into three percentiles: lower bound (driest possible change); normal bound (normal possible change); and the upper bound (wettest possible change).

Affiliation

¹Science Research Specialist, Isabela State University; ^{2,4}Professor, Isabela State University; ³Assistant Professor, Isabela State University; ⁵Associate Professor, Kyoto University; ⁶University Research Associate, Isabela State University; ⁷Science Research Assistant, Isabela State University



MAIN RESULTS

The table below shows the 17 most influential parameters and their values according to manual and SWAT-CUP calibrations. A study made by Arceo et.al. (2018) mentioned six parameters that were considered influential: Initial SCS runoff curve number (CN2), Base-flow alpha factor (ALPHA_BF), Groundwater delay time (GW_DELAY), Threshold depth of water in the shallow aquifer required for return flow to occur (GWQMN), Groundwater “revap” coefficient (GW_REVAP), and Soil evaporation compensation factor (ESCO). The same parameters were also found out to be influential to the inflow of the Magat Reservoir as seen in Table 1.

Table 1. Sensitive Parameters during the Calibration of the model

| Parameter | Description | Calibrated Value |
|--------------------|---|------------------|
| 1. CN2.mgt | Initial SCS curve number for moisture condition II | 35.65 |
| 2. ALPHA_BF.gw | Baseflow alpha factor | 1 |
| 3. GW_DELAY.gw | Groundwater delay | 0.1 |
| 4. GWQMN.gw | Threshold depth of water in the shallow aquifer required for return flow to occur | 600 |
| 5. GW_REVAP.gw | Groundwater "revap" coefficient | 0.02 |
| 6. ESCO.hru | Soil evaporation compensation factor | 1 |
| 7. EPCO.hru | Plant uptake compensation factor | 1 |
| 8. CH_K2.rte | Effective hydraulic conductivity in the main channel alluvium | 500 |
| 9. ALPHA_BNK.rte | Baseflow alpha factor for bank storage | 1 |
| 10. SOL_AWC ().sol | Available water capacity of the soil layer | 0.01 |
| 11. SOL_K ().sol | Saturated hydraulic conductivity | 2000 |
| 12. SOL_BD ().sol | Moist bulk density | 2.5 |
| 13. OV_N.hru | Manning's value for overland flow | 0.01 |
| 14. RCHRG_DP.gw | Deep aquifer percolation factor | 0.01 |
| 15. HRU_SLP.hru | Average slope steepness | 0.6 |
| 16. SURLAG.bsn | Surface runoff lag coefficient | 4 |
| 17. LAT_TIME.hru | Lateral flow travel time | 30 |

The calibration and validation result in a satisfactorily acceptable model. Calibration shows that the model has an NSE of 0.73, R2 of 0.745, RSR of 0.52, and PBIAS of 8.24, which are all considered statistically acceptable when compared to the indices that were set. The validated model has an NSE of 0.57, R2 of 0.62, RSR of 0.47, and a PBIAS of 9.90. Figure 1 shows that the model generally underestimated the peak flows. This is one of the known limitations of the SWAT model. Alejo, L. (2019) also satisfactorily calibrated and validated a SWAT model in Maasin River Watershed in Laguna, the Philippines using actual streamflow. Her calibration process had 0.82 R2, 82% NSE, 0.024 RSR, and a PBIAS of 3.7%. This suggests that SWAT can be locally applied in river basin conditions in the country.

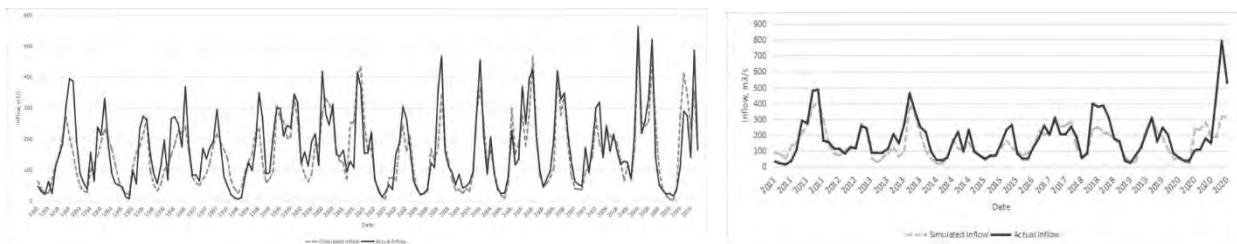


Figure 1. Calibration (left) and validation (right) results of the SWAT model.

Affiliation

¹ Science Research Specialist, Isabela State University; ² Professor, Isabela State University; ³ Assistant Professor, Isabela State University; ⁴ Associate Professor, Kyoto University; ⁵ University Research Associate, Isabela State University; ⁶ Science Research Assistant, Isabela State University



The simulation results incorporating the climate change scenarios showed that under the RCP 4.5 scenario for the mid-21st century, there would be a 27.08% and 7.9% decrease of inflow for dry and normal years while there would be an increase by 10.08% in the wet year. Under RCP 8.5 Mid-21st century scenario, there would be a decrease of inflow by 18.46% during the dry years and an increase of inflow by 0.72% and 18% during the normal and wet years, respectively. Under the RCP 4.5 scenario in the late 21st century, there was an anticipated decrease of inflow by 21.73% and 4.7% during the dry and normal years, while there was an increased inflow by 15.89% for wet years. Under the RCP 8.5 scenario for the Late 21st century, there would be a decrease of inflow for both dry and normal years by 24.01% and 11.31%, respectively, while there was an anticipated increase of the inflow during the wet years by 20.42%. Furthermore, the simulation results showed that at least 119.61 m³/s, 140.86 m³/s, and 169.06 m³/s can be expected as monthly peak inflows in the Mid-21st century under RCP 4.5 for dry, normal, and wet years, respectively. On the other hand, at least 211.3675 m³/s, 256.87 m³/s, and 297.285 m³/s can be expected as monthly peak inflows of the Magat reservoir in the years 2036-2065 (mid-21st century) under RCP 8.5 for dry, normal, and wet years, respectively. Meanwhile, in the Late 21st century under RCP 4.5, at least 203.19 m³/s, 238.13 m³/s, and 287.06 m³/s can be expected as monthly peak inflows for dry, normal, and wet years, respectively. Conversely, under RCP 8.5 Late 21st century scenario, at least 192.61 m³/s, 214.85 m³/s, and 317.12 m³/s can be expected as monthly peak inflows for dry, normal, and wet years, respectively. In addition, the highest inflow of water to the reservoir is anticipated from September and October.

CONCLUSION

Climate change will lead to increase in inflow during wet years and decrease in inflow during dry years. The results of the model could be used as a basis for the development of long-term plans of NIA-DRD, RBC, and LGUs to prepare and respond to future climate change impacts and resolve the risks related to water resources especially in the reservoir. Also, the results could pave the way towards the design of various interventions to take care of the watershed and its river networks and reduce the negative impacts of climate change on the Magat reservoir in the future.

Acknowledgment: The authors would like to thank the agencies and projects mentioned in this article, which generously shared their data. This work was supported by the Department of Science and Technology – Philippine Council for Industry, Energy, and Emerging Technology Research and Development in collaboration with Thuy Loi University of Vietnam and Kyoto University of Japan.

REFERENCES

- Alejo, L.A., Ella V.B. 2019.** “Assessing the impacts of climate change on dependable flow and potential irrigable area using the SWAT model. The case of Maasin River watershed in Laguna, Philippines”. *Journal of Agricultural Engineering* 2019; volume L:94.
- Arceo, Maria Graciela Anna S.; Cruz, Rex Victor O.; Tiburan, Cristino L.; Balatibat, Juancho B.; and Alibuyog, Nathaniel R. 2021.** "Modeling the hydrologic responses to land cover and climate changes of selected watersheds in the Philippines using soil and water assessment tool (SWAT) model" *Journal Article*. 1092.
- Arnold, J. G., Srinivasan, R., Muttiah, S., and Williams, J. R. 1998.** “Large-area hydrologic modeling and assessment: Part I. Model development.” *J. American Water Resour. Assoc.*, 34(1), 73-89.

Affiliation

¹Science Research Specialist, Isabela State University; ²Professor, Isabela State University; ³Assistant Professor, Isabela State University; ⁵Associate Professor, Kyoto University; ⁶University Research Associate, Isabela State University; ⁷Science Research Assistant, Isabela State University



EXTREME CLIMATE INDICES: TOOLS FOR ASSESSMENT OF SPATIO-TEMPORAL CLIMATE CHANGE RISK OVER CAGAYAN RIVER BASIN, PHILIPPINES

Khagendra P. Bharambe¹, Sameh A. Kantoush², Tetsuya Sumi², Mohamed Saber², Orlando Balderama³

^{1,2} Water Resources Center, Disaster Prevention Research Institute, Kyoto University, Japan, bharambe.khagendrapralhad.2k@kyoto-u.ac.jp, kantoush.samehahmed.2n@kyoto-u.ac.jp, sumi.tetsuya.2s@kyoto-u.ac.jp, mohamedmd.saber.3u@kyoto-u.ac.jp

³ College of Engineering, Isabela State University, Philippines, orly_isu@yahoo.com

ABSTRACT

Extreme climate events, such as heavy rainfall, heat waves, and drought, have become the most common natural disasters, exacting a high toll on people and economies. As a result, their frequency and losses increase, stressing governments' and humanitarian organizations' response capacities. Addressing the consequences and occurrence of these disasters always has a significant challenge in the Philippines, particularly at Cagayan River Basin, due to increasing population and the impacts posed by climate change. One of the many approaches to addressing this challenge is to make better use of climate information and tailor it to predict better the probability of occurrences and associated risk for such disasters before they occur. This study is conducted to help meet these challenges considering the spatio-temporal assessment of climate change impacts on extreme climate events based on comprehensive assessment of extreme rainfall and temperature indices using data for worst-case climate change scenarios MRI-AGCM3.2S. The results have shown an increased risk from the severe dry spell and wet spell in future period over CRB than past, which may lead to higher vulnerability for drought and flood.

Keywords: Extreme Climate Indices, Climate Risk, Climate Change Adaptation, Spatio-temporal modeling.

1. INTRODUCTION

Frequent heavy precipitation events and severe droughts are likely to increase due to the adverse effect of climate change and a greater degree of fluctuation in precipitation and temperature (IPCC, 2007; Carter et al., 2007). The most critical impacts are affecting water resources, which directly affect agricultural systems and food security. And, the Cagayan River Basin (CRB) in the Philippines is the largest, covering a total land area of 27,493.49 km², currently facing critical issues of rapid climate variability and frequent occurrences of hydroclimatic extremes events such as flood, drought, etc. These are the significant constraints that somehow prevent further development in CRB. By looking into climate change, the situation may worsen in the upcoming period over CRB, which is predicted to increase the magnitude and frequencies of droughts and floods. Therefore, given the significance of the current problems and future risk, there is a strong need for an integrated approach to study climate change, combing aspects of climate projections and predicting future potential risk towards achieving sustainable development goals (SDGs). This research has been conceptualized to explore the spatial and temporal changes in climate variability and extreme climate indices using long-term historical and future climate data to identify the present and future potential climate change risk over CRB.

The Spatio-temporal modeling approach by Sen's slope estimation using Mann Kendall's test was applied to analyze the variability and magnitude of change in climate variables and extreme climate

Affiliation

¹ Researcher, Kyoto University; ² Professor, Kyoto University; ³ Professor, Isabela State University



indices, using the meteorological variables obtained from high-resolution CMIP6 simulation data produced by MRI-AGCM3.2S over historical (1951-2014) and future (2015-2099) period. This study estimated the extreme climate indices such as CDD, CWD, R95p, TX90p, and TN90p, considering the most important and relevant for agriculture and water resource protection point of view to identify the level of climate change risk (**Table 1**)

Table 1: Indices for characterizing temperature and rainfall extremes (Source: ETCCDI)

| Precipitation Indices | | | Temperature Indices | | |
|-----------------------|--|-------|---------------------|--|------|
| Indices | Definition | Unit | Indices | Definition | Unit |
| PRCPTOT | Total Annual Precipitation | mm/yr | TX | Mean daily max. temperature | °C |
| CDD | Consecutive Dry Days: Number of Spell of five consecutive days with rainfall <1mm per year | days | TN | Mean daily min. temperature | °C |
| CWD | Consecutive Wet Days: Number of Spell of five consecutive wet per year with rainfall <1mm | days | TX90p | Amount of hot days: Percentage of days when TX>90 th percentile | % |
| R95p | Very wet days rainfall: Annual total rainfall when daily rainfall exceeds the 95 th percentile of wet days | Mm/yr | TN90p | Amount of warm nights: Percentage of days when TN>90 th percentile | % |

2. MAIN RESULTS

To investigate the variability and magnitude of change in climate variables and extreme climate indices over historical and future climate change, the relative changes over space and time were estimated and illustrated in **Figure 1**.

The analysis indicated some promising key results across each sub-basin. First, the intra-annual rainfall has shown an increasing trend over the future period, with a higher fluctuation rate in minimum and maximum annual rainfall. This will cause the top occurrences of droughts where precipitation has been observed decreasing trend over the sub-basins, namely Chico, Magat, Cagayan Segment1 during the future period. On the other hand, floods will like to occur where precipitation has shown an increasing trend over sub-basins like Siffu-Mallig, Ganano, and Addalam over the future period over the Cagayan River Basin (**Figure 1**). The findings also revealed that the Addalam sub-basin would experience an increase in average annual rainfall and an increase in the percentage of consecutive dry days in the future compared to the past. This indicates that there will be a higher probability of increasing risk for intense dry spells and heavy precipitation events that may cause severe drought and flood events in Addalam sub-basin at the Cagayan River Basin.

Understanding knowledge about the identification and probability of occurrences of extreme climate phenomena is always crucial for managing climate-related risks. Furthermore, as the world continues to warm, more extreme weather events can be expected in the future. Hence, these results would be an easy-to-use resource to tackle the high-risk zone and provide guidance to the disaster risk reduction authority to take an appropriate decision for implementing the adaptation strategies.

Affiliation

¹ Researcher, Kyoto University; ² Professor, Kyoto University; ³ Professor, Isabela State University

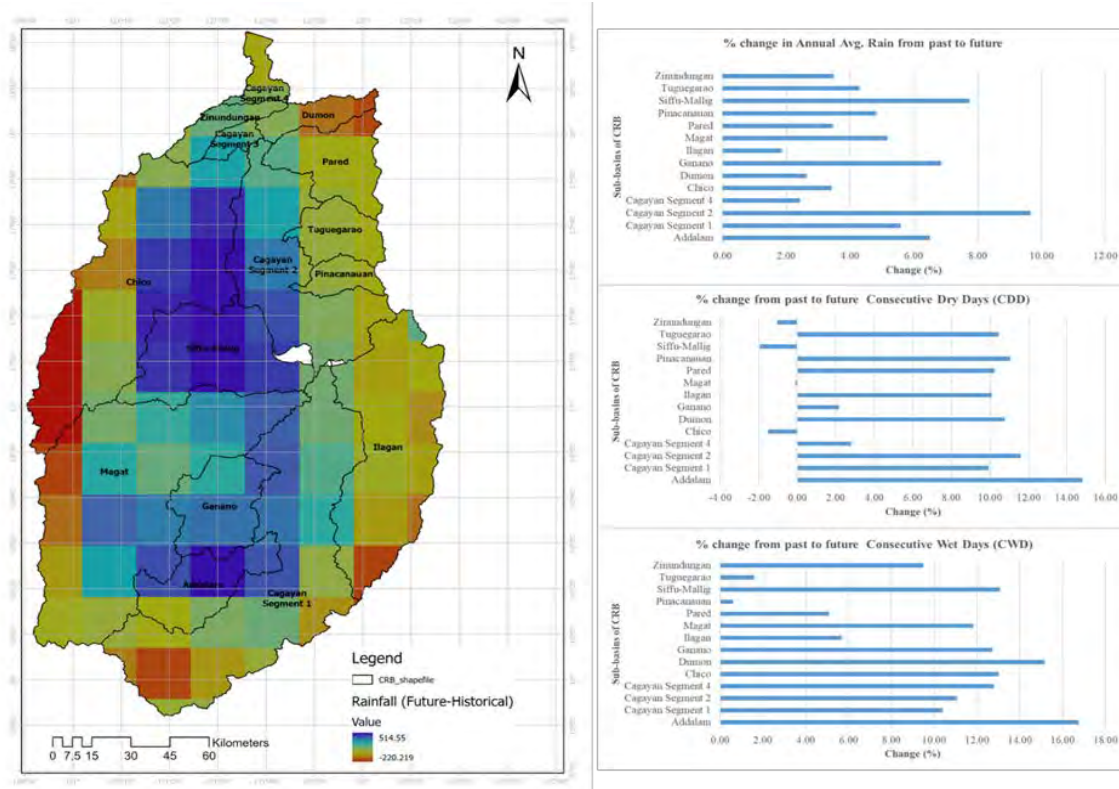


Figure 1: Spatio-temporal changes in rainfall and key extreme climate indices (CDD, CWD) at CRB.

3. CONCLUSION

A consistent increase in temperature and precipitation is likely to bring prolonged dry spells leading to droughts and wet spells leading to intensive floods at the Cagayan River Basin. However, the climate change risk will not be uniform; some sub-basins will experience higher vulnerability than the other sub-basins, significantly accelerating the different changes of hydroclimatic extremes. Therefore, spatiotemporal modeling is significant to determine the changes over space and time across river basins and is helpful for the effective implementation of adaptation strategies.

Acknowledgment:

This work was funded by APN "Asia-Pacific Network for Global Change Research" under project reference number CRRP2020-09MYKantoush (Funder ID: <https://doi.org/10.13039/100005536>).

4. REFERENCES

- Mizuta, Ryo; Yoshimura, Hiromasa; Ose, Tomoaki; Hosaka, Masahiro; Yukimoto, Seiji (2019). MRI MRI-AGCM3-2-S model output prepared for CMIP6 HighResMIP-Version1. Earth System Grid Federation. <https://doi.org/10.22033/ESGF/CMIP6.1625>
- Carter, T. R., et al. 2007. General guidelines on the use of scenario data for climate impact and adaptation assessment. Geneva: Intergovernmental Panel on Climate Change, Task Group on Data and Scenario Support for Impact and Climate Assessment.
- IPCC, 2007: Climate Change 2007: Synthesis Report. Contribution of Working Groups I, II and III to the Fourth Assessment Report of the Intergovernmental Panel on Climate Change
- Expert Team on Climate Change Detection and Indices (ETCCDI), available at <https://www.wcrp-climate.org/etccdi>

Affiliation

¹ Researcher, Kyoto University; ² Professor, Kyoto University; ³ Professor, Isabela State University



FLOOD RISK AND RESERVOIR SEDIMENTATION IN CAGAYAN AND VU GIA- THU BON RIVER BASINS

Sameh A. Kantoush¹, Doan Van Binh², Mohamed Saber¹, Khagendra P. Bharambe¹, Tetsuya Sumi¹, Orlando Balderama³, Duong Ngoc Vo⁴, Nga H. Pham⁵, Duong Du Bui⁶

¹Water Resources Center, Disaster Prevention Research Institute, Kyoto University, Japan, kantoush.samehahmed.2n@kyoto-u.ac.jp, mohamedmd.saber.3u@kyoto-u.ac.jp, bharambe.khagendrapralhad.2k@kyoto-u.ac.jp, sumi.tetsuya.2s@kyoto-u.ac.jp

²Faculty of Engineering, Vietnamese German University, Binh Duong Province, Vietnam, binh.dv@vgu.edu.vn

³College of Engineering, Isabela State University, the Philippines, orly_isu@yahoo.com

⁴The University of Danang – University of Science and Technology, 54 Nguyen Luong Bang Str., Danang City, Viet Nam, vnduong@dut.udn.vn.

⁵Thuyloi University, Hanoi, Vietnam, phamhongnga@tlu.edu.vn

⁶National Center for Water Resources Planning and Investigation (NAWAPI). Long Bien District, Ha Noi, Vietnam, duongdubui@gmail.com

ABSTRACT

Climate change threatens the security of communities, economic activities, ecological services, and water supply to a range of users in the Vu Gia-Thu Bon and Cagayan river basins, which are among the most important river basins in Vietnam, and the Philippines, respectively. Furthermore, human interventions such as deforestation, sand mining, dam construction, and expansion of irrigation systems have intensified the climate change impacts. On the other hand, sediment supply downstream will be beneficial to improve river geomorphology creating suitable habitat, reducing coastal erosion, and increasing the safety of hydraulic structures. Therefore, this project has been implemented for assessing the impacts of climate change and human interventions on reservoir sedimentation, flood inundation, agricultural practices, and river and coastal erosion in the Vu Gia-Thu Bon and Cagayan River basins. The ultimate goal is to transfer the results of the project to the stakeholders and policy decision-makers to implement into the national laws, with involved organizing some training courses, seminars, and workshops to train the young researchers, stakeholders, policymakers, local communities as well as to expand the collaborative network with other ASIAN countries and global change programs. In the end, this will help enhance networking and cooperation in Asia and the Pacific region to understand and resolve floods and sediments issues and foster the next generation of participating scientists to keep the specialist network in the future.

Keywords: Coastal erosion risk, Climate change, Flood and Sedimentation, River basin management

1. INTRODUCTION

Climate change poses a significant threat from devastating floods and droughts to the world. Vietnam and the Philippines are among the most affected countries by climate change and rainfall variability (Principe, 2012; Souvignet et al., 2014). It has been predicted to increase extreme floods and droughts (Hoanh et al., 2010). In recent years, flooding has become more common in the Vu Gia-Thu Bon river basin in Vietnam, with higher flood peaks and more severe inundation. (Do et al., 2018; Nga, 2019).



Reservoir sedimentation is a primary factor in the river and coastal erosion in Vietnam and the Philippines. **Figure 1** conceptualizes the main drivers facing the river basin from the watershed until the delta. Climate change causes alteration in hydrological patterns, resulting in accelerated reservoir siltation rates and loss of reservoir function. Therefore, optimizing dam operation and reservoir sediment management is highly crucial for the sustainability of a river basin. Therefore, sustainable development in a river basin requires an "integrated flood and sediment management" approach. All water-related issues must be addressed and managed appropriately collaboratively throughout the basin.

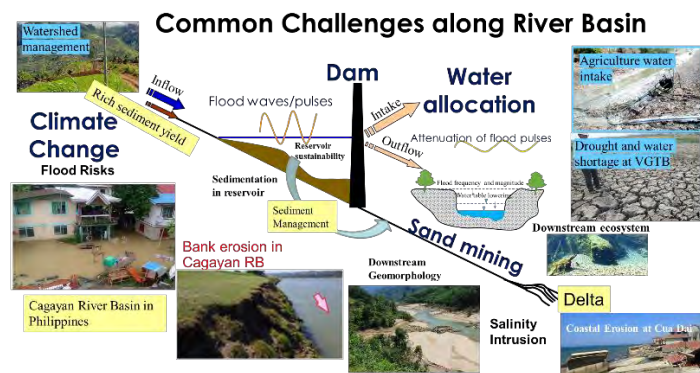


Figure 1. Challenges affect the river basin system due to anthropogenic effects caused by hydraulic infrastructure such as dams.

Figure 2 shows the map of the Cagayan River Basin, which is located in the northeastern part of the Philippines. The catchment area of 27,753 km² covers four regions. Cagayan is the longest river with more than 20 tributaries and the largest river by discharge volume of water in the Philippines. However, current water consumption is minimal, and water resources are sufficient to supply domestic, industrial, and irrigation needs.

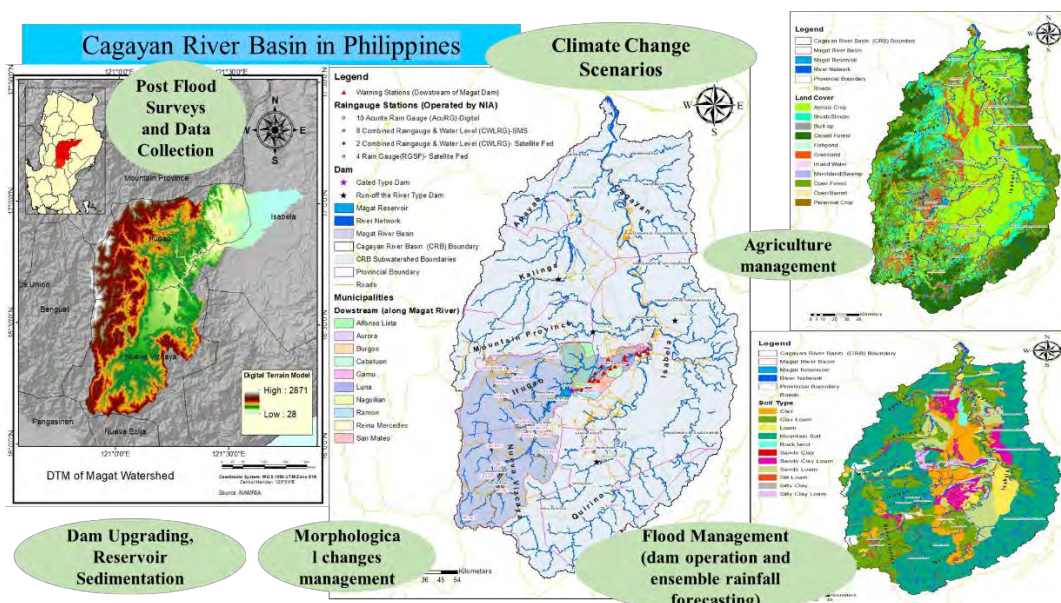


Figure 2. The study area of the Cagayan River Basin in the Philippines



Flood inundation, drought, and soil erosion are the major causes of slow economic development and environmental degradation intensified by anthropogenic activities. In 2020, five successive typhoons hit the basin before Ulysses caused a severe inundation at two central provinces, Cagayan, Isabela, Kalinga, and Ifugao.

To achieve integrated flood and sediment management, we apply field surveys, numeric simulation, remote sensing, training, workshop to share the results, and technology transfer. The general methodology of the proposed research starts with data collection of various data types. Then, data analyses are performed to understand the fundamentals of the study areas and preparation of inputs for modeling. Following that, numerical models are established to predict the future changes of the concerned problems so that countermeasures can be proposed, as shown in the methodology flowchart (**Figure 3**).

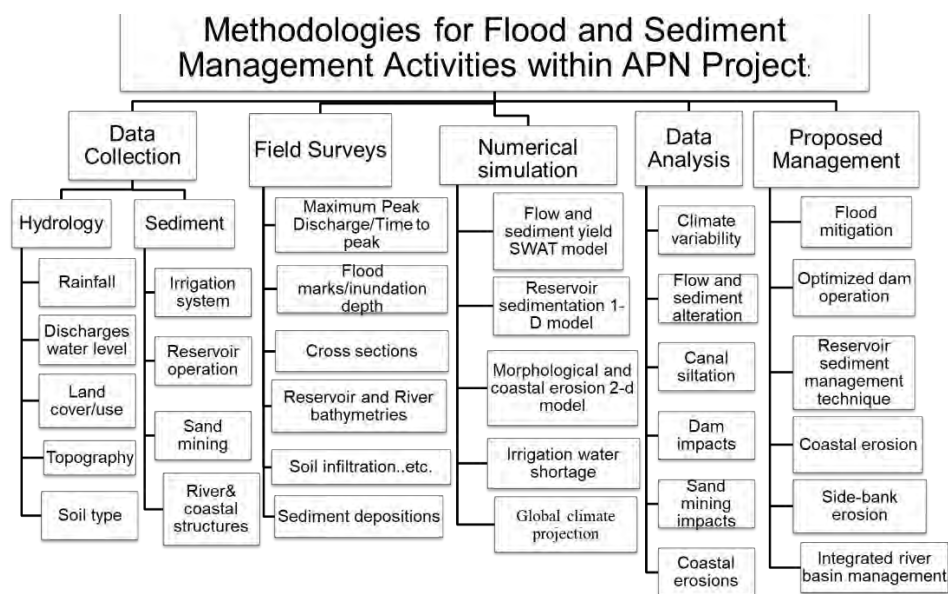


Figure 3. Methodology flowchart for Integrated flood and sediment management

2. MAIN RESULTS

The Vu Gia-Thu Bon River basin (VGTB-RB) in Vietnam and the Cagayan River Basin (C-RB) in the Philippines witnessed an extraordinary flood inundation from October to November 2020. Nine typhoons hit the central part of Vietnam, where VGTB-RB is located, with a prolonged heavy rain from 6 Oct. to 1 Dec. 2020 (Linfa brought 852 mm/day, total 3300 mm from 5-20 Oct. 2020). In the Philippines, five typhoons occurred successively before Ulysses lashed Luzon's main island on 11-12 November 2020, triggering extensive flooding in C-RB, as shown in **Figure 4(A)**. One of the leading causes of such extreme flooding is the successive rainfall events accompanied by heavy rainfall separated with short intervals. As a result, the soil moisture within the catchment increased, and surface runoff increased.

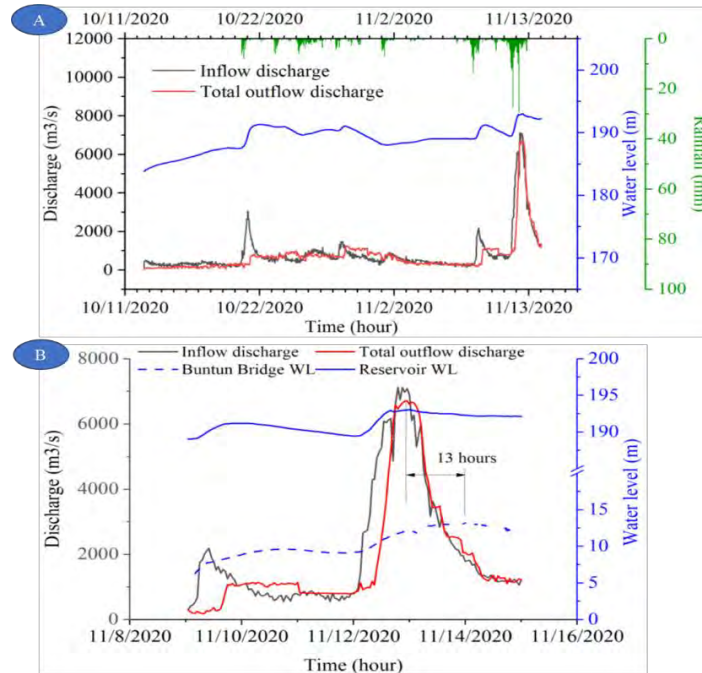


Figure 4. (A) Rainfall, Inflow, outflow, and reservoir elevation during the five successive typhoons in 2020, and (B) Magat dam operation during typhoon Ulysses 2020

3. CONCLUSION

Results suggest an urgent need to optimize dam pre-release to balance between required storage for droughts and management strategy in reducing flood impact. And, optimizing the sediment management is crucial to recover the reservoir volume and restore the original functions, which will be proposed.

Acknowledgment:

This work was funded by A.P.N. "Asia-Pacific Network for Global Change Research" under project reference number CRRP2020-09MY-Kantoush.

4. REFERENCES

- DO, A.T.K., Vries, S.D., Stive, M.J.F. "Beach evolution adjacent to a seasonally varying tidal inlet in central Vietnam", *Journal of Coastal Research*, 34(1), 6-25, 2018.
- Hoanh, C.T., Jirayoot, K., Lacomme, G., Srunetr, V. "Impacts of climate change and development on Mekong flow regimes-First assessment 2009", M.R.C. Technical paper No. 29. Mekong River commission, Vietnam, Lao P.D.R., 2010.
- Nga, P.H. "Flood risk assessment focusing on intangible vulnerability for rural floodplain area in Central Vietnam", Doctoral thesis, Kyoto University, Japan, 2019.
- Principe, J. A. "Exploring climate change effects on watershed sediment yield and land-cover based mitigation measures using SWAT model, R.S. and G.I.S.: case of Cagayan river basin, Philippines", *International Archives of the Photogrammetry, Remote Sensing and Spatial Information Sciences*, XXXIX-B8, Australia, 193-198, 2012.
- Souvignat, M., Laux, P., Freer, J., Cloke, H., Thinh, D.Q., Thuc, T., Cullmann, J., Nauditt, A., Flugel W. A., Kunstmann, H., Ribbe, L. "Recent climatic trends and linkages to river-discharge in Central Vietnam", *Hydrological processes*, 28, 1587-1601, 2014.



SPATIAL-TEMPORAL VARIATIONS OF SUSPENDED SEDIMENT IN THE VIETNAMESE MEKONG DELTA

Doan Nguyen Luyen Phuong¹, Doan Van Binh², Sameh A. Kantoush³, Quoc Hung Nguyen⁴, Trung La Vinh⁵, Mai Nguyen Thi Phuong⁶, Hung. T. Nguyen⁷, Tetsuya Sumi⁸

^{1,2,4} Faculty of Engineering, Vietnamese German University, Binh Duong Province, Vietnam, nguyendoan041297@gmail.com, binh.dv@vgu.edu.vn

^{3,8} Water Resources Centre, Disaster Prevention Research Institute, Kyoto University, Japan, kantoush.samehahmed.2n@kyoto-u.ac.jp, sumi.tetsuya.2s@kyoto-u.ac.jp

⁵ Research Management Department, Vietnamese German University, Binh Duong Province, Vietnam, trung.lv@vgu.edu.vn

⁶ Department of Civil Engineering, Thuyloi University, Hanoi Capital, Vietnam, maiswru@tlu.edu.vn

⁷ Sustainable Urban Development Program, Vietnamese German University, Binh Duong Province, Vietnam, hung.nt@vgu.edu.vn

ABSTRACT

Sediment depletion in the Vietnamese Mekong Delta (VMD) has brought threats to riverbed and riverbank dynamics. The main objective of this research is to make a relationship between turbidity and suspended sediment concentration (SSCs) and to assess temporal-spatial variations of SSCs in the VMD. In this regard, the SSCs were measured and monitored along the Tien and Hau Rivers under the Japan-ASEAN Science, Technology, and Innovation Platform (JASTIP) project. Particularly, we installed three monitoring stations in main rivers and conducted two field surveys to collect data for assessing SSC values in the VMD. The results show that the SSCs in the delta are changeable seasonally with high values in the high-flow season and low values in the low-flow season. The Tien and Hau Rivers can be divided into two reaches. The upper reach has high SSC, decreasing seaward, whereas the lower reach has lower SSC, increasing seaward.

Keywords: Sediment, VMD, erosion, turbidity, SSCs

1. INTRODUCTION

The Vietnamese Mekong Delta (VMD) is the third-largest delta worldwide with flat topography and a dense network of rivers and channels. Recently, the VMD is suffered from riverbank erosion, high sea-level rise, and a poured sediment decrease of about 74% due to dam development (Binh et al., 2020). Besides, sand mining contributes significantly to a decrease in the sediment budget of the VMD (Loc et al., 2021), reducing the sediment flux from the river to the sea. Declined sediment load in the delta has caused erosion of the coastlines and riverbank and incision of the riverbed (Binh et al., 2021). Dams and sand mining may cause changes in the erosion processes. Although the understanding of the flow regime and sediment load in the VMD, the understanding of spatial-temporal variations of the suspended sediment in the VMD is limited. Therefore, this study examines sediment dynamics in the VMD using the in-situ and historically measured data. The specific objectives are (1) establishing the relationship between turbidity

Affiliation

¹ Master student, Vietnamese-German University; ^{3,8} Professor, Kyoto University; ^{2,5,7} Lecturer, Vietnamese-German University; ⁴ Professor, Vietnamese-German University; ⁶ Lecturer, Thuyloi University



and the suspended sediment concentration (SSC) and (2) examining spatiotemporal variations of the SSC in the delta.

To achieve the objectives, we conducted two campaigns to install three stations that monitor turbidity in the VMD under the Japan-ASEAN Science, Technology, and Innovation Platform (JASTIP) project led by Kyoto University. In the first campaign (February 26-28, 2016), we set up two stations at Tan Chau and Vam Nao to measure the turbidity using an Infinity-ATU75W2-USB turbidity meter. In the second campaign (August 2017), we installed a turbidity station at Thot Not (about 20 km from the Can Tho City) (Fig 1). The measurement interval at these three stations is 30 minutes. On the other hand, we conducted two field surveys in August 2017 (high-flow season) and March-April in 2018 to measure the SSCs, river bathymetry, and flow parameters. The measurement was conducted along 570 km in the entire Tien and Hau Rivers and the Vam Nao diversion channel. The instrument used were an acoustic Doppler current profiler (ADCP) and an Infinity-ATU75W2-USB turbidity meter. In the second field survey, we also measured the vertical distribution of the SSCs and flow velocity using the Infinity turbidity and velocity meters, respectively.

2. MAIN RESULTS

2.1 Relationship between turbidity and suspended sediment concentration

The samples of suspended sediment were collected at 1 m below the water surface at My Thuan and Mang Thit which are located about 100 and 65 km from the river mouth of the Tien River, respectively. We determined the grain size distribution by using Shimadzu SALD-2300 Laser Diffraction Particle Size Analyzer to measure particle size between 17 nm and 2,500 μm . The results show that the suspended sediment diameters are 12.6 μm at My Thuan and 6.1 μm at Mang Thit. Approximately 95% of the suspended sediment is composed of silt and clay.

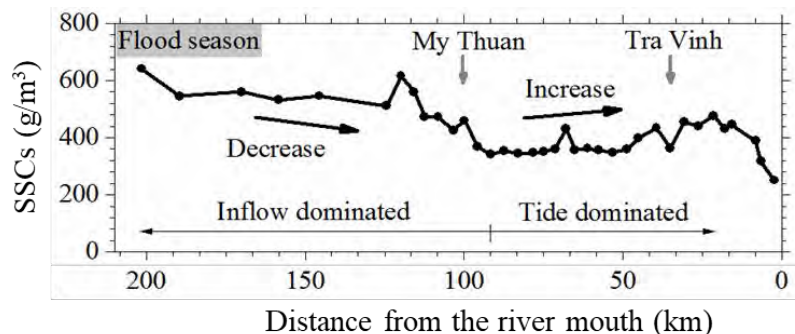


Figure 1: Longitudinal SSC variations in the Tien River in the high-flow season in March-April 2018

The data measured in the field campaigns are the turbidity with units of ppm and FTU. To synchronize with collected SSC data (unit is g/m^3); we converted the turbidity to SSCs. To form a relationship between the turbidity and SSC, we collected samples during the field surveys, and then analyzed them in the laboratory. The relationships between turbidity and SSC are in the forms of linear correlation shown in equations (1) and (2) with the coefficient of determinations (R^2) of 0.9925 and 0.9945, respectively.

$$\text{SSC} (\text{g}/\text{m}^3) = 1.9922 \times \text{Turbidity} (\text{ppm}) - 23.981 \quad (1)$$

Affiliation

¹Master student, Vietnamese-German University; ^{3,8}Professor, Kyoto University; ^{2,5,7}Lecturer, Vietnamese-German University; ⁴Professor, Vietnamese-German University; ⁶Lecturer, Thuyloi University



$$\text{SSC (g/m}^3\text{)} = 3.0572 \times \text{Turbidity (FTU)} - 6.8179 \quad (2)$$

2.2 Temporal and spatial variations of SSCs

In the VMD, the SSCs is changeable; it is usually high in the high-flow season and low in the low-flow season. At Tan Chau in the Tien River, the recorded SSCs got the highest value of 1,300 g/m³, and its range was from 5 to 70 g/m³ in the low-flow season (in March-April 2018). However, in the regions of the turbidity maximum, the SSCs were relatively similar in both high-flow and low-flow seasons. For example, the SSC at Tra Vinh (in the Tien River) was 364 g/m³ (in August 2017) and 295 g/m³ (in April 2018).

In the high-flow season, the SSCs in the Tien River were high from Tan Chau to My Thuan and decreased seaward, while they were low from My Thuan to the river mouth and decreased seaward. Similarly, the SSCs in the Hau River were high upstream of Can Tho and decreased seaward, while they were low from Can Tho to the river mouth and increased seaward (Fig. 1).

3. CONCLUSION

The sediment dynamics in the Tien and Hau Rivers are changeable reasonably. The SSCs are high in the high-flow season and low in the low-flow season. The VMD's main rivers can be divided into two reaches: upper and lower. In the flood season, the upper reach has high SSC, decreasing seaward, while the lower reach has lower SSC, increasing seaward.

Acknowledgment:

The research was funded by the Japan-ASEAN Science, Technology and Innovation Platform (JASTIP) and the Supporting Program for Interaction-Based Initiative Team Studies SPIRITS 2016 of Kyoto University, Japan.

4. REFERENCES

- Binh, D. V., Kantoush, S., & Sumi, T. (2020). Changes to long-term discharge and sediment loads in the Vietnamese Mekong Delta caused by upstream dams. *Geomorphology*, 353. <https://doi.org/10.1016/j.geomorph.2019.107011>
- Loc, H. H., Van Binh, D., Park, E., Shrestha, S., Dung, T. D., Son, V. H., Truc, N. H. T., Mai, N. P., & Seijger, C. (2021, Feb 25). Intensifying saline water intrusion and drought in the Mekong Delta: From physical evidence to policy outlooks. *Sci Total Environ*, 757, 143919. <https://doi.org/10.1016/j.scitotenv.2020.143919>
- Binh, D. V., Kantoush, S. A., Sumi, T., Mai, N. P., Ngoc, T. A., Trung, L. V., & An, T. D. (2021). Effects of riverbed incision on the hydrology of the Vietnamese Mekong Delta. *Hydrological Processes*, 35(2). <https://doi.org/10.1002/hyp.14030> .

Affiliation

¹Master student, Vietnamese-German University; ^{3,8}Professor, Kyoto University; ^{2,5,7}Lecturer, Vietnamese-German University; ⁴Professor, Vietnamese-German University; ⁶Lecturer, Thuyloi University



APPLICATION OF RAINFALL-RUNOFF- INUNDATION (RRI) MODEL FOR FLOOD MAPPING AT VU GIA THU BON RIVER BASIN IN VIETNAM

Thao Thi Phuong Bui^{1,2}, Sameh Kantoush¹, Mohamed Saber¹, Doan Van Binh³
SUMI Tetsuya¹, Duong Du Bui², Nguyen Quang Binh^{1,4}

¹Water Resource Center, Disaster Prevention Research Institute (DPRI), Kyoto
University, Kyoto 611-0011, Japan, bui.thaothiphuong.3e@kyoto-u.ac.jp,
Thaobtp26@wru.vn, kantoush.samehahmed.2n@kyoto-u.ac.jp,
mohamedmd.saber.3u@kyoto-u.ac.jp, sumi.tetsuya.2s@kyoto-u.ac.jp

²National Center for Water Resources Planning and Investigation (NAWAPI).
Long Bien District, Ha Noi, Vietnam, duongdubui@gmail.com

³Faculty of Engineering, Vietnamese German University, Binh Duong Province,
Vietnam, binh.dv@vgu.edu.vn

⁴The University of Danang - University of Science and Technology, 54 Nguyen
Luong Bang, Danang, Vietnam, nqbinh@dut.udn.vn

ABSTRACT

The Vu Gia Thu Bon (VGTB) River basin is one of the main river basins in Vietnam. The rapid development of dams with deforestation has resulted in many environmental challenges in the VGTB basin, especially floods. Frequent heavy rainfall due to typhoons between September to December causes floods to occur annually. Floods have become an extreme natural disaster in the basin which caused many people and economic loss. For flood mapping, this study aims to apply the Rainfall-Runoff-Inundation (RRI) model in the VGTB River basin. The first-hand setup for two flood events (2017 and 2020) shows a potential result. A flood hazard map can be continually developed using the RRI model in the VGTB river basin.

Keywords: RRI model, Discharge, Flood mapping, Vu Gia Thu Bon River basin, Vietnam

1. INTRODUCTION

Vietnam has been faced with various challenges related to water resources, such as transboundary water resources management, increasing water demand, degradation of water quality and quantity due to climate change, and human activities, especially flood, which has been a prevalent concern for farmers last decades. With over 3,200 kilometers of coastline, and 80% of the total population living along the coast, Vietnam is one of the most flood-prone and most affected countries by climate change (**Dasgupta S. et al., 2007**). Besides, human activities, such as watershed deforestation and construction of hydroelectric power plants, have the most visible impact on Vietnam's water quality and quantity. One of the most crucial issues from these human activities is extreme flood events, leading to poor water quality or inundation in the downstream areas.

We focus our study on the VGTB River basins located in Central, one of Vietnam's largest internal drainage systems. VGTB river basin covers 10,000 km² (**Firoz. et al., 2018**); this river system is formed by two major rivers of the Vu Gia and the Thu Bon (Vu Gia river is 204 km long, Thu Bon river is 152 km long). Most of the VGTB River basin area is situated in Quang Nam province and Da Nang city, and a very small proportion is located in Kon Tum province. It is characterized by topography from 0 m to 2598 m elevation



(Viet et al., 2017). Almost half of the land area is covered by forest, followed by agricultural land, urban and water. Within the VGTB River basin, 18 multipurpose dams (MOITb, 2015) are used for water supply, irrigation, and hydropower. Several observation stations within the VGTB River basin include two water discharge stations and 15 rainfall stations, as shown in **Figure 2**. The VGTB river basin is greatly decisive to the livelihood of residents concerning water, food, energy, cultural, and recreational activities. The rainfall occurs primarily in the four months of the wet season (from September to December); the heavy rain concentrates from October to December leads to an increase in flood risk in the catchment. At the same time, little rain occurs during the long dry season, which spans from February to August and often causes water shortages (MOITa, 2015). The recurrence of floods during the rainy season poses many severe challenges to local decision-makers.

We attempt to create a flood risk map to help managers and citizens better understand the flood situation in the VGTB River basin.

RRI model is a two-dimensional model used for rainfall-runoff and inundation simulation. RRI model can simulate flood extent using different surface and sub-surface flow conditions. RRI also deals with the lateral subsurface flow in mountainous areas and infiltration in flat regions separately. For a detailed explanation of RRI, refer to the literature (Sayama et al., 2012). Data used as input is MERIT Digital Elevation Model (MERIT DEM). It represents the terrain elevations at a 3sec resolution (~90m at the equator). Rainfall and river discharge data were collected from the rainfall stations and hydrology stations within the VGTB river basin.

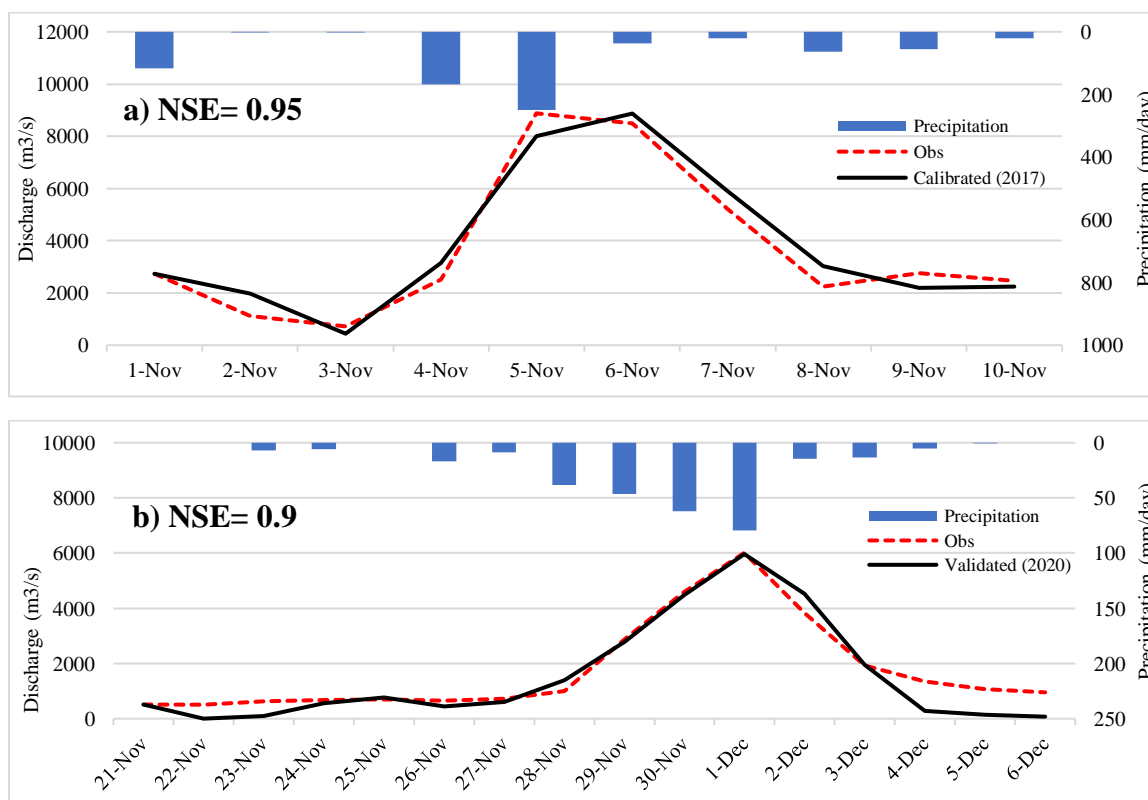


Figure 1. Observed and simulated discharge at Nong Son station in VGTB river basin **a)** calibration period- flood event 2017 and **b)** validation period- flood event 2020



2. MAIN RESULTS

RRI model was applied for daily discharge (m^3/sec) estimation in the Nong Son station. **Figure 1a)** and **1b)** show the results of the daily discharge estimation for flood events 2017 (calibration period) and 2020 (validation period) at Nong Son station, respectively. Model evaluation for the discharge by Nash–Sutcliffe model efficiency coefficient (NSE), the NSE value shows the acceptable performance of RRI in the VGTB River basin. The initial results of the simulated river discharge point out that the RRI model has great potential in estimating the released flow for the study area. RRI simulation results showed the flood inundation extent closely to the actual flood event 2020, as shown in **Figure 2**. The green points displayed in Figure 2 represent measured post-flood marks collected from our co-author's field trip. Correlation between 47 measured flood mark points and water depth by RRI was calculated for this flood event (**Figure 3**). The coefficient of determination R^2 shows how strong of a linear relationship is. The value of 0.503 presents a good relationship in simulating water depth by the RRI model compared to the actual value.

3. CONCLUSION

This study shows the potential of the RRI model in estimating the river discharge in the VGTB River basin. However, there is still a need to improve the model in terms of parameter setting and reservoir adding to achieve higher model accuracy. Therefore, RRI can simulate the flood hazard map in the VGTB river basin.

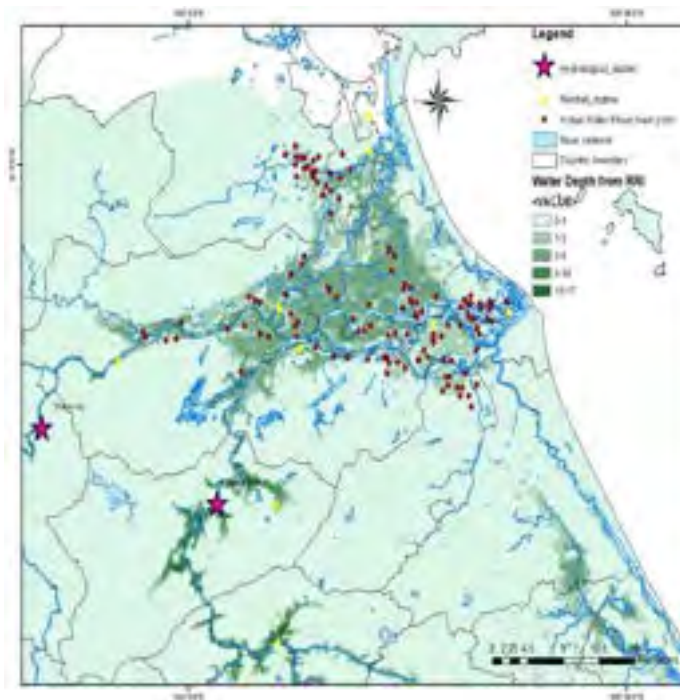


Figure 2. Correlation between Actual Flood mark and Water depth by RRI for flood event 2020 in VGTB river basin (m)

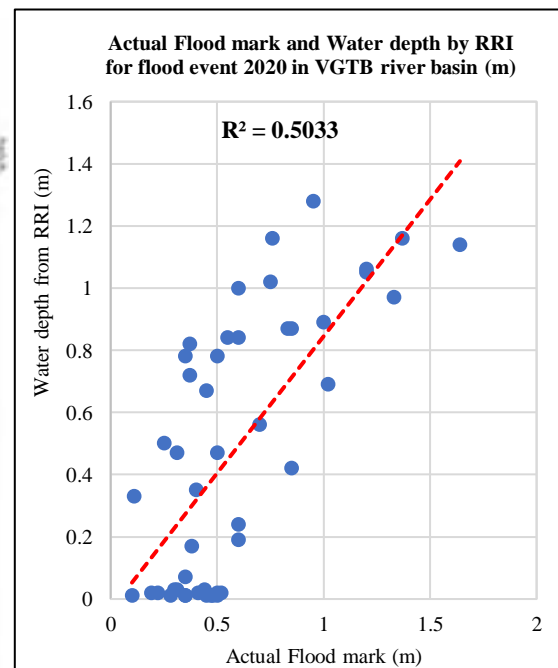


Figure 3. Correlation between Actual Flood mark and Water depth by RRI for flood event 2020 in VGTB river basin (m)



Acknowledgment: This work was funded by APN "Asia-Pacific Network for Global Change Research" under project reference number CRRP2020-09MYKantoush (Funder ID: <https://doi.org/10.13039/100005536>).

4. REFERENCES

- Dasgupta S, Laplante B, Meisner C, Wheeler D, Yan J (2007). *The impact of sea level rise on developing countries: A comparative analysis* (Washington: World Bank Policy Research Working Paper)
- Firoz, A. B. M., Nauditt, A., Fink, M., and Ribbe, L. (2018): *Quantifying human impacts on hydrological drought using a combined modelling approach in a tropical river basin in central Vietnam*, Hydrol. Earth Syst. Sci., 22, 547–565, <https://doi.org/10.5194/hess-22-547-2018>.
- Ribbe, L., Viet, T. C., Firoz, A., Nguyen, A. T., Nguyen, U., and Nauditt, A. (2017): *Integrated River Basin Management in the Vu Gia Thu Bon Basin*, in: *Land Use and Climate Change Interactions in Central Vietnam*: LUCCi, edited by: Nauditt, A. and Ribbe, L., Water Resources Management and Development, Springer Book Series.
- MOIT: *Decision for Hydropower Plant Operation* (2015a): Technical Document, Ministry of Investment and Trade, Socialist Republic of Vietnam (Vietnamese).
- MOIT: *Decision for Hydropower Plant Operation* (2015b): Technical Document, Ministry of Investment and Trade, Socialist Republic of Vietnam (Vietnamese).
- MERIT DEM, http://hydro.iis.u-tokyo.ac.jp/~yamadai/MERIT_Hydro/
- Sayama T, Ozawa G, Kawakami T, Nabesaka S, Fukami K. 2012. *Rainfall-runoff-inundation analysis of the 2010 Pakistan flood in the Kabul River basin*. Hydrological Science Journal 57: 298–312. DOI: 10.1080/02626667.2011.644245.



PREDICTION OF SUSPENDED SEDIMENT CONCENTRATION USING LONG SHORT-TERM MEMORY NETWORKS

Duy Vu LUU¹, Thi Ngoc Canh DOAN², Ngoc Duong VO³

¹ The University of Danang – University of Technology and Education, 48 Cao Thang, Danang, Vietnam

² The University of Danang – University of Economics, Danang, Vietnam

³ The University of Danang – University of Science and Technology, Danang, Vietnam

ldvu@ute.udn.vn

Abstract. Understanding changes in sediment dynamics can significantly impact the sustainable development of the world. Modelling suspended sediment plays a crucial role because it allows decision makers and managers to formulate solutions that can avert the blockage of the sediments in a watershed. Estimates of suspended sediment is useful for global ecosystem service assessments and identify vulnerable aspects under climate change. This research has proposed using the Long Short-Term Memory (LSTM) networks to forecast suspended sediment concentration (SSC) at the Vu Gia-Thu Bon catchment, Vietnam. Inputs include the monthly runoff data and the monthly suspended sediment concentration at the Thanh My station. The outputs are predicted suspended sediment concentrations compared with the observed data. In the training and testing sets, monthly data from 1978 to 2005 and data from 2006 to 2019 are used. The research evaluates many scenarios with different hyperparameters to find the optimal LSTM model for the catchment. The comparison shows that the LSTM model has the ability to predict SSC time series at the catchment.

1. Introduction

High sediment delivery ratios can lead to significant flood risks because sedimentation can reduce the cross sections [1]. Sediment transport is a nonlinear and complicated environmental phenomenon. The topic has attracted many researchers. There is a wide range of models adopted to simulate and predict river sediment dynamics, such as empirical, numerical and physically-based models. The empirical studies have been successfully applied to estimate sediment transport [2]. However, the empirical studies are expensive in comparison with other approaches. The empirical equations based on the input parameters with innate errors can lead to uncertainties in the results [3]. In addition, the equations require essential information about the flow and sediment characteristics to develop sediment load relations [4]. Because there is a wide range of flow conditions and dependent parameters of sediment characteristics at different points, the equations are not unique. Moreover, they adopt the simple linear structure which is not enough to model the nonlinear and complex processes of sediment load [5]. Therefore, empirical models do not often have the ability to predict SSL accurately. In terms of the theoretical governing equation, there are difficulties in obtaining knowledge of the overall processes because it uses the large



range of obscure parameters [6]. Physically-based models have been widely applied to estimate erosion and sediment load across the world [7]. However, they require many variables with spatial and temporal data. It is difficult, even impossible, to collect them in many areas.

In recent decades, numerous data driven models have been widely introduced for suspended sediment modelling, such as LSTM models. The data driven models have accurate results in modelling suspended sediment, although they are simplicity and do not require much prior knowledge. The extract approaches can identify the data patterns from the historical data to predict future events [8]. They can reduce the complexity of the processes because they do not require many algorithms and theory.

In this study, the LSTM models are adopted to estimate suspended sediment concentration (SSC) at Vu Gia – Thu Bon catchment, Vietnam.

2. Theoretical review

The LSTM network, a kind of Recurrent Neural Network (RNN), can overcome the problem of vanishing gradients of RNN models. LSTM is applied in many topics, from prediction to face detection. LSTM can remember prior important things and forget unnecessary information [9]. A basic LSTM model consists of three gates: an input gate, an output gate and a forget gate. The gates have different weights.

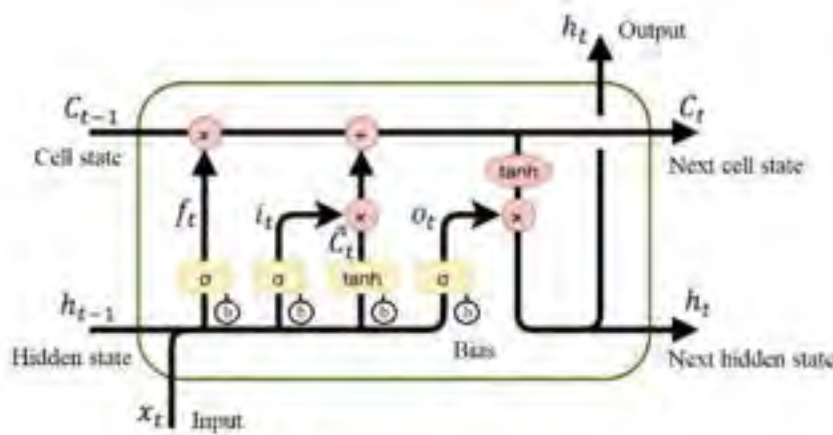


Figure 1. LSTM cell.

In the forget gate, f_t , input, h_{t-1} and x_t , are passed or forgot. Output of this gate being from 0 to 1 is computed as

$$f_t = \sigma(W_f \cdot [h_{t-1}, x_t] + b_f) \quad (1)$$

where σ is the sigmoid function, w_t is the weight value, h_{t-1} is output of the module at the last time (t-1), x_t is input at time t, and b_t is the bias value. When f_t is 1, the module completely stores the whole information. In contrast, when f_t is 0, the module completely forgets the received information.

The input gate controls what information is transferred to the cell state. The output is determined by using the following equations:

$$i_t \cdot \tilde{C}_t = \sigma(W_i \cdot [h_{t-1}, x_t] + b_i) \cdot \tanh(W_c \cdot [h_{t-1}, x_t] + b_c) \quad (2)$$

$$C_t = f_t \cdot C_{t-1} + i_t \cdot \tilde{C}_t \quad (3)$$

where C_t and C_{t-1} are the cell states at time t and t-1 respectively.

The output gate controls the data flow in the cell state transferred to the next step. The output value, h_t , is computed as

$$h_t = O_t \tanh(C_t) \quad (4)$$

$$O_t = \sigma(W_o [h_{t-1}, x_t] + b_o) \quad (5)$$



where b_0 is the bias value and w_0 is the weight value at the output gate.

3. Study area

The Thu Bon river with a drainage basin of over 10,000 km² is the main river in Quang Nam province and Da Nang city. The flood season lasts 3 months and contribute 80% of the annual flow. The dry season lasts 9 months but makes up only 20% of the annual flow. In the flood season, the river deliver sediment to the coast. The frequent landslides in the region usually occur, the river carries the high suspended sediment load. It increases suspended sediment amount. Sediment concentration can affect water quality, the plants and animals living in the river. Sediments can settle and develop sand bars on the river or stream bed.

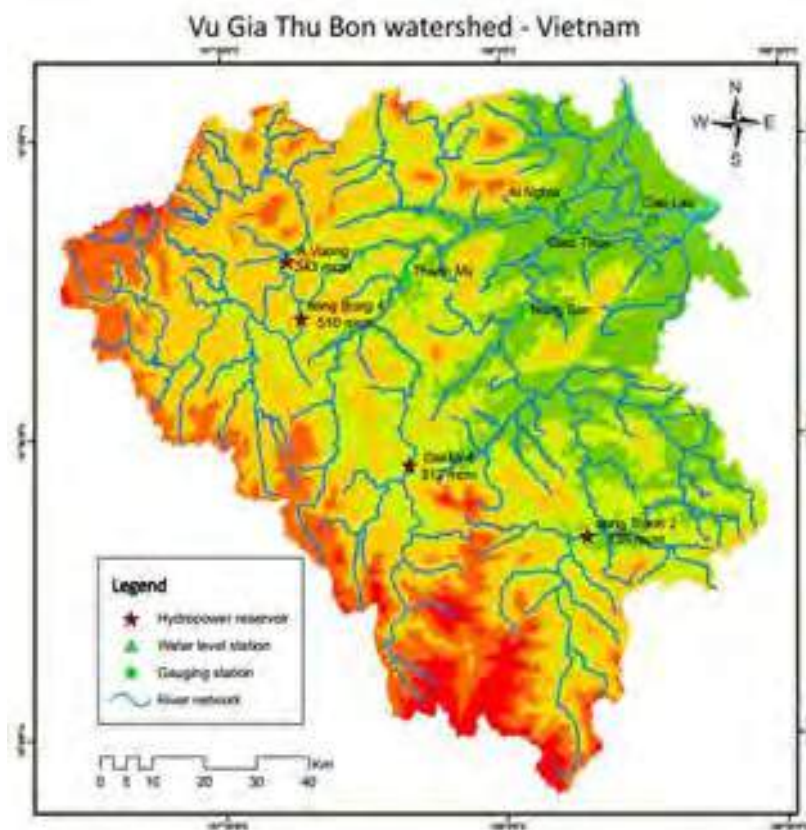


Figure 2. Vu Gia Thu Bon catchment.

4. Model development

The proposed model adopts uninterrupted time series data, including monthly discharge data (Q) and monthly suspended sediment concentration (SSC) at Thanh My for training and testing processes. In the training and testing sets, monthly data from 1978 to 2005 (27 years) and data from 2006 to 2019 (16 years) are used. The main reason why the first twenty-nine years are assigned to the training set is that this period has the highest values.

Tables 1 shows the input combinations. They allow the study to predict the SSC value in one month ahead at time t (SSC_t).



Table 1. The input combinations

| Model | The input combinations |
|-----------------|---|
| S ₁ | SSC _{t-1} |
| SQ ₁ | SSC _{t-1} , Q _{t-1} |
| S ₂ | SSC _{t-1} , SSC _{t-2} |
| SQ ₂ | SSC _{t-1} , SSC _{t-2} , Q _{t-1} , Q _{t-2} |
| S ₃ | SSC _{t-1} , SSC _{t-2} , SSC _{t-3} |
| SQ ₃ | SSC _{t-1} , SSC _{t-2} , SSC _{t-3} , Q _{t-1} , Q _{t-2} , Q _{t-3} |

The LSTM models, including one input layer, hidden layers and one output layer, are used to predict SSC. The Relu activation and the linear activation are used in the hidden layer and the output layer respectively.

The numbers of nodes in the input and output layers are equal to the number of input and output variables of a proposed model. The number of nodes in the hidden layer is an important consideration in training state. Fewer nodes within a hidden layer cannot allow the LSTM models to capture the intricate relationships between indicator parameters and the output. Too many hidden layer nodes can lead to overtraining.

The selection of parameters, such as the number of batch-size, epoches and hidden layers and nodes in the hidden layer (in training process) is based on the grid search (GS) method. In the GS processing, the grid range of batch-size is between 1 and 20 and a grid step is 1. The range of the number of epoch is from 1 to 1000. The grid range of nodes is from 2 to 10 with a grid step of 1. An early-stopping set allows us to select the optimal epochs. The early-stopping is set as 20 which means the algorithm will stop when there is no improvement within 20 steps.

The optimization algorithm is Adam presented by Diederik Kingma [10]. This algorithm is widely applied to many applications, specifically in training deep neural networks. Adam is a replacement for stochastic gradient descent for turning the weights iteratively based on training data. Adam helps the model increase computational efficiency and require little memory. To protect the LSTM model from overfitting, Dropout regularization is used in this study.

Table 2. The proposed MLP and LSTM models

| Items | Details |
|---------------------|---|
| Input variables | Monthly SSC and Q in Thanh My station |
| Output variable | Monthly SSC in Thanh My station |
| Training parameters | Number of input neurons: from 1 to 6 Number of hidden neurons: variety Number of hidden layer: 1 or 2 Learning rate 0.01 Transfer function of hidden layer: Relu Transfer function of output layer: Linear Training algorithm: Adam |



The number of epochs: variety

Early stopping: yes

The length of timesteps: 1, 2 and 3

The Nash–Sutcliffe model efficiency coefficient (NSE), Root Mean Squared Error (RMSE) and Mean Absolute Error (MAE) are the model evaluation criteria. The model's efficiency can be shown by the NSE. NSE is a number that ranges from -infinity to one. When NSE equals one, the modelled and actual data are a perfect match. The RMSE is a statistic that shows how prediction errors cluster around the line of best fit, or the discrepancies between predicted and observed values. The value of the RMSD is never negative. Theoretically, if the RMSD number is 0, the data is perfectly fit. In statistics, MAE is a measure of errors between two continuous variables. The lower the MAE number, the better the model fits.

$$NSE = 1 - \frac{\sum_{i=1}^n (\hat{y}_t - y_t)^2}{\sum_{i=1}^n (y_t - \bar{y})^2} \quad (6)$$

$$RMSE = \sqrt{\frac{1}{n} \sum_{i=1}^n (\hat{y}_t - y_t)^2} \quad (7)$$

$$MAE = \frac{\sum_{i=1}^n |y_t - \hat{y}_t|}{n} \quad (8)$$

Where \hat{y}_t is the observed discharge, y_t is the modeled discharge, and \bar{y}_t is the mean of observed discharge.

5. Model results

Table 3 displays the results of the LSTM models comprising of hidden neuron, epochs, and batch_size change. In the training of Thanh My station, the SQ₂ model produce the best MAE, RMSE and NSE (28.018, 48.786 and 0.407, respectively). In the testing phases, the SQ₂ also obtains the best RMSE, NSE and MAE values. Therefore, the SQ₂ model is selected for the catchment.

Table 3. Performance of the LSTM models

| Station | model | Model parameters | Training | | | Testing | | |
|-------------|-----------------|---|----------|--------|-------|---------|---------|-------|
| | | | MAE | RMSE | NSE | MAE | RMSE | NSE |
| Thanh My | S ₁ | Structure: 1-5-4-1 Epoch:30 Batch_size: 10 5-4 (e30) | 34.038 | 52.736 | 0.303 | 92.405 | 133.897 | 0.272 |
| | SQ ₁ | Structure: 2-4-3-1 Epoch: 75 Batch_size: 10 | 30.550 | 51.645 | 0.332 | 86.616 | 125.784 | 0.358 |
| | S ₂ | Structure: 2-2-3-1 Epoch: 50 | 34.080 | 55.887 | 0.222 | 99.266 | 143.480 | 0.170 |



| | | | | | | | |
|-----------------|---------------------|--------|--------|-------|--------|---------|--------|
| | Batch_size: 10 | | | | | | |
| SQ ₂ | Structure: 4-5-3-1 | 28.789 | 48.786 | 0.407 | 84.353 | 121.312 | 0.402 |
| | Epoch: 50 | | | | | | |
| | Batch_size: 10 | | | | | | |
| S ₃ | Structure: 3-5-3-1 | 31.756 | 51.990 | 0.326 | 96.368 | 137.224 | 0.243 |
| | Epoch: 50 | | | | | | |
| | Batch_size: 8 | | | | | | |
| SQ ₃ | Structure: 6-14-4-1 | 28.018 | 49.229 | 0.395 | 85.000 | 123.596 | 85.000 |
| | Epoch: 60 | | | | | | |
| | Batch_size: 10 | | | | | | |

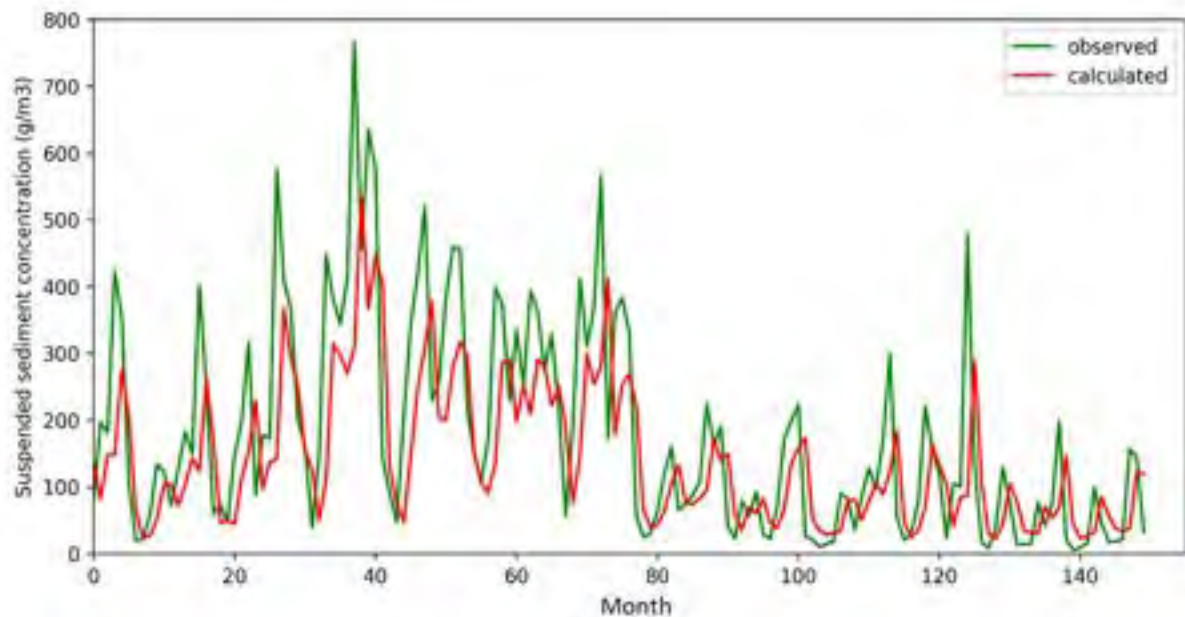


Figure 3. Comparison between the modelled and observed SSC for testing period (the SQ₂ model)

Figure 3 shows the relationship between the modelled SSC and the observed data from 1978 to 2007 in testing period based on the SQ₂ model. There is a similar trend between the observed data and the modelled data. The LSTM model has the ability to produce the same pattern as the observation. However, the LSTM model sometimes underestimates the SSC. The reason for this issue could be flood discharges in the upstream reservoirs at that time. Therefore, the flooding flow becomes more extraordinary.

6. Conclusion



This research introduces and develops the LSTM model to generate SSC. The six models are estimated to select the suitable one for the catchment. The model evaluation criteria are MEA, RMSE and NSE. The performances of all the scenarios are good and there are no significant differences in the results between the scenarios. The scenario SQ₂ is slightly better than others and was selected to test the model in the testing dataset that the model would face certainty.

The LSTM model can remember, update and also forget the information. Therefore, it can effectively solve problems with time series, for example SSC forecasting. Moreover, this method requires limited input data, only SSC and discharge, to produce accurate results. This is one advantage because there is not enough accurate data, such as topographical and hydrological information, in this catchment. Although there are discrepancies between the modelled data and observation, the model has the ability to generate quite accurate SSC. Therefore, the LSTM model is an effective approach to forecast discharge in the Vu Gia-Thu Bon catchment and is useful for giving early warning.

References

- [1] O. Korup, M. J. McSaveney, and T. R. Davies, "Sediment generation and delivery from large historic landslides in the Southern Alps, New Zealand," *Geomorphology*, vol. 61, no. 1-2, pp. 189-207, 2004.
- [2] J. Venditti, M. Church, M. Attard, and D. Haught, "Use of ADCPs for suspended sediment transport monitoring: An empirical approach," *Water Resources Research*, vol. 52, no. 4, pp. 2715-2736, 2016.
- [3] C. W. Rose, J. G. Shellberg, and A. P. Brooks, "Modelling suspended sediment concentration and load in a transport-limited alluvial gully in northern Queensland, Australia," *Earth Surface Processes and Landforms*, vol. 40, no. 10, pp. 1291-1303, 2015.
- [4] E. Shamaei and M. Kaedi, "Suspended sediment concentration estimation by stacking the genetic programming and neuro-fuzzy predictions," *Applied Soft Computing*, vol. 45, pp. 187-196, 2016.
- [5] K. Kamel, T. Mahmoud, Y. Le Bissonnais, and T. Mahmoud, "Assessment of the artificial neural networks to geomorphic modelling of sediment yield for ungauged catchments, Algeria," *Journal of Urban and Environmental Engineering*, vol. 8, no. 2, pp. 175-185, 2014.
- [6] C. T. Yang and S. Wan, "Comparisons of selected bed-material load formulas," *Journal of Hydraulic Engineering*, vol. 117, no. 8, pp. 973-989, 1991.
- [7] V. Nourani, "Using artificial neural networks (ANNs) for sediment load forecasting of Talkherood River mouth," *Journal of Urban and Environmental Engineering*, vol. 3, no. 1, pp. 1-6, 2009.
- [8] T. Rajaei, S. A. Mirbagheri, M. Zounemat-Kermani, and V. Nourani, "Daily suspended sediment concentration simulation using ANN and neuro-fuzzy models," *Science of the total environment*, vol. 407, no. 17, pp. 4916-4927, 2009.
- [9] Q. Yuan and S. Wei, "Aligning network traffic for serial consistency and anomalies with a customized LSTM model," in *2018 IEEE International Conference on Progress in Informatics and Computing (PIC)*, 2018, pp. 322-326: IEEE.
- [10] D. P. Kingma and J. Ba, "Adam: A method for stochastic optimization," *arXiv preprint arXiv:1412.6980*, 2014.



WATER STRESS INDEX: CASE STUDY ON VUGIA – THU BON RIVER BASIN IN VIETNAM

Duong Thi Thuy Mai¹, Duong Ngoc Vo¹, Thi Viet Nga Tran²

¹Ph.D. Student, The University of Danang – University of Science and Technology,
54 Nguyen Luong Bang Str., Danang City, Viet Nam.

mttduong@dut.udn.vn;

¹Professor, The University of Danang – University of Science and Technology, 54
Nguyen Luong Bang Str., Danang City, Viet Nam.

vnduong@dut.udn.vn.

² Professor, Hanoi University of Civil Engineering, 55 Giai Phong Str., HaNoi City,
Viet Nam.

ngattviet@nuce.edu.vn

ABSTRACT

The role of water security is the importance of sustainable development in a country. This study used the water stress index (WSI) to evaluate the status of water resources and water exploitation in the Vu Gia - Thu Bon river basin. In the study, the Vu Gia - Thu Bon river basin was divided into 9 areas to calculate the water stress index (WSI) through the following calculation: The water availability is calculated by the simulation software MIKE SHE; Demand water (domestic, industry, agriculture); Environmental water requirement (EWR) to maintain environmental stability of the river.

The findings have shown that 1) There is WSI differences between upper and lower Vu Gia Thu Bon; 2) In the downstream areas, water scarcity becomes more serious than in the middle and upstream areas, especially, the exploitation area to supply water for domestic and industry in Da Nang city.

Keywords: Water stress index; Environmental water requirement; Water availability; Demand water; Vu Gia - Thu Bon river basin.

1. INTRODUCTION

The total annual surface water is around 830-840 billion m³. Of this, 310-315 billion cubic meters per year is generated within the territory of Viet Nam, and accounts for 37%; while the volume of water runoff into the country is about 520-525 billion cubic meters per year, equal to 63%. Water resources are not evenly distributed over different regions and by different times of the year (The average volume of water in 3-5 months in the flood season makes up 70-80% of the total volume, while the 7-9 months of the dry season receives 20-30% of the year's water quantity). (Ministry of Natural Resources and Environment (MoNRE), 2006)

In Da Nang city, the demands for water from all sectors of the economy are increasing with an exploitation capacity of around 300.000 m³/day, and water demand grew 8% per year. According to the master plan on the water supply to 2030, vision to 2050, 100% of the urban population will have access to clean water (180 L/cap/day), 100% of the urban population with 150 L/cap/day [Da Nang, 2019]. The volume of water for municipal supply depends mostly on the amount of Vu Gia Thu Bon basin (97%) which is under a separate jurisdiction (Quang Nam Province) and is subject to strong competition from other water uses.

Affiliation

¹ Professor, University

² Student, University



With an expected reduction in dry season flows from the Song Vu Gia, the existing water supply intake at the Cau Do water treatment plant (WTP - Da Nang city) would be more vulnerable to salinity intrusion and increased concentration of pollutants as a result of the river's reduced flushing capacity. The early onset of the dry season has forced Da Nang Water Company (DAWACO) to pump water from An Trach due to salinity intrusion in the Vu Gia River, in turn, attributed to inadequate freshwater flows from the Vu Gia River (The salinity of water in WTP is 1119 mg/L on March 2nd, 2021 -DAWACO).

Da Nang features continuously strong and stable economic growth, ever-increasing living standards of its citizens. Da Nang's water demand is increasing rapidly, but available sources of water are very limited. With current and future challenges for water resources management, it is necessary to build the database in water sustainability assessment.

Metrics of water scarcity and stress have evolved over the years from simple to complex threshold indicators. Water scarcity can broadly be described as a shortage in the availability of renewable freshwater relative to demand (Damkjaer & Taylor, 2017). It is defined as the fraction of the total annual runoff available for human use. Water scarcity expresses insufficient freshwater resources to meet the human and environmental demands of a given area.

Water stress index (WSI) is typically defined as the relationship between total water use in domestic, industry, agriculture, and water availability. According to the map of water stress by the World Resources Institute, 17 countries currently face "extremely high" levels of water stress, in which, 12 countries belong to the Middle East and North Africa region. The studies show that climate change probably complicates the global water crisis.

There are many approaches to measure the WSI of a watershed. To assess the suitability of water resources, besides the evaluation of the water supply capacity and water demand, the required amount of water to maintain an ecosystem also needs to be considered. The relationship of the renewable water reserves (WR), total water use (WU), and the environmental water requirement (EWR) in that region are denoted by the water stress indicator (WSI) (Smakhtin et al., 2004).

$$WSI = \frac{WU}{WR - EWR}$$

WSI: Water stress index

WU: The water use (WU),

WR: water resource (WR)

EWR: Environmental Water Requirement

If:

WSI > 1: Overexploited (current water use is tapping into EWR)—environmentally water scarce basins.

0,6 ≤ WSI < 1: Heavily exploited

0,3 ≤ WSI < 0,6: Moderately exploited.

WSI < 0,3: Slightly exploited.

Research objectives

Water supply capacity assessment for domestic, industry, and agriculture of Vu Gia-Thu Bon river basin.

Calculating the water stress index and developing to map water stress index of the downstream region of the Vu Gia – Thu Bon river system.

Proposing some possible solutions to ensure water security for Danang City.

Methodology

Literature review and inheritance methods

Review of related theory aims to inherited researches at home and abroad that related to research contents. It can also help to provide an overview of areas in which the research is disparate and interdisciplinary a

Affiliation

¹ Professor, University

² Student, University



literature review is an excellent way of synthesizing research findings to show evidence on a meta-level and to uncover areas in which more research is needed, which is a critical component of creating theoretical frameworks and building conceptual models.

Methods of data collection and analysis

Data collection is a process of collecting information from all the relevant sources: water resources availability and demand, rainfall, weather...

Model methodology

The MIKE SHE Software will be applied for calculation.

2. MAIN RESULTS

15 regions of Vu Gia-Thu Bon river basin:

| No. | Areas | Area (km ²) |
|-------------------------|-----------------------|-------------------------|
| Region 1 (KV1) | Upper Vu Gia | 2411.61 |
| Region 2 (KV2) | Cai River basin | 865.21 |
| Region 3 (KV3) | Dak Mi River basin | 625.90 |
| Region 4 (KV4) | Tranh 2 River basin | 1062.69 |
| Region 5 (KV5) | Tranh 3 River basin | 1641.08 |
| Region 6 (KV6) | Middle Thu Bon | 725.11 |
| Region 7 (KV7) | Middle Vu Gia | 314.36 |
| Region 8 (KV8) | Con River basin | 616.88 |
| Region 9 (KV9) | Lower 1 Thu Bon | 332.90 |
| Region 10 (KV10) | Lower 2 Thu Bon | 186.47 |
| Region 11 (KV11) | Quang Hue River basin | 28.28 |
| Region 12 (KV12) | Yen River basin | 121.19 |
| Region 13 (KV13) | Tuy Loan River basin | 102.81 |
| Region 14 (KV14) | Cam Le River basin | 122.00 |
| Region 15 (KV15) | Lower Vu Gia | 189.65 |

Affiliation

¹ Professor, University

² Student, University

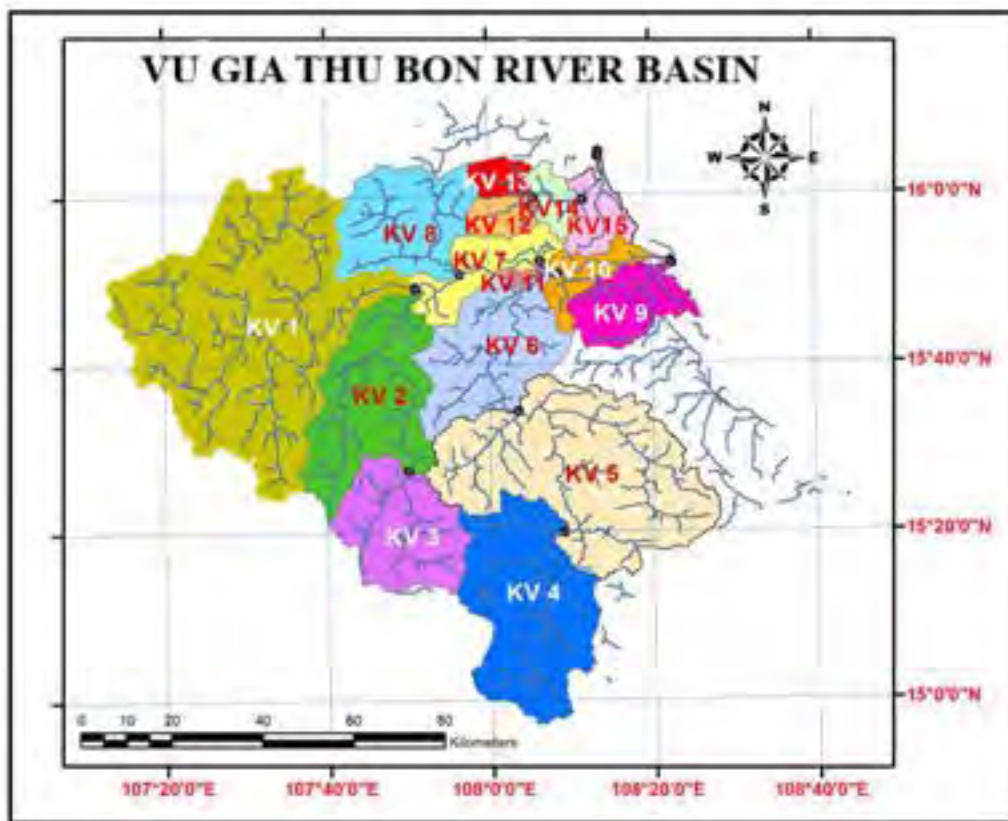


Figure 1: Map of dividing calculation regions on Vu Gia - Thu Bon River basin

The WSI differs dramatically within in other regions. In the upper areas, where $WSI < 0.3$ or $0.3 < WSI < 0.6$, indicating withdrawals which are environmentally safe, moderately exploited. While, the situations of environmentally water scarcity are occurring primarily in the lower Vu Gia - Thu Bon river basin, especially in Da Nang city.

3. CONCLUSION

The results of the research can be considered as one of the water resources management tools in the Vu Gia-Thu Bon river basin in general and Danang in particular. The water stress index is the basin of water supply planning in Danang City. Scarcity index is one technical numerical method developed to assist the parties to allocate the shared water resources and to assist in recovering the water gaps.

Acknowledgment: This work was supported by Vingroup scholarship program for Ph.D. student, 2021.

4. REFERENCES

- [1]. Ministry of Natural Resources and Environment (MoNRE). (2006). *National Water Resources Strategy. Towards the Year 2020*. 24.
- [2]. Challenges of water resources management in the current context in Da Nang city -August 2019.

Affiliation

¹ Professor, University

² Student, University



- [3]. Damkjaer, S., & Taylor, R. (2017). The measurement of water scarcity: Defining a meaningful indicator. *Ambio*, 46(5), 513–531. <https://doi.org/10.1007/s13280-017-0912-z>
- [4]. Smakhtin, V., Revenga, C., & Döll, P. (2004). A pilot global assessment of environmental water requirements and scarcity. *Water International*, 29(3). <https://doi.org/10.1080/02508060408691785>

Affiliation

¹ Professor, University

² Student, University



TURBULENT FLOW FIELD IN VEGETATION, FROM EXPERIMENT TO NUMERICAL MODEL

S.H, Truong¹, K.L., Phan², and N.H, Pham³

¹Thuyloi University, Hanoi, Vietnam

(truonghongson@tlu.edu.vn)

² Thuyloi University, Hanoi, Vietnam

(phankhanhlinh@tlu.edu.vn)

³ Thuyloi University, Hanoi, Vietnam

(phamhongnga@tlu.edu.vn)

ABSTRACT

The interaction between hydrodynamics, vegetation, and morphodynamics is the crux of nature-based solutions. The knowledge of these interaction processes is still in its infancy. Fundamental studies on this topic are usually based on small-scale laboratory experiments with a simple model of vegetation. Whether or not knowledge obtained can be applied for rivers, channels, and estuaries with natural scales has not yet been determined. Numerical models provide an effective tool to fill this knowledge gap. Numerical simulations were successfully captured the large coherent structures at the interface of a porous layer. Nevertheless, from a civil engineering perspective, utilizing detailed models on a large scale, e.g., river channels, coasts, or estuaries, is computationally costly. This study introduces some recent findings on this topic. A step-by-step approach including experiments, the analytical model, and numerical techniques was presented. The results focus on the presence of a shallow flow field and the transverse exchange of mass and momentum at the edge of the vegetation area.

Keywords: Natural-based solution; Vegetation; Flow Field; Physical model; Numerical Model.

1. INTRODUCTION

Vegetation provides effective protective tools for rivers, estuarine and coastal regions. The roots, stems, and canopy system of vegetation divert and retard the flow field within and surrounding vegetation region (Truong et al., 2019). In addition, mangroves and saltmarshes absorb external forces such as waves and currents (Phan et al., 2020). As a result, sediment tends to be deposited in and around the vegetation region (Vargas Luna et al., 2015). The sediment deposited then may have large influences on the shallow flow field and the growth conditions of the vegetation (Truong et al., 2017). These mutual interactions between ecological area (vegetation), hydrodynamic conditions (shallow flow field), and morphological conditions (sediment transport) are the crux of nature-based solutions (Nbs).

Many studies have been published in this context, focusing on understanding the hydrodynamic processes in and around the forest and the defensive role of vegetation in coastal and estuarine regions. For example, Truong et al., 2017 and Phan et al., 2015 observed the development of mangroves along the Mekong Delta estuaries and Mekong Deltaic Coast and linked the degradation of those ecological systems to the squeeze phenomenon. It is hypothesized that the ecological system needs certain accommodation spaces for its cyclic evolution under the stresses of human construction and increased water levels induced by sea-level rises. From a hydrodynamic perspective, this hypothesis was clarified by the penetration of

Affiliation

¹ Ph.D., Thuyloi University

² Ph.D., Thuyloi University

³ Ph.D., Thuyloi University



large turbulent flow structures in the mixing layer into the vegetation region (Truong et al., 2019). These turbulent structures caused by the Kelvin-Helmholtz instability are large compared to the water depths and are termed as large horizontal coherent structures (LHCSs).

The presence of turbulent structures at the interface of the vegetation region is recognized in a small-scale flume (Truong et al., 2019). As the LHCSs move along the vegetation-open channel interface, they generate cycloid flow events, including sweeps, ejections, the stagnant and reverse flows (Truong et al., 2019). These flow events split the shallow flow field into different regions associated with different length scales. These flow events have large influences on the transverse exchange of momentum in and around the vegetation region. It is suggested that Reynolds Shear stresses (RSs) induced by these LHCSs contribute more than 90% to the total turbulent shear stress (Truong & Uijtewaal 2019). In other words, these turbulent structures contribute up to 90% of the amount of transverse momentum exchange between the vegetation region and the open channel areas.

In order to model this phenomenon using the Unsteady Reynolds-Averaged Navier-Stokes (URANS) models, a new momentum exchange model was developed and verified using different data sets. This viscosity model could be used as a turbulent model in a numerical simulation to enhance the capability of the simulations.

2. MAIN RESULTS

A new hybrid eddy viscosity model was proposed by Truong & Uijtewaal 2019. The total eddy viscosity model can be determined according to the equations:

$$v_t = \begin{cases} \alpha \sqrt{c_f} \langle \bar{u} \rangle_d D + \frac{Dm}{D(y)} D_r^2 \beta^2 \delta^2 \left| \frac{d\langle \bar{u} \rangle_d}{dy} \right| & (y > 0) \\ \underbrace{\alpha \sqrt{c_f} \langle \bar{u} \rangle_d D}_{Elder} + \underbrace{\frac{1}{8} C_t^{-2} C_d d \langle \bar{u} \rangle_d}_{vegetationdrag} + \underbrace{\frac{Dm}{D(y)} D_r^2 \beta^2 \delta^2 \left| \frac{d\langle \bar{u} \rangle_d}{dy} \right|}_{LHCSs} & (y \leq 0) \end{cases}$$

In which α is a constant of the order of 0.1; Dm and $D(y)$ is the mean water depth and local water depth respectively; C_t is constant of proportionality and C_d is the drag coefficient of a single stem; β is a proportionality constant, and β is the mixing length.

Affiliation

¹ Ph.D., Thuyloi University

² Ph.D., Thuyloi University

³ Ph.D., Thuyloi University

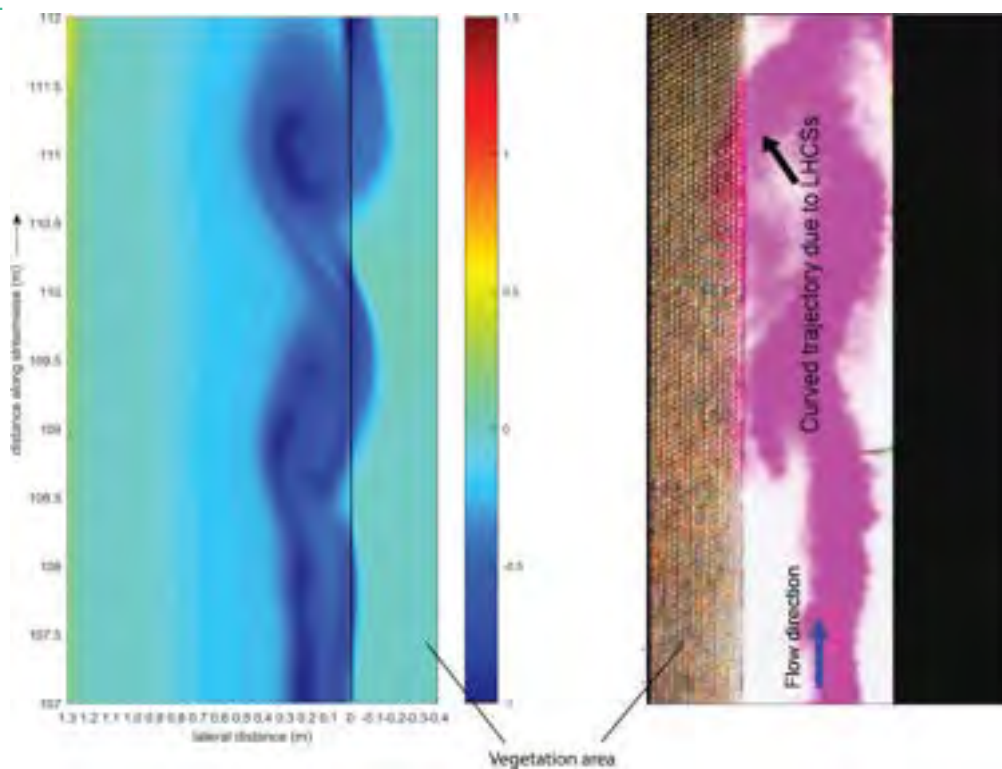


Figure 1. The pattern of the LHCSSs is captured in the numerical model (vorticity fields) (left panel) and the small-scale physical model (right panel).

One of the most difficult tasks of utilizing a depth-averaged two-dimensional in the horizontal model (2DH model) is to provide an adequate turbulent viscosity model. This turbulent closure model needs to represent horizontal mixing or bed-generated turbulence. After demonstrating the hybrid eddy viscosity model's applicability (Truong & Uijtewaal 2019), it can be imposed in a numerical model of compound channels to enhance the numerical results. The numerical model was run first with eddy viscosity calculated from Elder formulations. Based on the simulation results, the parameters required to determine the hybrid eddy viscosity model, such as shear-layer width, vegetation drag, and velocity gradient, can be determined. This new eddy viscosity model was then imposed into the numerical model to improve the simulation results. The figure above illustrates the comparison between the numerical model and the physical model regarding the presence of the LHCSSs.

3. CONCLUSION

This paper summarised some new findings in the flow in and around the vegetation region. The presence of large vortex structures moving along the vegetation edge can be observed. These structures generate a cyclic flow field in which different flow events. These flow events, especially sweeps and ejections, contribute more than 90% to the transverse exchange of mass and momentum between the vegetation and the adjacent open channels. In order to capture this phenomenon in the 2DH model, a new hybrid eddy

Affiliation

¹ Ph.D., Thuyloi University

² Ph.D., Thuyloi University

³ Ph.D., Thuyloi University



viscosity was developed and then prescribed into the numerical model. The model was validated with different data sets and can improve the simulation results. Future works will focus on validating this momentum exchange model on large-scale experiments, natural river channels, and the morphological of the vegetated channel.

4. REFERENCES

- Phan, L. K., van Thiel de Vries, J. S., and Stive, M. J. (2015). Coastal Mangrove Squeeze in the Mekong Delta. *Journal of Coastal Research*, 300:233–243.
- Phan, K. L., Stive, M. J. F., Zijlema, M., Truong, H. S., and Aarninkhof, S. G. J. (2019). The effects of wave non-linearity on wave attenuation by vegetation. *Coastal Engineering*. 147 (2019), 63-74. <https://doi.org/10.1016/j.coastaleng.2019.01.004>
- Truong, S.H., Ye, Q., and Stive, M. J. F. (2017). Estuarine mangrove squeeze in the Mekong delta, Vietnam. *Journal of Coastal Research*, 33(4):747–763.
- Truong, S. H., Uijttewaai, W. S. J., and Stive, M. J. F. (2019). Exchange Processes Induced by Large Horizontal Coherent Structures in Floodplain Vegetated Channels. *Water Resources Research* (WRR). 55(3), 2014-2032. <https://doi.org/10.1029/2018WR022954>
- Truong, S. H. and Uijttewaai, W. S. J (2019). Transverse Momentum Exchange Induced by Large Coherent Structures in a Vegetated Compound Channel. *Water Resources Research* (WRR). 55(1), 589-612. <https://doi.org/10.1029/2018WR023273>
- Vargas-Luna A, Crosato A, Uijttewaai, W. S. J. (2015). Effects of vegetation on flow and sediment transport: comparative analyses and validation of predicting models. *Earth Surface Processes and Landforms*, 40(2), 157-176.

Affiliation

¹ Ph.D., Thuyloi University

² Ph.D., Thuyloi University

³ Ph.D., Thuyloi University



**1st International symposium on Integrated Flood and
Sediment Management in River Basin
for Sustainable Development** **2022**

FSMaRT

ABSTRACTS

**18-20th December 2022, R. S02.06 - Smart Building, DUT
Da Nang, Viet Nam**



Contents

| | |
|---|-----------|
| 1st Session on Hydrological Modelling and Sediment Management – A | 1 |
| Impact assessment of Son Tra wastewater treatment to the coast of Danang city, Vietnam | 2 |
| Application of Rainfall-Runoff Inundation model to forecast Magat dam inflow and water elevation | 3 |
| Ceres – A Citizen Science Approach Monitoring Reservoir Operation from space for poorly gauged reservoirs: A case study in Vu Gia Thu Bon. | 4 |
| Vulnerability assessment of riverbank erosion: a case study of Vietnamese Mekong Delta | 5 |
| Hydropeaking process in Vu Gia Thu Bon River basin: Causes, consequences, and main driven | 6 |
| Reviewing on flood simulation using hydrological models | 7 |
| Monitoring the shoreline change in the coastal area of Da Nang City, Vietnam using time-series satellite imageries and Google Earth Engine platform | 8 |
| Evaluation of urbanization and climate change on urban water drainage system in central of Vietnam | 9 |
| Comparison of 2D and 3D modelling for T-junction channel with different turbulence model | 10 |
| Sediment Nutrient Fluxes and Links to Harmful Algal Blooms in a Eutrophic Lake using Diagenetic Modeling | 11 |
| Riverbank erosion assessment using Mike 21C modeling in Vu Gia – Thu Bon river (Quang Nam provincial region) | 12 |
| Overview of reservoir sedimentation in Batu Dam, Selangor, Malaysia..... | 13 |
| Dynamic of Salinity Intrusion in Dinh An and Tran De Branches of Mekong estuaries | 14 |
| | |
| 2nd Session on Hydrological Modelling and Sediment Management – B | 15 |
| Impacts of Reservoirs on Sediment concentration in the transboundary Srepok River Basin, Vietnam | 16 |
| Integrated flood and sediment management in river basins for sustainable development: The case of Cagayan River Basin | 17 |
| A conceptual approach to study influences of river sand mining on the depth-averaged velocity in vegetated compound channels | 18 |
| Optimization of Magat dam operation rule for flood risk management in the Cagayan river basin | 19 |
| Magat Dam science-based initiatives for long-term flood and sediment management..... | 20 |
| | |
| 3rd Session on Artificial Intelligence for Hydrological Application | 21 |
| Water level prediction model of Kien Giang river based on regression techniques | 22 |
| Water level prediction of Kien Giang river using deep learning models | 23 |
| A real-time flood forecasting hybrid machine learning hydrological model for Krong H’ngang hydropower reservoir | 24 |

Machine Learning Techniques and hydrological Modeling for Flood Susceptibility and Inundation Mapping: Case study VGTB River Basin, Vietnam 25

4th Session on Flood Risk Assessment 27

Urban flood forecasting based on hydraulic model by coupling of MIKE Flood and MIKE Urban: A case study of Tam Ky city, Vietnam 28

Flood modelling in the Ba River basin using a coupled hydrodynamic model- MIKE FLOOD..... 29

Study on flood mitigation operation of cascading dams, including hydropower dams in Ohi river 30

Flood Vulnerability Indicators of Transportation System Concerning Climate Change 31

Stakeholders forum on integrated flood risk management in Cagayan River Basin: Basis in writing policy recommendations 32

Development of a localized integrated disaster risk index – A Malaysia case study of Langat River Basin..... 33

Mapping Open Fire Susceptibility and Nearest Water Resources For Fire Fighting -A Case Study in Johor Malaysia 34

Response of long-term hydrological to land use/land cover change in Vu Gia Thu Bon River basin 35

Modeling the urban flood during the heavy rain in October 2022 for Ngu Hanh Son District, Da Nang City using SWMM model..... 36

Nonparametric estimation approach for evaluating the trend of hydro-meteorological factors in Lai Giang, Binh Dinh 0

Impacts of drought on water resources in Central Vietnam. A case study of Vu Gia Thu Bon River basin 1

Quantification of GPM IMERG and SM2RAIN-ASCAT rainfall products over complex terrain under impacts of reservoirs. A case study for Srepok River basin 2

River System's Behavioral Changes in Response to Manmade disturbances..... 3

Analysis of spatial and temporal variation in rainfall trend of Vu Gia Thu Bon River Basin, Vietnam 4

Spatio-temporal variability and trends of extreme rainfall and temperature events over Cagayan River Basin, Philippines 5

Trends of low flow in the Vu Gia-Thu Bon River basin, Central Vietnam..... 6

5th Session on Remote Sensing and GIS for Flood and Water Security 7

Evaluation of water indices for dynamic monitoring reservoir surface water using Landsat 8 data..... 8

Impact of different types of vegetation in reducing roof runoff 9

Impacts of anthropogenic activities on riverbed elevation. A case study in Central Vietnam 10

Livelihood resilience: salinity intrusion hazard assessment of and adaptation strategy for socio-economic development in Ben Tre Province 11

GIS-based flood susceptibility mapping using AHP approach: A case study of Kien Giang river basin, Quang Binh province 12

| | |
|--|-----------|
| 6th Session on Hydrological Modelling and Sediment Management - C | 13 |
| Hydrodynamic modelling of Magat dam and reservoir during extreme conditions using Telemac 2D | 14 |
| Evaluation of coastline change in Quang Nam under the influence of jetty construction | 15 |
| Evaluation of hydrodynamic and sediment transport under construction of Cua Lo's navigation channel..... | 16 |
| Two-dimensional numerical models in simulating hydro-sediment-morphodynamics for the Vu Gia Thu Bon River basin..... | 17 |
| Assessment of salinity intrusion trends along main rivers and coastal zones in the Vietnamese Mekong Delta | 18 |
| Assessment of water scarcity under the impact of climate change in the downstream Vu Gia-Thu Bon river basin, Vietnam..... | 19 |
| Probable maximum precipitation estimates considering homogeneous regions of Malaysia..... | 20 |
| Climate change intensifies drought vulnerability of magat sub basin in the Philippines | 21 |

Symposium Agenda of 1st FSMaRT 2022

| Time | | Activity |
|---|----------------------|--|
| 1st day of FSMaRT2022 (Sunday, 18th of December) | | |
| 1 | 08:30 – 09:00 | Registration |
| 2 | 09:00 – 09:30 | Opening Session |
| | 09:00 – 09:05 | Welcome Message from Assoc. Prof. Duong Vo Ngoc (Da Nang University of Science and Technology, Vietnam) |
| | 09:05 – 09:10 | Special Message from Mr. Suzuki Takashi (JICA representative in Vietnam) |
| | 09:10 – 09:15 | Special Message from Mr. Nobuyuki Ichihara (Director International Affairs Division, Japan Water Agency) |
| | 09:15 – 09:20 | Special Message from Prof. Ricmar P. Aquino (President of Isabela State University, Philippines) |
| | 09:20 – 09:25 | Special Message from Prof. Tetsuya Sumi (Kyoto University, Japan) |
| | 09:25 – 09:30 | Special Message from Prof. Thai Nguyen Canh (Thuyloi University, Vietnam) |
| | 09:30 – 09:35 | Special Remarks from Assoc. Prof. Doan Quang Vinh (The Rector of the Da Nang University of Science and Technology, Vietnam) |
| 3 | 09:35 – 09:50 | Final Report of Research Achievements of Integrated Flood and Sediment Management (FSMaRT) by Prof. Sameh Kantoush |
| | 09:50 – 10:00 | MOU Signature between Isabela State University and Da Nang University of Science and Technology |
| 4 | 10:00 – 10:15 | Group Photo and Coffee Break |
| 5 | 10:15 – 10:30 | Keynote #1: Situation over Vu Gia-Thu Bon (VGTB), Vietnam by Dr. Nguyen Van Hoang , Vietnam disaster management authority |
| | 10:30 – 10:45 | Keynote #2: Prof. Tetsuya Sumi , Kyoto University, Japan |
| | 10.45 – 11.30 | Open Session for Plenary Discussion |

| | | |
|---|---------------|---|
| 6 | 11:30 – 12:00 | Poster Program: Session A |
| | 12:00 – 13:00 | Extension of Poster Session with Lunch |
| 7 | 13:00 – 14:30 | Session 1: Hydrological Modelling and Sediment Management-A |
| 8 | 14:30 – 16:00 | Session 2: Hydrological Modelling and Sediment Management-B |
| 9 | 16:00 – 16:15 | Coffee Break |
| 10 | 16:15 – 17:30 | Session 3: Artificial Intelligence for Hydrological Application |
| 11 | 18:00 – 20:00 | Dinner |
| 2nd day of FSMaRT2022 (Monday, 19th of December) | | |
| 12 | 09:00 – 09.15 | Keynote #3: Prof. Orlando F. Balderama , Isabela State University, Philippines |
| | 09:15 – 09.30 | Keynote #4: Prof. Hung The Nguyen , the University of Science and Technology in Danang, Viet Nam |
| 13 | 09:30 – 09.45 | Coffee Break |
| 14 | 09:45 – 11.15 | Session 4: Flood Risk Assessment |
| 15 | 11:15 – 12.00 | Poster Program: Session B |
| 16 | 12:00 – 13.00 | Lunch |
| 17 | 13:00 – 14.30 | Session 5: Remote Sensing and GIS for Flood and Water Security |
| 18 | 14:30 – 16.00 | Session 6: Hydrological Modelling and Sediment Management-C |
| 19 | 16:00 – 17.00 | Session 7: Climate Change and Sustainability |
| 20 | 17:00 – 17.30 | Presentation of Awards and Closing Remarks |
| 21 | 18:30 – 21.00 | Gala Dinner at Hotel |

3rd day of FSMaRT2022
(Tuesday, 20th of December)

Field Excursion

| | |
|---------------|---|
| 08.00 | 1 st Meeting Place at Hotel Lobby |
| 08.15 | 2 nd Meeting Place at University of Science and Technology |
| 09:15 | Departure from University of Science and Technology by bus |
| 11:15 | Arrival at A Vuong Hydropower at Thanh My Town, Nam Giang District, Quang Nam |
| 12:30 | Lunch |
| 13:00 | Departure from A Vuong Hydropower |
| 14:30 | Arrival at CuaDai river mouth in Cam An ward, Hoi An city, Quang Nam province |
| 16:45 – 18:30 | Visit Hoi An Ancient town, Japanese bridge, Tan Ky ancient house, Phuc Kien Assembly hall, Museum of Trade Ceramics, CamPho communal house, etc |
| 18:30 | Dinner |
| 19:00 | Return to Danang city |
| 20:00 | Arrival at Danang city |

Detailed Program of 1st FSMaRT 2022

18th December 2022 (Sunday), at the Conference Hall of F Building

| 08:30 – 09:00 | Registration | |
|--|---|---|
| Opening Sessions | | |
| <i>Chaired by: Prof. The Hung Nguyen</i> | | |
| Time | Title of presentation | Presenter |
| 09:00 – 09:05 | Welcome Message | Assoc. Prof. Duong Vo Ngoc , (Da Nang University of Science and Technology, Vietnam) |
| 09:05 – 09:10 | Opening Speech | Mr. Suzuki Takashi (JICA representative in Vietnam) |
| 09:10 – 09:15 | Opening Speech | Mr. Nobuyuki Ichihara (Director International Affairs Division, Japan Water Agency) |
| 09:15 – 09:20 | Opening Speech | Prof. Ricmar P. Aquino (President of Isabela State University, Philippines) |
| 09:20 – 09:25 | Opening Speech | Prof. Sameh A. Kantoush (DPRI, Kyoto University, Japan) |
| 09:25 – 09:30 | Opening Speech | Prof. Thai Nguyen Canh (Thuyloi University, Vietnam) |
| 09:30 – 09:35 | Special Remarks | Assoc. Prof. Doan Quang Vinh , (The Rector of the Da Nang University of Science and Technology, Vietnam) |
| 09:35 – 09:50 | Final Report on Research Achievements of Integrated Flood and Sediment Management (FSMaRT) | Prof. Sameh A. Kantoush (DPRI, Kyoto University, Japan) |
| 09:50 – 10:00 | MOU Signature between Isabela State University and Da Nang University of Science and Technology | |
| 10:00 – 10:15 | Group Photo and Coffee Break | |
| Special Session | | |
| <i>Chaired by: Prof. Sameh A. Kantoush</i> | | |
| Time | Title of presentation | Presenter |
| 10:15 – 10:30 | 1#: Keynote Speaker | Dr. Nguyen Van Hoang (Vietnam disaster management authority) |
| 10:30 – 10:45 | 2#: Keynote Speaker | Prof. Tetsuya Sumi (DPRI, Kyoto University, Japan) |
| 10:45 – 11.30 | Open Session for Plenary Discussion | |

Poster Program – Session A B (11.30 -12.00)

Chaired by: Dr. Son Truong Hong

Note: Allocated time for Poster Presentations: 03 min. talk + 02 min. discussion

| Poster Code | Title | First Author/Presenter |
|---------------|---|------------------------|
| A1 | Impact assessment of Son Tra wastewater treatment to the coast of Danang city, Vietnam | Nguyen Phuoc Quy An |
| A2 | Application of Rainfall-Runoff Inundation model to forecast Magat dam inflow and water elevation | Arlen Alejandro |
| A3 | Ceres – A Citizen Science Approach Monitoring Reservoir Operation from space for poorly gauged reservoirs: A case study in Vu Gia Thu Bon. | Tien Du |
| A4 | Vulnerability assessment of riverbank erosion: a case study of Vietnamese Mekong Delta | Menna Ahmed |
| A5 | Hydropeaking process in Vu Gia Thu Bon River basin: Causes, consequences, and main driven | Binh Quang Nguyen |
| A6 | Reviewing on flood simulation using hydrological models | Son Nguyen Thien |
| A7 | Monitoring the shoreline change in the coastal area of Da Nang City, Vietnam using time-series satellite imageries and Google Earth Engine platform | Van An Nguyen |
| A8 | Evaluation of urbanization and climate change on urban water drainage system in central of Vietnam | Duc Phuoc Vo |
| 12:00 – 13:00 | Extension of Poster Session with Lunch | |

1st Session on Hydrological Modelling and Sediment Management – A**Chaired by: Prof. Mohamed Saber****Note: Allocated time for Oral Presentations: 15 min. talk**

| Time | Title of presentation | First Author/Presenter |
|---------------|---|--------------------------|
| 13:00– 13:15 | Comparison of 2D and 3D modelling for T-junction channel with different turbulence model | Mohamad Faizal Ahmad |
| 13:15 – 13:30 | Sediment Nutrient Fluxes and Links to Harmful Algal Blooms in a Eutrophic Lake using Diagenetic Modeling | Phuong Doan |
| 13:30 – 13:45 | Riverbank erosion assesment usung Mike 21C modeling in Vu gia – Thu Bon river (Quang Nam provincial region) | Tuan An Bui |
| 13:45– 14:00 | Overview of reservoir sedimentation in Batu Dam, Selangor, Malaysia | Siti Saimah Abdul Rahman |
| 14:00 – 14:15 | Dynamic of Salinity Intrusion in CoChien and CungHau branches of Mekong estuaries | Nguyen Phuong Mai |
| 14:15 – 14:30 | Open Discussion (Q&A) | |

2nd Session on Hydrological Modelling and Sediment Management - B**Chaired by: Dr. Doan Van Binh****Note: Allocated time for Oral Presentations: 15 min. talk**

| Time | Title of presentation | First Author/Presenter |
|---------------|--|------------------------|
| 14:30 – 14:45 | Impacts of Reservoirs on Sediment concentration in the transboundary Srepok River Basin, Vietnam | Thao Bui Thi Phuong |
| 14:45 – 15:00 | Integrated flood and sediment management in river basins for sustainable development: The case of Cagayan River Basin | Lanie Alejo |
| 15:00 – 15:15 | A conceptual approach to study influences of river sand mining on the depth-averaged velocity in vegetated compound channels | Son Hong Truong |
| 15:15 – 15:30 | Optimization of Magat dam operation rule for flood risk management in the Cagayan river basin | Hikaru Goto |

| 15:30 – 15:45 | Magat Dam science-based initiatives for long-term flood and sediment management | Carlo Ablan |
|--|---|-------------------------------|
| 15:45 – 16:00 | Open Discussion (Q&A) | |
| 16.00 – 16.15 | Coffee Break | |
| 3rd Session on Artificial Intelligence for Hydrological Application <i>Chaired by Dr. Pham Hong Nga</i> | | |
| Note: <i>Allocated time for Oral Presentations: 15 min. talk</i> | | |
| Time | Title of presentation | First Author/Presenter |
| 16.15 – 16.30 | Water level prediction model of Kien Giang river based on regression techniques | Quang Chieu Ta |
| 16.30 – 16.45 | Water level prediction of Kien Giang river using deep learning models | Trung Hieu Trieu |
| 16.45 – 17.00 | A real-time flood forecasting hybrid machine learning hydrological model for Krong H'ngang hydropower reservoir | Phuoc Sinh Nguyen |
| 17.00 – 17.15 | Machine Learning Techniques and hydrological Modeling for Flood Susceptibility and Inundation Mapping: Case study VGTB River Basin, Vietnam | Mohamed Saber |
| 17.15 -17.30 | Open Discussion (Q&A) | |
| 18.00 – 20.00 | 1st Day Dinner | |

19th December 2022 (Monday), at the Conference Hall of F Building

| Special Session <i>Chaired by: Prof. Tetsuya Sumi</i> | | |
|---|------------------------------|--|
| Time | Title of presentation | Presenter |
| 09:00 – 09:15 | 3#: Keynote Speaker | Prof. Orlando F. Balderama (Isabela State University, Philippines) |
| 09:15 – 09:30 | 4#: Keynote Speaker | Prof. Hung The Nguyen (University of Science and Technology in Danang, Vietnam) |
| 09.30 – 09.45 | Coffee Break | |

4th Session on Flood Risk Assessment
Chaired by: Prof. Orlando Balderama

Note: *Allocated time for Oral Presentations: 15 min. talk*

| Time | Title of presentation | First Author/Presenter |
|---------------|---|---------------------------|
| 09:45 – 10:00 | Urban flood forecasting based on hydraulic model by coupling of MIKE Flood and MIKE Urban: A case study of Tam Ky city, Vietnam | Cong Nguyen Chi |
| 10:00 – 10:15 | Flood modelling in the Ba River basin using a coupled hydrodynamic model - MIKE FLOOD | Tuan Luc Anh |
| 10:15 – 10:30 | Study on flood mitigation operation of cascading dams, including hydropower dams in Ohi river | Yuki Okamoto |
| 10:30 – 10:45 | Flood Vulnerability Indicators of Transportation System Concerning Climate Change | Hamizah Amalina Amlan |
| 10:45 – 11:00 | Stakeholders forum on integrated flood risk management in Cagayan River Basin: Basis in writing policy recommendations | Orlando Balderama |
| 11:00 – 11:15 | Development of a localized integrated disaster risk index – A Malaysia case study of Langat River Basin | Muhammad Wafiy Adli Ramli |
| 11:15 – 11:30 | Open Discussion (Q&A) | |

Poster Program- Session B (11.15 -12.00)

Chaired by: Dr. Pham Hong Nga

Note: *Allocated time for Poster Presentations: 03 min. talk + 02 min. discussion*

| Poster Code | Title | First Author/Presenter |
|-------------|--|------------------------|
| B1 | Mapping Open Fire Susceptibility and Nearest Water Resources For Fire Fighting -A Case Study in Johor Malaysia | Fara Aiza Md Sanin |
| B2 | Response of long-term hydrological to land use/land cover change in Vu Gia Thu Bon River basin | Thanh-Nhan-Duc Tran |

| | | |
|--|---|-------------------------------|
| B3 | Modeling the urban flood during the heavy rain in October 2022 for Ngu Hanh Son District, Da Nang City using SWMM model | An Tran |
| B4 | Nonparametric estimation approach for evaluating the trend of hydro-meteorological factors in Lai Giang, Binh Dinh. | Thi Ngoc Canh Doan |
| B5 | Impacts of drought on water resources in Central Vietnam. A case study of Vu Gia - Thu Bon River basin | Binh Quang Nguyen |
| B6 | Quantification of GPM IMERG and SM2RAIN-ASCAT rainfall products over complex terrain under impacts of reservoirs. A case study for Srepok River basin | Thanh-Nhan-Duc Tran |
| B7 | River System's Behavioral Changes: Response to Climate Change or Manmade? | Kogila Vani Annammala |
| B8 | Analysis of spatial and temporal variation in rainfall trend of Vu Gia Thu Bon River Basin, Vietnam | Thao Bui Thi Phuong |
| B9 | Spatio-temporal variability and trends of extreme rainfall and temperature events over Cagayan River Basin, Philippines | Khagendra Bharambe |
| B10 | Trends of low flow in the Vu Gia - Thu Bon river basin, Central Vietnam | Thi Ngoc Uyen Nguyen |
| 12:15 – 13:00 | Extension of Poster Session with Lunch | |
| <p>5th Session on Remote Sensing and GIS for Flood and Water Security Chaired by: Prof. Thai Nguyen Canh</p> | | |
| <p>Note: Allocated time for Oral Presentations: 15 min. talk</p> | | |
| Time | Title of presentation | First Author/Presenter |
| 13:00 – 13:15 | Evaluation of water indices for dynamic monitoring reservoir surface water using Landsat 8 data | Anh Minh Vu |

| | | |
|--|---|-------------------------------|
| 13:15 – 13:30 | Impact of different types of vegetation in reducing roof runoff | Noraliani Alias |
| 13:30 – 13:45 | Impacts of anthropogenic activities on riverbed elevation. A case study in Central Vietnam | Binh Quang Nguyen |
| 13:45 – 14:00 | Livelihood resilience: salinity intrusion hazard assessment of and adaptation strategy for socio-economic development in Ben Tre Province | Doan Van Binh |
| 14:00 – 14:15 | GIS-based flood susceptibility mapping using AHP approach: A case study of Kien Giang river basin, Quang Binh province | Ngan Vu Huong |
| 14:15 – 14:30 | Open Discussion (Q&A) | |
| 6th Session on Hydrological Modelling and Sediment Management - C <i>Chaired by Dr. Nor Eliza Alias</i> | | |
| Note: <i>Allocated time for Oral Presentations: 15 min. talk</i> | | |
| Time | Title of presentation | First Author/Presenter |
| 14.30 – 14.45 | Hydrodynamic modelling of Magat dam and reservoir during extreme conditions using Telemac 2D | Jeoffrey Lloyd R. Bareng |
| 14.45 – 15.00 | Evaluation of coastline change in Quang Nam under the influence of jetty construction | Tran Tieu Long Trinh |
| 15.00 – 15.15 | Evaluation of hydrodynamic and sediment transport under construction of Cua Lo's navigation channel | Cong Phuc Dang |
| 15.15 – 15.30 | Two-dimensional numerical models in simulating hydro-sediment-morphodynamics for the Vu Gia Thu Bon River basin | Binh Quang Nguyen |
| 15.30 – 15.45 | Assessment of salinity intrusion trends along main rivers and coastal zones in the Vietnamese Mekong Delta | Doan Nguyen Luyen Phuong |
| 15.45 – 16.00 | Open Discussion (Q&A) | |

7th Session on Climate Change and Sustainability
Chaired by Prof. Hung The Nguyen

Note: *Allocated time for Oral Presentations: 15 min. talk*

| Time | Title of presentation | First Author/Presenter |
|----------------------------|---|------------------------|
| 16.00 – 16.15 | Assessment of water scarcity under the impact of climate change in the downstream Vu Gia Thu Bon river basin, Vietnam | Mai Thi Thuy Duong |
| 16.15 – 16.30 | Probable maximum precipitation estimates considering homogeneous regions of Malaysia | Nor Eliza Alias |
| 16.30 – 16.45 | Climate change intensifies drought vulnerability of magat sub basin in the Philippines | Christian Alec Managa |
| 16.45 – 17.00 | Open Discussion (Q&A) | |
| Awards and Closing Remarks | | |
| 17.00 – 17.30 | Presentation of Awards and Closing Remarks | |
| 18.30 – 21.00 | 2nd Gala Dinner at Hotel | |

Committee for Poster: *Prof. Mohamed Saber, Dr. Doan Van Binh, Dr. Pham Hong Nga, Dr. Lanie Alejo*

3rd day of FSMaRT2022
(Tuesday, 20th of December)

Field Excursion

| | |
|---------------|---|
| 08.00 | 1 st Meeting Place at Hotel Lobby |
| 08.15 | 2 nd Meeting Place at University of Science and Technology |
| 09:15 | Departure from University of Science and Technology by bus |
| 11:15 | Arrival at A Vuong Hydropower at Thanh My Town, Nam Giang District, Quang Nam |
| 12:30 | Lunch |
| 13:00 | Departure from A Vuong Hydropower |
| 14:30 | Arrival at CuaDai river mouth in Cam An ward, Hoi An city, Quang Nam province |
| 16:45 – 18:30 | Visit Hoi An Ancient town, Japanese bridge, Tan Ky ancient house, Phuc Kien Assembly hall, Museum of Trade Ceramics, CamPho communal house, etc |
| 18:30 | Dinner |
| 19:00 | Return to Danang city |
| 20:00 | Arrival at Danang city |

1st Session on Hydrological Modelling and Sediment Management – A

Impact assessment of Son Tra wastewater treatment to the coast of Danang city, Vietnam

Phuoc Quy An Nguyen^{1,*}, Philippe Gourbesville¹, Philippe Audra¹, Ngoc Duong Vo²

¹ Polytech'Lab, University of Nice Sophia Antipolis, 930 route des Colles, 06410 Biot, France

²The University of Danang, University of Science and Technology, 54 Nguyen Luong Bang, Danang, Vietnam

*Corresponding author: npqan@dut.udn.vn

Abstract. Son Tra wastewater treatment plant (WWTP) is one of four WWTPs in Danang City. In most of the cases, the wastewaters are treated by WWTPs before discharging into the natural environment that is the coastal area or rivers. However, the treatment level does not ensure a sufficient performance for maintaining the quality of the receptive environment. This situation is currently faced in the Danang area where the significant impact has been detected in the receiving environment. In this study, Mike 21 FM Hydrodynamics module coupled to a water quality model using Mike 21 FM ECOLab module is applied to simulate the water quality and to identify the spreading of NH_4^+ , which is used as a pollutant tracer. The study suggests three scenarios of NH_4^+ concentration in the wastewater of the Son Tra WWTP outlet are used to simulate the impact in the coastal area. The first scenario is that wastewater discharges from the outlet with the current NH_4^+ concentration (15 mg/l). Second, after some failure with Son Tra WWTP because of power outage or damages, therefore, wastewater discharge directly to the coast with a higher NH_4^+ concentration (25 mg/l) for 24 hours. Third, wastewater is treated to follow the regulation of industrial wastewater (10 mg/l). Out of the three proposed scenarios, the polluted area of scenario 1 is similar to scenario 2. However, scenario 2 generates the largest polluted area with NH_4^+ concentration > 1.9 mg/l. Scenario 3 has the smallest polluted area along the coast and the NH_4^+ peak concentration is lower than 1.7 mg/l.

Keywords. Son Tra WWTP, NH_4^+ concentration, Mike 21 FM ECOLab, coastal area, scenario

Application of Rainfall-Runoff Inundation model to forecast Magat dam inflow and water elevation

Arlen S. Alejandro¹, Lanie A. Alejo², Carlo C. Ablan³, Orlando F. Balderama⁴
Tetsuya Sumi⁵, and Sameh Ahmed Kantoush⁶

^{1,3} National Irrigation Administration, Magat River Integrated Irrigation System, Dam and Reservoir Division, Ramon, Isabela, Philippines

^{2,4} College of Engineering, Isabela State University, Echague, Isabela, Philippines ^{5,6} Water Resources Research Center - Disaster Prevention Research Institute Kyoto University, Kyoto, Japan

*Corresponding author: arlenalejandro001@gmail.com

Short abstract. Flood forecasting is vital in preventing and mitigating flood damage. Flood inundation can be simulated to forewarn the affected areas of the possible effect of floods brought by heavy rainfall events. Rainfall-runoff models need precise forecast rainfall. In this paper, the fully calibrated and validated Rainfall-Runoff Inundation Model utilized the 3-ensemble rainfall forecast that gives high, mid, and low forecast scenarios. It was tested on extreme weather events, typhoon Karding and Maymay. The result shows RRI simulated inflows and statistical values indicate unacceptable agreement with the actual inflow. However, it was satisfactory in terms of predicted water level. The ensemble is yet to be bias corrected. Generally, the use of the hourly prediction from the ensemble gave quite good results when translated to inflow and water elevation using the RRI.

Keywords. Forecasting, runoff, ensemble

Ceres – A Citizen Science Approach Monitoring Reservoir Operation from space for poorly gauged reservoirs: A case study in Vu Gia Thu Bon.

Du Le Thuy Tien¹, Hyongki LEE¹, Duong Du Bui², Son K. DO^{1,*}, Ngoc Thi Nguyen¹, Thao Thi Phuong Bui³, Nuong Thi Bui⁴, Tra T.T. NGUYEN²

¹ Department of Civil and Environmental Engineering, University of Houston, Texas, U.S.A.

² National Center for Water Resources Planning and Investigation (NAWAPI). No.93, lane 95, Vu Xuan Thieu Street, Sai Dong Ward, Long Bien District, Ha Noi, Vietnam.

³ Department of Urban Management, Water Resource Center, Disaster Prevention Research Institute (DPRI), Kyoto University, Kyoto 611-0011, Japan.

⁴ Hanoi University of Natural Resources and Environment (HUNRE), Hanoi, Vietnam

*Corresponding author: thuytien1025@gmail.com

Abstract. This study creatively employs a well-known citizen science approach to constantly further improve our satellite based reservoir operation monitoring (CERES) tool, enhance end-users' trust, acceptance and uptake of the tool and consequently support water resources decision making processes for users. Our CERES is a cloud-based interactive web app with freely available datasets for non-commercial uses based on multi-mission satellite datasets, including Sentinel-1 C-band Synthetic Aperture Radar Ground Range Detected (SAR GRD), Shuttle Radar Topography Mission (SRTM) Digital Elevation Models (DEM), Advanced Land Observing Satellite (ALOS) and Multi-Error-Removed Improved-Terrain (MERIT) DEM. Its graphical user interface design allows non programming users to interact with maps, generate results, evaluate them with provided templates and optionally email performance metrics and figures back to developers for further improvement without granting developers of access to the local observed data.

Keywords. Monitoring, remote sensing, citizen science, reservoirs, poorly-gauged, Vu Gia Thu Bon River basin

Vulnerability assessment of riverbank erosion: a case study of Vietnamese Mekong Delta

Menna F.AHMED¹, Doan Van BINH², Nguyen Phuong MAI³, Sameh A.KANTOUSH¹, and Tetsuya SUMI¹

¹ Water Resources Research Center, Disaster Prevention Research Institute, Kyoto University (Goka-sho, Uji-shi, 611-011, Kyoto), Japan

² Faculty of Engineering, Vietnamese –German University, (Ben Cat Town, Binh Duong Province), Vietnam

³ Thuyloi University-Southern Campus (No.2 TruongSa Street, HoChiMinh City), Vietnam

*Corresponding author: Menna F. Ahmed, Email: ahmed.zaki.27d@st.kyoto-u.ac.jp

Abstract. Over decades, the Vietnamese Mekong Delta (VMD) has suffered severe coastal and riverbank erosions resulting in serious social, economic, and environmental impacts. Several natural and anthropogenic key factors contribute to the rising riverbank erosion rate in VMD, such as flood depletion, rainfall extremes, high water waves and currents, soft alluvial soils, excessive sand mining, increasing river traffic, and sediment reduction caused by upstream river damming. Although few studies have estimated the long-term riverbank erosion in VMD using remote sensing and numerical models, no study has assessed the eroded sediment volume due to the riverbank. In this paper, we quantitatively evaluated the eroded volumes due to riverbank erosion along VMD by field survey, remote sensing, and a two-dimensional (2D) hydromorphodynamic numerical model. The model combines the river hydro and morpho-dynamics computer models TELEMAC-2D and GAIA of the open source TELEMAC-MASCARET for investigating flow and sediment transport in open channels at large temporal and spatial scales. The field surveys revealed that the riverbanks near the estuaries (about 50-80km from the river mouth) are alternately eroded and deposited; however, erosion is dominant (Fig. 1). Erosion takes place even in some vegetated areas. We also found that some aquaculture ponds had to leave redundant due to riverbank erosion that cut off some ponds (Fig. 1, left panel). The results show changes in riverbank position for the next 50 years within the study area due to riverbank migration, i.e., accretion and erosion. It also shows that the general patterns of erosion and deposition at the main rivers and channels are represented reasonably well when seasonal river discharge is used. The model has been calibrated and validated with the collected field data between 2014 and 2019. This research serves as a developed reference in predicting the riverbank instability numerically, as to be considered in decision support strategies of the river system.

Keywords. Mekong delta, Riverbank erosion, 2D numerical modeling

Hydropeaking process in Vu Gia Thu Bon River basin: Causes, consequences, and main driven

Binh Quang Nguyen^{1,2,*}, Thinh Hung Nguyen², Thanh-Nhan-Duc Tran³, Ngoc Duong Vo², Sameh A. Kantoush¹, Tetsuya Sumi¹

¹ Water Resource Center, Disaster Prevention Research Institute (DPRI), Kyoto University, Kyoto 611-0011, Japan

² The University of Danang - University of Science and Technology, 54 Nguyen Luong Bang, Danang, Vietnam

³ Department of Engineering Systems and Environment, University of Virginia, Charlottesville, VA 22904, USA

*Corresponding author: Binh Quang Nguyen (nqbinh@dut.udn.vn)

Abstract. Quantifying river flow change is important to understand the impacts of hydropower generation to water resources. Energy demand fluctuates at sub-daily scales, which may cause changes in regulated river flow (e.g., hydropeaking) resulting in the decrease of water supply and the increase of salinity intrusion. In this study, we investigated the influence of increasing hydropower generation on hydropeaking for the Vu Gia Thu Bon (VGTB) River basin, Central Vietnam. We used the analytical method to quantify the difference of water level in daily scale including the reservoir operation. This study used hourly water level data between 2018 and 2022 from seven hydrological stations within the VGTB River basin. Our key findings indicated that hydropeaking is at high levels in the VGTB River and has seen an increase over the last decade, especially over the past few years.

Keywords. Hydropeaking, Reservoir, Water level, Salinity intrusion, Water supply, Vu Gia Thu Bon River

Reviewing on flood simulation using hydrological models

Nguyen Thien Son¹, Huang Guangwei¹

¹ Graduate School of Global Environmental Studies, Sophia University, Tokyo, 102-8554, Japan

*Corresponding author: sonnt01.iwe@gmail.com

Abstract. Since ancient times, people over the world have often faced the dangers caused by various types of natural disasters including floods. Along with the development of modern science and technology facilities, flood disaster events have been increasingly studied and modeled, thereby developing preparedness, minimization and early warning systems. In this paper, we evaluate the available recent research on flood simulation on river basins using hydrological models. We distinguish between studies focusing on flood flow simulations using (i) rainfall-runoff models, (ii) hydrological models combining hydraulic models, remote sensing images and (iii) the models take into account land use changes, climate change and the operation of hydropower dams in the basin. We discuss the differences in the model's inputs and the accuracy in flood flow simulation mentioned in the studies. This allows to clarify the influence of the model's inputs on the flood flow simulation results to improve the accuracy in process of flood flow simulation. We also emphasize the characteristics and scale of the simulated watershed. The purpose of this assessment is to find out limitations in existing flood simulation methods to improve not only methodologies but also network design and monitoring system in order to increase the simulation accuracy and especially in flood forecasting to minimize flood risks and optimize the use of water resources in the basin.

Keywords. Flood simulation, hydrological models, accuracy, watershed

Monitoring the shoreline change in the coastal area of Da Nang City, Vietnam using time-series satellite imageries and Google Earth Engine platform

Van An Nguyen, Thi An Tran, Ngoc Hanh Le and Thi Ngoc Nguyen

Abstract. Shorelines are sensitive and vulnerable to human activities including urbanization, land reclamation and sediment loading. The deterioration of coastal ecosystems brought on by human activity may be reflected in shoreline changes. Therefore, it is important to understand shoreline dynamics. A significant source for analyzing changes in coastal ecosystems is earth observation data, such as multitemporal satellite imageries. In this research, we used Google Earth Engine (GEE) to monitor and map historical shoreline dynamics in the coastal zone of Da Nang City which is currently an attractive tourism destination of Viet Nam. Landsat imagery from 1986 to 2022 was processed in Google Earth Engine to calculate the MNDWI. Subsequently, applying a thresholding method, we have determined the water bodies that extracted the shoreline by different times. The change detection method in remote sensing has been employed to evaluate the shoreline dynamics in Da Nang coastal area. The results indicate that in the study area, the shoreline has moved by more than 5 km in the last decades, accounting for approximately 500 km² of land accretion. The proposed methodology can be applied to other coastal zones in various regions and scaled up to larger areas.

Keywords. Google Earth Engine, remote sensing, shoreline dynamics, Da Nang city

Evaluation of urbanization and climate change on urban water drainage system in central of Vietnam

Hoang Nghia Le¹, Duc Phuoc Vo^{2*}, Quang Dinh Nguyen³, Binh Quang Nguyen², Chi Cong Nguyen²

¹Institute of Social Sciences of Central Highland

²University of Science and Technology, University of Danang

³Thua Thien Hue investment and construction consultants joint stock company

*Corresponding author: Duc Phuoc Vo (email: vnducphuoc@dut.udn.vn)

Abstract. Urban flooding is one of the significant issues that many cities are dealing with. Upgrading of the drainage systems is a common measure that is often used to address the risk of flooding. However, due to the effects of climate change, global sea levels are rising and extreme rainfall is increasing in both frequency and intensity. These has affected the flow, resulting in flooding in many cities worldwide. Among the types of models, the storm water management model (SWMM) is chosen for this research because it is widely accepted in academic and engineering communities. This research assessed the impacts of urbanization on the formulation of the flow at an urban catchment in An Ha, Tam Ky, Quang Nam. The results showed that urbanization contributes to reduce the flow loss through infiltration into the ground. When the degree of urbanization increases by more than 70%, the efficiency of flow reduction decreases rapidly, and the effects of urbanization are clearer for long rain duration.

Keywords. LID, urban flooding, urbanization, Tam Ky, storm water management

Comparison of 2D and 3D modelling for T-junction channel with different turbulence model

*M Faizal Ahmad¹, Siti Aimi Asyarah Zakaria¹, Mohd Ridza Mohd Haniffah¹, Nor Eliza Alias¹

¹ Faculty of Civil Engineering, Universiti Teknologi Malaysia, Johor Bahru, 81310, Malaysia

*Corresponding author: faizal_9273@yahoo.com

Short abstract. The modelling of water flow at a T-junction is challenging due to complex fluid dynamics behavior. The flow mechanisms and dynamics need to be quantified before they can be used for river analysis such as riverbed scouring, riverbank erosion and water overtopping at the T-junction. This paper presents some validation and verification results of 2D and 3D modelling of the T-junction then compared with previous experimental works. The 2D simulation used the Menter's Shear Stress Transport $k-\omega$ (SST) and Low Reynolds $k-\varepsilon$ (LRE) turbulence models which solved by finite element method (FEM) using COMSOL Multiphysics. The 3D simulation used the Re-Normalization Group (RNG) turbulence model solved by finite volume technique (FVM) through FLOW-3D. The 2D simulation result was validated and verified using separation length (SL) that occurred at the branch channel of the T-junction. The results of 3D simulation were validated and proved the 3D RNG turbulence model can replicate the previous experimental result in term of discharge ratio (Q_r) which is the ratio of discharge in the branch to the upstream discharge with minimal difference from experimental work. The 2D SST turbulence model shows better result compared to the 3D RNG simulation and experimental data. The dynamics behavior of the water in term of pressure and velocity of the T-junction were discussed. The study shows that 2D turbulence model is sufficient for riverbank and river details analysis with some limitations.

Keywords. Turbulence modelling, RNG, SST, Low Reynolds $k-\varepsilon$, T-junction

Sediment Nutrient Fluxes and Links to Harmful Algal Blooms in a Eutrophic Lake using Diagenetic Modeling

Phuong Doan^{1*}, Thao Van Le¹

¹The University of Da Nang-University of Science and Technology, Da Nang, Vietnam.

*Corresponding author: Phuong Doan (email: dtkphuong@dut.udn.vn)

Abstract. In this study, we investigated a linkage between sediment diagenesis and harmful algal blooms in the Bay of Quinte, an embayment of Lake Ontario, Canada. Although a strong decline of external P loading to the Bay of Quinte during last decades, it still experiences harmful cyanobacterial algal blooms, which were hypothesized to be connected to nutrient loading from sediments. However, the linking sediment diagenesis with harmful algal blooms remain largely unknown. Our modelling framework integrated physical and biogeochemical processes at the sediment water interface (SWI) and incorporated dynamic boundary conditions, such as oxygen, soluble reactive phosphorus concentrations and organic matter sedimentation at the SWI. In the model, total P was divided into adsorbed, redox-sensitive, organic, aluminum-bound, and apatite forms. In this study, the Aquasim model was used and applied to link sediment diagenesis with harmful algal blooms of a eutrophic system, the Bay of Quinte, Canada. Our sediment diagenesis modelling results show that P burial efficiency critically increased after the period of external P loading reduction in 1970s corresponding to the decrease in total P, chlorophyll and most major phytoplankton groups in the water column.

Keywords. Phosphorus release, phosphorus burial efficiency, sediments, diagenetic modelling

Riverbank erosion assessment using Mike 21C modeling in Vu Gia – Thu Bon river (Quang Nam provincial region)

Son Hoang Thanh¹, Lan Vu Thi Thu², Tuan Bui Anh^{1,*}, Hanh Le Duc¹, Tuan Tong Phuc¹, Dang Vu Hai³, Chi Tran Thuy⁴

¹ Institute of Geography, VAST

² Department of Application & Development of Technology, VAST

³ Institute of Marine Geology and Geophysics, VAST

⁴ Hanoi University of Natural Resources and Environment

*Corresponding author: igtuan253@gmail.com

Abstract. The riverbank erosion-accretion is mainly a physical process of river dynamics, reflecting the correlation between the flow and the channel, linked to the sediment balancy. Prediction of riverbank erosion-accretion plays crucial role for localy riverbank social economic development as well as for whole region. This study presents the results of Mike models (Mike11RR, HD, ST and Mike 21C) application to simulate the riverbed evolution (erosion, accretion). Compared with realistic changes, the results showed that the ability of simulation modelling is acceptable for Vu Gia – Thu Bon River basin. The riverbed change prediction according to the scenario of development and real-time approaches was calculated with updating boundary conditions of rain and erosion. From the simulation results, a map of the erosion risk was built to help risk management authorities and communities in riverbank erosion disasters proactive responding.

Keywords. Riverbank erosion, MIKE 21C, MIKE 21C, Vu Gia – Thu Bon

Overview of reservoir sedimentation in Batu Dam, Selangor, Malaysia

Siti Saimah Abdul Rahman^{1,2*}, Faizah Che Ros¹

¹Department of Chemical and Environmental Engineering, Malaysia-Japan International Institute of Technology (MJIIT), Universiti Teknologi Malaysia, Malaysia Jalan Sultan Yahya Petra, 54100 Kuala Lumpur, Malaysia

² Department of Irrigation and Drainage Malaysia, Jalan Sultan Salahuddin, 50626 Kuala Lumpur, Malaysia

*Corresponding author: sitisaimah.abr@gmail.com

Abstract. Reservoir sedimentation reduces storage capacity and shortens the lifespan of the dams. This paper seeks to the potential risk of reservoir sedimentation in Batu Dam, Malaysia. It is based on literature and findings from related studies on the sedimentation of the Batu Dam reservoir. Based on the feasibility study in 1980, the allowable annual sediment trapped was 40,000 m³/year as designed. Sediment accumulation for 50-year and 100-year sediment analysis is 1.85 m³ x 10⁶ and 3.70 m³ x 10⁶ respectively. According to the bathymetric survey in 2013, sedimentation occurs upstream of Batu Dam. Followed by the Formal Safety Inspection in 2015 reported that sedimentation was trapped at the lowest screen of the intake tower. It is proven by a previous sampling study in 2016 that most of the sedimentation categories as course material accumulated at the river mouth of Batu River upstream of the reservoir. Historical satellite images also capture the increase of area by sedimentation. An earlier remote sensing study in 2018 reported that sediment volume from 1987 until 2017 was about 7.31 million m³. Although this dam reservoir is designed to accommodate a certain amount of sedimentation, it is essential to keep monitoring sedimentation to manage a sustainable reservoir. The overall findings of this paper can assist in making better decisions for reservoir management.

Keywords. reservoir sedimentation, bathymetric survey, sediment sampling, satellite image, Batu Dam

Dynamic of Salinity Intrusion in Dinh An and Tran De Branches of Mekong estuaries

Mai Nguyen¹, Hai D. Do², Sameh Kantoush³, Sumi Tetsuya⁴, and Thang D. Tang⁵

¹ Thuyloi University-Southern Campus (No.2 Truong Sa Street, Binh Thanh district HoChiMinh City), Vietnam

^{2,5} Southern Institute of Water Resources Research (No. 658 VoVanKiet street, District 5, HoChiMinh City), Vietnam

^{3,4} Water Resources Research Center, Disaster Prevention Research Institute, Kyoto University (Goka-sho, Uji-shi, 611-011, Kyoto), Japan

*Corresponding author: maiswru@tlu.edu.vn

Abstract. The increase of salt intrusion in recent years in the DinhAn and TranDe branches two of seven estuaries of the Mekong estuaries, has threatened the freshwater supply in the coastal regions, of Tra Vinh province. Combining the field survey and numerical modelling to investigate the salt transport mechanisms and the response of salt intrusion to changes in river discharge and tidal mixing have been conducted. The results of this research in the daily tidal cycle are that maximum salinity concentration (Smax) occurs at the bottom and later maximum water level from 1 to 2 hours. While Smax in the fortnight cycle appears during the transition period from neap tide to spring tide. The response of the salinity intrusion mechanism to the tidal velocity change is less than the river flow. However, when river flow increases, the impact of tidal velocity increases and the phase lag of response time decreases. The asymmetries of salt intrusion responding to increasing and decreasing river flow or tidal velocity are observed in the estuary.

Keywords. Salinity intrusion, Mekong estuary, tidal regime, tidal velocity

2nd Session on Hydrological Modelling and Sediment Management – B

Impacts of Reservoirs on Sediment concentration in the transboundary Srepok River Basin, Vietnam

Thao Thi Phuong Bui^{1,2,*}, Sameh Ahmed Kantoush¹, Akira Kawamura³, Tien L.T. Du⁴, Nuong Thi Bui⁵, Mohamed Saber¹, Ngoc T. Nguyen⁴, Duong Du Bui², Sumi Tetsuya¹, Doan Van Binh⁶, Binh Quang Nguyen⁷, Tra T.T. Nguyen²

¹ Department of Urban Management, Water Resource Center, Disaster Prevention Research Institute (DPRI), Kyoto University, Kyoto 611-0011, Japan

² National Center for Water Resources Planning and Investigation (NAWAPI). No.93, lane 95, Vu Xuan Thieu Street, Sai Dong Ward, Long Bien District, Ha Noi, Vietnam

³ Department of Civil and Environmental Engineering, Tokyo Metropolitan University, 1-1 Minami-Ohsawa, Hachioji, Tokyo 192-0397.

⁴ Department of Civil and Environmental Engineering, University of Houston, Texas, U.S.A.

⁵ Hanoi University of Natural Resources and Environment (HUNRE), Hanoi, Vietnam

⁶ The University of Danang - University of Science and Technology, 54 Nguyen Luong Bang, Danang, Vietnam

⁷ Master Program in Water Technology, Reuse, and Management, Vietnamese- German University. No 10 Hoang Dieu Street, Phu Nhuan District, Ho Chi Minh City, Vietnam

*Corresponding author: thaobtp26@wru.vn

Abstract. In the Upper Srepok River Basin (USRB), one of the major tributaries with four cascade reservoirs already in place that may have negative effects on the downstream ecosystems, particularly the world's rice bowl in the Mekong Delta and the world's most productive inland fisheries in the Tonle Sap Lake, a process-based hydrological model was established. Changes in simulated streamflow and suspended sediment concentration (SSC) can therefore be linked to modifications in reservoir operations by maintaining the same climatic conditions, altering topographic factors associated to reservoirs, and introducing a reservoir management module. Both the annual and seasonal periods saw a sharp decline in the average and peak SSC. Sediment loads at the Ban Don station were 15% (140 000 tons/year) lower than they were before the dam was built.

Keywords. Srepok, HYPE, reservoirs, suspended sediment concentration

Integrated flood and sediment management in river basins for sustainable development: The case of Cagayan River Basin

Lanie A. Alejo^{1*}, Orlando F. Balderama¹, Jeffrey Lloyd R. Bareng¹, Czarimah L. Singson¹, Elmer A. Rosete¹, Arlen S. Alejandro², Carlo C. Ablan², Sameh Ahmed Kantoush³, Tetsuya Sumi³, Mohamed Saber³, Doan Van Bihn⁴

¹ Isabela State University, Echague, Isabela, 3309 Philippines

² National Irrigation Administration, Magat River Integrated Irrigation System-Dam and Reservoir Division, Ramon, Isabela 3319 Philippines

³ Kyoto University, Japan

⁴ Thuyloi University, Vietnam

*Corresponding author: lhan1023@yahoo.com

Abstract. Climate change threatens the world with disastrous floods and droughts, with Japan, Vietnam, and the Philippines among the worst-affected countries. This management paper highlights collaboration with Japanese and Vietnamese universities in implementing the international project “Integrated Flood and Sediment Management in River Basins for Sustainable”. Kyoto University transferred its technologies on flood and sediment management to Isabela State University and Thuyloi University thru trainings. The impacts of climate change and human interventions were assessed in the Vu Gia-Thu Bon River basin (Vietnam) and Cagayan River basin (Philippines). Bathymetry survey in the Magat dam showed reduced capacity of the reservoir due to sedimentations. Hence, funding for the dredging of the Magat dam was secured. Also, it was projected that climate change and landuse changes will significantly reduce water resources during dry years leading to droughts, and will abruptly increase during wet years leading to flooding. The rainfall-runoff-inundation model was locally optimized as a decision support tool for flood inundation forecast and upgrade dam discharge protocol during extreme rainfall events. The International Association on Climate Change Adaptation and Disaster Risk Reduction Management was created and registered as a science- government-community association to address Integrated Flood and Sediment management in river basins.

Keywords. Flood and sediment management, river basins

A conceptual approach to study influences of river sand mining on the depth-averaged velocity in vegetated compound channels

S.H Truong ^{1*}, **K.L Phan** ¹, **Un Ji** ², **S.A. Kantoush** ³, **W.S.J Uijttewaal** ⁴

¹ Department of civil engineering, Thuy loi University, Hanoi, 10000, Vietnam

² Department of land, water and environment, Korea Institute of Civil Engineering and Building Technology, IILsan, South Korea

³ Water Resources Research Center, Disaster Prevention Research Institute, Kyoto University, 611-0011, Japan

⁴ Department of civil engineering, Delft University of Technology, Delft, The Netherlands

*Corresponding author: truonghongson@tlu.edu.vn

Abstract. In the Mekong Delta, riverbed sand and gravel are usually over-extracted due to the increasing demand for materials for the construction industry. As a result, the river bed is often deeper, about two to three meters. Numerous studies have been published focusing on the morphological response induced by river sand mining in the short and long term. Nevertheless, the impact of elevation loss on the hydrodynamic processes in the mixing layer of compound channels at the reach scale is unclear, especially during the flooding stage. In order to obtain more insight, a schematised model of a vegetated compound channel in the Tieu Estuary was constructed in Delft3D. Different riverbed elevations were considered together with different vegetation densities on the floodplain. The numerical results reveal a significant modification of the outer layer in the mixing layer due to river sand mining, which may create unfavorable conditions for the lateral exchange of nutrients and sediment between the floodplain region and the main open channel.

Keywords. Sand mining, compound channel, vegetation, hydrodynamic, numerical model, mixing layer

Optimization of Magat dam operation rule for flood risk management in the Cagayan river basin

Hikaru Goto¹, Mohamed Saber¹, Yasuhiro Takemon¹, Sameh Kantoush^{1,*}, and Tetsuya Sumi¹

¹ Department of Urban Management, Socio & Eco Environment Risk Management, Water Resources Research Center, Disaster Prevention Research Institute (DPRI), Kyoto University, Kyoto, 611-0011, Japan

*Corresponding author: kantoush.samehahmed.2n@kyoto-u.ac.jp

Abstract. The Philippines has experienced several intense and devastating typhoons imposing significant threats to human lives and urban development. Therefore, this study aims to understand the flood characteristics by simulating the extreme Typhoon Ulysses at the Cagayan River, focusing on the Magat dam. Several scenarios have been conducted, including an assessment of the contribution of each sub-catchment and dam operations during the typhoon and an examination of additional proposed dams at the other sub-catchment. Rainfall-Runoff Inundation Model (RRI) was used and examined with four scenarios: a model without a dam, a constant discharge model and a constant rate discharge model for the operation of the Magat dam, and a case where the Magat dam and a new additional dam were installed. We found that some sub-basins had higher runoff than others. As for the operation of the Magat dam, the sedimentation countermeasures and pre-release of the Magat dam have flood control effects, but they are insufficient. It is expected that a proposed dam at the Cagayan Segment 1 could improve the flood risk in the downstream regions. Further scenarios considering the ensembled Rainfall data are needed to enhance dam operations and control flood impacts.

Keywords. Cagayan River Basin, Magat dam, dam operation, RRI model

Magat Dam science-based initiatives for long-term flood and sediment management

Carlo C. Ablan^{1*}, Arlen S. Alejandro², Lanie A. Alejo³, Orlando F. Balderama⁴ and Sameh Ahmed Kantoush⁵

^{1,2} National Irrigation Administration, Magat River Integrated Irrigation System, Dam and Reservoir Division, Ramon, Isabela, Philippines

^{3,4} College of Engineering, Isabela State University, Echague, Isabela, Philippines ⁵ Water Resources Research Center - Disaster Prevention Research Institute Kyoto University, Kyoto, Japan

*Corresponding author: carlo.ablan14@gmail.com

Abstract. Addressing sedimentation problems in dam reservoirs is a process that involves identifying its sources and application of different techniques to monitor and reduce the further accumulation of sediment yield. This paper explains the results of the initiatives and collaborative efforts to focus on the issue of sedimentation in the Magat Dam reservoir. Recent 2021 bathymetric survey revealed that there is a reduction in the storage capacity by 65.34 MCM. From the turbidity measurements, results showed an average volume of 202,187.90 m³ of sediments for May. Structural and nonstructural ways to alleviate the impacts of sedimentation was done through the construction of sediment catchment structures and raising awareness on the importance of watershed resources through community extension seminar.

Keywords. Reservoir, sedimentation, techniques

3rd Session on Artificial Intelligence for Hydrological Application

Water level prediction model of Kien Giang river based on regression techniques

Ta Quang Chieu^{1,*}, Nguyen Thi Phuong Thao¹, Dao Thi Hue², Nguyen Thi Thu Huong¹

¹ Faculty of Computer Science and Engineering, Dong Da, Thuyloi University, Hanoi, 100000, Vietnam

² Faculty of Water Resources Engineering, Thuyloi University, Dong Da, Hanoi 10000, Vietnam

*Corresponding author: quangchieu.ta@tlu.edu.vn

Abstract. Model accuracy and running speed are the two key issues for flood warnings in rivers. Traditional hydrodynamic models, which have a rigorous physical mechanism for flood routine, have been widely adopted for water level prediction in the river, lake, and urban areas. However, requiring various types of data, some expertise and experience with models and intensive computation time limits short-term or real-time prediction of the traditional models. To achieve a real-time prediction for the water level, a new framework based on a machine learning method was proposed in this paper. We develop a water level prediction model using various machine learning models such as linear regression (LR), support vector regression (SVR), random forest regression (RFR), multilayer perceptron regression (MLPR), and light gradient boosting machine regression (LGBMR). The models compared to predict the hourly water levels in Kien Giang station of Kien Giang river based on collected data of 2012, and 2020. Three evaluation criteria, i.e., R², MAE, and RMSE, were employed to examine the reliability of the proposed models with others. The results show that the LR model outperforms the SVR, RFR, MLPR, and LGBMR models.

Keywords. LGBMR, linear regression, machine learning, MLPR, SVR, RFR, water level

Water level prediction of Kien Giang river using deep learning models

Trieu Trung Hieu^{1,2}, Ta Quang Chieu^{3,*}, Nguyen Dac Hieu³, Dinh Nhat Quang⁴ and Nguyen Thanh Tung³

¹ Viettel Digital Services, Hanoi, 100000, Vietnam

² VCREME Center of Research, Hanoi, 100000, Vietnam

³ Faculty of Computer Science and Engineering, Thuyloi University, Dong Da, Hanoi, 100000, Vietnam

⁴ Faculty of Civil Engineering, Thuyloi University, Dong Da, Hanoi, 10000, Vietnam

*Corresponding author: quangchieu.ta@tlu.edu.vn

Abstract. Time-series prediction of a river stage during natural disasters (such as typhoons and storms) is crucial for both flood control and flood disaster prevention. Data-driven models using deep learning (DL) techniques have proven to be an attractive and effective approach for water level prediction. This paper proposes a novel data-driven approach using deep learning network structures of Gated Recurrent Unit (GRU), Long Short-Term Memory (LSTM), and Bidirectional Long-Short Term Memory (Bi-LSTM). The models were implemented and validated based on an experimental dataset including observed data of hourly rainfall and water level at several meteorological and hydrological stations along the Kien Giang river. Two time leads scenarios of one and three hours were established to compare the prediction capability of three proposed models for the water level at Le Thuy station. Three evaluation metrics, i.e. R2, MAE, and RMSE, are used to evaluate DL models. The results reveal that the LSTM model overperformed the Bi-LSTM and GRU models with the values of three metrics are 0,98; 0,068; 0,096 respectively.

Keywords. Bi-LSTM, Deep learning, GRU, LSTM, Le Thuy, Water level prediction

A real-time flood forecasting hybrid machine learning hydrological model for Krong H'ngang hydropower reservoir

Phuoc Sinh Nguyen^{1,2*}, Truong Huy Nguyen^{1,3}, The Hung Nguyen²

¹ Faculty of Water Resources Engineering, University of Science and Technology-The University of Da Nang, 50000, Vietnam.

² Song Ba JSC, 573 Nui Thanh, Hai Chau, Da Nang, 50000, Vietnam.

³ Department of Civil Engineering, McGill University, 817 Sherbrooke Street West, Montreal, Quebec H3A 2K6, Canada

*Corresponding author: phuocsinhbk@gmail.com

Abstract. Flood forecasting is critical for mitigating flood damage and ensuring a safe operation of hydroelectric power plants and reservoirs. The authors introduce a hybrid hydrological model based on the combination of the HEC-HMS hydrological model and an Encoder-Decoder-Long Short-Term Memory network in this study to enhance the accuracy of a real-time flood forecasting. The proposed hybrid model has been applied to the Krong H'ngang hydropower reservoir. The observed data from 33 floods monitored between 2016 and 2021 are used to calibrate, validate, and test the hybrid model. Results show that the HEC-HMS-ANN hybrid model significantly improves the forecast quality, especially for long forecasting time steps. The KGE efficiency index, for example, increased from $\Delta KGE = 16\%$ at time $t + 1$ to $\Delta KGE = 69\%$ at time $t + 6$ hours, similar to other indicators (such as peak error and volume error). The computer program developed for this study is being used at the KrongHngang hydropower to aid in reservoir planning, flood control, and water resource efficiency.

Keywords. Hydrological hybrid model, HEC-HMS, machine learning, KrongH'ngang, real-time flood forecasting

Machine Learning Techniques and hydrological Modeling for Flood Susceptibility and Inundation Mapping: Case study VGTB River Basin, Vietnam

Mohamed Saber^{1, *}, Tayeb Boulmaiz², Mawloud Guermoui³, Karim I. Abdrabo⁴, Sameh A. Kantoush¹, Tetsuya Sumi¹, Hamouda Boutaghane⁵, Doan Van Binh⁶, Binh Quang Nguyen^{1,7}, Thao T. P. Bui¹, Ngoc Duong Vo⁷, Emad Habib⁸, Emad Mabrouk^{9,10}

¹Disaster Prevention Research Institute (DPRI), Kyoto University, Kyoto 611-0011, Japan; *mohamedmd.saber.3u@kyoto-u.ac.jp, kantoush.samehahmed.2n@kyoto-u.ac.jp, sumi.tetsuya.2s@kyoto-u.ac.jp,

²Materials, Energy Systems Technology and Environment Laboratory, Ghardaia University, Ghardaia, Algeria; boulmaiz.tayeb@univ-ghardaia.dz

³Unité de Recherche Appliquée en Energies Renouvelables, URAER, Centre de Développement des Energies Renouvelables, CDER, 47133 Ghardaïa, Algeria; gue.mouloud@gmail.com ⁴Faculty of Urban and Regional Planning, Cairo University, Giza 12613, Egypt; m.karim.ibrahim@cu.edu.eg

⁵Hydraulic Department, Badji Mokhtar-Annaba University, P.O. Box 12, Annaba, Algeria; hamouda.boutaghane@univ-annaba.dz

⁶Master Program in Water Technology, Reuse, and Management, Faculty of Engineering, Vietnamese German University, 2-Le Lai Street, Hoa Phu Ward, Thu Dau Mot City, Binh Duong Province 820000, Vietnam; binh.dv@vgu.edu.vn

⁷The University of Danang -University of Science and Technology, 54 Nguyen Luong Bang, Danang, Vietnam; nqbinh@dut.udn.vn

⁸Department of Civil Engineering, University of Louisiana at Lafayette, PO Box 42291, Lafayette, LA 70504, USA, Email; habib@louisiana.edu

⁹College of Engineering and Technology, American University of the Middle East, Egaila 54200, Kuwait; emad.mabrouk@aum.edu.kw

¹⁰Department of Mathematics, Faculty of Science, Assiut University, Assiut 71516, Egypt; mabrouk@aun.edu.eg

*Corresponding author: mohamedmd.saber.3u@kyoto-u.ac.jp

Abstract. Vietnam has experienced many natural disasters, particularly typhoons. This study aims to examine three machine learning (ML) approaches—random forest (RF), LightGBM, and CatBoost—for flooding susceptibility maps (FSMs) in the Vu Gia-Thu Bon (VGTB) River Basin of Vietnam. The results of ML are compared with those of the rainfall–runoff model. Ten independent factors that influence the FSMs in the study area, namely, aspect, rainfall, curvature, DEM, horizontal distance from the river, geology, hillshade, land use, slope, and stream power index, are assessed. An inventory map that includes approximately 850 flooding sites is considered based on several post-flood surveys. The inventory dataset is randomly divided into two sets: training (70%), and testing (30%). The AUC- ROC results are 97.9%, 99.5%, 99.5% for CatBoost, LightGBM, and RF, respectively. The FSMs

developed by the ML methods show good agreement in terms of extension with flood inundation maps developed using the rainfall-runoff model. The FSMs show that downstream areas (both urbanized and agricultural) are under “high” and “very high” levels of susceptibility. The developed FSMs for such typhoon-prone regions can be used by decision-makers and planners in Vietnam to propose effective mitigation measures for community resilience and development.

Keywords. Machine learning, random forest, LightGBM, CatBoost, flood susceptibility mapping, rainfall-runoff inundation model

4th Session on Flood Risk Assessment

Urban flood forecasting based on hydraulic model by coupling of MIKE Flood and MIKE Urban: A case study of Tam Ky city, Vietnam

Chi Cong Nguyen^{1*}, Binh Quang Nguyen¹, Xuan Cuong Le¹, Ly Trieu Pham¹, Thanh Hai Nguyen¹, Ngoc Duong Vo¹

¹The University of Da Nang-University of Science and Technology, Da Nang, Vietnam.

*Corresponding author: Chi Cong Nguyen (email: nccong@dut.udn.vn)

Abstract. Tam Ky city is located downstream of Ban Thach and Tam Ky rivers in central Vietnam. According to annual statistics, this area is affected by heavy rains from tropical storms, so flooding is quite common here. This study establishes a flood forecasting model for Tam Ky city based on forecasted rainfall data and tidal level. A flood forecasting model is based on a proceeding of rainfall-runoff and is connected between the river basin and the city. The parameters of the flood forecasting model are calibrated and verified for floods that have occurred on rivers as well as in urban areas. An experimental flood forecast for Typhoon Nuru has just occurred on September 28, 2022. The forecast results of location and depth flooding in the city reflect the reality very well.

Keywords. MIKE Flood, MIKE Urban, Tam Ky City.

Flood modelling in the Ba River basin using a coupled hydrodynamic model- MIKE FLOOD

Luc Anh TUAN¹, Can Thu VAN², Doan Van BINH³, Sameh A. KANTOUSH⁴, and Tetsuya SUMI⁵

^{1, 2} Ho Chi Minh City University of Natural Resources and Environment, (236B Le Van Sy Street, Ward 1, Tan Binh District, Ho Chi Minh City), Viet Nam

³Faculty of Engineering, Vietnamese –German University, (Ben Cat Town, Binh Duong Province), Viet Nam

^{4,5}Water Resources Research Center, Disaster Prevention Research Institute, Kyoto University (Goka-sho, Uji-shi, 611-011, Kyoto), Japan

*Corresponding author: latuan@hcmunre.edu.vn

Abstract. The problem of flooding in the Central Vietnam in general and the lower Ba River in particular is one of the natural disasters that frequently threatens people's lives and socio-economic development in the region. Especially, climate change is becoming ever more prominent and hotter, making extreme natural disasters more unusual and unpredictable. Many methods have been applied and shown to be effective in calculating floods. Under the development of science and technology, many hydrodynamic models were developed, and they have become speedy in the era of competitive computer industry leading to parallel computation. In this study, the MIKE-FLOOD model - a model that connects a 1-dimensional (1-D) MIKE 11 Hydrodynamics (HD) model with a 2-dimensional (2-D) MIKE 21 HD model was used to set up, calculated for 3 floods: (1) flood in October 1993, (2) flood in November 2003, (3) flood in November 2007, these are floods with frequency large and relatively large floods, especially the October 1993 flood is considered a historic flood in the region. The model testing correction indexes such as flood peak error (%), Nash index, correlation index R², are in good range and reliable enough to simulate large and relatively large floods for the area. The results of calculation and analysis of the flooded area compared with the inundation time of the October 1993 flood, show that the flood rises quickly and recedes quickly. When the flood water level reaches the maximum value, the total area affected by inundation corresponding to the flood water level is 22,600 hectares, accounting for 52% of the natural area, up to 16,500 hectares are flooded deeper than 1 meter, 11,000 hectares are flooded deeper 2 meters, 7,000 hectares were flooded more than 3 meters deep, 4,200 hectares were flooded more than 4 meters deep and the area flooded more than 5 meters deep was 2,200 hectares. The 2003 flood and the 2007 flood are two frequent floods in the basin, with a frequency of 20%, the flooded area when H max occurs at points in the study area is not much different compared with the exceptionally large flood of 1993 with a frequency of 5%, differing only in the value of each point. Especially in the center of Tuy Hoa city, the flooded area at the time of H max is almost 100%.

With the set of parameters set up in this paper, it gives us relatively accurate results in terms of quantity, type of flood and time of occurrence. Therefore, it can be used to simulate and predict floods for the Ba River downstream.

Key words. Flooding, coupled hydrodynamic model, MikeFlood model, Ba River basin

Study on flood mitigation operation of cascading dams, including hydropower dams in Ohi river

Yuki Okamoto^{1,*}, Takahiro Koshiba², Mohamed Saber¹, Yasuhiro Takemon¹, Sameh Kantoush¹ and Tetsuya Sumi¹

¹ Disaster Prevention Research Institute, Kyoto University, Kyoto, Japan

² Ujigawa Open Laboratory, Kyoto University, Kyoto, Japan

*Corresponding author: okamoto.yuki.75a@st.kyoto-u.ac.jp

Abstract. Dam pre-release is an effective measure against large-scale floods, whereas its implementation period is limited. In addition, there are a few considerations of pre-release in cascading dams, including hydropower dams. This study investigated the effect on the maximum discharge of each dam as the flood control effects and the discharge loss of hydropower dams, which directly connect to hydropower generation, by changing the start time and target water level of pre-release in cascading dams. By advancing the start time and increasing the target water level drawdown, the pre-release effects on flood control and water utilization have increased.

Keywords. Pre-release, cascading dams, hydropower, RRI model

Flood Vulnerability Indicators of Transportation System Concerning Climate Change

Hamizah Amalina Amlan¹, Sitti Asmah Hassan^{1*} and Nor Eliza Alias¹

¹ Faculty of Civil Engineering, Universiti Teknologi Malaysia, 81310, Johor, Malaysia

*Corresponding author: hamalina2@graduate.utm.my, *sasmah@utm.my, noreliza@utm.my

Abstract. Transportation moves people and goods to different neighborhoods, cities, states, and countries. Transportation systems have included the concept of vulnerability, which has piqued the interest of academics in numerous disciplines of transportation. This is intended to increase the efficiency of transportation systems and mitigate the effects of disruptions. However, climate change is likely to impair transportation infrastructure by increasing temperatures, causing more severe storms and flooding, and increasing storm surges, compromising the reliability and capacity of transportation systems. Past works relating to transportation vulnerability had focused on different elements of vulnerability indicators and they have developed a more comprehensive concept. As a result, this paper offers a comprehensive review of vulnerability indicators concerning climate change. The primary focus of the study is to explore the flood vulnerability indicators considering the tropical climate in Malaysia. Based on this, prior research on transportation system vulnerabilities is examined in order to define the criteria required to assess transportation system vulnerability as well as the future directions of transportation vulnerability assessment.

Keywords. Climate Change, Flood, Indicator, Transportation System, Vulnerability

Stakeholders forum on integrated flood risk management in Cagayan River Basin: Basis in writing policy recommendations

Orlando F. Balderama¹, Lanie A. Alejo², Jeffrey Lloyd R. Bareng³, Jennelyn L. Raymundo⁴

¹College of Engineering, Isabela State University, Echague, 3309, Philippines

²College of Engineering, Isabela State University, Echague, 3309, Philippines

³College of Engineering, Isabela State University, Echague, 3309, Philippines

⁴ College of Education, Isabela State University, Echague, 3309, Philippines

*Corresponding author: orly_isu@yahoo.com

Abstract. The stakeholders forum aimed to enhance the capacities of policymakers, managers, and practitioners of river basin organizations on flood management through knowledge sharing of new approaches, techniques, methodologies, and good practices from partners here and abroad to help achieve effective implementation of integrated flood risk management as a component of integrated water resources management. Considering the designed series of activities, the forum highlighted the partnership of the Japan Water Agency and the Cagayan River Basin Management Council, a multipartite information exchange among the Philippine government agencies' dignitaries, political leaders and legislators, and Japanese stakeholders, and the update reports conveyed by numerous Philippine government agencies as well as their collaborative workshop engagement to scale up international community linkages. It also underscored the inauguration of the International Organization on Climate Change Adaptation and Disaster Risk Reduction Management Office, stakeholders' collaboration for technology transfer and knowledge-sharing activities at NIA stations, and the newly forged partnership between JWA and City of Santiago to promote UN-SDG 6 and water security. Thus, the forum served as a channel that bridged what the government agencies and organizations know about flood and sedimentation management and what the community partners need to understand to revitalize science-community-government-academe collaboration.

Keywords. knowledge sharing, technology transfer, water security, integrated water resources management, flood and sedimentation management

Development of a localized integrated disaster risk index – A Malaysia case study of Langat River Basin

Nor Eliza Alias^{1,2, *}, M Wafiy Adli Ramli¹, Zulkifli Yusop^{1,2}

¹Center for Environment Sustainability and Water Security (IPASA), Universiti Teknologi Malaysia, Johor Bahru, 81310, Malaysia

²Faculty of Civil Engineering, Universiti Teknologi Malaysia, Johor Bahru, 81310, Malaysia

*Corresponding author: noreliza@utm.my

Abstract. Multiple disasters in Malaysia are observed to occur more frequently. This is due to impact of urbanization and climate change. Flood, landslide, debris flow and earthquakes are among distinct natural disaster seems to have great impact to the community. When it comes to community resilience, multi-vulnerability assessment is needed for a proper disaster management strategy. The index was developed by expanding on the multi-hazard spatial overlapping and Methods for the Improvement of Vulnerability Assessment in Europe (MOVE) theoretical framework. Two common hazards in Malaysia: floods and landslides were combined for the multi-hazard assessment. Multidimensional vulnerability combined six dimensions: social, economic, physical, institutional, environmental and cultural. A spatial vulnerability assessment is presented by mapping the risk val. The findings indicate that of the total areas in Langat River Basin, 14% has very high risk in which are urban areas. A validation of the index model was able to be done when a disastrous flood in December 2021 occurred at Langat River Basin. Assessment from the disaster impact data shows that one of the vulnerability dimensions which is areas with high institutional vulnerability were well correlated to the poor coordination or late emergency aid during the disaster.

Keywords. Multi-hazard, multi-vulnerability, disaster risk, Risk map

Mapping Open Fire Susceptibility and Nearest Water Resources For Fire Fighting -A Case Study in Johor Malaysia

Fara Aiza Md Sanin^{1,*}, Nor Eliza Alias^{1,2}, Kasturi Devi Kanniah³

¹ Faculty of Civil Engineering, Universiti Teknologi Malaysia, Johor Bharu, 81310, Malaysia.

² Center for Environment Sustainability and Water Security (IPASA), Universiti Teknologi Malaysia, Johor Bharu, 81310, Malaysia.

³ Tropical Map Research Group, Faculty of Built Environment & Surveying, Universiti Teknologi Malaysia, 81310 Johor Bahru, Johor, Malaysia.

*Corresponding author. E-mail: noreliza@utm.my

Abstract. Open fire releases toxic gasses and pollutant to air and can be destructive to the ecological, environmental and human infrastructure. Different methods and techniques for open fire susceptibility mapping are introduced according to the literature and can be classified into three groups: Probabilistic, statistical, and machine learning methods. In this research, we utilized the Random Forest (RF) machine learning approach for identifying the role of climatic and anthropogenic factors in influencing fire occurrence probability and mapping the open fire susceptibility for Johor State: Malaysia. A geo-database was established with 1726 Open fire sample locations and 12 predictor variables in total. Factor importance analysis was performed to identify the important factors of the occurrence of open fire in Johor state. The results show that the most important factor in the johor state region is distance to peatland. Additionally mean maximum temperature and distance to residential area are relatively important to open fire in Johor state. The model performance was evaluated using the receiver operating characteristic (ROC) curve method with AUC (Area under curve) value 0.86. The values of AUC using the best models are greater than 0.8, demonstrating that the model's predictive abilities are acceptable. The susceptible map can support future efforts in battling open fire and help local authorities in emergency planning. River and water body map overlaid on open fire map to calculate the distance of susceptible area to the nearest water resources.

Keyword. Open fire, susceptibility, random forest, fire fighting

Response of long-term hydrological to land use/land cover change in Vu Gia Thu Bon River basin

Thanh-Nhan-Duc Tran¹, Binh Quang Nguyen^{2,3*}, Ngoc Duong Vo³, Sameh A. Kantoush², Tetsuya Sumi²

¹Department of Engineering Systems and Environment, University of Virginia, Charlottesville, VA 22904, USA

²Water Resource Center, Disaster Prevention Research Institute (DPRI), Kyoto University, Kyoto 611-0011, Japan

³The University of Danang - University of Science and Technology, 54 Nguyen Luong Bang, Danang, Vietnam

*Corresponding author: nqbinh@dut.udn.vn

Abstract. The Vu Gia Thu Bon River basin, Vietnam, is an important watershed supporting drinking water, and agricultural activities in Central Vietnam. However, the potential hydrological impacts of LULC change in recent decades, are not quantified. Therefore, assessing long-term hydrological impacts of land use/land cover (LULC) change is of critical importance for land use planning and water resource management. This work would assess the long-term impacts of LULC change on streamflow and suspended sediment concentration. LULC records are collected annually from Launch Regional Land Cover Monitoring System (RLCMS) from SERVIR–Mekong between 1987 – 2018. Our key findings indicate interesting results, in which the simulated streamflow and sediment loads within this river basin have decreased due to deforestation. Thus, these findings would serve as a scientific basis for future management plans of stakeholders and decision-makers regarding water resources management.

Keywords. Land use/land cover (LULC) change, streamflow, suspended sediment concentration, vu gia thu bon, vietnam

Modeling the urban flood during the heavy rain in October 2022 for Ngu Hanh Son District, Da Nang City using SWMM model

Nguyen Thi Ngoc¹, Tran Thi An², Kieu Thi Kinh¹, Le Ngoc Hanh¹

¹ Master course of Environmental Management, University of Science and Education, The University of Da Nang, Viet Nam.

² Thu Dau Mot University, Binh Duong province, Viet Nam.

³ University of Science and Education, The University of Da Nang, Viet Nam.

*Corresponding author: nguyennhocchemical@gmail.com

Abstract. Urban flooding is one of the challenges by large cities in Vietnam, especially in Ha Noi, Ho Chi Minh, and Da Nang cities which are the largest cities in the country. The process of urbanization under the context of climate change is one of the causes of urban flooding in recent years. Therefore, the simulations of urban flood and drainage systems in typical rain are important to build the warning map of the risk to the local community. The main objective of this study is to use GIS modeling to warn of the risk of local flooding in some routes in Ngu Hanh Son district, Da Nang City during the heavy rain in October 2022 which is considered the most severe rainfall in the past 20 years. The main purpose of the simulation of urban drainage in Ngu Hanh Son through the October 2022 rain is to determine a reasonable set of hydrological- hydraulic parameters for the construction of hazard warning maps for flooding due to rain. Within the scope of the paper, we will present the results of the urban drainage simulation for Ngu Hanh Son district by using the Storm Water Management Model (SWMM) model with in- situ rainfall data on October 14th, 2022.

Keywords. Da Nang City, Ngu Hanh Son, urban flood, heavy rain, SWMM

Nonparametric estimation approach for evaluating the trend of hydro-meteorological factors in Lai Giang, Binh Dinh

Thi Ngoc Canh Doan¹, Ngoc Duong Vo², Cong Phong Nguyen³, Trung Quan Nguyen⁴,
Huu Phuoc Tran⁵

¹ The University of Danang, University of Economics, Viet Nam

² The University of Danang, University of Science and Technology, Viet Nam

³ Sourthen institute of Water resources research, Viet Nam

⁴ Vietnam disaster management authority

⁵ Binh Dinh irrigation works exploitation company

*Corresponding author: canhdtm@due.edu.vn

Abstract. With the purpose of analyzing trend variations of hydro-meteorological factors in Lai Giang catchment, as a basis for the planning as well as socio-economic development of the locality in the future, the research uses the nonparametric estimation method to evaluate the tendency of changes in rainfall, runoff and temperature at stations in the basin. Based on data of more than 40 years, from 1980 to 2020, hydro-meteorological factors are analyzed with different parameters, such as annual average, annual maximum, annual minimum, dry season average, and maximum daily rainfall, three-day maximum rainfall, etc. Research results show the change of factors in space as well as over time. At the same time, the study also builds up the trend equation of the research quantities, as a basis for future scenario assessment.

Keywords. Nonparametric estimation; rainfall; runoff, Mann-Kendall

Impacts of drought on water resources in Central Vietnam. A case study of Vu Gia Thu Bon River basin

Binh Quang Nguyen^{1,2*}, Thanh-Nhan-Duc Tran³, Ngoc Duong Vo², Sameh A. Kantoush¹, Tetsuya Sumi¹

¹Water Resource Center, Disaster Prevention Research Institute (DPRI), Kyoto University, Kyoto 611-0011, Japan

²The University of Danang - University of Science and Technology, 54 Nguyen Luong Bang, Danang, Vietnam

³Department of Engineering Systems and Environment, University of Virginia, Charlottesville, VA 22904, USA

*Corresponding author: nqbinh@dut.udn.vn

Abstract. Severe droughts cause substantial damage to different socio-economic sectors, and even Vietnam, which has abundant water resources, is not immune to their impacts. To assess the implications of a severe drought in Central Vietnam, we carried out a regional-scale drought impact analysis. We have assessed extreme to moderate drought events starting from 1980 to 2020 using the Standardized Runoff Index (SRI) drought classification. The runoff is collected from observation and the results of the Soil and Water Assessment Tool (SWAT) hydrological model. The results indicate that the long-lasting drought caused a significant decrease every year. Thus, we suggest that the resilience to droughts could be improved with region-specific drought management plans and by including droughts in existing regional preparedness exercises.

Keywords. Central Vietnam, drought, Standardized Runoff Index (SRI), SWAT

Quantification of GPM IMERG and SM2RAIN-ASCAT rainfall products over complex terrain under impacts of reservoirs. A case study for Srepok River basin

Thanh-Nhan-Duc Tran¹, Binh Quang Nguyen^{2,*}

¹ Department of Engineering Systems and Environment, University of Virginia, Charlottesville, VA 22904, USA

² Faculty of Water Resources Engineering, The University of Da Nang-University of Science and Technology, Da Nang 550000, Vietnam

*Corresponding author: nqbinh@dut.udn.vn

Abstract. Precipitation has a direct link to the water cycle and remains the primary driver to study climatic extremes. The impact of precipitation on key variables such as soil moisture is complicated to observe in nature and is often poorly represented. In this work, we validate two precipitation products namely (i) the Global Precipitation Measurement mission (GPM) integrated Multi-satellite Retrievals (IMERG), (iii) SM2RAIN-Advanced SCATerometer (SM2RAIN-ASCAT over Asia). The IMERG precipitation product is derived from multi-satellite precipitation product (top-down approach) and the SM2RAINASCAT is derived from surface satellite soil moisture (bottom up approach). Our key findings indicate the superior performance by GPM IMERG product over the Srepok River basin, in which impacts of new- built reservoirs were also included.

Keywords. Precipitation, SM2RAIN-ASCAT, GPM IMERG, Srepok River basin, Vietnam

River System's Behavioral Changes in Response to Manmade disturbances

Kogila Vani Annammala ^{1,2*}, Yun Qi Liang ¹, Yong Ee Ling ², Kawi Bidin ³, Nor Eliza Alias^{1,2} & Anand Nainar⁴

¹ Center for Environment Sustainability and Water Security (IPASA), Universiti Teknologi Malaysia, Johor Bahru, 81310, Malaysia

² Faculty of Civil Engineering, Universiti Teknologi Malaysia, Johor Bahru, 81310, Malaysia

³ Faculty of Science and Natural Resources, Universiti Malaysia Sabah, 88999 Kota Kinabalu, Malaysia

³ Faculty of Tropical Forestry, Universiti Malaysia Sabah, 88999 Kota Kinabalu, Malaysia

*Corresponding author: kogila@utm.my

Abstract: Modification of landscape directly implicate to the stream water quality by increasing the sediment and pollutants run off into river. The elevated terrestrial sediment deposition has impacted river morphologies, channel patterns, and affected its quality. This has emerged as a matter of concern in terms of water security and catastrophic flooding especially in developing nations. Thus, a better understanding of sediment dynamics and distribution is crucial to advance the knowledge of fluvial systems and its behavioural changes particularly in the tropics: a case study from Malaysia on the reconstruction of temporal sediment dynamics, identification of sediment sources, and quantification of the respective contributing sediment sources is presented, alongside with the impacts to river water quality. Storm events are one of the main causes of mobilization and transport of solutes into and within stream channels. The nonlinearity of solute transport during storm events is evident. Land-use and land cover changes related to timber harvesting and conversion into agricultural plantation under various national economic plans and initiatives have been recognised as a major driver of sediment yield and delivery in studied watersheds.

Keywords. Water quality index, sediment fingerprinting, multi proxy sediment, sedimentation

Analysis of spatial and temporal variation in rainfall trend of Vu Gia Thu Bon River Basin, Vietnam

Thao Bui Thi Phuong^{1,3}, Kantoush Ahmed Sameh^{1,*}, Binh Quang Nguyen^{1,2}, Duong Bui Du³, Sumi Tetsuya¹, Mohamed Saber¹, Tien Du Le Thuy⁴ and Doan Van Binh⁵

¹ Department of Urban Management, Water Resource Center, Disaster Prevention Research Institute (DPRI), Kyoto University, Kyoto 611-0011, Japan

² The University of Danang - University of Science and Technology, 54 Nguyen Luong Bang, Danang, Vietnam

³ National Center for Water Resources Planning and Investigation (NAWAPI). No.93, lane 95, Vu Xuan Thieu Street, Sai Dong Ward, Long Bien District, Ha Noi, Vietnam

⁴ Department of Civil and Environmental Engineering, University of Houston, Texas, U.S.A

⁵ Master Program in Water Technology, Reuse, and Management, Vietnamese- German University. No 10 Hoang Dieu Street, Phu Nhuan District, Ho Chi Minh City, Vietnam

*Corresponding author: kantoush.samehahmed.2n@kyoto-u.ac.jp

Abstract. This study examines rainfall spatial and temporal variation in the Vu Gia Thu Bon River basin from 1979 to 2021. The Mann-Kendall (MK) and Sen's Slope estimator test, which can determine rainfall variability and long-term monotonic trends, were utilized to analyze 16 rainfall stations that are distributed all over the river basin. The results showed that the pattern of annual rainfall was prevalent everywhere. Every location has a tendency to grow or to be insignificant. This pattern suggests that Vu Gia Thu Bon will have significantly more rainfall in the coming years. The examination of monthly rainfall yielded findings that 10 areas had noticeable rising tendencies. Trends in rainfall suggest that this area has seen climate change.

Keywords. Vu Gia Thu Bon River basin, rainfall, Mann-Kendall test, Sen's Slope

Spatio-temporal variability and trends of extreme rainfall and temperature events over Cagayan River Basin, Philippines

Khagendra Bharambe^{1*}, Sameh Kantoush², Tetsuya Sumi², Mohamed Saber² and Orlando Balderama³

^{1,2} Water Resources Center, Disaster Prevention Research Institute, Kyoto University, Uji-city, 6110011, Kyoto, Japan.

³ College of Engineering, Isabela State University, San Fabian, Echague, Isabela 3309 Philippines

*Corresponding author: bharambe.khagendrapralhad.2k@kyoto-u.ac.jp

Abstract. Extreme climate events, such as heavy rainfall, drought, flood, and heat waves, have become the most common natural disasters over the Cagayan River Basin. Addressing the consequences and the occurrence of these disasters has always a major challenge, due to increasing population and the impacts posed by extreme climate events. In order to help meet these challenges, this study has been undertaken considering the aim of evaluating of spatio-temporal variation of extreme climate events based on comprehensive assessment of extreme rainfall and temperature indices using long-term high-spatial-resolution climate data for worst-case (RCP8.5) climate change scenarios of MRI-AGCM3.2S data. The findings indicate an increased risk of extreme climate events such as extreme dry spells and extreme wet spells in future, which may lead to greater vulnerability to drought and flood over CRB. These findings would be a straightforward resource for addressing the high-risk zone and guiding disaster risk reduction authorities in making appropriate decisions for implementing adaptation strategies.

Keywords. Extreme Climate Events, flood risk, drought risk, climate change adaptation, spatio-temporal changes

Trends of low flow in the Vu Gia-Thu Bon River basin, Central Vietnam

Thi Ngoc Uyen Nguyen^{1,2}, Schneider, K¹, Ribbe, L², Duc Phuoc Vo³

¹ University of Cologne, Cologne, 50678, Germany

² Cologne University of Applied Science, Cologne, 50923, Germany

³ The University of Science and Technology, Da Nang, 55500, Viet Nam

*Corresponding author: ntngocuyen.dn@gmail.com

Abstract. Analysis of trends in low flow plays a significant role in water resource planning and operation. The main objective of this study is to examine the low flow trends as well as precipitation trends in the Vu Gia – Thu Bon during the period 1976 – 2014 non-parametric test Mann – Kendall. The analysis was carried out on monthly and annual time scales. Besides, the regime shift assessment was conducted to detect any abrupt change in the flow regimes. In addition, SPEI03 and SPEI06 were calculated in order to understand the drought situation in the same period. The results revealed that there is a significant upward linear trend in the annual precipitation by 17.03 mm/year between 1976 and 2014. However, the month-by-month analysis revealed that the increased precipitation primarily was during the rainy season. For the flows in Vu Gia and Thu Bon rivers, there are similar increasing trends in the discharges at the Thanh My station by approximately 1.617 m³/s and Nong Son station by 2.725 m³/s, respectively. Still, the increasing trends with the most significant ones being identified at seasonal rather than annual scale. Regarding the regime shifting, there were prominent alterations in some months during the dry season in 1999 which was recorded in February at Nong Son station (Thu Bon river) and in February, April, May, and July at Thanh My station (Vu Gia river). Additionally, the examination of drought identified a decline in drought occurrences' frequency, duration, and intensity for the period post-2000. These findings will contribute numerous values to improve the integrated water resource management in the region.

Keywords. Low flow, drought, Mann – Kendall test, Standardized Precipitation Evapotranspiration Index (SPEI)

5th Session on Remote Sensing and GIS for Flood and Water Security

Evaluation of water indices for dynamic monitoring reservoir surface water using Landsat 8 data

Vu Anh Minh¹, Dinh Nhat Quang^{2,*}, Nguyen Phuong Dung²

¹ Thuyloi University, 175 Tay Son, Dong Da, Hanoi 10000, Vietnam

² Faculty of Civil Engineering, Thuyloi University, 175 Tay Son, Dong Da, Hanoi 10000, Vietnam

*Corresponding author: quang.dinh@tlu.edu.vn

Abstract. Consistent dynamic monitoring of surface water area is significantly essential for reservoirs operation and management. Threshold segmentation method is mostly used for surface water extraction by applying fixed water index thresholds, which can be incompatible for regions with distinct characteristics. This study aims to evaluate the most suitable thresholds for three widely used water indices, i.e. Normalized Difference Water Index (NDWI), Modified NDWI (MNDWI) and Automated Water Extraction Index (AWEI) for detecting and extracting surface water of Phu Hoa reservoir in Quang Binh province from Landsat-8 imagery. Google Earth Engine platform is used to automatically collect low cloudiness scenes, compute three proposed indices, then detect and extract water surface using different threshold values. Accuracy evaluation of the extraction results is carried out by calculating Overall Accuracy (OA) and Kappa coefficient (kappa) based on observed water level and reservoir characteristics curve. The results show that the most effective thresholds for NDWI, MNDWI and AWEI are -0.4, -0.25 and -0.55; with OA and Kappa vary from 92÷96% and 0.84÷0.89 respectively. Chosen thresholds are then adopted for monitoring the dynamic of surface water of Phu Hoa reservoir over the period 2013-2021 that supports decision makers in process of reservoir operation and management.

Keywords. Landsat 8; Phu Hoa reservoir; Surface water extraction; Water indices

Impact of different types of vegetation in reducing roof runoff

Noraliani Alias¹ Nur Shazwani Baha Uddin², Mohammad Nurhadi Mohd Salim³ Nor Eliza Alias⁴

^{1,2,3,4} Faculty of Civil Engineering, Universiti Teknologi Malaysia, 81310 Johor Bahru, Johor, Malaysia

*Corresponding author: noraliani@utm.my

Abstract. Rapid development in urban area increased the flash flood occurrence. This is due to increasing of impervious surface in the urban area. Therefore, vegetated roof is introduced in order to reduce the peak discharge, velocity and quantity of the runoff generated during rainy season thus reducing flash flood occurrence. The objective of this study is to investigate the impact of different types of vegetation on roof runoff. Cow grass, carpet and pearl grass were selected to be installed on the roof. The vegetated roof was constructed in the laboratory and rainfall simulator was used in order to imitate the rainfall event. High intensity rainfall was implemented in this study. The results found that pearl grass was the best in reducing the volume of the roof runoff compared to cow and carpet grass.

Keywords. Flash flood, vegetated roof, roof runoff, peak discharge, pearl grass, cow grass, carpet grass

Impacts of anthropogenic activities on riverbed elevation. A case study in Central Vietnam

Binh Quang Nguyen^{1,2,*}, Sameh A. Kantoush¹, Doan Van Binh³, Ngoc Duong Vo², Mohamed Saber¹, Tetsuya Sumi¹

¹Water Resource Center, Disaster Prevention Research Institute (DPRI), Kyoto University, Kyoto 611-0011, Japan

²The University of Danang - University of Science and Technology, 54 Nguyen Luong Bang, Danang, Vietnam

³Master Program of Water Technology, Reuse and Management, Faculty of Engineering, Vietnamese German University, Binh Duong, Vietnam

*Corresponding: Binh Quang Nguyen (nqbinh@dut.udn.vn)

Abstract. Anthropogenic activities such as dams and sand mining are considered as one of the main driving causes changes of in riverbed elevation in the Vu Gia Thu Bon (VGTB) River basin. Therefore, assessing the impact of human activities on riverbeds can provide scientific insight to understand the morphological change and complex hydrological as well as to develop strategies for VGTB river basin management and sustainability. In this study, the riverbed data (in 2010, 2015, 2018, and 2021) and sediment size (in 2021) were analyzed to further clarify the changes of dams upstream and sand mining. We find that the riverbed elevation changes from downstream dams on Vu Gia and Thu Bon Rivers by 68 km and 74 km, respectively. The riverbed changes are greatly concentrated in the sand mining sites. The water level was driven by riverbed incision, and this is likely one of the main causes of the enhanced salinity intrusion.

Keywords. Dams, sand mining, riverbed elevation, vu gia thu bon river

Livelihood resilience: salinity intrusion hazard assessment of and adaptation strategy for socio-economic development in Ben Tre Province

Doan Van BINH¹, Nguyen Huu Minh TRI², Nguyen Trung NAM³, Ly Truong GIANG⁴, Sameh A. KANTOUSH⁵, and Tetsuya SUMI⁶

^{1,2,4} Faculty of Engineering, Vietnamese –German University, (Ben Cat Town, Binh Duong Province), Vietnam

³ Southern Institute of Water Resources Planning, (Ho Chi Minh City), Vietnam

^{5, 6} Water Resources Research Center, Disaster Prevention Research Institute, Kyoto University (Goka-sho, Uji-shi, 611-011, Kyoto), Japan

*Corresponding author: binh.dv@vgu.edu.vn

Abstract. The impacts of climate change and human activities have caused several hydrology-related challenges, such as severe drought and salinity intrusion, in the Vietnamese Mekong Delta. The study attempts to assess livelihood resilience in the Ben Tre Province under the increasing frequency of drought and salinity intrusion and to correlate salinity intrusion with resilience level geographically in four dimensions: social (community-based); economic (finance-based); institutional (governance-based); and infrastructure (technical-based). These objectives were achieved by field surveys, questionnaires, and one-dimensional hydrodynamic modelling. The results show that total community resilience in Ben Tre is a function of its subcomponents in social, economic, infrastructural, and institutional dimensions. The contribution of each subcomponent to the aggregated community resilience is relatively similar, indicating that it might necessitate a uniform change of all subcomponents to change the tendency of the overall resilience. Both overall and subcomponent resilience is inversely proportional to salinity concentration. The governance capacity in geographically challenged areas is less likely to receive the benefits of aid and local assistance, thus reducing their resilience and increasing their vulnerability. To improve the livelihood resilience for sustainable development in Ben Tre, not only technical measures but also governance capacity, institutional coordination, and community media need to be integrated.

Keywords. Ben Tre, livelihood resilience, salinity intrusion

GIS-based flood susceptibility mapping using AHP approach: A case study of Kien Giang river basin, Quang Binh province

Vu Huong Ngan¹, Dinh Nhat Quang^{2,*}, Pham Hong Nga²

¹ The Alliance of Bioversity International and Centre of International Agriculture, Tu Liem, Hanoi 10000, Vietnam

² Faculty of Civil Engineering, Thuyloi University, Dong Da, Hanoi 10000, Vietnam

*Corresponding author: quang.dinh@tlu.edu.vn

Abstract. Flood is the most devastating and unpredictable risk in Vietnam. As flood defence measures are becoming increasingly popular, researches on comprehensive flood assessment and management are still limited at local and national levels. This paper focuses on flood assessment in the Kien Giang river basin, which suffers from particularly severe floods, using the combination between flood susceptibility mapping and Analytical Hierarchy Process (AHP). While susceptibility map provides holistic levels and extent of the flood-affected area, based on the main flood-causing criteria; the AHP technique give the pair-wise comparison matrix to calculate the factor weights. Flood-related factors include TWI, land use, land cover, elevation, slope, precipitation, NDVI were considered and defined as raster dataset with the resolution of 10m. The levels of flood susceptibility are classified into five classes, i.e. very low, low, moderate, high and very high. The results indicate that 35.2% of Kien Giang river basin is considered as high and very high level of susceptibility while moderate susceptibility accounts for 40.5%. The AHP results also show that elevation and precipitation influence the most to find areas susceptible to flooding. This research constitutes a qualitative and quantitative tool that can be widely applied to localities, therefore helps local authorities to mitigate damage caused by floods.

Keywords. Analytical Hierarchy Process, flood susceptibility, GIS, Kien Giang river basin

6th Session on Hydrological Modelling and Sediment Management - C

Hydrodynamic modelling of Magat dam and reservoir during extreme conditions using Telemac 2D

Orlando F. Balderama¹, Jeffrey Lloyd R. Bareng², Lanie A. Alejo³, Englebert O. Manmano⁴

¹ Vice President for Research, Development, Extension and Training, Isabela State University, Echague, Isabela, 3309, Philippines

² University Director/ Research and Development Services, Isabela State University, Echague, Isabela, 3309, Philippines

³ Director/ Water Research and Development Center, Isabela State University, Echague, Isabela, 3309, Philippines

⁴ SRS/Water Research and Development Center, Isabela State University, Echague, Isabela, 3309, Philippines

*Corresponding author: orly_isu@yahoo.com

Abstract. In the case of Magat dam and reservoir, the significant storage capacity loss will indefinitely affect the agricultural production under the areas serviced by the said reservoir. This is in addition to the communities that depend on the reservoir for their domestic uses. Based on the accumulated sediment volume for the past five (5) years, the remaining storage capacity for the Magat Reservoir is now at around 570 MCM, in contrast with its 1.08 BCM designed capacity. With these data, it is only expected to get worse if no effective sediment management is employed. A purely hydrodynamic modelling is performed on Magat reservoir to evaluate the ability of Telemac 2D in simulating the actual flow during extreme events. The hydrodynamic behavior in the reservoir level was accurately reproduced using Telemac 2D. This model was calibrated and validated using flow data during typhoons Rolly and Ulysses (November 2020) and Severe Tropical Storm Florita (August 2022). The simulated results showed that the applied model could precisely reproduce the outflow events. The hydrodynamic model is planned to be coupled with the sediment transport module “Gaia” to potentially understand the sediment transport dynamics of the Magat Dam and Reservoir.

Keywords. hydrodynamic modelling, Magat dam and reservoir, Telemac 2D

Evaluation of coastline change in Quang Nam under the influence of jetty construction

Trinh Tran Tieu Long¹, Ho Sy Tam^{2,*}, Nguyen Quang Duc Anh³, Nguyen Hiep^{1,4}, Dinh Nhat Quang² and Nguyen Trung Viet²

¹Thuyloi University, Dong Da, Hanoi 10000, Vietnam

²Faculty of Civil Engineering, Thuyloi University, Dong Da, Hanoi 10000, Vietnam

³Institute of Civil Engineering, Thuyloi University, Dong Da, Hanoi 10000, Vietnam

⁴Vietnam Disaster Management Authority, Ministry of Agriculture and Rural Development, Ba Dinh, Hanoi 10000, Vietnam

*Corresponding author: tamhs.cctl@tlu.edu.vn

Abstract. In recent years, coastal erosion and accretion have been observed and amplified along Quang Nam coast, which causes serious adverse impacts to inhabitants as well as rich ecological values along the coast. In the master plan for Cua Lo port, a jetty is constructed in the north of Cua Lo estuary to protect the harbor basin of the port from sediment deposition. In this study, the numerical model GENCADE is used to evaluate the changes of Quang Nam coastline, i.e. from Cua Dai estuary to Cua Lo estuary. Different values of model-specific parameters K1 and K2 have been examined to compare the calculated coastlines with the image-analyzed ones for evaluating the accuracy of the model. The results reveal that 0.4 and 0.2 are the optimal values for the study area's empirical coefficients K1 and K2. The well-validated model is then adopted to evaluate the coastline change under the influence of jetty construction. The GENCADE results indicate that after 10 years, 20 years and 50 years of operation, shoreline modifications reach a distance of 250 m, 360 m and 450 m toward the sea respectively. Finally, the length of the jetty will be proposed based on these accretion predictions.

Keywords. Cua Lo port, GENCADE, Quang Nam coastline, sediment transport, shoreline change

Evaluation of hydrodynamic and sediment transport under construction of Cua Lo's navigation channel

Dang Cong Phuc¹, Ho Sy Tam^{2,*}, Nguyen Quang Duc Anh³, Trinh Thanh Tung¹, Dinh Nhat Quang² and Nguyen Trung Viet²

¹ Thuyloi University, Dong Da, Hanoi 10000, Vietnam

² Faculty of Civil Engineering, Thuyloi University, Dong Da, Hanoi 10000, Vietnam

³ Institute of Civil Engineering, Thuyloi University, Dong Da, Hanoi 10000, Vietnam

*Corresponding author: tamhs.cctl@tlu.edu.vn

Abstract. Cua Lo is one of the most potential areas for port economic development in Chu Lai Open Economic Zone, Quang Nam province. To protect navigation channel from sedimentation and waves, according to master plan, two jetties are constructed in the North and South Cua Lo by dredging and cutting through the sand spit in the North bank. Prediction the impacts of navigation channel construction and its protections on the hydrodynamic regime and deposition process plays an important role for the success of a port project. In this study, the numerical model Delft3D is developed to evaluate the morphodynamic change of Cua Lo, then calibrated and validated using the observed data in two survey campaigns in 2019. The simulation results reveal that, in the positions with the highest wave height, the construction has had a significant effect of reducing wave height, the reduction is about $0.8\div 0.9$ m, equivalent to 50% compared to the absence of jetties during Northeast monsoon period and $1\div 1.16$ m in adverse conditions, such as floods and storms. In addition, the structures have flood drainage effect with the reduction of maximum water level of $0.8\div 1.2$ m in comparison to the current situation. Moreover, in terms of deposition process, for the area of the new navigation channel between the two jetties, the constructions have effectively reduced the fluctuation of accretion and erosion, about $2500\text{m}^3/\text{year}$.

Keywords. Cua Lo port, DELFT3D, hydrodynamics, sediment transport

Two-dimensional numerical models in simulating hydro-sediment-morphodynamics for the Vu Gia Thu Bon River basin

Binh Quang Nguyen^{1,2,*}, Sameh A. Kantoush¹, Doan Van Binh³, Ngoc Duong Vo², Mohamed Saber¹, Tetsuya Sumi¹

¹Water Resource Center, Disaster Prevention Research Institute (DPRI), Kyoto University, Kyoto 611-0011, Japan

²The University of Danang - University of Science and Technology, 54 Nguyen Luong Bang, Danang, Vietnam

³Master Program of Water Technology, Reuse and Management, Faculty of Engineering, Vietnamese German University, Binh Duong, Vietnam

*Corresponding author: Binh Quang Nguyen (nqbinh@dut.udn.vn)

Abstract. This study aims to establish a complete hydro-sediment-morphodynamics model (TELEMAC-2D + GAIA + NESTOR) and ensure the accuracy of the Vu Gia Thu Bon (VGTB) River basin located in Central Vietnam. The model has been calibrated and validated at six hydrological stations along the river system in 2019, 2020, 2021 and statistical indicators perform good results. The model is able to capture the peaks of water levels in all stations during flood events. The performance R^2 are 0.78, 0.81, 0.95, 0.94, 0.92, and 0.96 at Hoi Khach, Ai Nghia, Cam Le, Giao Thuy, Cau Lau, Hoi An. Similarly, NSE values range from 0.74 at Ai Nghia station to 0.94 at Hoi An station. Moreover, RMSE values vary from 0.041 m to 0.238 m. The simulation results of suspended sediment concentration also have good performance compared with data from turbidimeter and GoogleEarth Engine. The model has well simulated riverbed elevation changes from 2018 to 2021. The results of this study would serve as the primary reference for water resource and sediment management, flood control, hydropower development, and agricultural production. Meanwhile, it provides reliable research data and results for scientists, stakeholders, decision-makers, and local communities, to quickly adapt to climate change and ensure sustainable development for the VGTB River basin.

Keywords. Two-dimensional, hydro-sediment-morphodynamics model, TELEMAC-2D, GAIA, NESTOR, Vu Gia Thu Bon River

Assessment of salinity intrusion trends along main rivers and coastal zones in the Vietnamese Mekong Delta

Nguyen Luyen Phuong DOAN¹, Doan Van BINH², Sameh A. KANTOUSH³, Nguyen Dinh VUONG⁴, Tetsuya SUMI⁵

^{1,2} Faculty of Engineering, Vietnamese –German University, (Ben Cat Town, Binh Duong Province), Vietnam

⁴ Southern Institute of Water Resources Research, (Ho Chi Minh City), Vietnam

^{3,5} Water Resources Research Center, Disaster Prevention Research Institute, Kyoto University (Goka-sho, Uji-shi, 611-011, Kyoto), Japan

*Correspondence to: nguyendoan041297@gmail.com

Abstract. Research on the vulnerability assessment of the Vietnamese Mekong Delta (VMD) is a long story due to the booming challenges of climate change, sea level rise, and salinity intrusion. Remarkably, the salinity intrusion level in this delta has peaked at the highest level in the 21st century, minimizing the available farming productivity and continuously reducing agriculture's economic benefits. Therefore, this research attempts to assess the salinity intrusion trends along main rivers (i.e., Tien, Hau, Co Chien, Ham Luong) and coastal zones (i.e., East and West Vietnam Seas) to understand spatiotemporal variations of salinity intrusion in the VMD. To this end, we analyzed daily salinity concentration at various monitoring stations for more than two decades using several statistical analyses for different indicators of salinity levels. We found that the maximum salinity concentration at Tran De in the Hau River and Vam Kenh in the Tien River (which are near the river mouths) statistically decreased by 0.45 and 0.2 mg/L/year ($p < 0.05$), respectively. At other stations near the river mouth, salinity concentration was relatively stable over the period analyzed. However, salinity concentration statistically increased at stations far upstream from river mouths. This indicates that upstream development, such as river damming and sand mining, is the driving force of the intensifying salinity intrusion in inland areas through morphological degradation.

Assessment of water scarcity under the impact of climate change in the downstream Vu Gia-Thu Bon river basin, Vietnam

Mai Thi Thuy Duong^{1, *}, Võ Ngọc Duong¹, Tran Thi Viet Nga², Le Tran Minh Dat¹

¹The University of Danang – University of Science and Technology, 54 Nguyen Luong Bang Str., Danang City, 50 000, Viet Nam.

²Hanoi University of Civil Engineering, 55 Giai Phong Str., Hanoi City, 100 000, Viet Nam.

*Corresponding author: mttduong@dut.udn.vn

Abstract. The downstream Vu Gia-Thu Bon river basin supplies more than 90% of the water needed for home and industrial use in Da Nang. The water extraction point used to supply the Cau Do - Da Nang clean water factory has experienced an increase in salinization since 2012, which has had a significant influence on water use in the downstream area. The water at the Cau Do factory's extraction site has been salty for 119 days in the first half of 2019, necessitating additional pumps from the An Trach dam. The study used the following computation to get the water stress index (WSI) for 15 areas that make up the Vu Gia-Thu Bon river basin. In the assessment, the water demand for the ecosystem is also considered as a required amount of water in the basins. The MIKE SHE hydrological model with the full major processes in the hydrologic cycle including process models for evapotranspiration, overland flow, unsaturated runoff, groundwater flow, channel runoff and others are used to simulate river flows in the study area for the period of 1980– 2020 and to forecast for 2030. The study also found it important to distinguish subsurface from surface water when calculating the impact of freshwater extraction. The results show that: (1) Water shortages are more severe in the downstream regions than they are in the middle and upstream, particularly where water is being exploited for domestic and industrial use in Da Nang city. (2) Except for the times when the reservoirs release water, the majority of the WSI values between March and May 2020 are higher than 0.6, with a peak of a WSI of more than 3.4, signifying severe scarcity. The Quang Nam-Da Nang region's summer rainfall change in 2030 will drop from 1.9 to 2.1% under the B1 low emission scenario, and the region is likely to experience more severe and extreme droughts. In comparison to 2020, the WSI grew by two times. Water shortages are expected to start earlier and remain longer in 2030, lasting from the beginning of February through September. (3) To address issues with drought, water scarcity, and salinity prevention in the context of climate change and sea level rise, the region needs proactive, suitable adaptation and planning for water resource management. In the downstream region of the Vu Gia river, alternatives for a safe water supply have also been suggested by the research.

Keywords. Downstream Vu Gia – Thu Bon river basin, MIKE SHE model, Environmental Water Requirement, water stress index

Probable maximum precipitation estimates considering homogeneous regions of Malaysia

Nor Eliza Alias^{1,2, *}, Rasnavi Paramasivam¹, Noraliani Alias²

¹ Center for Environment Sustainability and Water Security (IPASA), Universiti Teknologi Malaysia, Johor Bahru, 81310, Malaysia

² Faculty of Civil Engineering, Universiti Teknologi Malaysia, Johor Bahru, 81310, Malaysia

*Corresponding author: noreliza@utm.my

Abstract. Probable maximum precipitation (PMP) values adopted using state boundaries had reported to increase due to substantial increase in atmospheric moisture content and consequent higher levels of moisture transport into storms. Homogeneous regions with similar rainfall characteristics are formed using L-moments method and adopted in the statistical PMP estimation for Malaysia. This research aims to assess the differences between the PMP values estimated using the extreme rainfall homogeneous regions compared to PMPs value estimated using conventional state-boundaries for 1-hour and 24-hour storm duration. The results were compared to projected rainfall from the Non-Hydrostatic Regional Climate Model (NHRCM). Results show that using rainfall data from 1969 to 2012, the PMP estimated using the homogeneous region have higher values compared to the PMP estimated using the state-boundaries. Moreover, the highest historical rainfall up to 2020 exceeds the PMP estimated using the state boundary but were not exceeded by the PMP estimated using the homogenous regions. The PMP estimated using the homogeneous region also have higher values than the highest projected rainfall obtained from NHRCM data (2079-2099).

Keywords. Extreme-rainfall, homogeneous regions, probable maximum precipitation

Climate change intensifies drought vulnerability of magat sub basin in the Philippines

Orlando Balderama¹, Lanie Alejo^{1,3}, Jeffrey Lloyd Bareng², Elmer Rosete⁴, Alvin John B. Felipe^{3*}, Alissandra Pauline Mariano³, and Carluz Bautista³, Christian Alec Managa³

¹ College of Engineering, Isabela State University, Echague, 3309, Philippines

² Water Research and Development Center, Isabela State University, Echague, 3309, Philippines

³ Philippine Council for Industry, Energy, and Emerging Technology Research and Development, 1631, Taguig, Metro Manila, Philippines

⁴ University Research Department, Isabela State University, Echague, 3309, Philippines

*Corresponding author: alvinjohn316felipe@gmail.com

Abstract. This study was conducted to assess the socio-economic impacts of climate change on the vulnerability of a significant river basin in the Philippines, the Magat River Basin, to drought by considering agriculture as the major sector of focus. The results of this study imply that the current drought susceptibility of Magat Watershed is at 1.9 – 3.39 min-max scale or from low to above moderate, where the basin's Sensitivity and Exposure, account for 57% and 31% of the total vulnerability, respectively. And that the resulting adaptive capacity has a mitigating factor of only 12%, thereby construed to be very low. And is projected to increase in the future by up to 30% under climate change scenarios.

Keywords. Climate change, drought, GIS, indicator, Magat watershed, vulnerability



2022
FSMaRT

